教学成果奖申请支撑材料

序号	附件名称
1	优秀论文
2	奖励（优秀毕业生、国奖、优秀毕业论文等）
3	新闻报道

1. 优秀论文

生态环境学报 2019, 28(8): 1613-1621
Ecology and Environmental Sciences
http://www.jeesci.com
E-mail: editor@jeesci.com

基于 ENVI-met 的城市居住区空间形态与 $PM_{2.5}$ 浓度关联性研究

祝玲玲[1]，顾康康[1,2*]，方云皓[1]

1. 安徽建筑大学建筑与规划学院，安徽 合肥 230022；2. 安徽省城镇化发展研究中心，安徽 合肥 230022

摘要：探讨城市居住区空间形态与 $PM_{2.5}$ 浓度关联性，对改善城市居住区空气质量具有重要意义。将居住区空间形态指标归纳为住宅群体组合形式、风向角度、容积率、绿地率等要素，采用 ENVI-met 软件模拟不同居住区空间形态指标下的 $PM_{2.5}$ 浓度，探讨城市居住区空间形态与 $PM_{2.5}$ 浓度关联性。结果表明，不同住宅群体平面组合形式的居住区 $PM_{2.5}$ 浓度分布呈现出较大的差异，周边式和混合式较其他形式居住区内部 $PM_{2.5}$ 难以扩散，行列式与点群式的居住区内部没有出现 $PM_{2.5}$ 聚集的现象，但是点群式居住区外西南角较行列式 $PM_{2.5}$ 积聚的面积大，其平均浓度分别为：171.78、170.021、169.255、172.365 $\mu g \cdot m^{-3}$，综合分析，合肥市居住区住宅群体平面组合形式的最佳方式为行列式，其次为点群式，混合式和周边式不利于居住区 $PM_{2.5}$ 扩散；不同风向角度的居住区 $PM_{2.5}$ 浓度分布呈现较为复杂的变化状况，当风向角度为 15º－30º 时，$PM_{2.5}$ 浓度随着风向角度的增大而增大，十分显著，平均浓度从 136.796 $\mu g \cdot m^{-3}$ 增至 140.796 $\mu g \cdot m^{-3}$，但是增至 45 度时，$PM_{2.5}$ 浓度有所减小，平均浓度为 135.605 $\mu g \cdot m^{-3}$，当风向角度为 60º－90º 时，$PM_{2.5}$ 浓度随着风向角度的增大而增大，变化较小，其平均浓度依次为 132.025、133.87、141.334 $\mu g \cdot m^{-3}$，综合分析，风向角度最优方案为 60º，而 45º、75º 为可选方案，15º、30º、90 º 为不可选方案；$PM_{2.5}$ 浓度较低的为容积率 0.8、其次为 1.2，容积率为 1.6 和 2 的居住区 $PM_{2.5}$ 浓度较高，容积率由小到大其平均浓度分别为 131.678、139.402、159.906、154.638 $\mu g \cdot m^{-3}$，可以基本认为居住区整体空间内的 $PM_{2.5}$ 浓度随着居住区容积率的增大而逐渐增大；增加绿地率可缓解 $PM_{2.5}$ 污染，当绿地率大小超过 35%，$PM_{2.5}$ 浓度随着绿地率的增大而减小的趋势逐渐减缓，综合分析，绿地率应该在 35%以上，才能有效降低居住区的 $PM_{2.5}$ 浓度。

关键词：ENVI-met；居住区；空间形态；$PM_{2.5}$；合肥

DOI: 10.16258/j.cnki.1674-5906.2019.08.014

中图分类号：X16　　**文献标志码：**A　　**文章编号：**1674-5906（2019）08-1613-09

引用格式：祝玲玲, 顾康康, 方云皓, 2019. 基于 ENVI-met 的城市居住区空间形态与 $PM_{2.5}$ 浓度关联性研究[J]. 生态环境学报, 28(8): 1613-1621.

ZHU Lingling, GU Kangkang, FANG Yunhao, 2019. Study on the correlation between space form of urban residential areas and $PM_{2.5}$ concentration based on Envi-met [J]. Ecology and Environmental Sciences, 28(8): 1613-1621.

随着城市化与工业化的快速推进，中国关于城市发展的重点在增加城市数量而忽略提升城市质量，城市开发强度、人口密度不断增长，城市发展面临着交通拥堵、环境污染、空气质量下降等现实问题，其中，$PM_{2.5}$ 污染已经成为世界各国面临的巨大挑战，对维护城市可持续发展产生严重威胁。$PM_{2.5}$ 来源广泛、扩散范围广、危害大，已成为影响我国城市空气质量的首要污染物，不仅降低空气品质、危害人们安全健康，作为形成雾霾天气的主要因素严重阻碍了城市运转（葛跃等，2017；李名升等，2016）。城市土地利用格局决定了城市污染物的空间分布特征，空间形态决定了污染物的扩散特征（顾康康等，2018；牛慧敏等，2016；Li et al.，2017）。居住用地自身造成的污染物浓度较低，但容易受周边污染扩散影响（于静等，2011）。城市居住区较比其他类型用地构成要素多样，进而居住区空间形态差异较大，不同的城市居住区空间形态直接影响污染物扩散状态（吴正旺等，2016a；吴正旺等，2016b）。因此，在研究城市污染物扩散中，无法完全消除污染源的存在，但是可人为调控空间形态，营造良好的通风环境，降低污染物浓度。

目前，国内外关于 $PM_{2.5}$ 污染模拟研究，主要采用 CFD 软件模拟居住区、街区的 $PM_{2.5}$ 污染特征及其影响因素（马西娜等，2017；裴晶晶，2006；裴会义，2016；袁磊等，2019），采用 ENVI-met 软件模拟道路两旁的植被对 $PM_{2.5}$ 浓度的影响

基金项目：2018 年度安徽省教育厅高校自然科学项目（KJ2018ZD047；KJ2018A0504）

作者简介：祝玲玲（1990 年生），女，硕士研究生，研究方向为区域发展与规划。E-mail: linglzhugrd@163.com

*通信作者，顾康康，E-mail: kangkanggu@163.com

收稿日期：2019-06-17

(Skelhorn et al., 2014; 王佳等, 2018; Morakinyo et al., 2016; Li et al., 2016), 较少采用 ENVI-met 软件模拟居住区 $PM_{2.5}$ 扩散, 本论文运用 ENVI-met 软件模拟不同居住区空间形态指标下的 $PM_{2.5}$ 浓度, 为研究居住区 $PM_{2.5}$ 扩散提供新的模拟方法。

1 研究区域与方法

1.1 研究区域

合肥 (30°57′－32°32′N、116°41′－117°58′E) 地处中国华东地区、长江三角洲西沿, 海拔平均高度 8 m, 地势以丘陵岗地为主。位于中纬度地带, 气候属于北亚热带湿润季风气候, 四季分明, 春秋季短而潮湿, 夏季长而闷热, 冬季寒冷、干燥, 全年主导风向以西北风为主, 年均相对湿度为 77%, 年均气温 15.7 ℃, 年均降水量约 1 000 mm。

1.2 测试内容及仪器

测试指标包括大气颗粒物 $PM_{2.5}$ 浓度和气候要素指标气温、相对湿度、风速。选择 2018 年 12 月 2 日的测试, 测试时间为 09:00－17:00, 每隔半小时进行测试。采用中国 ETEST-100 $PM_{2.5}$ 空气质量检测仪测定气温、相对湿度、$PM_{2.5}$ 浓度。采用美国 Kestrel 5500 风速气象仪器测定空气风速。

1.3 测点布置

选择位于合肥市老城区的宝业城市绿苑西区为研究对象, 在居住区内部设置两个测点进行实地监测, 监测点 1 处于建筑间, 监测点 2 处于中心广场, 其具体位置如图 1。



图 1 宝业城市绿苑西区居住区监测点布置图

Fig. 1 Baoyechengshilvyuanxiqu monitoring point distribution map

红色标志为监测点 The red mark is the monitoring point

1.4 研究方法

对合肥市老城区宝业城市绿苑西区进行 $PM_{2.5}$ 浓度监测, 并采用 ENVI-met 数值模拟方法模拟宝业城市绿苑西区的 $PM_{2.5}$ 浓度, 将模拟数据与实测数据进行对比, 从而验证数值模拟的可行性, 为进一步研究提供可靠的方法。在实地调研基础上归纳总结合肥市居住区空间形态特征, 凝练居住区空间形态指标, 包括居住区住宅群体平面组合形式、风向角度、容积率、绿地率等。运用 ENVI-met 软件模拟不同居住区空间形态指标下的 $PM_{2.5}$ 浓度, 定量比较各项空间形态指标包括容积率、绿地率、住宅群体平面组合、风向角度对 $PM_{2.5}$ 浓度的影响机理。

2 结果与分析

2.1 宝业城市绿苑西区 $PM_{2.5}$ 浓度模拟

2.1.1 模型构建

将宝业城市绿苑西区的平面图导入 ENVI-met 软件里面就可以在此基础上准确建模(图 2、图 3), 进而对居住区温湿度、风速、$PM_{2.5}$ 浓度模拟。



图 2 宝业城市绿苑西区的卫星图

Fig. 2 Satellite image of Baoyechengshilvyuanxiqu

红色虚线框内为宝业城市绿苑西区 Inside the red dotted line is the Baoyechengshilvyuanxiqu

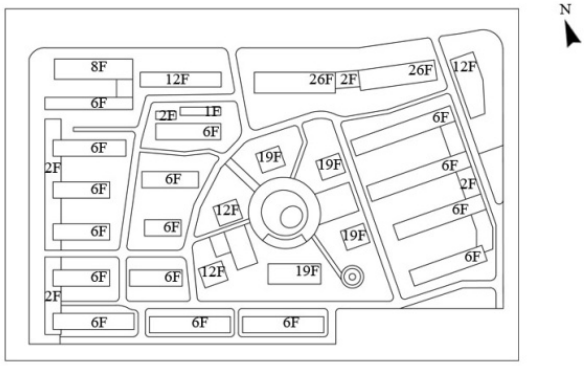


图 3 宝业城市绿苑西区的平面图

Fig. 3 Floor plan of Baoyechengshilvyuanxiqu

2.1.2 模拟数据与实测数据对比

图 4 是冬季以宝业城市绿苑西区为对象进行模拟后, 获得的 2018 年 12 月 2 日 15:00, 水平高度在 1.4 m 的 $PM_{2.5}$ 浓度分布图。数值变化随颜色变化, 由数值较大区域显示颜色黑色向数值较小区域蓝色递进变化。从图 4 可以看出, 在当地湿度、风向、云层厚度等天气条件下, 居住区内不同的空间

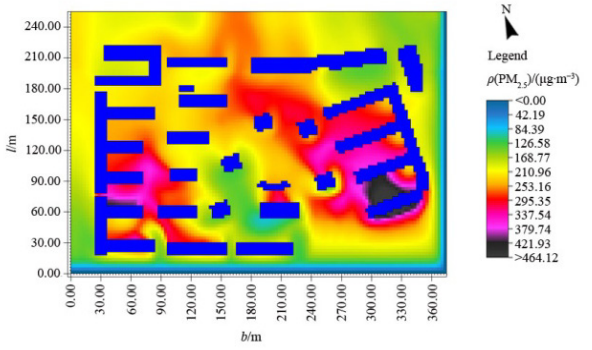


图 4　宝业城市绿苑西区 $PM_{2.5}$ 浓度分布图

Fig. 4　$PM_{2.5}$ concentration distribution map of Baoyechengshilvyuanxiqu

$PM_{2.5}$ 浓度存在较大差异。分析发现，在东南风的条件下，在居住区的下风向容易形成 $PM_{2.5}$ 浓度集聚与沉积的高值区域，从而该区域呈现紫红色、红色；周边式布局的居住区内部 $PM_{2.5}$ 浓度明显增加，该区域呈现紫红色。在建筑的背风向 $PM_{2.5}$ 浓度较大，且当建筑密集排列时十分明显；在建筑稀疏的空间开阔区域，$PM_{2.5}$ 浓度逐渐被疏散，$PM_{2.5}$ 浓度较低，呈现黄色、绿色。

图 5 是对宝业城市绿苑西区的 9:00－17:00 的模拟 $PM_{2.5}$ 浓度与实测 $PM_{2.5}$ 浓度对比图，模拟 $PM_{2.5}$ 与实测 $PM_{2.5}$ 数值都是先下降后上升。模拟与实测测点 1 平均 $PM_{2.5}$ 浓度都要低于测点 2 的平均 $PM_{2.5}$ 浓度，测点 1 与 2 模拟的平均 $PM_{2.5}$ 浓度分别为 194.85、229.21 $\mu g \cdot m^{-3}$，两者相差 35 $\mu g \cdot m^{-3}$，测点 1 与测点 2 实测平均 $PM_{2.5}$ 浓度分别为 216.41，235.53 $\mu g \cdot m^{-3}$，两者相差 19 $\mu g \cdot m^{-3}$；测点 1 与测点 2 模拟 $PM_{2.5}$ 浓度与实测 $PM_{2.5}$ 浓度误差分别为 11.06%、2.8%。由于实测环境为复杂的城市建设环境，而模拟建立的模拟环境更加简单，使得实测值高于模拟值，此外，当天实测天气属于雾霾天气，加剧了这种现象，但两者 $PM_{2.5}$ 浓度空间分布和趋

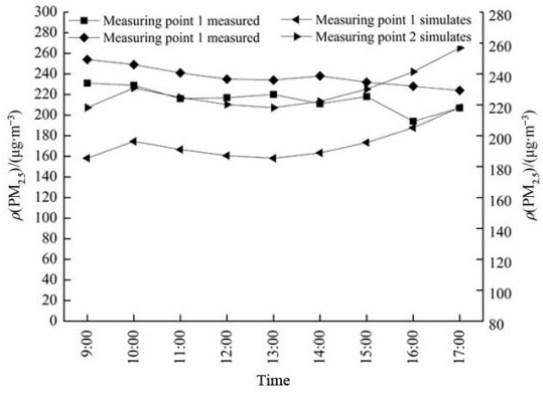


图 5　宝业城市绿苑西区实测 $PM_{2.5}$ 与模拟 $PM_{2.5}$ 浓度对比图

Fig. 5　Comparison of measured $PM_{2.5}$ and simulated $PM_{2.5}$ concentrations in Baoyechengshilvyuanxiqu

势变化基本一致，因此模拟能够反映居住区 $PM_{2.5}$ 浓度的分布与扩散。

2.2　平面布局模拟

2.2.1　住宅群体平面组合形式

图 6 是东北风的条件下，时间为冬季 15:00 点，不同住宅群体平面组合形式的居住区 1.4 m 高度的 $PM_{2.5}$ 浓度分布图。图 7 是在不同住宅群体平面组合形式的居住区内 1.4 m 高度西侧到东侧建筑间 $PM_{2.5}$ 浓度对比图。从图可以看出，不同住宅群体平面组合形式的居住区 $PM_{2.5}$ 浓度分布呈现出较大的差异。

从图 6 可以看出，在周边式的居住区内部的西侧与西南角 $PM_{2.5}$ 容易积聚，且面积较大，模拟分析图中呈现红色、黄色，而混合式与之类似，略低于周边式，表明周边式和混合式较其他形式居住区内部 $PM_{2.5}$ 难以扩散。行列式与点群式的居住区内部没有出现 $PM_{2.5}$ 聚集的现象，且 $PM_{2.5}$ 浓度分布较为稳定，但是点群式居住区外西南角较行列式 $PM_{2.5}$ 积聚的面积大，紫红色部分。由图 7 的数据对比发现，周边式与混合式的浓度较高且非常接近，周边式略高于混合式，其次为行列式，浓度最低的为点群式，其平均浓度分别为：171.78、170.0213、169.255、172.365 $\mu g \cdot m^{-3}$，在西侧开阔地间十分明显，且 4 种布局方式浓度均达到最高，分别是 265.51、25.91、174.96、203.7 $\mu g \cdot m^{-3}$。综上所述，最有利的布局模式为：行列式。因此，居住区住宅群体平面组合的最佳方式为行列式，其次为点群式，混合式和周边式不利于居住区的 $PM_{2.5}$ 扩散。

在对合肥市居住区住宅群体平面组合形式进行分析总结，提炼最常见的 4 种住宅群体平面组合形式，对 4 种住宅群体平面组合形式的居住区 $PM_{2.5}$ 浓度分别进行数值模拟，最终得到居住区住宅群体平面组合的最佳方式为行列式，其次为点群式，混合式和周边式不利于居住区的 $PM_{2.5}$ 扩散。

2.2.2　风向角度

图 8 是风向角度分别为 15°、30°、45°、60°、75°、90° 的情况下，居住区 1.4 m 高度的 $PM_{2.5}$ 浓度分布图。图 9 是风向角度分别为 15°、30°、45°、60°、75°、90° 的居住区内 1.4 m 高度西侧到东侧建筑间 $PM_{2.5}$ 浓度对比图。从图可以看出，不同风向角度的居住区 $PM_{2.5}$ 浓度分布呈现较为复杂的变化状况。

从图 8 可以看出，当风向角度达到 45° 的时候，居住区的整体风环境随着迎风口的方向改变而转变，从而对整个居住区内部的 $PM_{2.5}$ 浓度产生影响。从图 8 看出，当风向角度小于 30° 时，$PM_{2.5}$ 得不到有效的扩散，尤其是在居住区南边建筑间，此时，$PM_{2.5}$ 浓度随着风向角度的增大而增大，浓度较大的

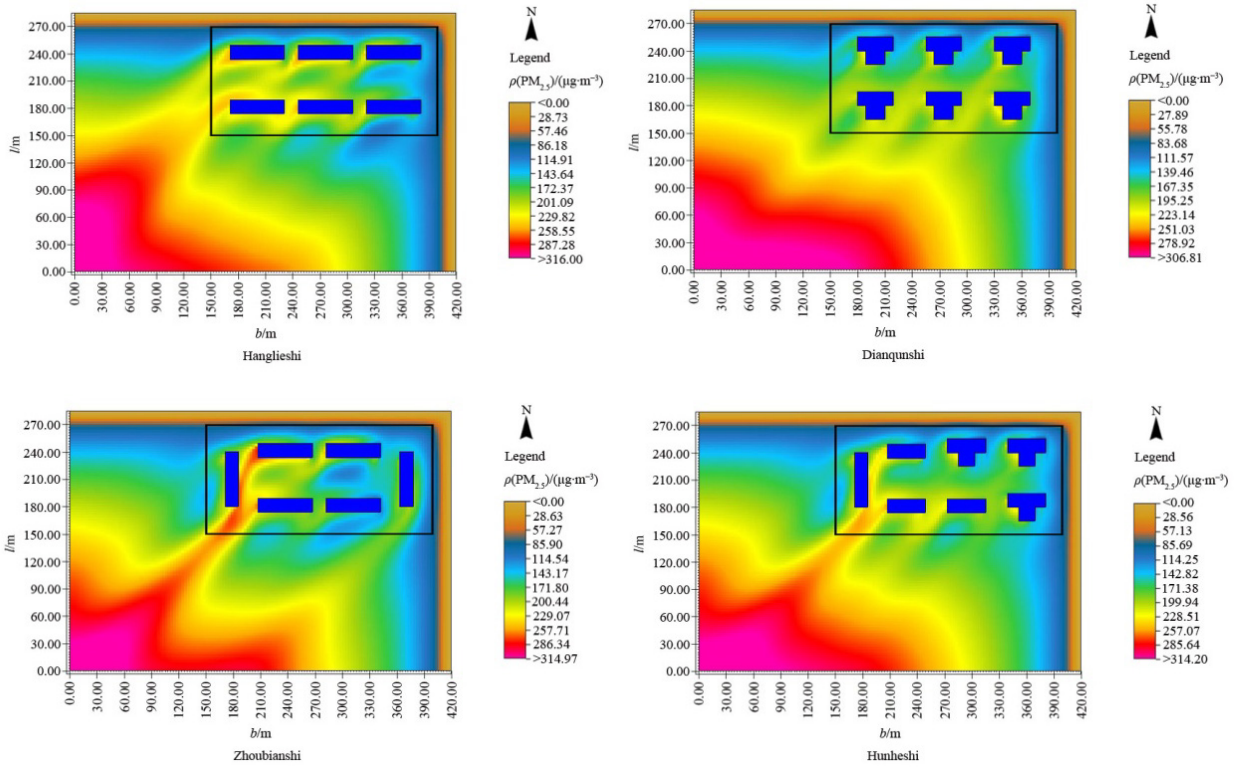


图 6 不同住宅群体平面组合形式的居住区 $PM_{2.5}$ 浓度分布图

Fig. 6 Distribution of $PM_{2.5}$ concentration in residential areas with different combinations of residential groups

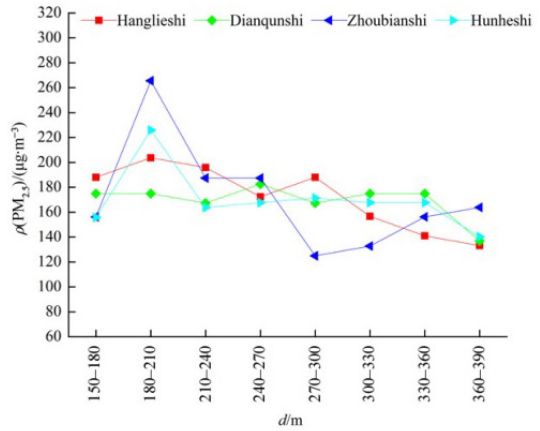


图 7 不同住宅群体平面组合形式的居住区内西侧到东侧建筑间 $PM_{2.5}$ 浓度对比图

Fig. 7 Comparison of $PM_{2.5}$ concentrations between buildings on the west to east side in residential areas with different combinations of residential groups

红色区域增大程度明显；从 30º—45º 时，居住区内部空间的 $PM_{2.5}$ 浓度逐渐降低，浓度较大的红色区域明显减小，且整个居住区 $PM_{2.5}$ 浓度分布较为平稳；风向角度达到 60º 之后，整个居住区内部 $PM_{2.5}$ 浓度分布很不均匀，空间差异明显，呈现阶梯状色块。由图 9 的数据对比发现，当风向角度从 15º—30º 时，其浓度排序为 15º<30º，平均浓度分别为 136.796 2、140.796 2 μg·m^{-3}，由此可知，$PM_{2.5}$ 浓度随着风向角度的增大而增大，十分显著；增加到 45º 时，其浓度有所降低，平均浓度为 135.605 4 μg·m^{-3}，由此可知，$PM_{2.5}$ 浓度随着风向角度的增大而降低；当风向角度从 60º—90º 度时，其浓度排序为 60º<75º<90º，平均浓度分别为 132.025 4、133.87、141.333 8 μg·m^{-3}，由此可知，居住区内部空间的 $PM_{2.5}$ 浓度随着风向角度的增大逐渐递增，但增幅较小。此外，若风向角度过大，冷空气直接贯穿居住区，从而增大居住区的热工耗能，人为增加 $PM_{2.5}$ 污染，因此，在选择最优方案时，综合考虑各项因素。

风环境是 $PM_{2.5}$ 浓度的主要影响因素（贾小芳等，2019）。通过数值模拟，随着风向投射角度的改变，在居住区的 $PM_{2.5}$ 浓度分布呈现出较为复杂的变化。可以看出，风经过居住区的内部空间，会带走居住区内部的 $PM_{2.5}$，但是随着居住区风向角度不同，主导风被建筑不同程度的阻挡，居住区内部空间的 $PM_{2.5}$ 呈现出不同的浓度状况。

对不同风向角度的居住区 $PM_{2.5}$ 浓度进行模拟，当风向角度为 15º—30º 时，$PM_{2.5}$ 浓度随着风向角度的增大而增大，十分显著，但是 45º 时，$PM_{2.5}$ 浓度有所减小，当风向角度为 60º—90º 时，$PM_{2.5}$ 浓度随着角度的增大而增大，变化幅度较小。综合分析，最终得到风向角度最优方案为 60º，而 45º、

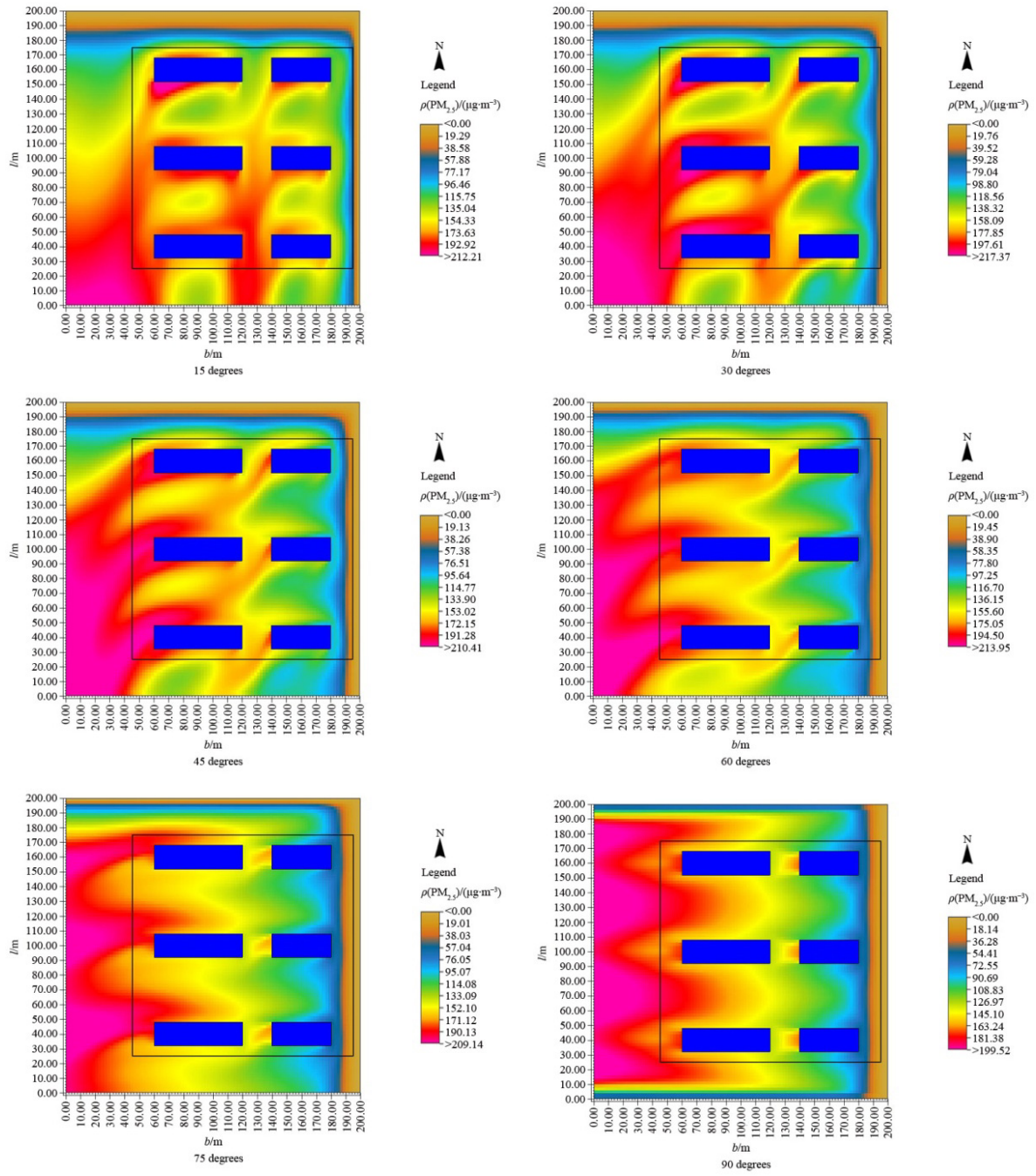


图 8　不同风向角度的居住区 $PM_{2.5}$ 浓度分布图

Fig. 8　Distribution of $PM_{2.5}$ concentration in residential area with different wind direction angle

75º 为可选方案，15º、30º、90º 为不可选方案。

2.3　开发强度模拟

2.3.1　容积率

图 10 是在以东北风为主导风向，时间为冬季下午 3 点，容积率分别为 0.8、1.2、1.6、2 的居住区 1.4 m 高度的 $PM_{2.5}$ 浓度分布图。图 11 是容积率分别为 0.8、1.2、1.6、2 的居住区 1.4 m 高度西侧到东侧建筑间 $PM_{2.5}$ 浓度对比图。整体来看，不同容积率的居住区的 $PM_{2.5}$ 浓度变化较为明显。

从图 10 可以看出，随着容积率的增大，建筑间距的减小，居住区整体空间内的 $PM_{2.5}$ 浓度增加较为明显，浓度较低的蓝色区域缩减程度明显，在居住区建筑间尤其明显；居住区外西南角重度污染区（紫色、红色）面积随着容积率的增大而增大。此外，建筑背风向的 $PM_{2.5}$ 浓度较大，尤其是贴近建筑处的区域 $PM_{2.5}$ 浓度，建筑间开阔地空间浓度较建筑附近的浓度小。由图 11 的数据对比可以发现，$PM_{2.5}$ 浓度较低的为容积率 0.8、其次为 1.2，容积率为 1.6 和 2 的居住区 $PM_{2.5}$ 浓度较高，其平均浓度分别为 131.678、139.402、159.906、154.638 $\mu g \cdot m^{-3}$。综上

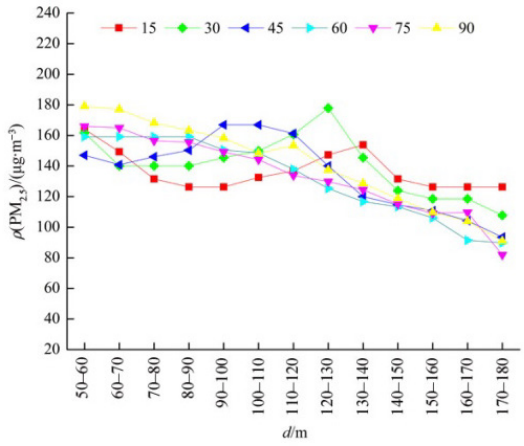


图 9 不同风向角度的居住区西侧到东侧建筑间 $PM_{2.5}$ 浓度对比图

Fig. 9 Comparison of $PM_{2.5}$ concentrations between the west and east sides of the residential area with different wind direction angles

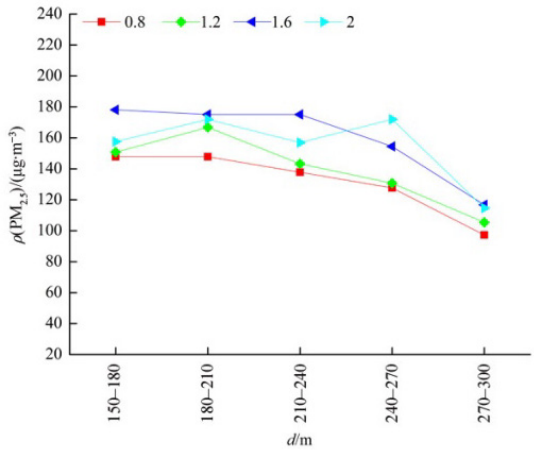


图 11 不同容积率的居住区内西侧到东侧建筑间 $PM_{2.5}$ 浓度对比图

Fig. 11 Comparison of $PM_{2.5}$ concentrations between the west and east sides of the residential area with different floor area ratios

所述，可以基本认为居住区整体空间内的 $PM_{2.5}$ 浓度随着居住区容积率的增大而逐渐增大。

对不同容积率的城市居住区 $PM_{2.5}$ 浓度进行模拟，从而对其 $PM_{2.5}$ 浓度进行比较分析，在居住区内建筑间 1.4 m 高度下，居住区整体空间内的 $PM_{2.5}$ 浓度随着居住区容积率的增大而逐渐增大。

2.3.2 绿地率

图 12 是绿地率分别为 20%、25%、30%、35%、40%的居住区 1.4 m 高度的 $PM_{2.5}$ 浓度分布图。图 13 是绿地率分别为 20%、25%、30%、35%、40%

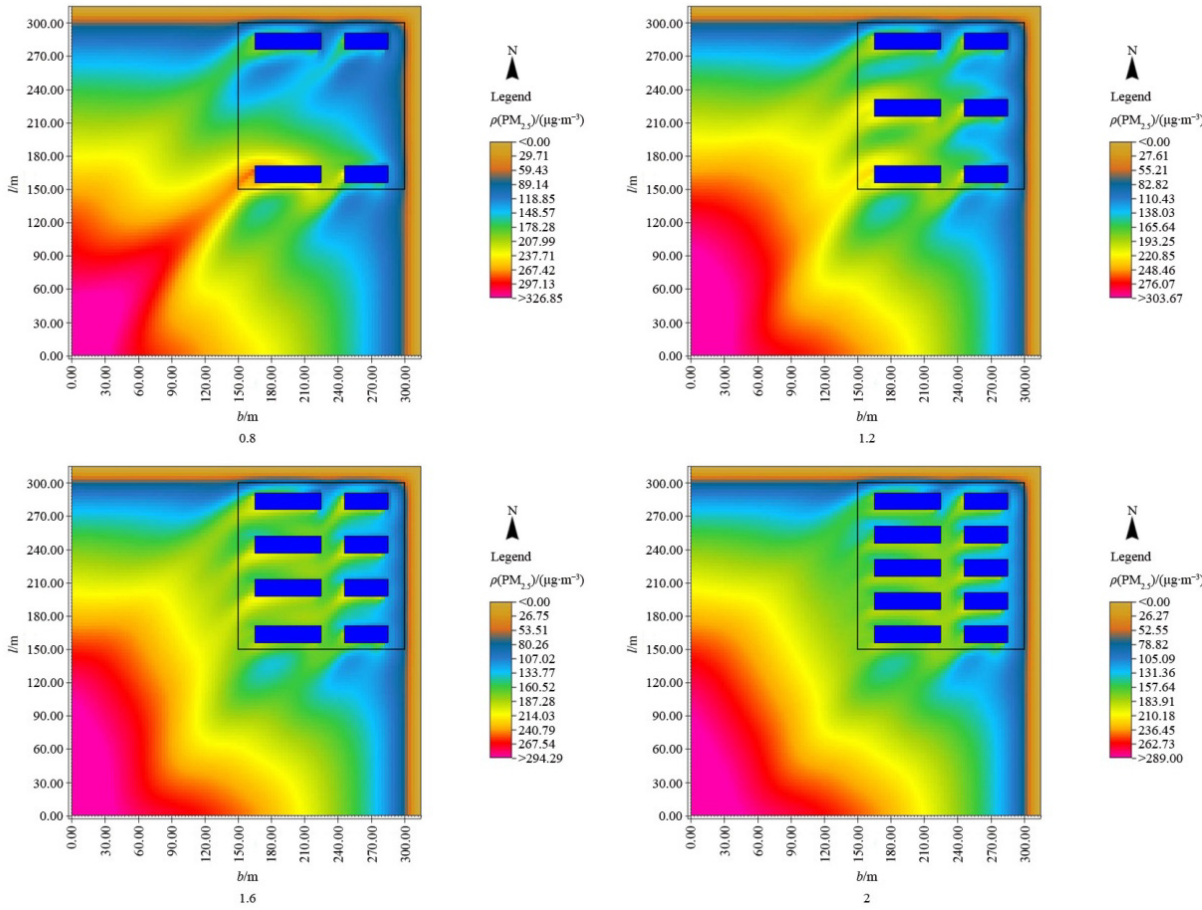


图 10 不同容积率的居住区的 $PM_{2.5}$ 浓度分布图

Fig. 10 Distribution of $PM_{2.5}$ concentration in residential areas with different floor area ratios

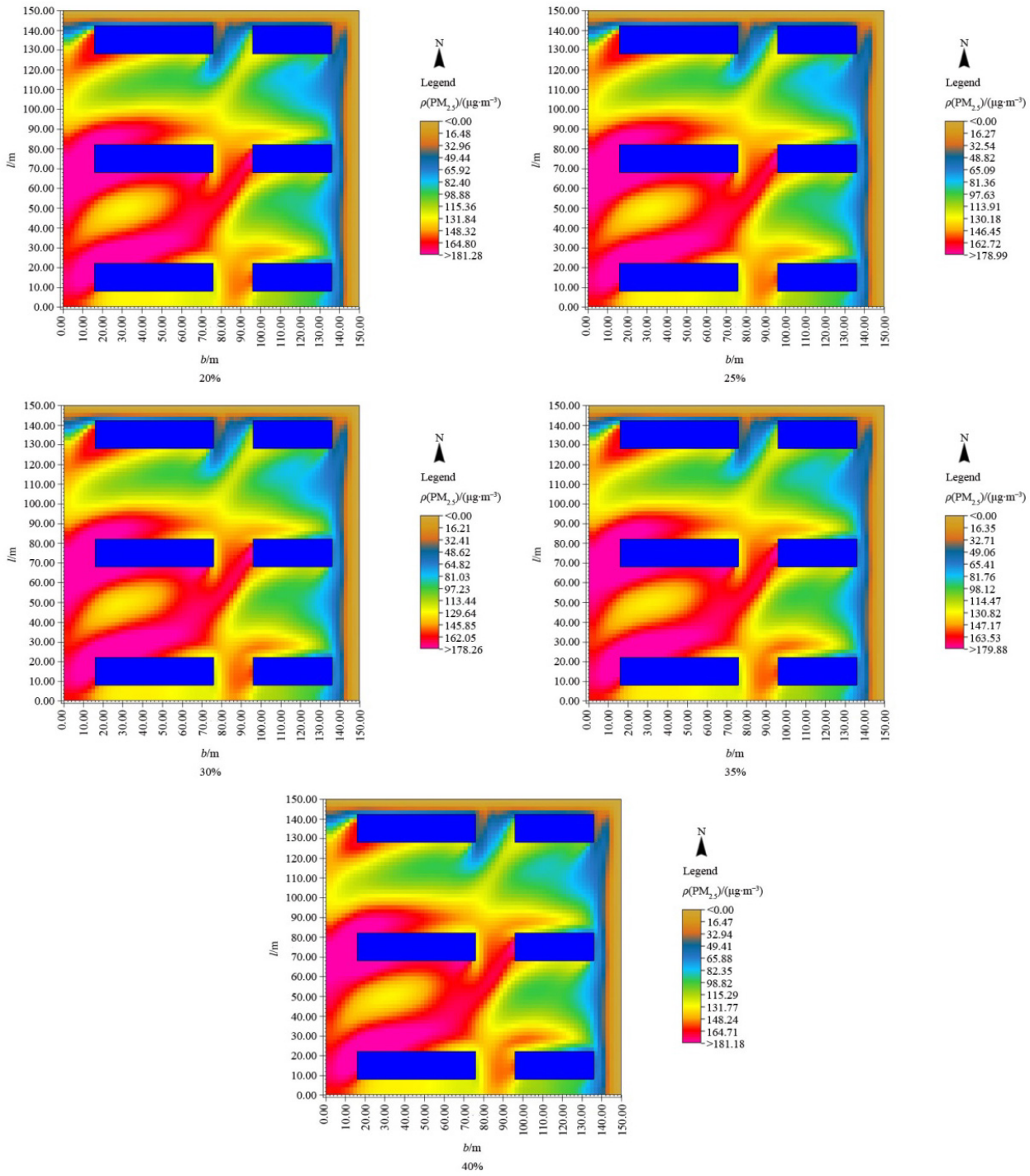


图 12　不同绿地率的居住区 $PM_{2.5}$ 浓度分布图

Fig. 12　Distribution of $PM_{2.5}$ concentration in residential areas with different green rates

的居住区内 1.4 m 高度西侧到东侧建筑间 $PM_{2.5}$ 浓度对比图，$PM_{2.5}$ 浓度随着绿地率大小不同呈现出一定的规律。

从图 12 可以看出，建筑背风向的 $PM_{2.5}$ 浓度较大，尤其是贴近建筑处的 $PM_{2.5}$ 浓度，$PM_{2.5}$ 浓度较小的为建筑间的开阔地带，居住区的西南侧 $PM_{2.5}$ 浓度较大。由图 13 的数据对比可以发现，呈现出 $PM_{2.5}$ 浓度随着绿地率的增大而减小的趋势，其浓度分别为：104.076、105.676、107.496、108.878、106.764 $\mu g \cdot m^{-3}$。但是当绿地率大小超过 35%，$PM_{2.5}$ 浓度随着绿地率的增大而减小的趋势逐渐减缓。绿地植被通过植物表面体吸附颗粒物，降低 $PM_{2.5}$ 的浓度（乔冠皓等，2017；Lu et al.，2018；Xie et al.，2018）；此外，绿地能改善居住区温湿环境，也可防止扬尘的二次污染。但是植被密度过大能阻挡风的流动，使得居住区内空间内的 $PM_{2.5}$ 处于稳定的

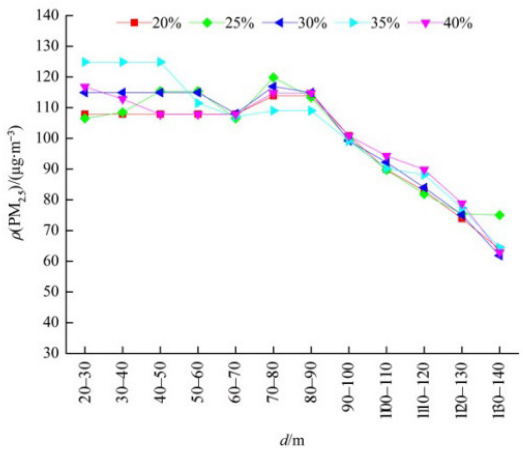


图 13 不同绿地率的的居住区内西侧到东侧建筑间 $PM_{2.5}$ 浓度对比图

Fig. 13 Comparison of $PM_{2.5}$ concentrations between the west and east sides of the residential area with different green rates

环境中，不利于扩散（Sanchez et al.，2015；马杰等，2013）。

增加绿地率可缓解 $PM_{2.5}$ 污染。通过综合分析，绿地率应该在 35%以上，才能有效缓解居住区的 $PM_{2.5}$ 浓度。绿化植被具有滞留吸纳颗粒物的能力，可改善热岛效应，此外，绿地植被可以防止扬尘的二次污染。但是，植被郁闭度过大能阻挡空气中的风，使得大气颗粒物处于一个稳定的环境中。

3 结论

本文在实地调研基础上归纳总结合肥市居住区空间形态特征，凝练居住区空间形态指标，包括居住区住宅群体平面组合形式、容积率、绿地率等。运用 ENVI-met 软件模拟不同居住区空间形态指标下的 $PM_{2.5}$ 浓度，定量比较各项城市居住区空间形态与 $PM_{2.5}$ 浓度的相关性，主要结论如下：

（1）居住区住宅群体平面组合形式的最佳方式为行列式，其次为点群式，混合式和周边式不利于居住区的 $PM_{2.5}$ 扩散。

（2）当风向角度为 15º－30º 时，$PM_{2.5}$ 浓度随着风向角度的增大而增大，十分显著，但是 45º 时，$PM_{2.5}$ 浓度有所减小，当风向角度为 60º－90º 时，$PM_{2.5}$ 浓度随着风向角度的增大而增大，但变化幅度较小。综合分析，最终得到风向角度最优方案为 60º，而 45º、75º 为可选方案，15º 为不可选方案。

（3）居住区整体空间内的 $PM_{2.5}$ 浓度随着居住区容积率的增大而逐渐增大。因此，控制居住区开发强度指标有利于居住区整体人居环境的提升。

（4）绿地率与 $PM_{2.5}$ 浓度负相关。但是，植被密度过大能阻挡风的流动，使得大气颗粒物处于一个稳定的环境中。通过分析，绿地率应该在 35%以上，才能有效缓解居住区的 $PM_{2.5}$ 浓度。

参考文献：

LI L F, WU A H, CHENG I, et al., 2017. Spatiotemporal estimation of historical $PM_{2.5}$ concentrations using PM_{10}, meteorological variables, and spatial effect [J]. Atmospheric Environment, 166: 182-191.

LI X B, LU Q C, LU S J, et al., 2016. The impacts of roadside vegetation barriers on the dispersion of gaseous traffic pollution in urban street canyons [J]. Urban Forestry & Urban Greening, 17: 80-91.

LU S W, YANG X B, LI S N, et al., 2018. Effects of plant leaf surface and different pollution levels on $PM_{2.5}$, adsorption capacity [J]. Urban Forestry & Urban Greening, 34: 64-70.

MORAKINYO T E, LAM Y F, 2016. Simulation study of dispersion and removal of particulate matter from traffic by road-side vegetation barrier [J]. Environmental Science and Pollution Research, 23(7): 6709-6722.

SANCHEZ I A, MCCOLLIN D, 2015. A comparison of microclimate and environmental modification produced by hedgerows and dehesa in the Mediterranean region: A study in the Guadarrama region, Spain [J]. Landscape and Urban Planning, 143(1): 230-237.

SKELHORN C, LINDLEY S, LEVERMORE G, 2014. The impact of vegetation types on air and surface temperatures in a temperate city: A fine scale assessment in Manchester, UK [J]. Landscape and Urban Planning, 121: 129-140.

XIE C, KAN L, GUO J, et al., 2018. A dynamic processes study of PM retention by trees under different wind conditions [J]. Environmental Pollution, 233: 315-322.

顾康康, 祝玲玲, 2018. 合肥市主城区 $PM_{2.5}$ 时空分布特征研究[J]. 生态环境学报, 27(6): 1107-1112.
GU K K, ZHU L L, 2018. Study on the spatial-temporal distribution characteristics of $PM_{2.5}$ in Hefei urban areas [J]. Ecology and Environmental Sciences, 27(6): 1107-1112.

葛跃, 王明新, 孙向武, 等, 2017. 基于增强回归树的城市 $PM_{2.5}$ 日均值变化分析:以常州为例[J]. 环境科学, 38(2): 485-494.
GE Y, WANG M X , SUN X W, et al., 2017. Variation analysis of daily $PM_{2.5}$ concentrations based on boosted regression tree: A case study in Changzhou [J]. Environmental Science, 38(2): 485-494.

贾小芳, 颜鹏, 孟昭阳, 等, 2019. 2016 年 11－12 月北京及周边重污染过程 $PM_{2.5}$ 特征[J]. 应用气象学报, 30(3): 302-315.
JIA X F, YAN P, MENG Z Y, et al., 2019. Characteristics of $PM_{2.5}$ in heavy pollution events in Beijing and surrounding areas from November to December in 2016 [J]. Journal of Applied Meteorological Science, 30(3): 302-315.

李名升, 任晓霞, 于洋, 等, 2016. 中国大陆城市 $PM_{2.5}$ 污染时空分布规律[J]. 中国环境科学, 36(3): 641-650.
LI M S, REN X X, YU Y, et al., 2016. Spatiotemporal pattern of ground-level fine particulate matter ($PM_{2.5}$) pollution in mainland China [J]. China Environmental Science, 36(3): 641-650.

马杰, 李晓锋, 朱颖心, 2013. 住区微气候的数值模拟方法研究[J]. 太阳能学报, 34(12): 2132-2138.
MA J, LI X F, ZHU Y X, 2013. Numerical simulation of microclimate around residential buildings [J]. Acta Energiae Solaris Sinica, 34(12): 2133-2138.

马西娜, 马方, 赵敬源, 等, 2017. 庭院式居住组团平面形态对 $PM_{2.5}$ 扩散的影响[J]. 建筑科学与工程学报, 34(4): 120-126.
MA X N, MA F, ZHAO J Y, et al., 2017. Effect of Courtyard Housing Group Plane Shape on $PM_{2.5}$ Diffusion [J]. Journal of Architecture and Civil Engineering, 34(4): 120-126.

牛慧敏, 涂建军, 姚作林, 等, 2016.中国城市空气质量时空分布特征[J]. 河南科学, 34(8): 1317-1321.
NIU H M, TU J J, YAO Z L, et al., 2016. Spatial and Temporal Distrubution Characteristics of Air Quality in Chain Cities [J]. Henan Sciences, 34(8): 1317-1321.

裴会义, 2016. 石家庄雾霾与高层建筑规划布局探索[D]. 石家庄: 河北科技大学: 1-86.
PEI H Y, 2016. The Study on the Relationship between City [D].

Shijiazhuang: Hebei University of Science and Technology: 1-86.

裴晶晶, 2006. 废气污染对建筑小区空气质量影响的研究[D]. 天津: 天津大学: 1-72.
PEI J J, 2006. Research on the influence of waste gas pollution on residential area air quality [D]. Tianjin: Tianjin University: 1-72.

乔冠皓, 陈警伟, 刘肖瑜, 等, 2017. 两种常见绿化树种对大气颗粒物的滞留与再悬浮[J]. 应用生态学报, 28(1): 266-272.
QIAO G H, CHEN J W, LIU X Y, et al., 2017. Retention and resuspension of atmospheric particles with two common urban greening trees [J]. Chinese Journal of Applied Ecology, 28(1): 266-272.

王佳, 吕春东, 牛利伟, 等, 2018. 道路植被结构对大气可吸入颗粒物扩散影响的模拟与验证[J]. 农业工程学报, 34(20): 225-232.
WANG J, LU C D, NIU L W, et al., 2018. Simulation and verification of influence of different street vegetation structure on diffusion of atmosphere particulates [J]. Transactions of the Chinese Society of Agricultural Engineering, 34(20): 225-232.

吴正旺, 韩宇婷, 吴彦强, 2016. $PM_{2.5}$ 在北京几种典型居住区中的分布及扩散比较[J]. 华中建筑, 34(8): 38-41.
WU Z W, HANG Y T, WU Y Q, 2016. Distribution and diffusion comparison of $PM_{2.5}$ in several typical residential areas in Beijing [J]. Huazhong Architecture, 34(8): 38-41.

吴正旺, 王岩慧, 单海楠, 2016. 基于 $PM_{2.5}$ 分布不均现象的城市居住区景观格局分析[J]. 华中建筑, 34(2): 52-56.
WU Z W, WANG Y H, SHAN H N, 2016. Residential area landscape pattern optimization analysis on the based of uneven distribution of $PM_{2.5}$ [J]. Huazhong Architecture, 34(2): 52-56.

于静, 张志伟, 蔡文婷, 2011. 城市规划与空气质量关系研究[J]. 城市规划, 35(12): 51-56.
YU J, ZHANG Z W, CAI W T, 2011. Research on relationship between urban planning and air quality [J]. City Planning Review, 35(12): 51-56.

袁磊, 宛杨, 何成, 2019. 基于 CFD 模拟的高密度街区交通污染物分布[J]. 深圳大学学报, 36(3): 274-280.
YUAN L, YUAN Y, HE C, 2019. Distribution of traffic pollutants in high-density blocks based on CFD simulation [J]. Journal of Shenzhen University, 36(3): 274-280.

Study on the Correlation between Space form of Urban Residential Areas and $PM_{2.5}$ Concentration Based on Envi-met

ZHU Lingling[1], GU Kangkang[1, 2], FANG Yunhao[1]

1. School of Architecture & Planning, Anhui Jianzhu University, Hefei 230022, China;

2. Research Center of Urbanization Development in Anhui Province, Hefei 230022, China

Abstract: Exploring the correlation between space form of urban residential areas and $PM_{2.5}$ concentration is of great significance for improving the air quality of urban residential areas. In this paper, the space form index of residential area is summarized as the combination form of residential group, wind direction angle, floor area ratio, green rate. The $PM_{2.5}$ concentration under different space form index of residential area is simulated by ENVI-met software, and the correlation between the space form of urban residential area and $PM_{2.5}$ concentration is studied. The experimental results are as follows: the concentration distribution of $PM_{2.5}$ in different combination forms of residential group shows great difference. The $PM_{2.5}$ concentration in peripheral and mixed residential areas is more difficult to diffuse than that in other residential areas. There is no $PM_{2.5}$ aggregation in determinant and point-group residential areas. However, the aggregation area of $PM_{2.5}$ in the southwest corner of the point-group residential area is larger than that in determinant residential area. The average concentration of $PM_{2.5}$ is 171.78, 170.021, 169.255, 172.365 $\mu g \cdot m^{-3}$, respectively. Comprehensive analysis shows that the best way of the combination form of residential groups in residential areas in Hefei is determinant, followed by point-group, mixed type and peripheral type are not conducive to $PM_{2.5}$ diffusion in residential area. Meanwhile, the distribution of $PM_{2.5}$ concentration in residential areas with different wind direction presents complex changes. When the wind direction angle is 15º–30º, the $PM_{2.5}$ concentration increases with the increase of the wind direction angle, which is very significant. The average concentration increases from 136.796 $\mu g \cdot m^{-3}$ to 140.796 $\mu g \cdot m^{-3}$. However, when the wind direction angle increases to 45º, the $PM_{2.5}$ concentration decreases, and the average concentration is 135.605 $\mu g \cdot m^{-3}$. When the wind direction angle is 60º–90º, the $PM_{2.5}$ concentration increases with the increase of the wind direction angle, and the average concentration is 132.025, 133.87, 141.334 $\mu g \cdot m^{-3}$, respectively. Comprehensive analysis shows that the optimal scheme of wind direction angle is 60º, while 45º and 75º are optional, and 15º, 30º and 90º are not available. In addition, when the floor area ratio is 0.8, the concentration of $PM_{2.5}$ is lower, followed by 1.2. The concentration of $PM_{2.5}$ in residential area with floor area ratio of 1.6 and 2 is higher. When the floor area ratio changes from small to large, the average concentrations are 131.678, 139.402, 159.906, 154.638 $\mu g \cdot m^{-3}$, respectively. It can be basically considered that the $PM_{2.5}$ concentration in the whole space of residential area increases gradually with the increase of the floor area ratio of residential area. Moreover, $PM_{2.5}$ pollution can be alleviated by increasing the green space. When green rate exceeds 35%, $PM_{2.5}$ concentration decreases lowly with the increase of green space rate. Comprehensive analysis shows that the green rate should be above 35% in order to effectively reduce the $PM_{2.5}$ concentration in residential areas.

Key words: Envi-met; residential area; space form; $PM_{2.5}$; Hefei

基于 GIS 的采煤塌陷区生态恢复优先级评价
——以安徽省淮南市区为例

张 岸[1]，顾康康[1,2]
(1.安徽建筑大学 建筑与规划学院，合肥 230022；2.安徽省城镇化发展研究中心，合肥 230022)

摘要： 选取煤矿型城市淮南市区为研究区域，以 2017 年 12 月淮南市 Landsat-TM 影像、淮南市采煤塌陷地分布矢量图和全国第二次土地调查的土地利用数据为数据源，在 GIS 技术支撑下，从生态敏感性和生物多样性服务价值两个方面评价采煤塌陷区的生态恢复优先级，利用 GIS 中的自然断点法将生态恢复优先级分为非常低、低、中等、较高和高 5 个级别。结果表明：淮南市区生态恢复优先级高和较高的塌陷区面积所占比例为 27.34%，主要分布于潘集区采煤塌陷区的中南部、八公山区采煤塌陷区的大部分区域、谢家集区采煤塌陷区的西北部以及大通区采煤塌陷区的大部分区域，建议将这些区域予以优先恢复。

关 键 词： 采煤塌陷区；生态敏感性；生物多样性服务价值；GIS；生态恢复优先级；淮南市
中图分类号： TD88 **文献标志码：** A **文章编号：** 1003-2363(2019)04-0122-05
doi: 10.3969/j.issn.1003-2363.2019.04.020

0 引言

面对快速城镇化和工业化进程导致的严重生态退化问题，生态恢复已成为国内外学者普遍关注的热点话题。生态修复是避免生物多样性损失和生态系统破坏的关键方法之一。20 世纪 80 年代以来，国内外学者针对生态系统退化问题，开展了一系列生态恢复研究[1]。进入 21 世纪后，生态问题越来越受到政府和社会的重视。在党的十八大上，生态文明被纳入五位一体，正式上升到国家战略层面。党的十九大进一步强调了建设生态文明、提升城市环境品质的重要性。在此国家战略层面引导下，“城市更新”“城市双修”等概念被提出。基于城市双修背景，生态修复已刻不容缓。然而，生态恢复是一项费用高昂、建设周期较长的工作，常面临经费不足的困难和各利益主体之间的矛盾，急需确定生态恢复的重要等级，以确保生态恢复高效、有序地进行[2-4]。目前，生态恢复优先级的研究对象主要针对森林、湿地、海域等自然生态退化区域。如姜帆等运用主成分分析、典型相关方法来分析示范区植被恢复效果与影响因素之间的关系，并提出生态恢复措施[5]；何萍等根据海河流域生态系统退化的严重性等级和保护重要性等级构造判断矩阵，获取保护优先级[6]；董张玉等以 GIS/RS 为技术手段，从景观结构因子、湿度指数等影响因素对东北地区湿度恢复潜力进行空间分析，确定湿地恢复的优先区域[7]。相比较而言，针对矿区的研究成果较少，而矿区作为人工系统，生态恢复面临的问题更加复杂。因此，本研究选取煤矿型城市淮南市区作为研究区域，探讨采煤塌陷区的生态恢复优先等级。

采煤塌陷区生态恢复优先级评价的关键是生态恢复综合适宜度分析，一般从生态适宜性和生态敏感性等方面进行研究。目前，生态敏感性分析主要从自然和人为因素等方面开展多个生态敏感性因子加权叠加的综合分析，这对于城市建设用地的开发和生态环境的保护有重要意义[8-9]。然而，生态敏感性分析多是仅考虑生态和人为因素，缺少对经济方面的考量。鉴于此，本研究另外选取评价生物多样性服务价值的指标，以经济价值为基础来估算不同土地利用类型的经济价值，通过自然社会经济的系统研究实现对生态恢复优先级的评价，从生态敏感性和生物多样性服务价值两个方面来探讨采煤塌陷区的生态恢复优先级方法，并提出相应的分区管制措施，为煤炭型矿业城市的生态修复提供参考。

1 研究区域与数据来源

1.1 研究区概况

淮南市地处淮河中游，位于安徽省中部偏北，市域总面积 5 571 km^2，辖 6 个区、1 个县。年平均气温 16.6 ℃，较常年偏高 1.0 ℃，属于暖温带和亚热带的过渡地带。境内拥有淮河和众多的湖泊湿地，水域面积超过 400 km^2，占总面积的 7%。淮南矿产资源丰富，煤炭远景储量 444 亿 t，探明储量 153 亿 t，占华东地区的 32%，煤层气储量 5 928 亿 m^3。煤炭资源开采形成“三废一沉”，每年煤炭开发和发电留下的煤矸石和粉煤灰高达 500 多万 t，占用耕地 4 470 hm^2，因采煤造成塌陷 10 000 hm^2，造成许多村庄和建筑物被废弃，如今正以约每年 347 hm^2 的速度发展[10]。本研究限定于淮南市区，区内

收稿日期：2018-09-29；修回日期：2019-07-23
基金项目：2018 年度安徽省教育厅高校自然科学项目(KJ2018ZD047，KJ2018A0504)
作者简介：张岸(1992-)，男，湖北监利县人，硕士研究生，主要从事区域发展与规划研究，(E-mail) 434787352@qq.com。
通信作者：顾康康(1982-)，男，安徽蚌埠市人，副教授，硕士生导师，博士，主要从事城乡生态规划与区域可持续发展研究，(E-mail) kangkanggu@163.com。

(C)1994-2019 China Academic Journal Electronic Publishing House. All rights reserved. http://www.cnki.net

采煤塌陷区主要分布在潘集区、八公山区、谢家集区、田家庵区、大通区 5 个行政区(图 1),塌陷区面积已达到 304.17 km^2。

1.2　数据来源

数据包括 2017 年 12 月淮南市 Landsat-TM 影像(空间分辨率 30 m)、淮南市采煤塌陷地分布矢量图和土地利用数据。其中淮南市 Landsat-TM 影像从地理空间数据云获取,淮南市采煤塌陷地分布矢量图由淮南市城乡规划局提供,土地利用数据来自全国第二次土地调查。以全国第二次土地调查的土地利用数据为基础数据,参照土地利用分类体系[11]将土地利用分为园地、林地、草地、耕地、水体、建设用地和未利用地。通过对淮南市土地利用现状数据和卫星遥感影像等资料的修正和处理,结合淮南市区采煤塌陷区现状,更新数据,最终确定塌陷区土地利用图(图 1)。

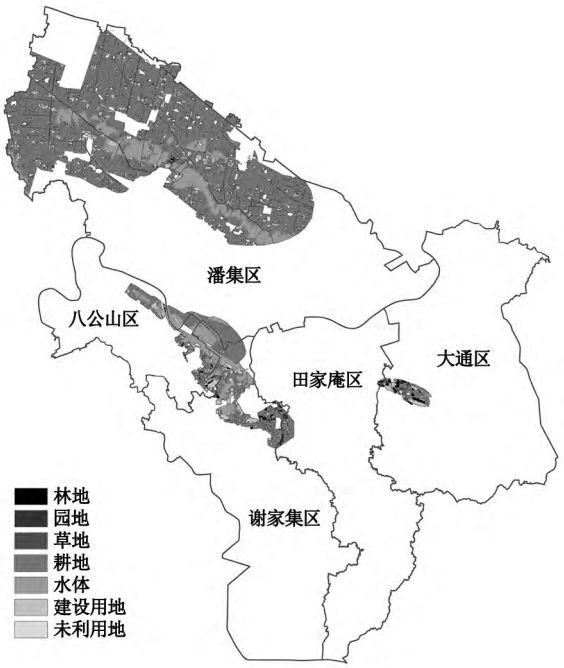


图 1　采煤塌陷区土地利用

Fig.1　Land use in coal mining subsidence areas

2　研究方法

2.1　生态敏感性评价

主要从人类因素和自然因素两个方面进行生态敏感性评价。结合采煤塌陷区特征及相关研究成果,人类因素选取了土地利用类型和交通干线两类评价因子,自然因素选取了植被覆盖指数、河湖水系、高程、坡度四类评价因子,构建生态敏感性评价指标体系(表 1)。各因子中不同要素的等级值采取特尔菲法确定分值,用1,3,5,7 来代表生态敏感性的高低,分值越高,敏感性越高[12]。分值的高低依据相关规范及淮南市相关规划来确定,运用层次分析法确定每个指数的权重。

利用 ArcGIS 10.2 软件的加权叠加工具得到生态敏感性值,公式为[13]:

表 1　采煤塌陷区生态敏感性评价因子等级划分标准

Tab.1　Criteria of ecological sensitivity evaluation factors in mining subsidence areas

因素	指标层	一级指标	二级指标	分值	分级依据
人类因素(0.333 3)	土地利用类型(0.222 2)	土地利用类型	林地	7	根据《生态环境状况评价技术规范》(HJ192—2015)中表征生境质量指数的各类生境类型的权重大小确定,林地最高,建设用地最低
			园地	6	
			水体	5	
			草地	4	
			耕地	3	
			未利用地	2	
			建设用地	1	
	交通干线(0.111 1)	铁路	>55 m 缓冲区	7	参考《城市道路设计规范》:道路红线宽度高速公路 60 m,铁路 10 m。根据淮南市总体规划(2005—2020 年)要求,高速公路、国道两侧各 50 m 范围内、铁路两侧各 50 m 范围内划定为禁建区。据此红线加绿带宽度:高速公路为 160 m、铁路 110 m
			0~55 m 缓冲区	1	
		高速公路	>80 m 缓冲区	7	
			0~80 m 缓冲区	1	
自然因素(0.666 7)	NDVI(0.327 9)	NDVI	0.2≤NDVI<0.4	7	通过对淮南市卫星遥感影像的修正和处理,得出淮南市区植被覆盖指数在-1~0.4 之间,然后通过 GIS 中的重分类工具进行分类
			0.1≤NDVI<0.2	5	
			0≤NDVI<0.1	3	
			-1<NDVI<0	1	
	河湖水系(0.203 7)	湖泊水库	0~300 m 缓冲区	7	王娟[14]
			>300 m 缓冲区	1	
		河流	0~40 m 缓冲区	7	蓝线 40 m,绿带 20 m,蓝线绿带范围总共 80 m
			>40 m 缓冲区	1	
	高程(0.083 2)	高程	>74 m	7	塌陷区内普遍高程低于 37 m,极少部分区域高程在 74 m 以上
			37~74 m	3	
			<37 m	1	
	坡度(0.051 9)	坡度	89.6°~90°	7	以《城市用地竖向规划规范》(CJJ83—2016)为基本依据,同时结合淮南市区地形地势而设置
			88.9°~89.6°	3	
			<88.9°	1	

说明:括号内数值为权重。

(C)1994-2019 China Academic Journal Electronic Publishing House. All rights reserved.　http://www.cnki.net

$$ES = \sum_{i=1}^{n} W_i X_i \quad 。$$

式中: ES 是生态敏感性值; X_i 是各项指标的分值; W_i 为各指标的权重。

2.2 生物多样性服务价值评价

使用生态系统服务评价指标来衡量生物多样性服务价值。中国生态系统服务评价指标由谢高地等在 2003 年问卷调查的基础上编制,涵盖了 200 名具有生态背景的专业人员[15-16]。在此基础上,李敏修订了淮南市的生态系统服务指标[11]:耕地、园地、林地、草地、水体、建设用地、未利用地的生物多样性服务价值系数分别设为 1 898.77,5 938.30,8 395.52,3 481.07,6 627.06,0.00,744.61 元/(hm^2 · a)。以此为参考,套用 R. Costanza 等[17]的方法来计算生物多样性服务价值,计算公式为:

$$ESV = \sum A_k \times VC_k \quad 。$$

式中: ESV 是生态系统服务价值(元); A_k 是研究区 k 类土地利用类型的面积(hm^2); VC_k 为生态系统服务功能的价值系数,即单位面积生态系统服务价值(元/ hm^2 · a)。通过计算得出园地、林地、草地、耕地、水体、建设用地和未利用地的生物多样性服务价值,服务价值越高的表明服务水平越高,在维持生物多样性方面发挥主导作用。由于其计算结果与生态敏感性值无法归一,为了归一化处理,同样采取特尔菲法对不同土地利用类型的生物多样性服务价值进行赋值,用 1,2,3,4,5,6,7 代表生物多样性服务价值的高低,分值越高,价值越高,对于分值高的区域应考虑优先恢复。

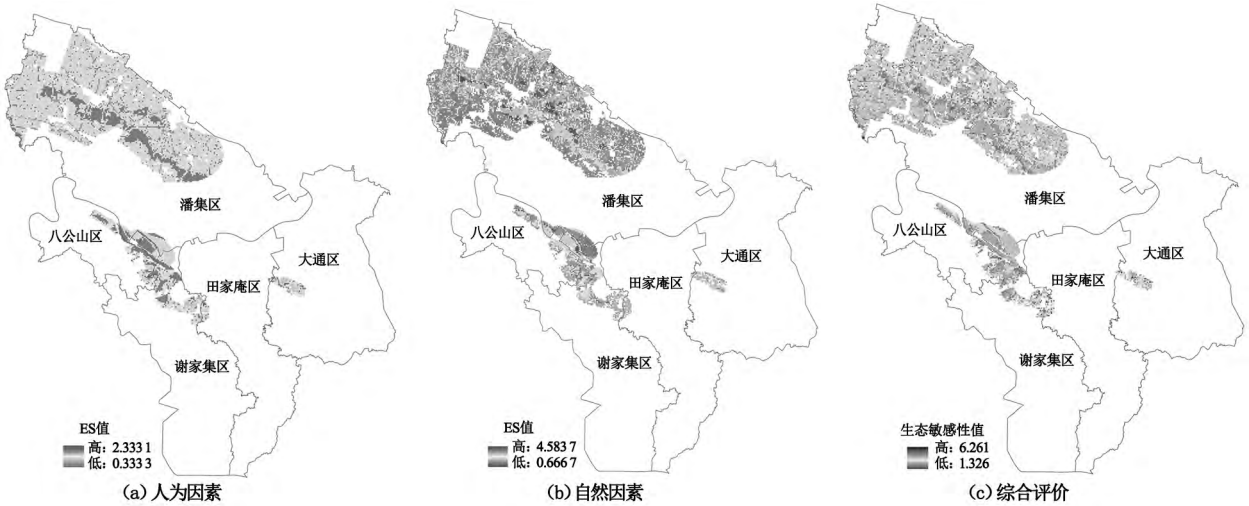
2.3 恢复优先级的确定

采煤塌陷区生态敏感性和生物多样性服务价值对采煤塌陷区生态恢复适宜性均具有重要影响,将二者结果通过 GIS 平台进行等权重叠加[13],得到采煤塌陷区的综合适宜度。采煤塌陷区的综合适宜度决定其生态恢复优先级的大小,适宜度越高,则生态恢复优先等级越高。利用自然断点法将综合适宜度值由小到大划分为 1~5 级,对应的生态恢复优先等级划分为非常低、低、中等、较高、高 5 个级别。

3 结果与分析

3.1 采煤塌陷区生态敏感性分析

通过 GIS 权重叠加分析,得出基于人为因素和自然因素的生态敏感性及其综合评价结果(图 2)。从人为因素来看,淮南市区生态敏感性值高分区域整体呈现出带状、块状和散点状的空间分布特征(图 2a),主要分布在潘集区采煤塌陷区的中南部、八公山区采煤塌陷区的大部分区域、谢家集区采煤塌陷区的西北部以及大通区采煤塌陷区的东部。这些高分区域的用地类型主要为林地、园地和水体,其在生境质量评价中所占权重值较高。在潘集区、八公山区和谢家集区采煤塌陷区内,因为两条内陆滩涂的贯穿,高分区域呈现明显的带状分布特点。以此为中心,由于大大小小的湖泊水库、坑塘水面、河流沟渠以及小部分园林地的存在,使得高分区域分布零散,以大小不同的块状和散点状分布。在潘集区采煤塌陷区的部分区域、八公山区采煤塌陷区的东南部和大通区采煤塌陷区西部,因为人为因素交通干线的干扰,这些区域生态敏感性值普遍较低。从自然因素来看,评价结果显示生态敏感性值波动于 0.67~4.58(图 2b),塌陷区生态敏感性值差异较大。生态敏感性值较高的区域比较零散,分布不集中,多以散点状存在,应考虑后期生态资源的整合。通常这些高分区域的植被覆盖率较高,而植被覆盖因子对于评价生态敏感性所占权重值较大。相比较而言,生态敏感性值在 2.6 左右,即处于中等水平的区域主要集中于潘集区采煤塌陷区的中部和大通区采煤塌陷区的东北部,表明这些塌陷区自然生态环境相对较好,可考虑优先恢复。综合分析人为因素和自然因素,可得出淮南市生态敏感性值高分区域的总体空间分布特征为两带、多核和多点。两带即两条贯穿的内陆滩涂,多核即以块状存在的湖泊、坑塘水面和园林地,多点即大大小小的沟渠水库。这些高分区域的用地主要为林地、园地、



(a) 人为因素 (b) 自然因素 (c) 综合评价

图 2 采煤塌陷区生态敏感性

Fig.2 Ecological sensitivity of coal mining subsidence areas

(C)1994-2019 China Academic Journal Electronic Publishing House. All rights reserved. http://www.cnki.net

水体以及某些植被覆盖率较高的耕地(图 2c),主要集中在潘集区采煤塌陷区的中南部、八公山区采煤塌陷区的大部分区域、谢家集区采煤塌陷区的西北部以及大通区采煤塌陷区的东部和中部,这些区域更适宜生态恢复。

3.2　生物多样性服务价值分析

通过计算得出林地、园地、草地、耕地、水体、建设用地和未利用地的生物多样性服务价值,分别为 482 亿元、39 亿元、19 亿元、393 亿元、405 亿元、0 亿元和 0.1 亿元,根据价值高低分别赋值 7,4,3,5,6,2,1(图 3)。其中林地具有最高的生物多样性服务价值,水体次之,表明林地系统对生物多样性的价值贡献最大。淮南市区生物多样性服务价值与价值系数即价值当量整体呈现出一致性,但其中耕地面积所占塌陷区总面积比例较大,使得其服务价值大于园地和草地的服务价值。分值为 7 和 6 的区域主要集中在潘集区采煤塌陷区的中南部、八公山采煤塌陷区的大部分区域、谢家集区采煤塌陷区的西北部以及大通区采煤塌陷区的西部,这些区域生物多样性服务价值较高,通常这些地区植物资源丰富,植被类型丰富。分值为 5 的区域主要集中在潘集区采煤塌陷区的大部分区域、谢家集区采煤塌陷区的东南部、田家庵区采煤塌陷区的大部分区域以及大通区采煤塌陷区的东部,这些区域生物多样性服务价值处于中等水平。建设用地和未利用地具有最低的生物多样性服务价值,对生物多样性基本无价值贡献。

3.3　生态恢复优先级

综合评价结果(图 4)可以看出,淮南市区采煤塌陷区综合适宜度值介于 1.16~5.37 之间,表明现有采煤塌陷区生态恢复的适宜程度具有较大差异。据此,将采煤塌陷区的综合适宜度由小到大依次划分为非常低、低、中等、较高、高,从而获得了淮南市区采煤塌陷区生态恢复优先级由低到高的顺序(图 5)。其中,高优先级塌陷区面积 4 216.54 hm^2,占总塌陷区面积的 15.17%;较高优先级塌陷区面积 3 381.04 hm^2,占总塌陷区面积的 12.17%;中等塌陷区面积 5 947.80 hm^2,占总塌陷区面积的 21.4%;低优先级塌陷区和非常低优先级塌陷区面积分别为 12 140.85 hm^2 和 2 103.35 hm^2,分别占总塌陷区面积的 43.69% 和 7.57%。高优先级和较高优先级塌陷区的用地类型总体上倾向于林地、水体。其中用地类型为林地和大面积连续水域的塌陷区具有明显的集聚特征,生态恢复成本较低,应最先考虑生态恢复。某些大面积湖泊和一些小面积沟渠水库的塌陷区分布较为零散,恢复顺序次之,但需相应加大生态恢复的投资。

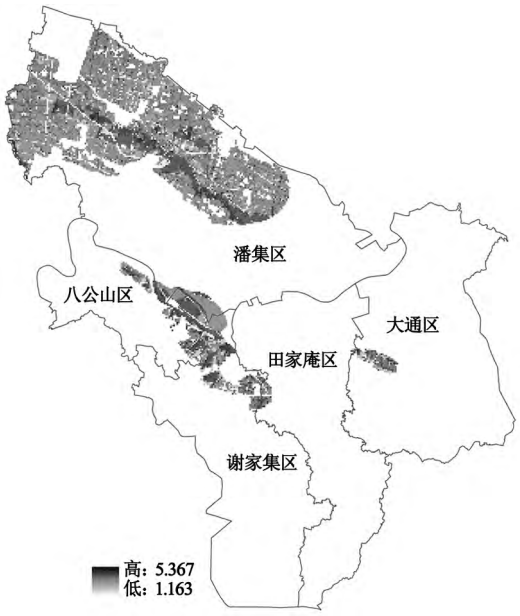


图 4　采煤塌陷区综合适宜度值

Fig.4　Value of comprehensive suitability of coal mining subsidence areas

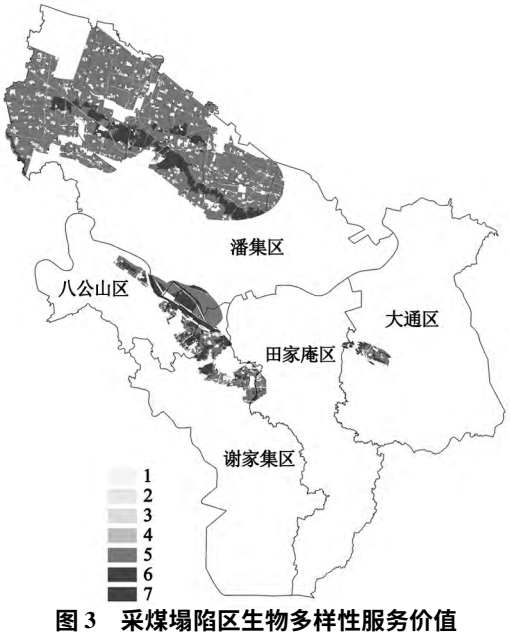


图 3　采煤塌陷区生物多样性服务价值

Fig.3　Biodiversity service value of coal mining subsidence areas

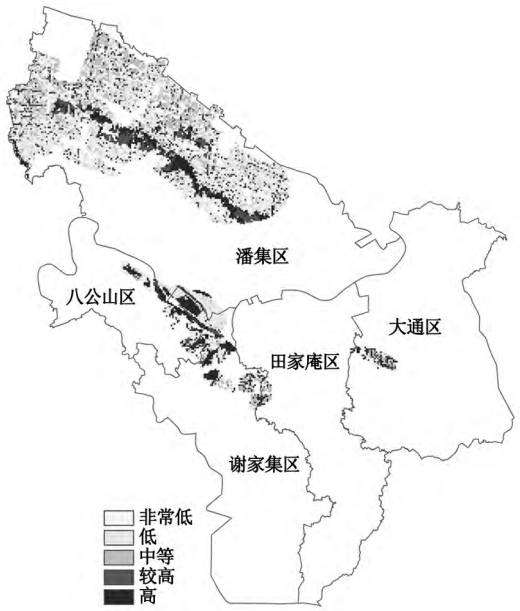


图 5　采煤塌陷区生态恢复优先级

Fig.5　Grades of restoration priorities for coal mining subsidence areas

(C)1994-2019 China Academic Journal Electronic Publishing House. All rights reserved.　http://www.cnki.net

3.4 采煤塌陷区生态恢复管制措施

采煤塌陷区应根据不同的恢复重点采取不同的生态恢复管制措施，从而确定不同的恢复区，并将其纳入到城市生态网络中。依据生态恢复优先次序从高到低分为保护恢复区、生态恢复区、农林恢复区、农田恢复区和建筑恢复区(表 2)。

表 2 采煤塌陷区生态恢复优先级分区及管制措施

Tab.2 Priority zoning and control measures for ecological restoration in coal mining subsidence areas

恢复优先级	分类	管制措施
高	保护恢复区	自然保护区
较高	生态恢复区	休闲公园; 景观公园; 生态湿地
中等	农林恢复区	瓜果采摘; 市民农园
低	农田恢复区	农用耕地
非常低	建筑修复区	城镇建设用地

保护恢复区(生态恢复优先级高)：这些区域对于改善城市生态环境至关重要，建议将其整合到城市生态网络中。通常这些区域的用地类型为林地、水体，具有连续、大面积的水域或较好的植被覆盖。应将这些地区保存完好并恢复到自然保护状态，以保证栖息地质量和生态系统服务价值，同时应禁止大规模的人类建筑活动。

生态恢复区(生态恢复优先级较高)：这些区域对改善城市生态环境具有明显的积极作用，建议将其纳入城市生态网络中。通常这些区域的用地类型为水体，具有大面积的湖泊和一些小面积的沟渠水库。建议避免在这些地区进行重要的人工活动和商业行为，并将其发展成休闲公园、景观公园和生态湿地等。

农林恢复区(生态恢复优先级中等)：这些区域对改善城市生态环境有一定的积极作用，可以融入城市生态网络中。通常这些区域的用地类型为耕地，且具有较好的植被覆盖。建议这些地区优先发展瓜果采摘、市民农园等观光体验型农业。

农田恢复区(生态恢复优先级低)：这些区域对改善城市生态环境没有明显的积极作用，可以在客观条件允许的情况下纳入城市生态网络中。通常这些区域的用地类型为耕地，为农田生态系统，但植被覆盖率较低。建议将这些地区恢复为农用耕地，打造农田景观。

建筑修复区(生态恢复优先级非常低)：这些区域对改善城市生态环境没有什么积极作用，不能考虑融入到城市生态网络中。这些地区通常具有良好的基础设施和区位条件，建议恢复为城镇建设用地，如商业办公、商业金融等功能。

4 结论与讨论

4.1 结论

(1) 为了实现自然-社会-经济复合目标下的系统性研究，从生态敏感性和生物多样性服务价值两个方面来评价采煤塌陷区的生态恢复优先级。塌陷区域生态恢复优先级等级越高，则实现生态恢复所消耗的人力、物力越低，越应予以优先恢复。淮南市区采煤塌陷区生态恢复高优先级塌陷区面积 4 216.54 hm^2，占总塌陷区面积的 15.17%，较高优先级塌陷区面积 3 381.04 hm^2，占总塌陷区面积的 12.17%，主要分布于潘集区采煤塌陷区的中南部、八公山区采煤塌陷区的大部分区域、谢家集区采煤塌陷区的西北部以及大通区采煤塌陷区的大部分区域，这些区域应最先予以生态恢复。

(2) 生态恢复优先等级高和较高的区域其用地类型主要为林地和水体，这些区域具有连续、大面积的水域或较好的植被覆盖，呈现明显的集聚特征。

(3) 不同采煤塌陷区生态恢复优先等级区域应具有不同的生态恢复目标及管制措施。生态恢复应强调生态恢复的整体控制和局部优先，突出城市整体生态功能的恢复和重建。

4.2 讨论

采煤塌陷区的形成和生态恢复是动态变化的长期过程，本研究缺乏对其动态内涵的考虑。未来研究应因时而异，采用更精确和新颖的方法和技术，如空间优化技术、大数据的分析方法及智能化分析，以此来完善生态恢复适宜性的评估。

参考文献:

[1] TAMBOSI L R, MARTENSEN A C, RIBEIRO M C, *et al*. A Framework to Optimize Biodiversity Restoration Efforts Based on Habitat Amount and Landscape Connectivity [J]. Restoration Ecology, 2014, 22(2): 169-177.

[2] 裴丹. 生态保护网络化途径与保护优先级评价——"绿色基础设施"精明保护策略 [J]. 北京大学学报(自然科学版), 2012, 48(5): 848-854.

[3] MENZ M H M, DIXON K W, HOBBS R J. Hurdles and Opportunities for Landscape-scale Restoration [J]. Science, 2013, 339: 526-527.

[4] 冯姗姗, 常江, 侯伟. GI 引导下的采煤塌陷地生态恢复优先级评价 [J]. 生态学报, 2016, 36(9): 2724-2731.

[5] 姜帆. 山地退化森林生态系统恢复效果评价 [D]. 哈尔滨: 东北林业大学, 2009.

[6] 何萍, 李向荣, 王东胜, 等. 海河流域水生态系统修复优先区筛选 [C]//水利部, 国家环保总局. 2009 年 GEF 海河流域水资源与水环境综合管理项目国际研讨会论文集. 北京: 环境保护部, 2009: 88-99.

[7] 董张玉, 刘殿伟, 王宗明, 等. 基于空间分析的东北地区湿地优先恢复 [J]. 应用生态学报, 2013, 24(1): 170-176.

[8] 邹洪坤, 李艳红, 王彬. 基于 GIS 的西宁市生态敏感性分析 [J]. 测绘与空间地理信息, 2018, 41(4): 21-24.

[9] 杨美玲, 米文宝, 李同昇, 等. 宁夏限制开发生态区生态敏感性综合评价与保护对策 [J]. 水土保持研究, 2014, 21(3): 103-108.

[10] 刘家乐. 资源型城市的现状分析及实现可持续发展的对策——以安徽省淮南市为例 [J]. 鸡西大学学报, 2008, 8(4): 41-43.

(下转第 131 页)

(C)1994-2019 China Academic Journal Electronic Publishing House. All rights reserved. http://www.cnki.net

Farmers' Environmental Awareness and Behavior in Ecologically Fragile Areas: Taking Typical Salinized Areas in Shandong Province as Example

LI Yaping , LIU Xiushuang , WANG Ping , XUE Shuhui

(*School of Geography and Tourism*, *Qufu Normal University*, *Rizhao* 276826, *China*)

Abstract: Taking the typical salinized areas in Dongying and Dezhou City, Shandong Province as study area, this paper investigated and analyzed farmers' environmental awareness and behavior with methods of questionnaire survey, interview and observation. The results showed that: (1) Farmers have a higher awareness of the environment, know common knowledge of saline-alkali land utilization, straw and mulch film treatment. Comprehensive scores of environmental concepts are not high, farmers are not familiar with professional terms of environmental pollution, and do not recognize that chemical fertilizers and pesticides bring pollution to the agricultural environment. (2) Comprehensive score of environmental behavior is high. Farmers dispose domestic refuse, animal manure and straw reasonably and can make comprehensive use of organic fertilizer and various saline-alkali land improvement technologies. (3) There are inconsistencies between farmers' environmental awareness and behavior, and the level of environmental behavior is also affected by rural basic conditions and national policies.

Key words: environmental awareness; environmental behavior; salinized area; farmer; Shandong Province

(上接第 126 页)

[11] 李敏.基于土地利用变化的生态系统服务价值研究[D].合肥:合肥工业大学,2015.

[12] 何丹,金凤君,周璟.资源型城市建设用地适宜性评价研究——以济宁市大运河生态经济区为例[J].地理研究,2011,30(4):655-666.

[13] CANG J,HU T H,LIU X X,*et al*.Construction of Green Infrastructure in Coal Resource-based City: A Case Study in Xuzhou Urban Area[J].International Journal of Coal Science & Technology,2018,5(1):92-104.

[14] 王娟.淮南市城乡建设用地布局适宜性评价研究[D].南京:南京农业大学,2010.

[15] 方明,吴次芳,沈孝强,等.杭州市生态系统服务价值演变分析[J].地域研究与开发,2014,33(2):153-158.

[16] 朱九龙.河南义马煤矿矿区生态系统服务价值动态演化过程分析[J].地域研究与开发,2016,35(2):145-149.

[17] COSTANZA R,D'ARGE R,DE GROOT R,*et al*.The Value of the World's Ecosystem Services and Natural Capital[J].Nature,1997,387:253-260.

Priority Evaluation of Ecological Restoration in Coal Mining Subsidence Area Based on GIS: A Case Study in the Huainan Urban Area

ZHANG An[1], GU Kangkang[1,2]

(1.*School of Architecture & Planning*, *Anhui Jianzhu University*, *Hefei* 230022, *China*;
2.*Research Center of Urbanization Development in Anhui Province*, *Hefei* 230022, *China*)

Abstract: This paper takes Huainan City as the research area, with the Landsat-TM image of Huainan City in December 2017, the vector distribution map of coal mining subsidence in Huainan City, the Huainan municipal area vector map and land use data for the second national land survey as data sources, under the support of GIS technology, comprehensively evaluates ecological restoration priorities in coal mining subsidence area from two aspects: the ecological restoration priority from low to high are very low, low, medium, high and very high by using the natural breakpoint method in GIS. The results show that the recovery in high priority and higher subsidence area accounted for 27.34%, mainly distributed in central and southern area in coal mining subsidence of Panji District, the northwestern part of the coal mining subsidence area of Xiejiaji area and most of the coal mining subsidence area in Datong and Bagongshan District, it is recommended that these areas be given priority recovery.

Key words: coal mining subsidence area; ecological sensitivity; value of biodiversity services; GIS; priority for ecological restoration; Huainan Gity

(C)1994-2019 China Academic Journal Electronic Publishing House. All rights reserved.　http://www.cnki.net

顾康康,朱鹏祥,宁杨,等.基于绿色出行理念的合肥市区空气污染分区调控研究[J].地理科学,2019,39(8):1312-1320.[Gu Kangkang, Zhu Pengxiang, Ning Yang et al. Zoning and Regulation of Air Pollution in Hefei City Based on the Concept of Green Travel. Scientia Geographica Sinica,2019,39(8):1312-1320.] doi: 10.13249/j.cnki.sgs.2019.08.013

基于绿色出行理念的合肥市区空气污染分区调控研究

顾康康[1,2],朱鹏祥[1],宁杨[1],汪斐[1]

(1.安徽建筑大学建筑与规划学院,安徽 合肥 230022;2.安徽省城镇化发展研究中心,安徽 合肥 230022)

摘要:空气污染是城市主要的环境问题之一,严重影响到城市人类健康,而交通尾气排放是空气污染的重要原因。绿色出行是基于城市可持续发展的要求,通过发展低碳、绿色、环保的出行方式,缓解城市交通拥堵、城市污染等问题的一种交通理念。基于绿色出行理念的城市空气污染分区调控研究,对于改善城市环境质量、提升人居环境品质具有重大意义。以合肥市区为例,构建基于绿色出行理念的城市空气污染评估框架,提出公共交通、步行及自行车的3类绿色出行评价指标,运用大数据分析绿色出行方式降低空气污染物排放的潜力。结果表明:合肥市区公共交通出行呈现东西、南北2条带状分布,步行及自行车出行集中于路网密度较高的城市二环内,"一核两轴"地区的绿色出行条件较好,改善空气污染物排放的潜力较强;城市空气污染空间呈现城市一环、滨湖新区核心区2个凹地;探讨绿色出行与城市空气污染的空间关系,发现两者存在一定的空间权衡关系;最后,基于绿色出行与城市空气污染的空间分布关系,将合肥市区分为绿色出行区、优化建设区、潜力提升区、出行限制区4类区域,并对不同区域提出城市空气污染优化策略。

关键词:绿色出行;空气污染;大分区调控;GIS;合肥

中图分类号:X513 **文献标识码**:A **文章编号**:1000-0690(2019)08-1312-09

随着中国城镇化速度不断提升,粗放型的城市发展方式带来了诸多城市问题,导致城市环境质量不断降低,城市环境问题越发突出[1~3]。空气污染便是城市环境问题的重要体现之一,已经成为制约城市可持续发展的重要因素[4~6]。20世纪50年代,国外因大力发展工业化而带来了严重城市空气污染,影响到城市发展与居民健康[7,8],解决城市空气污染问题成为重要的研究领域。21世纪以来,部分学者开始关注城市空气污染与城市类型的关系,探索城市空气污染空间分异特征[9~11]。近年来,城市空气污染与城市交通、土地利用、人群健康间的关系[12~15]研究日益加强。然而,关于城市空气污染的研究多以定性分析为主,探索空气污染变化趋势及影响机制的研究较多[16,17],空气污染量化分析研究相对较少,城市空气污染调控研究不足[18,19]。相关学者研究表明机动车尾气是空气污染的重要因素[20,21],中国环保部门曾对规模较大的城市进行空气污染气体调查(包括上海、北京等),研究结果显示[22],城市空气中的一氧化碳、氮氧化物等污染气体,其50%~90%来源于城市机动车尾气;步行、自行车出行及公共交通所代表的绿色出行能降低空气污染物排放,是降低空气污染的重要途径。而如何科学评估绿色出行方式降低空气污染物排放的潜力?绿色出行理念如何融入城市空气污染优化策略中?这些问题需要深入研究和探讨。因此,本文将绿色出行理念引入城市空气污染研究中,构建绿色出行理念下的城市空气污染评估指标体系,将评估结果对比城市空气污染空间分布图,划分城市空气污染减排分区,并针对不同类型区提出提升策略。

收稿日期:2018-09-08;**修订日期**:2018-11-02

基金项目:2018年度安徽省教育厅高校自然科学项目(KJ2018ZD047,KJ2018A0504)资助。[Foundation: Natural Science Project for Universities of Anhui Education Department in 2018 (KJ2018ZD047、KJ2018A0504)]

作者简介:顾康康(1982-),男,安徽蚌埠人,博士,副教授,主要从事城乡生态规划研究。Email: kangkanggu@163.com

1　研究区域与研究方法

1.1　研究区域

合肥位于中国华东地区,长三角西端,江淮之间。合肥是安徽省省会城市,2018年末常驻总人口808.7万人,GDP达到7 822.9亿元[23]。本文选择合肥市区作为研究区域,包括蜀山区、瑶海区、庐阳区、包河区、滨湖区,总面积472.33km^2(图1)。相关研究表明[24]:合肥市区$PM_{2.5}$浓度季节差异显著,污染天数呈现春冬多、夏秋少的规律,1月、2月、3月、11月和12月的污染天数比例均超过50%,重度以上污染天气主要出现在春冬季节,空气污染显著。

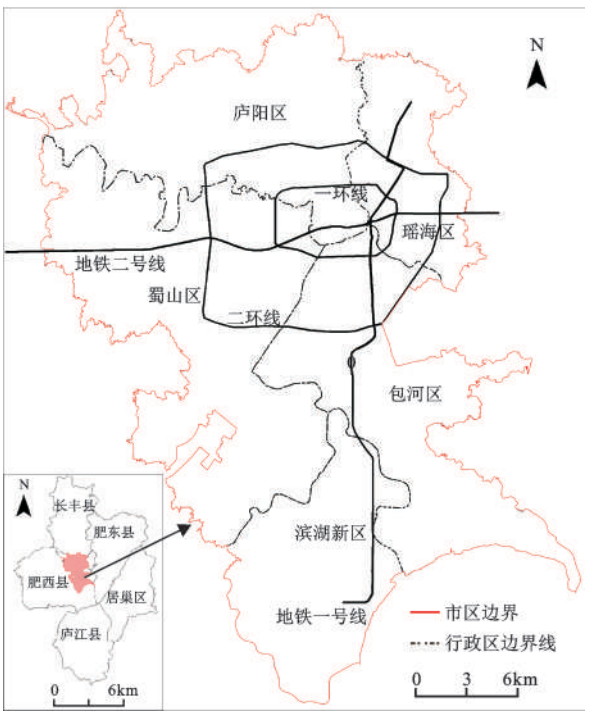


图1　研究区域

Fig.1　The area of study

1.2　研究方法

1.2.1　研究思路

相关研究[12]表明城市空气污染与机动车尾气排放有较大关联性,绿色出行理念提倡慢行交通和公共交通出行,可以降低机动车尾气排放,进而优化城市空气环境。本研究构建基于绿色出行理念的城市空气污染评估框架,提出公共交通、步行及自行车的3类绿色出行评价指标,运用大数据分析绿色出行方式降低空气污染物排放的潜力;利用$PM_{2.5}$浓度评估空气污染现状,明确哪些地区可以通过绿色出行降低城市空气污染。探讨基于绿色出行理念的空气污染物减排潜力、城市空气污染两者空间关系,进而划分城市空气污染减排分区并提出相关策略。

1.2.2　基于绿色出行理念的空气污染物减排潜力评估

2005年,美国旧金山发布《城市环境协定——绿色城市宣言》[25],提出绿色出行模式是实现绿色城市的重要前提,确保城市公共交通的优先权是其主要目标,并在此基础上大力发展快速公共交通和非机动交通,降低私人小汽车的使用率。基于绿色城市理论及国内外学者研究成果[26,27],本文认为降低交通污染物排放能缓解城市空气污染,步行、自行车出行及公共交通所代表的绿色出行可以降低交通相关的空气污染物排放,而绿色出行又与公共交通设施布局、可达性、土地利用、建成环境等指标相关。因此,本文从公共交通、步行、自行车出行3个方面构建基于绿色出行理念的空气污染物减排潜力评估框架,构建层次分析结构:包括目标层(降低交通相关的空气污染物潜力)、指标层(出行方式)及分指标层(评价指标),运用层次分析法[28]计算指标相应的权重(表1)。将分析得到的各类交通出行方式的减排潜力以自然断裂法(通过对分类间隔加以识别,可对相似值进行最恰当地分组,并可使各个类之间的差异最大化)进行分级表示,再进行分区对比。

1)公共交通的空气污染物减排潜力评估。公共交通因其运载量大、使用清洁能源等特征是降低城市空气污染的重要交通出行方式之一,利

表1　绿色出行的空气污染物减排潜力评价体系及权重

Table 1　The assessment system and weight of potential ability of green travel types to reduce emission atmospheric pollutants

目标层	出行方式	评价指标	权重
降低交通相关的空气污染物潜力	公共交通	公共交通通勤频数	0.43
	步行	土地利用混合度	0.11
		建筑密度	0.05
		服务设施密度	0.10
		单元连接度	0.08
	自行车出行	共享单车分布密度	0.11
		坡度变化率	0.05
		单元连接度	0.07

用“公共交通通勤频数”计算研究区公共交通降低交通相关的空气污染物排放潜力。公共交通包括公交车与地铁，通勤频数是每个站点公共交通一天通行次数。将研究区划为300 m × 300 m的网格，运用GIS进行核密度分析，最终得到公共交通的空气污染物减排潜力。

2）步行的空气污染物减排潜力评估。步行降低交通相关的空气污染物排放潜力体现在区域的可步行性，而可步行性与土地利用、建筑分布、设施配套等相关[28~32]。因此，本研究利用土地利用混合度、建筑密度、服务设施密度及单元连接度等指标，计算研究区步行的空气污染物减排潜力。

土地利用混合度。运用城市地理学信息论中熵的概念，用熵值反映土地利用混合程度[33]。计算公式为：

$$S = -\sum_{i=1}^{n} P_i \log_{10} P_i \left(\sum_{i=1}^{n} P_i = 1 \right) \quad (1)$$

式中: S为土地利用混合程度的熵值；n 为土地利用类型的划分数目；P_i为第 i类土地面积所占比例。

建筑密度。将研究区划为300 m×300 m的网格，运用合肥市建筑大数据计算网格内建筑面积的比例，进而得到建筑密度分布图。

服务设施密度。将研究区划为300 m×300 m的网格，运用合肥市POI大数据（教育设施、餐饮设施、医疗设施、金融服务设施、休闲娱乐设施、日常购物六大类）统计每个网格中服务设施点的个数，网格中服务设施点最高的单元得分为1，其他网格中服务设施点数量与最高数量的比例反映各网格中服务设施密度。

单元连接度。将研究区划为300 m×300 m的网格，网格中可步行道路交点数表示单元连接度。计算方法同服务设施密度。

3）自行车出行的空气污染物减排潜力评估。自行车出行降低交通相关的空气污染物排放潜力体现在自行车可获得性及地形条件，本研究利用共享单车分布密度、坡度变化率及单元连接度，计算自行车出行的空气污染物减排潜力。

共享单车分布密度。将研究区划为300 m×300 m的网格，选取合肥市共享单车分布位置及数量信息。计算方法同服务设施密度。

坡度变换率。将研究区划为300 m×300 m的网格，运用GIS表面分析工具计算坡度变化率。

单元连接度。将研究区划为300 m×300 m的网格，网格中可自行车通行道路交点数表示单元连接度。计算方法同服务设施密度。

4）绿色出行理念下的空气污染物减排潜力综合评估。计算公式如下：

$$S = \sum_{i=1}^{n} W_i \times X_i \quad (2)$$

式中，S表示综合评估得分，X_i表示各指标评价值，W_i为每个指标所对应的权重，i=1，2，…n。

1.3 数据来源

1）合肥市建筑轮廓数据：来源于水经注万能地图（www.rivermap.cn），包括2018年5月合肥城市矢量建筑轮廓数据。

2）单车数据：利用摩拜单车APP，通过网络爬虫爬取，数据时间为2018年5月26上午8点到次日上午8点，数据包括研究区每小时单车分布位置及数量信息。

3）公共交通数据：合肥市轨道交通数据来源于合肥城市轨道交通有限公司官网（www.haomifan.com），包括地铁站数量、站点位置、及每条地铁线运营时刻表；公交站点数据来源于高德地图的公交站点分布位置、数量、坐标。

4）服务设施数据：2018年5月高德地图的POI数据和公交站点数据，包括教育设施、餐饮设施、医疗设施、金融服务、休闲娱乐、日常购物六大类，74 517条数据。

5）坡度数据：来源于中国科学院计算机网络信息中心地理空间数据云（www.gscloud.cn）平台的GDEMDEM 30 m 分辨率数字高程数据，再通过GIS数据转换进行坡度分析。

6）污染物数据：来源于合肥市生态环境局（sthjj.hefei.gov.cn），其包括每个监测点连续的日污染物浓度数据及月污染物浓度数据。

2 结果与分析

2.1 基于绿色出行理念的空气污染物减排潜力评估

基于上述方法得到每个网格的“交通出行方式的减排潜力”，考虑数据中出现的特征点、转折点，通过统计数值分布规律，将研究的数据分成性质相似的群组，使各个群组之间的差异最大化，运用GIS自然断裂法进行分级，将“减排潜力”分成5级，分别是低潜力区、较低潜力区、中潜力区、较高潜力区、高潜力区。

1）公共交通出行的空气污染物减排潜力评

估。通过降低污染物潜力评价体系,分析合肥市区与交通相关的空气污染物减排潜力(图2a),结果显示城市二环内与滨湖新区公共交通出行频率远高于其他区域,该区域公共交通的空气污染物减排潜力较高,空气污染物减排高潜力区空间整体呈现出东西与南北两条带状分布。从公共交通的空气污染物减排潜力空间差异来看,高潜力区、较高潜力区分布较分散,位于地铁一号线、二号线周边,且面积仅占合肥市区7%;中潜力区集中于城市一环,面积占合肥市区6%;较低潜力区集中于城市一环和二环之间,低潜力区大量分布在城市新区,面积分别占合肥市区的26%和61%。总

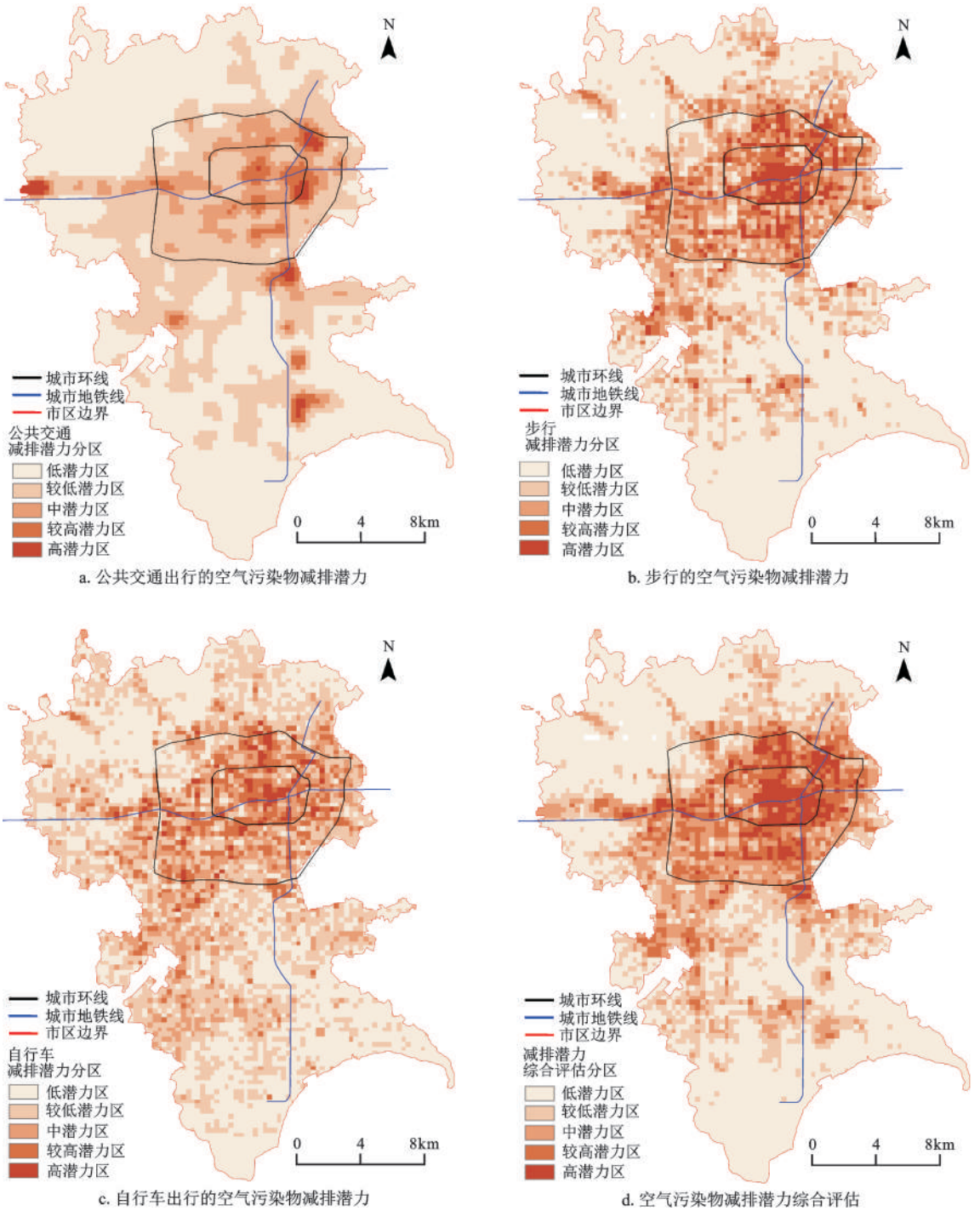


图2　合肥市区与交通相关的空气污染物减排潜力

Fig.2　The capacity to reduce emissions of traffic-related atmospheric pollutants in Hefei downtown

体而言，合肥市区公共交通的空气污染物减排潜力空间差异较大，高潜力区集中于地铁沿线，但辐射范围较小。

2）步行的空气污染物减排潜力评估。基于用地布混合度、建筑密度、道路连接度和城区服务设施等指标，得到步行的空气污染物减排潜力图（图2b）。步行适宜性好的地区主要分布在土地利用混合度高、建筑、道路和服务设施密度大区域，城市二环内作为老城区，道路网密度高且服务设施数量大，步行的空气污染物减排潜力较高。总体而言，合肥市区步行的空气污染物减排潜力较高区域分布在城市二环内，面积占市区13%；城市滨湖新区和北城新区步行的空气污染物减排潜力较低，面积占市区的73%。

3）自行车出行的空气污染物减排潜力评估。随着共享单车的投放，城市自行车出行率大幅度提高，基于共享单车分布密度、道路交通状况得出骑行的空气污染物减排潜力（图2c）。骑行的空气污染物减排高潜力区较少，面积仅占市区4%，空间分布分散在城市一环周边；骑行的空气污染物减排较高潜力区分布在城市二环内，面积占市区10%。总体而言，合肥市区自行车出行的空气污染物减排潜力一般，较高潜力区仅在城市二环内散点状分布，这与城市共享单车分布及慢行交通系统关系紧密。

4）绿色出行理念下的空气污染物减排潜力综合评估。综合公共交通、步行、自行车出行的空气污染物减排潜力，得出绿色出行理念下的空气污染物减排综合潜力（图2d）。可以看出，城市一环内、瑶海区中南部、南二环周边、滨湖新区紫云路周边等区域绿色出行条件较好，有较强的空气污染物减排潜力。

2.2 城市空气污染空间分析

利用2018年1月份合肥市生态环境局10个国控环境空气自动监测站24 h连续监测数据，运用GIS空间插值分析合肥市区$PM_{2.5}$空间分布格局（图3）。可以看出，合肥市区1月$PM_{2.5}$空间分布呈现“双峰多谷”的规律，城市一环和滨湖新区是$PM_{2.5}$质量浓度高峰区，属于重度污染区域，蜀山区、庐阳区的空气污染相对较低。对比合肥路网分布和交通流量，城市一环、滨湖新区核心区均属于路网密度高、交通流量大的区域，一定程度上反映了道路交通与城市空气污染的正关联性。

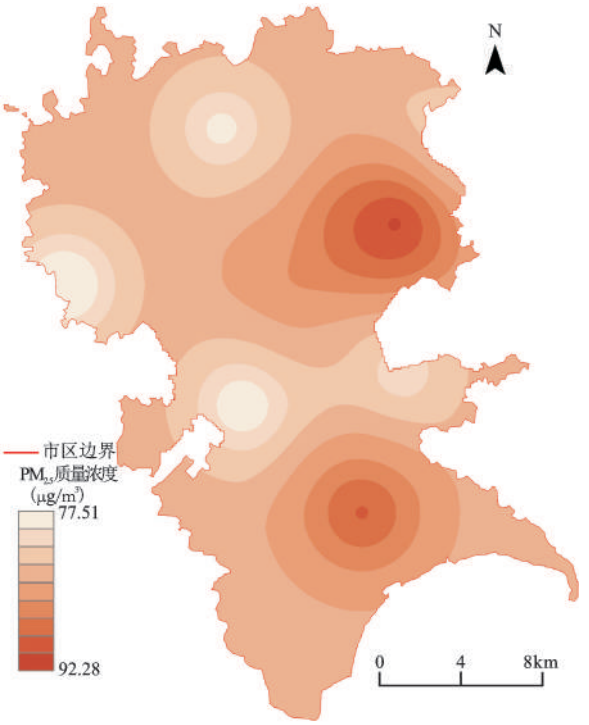


图3 合肥市区$PM_{2.5}$质量浓度分布

Fig.3 The concentration distribution of $PM_{2.5}$ in Hefei dawntown

对比分析绿色出行的空气污染物减排潜力与城市空气污染物的空间关系，绿色出行的空气污染物减排潜力与城市空气污染空间分布关系多样性显著，既存在空间相关区域，也有空间相异区域。如城市一环同时属于污染物减排潜力高和城市空气污染高的区域，而滨湖新区的核心区既属于低减排潜力区又属于高空气污染的区域。

2.3 城市空气污染减排分区及提升策略

依据绿色出行的空气污染物减排潜力与城市空气污染物的空间关系，图2、图3分析结果按照平均值分高和低两个区间，分别代表空气污染物减排潜力高和低，空气污染物浓度高和低，相互组合形成合肥城市空气污染减排分区，包括绿色出行区、优化建设区、潜力提升区、出行限制区（图4）划分合肥城市空气污染减排分区，包括绿色出行区、优化建设区、潜力提升区、出行限制区（图4）。基于分析结果，针对不同区域状况实行相应的管控措施，提出不同区域的提升策略。

1）绿色出行区：城市空气污染低且空气污染物减排潜力高的区域，属于城市生态环境较好的区域，如大蜀山国家森林公园、天鹅湖公园等休闲

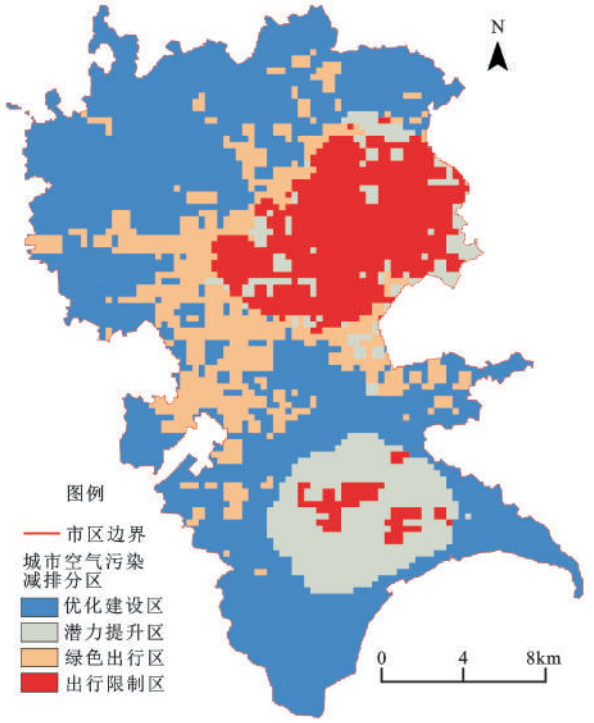


图4　合肥市区空气污染减排分区

Fig.4 The zoning of urban air pollution reduction in Hefei downtown

娱乐的区域,具有完善的基础设施,周边出行方式以步行及骑行为主。

该区在未来发展中应以生态保护为主,严格管控区域发展强度,坚持绿色发展,保存现状环境。结合当前交通现状,利用较好的出行环境与基础设施,推广并实行绿色出行理念,构建完善的区域慢行体系;如优化城市公共交通路线,增加城市公共交通站点及公共交通出行频率,利用共享单车的实行,合理布置自行车点,提高该地区绿色出行的可行性;同时作为城市实行绿色交通的示范区,还需提高该区域机动车通行及停放要求,严格控制该区域机动车数量的增长,可通过统一管理该地区机动车停靠地点,增加停车收费标准来进行管控。

2）优化建设区:城市空气污染低且空气污染物减排潜力也较低的区域,属于城市开发强度较低的区域,多位于城区外围,如滨湖新区西南部、庐阳区北部;城市开发建设强度相对较低使其周边空气环境并未受到太大影响,但区域的基础建设则较为缺失。

优化建设区是城市重点建设与开发的地区,为避免相同城市交通及空气问题的出现,需在建设的同时,需注重优化城市布局与基础设施建设,构建合理的绿色出行系统,并协调城市建设强度与城市环境的关系;因其具有较强的空间塑造性,可重点发展区域公共交通,建设成以公共出行为主、机动车出行为辅的生态建设区。

3）潜力提升区:城市空气污染高且空气污染物减排潜力较低的区域,属于城市基础设施缺失的街道和新建城区,如滨湖新区核心区,其具有较高的人群密度,机动车出行频率较高,但基础设施的缺失与不完善,严重影响到该地区绿色出行潜力。

潜力提升区属于交通体系不完善的区域,其在未来的发展中,首先需要重视和发展城市基础设施,包括在整体层面上适当增加城市公共交通运行强度、完善城市慢行交通路网等,并控制城市开发建设,合理安排城市功能建设。如改善公共交通系统,合理安排公共交通路线,设置城市BRT站点,提升城市公共服务设施水平;并整合区域步行道与自行车道,构建城市慢行通道,保障绿色出行安全;在保障该区域出行需求的基础上,再合理协调交通出行方式,适当较少机动车的出行频率,提升城市绿色出行方式。

4）出行限制区:城市空气污染高且空气污染物减排潜力高的区域,主要位于城市二环,属于商业、行政等服务功能聚集地,人们高强度活动使得机动车出行较为频繁,空气环境污染较为严重。同时高强度的开发建设也让该区域基础建设较为完善,具有良好的绿色出行条件,使得其成为空气污染较高的区域,也是绿色出行潜力较高的区域。

出行限制区是在城市空气环境优化中要严格进行管控的区域,需限制机动车的出行,并在现状基础上,进一步优化城市绿色出行体系。同时制定相关激励政策,鼓励该地区人们利用较好的绿色出行条件,可采取在人流较多的街道设立步行街区的方法,打造城市特色步行环境,来鼓励人们步行出行,同时在主要步行街口周边设立若干大型停车点,统一管理进入该区的车辆,来降低该地区机动车的使用,并增加公共交通站点、公共自行车点,提升公共交通出行服务,逐渐形成以公共交通、步行及自行车为主要出行方式,提高该区域绿色出行频率,来减少污染气体的排放,以达到优化空气环境目的。

3 结论

1）基于绿色出行理念的空气污染物减排潜力评估框架，运用大数据空间可视化分析绿色出行方式降低空气污染物排放的潜力，发现合肥市区一环内、瑶海区中南部、南二环周边、滨湖新区紫云路周边等区域绿色出行条件较好，有较强的空气污染物减排潜力。

2）本研究利用$PM_{2.5}$质量浓度反应空气污染，合肥市空气污染呈现“双峰多谷”的空间分布特征，形成城市一环、滨湖新区核心区2个凹地，蜀山区、庐阳区的空气污染相对较低。

3）绿色出行的空气污染物减排潜力与城市空气污染空间分布不匹配，存在空间权衡关系。利用两者空间关系划分合肥市空气污染减排分区为绿色出行区、优化建设区、潜力提升区、出行限制区。绿色出行区应以生态保护为主，作为城市实行绿色交通的示范区；优化建设区是城市重点建设与开发的地区，但需协调城市建设强度与城市环境的关系；潜力提升区需加强城市公共交通建设，合理规划慢行交通体系；出行限制区需限制机动车出行，鼓励居民绿色出行。

4）定量评估基于绿色出行的空气污染物减排潜力，进而提升城市空气质量，是城市研究的一种新尝试，对城市空间布局合理化具有重要意义。相关城市可依据城市特征划分不同的城市空气污染优化分区，参考合肥绿色出行分区提升策略制定管控要求。由于数据等局限，该本研究涉及的指标还有待完善。在未来进一步的研究中，需考虑到人群出行的主观意愿，并丰富研究内容和方法，进而提高评估结果的科学性和可实施性。

参考文献(References)：

[1] 王兴杰, 谢高地, 岳书平. 经济增长和人口集聚对城市环境空气质量的影响及区域分异——以第一阶段实施新空气质量标准的74个城市为例[J]. 经济地理, 2015, 35(2):71-76+91. [Wang Xingjie, Xie Gaodi, Yue Shuping. Impact of economic growth and population aggregation on urban environmental quality and its regional differentiation: A case study of 74 cities implemented the new standard for air quality during the first stage. Economic Geography, 2015, 35(2): 71-76+91.]

[2] 金春雨, 吴安兵. 工业经济结构、经济增长对环境污染的非线性影响[J].中国人口·资源与环境,2017, 27(10): 64-73. [Jin Chunyu, Wu Anbing. Nonlinear influence of industrial economic structure and economic growth on environmental pollution. China Population Resources and Environment, 2017, 27(10): 64-73.]

[3] 张同斌, 李金凯, 程立燕. 经济结构、增长方式与环境污染的内在关联研究——基于时变参数向量自回归模型的实证分析[J].中国环境科学, 2016, 36(7): 2230-2240. [Zhang Tongbin, Li Jinkai, Cheng Liyan. Intrinsic correlation of economic structure, growth mode and environmental pollution—An empirical analysis based on time-varying parameter vector autoregressive model. China Environmental Science, 2016, 36(7): 2230-2240.]

[4] 梅大伟, 修春亮, 冯兴华, 等. 中国城市脆弱性的时空变化及其内在机理——基于“五普”“六普”及《中国城市统计年鉴》数据的分析[J].城市问题, 2018(9): 13-19. [Mei Dawei, Xiu Chunliang, Feng Xinghua et al. Temporal and spatial changes of China's urban fragility and its internal mechanism—Based on the analysis of the data of “Five Pu”, “Six Pu” and “China Urban Statistical Yearbook”. Urban Problems, 2018(9):13-19.]

[5] 王琰. 多维度城市化对空气质量的影响:基于中国城市数据的实证检验[J].东南大学学报(哲学社会科学版),2017,19(4): 100-110+148. [Wang Yan. The impact of multi-dimensional urbanization on air quality: an empirical test based on Chinese urban data. Journal of Southeast University (Philosophy and Social Science), 2017, 19(4): 100-110+148.]

[6] 王翠平, 丁黎. 城市扩张背景下城市群环境问题的区域性特征分析[J].生态学报,2017,37(23):8058-8066. [Wang Cuiping, Ding Li. Analysis of regional characteristics of urban agglomeration environmental problems in the context of urban expansion. Acta Ecologica Sinica, 2017, 37(23): 8058-8066.]

[7] 王洪平. 基于国外经验的生态环境损害赔偿制度建设分析[J].生态经济,2018,34(9):192-196. [Wang Hongping. Analysis on the institution construction of ecological damage compensation on the basis of foreign experience. Ecological Economy, 2018, 34(9): 192-196.]

[8] 王开泳,颜秉秋,王芳,等. 国外防治城市病的规划应对思路与措施借鉴[J].世界地理研究,2014, 23(1):65-72. [Wang Kaiyong, Yan Bingqiu, Wang Fang et al. Countermeasures of urban planning to manage“Urban Disease”: The experiences from foreign countries. World Regional Studies, 2014, 23(1): 65-72.]

[9] 丁镭,刘超,黄亚林,等. 湖北省城市环境空气质量时空演化格局及影响因素[J].经济地理,2016,36(3):170-178. [Ding Lei, Liu Chao, Huang Yalin et al. Spatial and temporal evolution patterns of urban ambient air quality and its influencing factors in Hubei Province. Economic Geography, 2016, 36(3): 170-178.]

[10] 燕丽, 杜小申. 典型城市空气污染特征对比分析[J].中国环境管理,2018, 10(6):92-98. [Yan Li, Du Xiaoshen. Comparative analysis of typical urban air pollution characteristics. Chinese Journal of Environmental Management, 2018, 10(6):92-98.]

[11] 马春燕, 李璐池, 薛文燕. 空气污染特征与分布规律的可视化技术研究[J].西北工业大学学报,2017, 35(6):1073-1078. [Ma Chunyan, Li Luchi, Xue Wenyan. Study on visualization technology of air pollution characteristics and distribution law. Journal of Northwestern Polytechnical University,2017, 35(6):

1073-1078.]

[12] 刘铁军, 邱大庆, 孙娟. 城市交通拥堵与空气污染相关度的初步研究[J].中国人口·资源与环境,2017, 27(S2):58-60. [Liu Tiejun, Qiu Daqing, Sun Juan. A preliminary study on the correlation between urban traffic congestion and air pollution.China Population Resources and Environmen,2017, 27(S2):58-60.]

[13] 邹滨, 许珊, 张静. 土地利用视角空气污染空间分异的地理分析[J].武汉大学学报(信息科学版), 2017, 42(2):216-222. [Zou Bin, Xu Shan, Zhang Jing. Geographical analysis of spatial differentiation of air pollution from the perspective of land use. Geomatics and Information Science of Wuhan University,2017, 42(2):216-222.]

[14] 智路平, 张华歆, 周溪召, 等. 空气污染下居民出行风险感知影响因素实证研究[J].上海理工大学学报,2018, 40(1):56-64. [Zhi Luping, Zhang Huaxin, Zhou Xizhao et al. An empirical study on the factors affecting the risk of residents' travel risks under air pollution. Journal of University of Shanghai for Science and Technology,2018, 40(1):56-64.]

[15] Puett R C, Hart J E, Yanosky J D et al. Particulate matter air pollution exposure, distance to road, and incident lung cancer in the nurses' health study cohort[J]. Environmental Health Perspectives, 2014, 122(9): 926-932.

[16] 韩立建. 城市化与$PM_{2.5}$时空格局演变及其影响因素的研究进展[J].地理科学进展,2018, 37(8):1011-1021. [Han Lijian. Relation-ship between urbanization and urban air quality: An insight on fine particulate dynamics in China. Progress in Geography, 2018, 37(8):1011-1021.]

[17] Schwarz J, Pokorná P, Rychlík Š et al. Assessment of air pollution origin based on year-long parallel measurement of $PM_{2.5}$ and PM_{10} at two suburban sites in Prague, Czech Republic[J]. Science of the Total Environment,2019, 426:1107-1116.

[18] 宋英石, 李锋, 徐新雨,等. 城市空气颗粒物的来源、影响和控制研究进展[J].环境科学与技术,2013, 36(S2):214-221.[Song Yingshi, Li Feng, Xu Xinyu et al. Research progress on source, impact and control measurements of particulate matter in the urban air. Environmental Science & Technology, 2013, 36(S2): 214-221.]

[19] 张晓瑞,张琳雅, 方创琳. 概念、框架和测度:城市脆弱性研究脉络评述及其拓展[J].地理与地理信息科学, 2015, 31(4): 94-99. [Zhang Xiaorui, Zhang Linya, Fang Chuanglin. Concept, framework and measurement: Review on the research context of urban vulnerability and its development. Geography and Geo-information Science, 2015, 31(4):94-99.]

[20] 李惠娟, 周德群, 魏永杰. 中国主要城市空气污染的影响因素——基于污染源解析的研究[J].生态经济,2018, 34(4): 197-203. [Li Huijuan, Zhou Dequn, Wei Yongjie. Impact factors of air pollution in Chinese important cities: Based on source apportionment. Ecological Economy, 2018, 34(4):197-203.]

[21] 王丽. 汽车消费和空气污染相关性的面板数据分析[J].中国人口·资源与环境,2014, 24(2):462-466. [Wang Li. Panel data analysis on consumption behavior of car buyer and air pollution in China. China Population Resources and Environment, 2014, 24(S2):462-466.]

[22] 连荣源, 董洁霜. 机动车辆尾气CO污染控制研究[J]. 交通与运输，2013(1):142-144. [Lian Rongyuan, Dong Jieshuang. Study on motor vehi-cle exhaust pollution CO control. Traffic & Trans-portation,2013 (1):142-144.]

[23] 合肥市统计局,国家统计局合肥调查队. 合肥市 2018 年国民经济和社会发展统计公报[N/OL]. http://tjj.hefei.gov.cn/8726/8730/201903/W020190329394353247722.pdf.2019-03-29. [Hefei Statistical Bureau, Hefei Investigation Team of National Statistical Bureau. Statistical bulletin of national economic and social development of Hefei in 2018. http://tjj.hefei.gov.cn/8726/8730/201903/W020190329394353247722.pdf.2019-03-29.]

[24] 陈刚, 刘佳媛, 皇甫延琦, 等. 合肥城区PM_{10}及$PM_{2.5}$季节污染特征及来源解析[J].中国环境科学,2016, 36(7):1938-1946. [Chen Gang, Liu Jiayuan, Huangpu Yanqi et al. Seasonal variations and source apportionment of ambient PM_{10} and $PM_{2.5}$ at urban area of Hefei, China.China Environmental Science,2016, 36 (7):1938-1946.]

[25] 窦攀烽,左舒翟,任引,等.基于城市分类的绿色城市指标体系构建[J]. 生态学杂志, 2019, 38(6):1937-1948. [Dou Panfeng, Zuo Shuzhai, Ren Yin et al. Constraction of an index system for green cities based on urban classification. Chinese Journal of Ecology, 2019, 38(6):1937-1948.]

[26] Cariolet J M, Colombert M, Vuillet M et al. Assessing the resilience of urban areas to traffic-related air pollution: Application in greater Paris[J]. Science of the Total Environment, 2018, 615: 588-596.

[27] Basagaña X, Triguero-Mas M, Agis D et al. Effect of public transport strikes on air pollution levels in Barcelona (Spain) [J]. Science of the Total Environment, 2018,610-611:1076-1082.

[28] 闫敏慧,姚秀萍,王蕾,等. 用层次分析法确定气象服务评价指标权重[J]. 应用气象学报,2014, 25(4):470-475.[Yan Minhui, Yao Xiuping, Wang Lei et al. Determining weight coefficients of meteorological service evaluation criteria with AHP.Journal of Applied Meteorological Science ,2014, 25(4):470-475.]

[29] 韦亚平, 潘聪林. 大城市街区土地利用特征与居民通勤方式研究——以杭州城西为例[J].城市规划, 2012, 36(3):76-84+89. [Wei Yaping, Pan Conglin. Urban land-use characteristics and commuters' travel pattern: A case study of west Hangzhou. Urban Planning Review, 2012, 36(3):76-84+89.]

[30] Saelens B E, Sallis J F, Frank L D. Environmental correlates of walking and cycling: Findings from the transportation, urban design, and planning literatures[J]. Annals of Behavioral Medicine,2003, 25(2):80-91.

[31] Hajna S, Ross N A, Brazeau A S et al. Associations between neighbourhood walkability and daily steps in adults: A systematic review and meta-analysis[J]. BMC Public Health,2015, 15 (1):768.

[32] Taleai M, Taheri Amiri E. Spatial multi-criteria and multi-scale evaluation of walkability potential at street segment level: A

case study of tehran [J]. Sustainable Cities and Society,2017 (31):37-50.

[33] 许学强,周一星,宁越敏.城市地理学[M].北京:高等教育出版社,2004:219-221. [Xu Xueqiang, Zhou Yixing, Ning Yuemin. Urban geography. Beijing: Higher Education Press, 2004: 219-221]

Zoning and Regulation of Air Pollution in Hefei City Based on the Concept of Green Travel

Gu Kangkang[1,2], Zhu Pengxiang[1], Ning Yang[1],Wang Fei[1]

(1.*School of Architecture & Planning, Anhui Jianzhu University, Hefei* 230022, *Anhui, China*; 2. *Research Center of Urbanization Development in Anhui Province, Hefei* 230022, *Anhui, China*)

Abstract: Air pollution is one of the major environmental problems in cities, which seriously affects urban human health, and traffic exhaust emission is an important cause of air pollution. Green travel is a kind of traffic concept that aims to alleviate urban traffic congestion, urban pollution and other problems by developing low-carbon, green and environment-friendly travel modes based on the requirements of sustainable urban development. The assessment of zoning and regulation of air pollution based on the concept of green travel is significance for improving quality of urban environmental and human settlement environment. Taking the downtown of Hefei China as an example, an urban air pollution assessment framework was constructed based on green travel concept, evaluation indexes of three types were green travel for public transportation, walking and bicycle, the potentiality of green travel modes to improve air pollutant emissions were analyzed by using big data. The results showed that the public transportation had a banding distribution with East-west and North-south direction in the downtown area of Hefei, and the walking and bicycle trips were concentrated in the second ring of the city with high road network density. Green travel showed strong ability to improve air pollutant emissions in the 'one nuclear and two-axis' region; there are two high-vulnerability depressions of Hefei air pollution in first ring and the core area of Binhu; the relationship was explored among green transportation and urban air pollution , it was found that there was a certain spatial trade-off relationship among of them. Finally, the downtown of Hefei is divided into four areas: green travel zone, travel restriction zone, optimized construction zone and potential promotion zonebased on coordination of green transportation, urban air pollution. Optimization strategies were proposed for the air pollution in different regions.

Key words: green travel; air pollution; zonal regulation; GIS; Hefei

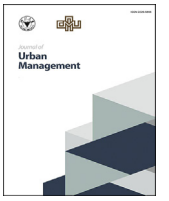
Journal of Urban Management 10 (2021) 3–15

HOSTED BY

Contents lists available at ScienceDirect

Journal of Urban Management

journal homepage: www.elsevier.com/locate/jum



Research Article

Performance evaluation on multi-scenario urban ventilation corridors based on least cost path



Yunhao Fang [a], Kangkang Gu [a,b,*], Zhao Qian [a], Zhen Sun [a], Yongzheng Wang [a], Ai Wang [a]

[a] School of Architecture & Planning, Anhui Jianzhu University, Hefei, 230022, China
[b] Collaborative Innovation Center of Urbanization Construction in Anhui Province, Hefei, China

ARTICLE INFO

Keywords:
Ventilation corridor
Vegetated areas
Waters
Least cost path (LCP)
Heat island effect

ABSTRACT

Ventilation Corridor is an important technique to mitigate local climate problems. Evaluating the benefits of ventilation corridors has gradually become the standard of its construction in cities. Previous studies have often analyzed the volume of ventilation from the perspective of geometric morphology, while there is a lack of discussion on its performance. Therefore, this study innovatively combined the roughness length (Z_0), 3-dimensional aerodynamics parameter, with NDVI and M-NDWI, 2-dimensional indices of land cover through the combination of remote sensing inversion and urban morphology analysis. Compared with the traditional ventilation method, the composite indicator could not only guarantee ventilation volume, but also consider the cooling benefits brought by waters and vegetated areas. In detail, this study was contextualized in four districts in the city core of Hefei, Anhui Province, China. Based on the method of least cost path, we set up four different schemes for comparison, including roughness, roughness + vegetated areas, roughness + waters, and roughness + vegetated areas + waters. Comparative results were effectively verified through land surface temperature retrieved from the Landsat Thematic Mapper. Results were as follows: (1) Different scenarios exerted different impacts on urban ventilation. Of the four regions, the ventilation corridor that only considers Z_0 presented the highest average land surface temperature. (2) The general temperature of ventilation corridors along the path of Z_0 + NDVI + M-NDWI was respectively 34.11 °C, 31.73 °C, 34.80 °C, and 34.93 °C, presenting a lowest temperature compared with other scenarios of the same region. (3) Among the four regions, ventilation corridors constructed based on the path of Z_0 + M-NDWI presented a slightly lower temperature that those based on Z_0+NDVI, with respective data of 34.22 °C < 34.55 °C, 31.85 °C < 31.91 °C, 34.81 °C < 34.82 °C, and 35.21 °C < 35.38 °C. The results provided methods and evidence for performance evaluation on urban land surface ventilation corridors.

1. Introduction

Traditional modifications of city structures and anthropogenic pollution have significantly altered the climate in urban areas. For instance, the phenomenon that urbanized areas suffer from warmer temperatures than their neighboring rural or suburban areas is known as urban heat island (UHI) (Oke, 1982; He et al., 2019). Optimal urban ventilation can enhance air flow capacity and reduce building energy consumption in the summer, which plays an important role in alleviating the urban heat island effect (Hong & Lin,

* Corresponding author. School of Architecture & Planning, Anhui Jianzhu University, Hefei, 230022, China.
E-mail address: kangkanggu@163.com (K. Gu).

https://doi.org/10.1016/j.jum.2020.06.006
Received 22 February 2020; Received in revised form 27 May 2020; Accepted 20 June 2020
Available online 28 August 2020
2226-5856/© 2020 The Authors. Published by Elsevier B.V. on behalf of Zhejiang University and Chinese Association of Urban Management. This is an open access article under the CC BY-NC-ND license (http://creativecommons.org/licenses/by-nc-nd/4.0/).

2015; Coccolo et al., 2016). Thus, the urban ventilation has been emphasized in practice and classified into key schemes of urban planning (Luo et al., 2017). However, actual urban planning often does not consider the efficiency of urban ventilation, which means that airflow cannot guarantee its effectiveness in mitigating climate issues such as the heat island effect (Cariolet et al., 2018; Yuan et al., 2014).

Urban morphology has been applied to explain urban climate change, which is also important for urban ventilation efficiency (Edussuriya et al., 2011; Stewart & Oke, 2012). Low horizontal wind speed is usually associated with high surface roughness, as the energy would be lost by vertical instability due to a high building density (Huang et al., 2014). The pressure difference along temperature gradients can also cause low-level breezes across the urban-rural boundary (Wong et al., 2010). In the previous studies, most data included in urban ventilation were from ground level instruments. The gathering of data over large regions such as a city, therefore, was a major challenge to these studies (Hang et al., 2012; Liu et al., 2019; Vernay et al., 2015). Currently, computer numerical simulation approaches such as computational fluid dynamics (CFD) are applied to analyze urban ventilation efficiency (Ding et al., 2017; Lyu et al., 2015). Specifically, it comprises a set of physical models which attempt to closely match the real urban geometry and thus simulate the air flow around buildings and along streets. The wind pressure and velocity are analyzed to provide feedback on the wind environment (Bajsanski et al., 2016; Guo et al., 2015; Hsieh & Huang, 2016). However, these simulations mostly focus strongly on the physical environment of some districts and buildings that cover small ranges (Badas et al., 2017). Therefore, for urban scale calculations, especially over densely urbanized regions with complex building structures, it is difficult to estimate ventilation efficiency.

The development of Geographic Information System (GIS) and remote sensing technology filled this gap (Yim et al., 2014). In addition, the mathematical model can simplify surface conditions by estimating roughness parameters of building structures (Li et al., 2019a; Wrobel-Niedzwiecka et al., 2019; Wen et al., 2017). Many morphological parameters and diffusion models have been applied to calculate the ground roughness in cities (Burian et al., 2002). The calculation methods include parameters such as building height, building area density, frontal area index, height-to-width ratio, roughness length, and displacement height, etc. Among these urban morphological parameters, the roughness length has been suggested as the most appropriate indicator of the roughness of urban surfaces

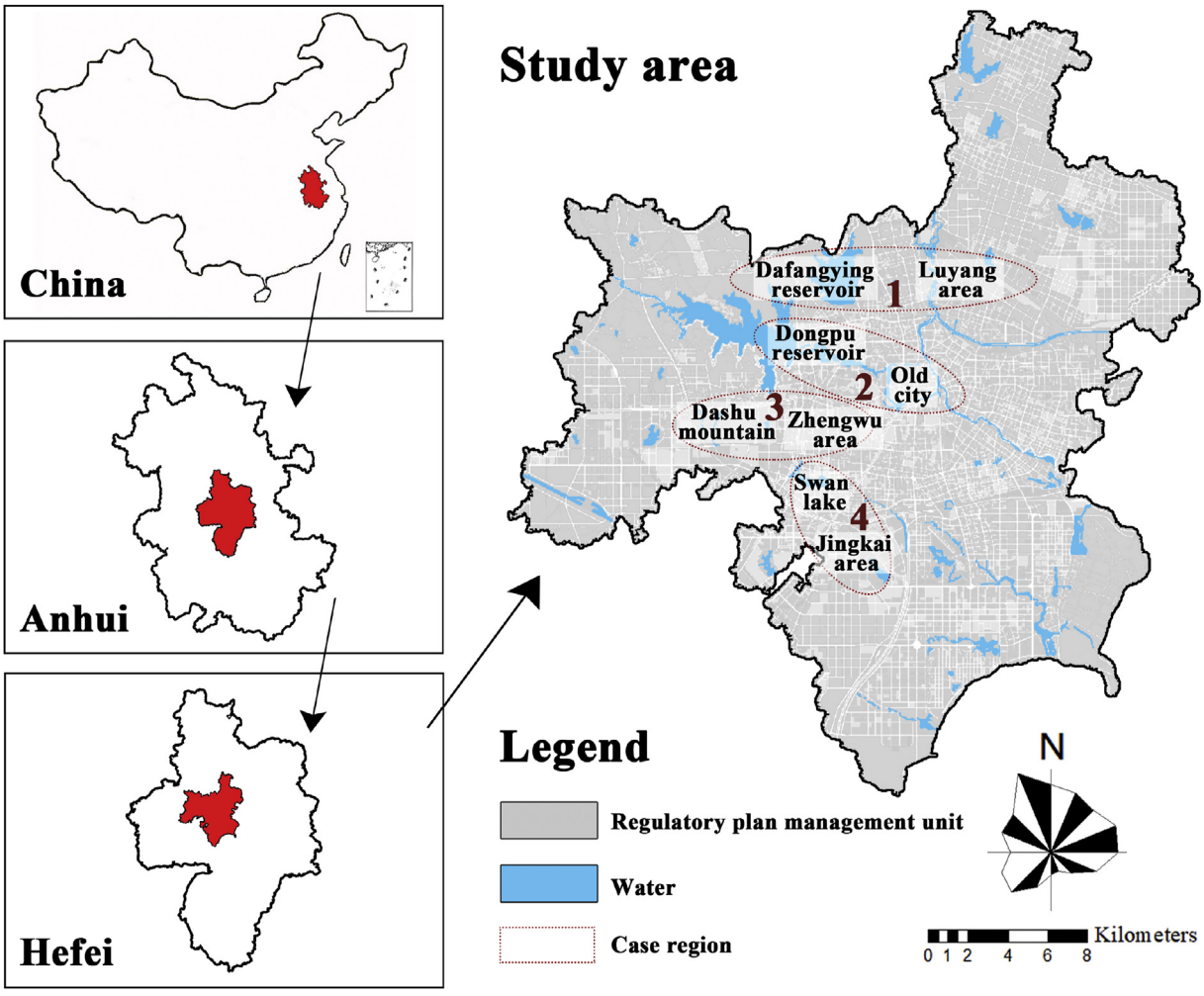


Fig. 1. Research area.

for meso-scale meteorological and urban dispersion models (Kent et al., 2017). Previous studies on urban planning applied a low roughness length to construct ventilation corridors, but the optimal ventilation benefits cannot be achieved by only considering urban morphology (Huang & Wang, 2019; Weng et al., 2015; He et al., 2020a). It is known that vegetated areas and waters have a strong cooling effect (Qiao et al., 2017; Zhang & Li, 2017; He et al., 2020b). As is expressed by the mathematical formula, they have the same low roughness length as road or open space. Specifically, this method can generate strong enough winds to maintain the volume and speed of the moving air, ignoring the benefits of the air temperature.

The purpose of this study is to design ventilation corridors addressing temperature influence according to land cover in order to improve urban ventilation efficiency. Accordingly, by combining 3-dimensional aerodynamics parameter with 2-dimensional indices through remote sensing inversion and the analysis of urban morphology, we chose the main area of Hefei as research object, based on the least cost path (LCP) method, to comprehensively compare the optimization cooling effect of urban vegetated areas and waters on land surface ventilation.

2. Research area and methods

2.1. Research area

Hefei (116°41′E−117°58′E, 30°57′N-32°37′N) locates in the eastern China, the middle latitude zone (Fig. 1). The terrain mostly consists of plains, hills and mountains. It belongs to humid subtropical climate, with distinctive four seasons and an average annual temperature of 15.7 °C. Its average annual precipitation is about 1000 mm, and average relative humidity 77%. An annual mainstream

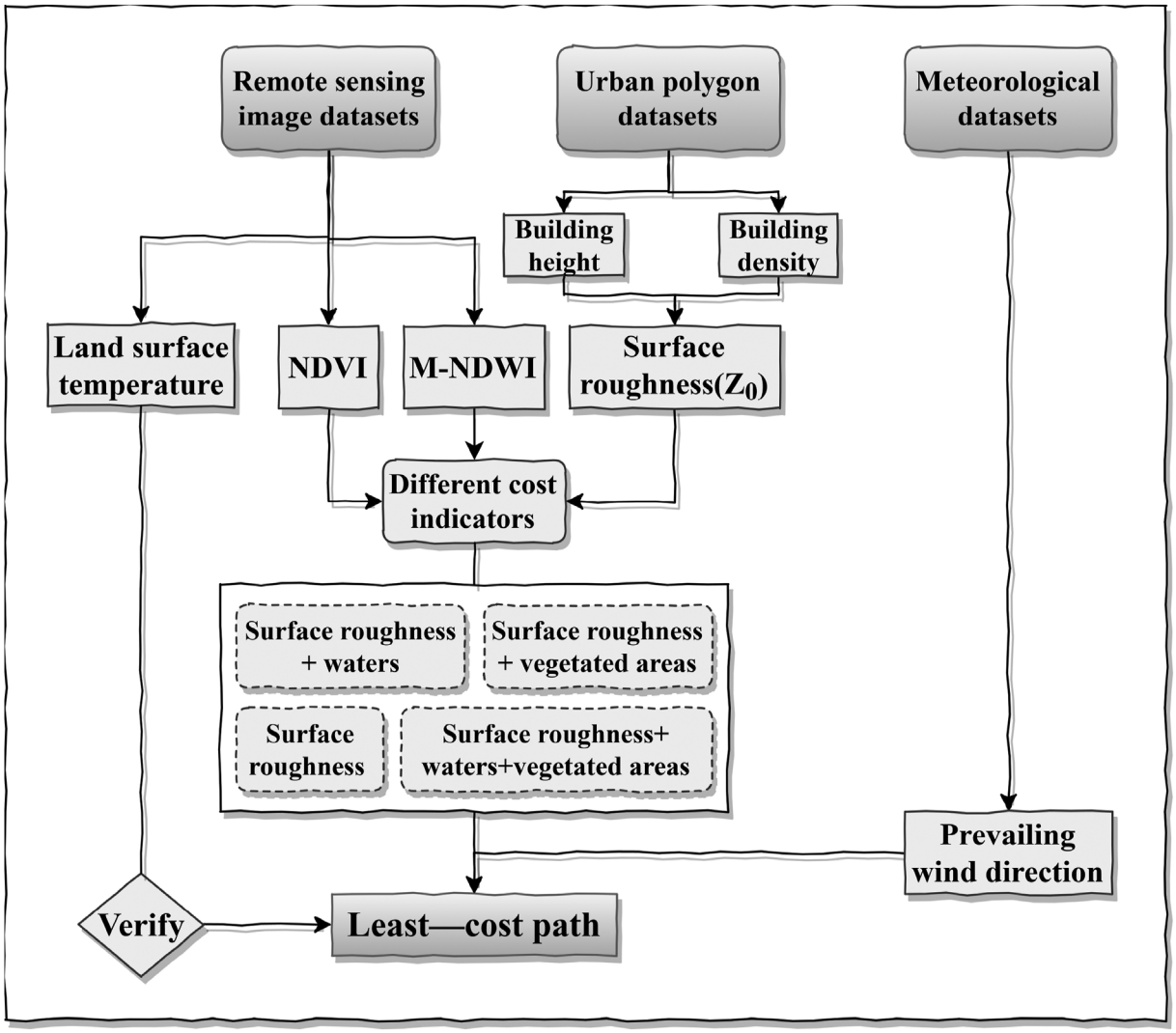


Fig. 2. Research framework.

prevails north and northwest throughout the year. By the end of 2018, Hefei had a resident population of 8.087 million. Meanwhile, farmland in the main urban area is the dominant landscape in this zone, accounting for 63.82%. Water area account for 6.03% and vegetation account for 2.68%. In addition, the construction area reached 460 km^2, accounting for 27.47%. In recent years, due to increasing infrastructure and haze weather, the pullulation of $PM_{2.5}$ increased significantly, and the urban heat island effect exacerbated annually. In Hefei, its heat island effect in winter is more intense than that in summer (Wang et al., 2019). In this study, we simulated and compared four regions in Hefei, which contain both vegetated areas, waters and region center. To be specific, the region 1 covered the Dafangying reservoir and Luyang area, the region 2 contained the Dongpu reservoir and Old city, the region 3 included the Dashu mountain and Zhengwu area, the region 4 covered the Swan Lake area and Jingkai area.

2.2. Research Framework

According to the German theory of ventilation corridor construction, the urban underlying land surface is divided into "the effective space" (Wirkungsraum), "the compensation space" (Ausgleichsraum), and "the ventilation path" (Luftleitbahn) (Liu & Shen, 2010). The effective space refers to area with thermal or air pollution. The compensation space, or say, compensation space for climate ecology, exchanges air with its adjacent space in order to generates regional air circulation. Furthermore, urban natural ventilation gets enhanced, thereby alleviating problems like urban heat island effect and other pollution. The ventilation path connects the effective space to the compensation space, with relatively low land surface roughness and less resistance to air flow (Weng et al., 2015). In this study, 30m*30m grids in Hefei were selected as samples. We calculated the intensity of the heat island using satellite remote sensing data, and identify the effective space and compensation space. In addition, data used in this study also includes Geographic Information System (GIS) data on land cover, and buildings for 2016 and relevant urban planning materials of Hefei. We used these data to analyze the urban wind environment and extract the parameters of urban spatial form. And then we used that data to build up the different costs, including roughness, roughness + vegetated areas, roughness + waters, and roughness + vegetated areas + waters. Then, this study is based on cost to construct urban land surface ventilation corridors between the effective space and compensation space applied LCP as the model to compare the ventilation efficiency of the four models. Finally, remote sensing images were applied to verify the ventilation potential of the four models. The specific process is exhibited in Fig. 2.

2.3. Analysis on least cost path (LCP)

2.3.1. Methods to extract cost index

2.3.1.1. Land surface roughness (Z_0). The roughness elements of urban underlying surface are complicated. Buildings work as resistance collection to ventilation, and thereby affect wind speed. Urban roughness elements and landform resist the flow of currents (Gál & Sümeghy, 2007). Therefore, urban land surface roughness Z_0 could partly reflect the ventilation potential near urban land surface (Bottema, 1997). According to relevant studies, roughness of urban land surface is mainly caused by buildings. Mainly determined by building density and building height (Bottema & Mestayer, 1998). Therefore, in the urban area, this study uses the morphological model to estimate the roughness of urban surface Z_0, including:

$$\frac{Z_d}{Z_h} = 1.0 - \frac{1.0 - \exp\left[-(7.5 \times 2 \times \lambda_F)^{0.5}\right]}{(7.5 \times 2 \times \lambda_F)^{0.5}} \tag{1}$$

$$\frac{Z_0}{Z_h} = \left(1.0 - \frac{Z_d}{Z_h}\right)\exp\left(-0.4 \times \frac{U_h}{u_*} + 0.193\right) \tag{2}$$

$$\frac{u_*}{U_h} = \min\left[(0.003 + 0.3 \times \lambda_F)^{0.5}, 0.3\right] \tag{3}$$

In the equation, Z_d (m) is the height of zero plane displacement; Z_0 (m) is the height of roughness degree; Z_h (m) is the height of building; Z_d/Z_h is the normalized height of zero plane displacement; Z_0/Z_h is the normalized height of roughness degree; U_h is wind speed; u^* is shear velocity; λF is building frontal area, which is closely related to the urban building density λP. In this study, when building density λP concentrates on the area of 0.35, Z_0/Z_h reached the peak. Then the relationship of λF and λP can be generated, that is, $\lambda F = 0.8\lambda P$ (Liu et al., 2017).

2.3.1.2. Normalized difference vegetation index (NDVI) and modified normalized difference water index (M-NDWI). Waters have a lower roughness length than the other land surfaces, which is also the case with the vegetation. This study relies on the ventilation corridors of urban vegetated areas and waters, which can not only ensure a certain amount of ventilation, but also form a blue-green cyberspace to effectively alleviate urban heat island effect. Besides, the two indicators can connect to natural system, purifying spatial pollution from the internal of city, compared with buildings with low roughness. Therefore, we consider the actual situation of Hefei and take vegetated areas and waters into the consideration of cost.

NDVI could accurately reflect the spatial distribution and growth details of plants (Zheng et al., 2018; Formica et al., 2017). M-NDWI performed better in exacting waters than NDWI, as it could better reflect the features and ranges of waters (Ghosh et al., 2015). The both indicators, range from −1 to 1, can effectively reflect the coverage of urban vegetated areas and waters. The larger the index, the higher

the vegetation coverage and water coverage. This study was conducted in main urban area of Hefei, based on Landsat8 OLI/TIRS data, and applied software ENVI5.3 to conduct band calculation after radiation correction. Spatial analysis ArcGIS was then applied to generate NDVI and M-NDWI, which are considered as important weighted indices of urban vegetated areas and waters.

2.3.2. Valuation under different ventilation corridor thresholds

The valuation of ventilation corridor costs is crucial for land surface ventilation corridor construction. Hefei is mainly a plain with an average elevation of 20–40 m, so that can be ignored in the selection of cost. For these reasons, we first apply normalization to each of the considered factors in this study. Specifically, three original variables Z_0, NDVI and M-NDWI were defined from 1 to 10 by using the reclassification Tool of ArcGIS. It is worth noting that the higher the value of Z_0, the higher the cost, while NDVI and M-NDWI represent the opposite, the higher the index value, the lower the cost. Then, for a multi-scene comparison, we not only consider the underlying land surface roughness (Z_0) factor, but also add different impact generated by vegetated areas (NDVI), waters (M-NDWI) and vegetated areas + waters (NDVI + M-NDWI). In this study, Analytic hierarchy process was applied to assess the factors and their accumulated contributions were listed in Table 1. The numerical settings in Table 1 not only take account into that the roughness of the land surface is higher than that of waters and vegetated areas, but also that the land coverage in the city is relatively wide, so the cumulative contribution cannot be too low.

2.3.3. The construction of ventilation corridor by LCP

The construction of ventilation corridor by LCP is to ensure ventilation corridor planning is conducted by path with least wind resistance, and to guarantee the comprehensive benefits of vegetated areas and waters could be truly brought to city. Generally speaking, LCP, as a kind of analytical model, needs to consider the different cost of grid surface to construct ventilation corridor paths. Compared to previous applications, we innovatively considered the selection of the dominant wind direction and the location of the LCP, that is the selection of the effective space and compensation space. This approach ensures maximum cost effectiveness of the ventilation corridors for the study area. The formula for calculating LCP is shown in equation (4) (Li et al., 2019b).

$$LCP = f_{min} \sum_{j=n}^{i=m} (D_{ij} \times R_i) \tag{4}$$

In equation (4), LCP is the minimum of accumulated resistance; D_{ij} is the weight coefficient of resistance factor i in pixel j; R_i is the resistance value to motion of factor i; n and m are the number of the type of source and cost factor.

2.3.4. Confirmation of ventilation efficiency

Heat island intensity is recognized as a significant factor influencing urban ventilation efficiency. The lower the air temperature, the greater the ventilation rate under normal conditions (Marzena et al., 2017; Morakinyo et al., 2013; Yin et al., 2018). But there are exceptions, for instance, the penetration of hot wind (derived from the inland desert area) with high ventilation efficiency results in the enhancement of land surface temperature (He, 2018). It really depends on whether the wind source is cool or not. Therefore, in order to ensure the cooling of the wind source, the study set it in the mountain or waters. Although the air temperature was a good reflection of the urban heat island phenomenon, the temperature measurement was time-consuming and labor-intensive, besides, the measurement range is difficult to cover. Therefore, we used the urban surface land temperature (LST) inversion from the Landsat TM thermal band to validate the ventilation efficiency. Relevant studies show that there is a certain difference between the surface temperature and the air temperature (Rao et al., 2019). In particular, the measurement object and diurnal variation rule of LST and air temperature are different. Despite the numerical differences, there was a strong correlation between LST and air temperature, and LST increased with the increase of air temperature (Sheng et al., 2017). In general, LST can describe the heat island intensity of a city. For the specific conversion method, please refer to formula (7).

According to Landsat8 OLI/TIRS remote sensing data on April 10th, 2018 and atmospheric correction, software ENVI5.3 was applied to conduct inversion on heat island intensity. The temperature generated was then coupled with cost paths to comprehensive analyze the ventilation potential of urban land surface (Marzena & Katarzyna, 2016; Qiao et al., 2017). This method removed the effects of atmospheric radiation on the surface based on real-time atmospheric sounding data to obtain a true ground heat radiation intensity. At the same time the algorithm also considers that the thermal infrared radiation brightness value (L_λ) comprises of the atmospheric upward radiance (L_u), the atmospheric downward radiance (L_d) and the true radiation received by satellite sensor from the ground.

$$L_\lambda = [\varepsilon L_T + (1 - \varepsilon) L_d]\tau + L_u \tag{5}$$

where ε is the surface specific emissivity; L_T is the radiant brightness of a black body with temperature (T (K)) in the thermal infrared band; τ is the atmospheric transmittance, which can be obtained using online values of L_u and L_d (https://atmcorr.Gsfc.nasa.gov/). Based

Table 1
The characteristic value of each principal component and its cumulative contribution rate.

Cost Factors	Land Surface Roughness	Land Surface Roughness + Vegetated Areas		Land Surface Roughness + Waters		Land Surface Roughness + Vegetated Areas + Waters		
Contribution Rate	Z_0	Z_0	NDVI	Z_0	M-NDWI	Z_0	NDVI	M-NDWI
	1	0.40	0.60	0.40	0.60	0.375	0.375	0.25

on the L_T obtained from formula (5), the surface temperature (T_s) was obtained using formula (6). The relevant parameters for each satellite are given in Table 2.

$$T_s = K_2 / ln[1 + K_1 / L_T] \tag{6}$$

The heat island intensity was then calculated using the UHI intensity index (UHII) algorithm, and the UHI scale index formula is shown in formula (7).

$$UHII_i = T_i - \frac{1}{n}\sum_{1}^{n} T_{crop} \tag{7}$$

where $UHII_i$ is the heat island intensity corresponding to the ith pixel on the image; T_i is the surface temperature; n is the number of effective pixels in the suburban farmland; and T_{crop} is the surface temperature in the suburban farmland, which means the average surface temperature of all surrounding agricultural and forest land.

3. Results and analysis

3.1. Spatial distribution features of cost indices

3.1.1. Analysis on land surface roughness

According to results, as is shown in Fig. 3, the general distribution demonstrated “two peaks and multiple bottoms”. To see from different ranges of roughness, Binhu area in the south and a small amount of Zhengwu area had relatively high land surface roughness, distributed in patches, belonging to “two peaks”. The land surface roughness in these areas were basically in the range between 9.09m to 13.95m. Old city and Luyang area in the north ranked the second, scattered in the figure, and the roughness was in the range of 2.79–5.66. The suburbs and part of Forest and Wetland parks had relatively low roughness, belonging to “multiple bottoms”, generally in the range of 0.40–2.79m. In general, roughness in the main urban area of Hefei reached peak in Binhu area in the south and Zhengwu area, and gradually reduced from the inside out.

3.1.2. Analysis on normalized difference vegetation index (NDVI) and modified normalized difference water index (M-NDWI)

It can be seen from spatial distribution (Fig. 4) that NDVI demonstrated the feature of “multiple peaks and two bottoms”. Areas with relatively high index were distributed in the surroundings of Dongpu reservoir and Dafangying reservoir in the northwest of main urban area, as well as Baohe area and Binhu area in the south, mostly in the range of 0.40–0.57. These areas were basically in patches, belonging to peaks of NDVI distribution. Shushan area in the west ranked the second, scattered in the figure. Dongpu reservoir and Dafangying reservoir in the northwest had the lowest index, mainly in the range of −0.20∼-0.01, belonging to “two bottoms”. The index generally rose from the inside out. M-NDWI had the feature of “two peaks and multiple bottoms”. “Two peaks” were in the area of Dongpu reservoir and Dafangying reservoir, with a general index between 0.16–0.35. The others were distributed in main rivers and lakes of the city.

3.2. Analysis on LCP

3.2.1. Overlay analysis on Different Cost Thresholds

In the main urban area of Hefei, based on urban land surface roughness, we respectively discussed the impact of vegetated areas, waters, vegetated areas and waters on ventilation corridors of the city. With the reference group of only considering land surface roughness (Z_0), we constructed three types of urban underlying land surface (roughness, roughness + vegetated areas, roughness + waters, and roughness + vegetated areas + waters). According to the difference of their accumulated contribution, we conducted overlay analysis to respectively generate four cost land surfaces, that is, Z_0, Z_0+M-NDWI, Z_0+NDVI and Z_0+M-NDWI + NDVI, thereby generating the general cost of four research areas, as is shown in Fig. 5.

3.2.2. Ventilation corridor construction by LCP

The ventilation corridor by LCP model can ensure the air flow between effective space and compensation space. In general, the construction of effective space and compensation space are not optional as the source points and destination points of the LCP model. The starting points should be set at the urban cold sources or the upwind of the prevailing wind all year round. The destination points, on the other hand, should be set to downwind of the prevailing wind in the case of dense heat sources in the city. Hefei is the perennial north and northwest direction, so we selected four typical regions and the source and destination points of the least-cost path within the

Table 2
Parameters used in the radiative transfer equation-based method.

Landsat type	K_1/(W/(m^2·sr·μm))	K_2/K
Landsat 5	607.76	1260.56
Landsat 7	666.09	1282.71
Landsat 8	774.89	1321.08

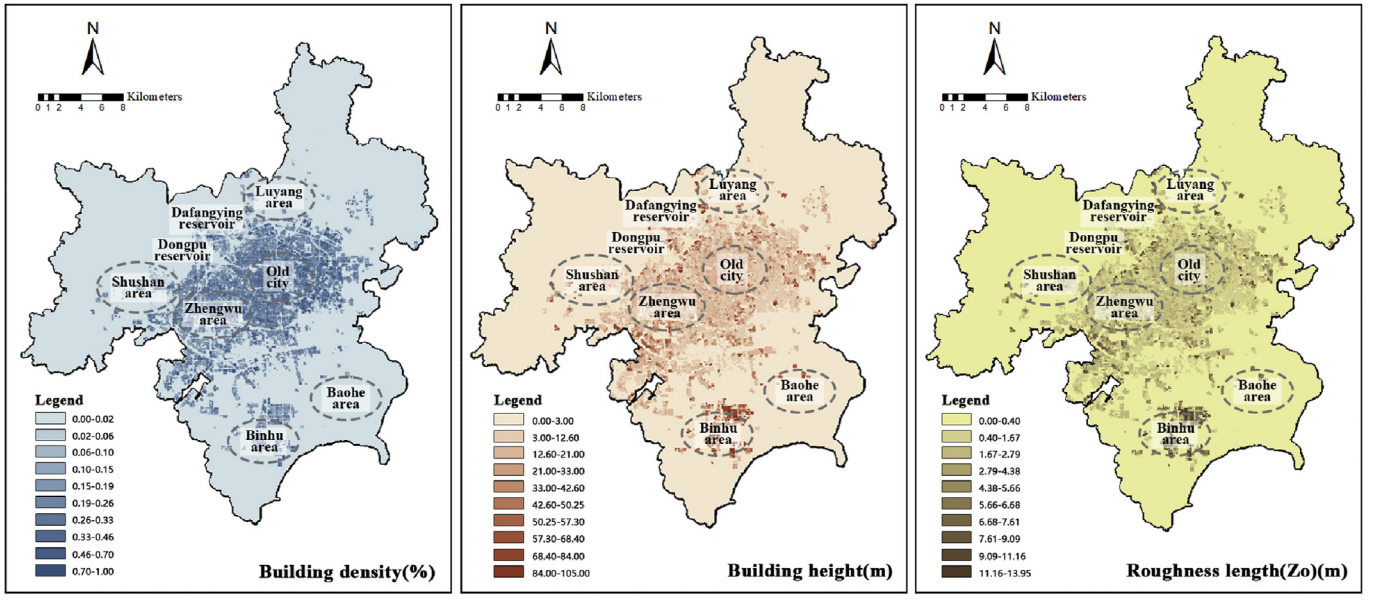


Fig. 3. Spatial Distribution of Density of Building (left), Height of Building (middle) and Land surface Roughness (right).

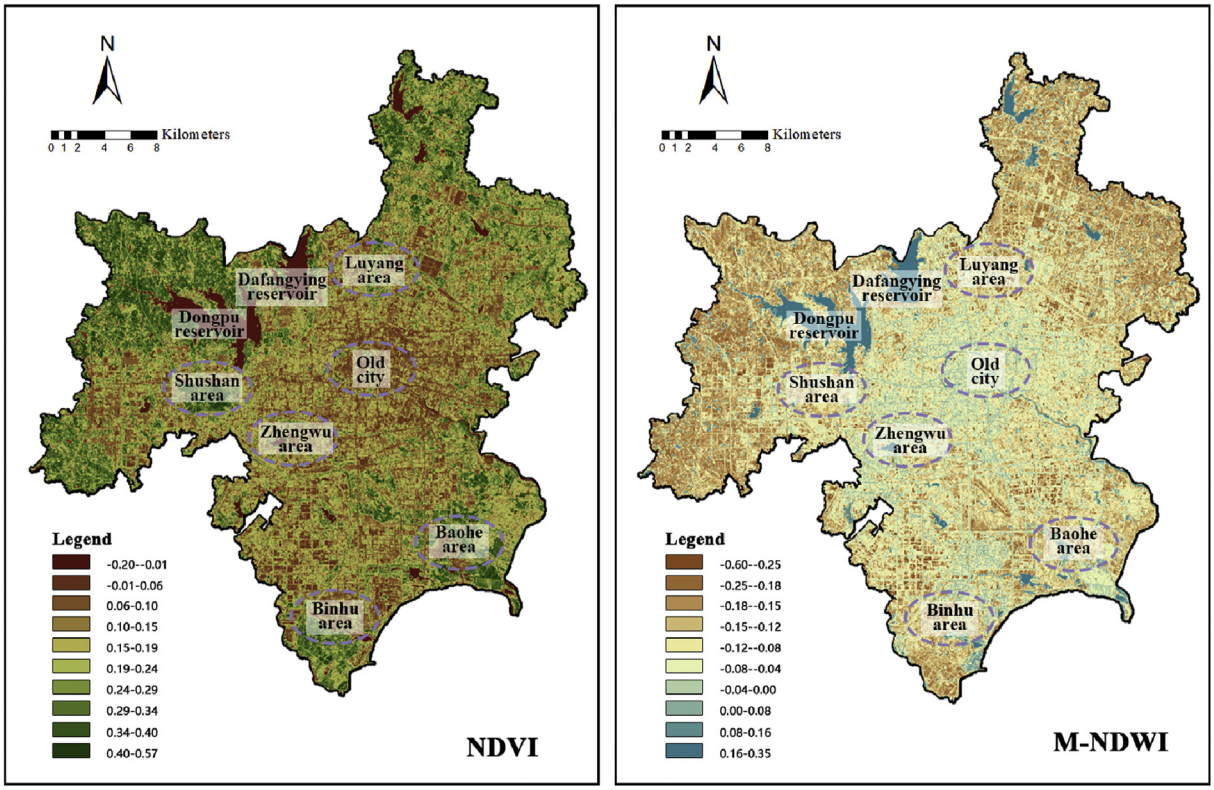


Fig. 4. Spatial distribution of NDVI and M-NDWI

region. Its starting points included Dongpu reservoir, Dafangying reservoir in the northwest, Dashu mountain and Swan Lake area. The destination points are determined in the area with high development intensity near the cold source, including the centers of Luyang area, Old city, Zhengwu area and Jingkai area. According to the sheet layers of different costs, the ventilation corridors constructed in this study are shown in Fig. 6.

Results showed that the general flows of four corridors were almost the same, and no resistance got in the way of north wind or northwest wind. Fresh air could flow from the compensation space through ventilation corridors to the effective space—centers of various main urban areas. However, different ventilation corridors generated different types of land surface paths at the regional level. Among four areas, ventilation corridor A mainly past trunk and secondary trunk roads and squares, consisting of cement and asphalt roads, as well as relatively open underlying land surface like vegetation. Ventilation corridor B mainly past urban green lands like shelter forest area and parks, and a few past non-permeable land surfaces like roads and low-rise buildings. Ventilation corridor C mainly past urban waters like moat, swan lake and reservoirs, and the others flowed to area with low intensity of development. Ventilation corridor D flow through urban natural environments like vegetated areas and waters, as well as artificial environments like buildings.

3.3. Simulation and confirmation

In order to determine the specific influence of ventilation corridors on urban space, constructed by different cost paths, the heat island intensity was used for inversion due to the correlation between the two. In addition, LST was used to represent the heat island intensity in this study because of the high consistency between the LST, obtained by remote sensing image, and weather temperature at that time (Sheng et al., 2017). Therefore, in order to prove different paths of ventilation efficiency, we conducted four cases of coupling ventilation path and surface temperature (Marzena et al., 2017; Qiao et al., 2017), and made statistics on the overlapping pixels in a grid of 30*30, as shown in Fig. 7.

It is indicated in results that heat island intensity of different areas were diversified. In general, it showed the pattern of “two bottoms and multiple peaks” with significant different in temperature. The land surface temperature of the compensation space was obviously lower than that of the effective space. Mountains and waters around the main urban area were generally of low temperature, mostly lower than 18.34 °C. Dongpu reservoir and Dafangying reservoir, located in the northwest of the main urban area, had the lowest temperature, 12.62 °C. And they were the two bottoms in the figure. In the meantime, all regions in the main urban area exhibited generally high temperature, higher than 31.78 °C in general. Peaks were scattered, and Luyang area in the north and Jingkai area in the south had the highest land surface temperature. In general, land surface temperature in the main urban area of Hefei demonstrated a spatial pattern of “cold outside but hot inside”, and temperature was gradually reducing from the inside out.

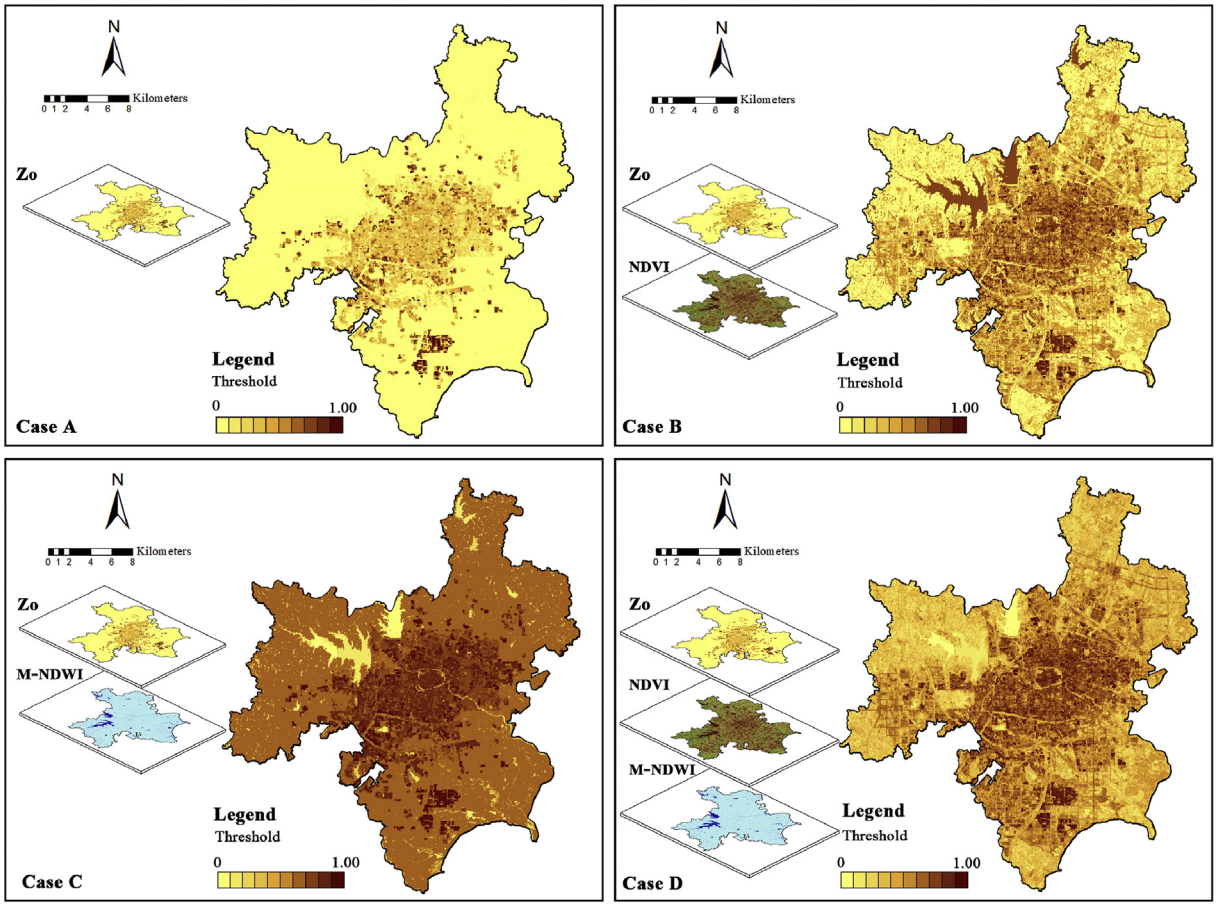


Fig. 5. Spatial distribution of different cost thresholds.

The average land surface temperature of ventilation corridors constructed by different costs in four regions was calculated and analyzed, as shown in Fig. 7 and Table 3. It is obviously that land surface temperature of different regions differed due to spatial distribution. Region 1, 3, and 4 had a generally high temperature, while the ventilation corridors in region 2, between Dongpu reservoir and Dafangying reservoir, had the lowest temperature in general, with an average temperature of 31.93 °C. The highest land surface temperature was in region 4, that is, the ventilation corridors between Swan Lake and Jingkai area, and the average temperature was 35.24 °C. The land surface temperature of the same region was within certain range, but temperature differs in different cases. The largest difference in temperature was in ventilation corridors of region 1, connecting Dafangying reservoir and the center of Luyang area, which was 0.78 °C. In general, whether it is the average comparison of a single region or the average comparison of an entire region, case A had the highest temperature, followed by case B and C, while case D had the lowest temperature.

4. Discussion

A more strategic and integrated process could help to ensure that multiple ventilation corridors are provided to the areas of the city that need them most. Most studies use urban morphology for reference to determine ventilation corridors, lacking of comprehensiveness. So we introduce the remote sensing inversion to improve the delineation of ventilation corridors (He et al., 2020). The method of combining 3-dimensional aerodynamics parameter with 2-dimensional indices was used to evaluate ventilation seeking to steer spatial planning about an integrated roughness length Z_0, NDVI, and M-NDWI. It is consistent with studying the ventilation corridors from a macro perspective, since they have conducted comprehensive research and judgment according to relevant criteria (Li et al., 2019; Marzena et al., 2017). But using different indicators produces different results. Therefore, in this study, in order to further study the rationality of index construction, we need to comprehensively compare the cooling effects of different indicators and their causes in the ventilation corridors. Based on this, we compared four scenarios in the study area. The statistical results of four schemes are shown in Table 3 and Fig. 7.

According to the case A with case B and C, the temperature of the ventilation corridors, constructed with roughness length Z_0, are the highest. In case A, the average temperature of the four regions is 34.37 °C, while in case B and C, the average temperature is 34.17 °C and 34.02 °C, respectively. Specifically, in case A only urban morphology is taken into account in the construction of ventilation corridors,

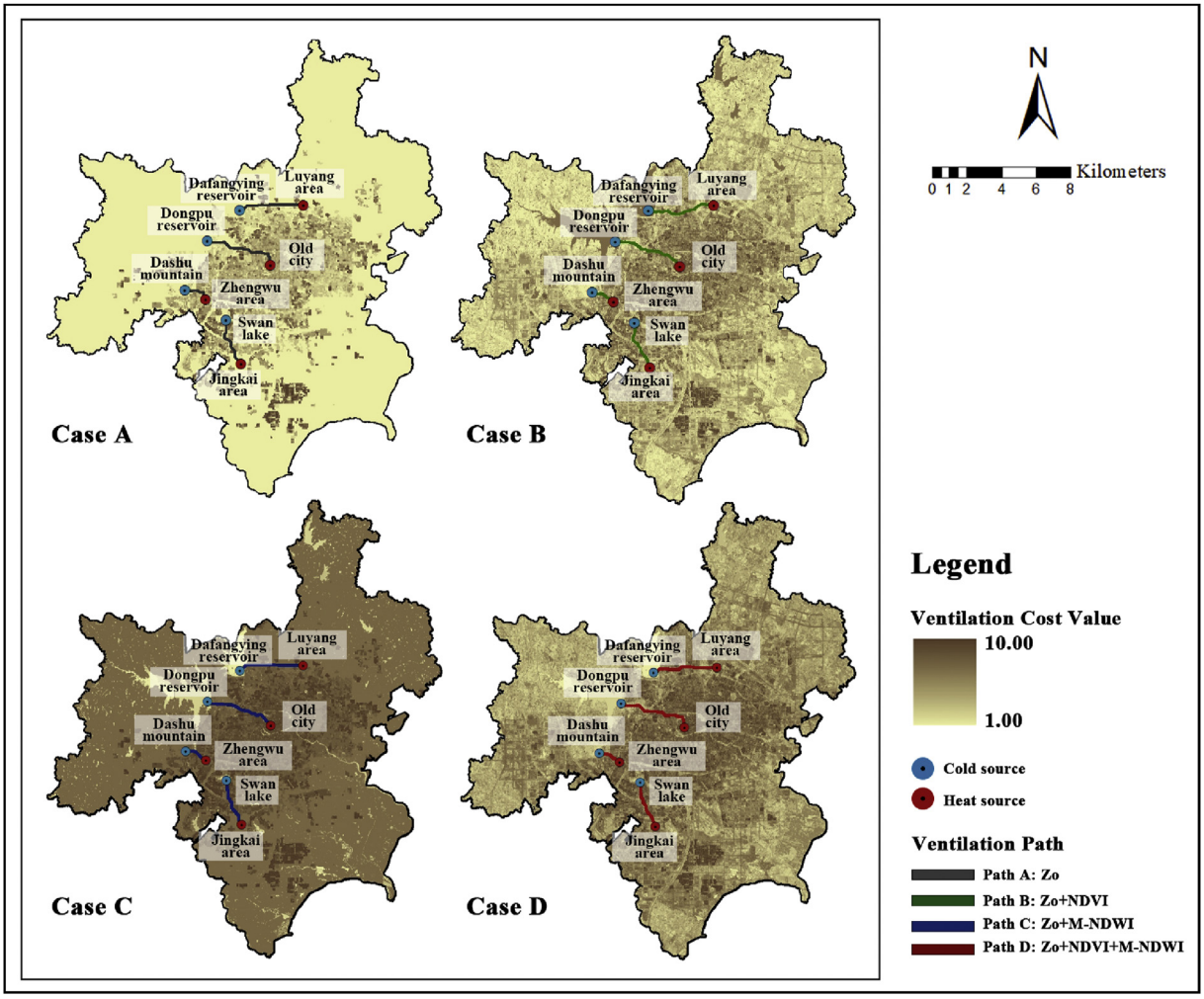


Fig. 6. Distribution of ventilation corridors by LCP

while in case B and case C the study considers the types of underlying land surface through remote sensing images on the basis of urban morphology including vegetated areas and waters. This comparison validates the former studies that the cooling effect of vegetated areas and waters is much greater than the concrete roads and hard paving bricks in cities at the same rough surface length (Li et al., 2013).

In addition, the study also compared case B and case C. As we can be seen from Table 3, the average temperature of each region in case B is not only higher than that of case C, but also the specific temperature in case B, including 34.55 °C, 31.91 °C, 34.82 °C and 35.38 °C, is higher than that of the ventilation corridor of case C in the same region, including 34.22 °C, 31.85 °C, 34.81 °C and 35.21 °C. The main reason for this is that the ventilation corridors of case C mainly passed through waters, while the ventilation corridors of case B mainly passed through vegetated areas. Relevant studies show that the cooling mechanism and cooling intensity of vegetated areas and waters are different in the construction of ventilation corridors. Specifically, waters mainly reduce the temperature of the ventilation corridors by evaporative heat dissipation, which tends to form a significant cold radiation effect on the surroundings, while vegetated areas influence temperature mainly by exchanging with the surrounding air, including photosynthesis and transpiration (Jan et al., 2013). The most important point is that when the wind body flows at a low altitude ($\leq$2m), the thermal mitigation capacity of vegetated areas is lower than the waters (Du, 2018).

Finally, we comprehensively compared the four schemes and found that the ventilation corridors in case D had the lowest average temperature 33.89 °C, showing the ventilation corridors passing through both vegetated areas and waters. Therefore, the combination of vegetated areas and waters can make up for the cooling area of the underlying land surface of the city in space and bring relatively cooling air to the surface of the city. In addition, related studies show that the combination of waters and vegetated areas can mitigate effect of heat island effect, forming a strong cooling island effect (Morakinyo et al., 2013).

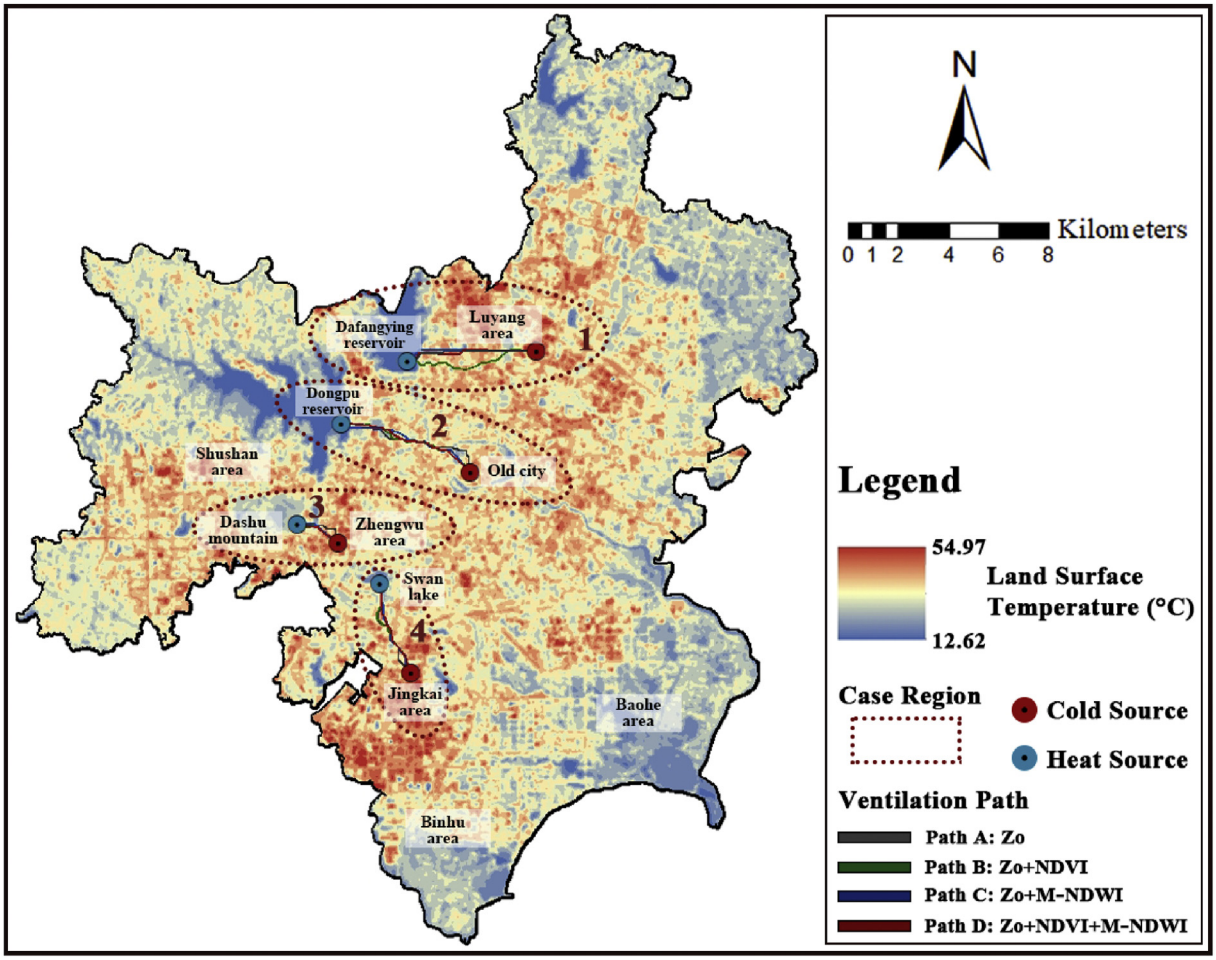


Fig. 7. Distribution of heat island effect intensity.

Table 3
Land surface temperature (LST) statistics in four areas under different paths.

Verification indicators	Regions	Cost indicators			
		Case A	Case B	Case C	Case D
		Z_0	Z_0+NDVI	Z_0+M-NDWI	Z_0+NDVI + M-NDWI
Average temperature(°C)	1	34.89	34.55	34.22	34.11
	2	32.21	31.91	31.85	31.73
	3	34.93	34.82	34.81	34.80
	4	35.45	35.38	35.21	34.93
Average value		34.37	34.17	34.02	33.89

5. Conclusion

Urban ventilation corridors can improve urban climate change, and the related planning needs to consider a variety of influencing factors, including adequate ventilation and wind benefits. In this paper, the least cost path LCP is used as the model to compare the ventilation corridors in multiple scenarios in Hefei (roughness, roughness + vegetated areas, roughness + waters, and roughness + vegetated areas + waters), combining urban heat island inversion with urban morphology. Through the comparison we can discover the optimal path for urban ventilation corridors. The main conclusions are as follows:

(1) The main urban area of Hefei exhibited relatively clear patterns of building heat source and ecological cold source. Above all, comprehensive assessment constructed based on LCP model could effectively optimize the ventilation corridors constructed based solely on urban morphological index.

(2) Different combinations of index showed different impacts on urban land surface ventilation, exhibiting the rule of land surface roughness < land surface roughness + vegetated areas < land surface roughness + waters < land surface roughness + vegetated areas + waters. Vegetated areas and waters could optimize urban ventilation and effectively reduce land surface temperature. Ventilation corridors constructed based on land surface roughness + vegetated areas + waters had the lowest temperature, and could generate the maximum of ventilation benefits.
(3) Waters had better efficiency on temperature reduction than vegetated areas on near-land surface level. Ventilation corridors constructed based on land surface roughness + waters had better capability of heat alleviation that based on land surface roughness + vegetated areas. Therefore, optimizing strategy of air quality should consider the spatial pattern of focusing more on waters while paying attention to vegetated areas.

Declaration of competing interest

The authors declared that they have no conflicts of interest to this work.

Acknowledgments

This research was funded by Natural Science Foundation of Anhui Province with the Grant reference No. 2008085ME160. We would like to thank the journal's editor and reviewers for their very useful comments, which greatly helped us to improve the paper; and to production editor for his support in the final proofreading of this publication.

References

Badas, M. G., Ferrari, S., Garau, M., & Querzoli, G. (2017). On the effect of gable roof on natural ventilation in two-dimensional urban canyons. *Journal of Wind Engineering and Industrial Aerodynamics, 162*, 24–34.
Bajsanski, I., Stojakovic, V., & Jovanovic, M. (2016). Effect of tree location on mitigating parking lot insolation. *Computers, Environment and Urban Systems, 56*, 59–67.
Bottema, M. (1997). Urban roughness modelling in relation to pollutant dispersion. *Atmospheric Environment, 31*(18), 3059–3075.
Bottema, M., & Mestayer, P. G. (1998). Urban roughness mapping-validation techniques and some first results. *Journal of Wind Engineering and Industrial Aerodynamics, 74*, 163–173.
Burian, S. J., Brown, M. J., & Linger, S. P. (2002). *Morphological analyses using 3D urban databases*. Los Angeles: Los Alamos National Laboratory.
Cariolet, J. M., Colombert, M., Vuillet, M., & Diab, Y. (2018). Assessing the resilience of urban areas to traffic-related air pollution: Application in Greater Paris. *The Science of the Total Environment, 615*, 588–596.
Coccolo, S., Kämpf, J., Scartezzini, J., & Pearlmutter, D. (2016). Outdoor human comfort and thermal stress: A comprehensive review onmodels and standards. *Urban Climate, 18*, 33–57.
Ding, C., Lam, K. P., & Feng, W. (2017). An evaluation index for cross ventilation based on CFD simulations and ventilation prediction model using machine learning algorithms. *Procedia Engineering, 205*, 2948–2955.
Du, H. Y. (2018). *The cool island effect of urban blue-green spaces and impact factors in mega city: A case study of Shanghai*. Shanghai: East China Normal University.
Edussuriya, P., Chan, A., & Ye, A. (2011). Urban morphology and air quality in dense residential environments in Hong Kong. Part I: District-level analysis. *Atmospheric Environment, 45*(27), 4789–4803.
Formica, A. E., Burnside, R. J., & Dolman, P. M. (2017). Rainfall validates MODIS-derived NDVI as an index of spatio-temporal variation in green biomass across non-montane semi-arid and arid Central Asia. *Journal of Arid Environments, 142*, 11–21.
Gál, T., & Sümeghy, Z. (2007). Mapping the roughness parameters in a large urbanarea for urban climate applications. *Acta Climatologica et Chorologica, 40*, 27–36.
Ghosh, M. K., Kumar, L., & Roy, C. (2015). Monitoring the coastline change of Hatiya Island in Bangladesh using remote sensing techniques. *ISPRS Journal of Photogrammetry and Remote Sensing, 101*, 137–144.
Guo, W., Liu, X., & Yuan, X. (2015). A case study on optimization of building design based on CFD simulation technology of wind environment. *Procedia Engineering, 121*, 225–231.
Hang, J., Li, Y., Sandberg, M., Buccolieri, R., & Di Sabatino, S. (2012). The influence of building height variability on pollutant dispersion and pedestrian ventilation in idealized high-rise urban areas. *Building and Environment, 56*, 346–360.
He, B. J. (2018). Potentials of meteorological characteristics and synoptic conditions to mitigate urban heat island effects. *Urban Climate, 24*, 26–33. https://doi.org/10.1016/j.uclim.2018.01.004
He, B. J., Ding, L., & Prasad, D. (2019). Enhancing urban ventilation performance through the development of precinct ventilation zones: A case study based on the greater Sydney, Australia. *Sustainable Cities and Society, 47*, 101472.
He, B. J., Ding, L., & Prasad, D. (2020a). Urban ventilation and its potential for local warming mitigation: A field experiment in an open low-rise gridiron precinct. *Sustainable Cities and Society, 55*, 102028. https://doi.org/10.1016/j.scs.2020.102028
He, B. J., Ding, L., & Prasad, D. (2020b). Wind-sensitive urban planning and design: Precinct ventilation performance and its potential for local warming mitigation in an open midrise gridiron precinct. *Journal of Building Engineering, 29*, 101145. https://doi.org/10.1016/j.jobe.2019.101145
Hong, B., & Lin, B. (2015). Numerical studies of the outdoor wind environment and thermal comfort at pedestrian level in housing blocks with different building layout patterns and trees arrangement. *Renewable Energy, 73*, 18–27.
Hsieh, C., & Huang, H. (2016). Mitigating urban heat islands: A method to identify potential wind corridor for cooling and ventilation. *Computers, Environment and Urban Systems, 57*, 130–143.
Huang, H. C., Lin, F. T., & Hsieh, C. M. (2014). A simple method for designation of urban ventilation path by using agent analyst in GIS — a study of Tainan, Taiwan. In *Conference on sustainable business, energy and development in Asia* (Hiroshima, Japan).
Huang, X., & Wang, Y. (2019). Investigating the effects of 3D urban morphology on the surface urban heat island effect in urban functional zones by using high-resolution remote sensing data: A case study of wuhan, Central China. *ISPRS Journal of Photogrammetry and Remote Sensing, 152*, 119–131.
Jan, F. C., Hsieh, C. M., Ishikawa, M., & Sun, Y. H. (2013). The influence of tree allocation and tree transpiration on the urban microclimate: An analysis of a subtropical urban park. *Environment and Urbanization ASIA, 4*(1), 135–150.
Kent, C. W., Grimmond, S., & Gatey, D. (2017). Aerodynamic roughness parameters in cities: Inclusion of vegetation. *Journal of Wind Engineering and Industrial Aerodynamics, 169*, 168–176.
Li, J., Deng, W., & Zhang, J. F. (2019b). Evaluating mountain water scarcity on the county scale: A case study of Dongchuan district, Kunming, China. *Journal of Mountain Science, 16*(4), 744–754.
Li, B., Jiang, C. Y., Wang, L., Cai, W. H., & Liu, J. (2019a). A parametric study of the effect of building layout on wind flow over an urban area. *Building and Environment*, 160.
Liu, S. M., Pan, W. X., & Cao, Q. (2019). CFD simulations of natural cross ventilation through an apartment with modified hourly wind information from a meteorological station. *Energy and Buildings, 195*, 16–25.

Liu, S. Y., & Shen, J. H. (2010). Urban ventilation channel planning method based on local circulation: A case study of Stuttgart, Germany. *Journal of Zhejiang University (Engineering Science), 44*(10), 1985–1991.
Liu, Y. H., Zhang, S., Cheng, P. F., Chen, P., Wei, L., & Fang, X. Y. (2017). Research and application of heat and ventilation environment assessment for city planning: A case study of Jinan central urban area. *Ecology and Environmental Sciences, 26*(11), 1892–1903.
Li, X. M., Zhou, W. Q., & Ouyang, Z. Y. (2013). Relationship between land surface temperature and spatial pattern of greenspace: What are the effects of spatial resolution? *Landscape and Urban Planning, 114*, 1–8, 0.
Luo, Y. W., He, J., & Ni, Y. L. (2017). Analysis of urban ventilation potential using rule-based modeling. *Computers, Environment and Urban Systems, 66*, 13–22.
Lyu, T., Buccolieri, R., & Gao, Z. (2015). A numerical study on the correlation between Sky view factor and summer microclimate of local climate zones. *Atmosphere, 10*, 8.
Marzena, W., Andreas, W., & Katarzyna, O. S. (2017). Detection of ventilation corridors using a spatio-temporal approach aided by remote sensing data. *European Journal of Remote Sensing, 50*(1), 254–267. https://doi.org/10.1080/22797254.2017.1318672
Marzena, W., & Katarzyna, O. S. (2016). Temporal analysis of urban changes and development in Warsaw's ventilation corridors. *Miscellanea Geographica, 20*(4), 11–21. https://doi.org/10.1515/mgrsd-2016-0021
Morakinyo, T. E., Balogun, A. A., & Adegun, O. B. (2013). Comparing the effect of trees on thermal conditions of two typical urban buildings. *Urban Climate, 3*, 76–93.
Oke, T. R. (1982). The energetic basis of the urban heat island. *Quarterly Journal of the Royal Meteorological Society, 108*(455), 1–24.
Qiao, Z., Xu, X. L., Wu, F., Luo, W., Wang, F., Liu, L., & Sun, Z. Y. (2017). Urban ventilation network model: A case study of the core zone of capital function in Beijing metropolitan area. *Journal of Cleaner Production, 168*, 526–535.
Rao, Y. H., Liang, S. L., Wang, D. D., Yu, Y. Y., Song, Z., Zhou, Y., Shen, M. G., & Xu, B. Q. (2019). Estimating daily average surface air temperature using satellite land surface temperature and top-of-atmosphere radiation products over the Tibetan Plateau. *Remote Sensing of Environment, 234*(1), 111462.
Sheng, L., Tang, X. L., You, H. Y., Gu, Q., & Hu, H. (2017). Comparison of the urban heat island intensity quantified by using air temperature and Landsat land surface temperature in Hangzhou, China. *Ecological Indicators, 72*, 738–746.
Stewart, I. D., & Oke, T. R. (2012). Local climate zones for urban temperature studies. *Bulletin of the American Meteorological Society, 93*(12), 1879–1900.
Vernay, D. G., Raphael, B., & Smith, lanF. C. (2015). Improving simulation predictions of wind around buildings using measurements through system identification techniques. *Building and Environment, 94*, 620–631.
Wang, X., Zhou, T., Tao, F., & Zang, F. Y. (2019). Correlation analysis between UBD and LST in Hefei, China, using Luojia1-01 night-time light imagery. *Applied Sciences, 9*(5224), 1–2. https://doi.org/10.3390/app9235224
Weng, Q. P., Zhang, H., Bao, H. X., Liu, J. G., & Wu, H. (2015). Study on ventilation channels of Nanjing city. *Science Technology and Engineering, 15*(11), 89–94.
Wen, C. Y., Juan, Y. H., & Yang, A. S. (2017). Enhancement of city breathability with half open spaces in ideal urban street canyons. *Building and Environment, 112*, 322–336.
Wong, M. S., Nichol, J. E., To, P. H., & Wang, J. Z. (2010). A simple method for designation of urban ventilation corridors and its application to urban heat island analysis. *Building and Environment, 48*(8), 1880–1889.
Wrobel-Niedzwiecka, I., Drozdowska, V., & Piskozub, J. (2019). Effect of drag coefficient formula choice on wind stress climatology in the North Atlantic and the European Arctic. *Oceanologia, 61*(3), 291–299.
Yim, S. H. L., Fung, J. C. H., & Ng, E. Y. Y. (2014). An assessment indicator for air ventilation and pollutant dispersion potential in an urban canopy with complex natural terrain and significant wind variations. *Atmospheric Environment, 94*, 297–306.
Yin, C. H., Yuan, M., Lu, Y. P., & Liu, Y. F. (2018). Effects of urban form on the urban heat island effect based on spatial regression model. *The Science of the Total Environment, 634*, 696–704.
Yuan, C., Ren, C., & Ng, E. (2014). GIS-based surface roughness evaluation in the planning system to improve the wind environment — a study in Wuhan, China. *Urban Climate, 10*(3), 585–593.
Zhang, Y. L., & Li, X. (2017). Study on urban ventilation channels planning based on optimization of the spatial layout in urban green space:a case study of Jinzhong. *Urban Development Studies, 24*, 35–41, 05.
Zheng, Y. T., Han, J. C., Huang, Y. F., Fassnacht, S. R., Xie, S., Lv, E. Z., & Chen, M. (2018). Vegetation response to climate conditions based on NDVI simulations using stepwise cluster analysis for the Three-River Headwaters region of China. *Ecological Indicators, 92*, 18–29.

引用格式：方云皓,顾康康.基于多元数据的中国地理空间疫情风险评估探索——以2020年1月1日至4月11日COVID-19疫情数据为例[J].地球信息科学学报,2021,23(2):284-296. [Fang Y H, Gu K K. Exploration on geospatial risk assessment in China based on multiple data: A case study of COVID-19 data from January 1 to April 11, 2020[J]. Journal of Geo-information Science, 2021,23(2):284-296.]
DOI:10.12082/dqxxkx.2021.200273

基于多元数据的中国地理空间疫情风险评估探索——以2020年1月1日至4月11日COVID-19疫情数据为例

方云皓[1],顾康康[1,2*]

1. 安徽建筑大学建筑与规划学院,合肥 230022; 2. 安徽省城镇化建设协同创新中心,合肥 230022

Exploration on Geospatial Risk Assessment in China based on Multiple Data: A Case Study of COVID-19 Data from January 1 to April 11, 2020

FANG Yunhao[1], GU Kangkang[1,2*]

1. School of Architecture and Planning, Anhui Jianzhu University, Hefei 230022, China;
2. Research Center of Urbanization Development in Anhui Province, Anhui Jianzhu University, Hefei 230022, China

Abstract: COVID-19 has a spatial transmission risk and poses a threat to the safety and health of the city. Preventing the spread of COVID-19 is therefore the urgent need for society now. The COVID-19 experienced a process that occurred, developed rapidly and stabilized from January 1 to April 11, 2020. Using the initial COVID-19 data for macro-level epidemic risk assessment can provide a certain reference for epidemic prevention and control measures. In this study, by using multiple data, including administrative division data, designated hospital data, epidemic community data, and road traffic data, we proposed a macro-level geospatial risk assessment and validated its effectiveness in China. Based on this, this study also analyzed the construction factors of geospatial risk assessment in order to explore its distribution rules. The following four conclusions showed that: ① Geospatial risk assessment of Covid-19 in China is effective to some extent. ② The spatial distribution of global Moran's I index of geospatial risk in China was 0.758, which had significant spatial agglomeration characteristics. At the same time, the LISA index in different provinces showed spatial differences. Some regions, including Hubei, Henan, Hunan, Jiangxi, Anhui, Zhejiang, Jiangsu, and Shanghai, were identified as high-high clusters and accounted for 25.81% of the provinces in China. The geospatial risk of these provinces was higher. Regions like Qinghai, Tibet, and Xinjiang, with a low degree of geospatial risk, accounted for 9.68% of the provinces in the country. ③ Some indicators, including geographic location indicators, road traffic indicators, medical and health indicators, and epidemic status indicators, were related to the distribution of geospatial risk. According to the statistical Pearson correlation analysis, there were differences in the correlation index R^2. In terms of numerical values, the epidemic status indicators, geographic location indicators, road traffic indicators, and medical and health indicators were ranked from highest to

收稿日期：2020-05-31；**修回日期：**2020-08-22.
基金项目：安徽省自然科学基金面上项目(2008085ME160)。[**Foundation item:** Natural Science Foundation of Anhui Province, No.2008085ME160.]
作者简介：方云皓(1995—),男,安徽合肥人,硕士生,主要从事地理信息系统方面研究。E-mail: 1198321182@qq.com
***通讯作者：**顾康康(1982—),男,安徽蚌埠人,博士,教授,主要从事城乡生态与环境规划研究。E-mail: kangkanggu@163.com

(C)1994-2021 China Academic Journal Electronic Publishing House. All rights reserved. http://www.cnki.net

lowest. Different secondary factors were composed of four indicators, and they exhibited two effects of positive and negative correlation. Specifically, the factor of geographic distance from Wuhan, the designated hospital density factor, and the resident-hospital geographical distance factor showed significant negative correlations, with R^2 of 0.813, 0.545, and 0.436, respectively. However, the remaining factors showed significant positive correlations, including railway network density factor, road network density factor, and epidemic community density factor, and their R^2 were 0.751, 0.792, and 0.825, respectively. ④ The components of geospatial risk were intricate and complicated by multiple factors. According to the spatial stratified heterogeneity analysis, we found that there were interactions between different factors. Among them, the resident-hospital geographic distance factor interacted strongly with the railway network density factor and the road network density factor, and their q values were 0.9842 and 0.9837, respectively. This study not only explored the spatial resource allocation of major epidemics in urban management, but also provided a basis for regional spatial prevention and control strategies.

Key words: COVID-19; multivariate data; geospatial epidemic risk; spatial autocorrelation; pearson correlation; spatial stratified heterogeneity; influencing factors; epidemic prevention and control

***Corresponding author:** GU Kangkang, E-mail: kangkanggu@163.com

摘要：新冠肺炎（COVID-19）在空间上具有一定的传播风险，对城市的安全健康构成了威胁，防止疫情传播成为紧迫的任务。在2020年1月1日至4月11日，COVID-19疫情经历了发生、迅速发展和趋于稳定的发展过程，利用初期的COVID-19数据进行宏观层面的疫情风险评估，为防疫控制措施提供一定的参考。因此本研究基于行政区划、定点医院、疫情小区以及道路交通等多元数据，在宏观层面提出并构建全国地理空间疫情风险性评估，对疫情风险分布探讨的同时进行评估效果验证，并根据构建指标揭示影响风险的因素及其机理，主要结论：① 地理空间风险评估具有有效的可行性。② 地理空间疫情风险分布全局Moran's I指数为0.758，具有显著的空间集聚特征。同时，不同的省区市之间的局部LISA值呈现空间差异性，其中高—高聚类省区市占比全国25.81%，风险程度较高，主要分布在湖北、河南、湖南、江西、安徽、浙江、江苏、上海，低—低聚类省区市占比全国9.68%，风险程度较低，主要分布在青海、西藏、新疆。③ 地理空间疫情风险分布与地理区位、道路交通、医疗卫生、疫情现状指标均存在一定的相关性。根据统计学的Pearson相关性分析，其相关指标R^2存在差异，在数值上由高到低依次为疫情现状、地理区位、道路交通、医疗卫生，在属性上其相关因子存在正负2种效应，地理空间疫情风险与武汉市地理距离、定点医院密度以及居民-医院地理距离呈现显著的负相关，其R^2分别为0.813、0.545、0.436，与铁路网密度、公路网密度以及疫情小区密度呈现显著的正相关，其R^2分别为0.751、0.792、0.825。④ 地理空间疫情风险的构成因素错综复杂，其受到多种因子的共同作用，根据空间分层异质性分析，不同因子之间均存在交互作用，其中居民—医院地理距离与公路网密度、铁路网密度交互作用较强，q值分别为0.9842、0.9837。本研究在宏观层面为城市管理中重大疫情的空间资源分配以及区域空间的联防联控策略提供了相应的依据。

关键词：COVID-19；多元数据；地理空间疫情风险；空间自相关；Pearson相关性；空间分层异质性；影响因素；疫情防控

1 引言

新型冠状病毒（COVID-19），又命名为SARS-CoV-2，其导致的新型冠状病毒肺炎疫情已经构成了2020年以来全球性的健康安全威胁，并继续呈现蔓延态势[1]。世界卫生组织在2020年1月30日宣布其形成了新的全球性“国际公共卫生突发事件（PHEIC）”，在2月28日将其在全球传播风险和影响风险级别上调为“非常高”并在3月11日宣布新冠肺炎疫情已构成全球大流行[2]。此次疫情对我国的居民健康以及社会经济发展造成了重要的影响，经过党、政府、组织以及个人的全社会共同协作，我国的疫情态势已经得到有效的控制（截至4月11日），相关新冠肺炎的研究逐渐上升到了重要的课题。

越来越多的研究证实，城市空间管理与城市健康以及疾病防控存在联系[3]，具体包括特征解析、机理解释、综合评估以及规划管控4个层面。① 在特征解析层面，丁晓彤等[4]利用Shannon信息熵理论和空间自相关方法，根据2014—2015年14种自然疫源性疾病的发病数，对中国自然疫源性疾病空间分布特征进行分析，高芳旭等[5]用自回归求和移动平均（ARIMA）模型，探索了天津地区细菌性痢疾发病率的时空聚集性表征，而陈会宴等[6]

(C)1994-2021 China Academic Journal Electronic Publishing House. All rights reserved. http://www.cnki.net

通过贝叶斯时空建模方法，在对山西省原平市神经管畸形人群的时空格局进行解剖的同时，对其规律进行挖掘。时空特征趋势可以揭示城市疫情的潜在风险因子。② 在机理解释层面，张湘雪等[7]采用地理探测器对2009—2013年京津唐地区HFMD发病率的时空异质性进行分析，并以此为根据量化各影响因子及其两两交互作用对HFMD发病率的解释力，Cao等[8]对深圳市HFMD发病情况与地理环境要素进行回归建模，从道路密度、人口密度、NDVI等空间环境要素探索机理因素。综合评估构建以机理因素的阐述为基础。③ 在综合评估层面，叶莹等[9]利用探索性数据分析方法，在区县尺度上对河南省新冠肺炎疫情的时空扩散特征与人口流动风险进行评估，此外，Wang等[10]利用地理空间回归模型探究登革热等蚊媒传染病及其空间分布，在评估的基础上进行预测。④ 在规划管控层面，唐燕[11]结合新冠肺炎疫情从社区规划与基层治理方向提供研究视角，杨俊宴等[12]结合高密度城市传播的特征，提出城市-社区-建筑的多尺度空间防疫体系。

综上，过往的研究尺度往往集中于区县尺度的精细化探讨，对于全国层面的研究较少，而在新冠疫情的专题研究上，较多以时间序列为主线而缺少空间特征的解读，此外在空间分析上通常停留在单一层面，关于特征、机理、评估的系统性研究不足。因此，本研究基于多元数据在宏观层面构建全国地理空间疫情风险性评估，并根据相关构建指标因素进行机理上的探索，为城市管理中的疫情空间防控提供依据并为区域大尺度的疫情研判提供经验。

2 数据与方法

2.1 数据来源

基于全国尺度的COVID-19疫情风险分析，本研究以各省为空间单元并旨在综合考虑空间总体分布情况，故选择相对稳定的数据源。需要特别说明的是，截至2020年4月11日全国疫情已趋于总体平稳，呈现稳中向好的态势，其新增病例主要来源于国外，4月11日后国内新增病例数据量小，对总体数据影响较小。具体研究数据主要分为2类：相关疫情统计数据；风险评估数据。而我国港澳台等地相应数据获取困难，因此不计入统计。

2.1.1 用于疫情统计的基础数据

本研究的疫情统计基础数据主要包括：中华人民共和国国家卫生健康委员会（国家卫健委）获取的2020年1月1日至4月11日的相关COVID-19疫情数据，具体涵盖各省累积确诊人数和累积死亡人数（http://www.nhc.gov.cn/）[13]；全国2019年常住人口数量[14]，其来源于国家统计局统计的各地官方公报（http://data.stats.gov.cn/search.htm?s/）；全国疾控机构基本信息数据[15]，具体涵盖各省疾控机构的达标情况、平均使用面积、机构数、总编制人数以及使用仪器情况（http://www.phsciencedata.cn/Share/en/index.jsp）。

2.1.2 用于风险评估的基础数据

综合新冠疫情的空间防控机制，应用在宏观层面风险评估类的基础数据主要包括：中国省级行政区划数据与道路交通数据[16]，其来源于OpenStreetMap开源地图获取的矢量数据（http://download.geofabrik.de/），其中道路交通数据具体分为主要公路数据以及铁路数据；定点医院与疫情小区数据[17]，根据Harvard Dataverse公布的COVID-19开源研究数据集对中国定点医院信息以及截至2020年4月11日已公布的疫情小区信息进行收集与空间统计，如图1所示。

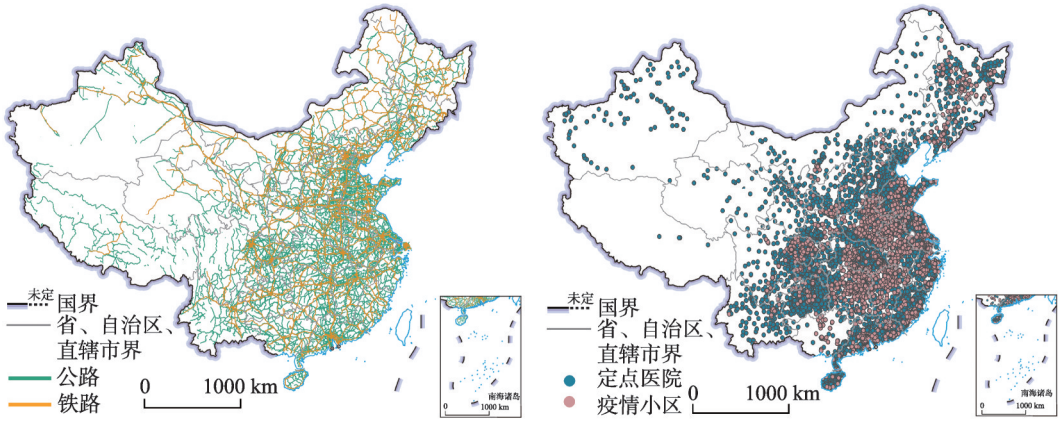
2.2 研究方法

2.2.1 空间风险评估

综合考虑自然地理、社会经济等多重因素以及疫情风险的特性，结合相关空间理论本研究判断影响地理空间疫情风险主要来源于疫情本身风险以及疫情传播（阻断）风险[18]，并利用ArcGIS软件提出并构建综合空间风险指数（Comprehensive Spatial Risk Index，CSRI）[19]。具体权衡4种指标及因子权重，如表1所示，包括地理区位指标[20]、道路交通指标[21]、医疗卫生指标以及疫情现状指标[22]。

综合空间风险指数（CSRI）是空间风险性评估的关键，本研究先采取等权重的设置处理（表1），其设置原因一方面是假设不同单项指标（因子）对于地理空间疫情风险都分别存在影响，表征其在综合空间风险指数（CSRI）的构建中都具有重要性，另一方面是为了避免综合构建结果受主观权重值设置带来的不确定性干扰，导致部分指标权重值失衡影响综合评估[23]。再按自然断裂法对因子阈值重新进行1-10分级，基于因子的权重情况，采取加法合成法[24]进行综合空间风险指数（CSRI）的分析，其适用于指标信息内容不重复的情况，通过指标因子与相应权重的乘积之和的计算，在强调客

(C)1994-2021 China Academic Journal Electronic Publishing House. All rights reserved. http://www.cnki.net



(a) 公路与铁路基础数据空间分布　　(b) 定点医院与疫情小区数据空间分布 (截至2020年4月11日)

注：该图基于自然资源部标准地图服务网站下载的审图号为GS(2019)1653号的标准地图制作，底图无修改；由于数据获取困难，本研究不包括香港、台湾和澳门。

图1　2020年中国公路、铁路基础数据及定点医院、疫情小区基础数据空间分布

Fig. 1　The spatial distribution basic data of roads and railways, designated hospitals and epidemic communities in China in 2020

表1　中国综合空间风险评估因子及其权重

Tab. 1　Comprehensive spatial risk assessment factors and their weights in China

评估因子	地理区位	道路交通		医疗卫生		疫情现状
	与武汉市地理距离	公路网密度	地铁网密度	定点医院密度	居民-医院地理距离	疫情小区密度
权重	0.250	0.125	0.125	0.125	0.125	0.250

观实际的同时更能反映评价对象的综合水平，其具体方法见式(1)。

$$CSRI_i = \sum_{j=1}^{n} x_{ij} w_{ij} \tag{1}$$

式中：$CSRI_i$代表第i个评价对象的综合空间风险指数值，数值越高表明该个评价对象各类因子的综合作用程度越高，地理空间疫情风险越大；n代表评估因子的数量，本研究取值n=6；X_{ij}代表第i个评价对象j因子的归一化值，其取值范围为[1, 10]，采取归一化处理以平衡数据量纲差距使不同数据能够在相同条件下统计；W_{ij}代表第i个评价对象j因子的权重。

2.2.2　空间自相关评估

全局空间自相关[25]通常运用Moran's I进行测度，根据整个区域的空间分布模式对子区域地理空间疫情风险的聚集性进行判断。Moran's I的取值范围为[−1, 1]，其值越高表明相邻区域之间的属性越相似，呈正相关或负相关，即CSRI指数存在明显的空间聚集特征，当全局Moran's I为0时，表示完全随机，其具体的计算公式为：

$$\text{Moran's } I = \frac{n\sum_{i=1}^{n}\sum_{j=1}^{n} w_{ij}(x_i-\bar{x})(x_j-\bar{x})}{\sum_{i=1}^{n}\sum_{j=1}^{n} w_{ij}\sum_{i=1}^{n}(x_i-\bar{x})^2} \quad (i\neq j) \tag{2}$$

式中：n为全国省份(或市、自治区)的数量；x_i和x_j分别代表第i个区域以及第j个区域的CSRI值；$\bar{x}$代表全国CSRI的平均值；W_{ij}代表空间权重矩阵。

局部空间自相关[26]能够揭示局部空间的异质性，弥补整个区域中局部地区的非典型特征，充分反映局部地理空间疫情风险的变化趋势。本研究采用LISA指数(Local Indicators of Spatial Association)来衡量CSRI的空间差异，其计算公式如下：

$$LISA_i = z_i \sum_{j} w_{ij} z_j \tag{3}$$

式中：z_i和z_j分别代表第i个区域以及第j个区域的CSRI标准化值；W_{ij}代表空间权重矩阵。在局部空间自相关的LISA指数中，CSRI值分为4类：高-高聚类(H-H)，高值集聚；低-低聚类(L-L)，低值集聚；高-低聚类(H-L)，高值主要由低值围绕的异常值；低-高聚类(L-H)，低值主要由高值围绕的异常值。

(C)1994-2021 China Academic Journal Electronic Publishing House. All rights reserved.　http://www.cnki.net

2.2.3 Pearson相关性评估

为了研判空间风险的评估效果，需要对综合空间风险指数（CSRI）的构建合理性进行验证。基于各省疫情累计归一化患病率指数、归一化死亡率指数以及疾控机构资源指数分别作为一种自变量，根据统计学的Pearson相关性[27]分析，综合衡量因变量CSRI值的准确度，其具体公式参照式（4），其中疾控机构资源指数作为疫情防控的重要依据，通过5类指标进行加权构建，其不同的指标类型及权重见表2。

$$r=\frac{\sum_{i=1}^{n}\left(x_i-\bar{x}\right)\left(y_i-\bar{y}\right)}{\sqrt{\sum_{i=1}^{n}\left(x_i-\bar{x}\right)^2\sum_{i=1}^{n}\left(y_i-\bar{y}\right)^2}} \quad (4)$$

式中：r代表相关程度，取值范围为[−1, 1]，其绝对值越大，表示相关性越强；x_i和y_i分布代表因变量CSRI值与自变量；$\bar{x}$与$\bar{y}$分别为2个变量的平均值。

2.2.4 空间分层异质性评估

空间分层异质性[28]，作为地理的一个基本现象之一，用于表示层内方差小于层间方差的量化指标，可用于表现指标因子相互之间的关系对空间分布的影响是否有显著的差异，用q值（q Statistics）度量，值域为[0, 1]。若分层对CSRI值划分，其值越高表明CSRI值的空间分异程度越高，若分层根据影响指标对CSRI值划分，其值越高表明该影响指标对CSRI值的解释程度越高，此外当q值为0时表示没有空间分异性。本研究采用地理探测器软件（GeoDetector）进行因子交互探测，其表达式为：

$$q=1-\frac{\sum_{h=1}^{L}N_h\sigma_h^2}{N\sigma^2}=1-\frac{SSW}{SST} \quad (5)$$

其中，$SSW=\sum_{h=1}^{L}N_h\sigma_h^2$，$SST=N\sigma^2$。

式中：将研究区划分为h个层（Strata），h=1，…，L；N_h和N分别代表层h和全区的单元数；σ^2代表CSRI的方差，σ_h代表层内指标方差；SSW和SST分别为层内方差之和（Within Sum of Squares）和全区总方差（Total Sum of Squares）。

3 结果

3.1 空间风险性格局

基于地理区位、道路交通、医疗卫生、疫情现状4项指标，由式（1）构建综合空间风险指数（CSRI），如图2所示。其中地理区位指标包括与武汉市地理距离，总体呈现由武汉市向外不断减弱的趋势；道路交通指标包括公路网密度和铁路网密度，形成交通枢纽集中在上海、浙江、江苏、北京、广东等，而在湖北、重庆、河南等形成交通副中心；医疗卫生指标包括定点医院密度以及居民—定点医院距离，其中江苏、上海、广东以及川渝地区的医疗点中心聚集性较强，其余主要分布于胡焕庸线以东的人口密集区域并集中于省会城市，总体来说全国大部分区域均存在相对完善的医疗救助点；疫情现状指标具体包括确诊疫情小区密度，截至2020年4月11日全国各省均存在疫情确诊情况，其中湖北省集聚性最为严重，广东、河南、浙江等省份为次级严重区域，湖南、安徽、江西、黑龙江等省份为第三级疫区，其余各省份疫情小区空间集聚性较弱。

根据空间风险分析的结果，不同区域的CSRI值呈现明显的空间异质性，其平均值为5.55。综合空间风险指数最高的区域分布在湖北省，其CSRI值达到8.69；其次为湖北邻近省份，包括河南、安徽、江西、湖南4省，其CSRI值普遍较高维持在7.81~8.35之间，北京、广东、浙江、江苏、上海等东南沿海各省市虽与湖北具有地理区位，但CSRI值总体较高处于6.33~7.48之间；而我国西南部包括四川、云南等省份，北部辽宁、河北、山西等省份CSRI值相对较低，范围为3.86~5.79之间，其中综合空间风险指数最低的区域集中分布于新疆、西藏2个自治区，CSRI值低于2.45。总体而言，全国的综合空间风险指数（CSRI）空间分布上形成“中强外弱”的结构，由湖北省向外逐渐降低的规律。

如上所述，通过对综合空间风险指数（CSRI）的空间聚类分析来看（图3），全局Moran's I指数为0.758（P-value=0.001；Z=6.705），显示CSRI值存在

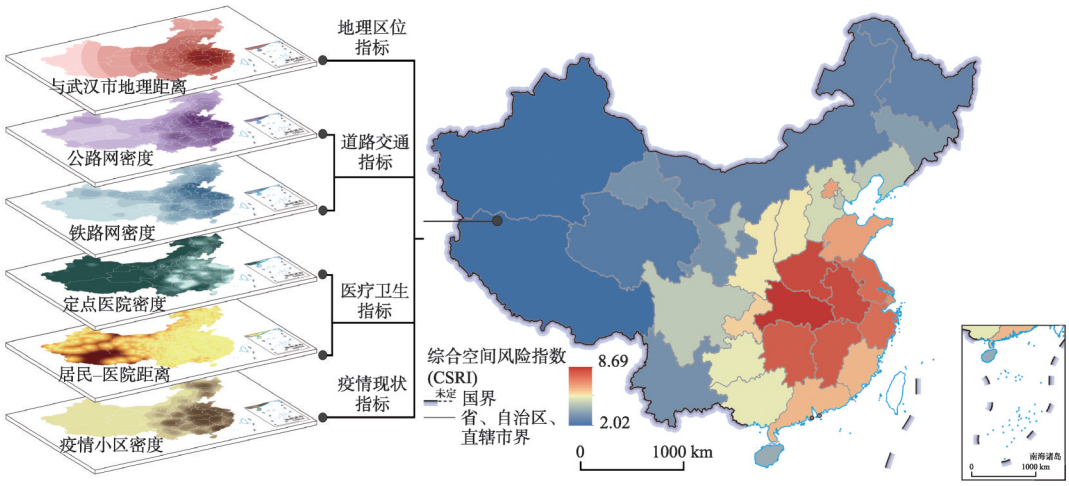
表2 中国疾控机构资源指标及其权重

Tab. 2 Disease control agency resource indicators and their weights in China

指标	达标情况	平均使用面积	机构数	总编制人数	使用仪器情况
属性	+	+	+	+	+
权重	0.2	0.2	0.2	0.2	0.2

注：表中“+”表示其指标与全国疾控机构资源呈正相关。

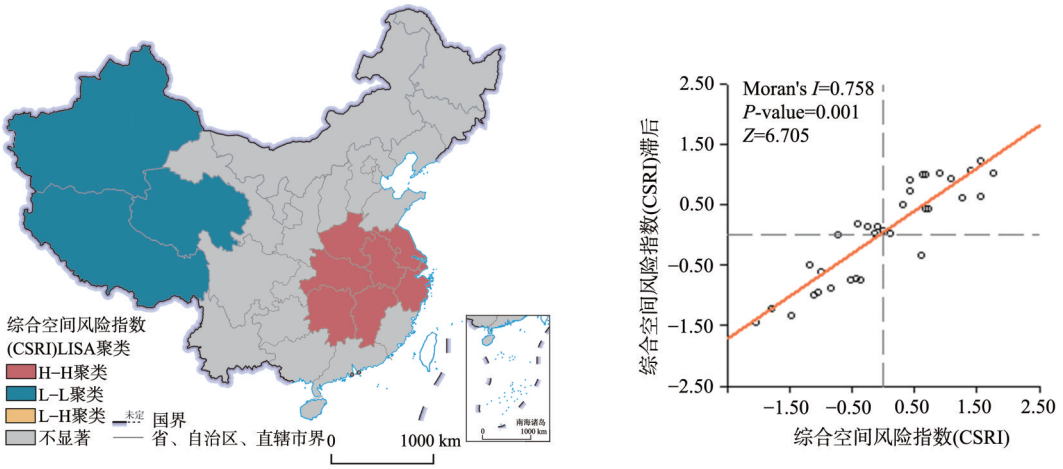
(C)1994-2021 China Academic Journal Electronic Publishing House. All rights reserved. http://www.cnki.net



注：该图基于自然资源部标准地图服务网站下载的审图号为GS(2019)1653号的标准地图制作，底图无修改；由于数据获取困难，本研究不包括香港、台湾和澳门。

图2　2020年1月1日至4月11日中国综合空间风险指数构成及其空间分布

Fig. 2　The composition and spatial distribution of Comprehensive Spatial Risk Index (CSRI) in China from January 1 to April 11, 2020



(a) 综合空间风险指数空间自相关分布　　(b) 综合空间风险指数全局Moran's *I*散点图

注：该图基于自然资源部标准地图服务网站下载的审图号为GS(2019)1653号的标准地图制作，底图无修改；由于数据获取困难，本研究不包括香港、台湾和澳门。

图3　2020年1月1日至4月11日中国综合空间风险指数空间自相关分布

Fig. 3　Spatial autocorrelation distribution of Comprehensive Spatial Risk Index (CSRI) in China from January 1 to April 11, 2020

显著的空间聚集模式，表明疫情风险空间分布并非随机，在一定程度上受到相邻地区空间传播的影响，政府部门“封城”、限制出行等举措在较大程度上能够遏制疫情的空间传播。此外，根据LISA聚类空间分布，CSRI值呈现显著的局部空间自相关性，其中L-L聚类(3个)主要分布在青海、西藏、新疆，占比9.68%，表明这些省份(自治区)综合空间风险持续暴露较弱，H-H聚类(8个)主要分布在湖北、河南、湖南、江西、安徽、浙江、江苏、上海，占比25.81%，表明这些省份(直辖市)是综合空间风险持续暴露较严重的区域，各级地方政府部门的联防联控举措对疫情防控具有重要的积极作用。总的来说，综合空间风险指数(CSRI)的分布遵循与湖北省的地理邻近和网络邻近特征。

3.2　空间风险性验证

基于全国疫情归一化患病率指数、归一化死亡率指数以及疫情机构资源指数空间分布，进行综合

(C)1994-2021 China Academic Journal Electronic Publishing House. All rights reserved.　http://www.cnki.net

空间风险指数(CSRI)验证,根据CSRI指数与各变量数据的划分类型及标准,进行残差统计如表3所示,各变量的残差具有一定的差异性,其中疾控机构指数残差绝对值在5以内的有15个(除香港、澳门、台湾),占比48.39%;归一化患病率指数残差绝对值在5以内的有21个,占比67.74%;归一化死亡率指数残差绝对值在5以内的有13个,占比41.94%。总体来说,各变量的残差对比统计表明CSRI指数具有一定的可靠性,也存在不确定性。

通过各变量的空间统计结果,归一化患病率指数与归一化死亡率指数的总体空间分布对比CSRI指数分别具有一定的相似性,呈现由湖北向外围降低的趋势(图4(b)、图4(c))。其中河南、安徽、江西等与湖北相邻接壤的地区与CSRI指数呈现显著的区位关联性,其归一化患病率指数与归一化死亡率指数分别为0.39、0.38、0.39以及0.17、0.10、0.06,对应的CSRI指数分别为8.35、8.32、8.05,表明地理区位在影响疫情的空间风险上具有一定正向效应。而北京、上海以及广东虽然与湖北有一定距离,但统计结果也具有一定的空间相关性,在空间分布上

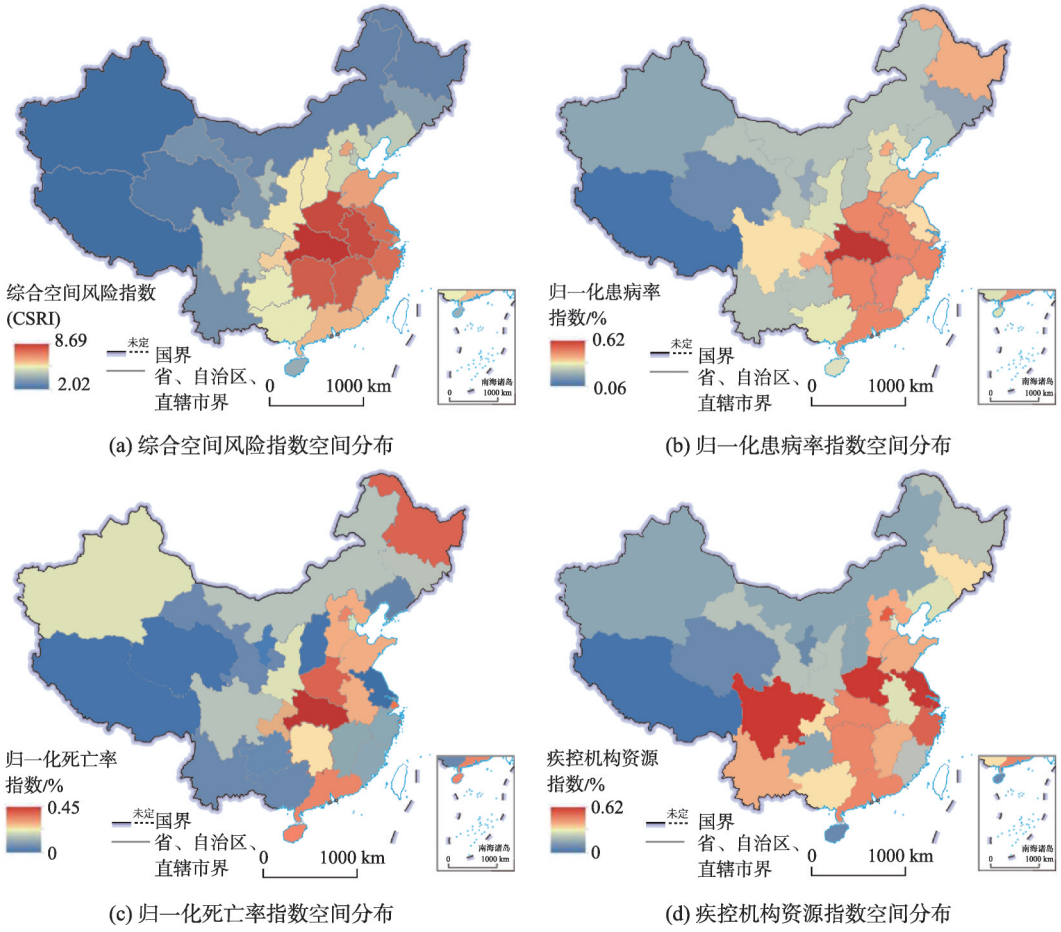
表3 2020年1月1日至4月11日中国综合空间风险指数(CSRI)与各变量对比统计

Tab. 3 Comparative statistics of Comprehensive Spatial Risk Index (CSRI) and various variables in China from January 1 to April 11, 2020

地区	CSRI	排名	疾控机构资源指数	残差	归一化患病率指数	残差	归一化死亡率指数	残差
湖北	8.69	1	0.49	−6	0.62	0	0.45	0
河南	8.35	2	0.59	0	0.39	−2	0.17	0
安徽	8.32	3	0.33	−14	0.38	−4	0.10	−6
江西	8.05	4	0.40	−9	0.39	−3	0.06	−11
湖南	7.81	5	0.49	−3	0.28	−20	0.08	−7
江苏	7.48	6	0.57	+2	0.36	−5	0.00	−21
浙江	7.18	7	0.54	+2	0.40	+5	0.06	−7
上海	6.76	8	0.61	+7	0.37	0	0.11	+2
山东	6.68	9	0.44	−1	0.36	−3	0.11	+2
北京	6.68	10	0.53	+4	0.38	+4	0.12	+6
广东	6.33	11	0.49	+2	0.40	+8	0.11	+6
福建	6.33	12	0.31	−9	0.33	−2	0.06	−5
重庆	6.13	13	0.37	−1	0.37	+4	0.10	+3
山西	5.79	14	0.25	−9	0.30	−6	0.00	−14
陕西	5.58	15	0.31	−7	0.32	−1	0.06	−3
广西	5.45	16	0.37	+1	0.31	−2	0.04	−6
贵州	5.33	17	0.25	−7	0.29	−6	0.04	−7
河北	5.14	18	0.41	+6	0.32	+3	0.10	+7
辽宁	4.95	19	0.33	+1	0.28	−7	0.04	−7
天津	4.89	20	0.33	+1	0.31	+1	0.07	+7
四川	4.83	21	0.58	+18	0.35	+8	0.06	+5
宁夏	4.67	22	0.13	−6	0.27	−6	0.00	−7
海南	4.32	23	0.10	−6	0.32	+6	0.11	+15
吉林	4.13	24	0.36	+8	0.27	−3	0.06	+4
云南	3.86	25	0.44	+14	0.29	+3	0.04	+2
甘肃	3.75	26	0.20	−1	0.29	+2	0.04	+1
黑龙江	3.66	27	0.32	+7	0.37	+17	0.15	+24
内蒙古	3.53	28	0.22	2	0.30	+7	0.06	+9
青海	3.00	29	0.04	−1	0.19	−1	0.00	−1
西藏	2.45	30	0.00	−1	0.07	−1	0.00	−1
新疆	2.02	31	0.23	6	0.25	+2	0.06	+10

注:残差表示与CSRI指数排名差异;各变量指数均经过归一化处理,非真实数字;由于数据获取困难,本研究不包括港香港、台湾和澳门。

(C)1994-2021 China Academic Journal Electronic Publishing House. All rights reserved. http://www.cnki.net



(a) 综合空间风险指数空间分布　(b) 归一化患病率指数空间分布

(c) 归一化死亡率指数空间分布　(d) 疾控机构资源指数空间分布

注：该图基于自然资源部标准地图服务网站下载的审图号为GS(2019)1653号的标准地图制作，底图无修改；由于数据获取困难，本研究不包括香港、台湾和澳门。

图4　2020年1月1日至4月11日中国综合空间风险指数(CSRI)与各变量空间分布

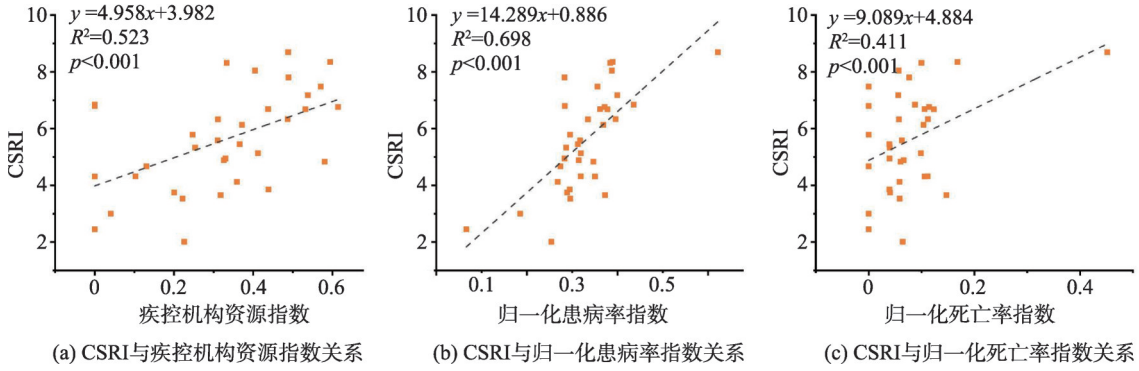
Fig. 4　Spatial distribution of Comprehensive Spatial Risk Index (CSRI) and various variables in China from January 1 to April 11, 2020

其归一化患病率指数分别为0.38、0.37、0.40，而CSRI指数分别为6.68、6.76、6.33，其原因可能为北京、上海和广东具备交通便利的属性带来的人口流动的影响加剧了疫情的空间风险，具体表现为人口流入和流出2个方面，人口流入，可能增加本地疫情风险，而人口流出尤其是重点疫区，则可能引致外部传播的风险。局部地区对比CSRI指数具有差异性，如黑龙江的归一化患病率指数与归一化死亡率指数较高，其可能主要受到境外输入病例影响，江苏、浙江归一化患病率指数与归一化死亡率指数较低，其可能由于当地政府的政策以及较高水平的定点医院数量导致。

综合对比疾控机构的资源指数空间分布（图4(d)），总体呈现出较明显的空间异质性，其中安徽、江西两地疾控机构资源指数较低分别为0.33、0.40，而CSRI指数较高分别为8.32、8.05，显示区域在面临高空间风险的同时其疾控资源却相较匮乏。部分地区如云南、四川疾控机构资源指数较高，分别为0.44、0.58，而CSRI指数较低分别为3.86、4.83，显示区域在面临低空间风险的同时其疾控资源却相对充裕。需要特别说明的是，湖北、北京、广东等省份（直辖市）虽然CSRI指数相对较高，分别为8.69、6.68、6.33，但是其疾控机构资源指数也相对较高分别为0.49、0.53、0.49，显示区域在面临高空间风险的同时依然有较强的疾控应急能力。总体来说，我国疾控机构资源在总体分布上能够覆盖绝大部分区域，与CSRI指数存在一定程度的区位关联性，但空间资源分布不均的现象依然存在。

综上，为进一步评估综合空间风险指数的精确度，系统比较CSRI与上述变量的相关程度。图5为综合空间风险指数(CSRI)与各变量的散点图，结果显示随着CSRI指数的增加，疫情机构资源指数、归

(C)1994-2021 China Academic Journal Electronic Publishing House. All rights reserved.　http://www.cnki.net



(a) CSRI与疾控机构资源指数关系 (b) CSRI与归一化患病率指数关系 (c) CSRI与归一化死亡率指数关系

图5 2020年1月1日至4月11日中国综合空间风险指数(CSRI)与各变量关系

Fig. 5 Relationship between Comprehensive Spatial Risk Index (CSRI) and various variables in China from January 1 to April 11, 2020

一化患病率指数以及归一化死亡率指数也存在增高的趋势,其回归方程均通过了p<0.001显著性检验,R^2分别为0.523、0.698、0.411,表明其与CSRI指数之间具有一定的相关性。基于以上综合结果,表明综合空间风险指数CSRI指数具有一定空间风险预警作用以及反映地理空间疫情风险的能力。

4 讨论

地理空间疫情风险评估对于全国疫情防控具有重要的作用。在宏观层面从空间尺度探索疫情评估的方法,为全国尺度研究疫情防控问题提供新的视角,其相较于传统的普查数据以及社会经济数据,具有更加快速、高效的特点。

但与相关的研究类似,尽管地理空间疫情风险评估的准确性得到了验证,但是实际情况较之复杂,宏观层面的评估仅仅提供评价方法的构建以及风险区域的识别,不足以为疫情防控提供具体的指导反馈[29]。因此本研究在地理空间疫情风险评估构建的基础上,将地理区位、道路交通、医疗卫生、疫情现状4种指标对CSRI指数影响程度的差异性做进一步分析,以探讨不同层面落实防控措施的必要性与权衡顺序。此外,不同指标之间在构建的过程中往往存在交互作用,会加剧对CSRI指数的影响,需要进一步研判指标之间的相互影响以在后续的疫情工作中避免相关因子的交叉造成的风险增加。

综合考虑以上情形,在全国范围通过划分100 km×100 km的网格,进行各指标数值统计并采用Pearson相关性予以探讨,如图6所示。

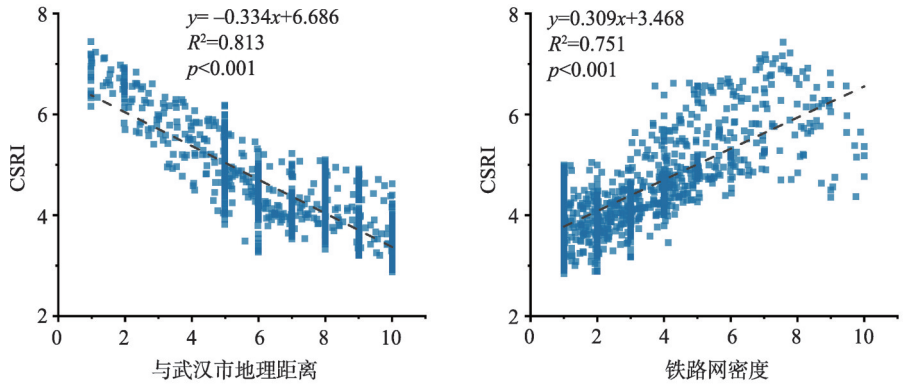
结合(图6(a))可知,CSRI指数与武汉市地理距离呈现较强的负相关性,其R^2为0.813,表明在中国本土的抗疫过程中,地理区位是疫情风险存在的重要因素。这与部分研究成果相一致[30],新冠疫情存在着地理空间传播的风险。同时也说明了武汉市作为疫情的暴风眼自然是疫情防控的重点,与武汉市相邻近的省市也保持了较高等级的社会防控,如安徽、河南等,其防控工作强度也相对较大。

同时,结合(图6(b)、图6(c))可知,铁路网密度、公路网密度与CSRI指数存在较强的正相关性,其R^2分别为0.751、0.792,表明道路交通因素对疫情的空间风险影响较大。公路、铁路包括地铁等在某种程度上突破了地理区位的隔阂,增加了疫情空间传播的范围,从而影响疫情风险的空间分布,如北京、广东等地,以道路交通为载体的人口流动加剧了国内疫情的空间风险程度,同时也在较大程度上表明我国在应对疫情防控中采取的部分高铁短时间停运等"限流"措施的有效性和科学性[31]。

而结合(图6(d)、图6(e))可知,定点医院密度、居民-医院地理距离与CSRI指数存在较强的负相关性,其R^2分别为0.545、0.436,表明医疗卫生因素对疫情的空间风险能够起到缓解的作用。定点医院的数量以及与周围居民的分布反映了各地区医疗资源情况,集中的医疗资源能够从源头上减少新冠病毒的存活时间并从空间上阻断疫情的传播,如江苏、浙江等地,同时也表明我国采取集中医疗资源于武汉等措施的必要性。但我国主要医疗资源分布在省会城市,在某种程度上其分布的不均衡会导致目前过多患者因在本地难以获得相应的治疗而汇集省城,增加交通成本和省城的医疗压力。

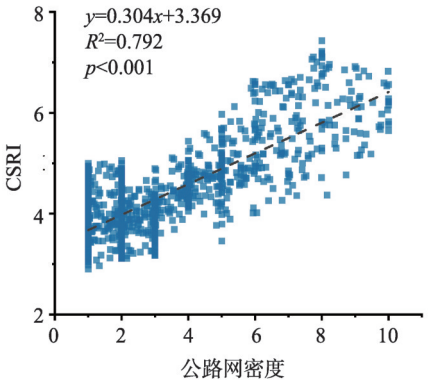
结合(图6(f))可知,CSRI指数与疫情小区密度则呈现较强的正相关性,其R^2为0.825,表明疫情本

(C)1994-2021 China Academic Journal Electronic Publishing House. All rights reserved. http://www.cnki.net

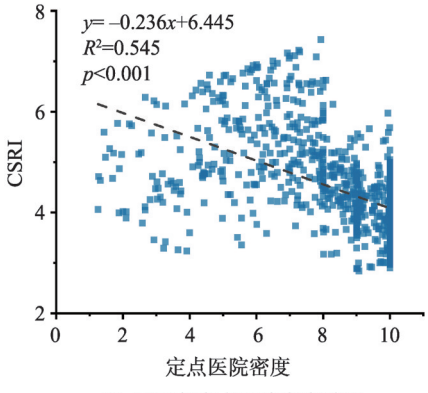


(a) CSRI与武汉市地理距离关系

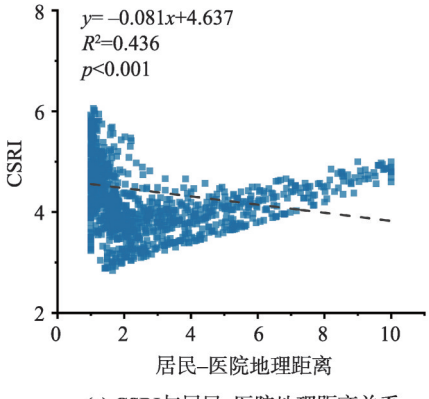
(b) CSRI与铁路网密度关系



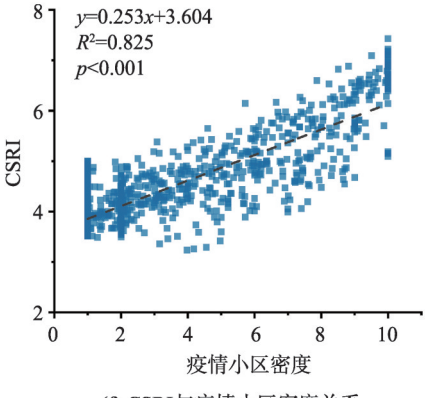
(c) CSRI与公路网密度关系



(d) CSRI与定点医院密度关系



(e) CSRI与居民–医院地理距离关系



(f) CSRI与疫情小区密度关系

图6　2020年1月1日至4月11日中国综合空间风险指数(CSRI)与评估因子关系

Fig. 6　Relationship between Comprehensive Spatial Risk Index (CSRI) and assessment factors in China from from January 1 to April 11, 2020

身的严重程度对疫情的空间风险构成仍有重要作用,在一定程度上解释我国在疫情防控初期部分城市“封城”的必要性,以及疫情防控取得阶段性成果(截至2020年4月11号)后,仍然落实和完善常态化疫情防控,防止疫情反弹举措的合理性[32]。

综上,4种指标与CSRI指数相关程度表征由高到低依次为疫情现状指标、地理区位指标、道路交通指标以及医疗卫生指标,表明在区域层面疫情的联防联控工作中,需要优先对疫情事发地以及武汉市重点区域采取“封城”(武汉“封城”2020年1月23日至4月7日)等隔离措施,防止疫情规模扩大,再从空间资源分配的角度,采取“限流”、“集中优势医疗资源”等防控措施。

此外,不同指标在影响综合空间风险指数(CSRI)

(C)1994-2021 China Academic Journal Electronic Publishing House. All rights reserved.　http://www.cnki.net

空间分布方面具有空间分层异质性。通过地理探测器的因子探测结果如表4所示，不同因子都具有较高的q值且均通过了$p<0.05$显著性检验，表明不同因子对于地理空间疫情风险均具有较强的解释力，也在一定程度上验证了综合空间风险指数（CSRI）构建的合理性。而根据交互作用探测结果（表5）可知，地理空间疫情风险并不只是由单一因子影响，其受到多种因子的共同作用，且任意2种因子的交互作用均大于单一因子，其中公路网密度与居民-医院地理距离的交互作用强度最大，q值达0.9842，铁路网密度与居民-医院地理距离的交互作用强度次之，q值达0.9837，反映了道路交通指标在居民前往定点医院治疗的过程中协调作用的结果要高于其单独作用的结果，会显著加剧空间疫情风险。

表4 2020年1月1日至4月11日中国地理空间疫情风险评估因子探测结果

Tab. 4 Detection results of geospatial epidemic risk factors in China from January 1 to April 11, 2020

因子	与武汉市地理距离	铁路网密度	公路网密度	定点医院密度	居民-医院地理距离	疫情小区密度
q统计值	0.8355	0.8103	0.8214	0.7649	0.6053	0.8139
p值	0.0000	0.0215	0.0343	0.0000	0.0127	0.0000

注：$p<0.05$具有统计意义。

表5 2020年1月1日至4月11日中国地理空间疫情风险评估因子交互作用结果

Tab. 5 Interaction results of geospatial epidemic risk factors in China from January 1 to April 11, 2020

因子	与武汉市地理距离	铁路网密度	公路网密度	定点医院密度	居民-医院地理距离	疫情小区密度
与武汉市地理距离	0.8355					
铁路网密度	0.9252(Y)	0.8103				
公路网密度	0.9309(Y)	0.9034(N)	0.8214			
定点医院密度	0.9210(Y)	0.8934(Y)	0.8957(Y)	0.7649		
居民-医院地理距离	0.9687(Y)	0.9837(Y)	0.9842(Y)	0.9781(Y)	0.6053	
疫情小区密度	0.9102(Y)	0.8834(N)	0.8908(N)	0.8755(Y)	0.9803(Y)	0.8139

注：Y代表有显著性差异，N代表没有显著性差异。

5 结论与展望

新冠疫情（COVID-19）风险依然存在且构成较复杂，涉及社会、经济、地理等多重维度。本研究基于中国行政区划、定点医院、疫情小区以及道路交通等多元数据在宏观层面构建全国地理空间疫情风险性评估，结合多尺度视角探讨疫情风险的空间分布表征，同时根据相关疫情统计数据进行评估效果验证，为后续城市管理中重大疫情的空间资源分配以及空间联防策略提供相应的依据，并提供如下结论：

（1）结合多元数据的地理空间风险评估在宏观层面精度较好，具有一定的可行性。

（2）地理空间疫情风险分布呈现显著的空间集聚特征，湖北省依然是疫情防控的重点（截至2020年4月11日），河南、湖南、江西、安徽、浙江、江苏、上海等省省份（直辖市）地理空间疫情风险分布遵循与湖北省的地理邻近和网络邻近特征。政府在落实常态化疫情防控举措过程中，需要外防输入、内防反弹，注重各区域的联防联控。

（3）地理空间疫情风险分布与地理区位、道路交通、医疗卫生、疫情现状均存在一定的相关性，且相关指标R^2存在差异，由高到低依次为疫情现状、地理区位、道路交通、医疗卫生，其中地理区位、医疗卫生呈现显著的负相关，道路交通、疫情现状呈现正相关。政府在应对疫情初期防控中优先采取的部分城市“封城”（武汉“封城”2020年1月23日至4月7日）等措施阻止疫情规模扩散，再采取部分交通“限流”以及集中医疗资源于武汉等措施，具有科学性、有效性、及时性。

（4）地理空间疫情风险的构成因素错综复杂，其往往受到多种因子的共同作用。在城市的疫情防控工作中需从多方面、多角度统筹考虑，综合多部门力量筑牢防线。

综合地理空间疫情风险分布，在一定程度上能够为今后城市疫情风险评估提供宏观的研究视

(C)1994-2021 China Academic Journal Electronic Publishing House. All rights reserved. http://www.cnki.net

角，然而在疫情防控工作中仍需要考虑人口的流动风险以及疫情的动态划分，这些因素也会影响评估的准确性，此外，区域的气候、生态环境对于疫情风险评估也具有重要的意义，后续将开展相关方面的研究。

参考文献(References)：

[1] Huang C, Wang Y, Li X, et al. Clinical features of patients infected with 2019 novel coronavirus in Wuhan, China [J]. The Lancet, 2020,395(10223):497-506.

[2] Wu F, Zhao S, Yu B, et al. A new coronavirus associated with human respiratory disease in China[J]. Nature, 2020, 579(7798):265-269.

[3] 朱斌,刘锦林,毛瑛.中国典型法定报告传染病发病率空间关联性分析[J].中国公共卫生,2018,34(1):4-8. [Zhu B, Liu J L, Mao Y. Spatial correlation of incidence rate of typical notifiable infectious diseases in China[J]. Chinese Journal of Public Health, 2018,34(1):4-8.]

[4] 丁晓彤,余卓渊,宋海慧,等.基于信息熵的中国自然疫源性疾病分布特征研究[J].地球信息科学学报,2019,21(12):1877-1887. [Ding X T, Yu Z Y, Song H H, et al. Research on the distribution of natural focus diseases based on information entropy[J]. Journal of Geo-information Science, 2019,21(12):1877-1887.]

[5] 高芳旭,齐秀英.天津市和平区细菌性痢疾流行特征及疫情预测[J].现代预防医学,2015,42(11):1951-1953. [Gao F X, Qi X Y. Epidemiologic characteristics and prediction of bacillary dysentery in Heping District, Tianjin[J]. Modern Preventive Medicine, 2015,42(11):1951-1953.]

[6] 陈会宴,廖一兰,张宁旭,等.山西省原平市神经管畸形时空分析[J].地球信息科学学报,2017,19(4):502-510. [Chen H Y, Liao Y L, Zhang N X, et al. Spatial and temporal analysis of neural tube defects in Yuanping County, Shanxi Province[J]. Journal of Geo-information Science, 2017,19(4):502-510.]

[7] 张湘雪,王丽,尹礼唱,等.京津唐地区HFMD时空变异分析与影响因子探测[J].地球信息科学学报,2019,21(3):398-406. [Zhang X X, Wang L, Yin L C, et al. Spatial-temporal variation analysis and risk determinants of hand, foot and mouth disease in Beijing-Tianjin-Tangshan, China[J]. Journal of Geo-information Science, 2019, 21(3):398-406.]

[8] Cao C, Li G, Zheng S, et al. Research on the environmental impact factors of Hand-Foot-Mouth disease in Shenzhen, China using RS and GIS technologies[C]. 2012 IEEE International Geoscience and Remote Sensing Symposium, 2012:7240-7243.

[9] 叶莹,范威,王海峰,等.河南省新型冠状病毒肺炎聚集性疫情流行病学特征分析[J].中国公共卫生,2020,36(4):465-468. [Ye Y, Fan W, Wang H F, et al. Clustering of 2019 novel coronavirus disease epidemic in Henan Province[J]. Chinese Journal of Public Health, 2020,36(4):465-468.]

[10] Wang C, Jiang B, Fan J, et al. A study of the dengue epidemic and meteorological factors in Guangzhou, China, by using a zero-inflated poisson regression model[J]. Asia-Pacific Journal of Public Health, 2014,26(1):48-57.

[11] 唐燕.新冠肺炎疫情防控中的社区治理挑战应对:基于城乡规划与公共卫生视角[J].南京社会科学,2020(3):8-14,27. [Tang Y. Challenges and responses of community governance in the prevention and control of novel coronary pneumonia: from perspectives of urban-rural planning and public health[J]. Nanjing Journal of Social Sciences, 2020(3):8-14,27.]

[12] 杨俊宴,史北祥,史宜,等.高密度城市的多尺度空间防疫体系建构思考[J].城市规划,2020,44(3):17-24. [Yang J Y, Shi B X, Shi Y, et al. Construction of a multi-scale spatial epidemic prevention system in high-density cities[J]. City Planning Review, 2020,44(3):17-24.]

[13] 中华人民共和国国家卫生健康委员会.截至4月11日24时新型冠状病毒肺炎疫情最新情况[EB/OL]. http://www.nhc.gov.cn/,2020-04-12. [National Health Commission, PRC. COVID-19 update as of 11 April 24:00[EB/OL]. http://www.nhc.gov.cn/,2020-04-12.]

[14] National data[DB/OL]. http://data.stats.gov.cn/search.htm?s/.

[15] The Data-center of China Public Health Science[DB/OL]. http://www.phsciencedata.cn/Share/en/index.jsp.

[16] Openstreetmap[DB/OL]. http://download.geofabrik.de/.

[17] China Data Lab Dataverse[DB/OL]. https://dataverse.harvard.edu/.

[18] 刘耀宝,曹俊.我国境外输入性疟疾防控策略对当前新型冠状病毒肺炎防控工作的启示[J].中国血吸虫病防治杂志,2020,32(2):113-118. [Liu Y B, Cao J. Management of coronavirus disease 2019 (COVID-9): experiences from imported malaria control in China[J]. Chinese Journal of Schistosomiasis Control, 2020,32(2):113-118.]

[19] Shi K F, Yang Q Y, Li Y Q, et al. Mapping and evaluating cultivated land fallow in Southwest China using multi-source data[J]. Science of the Total Environment, 2019, 654(1):987-999.

[20] 许小可,文成,张光耀,等.新冠肺炎爆发前期武汉外流人口的地理去向分布及影响[J].电子科技大学学报,2020,

(C)1994-2021 China Academic Journal Electronic Publishing House. All rights reserved. http://www.cnki.net

49(3):324-329. [Xu X K, Wen C, Zhang G Y, et al. The geographical destination distribution and effect of outflow population of Wuhan when the outbreak of COVID-19[J]. Journal of University of Electronic Science and Technology of China, 2020,49(3):324-329.]

[21] 张宇,田万利,吴忠广,等.基于改进SEIR模型的新冠肺炎疫情沿交通线路传播机制[J].交通运输工程学报,2020,20(3):150-158. [Zhang Y, Tian W L, Wu Z G, et al. Transmission mechanism of COVID-19 epidemic along traffic routes based on improved SEIR model[J]. Journal of Traffic and Transportation Engineering, 2020,20(3):150-158.]

[22] 李欣,周林,贾涛,等.城市因素对COVID-19疫情的影响——以武汉市为例[J].武汉大学学报·信息科学版,2020,45(6):826-835. [Li X, Zhou L, Jia T, et al. Influence of urban factors on the COVID-19 epidemic: A case study of Wuhan City[J]. Geomatics and Information Science of Wuhan University, 2020,45(6):826-835.]

[23] Shi K, Chang Z, Chen Z, et al. Identifying and evaluating poverty using multisource remote sensing and Point of Interest (POI) data: A case study of Chongqing, China[J]. Journal of Cleaner Production, 2020,255:120245.

[24] 李刚,李建平,孙晓蕾,等.主客观权重的组合方式及其合理性研究[J].管理评论,2017,29(12):17-26,61. [Li G, Li J P, Sun X L, et al. Research on a combined method of subjective-objective weighing and the its rationality[J]. Management Review, 2017,29(12):17-26,61.]

[25] 郑斓,任红艳,施润和,等.珠江三角洲地区登革热流行风险空间模拟与预测[J].地球信息科学学报,2019,21(3):407-416. [Zheng L, Ren H Y, Shi R H, et al. Spatial simulation and prediction of dengue fever transmission in Pearl River Delta[J]. Journal of Geo-information Science, 2019,21(3):407-416.]

[26] 张永树,杨振凯,訾璐,等.中国艾滋病空间格局和时空演化分析[J].地球信息科学学报,2020,22(2):198-206. [Zhang Y S, Yang Z K, Zi L, et al. Spatio-temporal evolution of the AIDS pattern in China[J]. Journal of Geo-information Science, 2020,22(2):198-206.]

[27] 张新,林晖,朱长明,等. COVID-19疫情早期中国确诊时间的时空特征及动态过程分析[J].武汉大学学报·信息科学版,2020,45(6):791-797. [Zhang X, Lin H, Zhu C M, et al. Spatiotemporal characteristics and dynamic process analysis of epidemic diagnosis time of COVID-19 at early stage in Chinese mainland[J]. Geomatics and Information Science of Wuhan University, 2020,45(6):791-797.]

[28] Wang J F, Zhang T L, Fu B J. A measure of spatial stratified heterogeneity[J]. Ecological Indicators, 2016,67:250-256.

[29] 张婷,程昌秀.顾及空间集聚程度的中国高温灾害危险性评价[J].地球信息科学学报,2019,21(6):865-874. [Zhang T, Cheng C X. Assessment of China's high-temperature hazards: Accounting for spatial agglomeration[J]. Journal of Geo-information Science, 2019,21(6):865-874.]

[30] 陈芳,吴家兵,姜静静,等.安徽省新型冠状病毒肺炎聚集性疫情流行特征与防控措施分析[J].中国公共卫生,2020,36(4):469-472. [Chen F, Wu J B, Jiang J J, et al. Epidemiological characteristics of clusters of COVID-19 in Anhui Province[J]. Chinese Journal of Public Health, 2020,36(4):469-472.]

[31] 刘勇,杨东阳,董冠鹏,等.河南省新冠肺炎疫情时空扩散特征与人口流动风险评估——基于1243例病例报告的分析[J].经济地理,2020,40(3):24-32. [Liu Y, Yang D Y, Dong G P, et al. The spatio-temporal spread characteristics of 2019 novel coronavirus pneumonia and risk assessment based on population movement in Henan Province: Analysis of 1243 individual case reports[J]. Economic Geography, 2020,40(3):24-32.]

[32] Layne S P, Hyman J M, Morens D M, et al. New coronavirus outbreak: Framing questions for pandemic prevention[J]. Science, 2020,12(534):eabb1469.

(C)1994-2021 China Academic Journal Electronic Publishing House. All rights reserved. http://www.cnki.net

Hindawi
Computational Intelligence and Neuroscience
Volume 2022, Article ID 9799054, 11 pages
https://doi.org/10.1155/2022/9799054

Research Article

Analysis of Spatial Distribution of CVD and Multiple Environmental Factors in Urban Residents

Beichen Wang,[1] Kangkang Gu,[1] Dong Dong,[1] Yunhao Fang,[2] and Lingling Tang[3]

[1]*School of Architecture & Planning, Anhui Jianzhu University, Hefei, Anhui 230022, China*
[2]*School of Architecture and Urban Planning, Huazhong University of Science and Technology, Wuhan, Hubei 430000, China*
[3]*College of Architecture and Art, Hefei University of Technology, Hefei, Anhui 230009, China*

Correspondence should be addressed to Kangkang Gu; kangkanggu@ahjzu.edu.cn

Received 29 October 2021; Accepted 20 January 2022; Published 16 March 2022

Academic Editor: Akshi Kumar

Copyright © 2022 Beichen Wang et al. This is an open access article distributed under the Creative Commons Attribution License, which permits unrestricted use, distribution, and reproduction in any medium, provided the original work is properly cited.

Cardiovascular disease (CVD) poses a serious threat to urban health with the development of urbanization. There are multifaceted and comprehensive influencing factors for CVD, so clarifying the spatial distribution characteristics of CVD and multiple environmental influencing factors is conducive to improving the active health intervention of urban environment and promoting the sustainable development of cities The spatial distribution characteristics of CVD deaths in a certain district, Bengbu City, Huaihe River Basin, China, in 2019 were explored, and the correlation between multiple environmental factors and CVD mortality was investigated in this study, to reveal the action mechanism of multiple environmental factors affecting the risk of mortality. Relevant studies have shown that (1) CVD deaths are characterized as follows: male deaths are more than females; the mortality is higher in those of higher age; most of them are unemployed; cardiocerebral infarction is the main cause of death; and the deaths are mainly distributed in the central city and near the old urban area. (2) The increased CVD mortality can be attributed to the increased density of restaurants and cigarette and wine shops around the residential area, the increased traffic volume, the dense residential and spatial forms, the low green space coverage, and the distance from rivers. Therefore, appropriate urban planning and policies can improve the active health interventions in cities and reduce CVD mortality.

1. Introduction

A great number of studies have demonstrated the high mortality and disability rate of cardiovascular disease (CVD) [1] and the resulting global burden of diseases [2]. The traditional risk factors for CVD include hypertension, diabetes, dyslipidemia, obesity, smoking, alcohol consumption, and lack of physical exercise. However, under the biological-psychosocial medical model, the influencing factors on health are multifaceted and comprehensive, including environmental factors. Previous studies have shown that the urban population is more likely to suffer from cardiovascular diseases than the rural population in some developing countries [3]. Industrialization, urbanization, aging, and constant changes in the ecological environment and lifestyle have brought challenges to people's health in the rapid urban development. A lot of cities are experiencing a major shift in the disease spectrum from infectious diseases to chronic noncommunicable diseases. Therefore, it is conducive to improving active health interventions in urban environment and promoting sustainable urban development in the future to identify the mortality distribution characteristics of CVD and environmental influencing factors.

Previous studies have shown that unreasonable diet, excessive oil, and salt intake will increase the pressure of human circulatory system [4], thereby leading to CVD morbidity and mortality. The increase in the amount of physical activity, such as work, commuting, and leisure, will appropriately reduce the risk of CVD-related death [5], and the accessibility of sports and leisure activity facilities and open space will also have an influence on the level of physical activity of residents [6]. Residents will tend to commute by non-motor vehicles and increase daily activities provided that the urban road slow traffic system is perfect and the bus

stops are dense [7]. In addition, residents engaged in manual work will have increased daily activities [8], thus reducing the risk of death. Air pollution [9–11] and noise pollution [12] constitute the important risk factors for CVD, of which long-term air pollution has a greater impact on CVD than short-term one [13]. The closer distance to the pollution source or the greater density of the surrounding pollution sources will increase the possibility of exposure to pollutants [14, 15], including a large number of industrial pollutants [16], the cooking fumes from [17], the exhaust gas emissions of motor vehicles, and urban transportation facilities, such as railways, subway lines, and airports [18]. Roads and restaurants produce noise pollution while causing air pollution, thereby leading to the occurrence of cardiovascular diseases [19]. The nearer distance from rivers and the higher green space coverage can effectively reduce the concentration of particulate matter (Douglas, W., and [20–22]) and lower CVD mortality. Cold weather and sudden temperature drop in winter are prone to causing overreaction of human function, resulting in death from acute CVD [23, 24]. The difference in temperature in different urban regions will lead to the difference in mortality.

In general, current studies focus on the macro-level of county [25], prefecture [26], and state [25], but neglect the small scales, such as communities and streets; meanwhile, the consideration of environmental factors is relatively simple, and the influence of aging population and old urban areas is relatively ignored. A large number of people in the Huaihe River Basin in Central China died of chronic diseases caused by the environment many years ago [27]. The urban environmental pollution is relatively serious now, seriously endangering the physical and mental health of residents. In view of this, the distribution characteristics of CVD deaths were analyzed, and the influences of multiple environmental factors on CVD were systematically investigated in this study with the old urban area in Bengbu City of Huaihe River Basin as the subject, to reduce CVD mortality by proper urban planning and policies, and provide certain research ideas for healthy city construction in other areas of Huaihe River Basin.

2. Materials and Methods

2.1. Study Area. Bengbu City, located in the south of Huaihe River Basin, China, is characterized by high population density and rapid urbanization [28]. Bengbu was an important industrial city and traffic hub in China before, where a large number of chemical, pharmaceutical, and building materials enterprises and the heavy traffic pressure have produced a large amount of pollution in Bengbu, seriously affecting the physical and mental health of residents. A certain district is located in the Western old urban area of Bengbu City, adjacent to the commercial and cultural center of the city in the east and the Huaihe River (one of the seven major rivers in China) in the north, and it is also the administrative area with the largest population in Bengbu City, so it is suitable for the research on urban environment and population health. The study area consisted of 12 blocks numbered YH01-YH12 in a certain district, which were divided into 2,744 spatial units by 100 m grid (Figure 1). The study area is located in the mid-latitude region, where northeasterly wind is the most prevalent throughout the year, the average temperature in January is 1°C, and it is susceptible to cold waves in winter.

2.2. Data Sources

2.2.1. Sources of Data Related to CVD. The data of cardiovascular disease (CVD) mortality were collected from the population whose cause of death was cardiovascular disease (ICD-10 code I00-I99) determined by Bengbu Health Commission in 2019, including detailed address, age, gender, and occupation before death. Inpatients whose home addresses and affiliations were not within the study area were excluded, so the final number was 469 in total. The number of resident population in a certain district in 2019 was derived from the official bulletin of Bengbu National Bureau of Statistics.

2.2.2. Environmental Data Sources. The land use data and built environment data in environmental data were obtained from the Anhui Urban & Rural Planning and Design Institute, and the data contained the main uses of each land in a certain district in 2019, as shown in Figure 2(a), which included roads, green space and river, residential land, industrial land according to urban land classification, and the base area and floor number of each building. Commercial and bus stops are derived from open-source point-of-interest (POI) data, which are characterized by large sample size, wide coverage, and detailed spatial resolution, making spatial analysis more comprehensive, objective, and in-depth, as shown in Figure 2(b). Data of environmental pollution indexes were obtained from the Bengbu Bureau of Ecology and Environment, and the pollution values of each spatial unit were obtained by the interpolation method for the pollution monitoring point data. Data of land surface temperature and vegetation coverage were derived from Landsat 8 remote sensing data in January 2019 provided by USGS and coded LC81210372019023LGN00.

2.3. Influencing Factor Index System. To explore the distribution characteristics of cardiovascular disease (CVD) and environmental influencing factors in urban residents, the basic characteristics and spatial distribution characteristics of CVD deaths were analyzed, and the correlation between various environmental influencing factors and CVD mortality was explored (Figure 3). Environmental influencing factors included land use, road traffic, spatial form, and natural environment, with their potential impacts on CVD shown in Table 1. The calculation formula for CVD mortality is as follows:

$$\text{Mortality} = \frac{\text{Nc}}{\text{Np}} \times 100\%, \tag{1}$$

where Nc is the number of deaths due to CVD in a unit and Np is the total population in a unit.

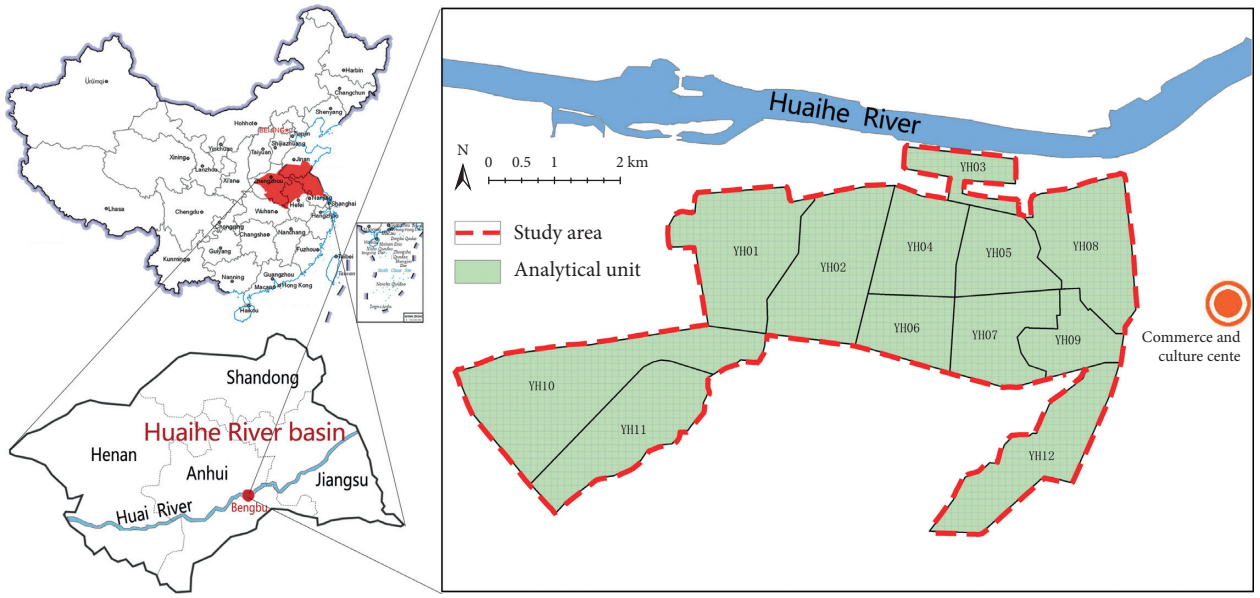


Figure 1: Area bitmap.

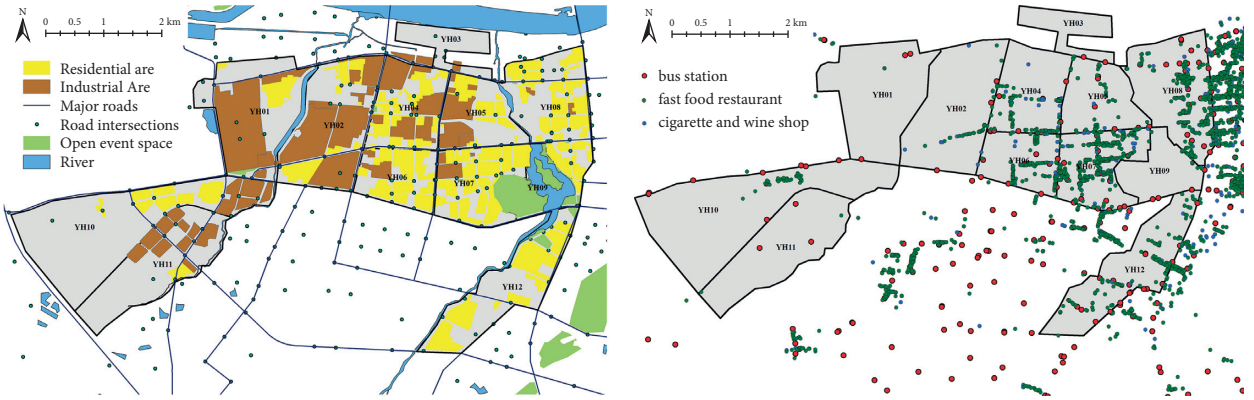


Figure 2: Present distribution.

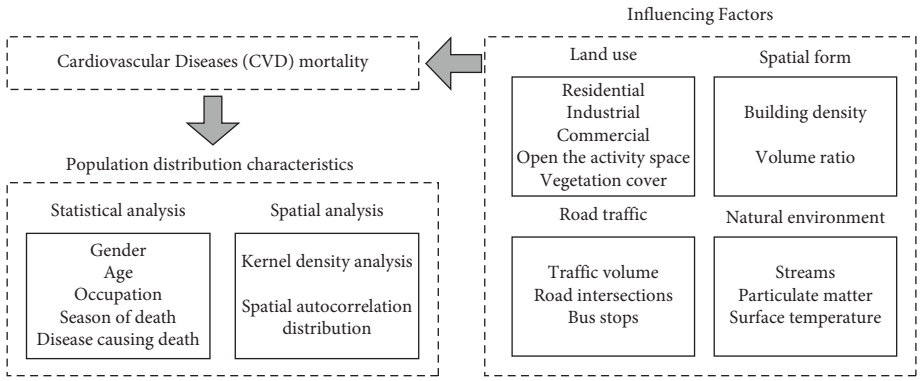


Figure 3: Conceptual framework.

2.4. Study Methods

2.4.1. Spatial Autocorrelation Assessment. Global spatial autocorrelation [29] is usually measured by Moran's *I*, and the aggregation of subregional geospatial CVD deaths is judged according to the spatial distribution pattern of the whole region. Moran's *I* range is [−1, 1], and the larger value indicates the more obvious spatial correlation, and the

Table 1: Environmental influencing factors.

Category	Subcategory	Variable	Unit	Definition	Potential impact of hypothesis
Land use	Live	Residential density	%	Living area/total land area	Cause pollution and physical and mental stress
	Industry	Distance from the nearest industry	m	Distance from the nearest industry	The closer you are to industry, the more pollution you get
	Business	Fast-food restaurant density	Pcs/ha	Number of fast-food restaurants in 500 m buffer zone/buffer zone area	Intake relatively high salt and oil
		Tobacco and liquor shop density	Pcs/ha	Number of tobacco and liquor stores in 500 m buffer zone/buffer zone area	Increase the risk of alcohol and smoking
	Open the activity space	Distance from the nearest open space	m	Distance from the nearest open space	It is more convenient to exercise and relax
	Vegetation cover	Normalized difference vegetation index (NDVI)	—	NDVI in 2019	Vegetation coverage can reduce air pollution, increase green vision rate, and delight body and mind
Road transport	Traffic	Road network density	m/ha	Road length/total land area	Increase air and noise pollution
	Road intersection	Road intersection density	Pcs/ha	Number of road intersections in 500 m buffer zone/buffer zone area	More air and noise pollution
	Bus stop	Bus stop density	Pcs/ha	Number of bus stops in 500 m buffer zone/buffer zone area	It is more convenient to travel and increase the amount of activities
Spatial form	Building density	Building coverage	%	Total area of building basement/total area of land	High density reduces the wind speed, which increases the concentration of air pollutants and makes people depressed
	Volume fraction	Volume fraction	—	Total construction area/total land area	High density reduces the wind speed, which increases the concentration of air pollutants and makes people depressed
Natural environment	River	Distance from the nearest river	m	Distance from the nearest river	Adsorption of air particles by water body
	Particulate matter (PM)	Mean $PM_{2.5}$	Ug/m^3	Average $PM_{2.5}$ in 2019	Increase air pollution
		Mean PM_{10}	Ug/m^3	Average PM_{10} in 2019	Increase air pollution
	(Ground) surface temperature	Mean surface temperature	°C	Surface temperature in January 2019	Cold winter temperatures increase the risk of death

smaller value indicates the greater spatial difference, with the specific calculation formula as follows:

$$\text{Moran's } I = \frac{n\sum_{i=1}^{n}\sum_{j=1}^{n} w_{ij}\left(x_i - \overline{x}\right)\left(x_j - \overline{x}\right)}{\sum_{i=1}^{n} w_{ij}\sum_{j=1}^{n}\sum_{i=1}^{n}\left(x_i - \overline{x}\right)^2} (i \neq j), \quad (2)$$

where n is the number of study units; x_i and x_j represent the CVD mortality in area i and area j, respectively. $\overline{x}$ represents the average CVD mortality; W_{ij} represents the spatial weight matrix.

Local spatial autocorrelation [30] can reveal the heterogeneity of local space, make up for the atypical characteristics of local areas in the whole region, and fully reflect the variation trend of local geospatial epidemic risk. The spatial difference in CVD mortality was measured by local indicators of spatial association (LISA) in this study, with the calculation formula shown as follows:

$$\text{LISA}_i = z_i \sum_j w_{ij} z_j, \quad (3)$$

where z_i and z_j represent the standardized values of CVD mortality in area i and area j, respectively. W_{ij} represents the spatial weight matrix. In the LISA of local spatial autocorrelation, CVD mortality can be divided into four categories: high-high clustering (H-H), high-value clustering; low-low clustering (L-L), low-value clustering; high-low clustering (H-L), outliers with high values mainly surrounded by low values; and low-high clustering (L-H), outliers with low values mainly surrounded by high values.

2.4.2. Spearman's Rank Correlation. To investigate the relationship between CVD and environmental factors, the correlation between the mortality rate of CVD (dependent variable) and the values of various environmental factors (independent variables) was comprehensively measured by Spearman's rank correlation [31], with the specific formula referred to formula (3). Compared with Pearson's correlation, Spearman's rank correlation can make up for the fact that the correlation of environmental factor values may not be linear and are interfered with detection error and other factors, thus making the correlation more significant [32]. CVD mortality and environmental factor values were subject

to normalized processing (value range of [0, 1]), which was used to balance the dimensional gap of data and enable different data to be counted under the same conditions.

$$\rho = 1 - \frac{6\sum_{i=1}^{n} d_i^2}{n\left(n^2 - 1\right)}, \quad (4)$$

where ρ is Spearman's correlation coefficient, with the value range of [−1, 1], and the larger absolute value indicates the stronger correlation. n represents the number of areas of CVD mortality, and d_i represents the rank difference between dependent variable (CVD mortality) and independent variable (environmental influencing factor values).

3. Results

3.1. Basic Characteristics of CVD Deaths. A total of 469 people died of cardiovascular disease (CVD) in the study area in 2019 according to the statistics of collected death data, with the basic characteristics of death population, such as gender, age, occupation, death season, and specific diseases leading to death, shown in Table 2.

The analysis results showed that the mortality among male CVD patients was significantly higher than female patients, with a ratio of about 1.18 : 1. The elderly over 80 years accounted for 54.15% of CVD deaths, and those under 60 years only accounted for about 10%, indicating that the higher the age, the higher the mortality. Winter (December to February of the following year) and autumn (September to November) were the most frequent periods of CVD deaths, accounting for 27.93% and 27.72% of the total number of deaths, respectively, and the mortality in autumn and winter was 1.25 times higher than that in spring and summer. The largest number of CVD deaths was among the unemployed (26.01%), followed by workers (6.61%), freelancers (5.54%), and farmers (2.56%). Among the specific diseases causing death, cerebral infarction and myocardial infarction accounted for 24.09% and 19.62%, followed by coronary heart disease (17.70%).

3.2. Spatial Distribution of CVD Deaths. In 2019, there was a significant difference in the number of CVD deaths among different units in the study area. YH07 and YH08 accounted for 73.56% in terms of deaths, of which YH08 had the largest number of CVD deaths, namely 180, followed by 165 deaths in YH07 and no deaths in YH10 and YH11. The kernel density analysis of CVD deaths was conducted with ArcGIS software (Figure 4), and unit density of CVD deaths in the study area could be calculated, which could intuitively reflect the distribution of CVD deaths in a continuous area [33]. The analysis results suggested that CVD deaths were mainly distributed in the vicinity of Unit YH09 in Zhanggongshan Park and the north of Unit YH08 near the Huaihe River. The area near YH09 was an old urban area of Bengbu, characterized by high population density and serious aging. A total of 365 people died within the 1 km buffer zone of Zhanggongshan Park, accounting for 77.82% of the total deaths; moreover, the density of deaths was lower in the area farther away from Zhanggongshan Park. The north of YH08 is also a large population gathering area, close to the central city of Bengbu and Huaihe River in the east.

Among 2,744 study units, 1,053 units containing residential land (i.e., unit population greater than 0) were taken as the research samples after the outlier samples were excluded. The normalized mean value of the calculated CVD mortality values of all study units was normalized to be 0.008, with the standard deviation of 0.055, indicating that there were significant spatial differences in the CVD mortality. Global Moran's I index analysis showed that the spatial distribution of normalized mortality index was of spatial autocorrelation (Moran's $I > 0$, $Z = 2.192$, $P < 0.05$), indicating that there was a significant spatial aggregation phenomenon in the distribution of CVD deaths. In addition, there was a local spatial autocorrelation in the normalized mortality index according to the spatial distribution of LISA clustering (Figure 5), in which H-H clustering (22) was mainly distributed in the middle of YH08, forming a significant H-H clustering of CVD mortality. L-L clusters (121) were mainly distributed in YH05, YH10, and YH12, with a few scattered clusters in other units, showing more L-L clusters in the CVD mortality.

3.3. Relationship between Environmental Factors and CVD Mortality. The results of Spearman's rank correlation analysis are shown in Table 3. Among land use, road traffic, spatial form, and natural environment, there are 14 environmental factors showing significant correlation and statistical significance with CVD mortality ($P < 0.05$). There was no correlation between industry and CVD mortality ($P > 0.05$). The spatial distribution of environmental influencing factors is shown in Figure 6.

3.3.1. Land Use. The model showed that the residential density was positively correlated with the CVD mortality ($\rho = 0.127$), indicating that the higher the residential density, the higher the CVD mortality. The density of fast-food restaurants and the density of cigarette and wine shops showed a significant positive correlation with the CVD mortality in the 500 m buffer zone ($\rho = 0.287$, $\rho = 0.286$), indicating that the higher the density of fast-food restaurants and cigarette and wine shops, the higher the mortality. There was a significant negative correlation between the nearest distance to the open space and the CVD mortality ($\rho = -0.189$), indicating that the farther from the park, the lower the CVD mortality. The normalized difference vegetation index (NDVI) in January showed a significant negative correlation with CVD mortality ($\rho = -0.179$), indicating that the higher the vegetation coverage, the lower the CVD mortality.

3.3.2. Road Traffic. The model showed that the road network density and the intersections within the 500 m buffer zone were significantly positively correlated with the CVD

Table 2: Statistics of CVD death population.

Category	Classify	Death toll	Proportion of deaths (%)
Gender	Man	254	54.16
	Woman	215	45.84
Age	≥80 years old	254	54.15
	70–79 years old	109	23.24
	60–69 years	58	12.37
	<60 years old	48	10.23
Occupation	Unemployed	122	26.01
	Worker	31	6.61
	Individual operator	26	5.54
	Farmer	12	2.56
	Other	278	59.27
Dead season	Spring (March–May)	110	23.45
	Summer (June–August)	98	20.90
	Autumn (September–November)	130	27.72
	Winter (December–February of the following year)	131	27.93
Specific diseases leading to death	Cerebral infarction	113	24.09
	Cardiac infarction	92	19.62
	Coronary heart disease	83	17.70
	Encephalorrhagia	55	11.73
	Pulmonary heart disease	43	9.17
	Other	83	17.70

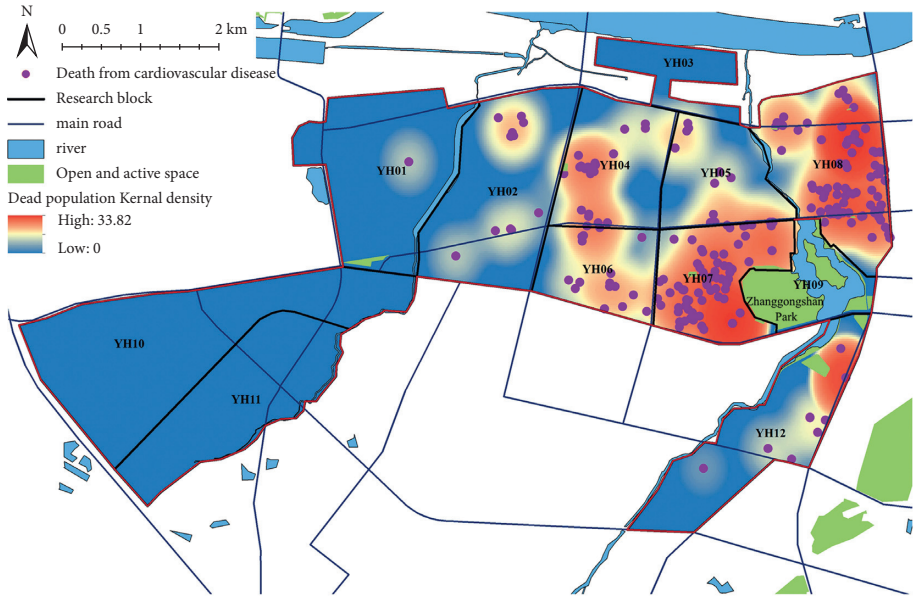


Figure 4: Distribution map of CVD death population.

mortality ($\rho = 0.138$, $\rho = 0.220$), indicating that the greater the traffic volume, the higher the CVD mortality. Meanwhile, there was a significant positive correlation between the density of bus stops and the CVD mortality within the 500 m buffer zone ($\rho = 0.238$), indicating that there was a lower risk of death among the people living in the area with sparse bus stops.

3.3.3. Spatial Form. The model showed that building density and floor area ratio were significantly positively correlated with CVD mortality, with the correlation coefficients of 0.104 and 0.115, indicating that high-density space would increase the CVD mortality.

3.3.4. Natural Environment. There was a significant positive correlation between the distance to the nearest river and the CVD mortality ($\rho = 0.121$), indicating that the closer to the river, the lower the CVD mortality. The average annual $PM_{2.5}$ and PM_{10} were significantly positively correlated with the CVD mortality, with the correlation coefficients of 0.088 and 0.072, indicating that the higher the average annual particulate matter (PM) concentration, the higher the CVD

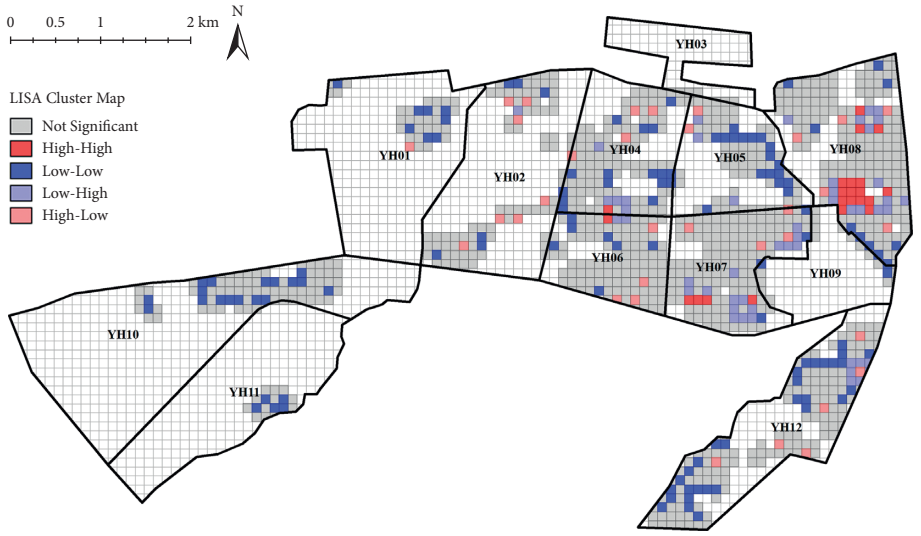


Figure 5: Spatial autocorrelation distribution of CVD normalized mortality index.

Table 3: Correlation between environmental factors and CVD mortality.

Category	Subcategory	Variable	P (correlation coefficient)	P value (double side)
Land use	Live	Residential density	0.127*	0.000
	Business	Density of fast-food restaurants in 500 m buffer zone	0.287**	0.000
		Density of tobacco and liquor stores in 500 m buffer zone	0.286**	0.000
	Industry	Distance from the nearest industry	-0.011	0.717
	Open the activity space	Distance from the nearest open space	−0.189**	0.000
	Vegetation cover	Normalized difference vegetation index (NDVI)	−0.179**	0.000
Road transport	Traffic	Road network density	0.138**	0.000
		Road intersection density in 500 m buffer zone	0.220**	0.000
	Bus stop	Density of bus stops in 500 m buffer zone	0.238**	0.000
Spatial form	Building density	Building coverage	0.104**	0.001
	Volume fraction	Volume fraction	0.115**	0.000
Natural environment	River	Distance from the nearest river	0.121**	0.000
	Particulate matter (pm)	Average annual $pm_{2.5}$	0.088**	0.004
		Average annual pm_{10}	0.072*	0.020
	(Ground) surface temperature	Surface temperature in January 2019	−0.135*	0.000

* $P < 0.05$, ** $P < 0.01$.

mortality. The average temperature was negatively correlated with the CVD mortality, with a correlation coefficient of -0.135, indicating that the lower the temperature in winter would contribute to the increase in the CVD mortality.

4. Discussion

(1) The characteristics of CVD deaths were significant and of spatial clustering.

Consistent with the conclusions of previous international statistical studies, the CVD deaths were characterized as follows: male deaths were more than females; the mortality is higher in those of higher age; most of them are unemployed; and cardiocerebral infarction was the main cause of death. In addition, the deaths were mainly distributed in the old urban area, and there was a significant spatial clustering phenomenon [34]. Previous studies have shown that alcohol abuse [35] and smoking [36] can affect the cardiovascular system, and males are more likely to do alcohol abuse and smoking than females, causing the difference in mortality. The risk of cardiac arteriosclerosis will increase with age; that is, the mortality is higher in those of higher age [37]. Working can reduce the risk of CVD [8], and the risk of CVD is lower in residents engaged in manual work, but higher in those unemployed. Low temperature and sudden drop in air temperature will

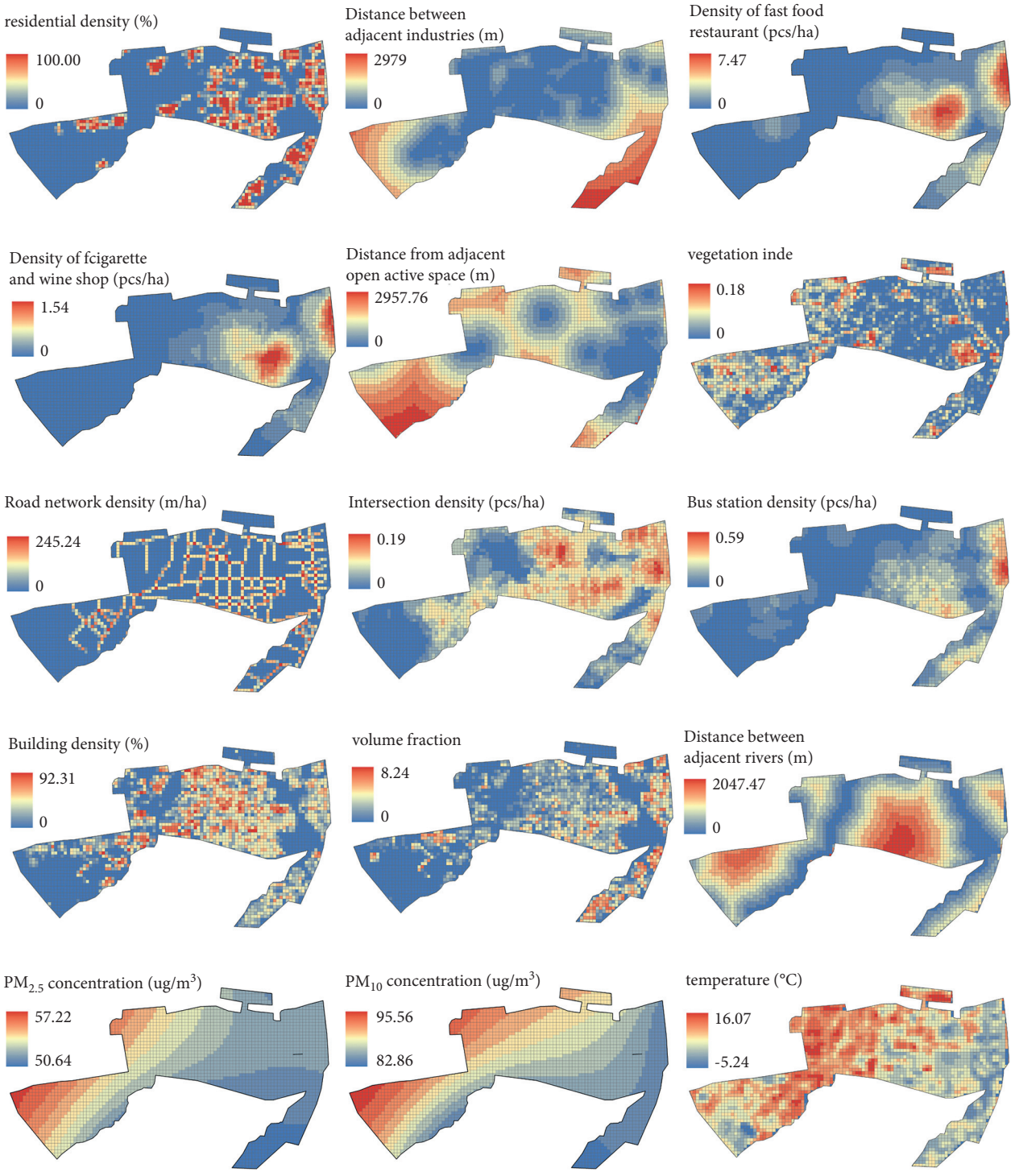


Figure 6: Spatial distribution of environmental influencing factors.

cause vasoconstriction and elevated blood pressure of human body, increasing the risk of sudden myocardial infarction [23, 24]; therefore, autumn and winter are the seasons of high incidence of CVD, and the mortality is higher in the urban areas with lower urban temperature [38].

(2) The higher density of restaurants and cigarette and wine shops will increase the CVD mortality.

It has been further confirmed in this study that the density of restaurants and smoking restaurants around the residential area showed a significant positive correlation with the CVD mortality. The daily activity distance that can meet the basic material and life needs of residents by 10-min walking is 500 m [39]. Handy et al. [40] found that the frequency of walking to businesses was positively

correlated with the number of businesses within the service radius; therefore, people in the areas with highly dense restaurants and cigarette and wine shop will have higher probability of dining out and buying cigarettes and wines. In the study area, located in northern Anhui, the restaurant diet contains high fat and salt, and the dense dining facilities will bring more cooking fumes, sewage, and other environmental pollution, in which a lot of fat and cholesterol oxide [17]will lead to hypertension, hyperlipidemia, and other metabolic disorder CVD, and the increased probability of buying alcohol and tobacco will raise the risk of alcoholism, thereby causing sudden death [17].

(3) The influence of environmental factors related to particulate matter concentration on the CVD mortality.

Consistent with the conclusion of previous studies abroad, long-term exposure to high levels of pollutants will affect the human circulatory system [41], thereby inducing CVD mortality. According to the data of disease burden from Barcelona, Spain, it was estimated that 849 cases of CVD could be prevented each year if the exposure level of air pollution could be reduced to the WHO recommended level [42]. There is a higher risk of death for residents in areas with high concentrations of particulate matter. The finding is further confirmed in this study: the increased traffic volume [43], dense bus stops [44], and dense residential and spatial forms [45, 46], low green space coverage [47], and longer distance from rivers [47] can increase the CVD mortality, of which the possible reason may be associated with the increased concentration of local particulate matter and other noise pollution and psychological harm.

(4) Discussion on the correlation between industrial and open activity space and CVD mortality.

Different from general studies, it is found that there is no significant relationship between CVD mortality and industry in this study, for which reason may lie in that northeasterly wind is the most prevalent in the study area throughout the year, and there are few residential areas located downwind of industry, only accounting for less than 10% of the study units; therefore, the influence of industry on the study unit is not significant. Meanwhile, this study also reveals that CVD mortality is lower in the areas farther from open space area, and the possible reason is that the study area is an old urban area that lacks green space, there are only 3 parks with the area of more than 1 ha within or 500 m from the study area (aggregated distribution), and there is relatively little activity space, which also is the common fault of an old urban area. The elderly are at high risk of dying from CVD, and they will deliberately choose the area around the open activity space when choosing housing, which will have a certain impact on the conclusion.

5. Conclusions and Prospects

To explore the distribution characteristics of cardiovascular disease (CVD) in urban residents and the environmental influencing factors, this study analyzed the basic characteristics and spatial distribution characteristics of CVD death population, explored the correlation between multiple environmental factors and CVD mortality, and revealed the factors affecting the risk of death and its mechanism, with the main conclusions as follows:

(1) The correlation study conducted in this study is of good scientific nature and research significance, and the conclusions are consistent with international studies. Therefore, the study methods can provide some research ideas for the construction of healthy cities in the Huaihe River Basin or other regions.

(2) With obvious characteristics, CVD deaths are mainly distributed in the vicinity of Unit YH09 in Zhanggongshan Park and the north of Unit YH08 near the Huaihe River. Therefore, attention should be paid to the key areas with the maximum number of CVD deaths and the population at high risk, and medical input should be increased to reduce the death risk.

(3) Because long-term exposure to high pollutants in the environment will cause CVD death, the following measures can be taken to reduce the CVD mortality in the construction of healthy cities in the future: increase traffic arterial roads around residential areas to reduce the traffic volume and vehicle exhaust emissions in residential areas; increase open space to reduce living and spatial density; plant more plants and building more rivers to reduce the local air pollution; and make dispersed layout of commercial facilities, such as restaurants and cigarette and wine shops, around residential areas to effectively reduce the risk of CVD death. Meanwhile, attention should also be paid to the influence of the areas with a higher density of the elderly on the analysis results.

Appropriate urban planning and policies can improve the active health interventions in cities and reduce the CVD mortality. To a certain extent, it can also provide more research perspectives for the construction of healthy cities in the future, and promote the development of healthy cities. In addition, this study is based on panel data, and little consideration is given to the changes of built environment and CVD mortality caused by time changes, so time series related research will be carried out in the future. At the same time, different lifestyles will affect CVD mortality, so further research on the correlation between residents' lifestyles and CVD mortality will be conducted in the future.

Data Availability

The datasets used during this study are available from the corresponding author on reasonable request.

Disclosure

An earlier version of this work was presented as an abstract at 57th ISOCARP World Planning Congress, 2021.

Conflicts of Interest

The authors declared that they have no conflicts of interest in this work.

Acknowledgments

This research was funded by Natural Science Foundation of Anhui Province with grant reference no. 2008085ME160.

References

[1] H. Beltránsánchez, S. Soneji, and E. M. Crimmins, "Past, present, and future of healthy life expectancy," *cold spring harbor perspectives in medicine*, vol. 5, no. 11, 2015.

[2] H. H. A. Kyu, D. Abate, K. H. Abay et al., "Global, regional, and national disability-adjusted life-years (DALYs) for 359 diseases and injuries and healthy life expectancy (HALE) for 195 countries and territories, 1990–2017: a systematic analysis for the Global Burden of Disease Study 2017," *The Lancet*, vol. 392, pp. 1859–1922, Article ID 10159, 2018.

[3] S. S. A. S. Jiaying Zhao, "Timing of urbanisation and cardiovascular risks in Thailand: evidence from 51 936 members of the Thai cohort study, 2005–2009," *Journal of Epidemiology*, vol. 24, no. 6, pp. 484–493, 2014.

[4] S. Rani and W. Anthony, "Current levels of salt knowledge: a review of the literature," *Nutrients*, vol. 6, no. 12, pp. 5534–5559, 2014.

[5] Y. Xu and F. Wang, "Built environment and obesity by urbanicity in the US," *Health & Place*, vol. 34, pp. 19–29, 2015.

[6] D. W. Barnett, A. Barnett, A. Nathan, J. V. Cauwenberg, A. Barnett, and au fnm, "Built environmental correlates of older adults' total physical activity and walking: a systematic review and meta-analysis," *International Journal of Behavioral Nutrition and Physical Activity*, vol. 14, 2017.

[7] M. Stevenson, J. Thompson, S. á. De et al., "Land use, transport, and population health: estimating the health benefits of compact cities," *Lancet*, vol. 388, pp. 2925–2935, 2016.

[8] R. Ewing, G. Meakins, S. Hamidi, and A. C. Nelson, "Relationship between urban sprawl and physical activity, obesity, and morbidity – update and refinement," *Health & Place*, vol. 26, pp. 118–126, 2014.

[9] F. Ballester, J. Tenias, and M. Perez-Hoyos, "Air pollution and emergency hospital admissions for cardiovascular diseases in Valencia, Spain," *Journal of Epidemiology & Community Health*, vol. 55, pp. 57–65, 2001.

[10] Y. Guo, J. P. Teixeira, and N. Ryti, "Ambient particulate air pollution and daily mortality in 652 cities," *New England Journal of Medicine*, vol. 381, no. 8, pp. 705–715, 2019.

[11] M. E. Héroux, H. R. Anderson, R. Atkinson, B. Brunekreef, and H. Walton, "Quantifying the health impacts of ambient air pollutants: recommendations of a WHO/Europe project," *International Journal of Public Health*, vol. 60, no. 5, 2015.

[12] M. Oh, K. Shin, K. Kim, and J. Shin, "Influence of noise exposure on cardiocerebrovascular disease in Korea," *The Science of the Total Environment*, vol. 651, pp. 1867–1876, 2018.

[13] R. D. Brook, S. Rajagopalan, C. A. Pope, J. R. Brook, and J. D. Kaufman, "Particulate matter air pollution and cardiovascular disease: an update to the scientific statement from the American Heart Association," *Circulation*, vol. 121, no. 21, pp. 2331–2378, 2010.

[14] C. Hong-han, C. Hong-wei, H. F. Jiang-tao, L. Zhao-li, S. Bing, and S. Jing, "Health-based risk assessment of contaminated sites:Principles and methods," *Earth Science Frontiers*, vol. 13, no. 001, pp. 216–223, 2006.

[15] W. Lan, J. Xiji, S. Wenyao, Z. Xiaojing, and T. Jian, "Impact of urban built environment on respiratory health and its planning strategy: a case study of a district in shanghai," *China City Planning Review*, vol. 42, no. 06, pp. 15–22, 2018.

[16] S. S. Mehraj, G. A. Bhat, H. M. Balkhi, and T. Gul, "Health Risks for Population Living in the Neighborhood of a Cement Factory," *Academic Journals*, vol. 7, no. 12, pp. 1044–1052, 2013.

[17] T. D. K. Y. Fei-hong, "Analysis on oil fume particles in catering industry cooking emission," *Environmental science*, vol. 33, no. 006, pp. 1958–1963, 2012.

[18] P. Malambo, A. P. Kengne, A. De Villiers, E. V. Lambert, and T. Puoane, "Built environment, selected risk factors and major cardiovascular disease outcomes: a systematic review," *PLoS One*, vol. 11, no. 11, 2017.

[19] W. Babisch, "Road traffic noise and cardiovascular risk," *Noise and Health*, vol. 10, no. 38, pp. 27–33, 2008.

[20] W. D. Douglas, "Epidemiologic evidence of cardiovascular effects of particulate air pollution," *Environmental Health Perspectives*, vol. 109, pp. 483–486, 2001.

[21] M. Furuuchi, T. Murase, M. Yamashita et al., "Temperature distribution and air pollution in phnom penh, Cambodia-influence of land use and the mekong and tonle sap rivers," *Aerosol and Air Quality Research*, vol. 6, no. 2, pp. 134–149, 2006.

[22] S. Valdés, C. M. Araque, F. G. Torres et al., "Ambient temperature and prevalence of obesity in the Spanish population: the D i@bet.es study," *Obesity*, vol. 22, no. 11, 2014.

[23] K. Bhaskaran, S. Hajat, A. Haines, E. Herrett, P. Wilkinson, and L. Smeeth, "Short term effects of temperature on risk of myocardial infarction in England and Wales: daily time series regression analysis of the Myocardial Ischaemia National Audit Project (MINAP) registry," *BMJ British Medical Journal*, vol. 341, no. 7768, 2010.

[24] J. A. Patz, D. Campbell-Lendrum, T. Holloway, and J. A. Foley, "Impact of regional climate change on human health. Nature 438: 310-317 (17 november)," *Nature*, vol. 438, no. 7066, pp. 310–317, 2005.

[25] Y. Xu and L. Wang, "GIS-based analysis of obesity and the built environment in the US," *Cartography and Geographic Information Science*, vol. 42, no. 1, pp. 9–21, 2015.

[26] H. M. GriffithsC, G. M. A. Jordan, and H. Saunders, "Neighbourhood typologies and associations with body mass index and obesity: a cross-sectional study," *Preventive Medicine: An International Journal Devoted to Practice and Theory*, vol. 111, pp. 351–357, 2018.

[27] P. Zhang, J. Lee, G. Kang et al., "Disparity of nitrate and nitrite in vivo in cancer villages as compared to other areas in Huai River Basin, China," *The Science of the Total Environment*, vol. 612, pp. 966–974, 2018.

[28] Y. Juna, "Research on the spatial pattern of population destribution in the Huaihe River basin," *Journal of Xinyang Normal University*, vol. 30, no. 1, pp. 525–528, 2014.

[29] T. W. Hwang and F. B. Wang, "Dynamics OF a dengue fever transmission model with crowding effect IN human

population and spatial variation," *Discrete and Continuous Dynamical Systems - Series B*, vol. 1, no. 1, pp. 147–161, 2013.

[30] C. Varga, D. L. Pearl, S. A. Mcewen, J. M. Sargeant, F. Pollari, and M. T. Guerin, "Area-level global and local clustering of human Salmonella Enteritidis infection rates in the city of Toronto, Canada, 2007–2009," *BMC Infectious Diseases*, vol. 15, no. 1, p. 359, 2015.

[31] G. A. Colditz, W. C. Willett, M. J. Stampfer et al., "The influence of age, relative weight, smoking, and alcohol intake on the reproducibility of a dietary questionnaire," *International Journal of Epidemiology*, p. 392, 1987.

[32] W. Xiaoyanl and L. Meizhou, "The relationship of rank correlation coefficient and spearman rank correlation coefficient," *Journal of Guangdong Industry Technical Colleg*, vol. 5, no. 004, pp. 26-27, 2006.

[33] D. Khosrow, "Density estimation for statistics and data analysis," *Technometrics*, vol. 29, no. 4, p. 495, 2012.

[34] C. T. Y. Y. Liu Jie, "Exploratory spatial data analysis of patients with acute myocardial infarction from 2007 to 2014 year in Yangpu District, Shanghai," *Chin J Evid Based Cardiovasc Med*, vol. 8, no. 4, pp. 464–467, 2016.

[35] X. H. Ning, W. A. C. Cuan, and G. Hong, "Further research into relationship between alcohol consumption and plasma homocysteine," *Adv Cardiovasc Dis*, vol. 31, no. 03, pp. 445–448, 2010.

[36] S. Qian, Z. Nanbo, Y. Canqing, G. Yu, B. Zheng, and L. J. Chen Zhengming, "Sex-specific associations between tobacco smoking and risk of cardiovascular diseases in Chinese adult," *Chinese Journal of Epidemiology*, vol. 39, no. 001, pp. 8–15, 2018.

[37] L. Liu, J. G. Wang, L. Gong, G. Liu, and J. A. Staessen, "Comparison of active treatment and placebo in older Chinese patients with isolated systolic hypertension: Systolic Hypertension in China (Syst-China) Collaborative Group," *Journal of Hypertension*, vol. 16, no. 12, p. 1823, 1998.

[38] L. Q. Z. Z. Liu Xue-en, "Influence of temperature and cold air on mortality of cardio -and cerebral vascular diseases," *CHINA PUBLIC HE ALTH*, vol. 18, no. 8, 2002.

[39] L. Meng, "The planning strategies of a 15- minute community life circle based on behaviors of residents," *Urban Planning Forum01)*, vol. 1, pp. 111–118, 2017.

[40] S. Handy, X. Cao, and P. L. Mokhtarian, "Self-selection in the relationship between the built environment and walking: empirical evidence from northern California," *Journal of the American Planning Association*, vol. 72, no. 1, pp. 55–74, 2006.

[41] D. F. M. M. Chuan, "Association between ambient PM 10 / PM 2.5 levels and population mortality of circulatory diseases: a case-crossover study in Beijing," *Journal of Peking University*, vol. 45, no. 03, pp. 398–404, 2013.

[42] N. Mueller, D. Rojas-Rueda, X. Basagaa et al., "Health impacts related to urban and transport planning: a burden of disease assessment," *Environment International*, vol. 107, pp. 243–257, 2017.

[43] R. Sinharay, J. Gong, B. Barratt et al., "Respiratory and cardiovascular responses to walking down a traffic-polluted road compared with walking in a traffic-free area in participants aged 60 years and older with chronic lung or heart disease and age-matched healthy controls: a randomised, crossov," *Lancet (London, England)*, vol. 391, pp. 339–349, Article ID 10118, 2020.

[44] L. Zhao, X. Wang, Q. He et al., "Exposure to hazardous volatile organic compounds, PM10 and CO while walking along streets in urban Guangzhou, China," *Atmospheric Environment*, vol. 38, no. 36, pp. 6177–6184, 2004.

[45] L. Schweitzer and J. Zhou, "Neighborhood air quality, respiratory health, and vulnerable populations in compact and sprawled regions," *Journal of the American Planning Association*, vol. 76, no. 3, pp. 363–371, 2010.

[46] B. Tong, H. Lijian, H. Liang et al., "Impact of urban air pollution on surrounding areas in Beijing , Tianjin , and Hebei Provinces," *Acta Ecologica Sinica*, vol. 038, no. 012, pp. 4268–4275, 2018.

[47] D. Wang, K. L. Lau, R. Yu, S. Wong, T. Kwok, and J. Woo, "Neighbouring green space and mortality in community-dwelling elderly Hong Kong Chinese: a cohort study," *BMJ Open*, vol. 7, no. 7, 2017.

Environ. Eng. Res. 2022; 27(2): 200559
https://doi.org/10.4491/eer.2020.559

pISSN 1226-1025
eISSN 2005-968X

Research

Exploring coupling effect between urban heat island effect and $PM_{2.5}$ concentrations from the perspective of spatial environment

Yunhao Fang[1], Kangkang Gu[1,2†]

[1]*School of Architecture and Planning, Anhui Jianzhu University, Hefei 230022, China*
[2]*Anhui Collaborative Innovation Center for Urbanization and Construction, Hefei 230022, China*

ABSTRACT

The coupling effect between urban $PM_{2.5}$ concentrations and urban heat island effect has been paid more and more attention to. Previous studies mostly focused on the analysis of data correlations, lacking the interpretation of the formation texture. Taking Hefei as the subject, this study combined the spatial statistical model with the coupling coordination degree model to explore the influence of spatial environment-related indicators on the coupling effect of cities. In addition, at the micro level, the paper used grid unit to verify the relevance and made a comprehensive analysis on the formation texture of coupling effect. The results indicated that: (1) there is a significant coupling effect between the urban heat island intensity and $PM_{2.5}$ concentrations in the main urban area of Hefei with significant spatial heterogeneity. (2) to some extent, the indicators of urban spatial environment, including vegetated areas, buildings, residential land, commercial land, industrial land, building density, floor area ratio, building form ratio, the densities of road junctions and sub-arterial roads, have different effects on the coupling effect. In general, the higher the degree of human activity, the higher the degree of coupling effect. (3) the coupling effect may be influenced by a variety of spatial environment factors.

Keywords: Coupling coordination degree model, $PM_{2.5}$, Spatial statistical model, Urban heat island effect, Urban planning strategy, Urban spatial environment

1. Introduction

Climatic problems in cities are becoming increasingly serious, most which are urban heat island effect and air pollution [1, 2]. Multiple studies have confirmed that excessive heat and air pollution particles in the city such as $PM_{2.5}$ (particulate matter in the air that is less than 2.5 mm in aerodynamic diameter) will continue to affect the lives of the residents, and, in turn, lead to greater health risks [3-6]. Research on urban heat island and urban air quality has become a heated topic in relevant research.

Researchers in different fields are trying to find a solution to the urban heat island intensity (UHII) and air pollutant concentrations [7-10]. Part of the results indicate that there is a close coupling effect between the UHII and urban air pollutant concentrations, which has been confirmed by relevant research [11-13]. For instance, Estournel et al. [14] found out that the temperature of urban and rural areas in Toulouse varies with the aerosol based on the results of solar radiation. Similar results are reported by Jauregui and Luyando for Mexico City [15], Robaa for the Greater Cairo region and Wang et al. for Beijing [16, 17]. Total Suspended Particles (TSP) plays an important role in the UHII as well [18, 19]. Furthermore, this process depends on the urban form, e.g. on the multiple bounces that may occur inside canyons. In turn, temperature determines the concentration of aerosols. For example, Sarrat et al. [20] studied the results of Paris, proving urban heat islands change the spatial distribution of regional pollutants (ozone and nitrogen oxides) by changing the atmospheric boundary layer. Besides, ozone is produced by the photooxidation of VOC_S in the presence of nitrogen oxides (NO_X) [21]. Based on related research, the cluster effect is governed by the amount of population, which

This is an Open Access article distributed under the terms of the Creative Commons Attribution Non-Commercial License (http://creativecommons.org/licenses/by-nc/3.0/) which permits unrestricted non-commercial use, distribution, and reproduction in any medium, provided the original work is properly cited.

Copyright © 2022 Korean Society of Environmental Engineers

Received October 09, 2020 **Accepted** February 02, 2021

† Corresponding author
E-mail: kangkanggu@163.com
Tel: +86-0551-15855118329
ORCID: 0000-0001-7606-9651

is typically larger over dense urban areas [22]. Some researchers also used regression analysis to explore the correlation between changes in SO_2 and NO_2 concentrations and temperature from the perspective of data analysis [23]. However, the method only considers the influence of numerical value, ignoring the connections among various factors in the region [24-26]. Therefore, some scholars used the method of spatial statistics to combine the spatial distribution of air pollution and thermal pollution and performed correlation analysis because such method incorporates spatial factors in the analysis and can consider the impact of air pollution or thermal pollution on its neighborhood [27, 28].

With the understanding of climate issues deepens, the research focus on the relationship between the UHII and air pollutant concentrations has gradually shifted to forming texture. Theoretically, on the one hand, the temperature difference between urban areas and suburbs has led to atmospheric circulation and the pollutants removal, which has affected the distribution of pollutants [29, 30]. On the other hand, the spatial distribution of air pollutant concentrations indirectly affects the UHII by influencing the radiation within the city [31, 32]. And when the air quality is poor, the high concentration of pollutants reduces the radiation from the sun to the ground during the day and the long-wave radiation from the ground at night, thus reducing the heat emission, leading to the temperature rise in the city. In addition, some studies have shown that pollutants in the air will result in cooling [33]. The reason is that the "dust dome" formed by excessive particulate matter will affect the solar radiation, which will lead the temperature to drop [34, 35].

However, UHII and air pollution are not only the opposite side of the synergistic effect, the process of which is also affected by the underlying surface spatial environment [36]. Although a large number of studies in the past have shown that UHII or air pollution is related to the spatial environment, they all indicate the relationship between the two. For example, Yuan et al. [28] used the spatial measurement model to explore the impact of $PM_{2.5}$ and built environment, while Yin et al. [27] explored the impact of urban form and urban heat island effect. In a word, they focused on the spatial environment but neglected its impact on the interaction between UHII and air pollution.

The purpose of this study is to analyze the interaction between urban heat island and air pollution according to spatial environment in order to improve urban climate and human settlements. Accordingly, we choose the main urban area of Hefei as the subject research object and try to explore the influence of urban spatial environment on the coupling effect of UHII and $PM_{2.5}$ by combining the coupling coordination degree model and spatial statistical model. In addition, we also used the combined perspective of macro and micro to give further guidance on the optimization of urban spatial environment.

2. Research Area and Methods

2.1. Research Area

Hefei (116°41′E-117°58′E, 30°57′N-32°37′N) lies in the eastern China, the middle latitude zone (Fig. 1). The terrain mostly consists of

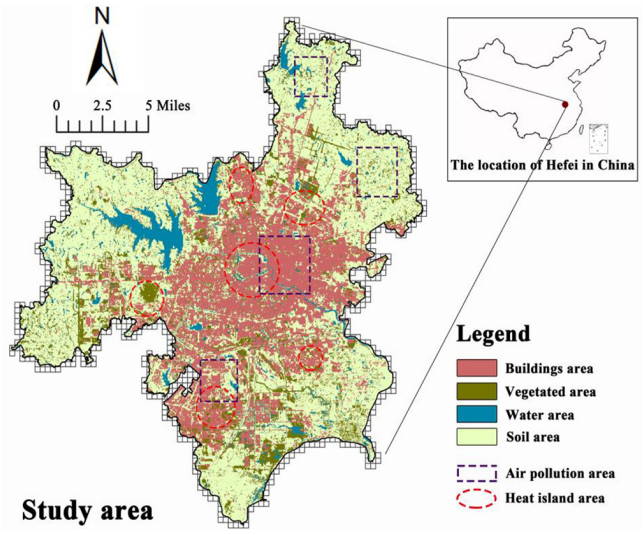


Fig. 1. Location and study area.

plains, hills and mountains. It has humid subtropical climate, with distinctive four seasons and an annual temperature average of 15.7℃. Its average annual precipitation is about 1,000 mm, and relative humidity 77%. An annual mainstream prevails north and northwest throughout the year. In the end of 2018, the number of the permanent residents in Hefei reached 8.087 million, and the building area 460 km^2. In recent years, with the expansion of cities and the increase in construction intensity, haze weather condition in urban areas has increased. According to the 2016 World Health Organization (WHO)'s air pollution statistics on Chinese cities, Hefei has serious air pollution, ranking 14th worst. In addition, the phenomenon of urban heat islands has intensified year by year, especially the long-lasting high temperature in summer. The data from China National Meteorological Observation Station showed that the average annual temperature increased in urban areas by 0.89℃/10 years, compared to the 0.44℃/10 years after 2,000 in the suburban areas, and the gap showed a trend of increasing. In general, the urban air pollution problem and the urban heat island effect have become the two major climatic problems in Hefei, and their interaction and impact pose a threat to the living environment of the urban residents.

2.2. Research Methods and Data

This study focused on the urban spatial environment and its influence on the interaction degree between thermal environment and air pollution. As Fig. 2 showed, we took the main urban area of Hefei as a sample and divided it into a grid of 500 m * 500 m. Urban remote sensing data and related urban air quality data were used to calculate UHII and $PM_{2.5}$ concentrations. It was worth noting that UHII referred to UHII at the surface rather than UHII in the atmosphere. Specifically, we analyzed the relationship between UHII and $PM_{2.5}$ concentrations through the coupling coordination degree model, and analyzed the size of the UHII -$PM_{2.5}$ coupling result CCD. Furthermore, spatial statistical model was used to explore the link between CCD and four spatial environmental

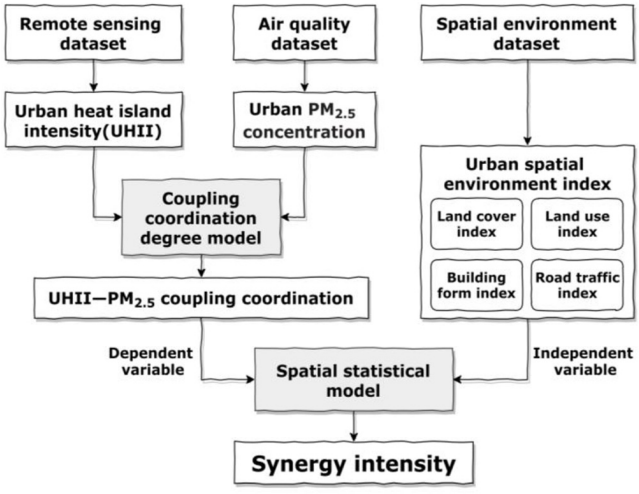


Fig. 2. Flowchart of the study.

indicators (including land cover indicators, land use indicators, building form indicators and road traffic indicators). Finally, we supplemented the effects of the mixed effects of spatial environmental indicators and other indicators uncovered in the analysis on the micro scale.

2.2.1. Urban heat indicators and air pollution indicators

Considering $PM_{2.5}$ and UHII in Hefei spring are obvious and easy to interact with others, we selected the data of April 2018 as samples for spatial processing. The sources and selection methods of each data are as follows:

Based on the remote sensing image data, we selected the Landsat8 Thermal Infrared Sensor (TIRS) data (https://atmcorr.Gsfc.nasa.gov/) at 2:42 am on April 11, 2018, which was a date with less cloud cover and no rainfall. At the same time, the atmospheric visibility was high, and it had the conditions for good surface temperature inversion [37, 38]. For the calculation of surface UHII, we used atmospheric correction. Landsat8 TIRS data were processed using Envi5.3 software to invert the surface temperature. This removed the effects of atmospheric radiation on the surface based on real-time atmospheric sounding data to obtain a true ground heat radiation intensity [39, 40]. The algorithm also considers that the thermal infrared radiation brightness value (L_λ) comprises of the atmospheric upward radiance (L_u), the atmospheric downward radiance (L_d) and the true radiation received by satellite sensor from the ground.

$$L_\lambda = [\varepsilon L_T + (1-\varepsilon)L_d]\tau + L_u \quad (1)$$

where ε is the surface specific emissivity; L_T is the radiant brightness of a black body with temperature (T (K)) in the thermal infrared band; τ is the atmospheric transmittance, which can be obtained using online values of L_u and L_d. Based on the L_T obtained from the formula (1), the surface temperature (T_s) was obtained using formula (2). The relevant parameters for each satellite are given in Table 1.

$$T_s = K_2/ln[1 + K_1/L_T] \quad (2)$$

Table 1. Parameters Used in the Radiative Transfer Equation-Based Method

Landsat type	K_1 /(W/(m^2·sr·μm))	K_2/K
Landsat 5	607.76	1,260.56
Landsat 7	666.09	1,282.71
Landsat 8	774.89	1,321.08

The heat island intensity was then calculated using the UHI intensity index (UHII) algorithm, and the UHI scale index formula is shown in formula (3).

$$UHII_i = T_i - \frac{1}{n}\sum_1^n T_{crop} \quad (3)$$

where $UHII_i$ is the heat island intensity corresponding to the ith pixel on the image; T_i is the surface temperature; n is the number of effective pixels in the suburban farmland; and T_{crop} is the surface temperature in the suburban farmland, which is meant to the average surface temperature of all surrounding agricultural and forest land.

$PM_{2.5}$, as the most commonly used air pollution detection indicator, can reflect the degree of urban air pollution [41]. The higher the $PM_{2.5}$ concentration, the higher the air pollution indicator, and the greater the harm to the human health [5]. At present, the 10 state-controlled ambient air automatic monitoring stations in Hefei cannot evaluate the spatial distribution of $PM_{2.5}$, and large-scale monitoring is not in line with the reality. However, related studies have shown that remote sensing images are of importance to the study of the spatial distribution of $PM_{2.5}$ in cities, especially in built-up areas [28, 42]. Specifically, the method combined aerosol optical depth (AOD) data with the scattering characteristics of the aerosol vertical profile through a CEOS-Chem transport simulation with good precision (r2 = 0.81; slope = 0.68) [43]. Therefore, we used this method to obtain 2018 $PM_{2.5}$ data from Atmospheric Composition Analysis Group (http://fizz.phys.dal.ca/~atmos/martin/?page_id=140) in Hefei. The study obtained processed China-wide $PM_{2.5}$ raster data from the above website, calibrated and adjusted by ArcGIS Software. In addition, we also clipped high-precision $PM_{2.5}$ spatial distribution data within the main urban area of Hefei.

2.2.2. Urban spatial environment-related indicators

In the study, the selection of spatial environmental indicators included two aspects that affect urban air environment and urban thermal environment. Specifically, we summarized four types of indicators: land cover, land use, building form, and road traffic to reflect the urban spatial environment through Geographic Information System (GIS) (Table 2). In addition, 500 m * 500 m grids in Hefei were selected as samples.

Land cover indicators influence urban climate through transpiration of vegetation and radiation of hardened land surface [44, 45]. It was obtained from high resolution remote sensing data. In this study, vegetated areas, waters, buildings and soils were counted in the study area, respectively.

The proportions of different land use indicators were used to reflect urban functions in each grid [46, 47]. We used Hefei urban planning dataset in 2016 to represent land use indicators because of the accuracy of their classification. Based on this, we counted

Table 2. Statistics of All the Variables

Category	Metrics	Min	Max	Mean	Std.D	Note
UHII	——	19.14	47.96	33.36	3.95	——
$PM_{2.5}$	——	55.23	115.07	78.95	4.15	——
Land cover	Vegetated areas	0	1.00	0.19	0.08	Sum of forest and grassland
	Waters	0	1.00	0.09	0.06	Sum of rivers, reservoirs and lakes
	Buildings	0	0.32	0.05	0.09	——
	Soils	0	0.54	0.27	0.29	——
Land use	AL	0	1.00	0.04	0.12	Administration land
	BL	0	0.92	0.02	0.08	Business land
	RL	0	0.97	0.10	0.19	Residential land
	ML	0	1.00	0.09	0.21	Industrial land
Building form	BH	0	90.00	7.39	12.86	Building height (m)
	BD	0	0.52	0.05	0.09	Building density (%)
	FAR	0	4.71	0.29	0.54	Floor area ratio
	BFR	0	0.97	0.15	0.21	Building form ratio
Road traffic	AD	0	2.00	0.35	0.08	Arterial road density (km/km^2)
	SAD	0	2.00	0.75	0.14	Sub-arterial road density (km/km^2)
	RJD	0	5.70	1.03	0.26	Road junction density

four types of indicators, including administration land (AL), business land (BL), residential land (RL), and industrial land (ML).

Building form indicators, including building height (BH), building density (BD), floor area ratio (FAR), and building form ratio (BFR), can not only change the ventilation performance of the block, but also affect the pollutant concentration and surface temperature around the buildings [48, 49]. They were also obtained from the Hefei urban planning dataset in 2016. It was worth noting that what we calculated was the average value within the grid, where BH and BD reflected the average height and density within the unit grid, FAR reflected the ratio of the total building area within the unit grid to the land area, and BFR reflected the ratio of the building surface area within the unit grid to the total volume.

Road traffic indicators reflected the influence of automobile exhaust emissions on street air and surface temperature [50]. We obtained the relevant vector from OpenStreetMap (http://download.geofabrik.de/), as the arterial road data and the sub-arterial road data. Based on this, we conducted intersection processing with road data through 500 m * 500 m grids in ArcGIS software to calculate the length of all arterial roads and sub-arterial roads in each grid. The ratio of the length to the area of all arterial roads in the grid will be regarded as the arterial road density (AD), and the ratio of the length to the area of all sub-arterial roads in the grid will be the sub-arterial road density (SAD). In addition, the study also counted the number of road intersections in the cell grid and set it as the road junction density (RJD).

2.2.3. Coupling coordination degree (CCD) model

The coupling coordination degree (CCD) of UHII-$PM_{2.5}$ represented the degree of interaction between urban thermal environment and urban air environment through different spatial elements. Besides, CCD ignores the pros and cons of the elements, which indicates the benign coupling in the interaction process, that is, the CCD performs numerical normalized analysis on the elements in the model [51]. The larger the value, the greater the degree of interaction between them [52]. In this study, CCD calculation was derived from remote sensing data and air quality data in April 2018. The consistency of the timing sequence avoids the construction indicators conflict, thus ensuring the accuracy of coupling results. By establishing a CCD model, we can not only explain the state of UHII and $PM_{2.5}$, but also analyze the texture and mechanism of interaction in the spatial environment. The CCD was calculated using the following expression:

$$C = 2 \times \left[\frac{U_1 \times U_2}{(U_1 + U_2)^2}\right]^{0.5} \tag{4}$$

$$T = aU_1 + bU_2 \tag{5}$$

$$CCD = (C \times T)^{0.5} \tag{6}$$

Where the *CCD* is between 0 and 1, a larger value indicates a stronger interaction between the UHII and $PM_{2.5}$ concentration; C is the general coupling degree, which can only reflect the strength of the interaction, but cannot filter out benign coupling. For example, when both $PM_{2.5}$ concentration and UHII are at a low level, there is also a high degree of coupling. Overall, it is difficult to reflect an accurate interaction compared to the *CCD*; T is the comprehensive evaluation value of $PM_{2.5}$ concentration and UHII; a and b are parameters to be determined. In this study, $a = b$ is set, which indicates that $PM_{2.5}$ concentration is as important as the UHII in the CCD model; U_1 represents the normalized value of UHII and

U_2 the normalized value of $PM_{2.5}$ concentration. Because of the inconsistency of dimensions, the above factors should be normalized with the following formula:

$$U_i = \frac{U - U_{min}}{U_{max} - U_{min}} \quad (7)$$

where U_i is a normalized value for the ith pixel (500 m spatial resolution), U represented the value of the $PM_{2.5}$ concentration or UHII, and U_{min} and U_{max} are the minimum and maximum values of these factors, respectively.

2.2.4. Spatial statistical model

The spatial statistical model was used because it incorporated spatial factors in statistical analysis, which made the results more accurate [25, 53]. Compared with traditional statistical methods (such as the Spearman correlation), the spatial statistical model can take into account the heat transfer and air flow on the land surface [54].

First, this study calculated a global autocorrelation index (Moran's I) using values for all the grids in the study area to evaluate whether patterns of spatial data distribution are clustered, dispersed, or random. We further used local Moran's I (LISA) to show the relationship of spatial data between each grid and its surrounding grids across the study area. The LISA is a space based on statistical technique which can give an indication of the extent to a significant spatial clustering of homogeneous values, existing around a particular observation [55]. Depending on the application, the high-high (HH) locations have been used to detect clusters of high CCD values, while high-low (HL) locations have been incorporated to locate local high outliers in the study area. The HH and HL locations are considered as hot spots whereas the low-low (LL) and low-high (LH) locations are indicative of the local cold spots and are not considered in detail in this study. Furthermore, The LISA can also serve as a prerequisite for the use of spatial statistical model.

Then, the study established a Queen contiguity weights matrix and used the test of Lagrange Multiplier (LM) index and the Robust Lagrange Multiplier (robust LM) index to select spatial statistical models, including spatial error model (SEM, Eq. (9)) and spatial lag model (SLM, Eq. (8)) [56, 57]. In detail, the test contains four statistical variables, including LM lag, LM error, Robust LM lag and Robust LM error. It also leads to an important parameter P, and the smaller the value is, the stronger the significance. In the process of modeling, SEM model is selected when LM-error statistics are significant, while SLM model is selected when LM-lag statistics are significant. If both of the two statistics are significant, we need to judge the remaining two statistics. SEM model is selected if the Robust LM-error statistics are significant, while SLM model is selected if the Robust LM-lag statistics are significant.

Finally, based on the appropriate spatial statistical model, we analyzed the statistical results. It should also be noted that all modelling was performed using GeoDa software and all variables were standardized before statistical analysis. Specific formulas included:

$$Y = \rho W_y + \sum a_i X_i + \varepsilon \quad (8)$$

$$Y = \sum a_i X_i + u(u = \lambda W_u + \varepsilon) \quad (9)$$

Where Y is dependent variable, representing the CCD of the grid; ρ is a spatial autocorrelation parameter; X_i is independent variable, representing the spatial environment-related indicator in the grid; a_i is the parameter of the corresponding independent variable; ε is the error term; u is the regression residual vector; λ is the spatial autocorrelation parameter reflecting the residual; W_y and W_u are the spatial matrices for Y and u, respectively.

3. Results and Analysis

3.1. Spatial Distribution Pattern of UHII and $PM_{2.5}$ Concentrations

It is indicated that UHII of different areas were diversified, showing the pattern of "double peaks and double bottoms" with significant difference in temperature (Fig. 3). Most main urban areas exhibited generally high temperature at about 31.78℃ in general. Specifically, the heat peak areas took the form of patches in the figure, clustered in the Luyang area in the north and the Jingkai area in the southwest of the city. Meanwhile, Dongpu Reservoir and Dafangying Reservoir were two bottoms in the figure, located in the northwest of the

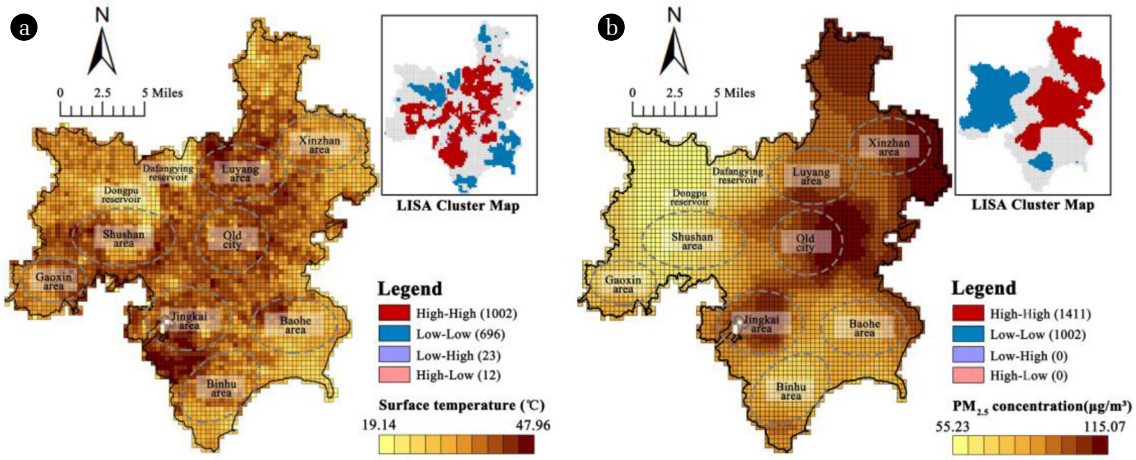


Fig. 3. Spatial distribution of UHII and $PM_{2.5}$ concentrations.

main urban area with the lowest temperature, namely 12.62°C. In general, the UHII in the main urban area of Hefei demonstrated a spatial pattern of "cold outside but hot inside", and temperature gradually decreased from the inside out.

In the study area, $PM_{2.5}$ concentrations ranged from 55.23 to 115.07 μg/m³ with a mean value of 78.95 μg/m³. It showed the pattern of "double bottoms and multiple peaks" in general, and the average value of some grids was higher than the national standard of 75.00 μg/m³. As Fig. 3 showed, the $PM_{2.5}$ concentrations were high in some areas, such as the center of Xinzhan area in the northeast and old city in the middle, with the highest concentration reaching 115.07 μg/m³. Jingkai area in the southwest ranked the second, and the $PM_{2.5}$ concentrations were in the range of 70.65~90.00 μg/m³.

This study prioritized the determination of Moran's I indicator before exploring the spatial correlation analysis between the UHII and $PM_{2.5}$ concentrations. According to the displayed results, some areas such as the Luyang area in the north, the Jingkai area in the southwest and the Gaoxin area in the west were considered the high-high clusters of the UHII, while other areas, such as the Old city in the central and the Xinzhan area in the northeast, demonstrated the spatial pattern of $PM_{2.5}$ concentration as high-high clusters. In addition, the Moran's I of the UHII and the Moran's I of $PM_{2.5}$ concentrations were 0.77 ($P < 0.001$) and 0.31 ($P < 0.001$) in the study area, respectively, which indicated that spatial autocorrelation for the UHII and $PM_{2.5}$ concentrations across all grids were significant. More importantly, the spatial distribution of the UHII and $PM_{2.5}$ concentrations in each grid was not random, and may also be affected by neighboring areas, which is consistent with the theory of the spatial statistical model [54].

3.2. Spatial Correlation Pattern of UHII and $PM_{2.5}$ Concentrations

The results of the spatial statistical analysis between UHII and $PM_{2.5}$ concentrations were shown in Table 3. Unexpectedly, either UHII or $PM_{2.5}$ concentration was taken as the independent variable, and both demonstrated a significant positive correlation. At the same time, the correlation parameters R^2 were 0.57 and 0.83, indicating that the UHII and $PM_{2.5}$ concentrations in cities were not spatially independent, and they often influenced each other [12]. Besides, the intensity of their interaction was significant, which was probably caused by the same reasons [7].

According to the results of spatial statistics, the analysis of the CCD of UHII-$PM_{2.5}$ was performed in this study, as shown in Fig. 4. The distribution of the CCD in the main urban area of Hefei had obvious spatial differences, and showed a spatial pattern of "double peaks and double bottoms". Furthermore, CCD ranged from 0 to 0.97 with the average value of 0.71, which means that UHII and $PM_{2.5}$ concentrations have a significant correlation in the study area. It also validated the analysis results obtained by the spatial statistical model.

It can also be seen from spatial distribution (Fig. 4) that Old city in the central and the Jingkai area in the southwest had the highest CCD value, mainly in the range of 0.81~0.97, belonging to "double peaks". The northern part of Xinzhan area ranked the second, and its range was maintained at 0.75~0.81, which was generally higher than the average. The "double bottoms" in the city, that was, grids with low CCD values, were mostly distributed in the Shushan area and the Binhu area, while a few were distributed in the Dongpu Reservoir and Dafangying

Table 3. Spatial Correlation between UHII and PM2.5 Concentrations

Type	Variable	Model	LM lag	Robust LM lag	LM error	Robust LM error	R^2	P
UHII	$PM_{2.5}$	SLM	0	0	0.12	0	0.57	0
$PM_{2.5}$	UHII	SLM	0	0	0.18	0	0.83	0

Note: The results indicate metrics statistically significant at $P < 0.01$ level.

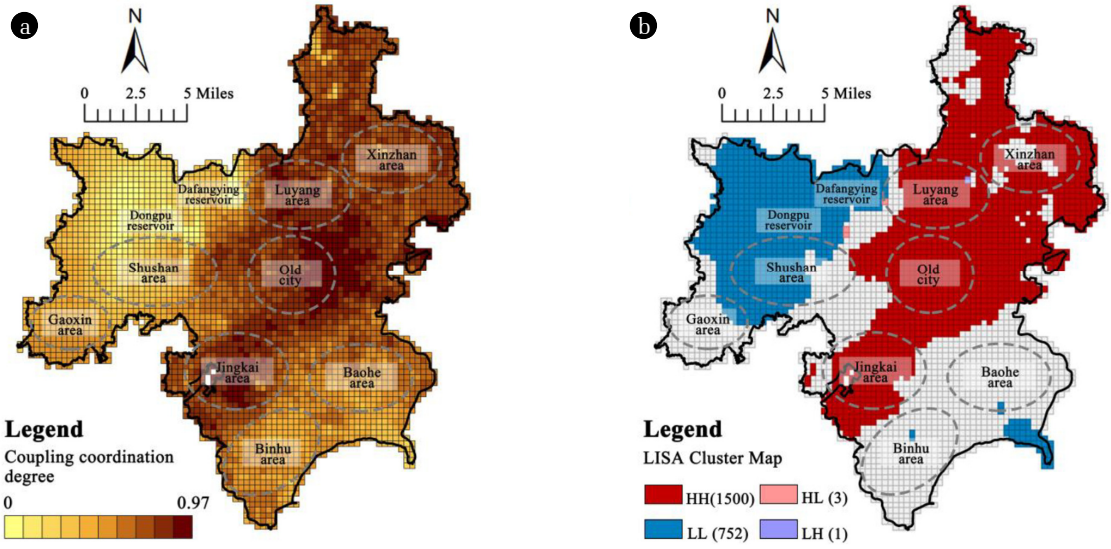


Fig. 4. CCD and spatial autocorrelation analysis.

Reservoir. Overall, the spatial distribution of CCD in the main urban area of Hefei formed a three-pole peak zone of "Xinzhan area-Old city-Jinkai area", which gradually decreased to the northwest and southeast sides.

LISA cluster distribution is found to be approximate and asymptotic while deriving the exact distribution for the global statistics [55]. According to LISA results, the Moran's I of CCD is 0.95 ($P < 0.001$), which means that a significant local cluster of CCD values locations is detected. Specifically, HH areas, such as Xinzhan area in the northeast, old city in the middle and Jingkai area in the southwest, on LISA map reflected the high-value clustering distribution of CCD while LL areas, such as Shushan area, on LISA map demonstrated the low-value clustering distribution of CCD. In addition, there were only three grids with a high level of CCD values surrounded by low levels of CCD (three high-low outliers) and one grid with a low level of CCD values surrounded by high levels of CCD (a low -high outlier).

3.3. Association between Urban Spatial Environment and UHII-$PM_{2.5}$ Coupling Coordination

3.3.1. Urban land cover indicators

The spatial statistical results of land cover indicators were shown in Table 4 and Fig. S1. Vegetated areas and CCD showed a significant negative correlation, with the corresponding coefficient R^2 of 0.75, which indicated that green vegetation can alleviate the degree of interaction between urban heat island effect and $PM_{2.5}$ [58]. Unexpectedly, the proportion of waters within grids was not correlated to CCD. On the one hand, the cooling effect of water can inhibit the UHII enhancement process caused by $PM_{2.5}$ [59]. Meanwhile, the space above water also reduced collisions among $PM_{2.5}$ particles caused by UHII. Both processes mean that they weaken the effects between UHII and $PM_{2.5}$. On the other hand, higher humidity around the water can provide an environment that intensified the interaction between UHII and $PM_{2.5}$ [60]. The results presented by buildings showed that building agglomeration had a positive effect on surface temperature and $PM_{2.5}$, with a correlation coefficient of 0.75. This also reflected that urban climate problems caused by the interaction between urban heat island effect and air pollution were closely related to human activities in built-up areas. In terms of soils, there was no significant correlation with spatial coupling coordination of UHII-$PM_{2.5}$.

3.3.2. Urban land use indicators

The spatial statistical results of land use indicators are shown in Table S1 and Fig. S2. There is no obvious correlation between administration land (AL) and CCD, which may be related to the geographical division of administration land itself. Both BL and RL have a significant positive correlation, with a correlation coefficient of 0.65 and 0.76, respectively. This may be because residential land and commercial land are more densely populated, intensifying the interaction between heat island effect and $PM_{2.5}$ in cities. At the same time, this result also indirectly indicates that a large number of crowded places are exposed to thermal pollution and air pollution [46]. While the proportion of industrial land (ML) in the grid has a positive correlation with the CCD, this is related to the industrial land itself having the function of emitting a large amount of pollutant haze and heat.

3.3.3. Urban building form indicators

The spatial statistical results of building form indicators are shown in Table S2 and Fig. S3. There is a low correlation between BH and CCD, reflecting the differentiation effect of building height. Specifically, when the building height is too low, polluted gas and heat cannot interact with each other; while when the city buildings exceed a certain height, the closed interval formed impedes the contact with other areas [61]. Meanwhile, BD and FAR affect the interaction between UHII and $PM_{2.5}$, with the correlation coefficients for 0.73 and 0.83. The reason for this is that when the index was too high, more building surfaces can store a lot of heat and block the movement of aerosol molecules, leading to the heat island effect in the region and the deterioration of air quality [62, 63]. Besides, the correlation coefficient R^2 of BFR is 0.78, reflecting the connection between surface area and volume. For example, it is more difficult for panel buildings to ventilate than point buildings. As a result, high thermal inertia and impermeability provide an interaction site for local heat islands and $PM_{2.5}$ [29].

3.3.4. Urban road traffic indicators

The spatial statistical results of road traffic indicators were shown in Table S3 and Fig. S4. The significance of AD was not high, with a P value of 0.05. Despite the roads developed rapidly in Hefei in recent years, traffic flows were still concentrated in Old city when the main roads were being built outward which can indirectly explain the current unbalanced development [64]. In addition, the densities of road junctions (RJD) and sub-arterial roads (SAD) showed significant positive correlation with CCD, and the corresponding correlation coefficients were 0.61 and 0.58, respectively. The above data indicated that cars in cities produced a large amount of heat energy while emitting exhaust gas, intensifying the interaction between temperature and $PM_{2.5}$ in cities [50].

Table 4. Statistical Results of Land Cover Indicators

Type	Variable	Model	LM lag	Robust LM lag	LM error	Robust LM error	R^2	P
Coupling coordination degree (CCD)	Vegetated areas	SLM	0	0	0	0	0.75	0
	Waters	SLM	0	0	0	0.13	0.31	0.25
	Buildings	SEM	0	0.45	0	0.01	0.75	0.02
	Soils	SLM	0	0.48	0	0.69	0.01	0.81

Note: The results indicate metrics statistically significant at $P < 0.01$ level.

4. Discussion

The interaction between urban heat island effect and $PM_{2.5}$ concentrations has become one of the most important phenomena in urban climate environment. Studies have shown that these interactions worsen urban climate. Exploring the influence of urban spatial distribution on this interaction provides a new research perspective for mitigating urban climate problems. The CCD between UHII and $PM_{2.5}$ concentrations indicated that there was a significant coupling effect between thermal environment and air environment. In this study, four types of urban spatial environment control group were selected, including land cover, land use, building form and road traffic. Specifically, vegetated areas, buildings, residential land, commercial land, industrial land, building density, floor area ratio, building form ratio, the densities of road junctions and sub-arterial roads all had an impact on the coupling effect to some extent. But the actual situation was often more complicated. In different regions, the CCD between UHII and $PM_{2.5}$ concentrations was affected by a variety of spatial environment indicators [36].

Taking the above situations into consideration, in order to further study the impact of urban spatial environment, the paper verified the impact of spatial environment on the CCD in a micro-scale grid. In terms of geographical location selection, according to the spatial distribution of CCD, we chose the area with a higher degree of interaction between UHII and $PM_{2.5}$, which was more representative. In terms of the selection of specific indicators, the paper selected the indicators of building form and road traffic. On the one hand, in the spatial layout strategy, these two indicators were more feasible and had more obvious benefits to urban development, while the cost of optimizing land cover and land use indicators was too high. On the other hand, there was no significant difference between the land cover indicators and the land use indicators of adjacent plots on the micro scale.

As shown in Fig. S5, the paper selected a set of adjacent grids in Old city to compare their building forms. After data statistical analysis, the CCD value of grid A and B is 0.87 and 0.76, respectively, and the value of A is greater than B. Meanwhile, we excluded the influence of floor area ratio, building density, the densities of road junctions and sub-arterial roads because the difference between FAR and BD values in the comparison was both relatively small, and both units were close to the main road except a few roads in the residential areas. By combining data and visualization results, the building form ratio (BFR) in grid A was 0.56 lower than the value of grid B (0.73), so the CCD between UHII and $PM_{2.5}$ had a significant negative effect, verified the previous spatial statistical analysis of the study area. Therefore, in the urban spatial planning and optimization strategy, we should reduce rough architecture, effectively improve the building form ratio, so as to optimize the climate environment.

The coupling effect of road traffic on UHII and $PM_{2.5}$ concentrations depends on the number of different types of roads and intersections. Under the same regional conditions, the more road intersections in the city, the more likely it is to generate vehicle exhaust and heat [64]. Based on this, we also selected the adjacent grids of Old city to compare with their road traffic. Meanwhile, we ensured that their urban building forms and other indicators were all similar (Fig. S6). The results showed that grid D has two more intersections than grid C, but its CCD is not very different. There are many reasons for this. On the one hand, the increase of road intersections means the increase of urban main roads, which can lead to the increase of open spaces, affecting the synergy between UHII and $PM_{2.5}$ concentrations. On the other hand, the pattern of streets and lanes under grid D may also change the microclimate, such as wind direction and wind speed. These local climate variations may weaken the interaction between $PM_{2.5}$ concentrations and UHII [65].

5. Conclusions

There is a coupling effect between the urban heat island intensity (UHII) and $PM_{2.5}$ concentrations, which will aggravate the deterioration of climate environment and endanger the health of residents. In the study, we selected the main urban area of Hefei as the research object. From the perspective of spatial environment, including land cover, land use, building form and road traffic, spatial statistical model and coupling coordination degree model were combined to explore the relationship between spatial environment and UHII-$PM_{2.5}$ coupling effect. This study provides a new perspective for the spatial layout strategies of urban planning and draws the following conclusions:

(1) There is a significant coupling effect between the urban heat island intensity and $PM_{2.5}$ concentrations in the main urban area of Hefei with significant spatial heterogeneity.

(2) Urban spatial environment can greatly influence the coupling effect between urban heat island intensity and $PM_{2.5}$ concentrations. The region with strong coupling effect has relatively strong spatial environment index significance, which means that the more intense the underlying surface activity is, the higher the synergistic effect is. To deal with this coupling effect, it is necessary for urban planners to develop a polycentric urban structure to balance high population density and reduce traffic emissions in downtown areas. Road and bus networks should be optimized simultaneously to reduce traffic jams, and more public transits (such as subways) should be built to link urban sub-centers to the downtown. In general, the exploration of spatial environmental indicators should be the focus of research to mitigate this coupling effect.

(3) The coupling effect between urban heat island intensity and $PM_{2.5}$ concentrations is complex, which may be influenced by a variety of spatial environmental indicators. Our study proposed some strategies based on relevant spatial environmental indicators, but there are still some limitations. Firstly, due to the time limitation of remote sensing image data, the timeliness of the research is affected to some extent. In addition, studies from the macro perspective may not be comprehensive enough, and the microclimate effects such as wind speed and direction are ignored. The combination of macro and micro methods can provide deeper comprehension of the mechanism of UHII-$PM_{2.5}$ coupling effect.

Acknowledgments

This research was funded by Natural Science Foundation of Anhui Province with the Grant Reference No.2008085ME160.

Author Contributions

Y.F. (PG. student) conducted all the data analysis and wrote the manuscript. K.G. (Professor) wrote and revised the manuscript.

References

1. Kan H. Climate change and human health in China. *Environ. Health Perspect*. 2011;119:60-61.
2. Azimi S, Moghaddam MS. Effect of Mercury Pollution on the Urban Environment and Human Health. *Environ. Ecol. Res*. 2013;1(1):12-20.
3. Kovats RS, Hajat S. Heat Stress and Public Health: A Critical Review. *Annu. Rev. Public Health*. 2008;29:41-55.
4. Hankey S, Marshall JD, Brauer M. Health impacts of the built environment: Within-urban variability in physical inactivity, air pollution, and ischemic heart disease mortality. *Environ. Health Perspect*. 2012;120(2):247-253.
5. Chen X, Shao S, Tian Z. Xie Z, Yin P. Impacts of air pollution and its spatial spillover effect on public health based on China's big data sample. *J. Clean. Prod*. 2017;142:915-925.
6. Liu H, Zhan Q, Yang C, Wang J. The multi-timescale temporal patterns and dynamics of land surface temperature using Ensemble Empirical Mode Decomposition. *Sci. Total Environ*. 2018;652:243-255.
7. Wang YT, Hu D, Huang JL, Fan LL. Influence of Urban Heat Island effect on C, N, P Concentration and Stoichiometry Characteristics of Plant Foliage. *Disaster Adv*. 2012;5(4):264-269.
8. He Y, Wang H. Analysis on the variation of urban heat island intensity and its relationships with air pollutants in Kunming, China. *Meteorol. Environ. Res*. 2013;1:26-28,35.
9. Zhu Y, Liu H, Shen J, Ji Y. Influence of urban heat island on pollution diffusion in Suzhou. *Plateau Meteorology*. 2016;35(6):1584-1594.
10. Wang C, Qiu G, Huang X. Relationship between urban heat island and PM2.5. *J. Arid Land Resour. Environ*. 2018;32(05): 191-195.
11. Lai LW, Cheng WL. Air quality influenced by urban heat island coupled with synoptic weather patterns. *Sci. Total Environ*. 2009;407:2724-2733.
12. Papanastasiou DK, Kittas C. Maximum urban heat island intensity in a medium-sized coastal Mediterranean city. *Theor. Appl. Climatol*. 2012;107:407-416.
13. Ulpiani G. On the linkage between urban heat island and urban pollution island: Three-decade literature review towards a conceptual framework. *Sci. Total Environ*. 2021;751(10):141727.
14. Estournel C, Vehil R, Guedalia D, Fontan J, Druilhet A. Observations and modeling of downward radiative fluxes (solar and infrared) in urban/rural areas. *J. Clim. Appl. Meteorol*. 1983;22:134-142.
15. Jauregui E, Luyando E. Global radiation attenuation by air pollution and its effects on the thermal climate in Mexico City. *Int. J. Climatol*. 1999;19(6):683-694.
16. Robaa SM. Urban-rural solar radiation loss in the atmosphere of greater Cairo region, Egypt. *Energ. Convers Manage*. 2009;50: 194-202.
17. Wang L, Gao Z, Miao S, et al. Contrasting characteristics of the surface energy balance between the urban and rural areas of Beijing. *Adv. Atmos. Sci*. 2015;32:505-514.
18. Crutzen PJ. New Directions: The growing urban heat and pollution “island” effect-impact on chemistry and climate. *Atmos Environ*. 2004;38(21):3539-3540.
19. Jonsson P, Bennet C, Eliasson I, Lindgren ES. Suspended particulate matter and its relations to the urban climate in Dar es Salaam, Tanzania. *Atmos Environ*. 2004;38(25):4175-4181.
20. Sarrat C, Lemonsu A, Masson V, Guedalia D. Impact of urban heat island on regional atmospheric pollution. *Atmos. Environ*. 2006;40:1743-1758.
21. Berezina E, Moiseenko K, Skorokhod A, et al. Impact of VOCs and NOx on Ozone Formation in Moscow. *Atmosphere* 2020;11(11):1262.
22. Cardelino CA, Chameides WL. Natural hydrocarbons, urbanization, and urban ozone. *J. Geophys Res*. 1990;95:971-979.
23. Yan ZY. Analysis on current situation and influencing factors of air quality in Shenzhen in recent years. *Environ. Sci. Manage*. 2014;39(8):125-129.
24. Li SC, Zhao ZQ, Xie MM, Wang YL. Investigating spatial non-stationary and scale-dependent relationships between urban surface temperature and environmental factors using geographically weighted regression. *Environ. Model. Softw*. 2010; 25(12):1789-1800.
25. Morabito M, Crisci A, Messeri A, et al. The impact of built-up surfaces on land surface temperatures in Italian urban areas. *Sci. Total Environ*. 2016;551-552:317-326.
26. Wan C, Su S. Neighborhood housing deprivation and public health: theoretical linkage, empirical evidence, and implications for urban planning. *Habitat. Int*. 2016;57:11-23.
27. Yin C, Yuan M, Lu Y, Huang Y, Liu Y. Effects of urban form on the urban heat island effect based on spatial regression model. *Sci. Total Environ*. 2018;634:696-704.
28. Yuan M, Song Y, Huang Y, Shen H, Li T. Exploring the association between the built environment and remotely sensed PM2.5 concentrations in urban areas. *J. Clean. Prod*. 2019;220:1014-1023.
29. Stone B. Urban sprawl and air quality in large US cities. *J. Environ. Manage*. 2008;86(4):688-698.
30. Guindon SM, Nirupama N. Reducting risk from urban heat island effects in cities. *Nat. Hazards*. 2015;77(2):823-831.
31. Civerolo K, Hogrefe C, Lynn B, et al. Estimating the effects of increased urbanization on surface meteorology and ozone concentrations in the New York City metropolitan region. *Atmos. Environ*. 2007;41(9):1803-1818.
32. Tan J, Zheng Y, Tang X, et al. The urban heat island and its impact on heat waves and human health in Shanghai. *Int. J. Biometeorol*. 2010;54(1):75-84.
33. Zhao WH, Gong HL, Zhao WJ, Tang T. Spatial distribution of urban IP pollution and CCA analysis between IP and meteorological factors :A Case Study in Beijing. *Geogr. Geo-Inf. Sci*. 2009;01:71-74.
34. Chen L, Zhu W, Zhou X, Zhou Z. Characteristics of the heat island effect in Shanghai and its possible mechanism. *Adv. Atmos. Sci*. 2003;20(6):991-1001.
35. Zhou K, Ye Y, Peng S, Wang Z, Liu H. Variations of urban heat island and its relationships with total suspended partic-

ulates in Guangzhou, China. *Ecol. Environ.* 2008;17(5):1861-1867.
36. Kotharkar R, Surawar M. Land use, land cover, and population density impact on the formation of canopy urban heat islands through traverse survey in the Nagpur urban area, India. *J. Urban Plan Dev*. 2016;142(1):04015003.
37. Sailor DJ, Lu L. A top-down methodology for developing diurnal and seasonal anthropogenic heating profiles for urban areas. *Atmos. Environ*. 2004;38(17):2737-2748.
38. Nichol JE, Fung WY, Lam KS, Wong MS. Urban heat island diagnosis using ASTER satellite images and 'in situ' air temperature. *Atmos. Res*. 2009;94(2):276-284.
39. Frey CM, Kuenzer C, Dech S. Quantitative comparison of the operational NOAA-AVHRR LST product of DLR and the MODIS LST product V005. *Int. J. Remote. Sens*. 2012;33(22):7165-7183.
40. Mackey CW, Lee X, Smith RB. Remotely sensing the cooling effects of city scale efforts to reduce urban heat island. *Build Environ*. 2012;49:348-358.
41. Shaltout AA, Boman J, Shehadeh ZF, Al-Malawi DR, Hemeda OM, Morsy MM. Spectroscopic investigation of PM2.5 collected at industrial, residential and traffic sites in Taif, Saudi Arabia. *J. Aerosol. Sci*. 2015;79:97-108.
42. Geng G, Zhang Q, Martin RV, et al. Estimating long-term PM2.5 concentrations in China using satellite-based aerosol optical depth and a chemical transport model. *Remote Sens. Environ*. 2015;166:262-270.
43. Van Donkelaar A, Martin RV, Brauer M, et al. Global estimates of fine particulate matter using a combined geophysical- statistical method with information from satellites, models, and monitors. *Environ. Sci. Technol*. 2016;50(7):3762-3772.
44. Rinner C, Hussain M. Toronto's urban heat island-exploring the relationship between land use and surface temperature. *Remote Sens*. 2011;3(6):1251-1265.
45. Hamada S, Tanaka T, Ohta T. Impacts of land use and topography on the cooling effect of green areas on surrounding urban areas. *Urban For. Urban Green*. 2013;12(4):426-434.
46. Sun Q, Wu Z, Tan J. The relationship between land surface temperature and land use/land cover in Guangzhou, China. *Environ. Earth Sci*. 2012;65(6):1687-1694.
47. Xu G, Jiao L, Zhao S, et al. Examining the impacts of land use on air quality from a spatio-temporal perspective in Wuhan, China. *Atmosphere* 2016;7(5):62.
48. Rodríguez MC, Dupont-Courtade L, Oueslati W. Air pollution and urban structure linkages: evidence from European cities. *Renew Sust. Energ. Rev*. 2016;53(1):1-9.
49. Xu Y, Ren C, Ma P, et al. Urban morphology detection and computation for urban climate research. *Landsc. Urban Plan*. 2017;167:212-224.
50. Liu H, He K. Traffic optimization: a new way for air pollution control in China's Urban Areas. *Environ. Sci. Technol*. 2012; 46(11):5660-5661.
51. Guo A, Zhao Z, Yuan Y, Wang Y, Li X, Xu R. Quantitative correlations between soil and plants in reclaimed mining dumps using a coupling coordination degree model. *R. Soc. Open Sci*. 2018;5(9):180484.
52. Xu Z, Zhang J, Li Z. Research on coupling coordination of resource-based city development system in Wu'an City. *Ecological. Economy*. 2017;33(08):124-128.
53. Hao Y, Liu YM. The influential factors of urban PM2.5 concentrations in China: aspatial econometric analysis. *J. Clean. Prod*. 2015;112:1443-1453.
54. Baltagi BH, Song SH, Jung BC, Koh W. Testing for serial correlation, spatial autocorrelation and random effects using panel data. *J. Econom*. 2007;140(1):5-51.
55. Anselin L. Local indicators of spatial association—LISA. *Geogr. Anal*. 1995;27(2):93-115.
56. Yang X, Jin W. GIS-based spatial regression and prediction of water quality in river networks: a case study in Iowa. *J. Environ. Manage*. 2010;91(10):1943-1951.
57. Su S, Pi J, Xie H, Cai Z, Weng M. Community deprivation, walkability, and public health: highlighting the social inequalities in land use planning for health promotion. *Land Use Pol*. 2017;67:315-326.
58. Park BJ, Furuya K, Kasetani T, Takayama N, Kagawa T, Miyazaki Y. Relationship between psychological responses and physical environments in forest settings. *Landsc. Urban Plan*. 2011; 102(1):24-32.
59. Amani-Beni M, Zhang B, Xie GD, Shi Y. Impacts of urban green landscape patterns on land surface temperature: Evidence from the adjacent area of Olympic Forest Park of Beijing, China. *Sustainability* 2019;11(2):1-16.
60. Cheng Y, He KB, Du ZY, Zheng M, Duan FK, Ma YL. Humidity plays an important role in the PM2.5 pollution in Beijing. *Environ Pollut*. 2015;197:68-75.
61. Yang X, Li Y. The impact of building density and building height heterogeneity on average urban albedo and street surface temperature. *Build. Environ*. 2015;90:146-156.
62. Dugord PA, Lauf S, Schuster C, Kleinschmit B. Land use patterns, temperature distribution, and potential heat stress risk-the case study Berlin, Germany. *Comput. Environ. Urban Syst*. 2014; 48(1):86-98.
63. Guo G, Zhou X, Wu Z, Xiao R, Chen Y. Characterizing the impact of urban morphology heterogeneity on land surface temperature in Guangzhou, China. *Environ. Modell. Softw*. 2016;84:427-439.
64. Pui DYH, Chen SC, Zuo Z. PM2.5 in China: Measurements, sources, visibility and health effects, and mitigation. *Particuology* 2014;13:1-26.
65. Bereitschaft B, Debbage K. Urban form, air pollution, and CO2 emissions in large US metropolitan areas. *Prof. Geogr*. 2013;65(4):612-635.

Chin. Geogra. Sci. 2022 Vol. 32 No. 5 pp. 867−882
https://doi.org/10.1007/s11769-022-1305-1

Springer Science Press
www.springerlink.com/content/1002-0063

Spatio-temporal Distribution Characteristics and Environmental Impact Factors of Lung Cancer Mortality: A Case Study of Yuhui District in Bengbu City, China

TANG Jingjing[1, 2], GU Kangkang[1, 2], MI Jing[3], ZHANG Wenhao[3], FANG Yunhao[4], LI Yuwei[1, 2], WANG Beichen[1, 2]

(1. *School of Architecture & Planning*, *Anhui Jianzhu University*, *Hefei* 230601, *China*; 2. *Research Center of Urbanization Development in Anhui Province*, *Anhui Jianzhu University*, *Hefei* 230601, *China*; 3. *Department of Epidemiology and Statistic*, *Bengbu Medical College*, *Bengbu* 233000, *China*; 4. *School of Architecture and Urban Planning*, *Huazhong University of Science and Technology*, *Wuhan* 430074, *China*)

Abstract: Among cancers, lung cancer is the most common cause of death in China. For the prevention and control of lung cancer, it is necessary to investigate the spatial and temporal distribution of lung cancer mortality, as well as the changes in the trend and the affecting mechanism. Based on statistics and auto-correlation analysis, this paper studied the spatial and temporal distribution of lung cancer mortality in Yuhui District, Bengbu, Huaihe River Basin, from 2017 to 2020. In addition, Spearman's Rank Correlation Assessment Model and Geographic Detector Model were used to examine the relationship between environmental factors and lung cancer mortality to identify impact factors and their mechanisms. The findings indicated that: 1) from the characteristics of temporal distribution, the number of lung cancer deaths exhibited a linear growth tendency, with the highest mortality in winter; 2) from the characteristics of spatial distribution, lung cancer mortality showed a strong spatial agglomeration form, concentrating on two clustering areas, located in the old city and the central city of Bengbu, near the Huaihe River; 3) from the point of view of the whole research area, there were 15 impact factors with significant correlation in the built and natural environment factors. The significant impacting factors in the built environment included land use, road traffic, spatial form and blue-green space, which could indirectly affect lung cancer mortality, while air pollution and temperature constituted the significant impacting factors in the natural environment; 4) the influence of screened environmental factors on lung cancer mortality was different. Spatial stratified heterogeneity assessment, the interaction among environmental factors demonstrated statistical significance, it was found that the interaction between environmental factors in pairs had a significant enhancement effect on lung cancer mortality. To some extent, urban planning and policies could reduce lung cancer mortality.

Keywords: lung cancer mortality; built environment; spatial auto-correlation; Spearman's Rank Correlation; Geographic Detector Model; Bengbu City, China

Citation: TANG Jingjing, GU Kangkang, MI Jing, ZHANG Wenhao, FANG Yunhao, LI Yuwei, WANG Beichen, 2022. Spatio-temporal Distribution Characteristics and Environmental Impact Factors of Lung Cancer Mortality: A Case Study of Yuhui District in Bengbu City, China. *Chinese Geographical Science*, 32(5): 867−882. https://doi.org/10.1007/s11769-022-1305-1

1 Introduction

Lung cancer is now the most common tumor with the highest mortality (World Health Organization, 2015; Wang et al., 2020; Huang et al., 2022), whose impacts have been extensively studied. Since the 1970s, the mortality rate of malignant tumors in China has steadily increased (World Health Organization, 2015), making it

Received date: 2021-11-01; accepted date: 2022-03-01
Foundation item: Under the auspices of Natural Science Foundation of Anhui Province (No. 2008085ME160), Provincial Natural Science Research Projects in Anhui Province-Postgraduate Projects (No. YJS20210500)
Corresponding author: GU Kangkang. E-mail: kangkanggu@ahjzu.edu.cn
© Science Press, Northeast Institute of Geography and Agroecology, CAS and Springer-Verlag GmbH Germany, part of Springer Nature 2022

one of the leading causes of death among both urban and rural residents (Cao and Chen, 2019; Yang et al., 2020). As reported in the Third China Residents Cause-of-Death Sample Survey, the mortality rate of malignant neoplasms in China is among the highest in the world, varying by gender and region, and shows a continuous upward trend (Lin and Lin, 2016). In China, lung cancer mortality has increased by 465% over the past 30 yr (Wang et al., 2012). The identification of the factors that influence lung cancer and the development of prevention policies that involve all relevant stakeholders is essential.

The risk factors for lung cancer are usually considered to smoking, occupational and environmental exposures, ionizing radiation, chronic lung infections, atmospheric pollution, and genetic factors (Wang et al., 2019). Nevertheless, the factors that influence lung cancer mortality have become more complex under the bio-psycho-social medicine model, which takes into account environmental factors. It has been reported that lung cancer is more prevalent in urban areas than in rural areas in some developing countries (Cao and Chen, 2019). Rapid urbanization and industrialization have resulted in air pollution and an unsuitable built environment, which pose serious health risks to both urban and rural residents (Pope et al., 2002; Loomis et al., 2013; Li et al., 2020a). Additionally, it affects social and economic development, causing widespread concern.

In recent years, there have been more and more studies on the spatial and temporal distribution of lung cancer and its influential factors. The spatial and temporal dynamic distributions and changing characteristics of lung cancer including factors such as age, gender, and geography (Thun et al., 2006; Samet et al., 2009), were discussed. On the basis of a long time series, more analysis of the degree of aggregation of mortality in different regions (Flores et al., 2017), the distribution of mortality of lung cancer in various age groups (Oliveira et al., 2013), gender differences (Xiao et al., 2022), *etc.* were discussed. But several studies have summarized the epidemiological characteristics of lung cancer from a preventive medicine perspective. Factors affecting lung cancer have been identified and analyzed: smoking is an important factor in lung cancer (Lu et al., 2019), but with effective tobacco control and promotion, the impact of smoking behavior on lung cancer has declined (Cao and Chen, 2019). Consequently, studies have begun to investigate other factors that may affect lung cancer. In 2013, outdoor air pollution was recognized as a carcinogenic factor by the International Agency for Research on Cancer (IARC). Lung cancer mortality in China has been associated with increased levels of SO_2 and suspended particles in the air (Liu et al., 2017a). Evidence suggests that the built environment has no direct impact on lung cancer rates (Wang et al., 2018). The built environment may indirectly affect lung cancer mortality through air pollution (Wang et al., 2016a; 2018), and epidemiological studies suggest that air pollution may increase lung cancer mortality (Hvidtfeldt et al., 2021). Studies on air pollution and lung cancer indicate that lung cancer is more prevalent in the developed industrial areas than in the less-developed industrial areas, and the prevalence of the urban population is higher than that of the rural areas in the suburbs (Li et al., 2020b). Thus, in order to validate the research findings, the study concentrated on the old, highly industrialized cities with high urbanization rates (Wang et al., 2019; Yang et al., 2019). A variety of spatial morphological factors affect the impact of the built environment on particulate matter concentrations. These factors include the use of land, the shape of the space, the traffic flow, the greenbelt, and the function of the environment, such as the growth of the city. The natural environment, which includes climate, air quality, and urban blue and green spaces, can effectively the reduce particulate matter and gaseous pollutants, and the more rivers and green spaces there are in an area, the lower the mortality rate for lung cancer (Fajersztajn et al., 2013; Wang et al., 2018). In winter, it is possible that the body will overreact when it is cold and the temperature falls, leading to the death of lung cancer. Differences in temperature between urban areas can affect mortality rates, *etc*. (Nielsen and Hansen, 2007; Tischer et al., 2017). However, the majority of studies have focused on the relationship between a single environmental factor and the prevalence of lung cancer. (Godden, 1958), and very few studies are classified as indicators, and they do not provide advice on how to optimize planning and design.

The effects of the built environment on air pollution and pollution exposure have typically been studied in previous studies, and due to the relatively independent

effects of air pollution and pollution exposure on lung cancer mortality and incidence, specific interventions cannot be recommended (Booth et al., 2005; Brownson et al., 2009). It should also be noted that, although lung cancer risk varies individually, genes and the environment work together best to explain lung cancer incidence and mortality when combined with biological factors within the body that ultimately determine health (Mackellar, 2015). It is possible to reduce lung cancer by improving the environment (Vandenbroucke, 1988; Wu et al., 2016). As a result of environmental factors, including the built environment, the natural environment, and social factors, as well as biological factors within the body, lung cancer develops over time. Thus, we should pay greater attention to the effects of multiple environments on lung cancer mortality, as well as examine factors that can provide references for the prevention and control of lung cancer, as well as reducing its risk.

The research on the spatial and temporal characteristics of lung cancer mortality is mainly in the field of preventive medicine, most of the research focuses on gender, age, cause of death of cancer, *etc.*, and usually based on a single characteristic. The majority of studies are carried out at the macro level, such as at the county level, while small-scale studies, for example, at the community and street level, are scarce. The relationship between environmental factors and variations in the degree of impact caused by various environmental factors is not taken into account in the majority of spatially distributed environmental impact factor analyses.

In summary, this article aims to investigate the factors affecting lung cancer mortality in Bengbu Yuhui District, Huaihe River Basin by analyzing lung cancer mortality data from January 2017 to December 2020. Based on statistical analysis, spatial auto-correlation methods, Spearman's rank correlation and Geodetector models, we investigate the characteristics of the spatial and temporal distribution of lung cancer mortality, as well as the impact of environmental factors on lung cancer mortality. This paper proposes a series of research ideas, which can be used to build healthy cities in Huaihe River Basin and elsewhere. Thus, it provides a theoretical basis and a practical guide to reduce the risk of respiratory disease in urban populations.

2 Materials and Methods

2.1 Study area

In this paper, Yuhui District of Bengbu City, Anhui Province, China is chosen as the study area (Fig. 1), which includes 12 study blocks in the Yuhui District, Bengbu City in the northeastern part of Anhui Province. It is an important industrial city in Anhui Province, with its central and northern area reaching the Huaihe River (Zhao et al., 2014; Ma and Gui, 2017). The study area is

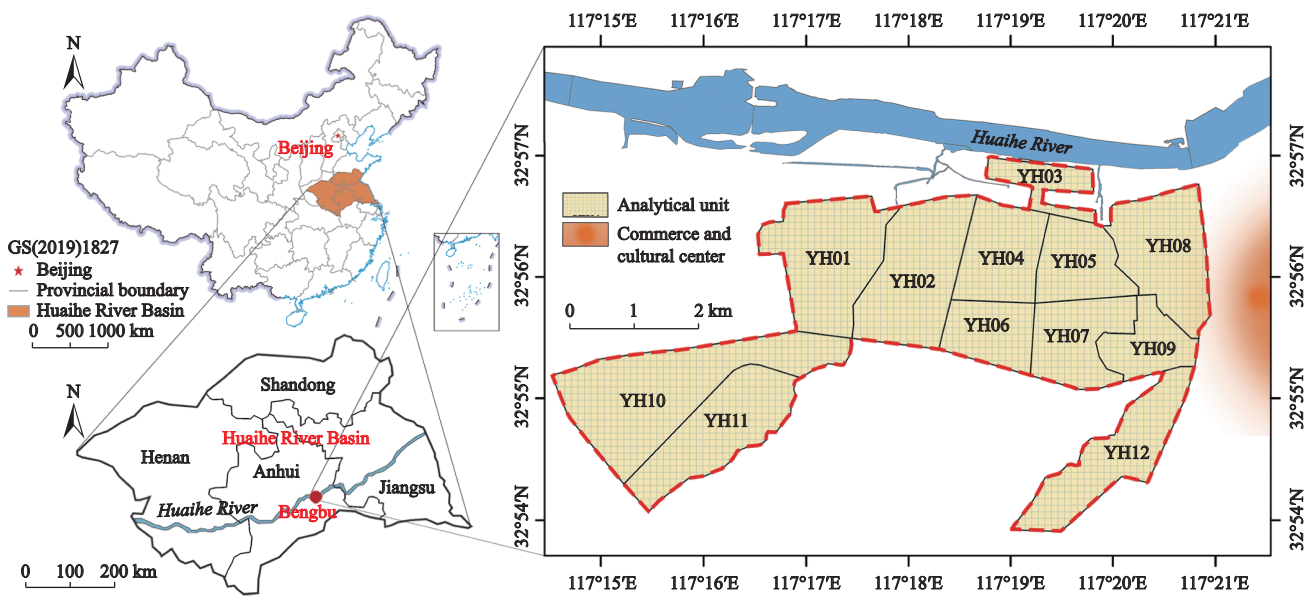


Fig. 1 The location of Yuhui District in Bengbu City, China

located in the western part of Bengbu City, on the south bank of the Huaihe River, and it is the old urban and most densely populated area in Bengbu City. The area is situated in the middle latitude area, with the prevailing northeasterly winds all year round, with an average temperature of 1°C in January and vulnerable to cold waves in winter. In 2019, it was estimated that there were 48.65 deaths from lung cancer for every 100 000 residents in China (National Health Commission of the People's Republic of China, 2020). The mortality in study area was 128/100 000 (data on lung cancer mortality rates collected from the Bengbu City Health Planning Commission), which was significantly higher than the national average value, so it is suitable for the study of population health and environmental impacting factor. The study area consist of 12 blocks numbered YH01–12, which are further divided into 2744 spatial units by 100 m grid, with the outliers excluded from the unavailable data.

2.2 Data source and processing

2.2.1 Dependent variable (*Data related to lung cancer death*)

The Bengbu City Health Planning Commission collected lung cancer deaths data from January 2017 to December 2020 from the ICD-10 (International Statistical Classification of Diseases and Related Health Problems 10th Revision) codes of C33-C34 (https://icd.who.int/browse10/2019/en#/U00-U49), including the deceased's address, age, and gender. Patients with an address and affiliation outside the study area were excluded, which made 343 patients in all. Based on the data entry, the patients were mainly elderly, and 86.88% of them were older than 60 years old. As a result, the mortality rate is calculated as follows:

$$M = \frac{Nc}{Np} \times K \tag{1}$$

where M represents the cumulative lung cancer mortality, Nc is the number of lung cancer deaths per unit in the same time period, and Np is the total number of patients with lung cancer at the same period; the proportionality factor K = 100 000/100 000 (The majority of lung cancers are relatively rare, and in medical practice, the cumulative rate or the cumulative mortality rate is often used, followed by a proportional factor, which is usually a decimal number). The unit of lung cancer mortality is the number of deaths per 100 000 people.

2.2.2 Independent variable (*Environmental data*)

Four types of environmental data were used in this study, including 1) land use data and built environment data obtained from the Anhui Urban & Rural Planning and Design Institute. In Bengbu, the landuse was classified according to *the Code for Urban Use Classes and Standards of Planning Construction Land* (GB 50137−2011) implemented on 1 January 2012, which included road, green space, river, residential land, and industrial land, as well as the number of floors for each building. 2) The data for commercial and bus stops for 2019 are derived from the Baidu Map Open Platform's point of interest (POI) data. Because the POI data has a large sample size, a wide coverage, and detailed spatial resolution, it makes spatial analysis more objective, comprehensive, and in-depth (Fig. 2). 3) Environmental pollution indicators data for 2019 were derived from Bengbu Bureau of Ecology and Environment. 4) Data of land surface temperature and vegetation coverage were derived from Landsat 8 remote sensing data in January 2019 provided by the United States Geological Survey website (USGS, https://www.usgs.gov/).

The data above were analyzed using GIS to determine evaluation indices for the environmental factors in the study, including POI density, building density, bus stop density, intersection density, and vegetation coverage. All variables related to lung cancer mortality are listed in Table 1.

2.3 Methods

2.3.1 Study framework

Firstly, the basic features and spatial distribution of the dead population of lung cancer were analyzed by means of Spatial Automatic Correlation Assessment, so as to find out the distribution features and impact hazards related to environment. Furthermore, the relationship between various environmental influencing factors and lung cancer mortality was examined by means of Spearman's rank correlation analysis, with lung cancer mortality as the dependent variable, and built environment and natural environment as independent variables, as shown in Fig. 3.

2.3.2 Spatial auto-correlation assessment

Spatial cluster analysis of diseases describes characteristics of disease spatial distribution, and determines whether there is a random distribution pattern in disease distribution.

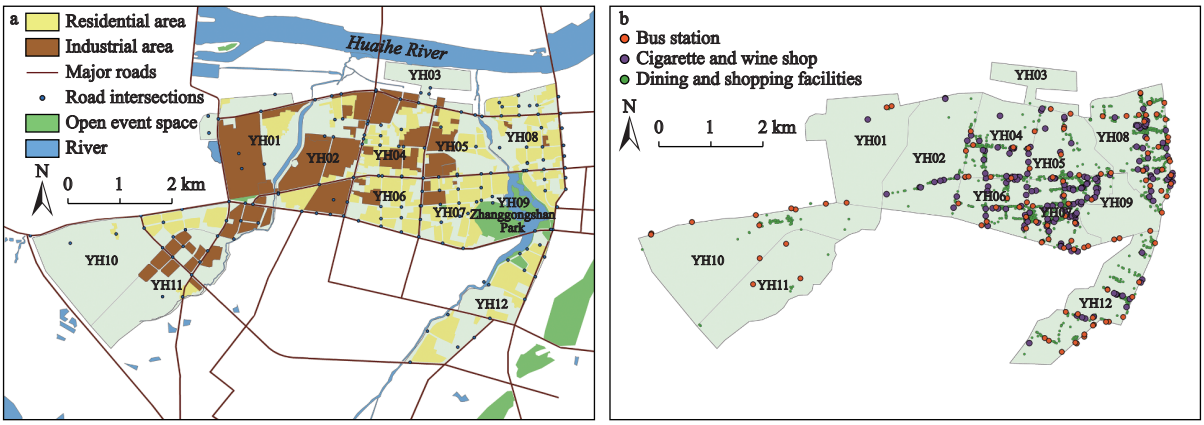


Fig. 2 Land uses categories (a) and POI (points of interest) type data (b) for 2019 in Yuhui District, Bengbu City, China

Table 1 Summary of environmental impact factors affecting lung cancer mortality in Yuhui District, Bengbu City, China

Environmental factor	Evaluation indicator	Impact factor	Scales and measurement method	Potential impact	Unit
Built environment	Land use	Residential density	Residential density; residential area/ total land area	Pollutant concentrations and open space (Frank et al., 2006)	%
		Commercial density	Catering facilities density; density of catering facilities in 500 m buffer zone	Motor vehicle emissions and environmental quality (Booth et al., 2005)	pcs/ha
			Alcohol and tobacco facilities density; density of alcohol and tobacco facilities in 500 m buffer zone	The effects of smoking and alcohol consumption on the body (Thun et al., 2006)	pcs/ha
	Road traffic	Road intersections density	Density of road intersections in 500 m buffer zone	Emissions of pollutants and noise impacts (Bidoliet al., 2016)	pcs/ha
		Bus stops density	Density of bus stops in 500 m buffer zone	Ease of travel and reduction of pollution emissions (Choi et al., 2018)	pcs/ha
	Spatial form	Building density	Building coverage ratio; the sum of the base area of buildings/ total planned construction land area	High density reduces ventilation corridors and increases exposure to pollutants (Wen and Malki-Epshtein, 2018)	%
		Volume ratio	Land use intensity, total building area/ total planned construction land area	High volume ratios reduce ventilation corridors and increase exposure to pollutants (Wen and Malki-Epshtein, 2018)	/
	Blue-green space	Vegetation cover	Normalized Difference Vegetation Index (NDVI)	Reduced air and noise pollution, high accessibility and pleasant mood (Nielsen and and Hansen, 2007)	/
		Distance to the river	Distance from the nearest river	Adsorption of airborne particulate matter by water bodies (Wang et al., 2018)	m
		Distance to the park	Distance from the nearest park	Accessibility, high openness (Tischer et al., 2017)	m
Natural environment	Air pollution	Particulate matter (PM) concentration	$PM_{2.5}$ and PM_{10} mean values, interpolated analysis	Air pollution exposure (Cao et al., 2018)	ug/m^3
		Gaseous pollutants concentration	SO_2, NO_2 and O_3 mean values, interpolation analysis	Air pollution exposure (Loomis et al., 2013)	ug/m^3
	Temperature	Surface temperature	Mean surface temperature, interpolation analysis	Cold winter temperatures increase the risk of disease and death (Hong et al., 2020)	°C

The global spatial auto-correlation of distribution (Liu et al., 2006; Mu and de Jong, 2012) is usually measured by Moran's *I*, with the value range of [–1, 1], and the higher value indicates the more remarkable spatial correlation, the lower value indicates the greater spatial difference, and the value 0 of global Moran's *I*

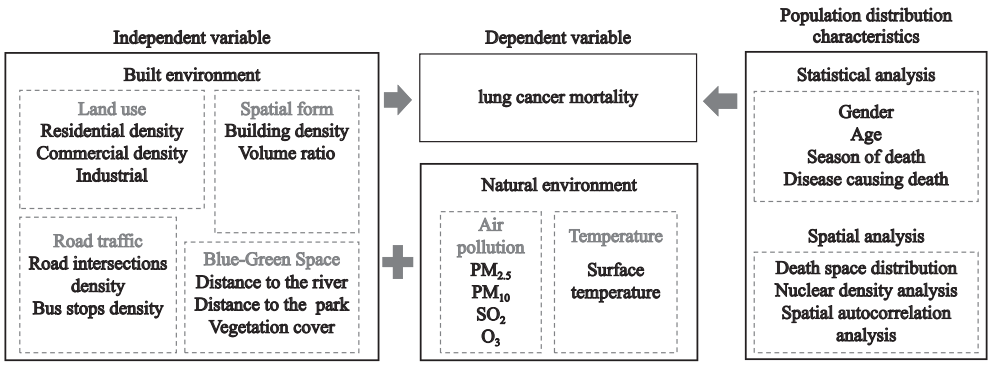


Fig. 3 Study framework of spatio-temporal distribution characteristics and environmental impact factors of lung cancer mortality analysis

indicates complete randomness (Hällfors et al., 2017; Li et al., 2018). The standardized statistic $Z(I)$ is usually used to test whether it is statistically significant after the Moran's I value is obtained. The null hypothesis was rejected when $Z > 1.96$ or $Z < -1.96$ and $P < 0.05$ at the significant level of spatial correlation $\alpha = 0.05$ of the statistical units (Pant et al., 2017), namely, there was spatial auto-correlation among the observed values of lung cancer mortality. The specific calculation formula is as follows:

$$\text{Moran's } I = \frac{n\sum_{i=1}^{n}\sum_{j=1}^{n} W_{ij}(x_i-\bar{x})\left(x_j-\bar{x}\right)}{\sum_{i=1}^{n}\sum_{j=1}^{n} W_{ij}\sum_{i=1}^{n}(x_i-\bar{x})^2}(i\neq j) \quad (2)$$

where n represents the number of study units in the study area; x_i and x_j represent the lung cancer mortality in area i and area j, respectively; $\bar{x}$ represents the average mortality of lung cancer in the study area; W_{ij} represents the spatial weight matrix. An analysis of the spatial weight matrix illustrates the degree of positional association between each of the study units, $W_{ij} = 1$ means study area i and area j are 'neighbours', otherwise $W_{ij} = 0$. The auto-correlations may differ significantly based on the spatial weight matrix used. A value of $I > 0$ indicates that lung cancer mortality is positively correlated overall, with high (low) value study units clustering together. $I = 0$ indicates that lung cancer mortality is randomly distributed; A value of $I < 0$ indicates that lung cancer mortality is negatively correlated overall.

Local spatial auto-correlation can detect local spatial aggregation, and spatial heterogeneity determines which units have the observed values with larger impact, and identifies the spatial clustering positions of elements with high or low values for lung cancer mortality (Moore et al., 2017; Fu et al., 2017). The spatial difference of lung cancer mortality was measured by local indicators of spatial association (LISA) in this study, with the calculation formula shown as follows:

$$LISA_i = z_i \sum_j W_{ij} z_j \quad (3)$$

where z_i and z_j represent the standardized values of lung cancer mortality in area i and area j, respectively. W_{ij} represents the spatial weight matrix. LISA of local spatial auto-correlation identifies four spatial association patterns for lung cancer mortality: High-High clustering, high-value clustering; Low-Low clustering, low-value clustering; High-Low clustering, excluding high values and focusing primarily on low values; Low-High clustering, excluding low values and focusing primarily on high values (Liu et al., 2017b).

2.3.3 Spearman's rank correlation assessment

Lung cancer mortality data are not continuously equidistant, and their forms of correlation and patterns of distribution are unknown. If Pearson's rank correlation coefficient is directly used for analysis, the results may be inaccurate. Therefore, this paper uses Spearman's rank correlation analysis to improve the accuracy of the analysis. Spearman's rank correlation coefficient (Liu et al., 2015; Song et al., 2021) is a non-parametric correlation coefficient. This coefficient has no requirements regarding the selection of raw data, the form of the correlation, and the pattern of distribution. It is typically used to measure the strength of a monotonic relationship or rank correlation between variables.

In order to investigate the relationship between lung

cancer and environmental influencing factors, the correlation between the mortality of lung cancer (dependent variable) and the values of various environmental factors (independent variables) was comprehensively measured by Spearman's rank correlation coefficient (Colditz et al., 1987). Lung cancer mortality and environmental influencing factors were subject to normalized processing (value range of [0, 1]), which was used to balance the dimensional gap between data, and enable different data to be counted under the same conditions, represented with the calculation formula:

$$r_s = 1 - \frac{6\sum_{i=1}^{n} d_i^2}{n(n^2-1)} \tag{4}$$

where r_s represents Spearman's rank correlation coefficient, with the value range of [–1, 1], and the larger absolute value indicates the stronger correlation. n represents the number of lung cancer mortality studied units, and $i = 1 \ldots n$. d_i represents the rank difference between the dependent variable (lung cancer mortality) and the independent variable (environmental influencing factor values) (Cao et al., 2018).

2.3.4 Assessment of spatial stratified heterogeneity

A stratified heterogeneity (Wang et al., 2016b) can not only refer to a quantitative index whose intra-layer variance is smaller than the inter-layer variance, but also a significant difference between factors on the spatial distribution as measured by q statistics. The higher the q value is, the greater its effect on lung cancer mortality. Additionally, a q value of 0 indicates that there is no spatial differentiation. Geodetector software was used to conduct factor interaction detection in this study, with the calculation formula as follows:

$$q = 1 - \frac{\sum_{h=1}^{L} N_h \sigma_h^2}{N\sigma^2} = 1 - \frac{SSW}{SST} \tag{5}$$

where $SSW = \sum_{h=1}^{L} N_h \sigma_h^2$, $SST = N\sigma^2$, and the study areas are divided into h strata, $h = 1 \ldots L$; N_h and N represent the number of units in layer h and the study area, respectively. σ^2 represents the variance of lung cancer mortality, and σ_h represents the variance of intra-layer index. SST and SSW represent the total quadratic sum and the inner quadratic sum, respectively.

3 Results and Analysis

3.1 Spatio-temporal distribution characteristics of lung cancer deaths

3.1.1 Temporal distribution characteristics of lung cancer deaths

From January 2017 to December 2020, 343 cases of lung cancer deaths were studied in the study area, with an incidence rate of 0–0.8 (per 100 000 people). A seasonal pattern is evident in the time distribution of lung cancer mortality over the period 2017–2020 (Fig. 4). There are a large number of patients in winter (December to February) every year, on the other hand, there is a small difference in the number of patients in other seasons. In light of Spearman's rank correlation analysis between different seasons and mortality, it can be concluded that winter is strongly correlated with mortality ($r_s = -0.690^{**}$, $P = 0.000$). Therefore, it shows that lung cancer death is vulnerable to climate conditions, mostly in winter (December to February). It can be inferred that the incidence trend based on time series may be closely related to temperature and humidity.

According to numerical statistical analysis, the mortality rate of male lung cancer patients was about 2.77:1 higher than that of female lung cancer patients. People over 80-year-old accounted for 27.12% of lung cancer deaths, while under 60 accounted for only 13.12% (Table 2). Thus, older patients have higher mortality.

3.1.2 Spatial distribution of lung cancer deaths

In the study area, lung cancer deaths occurred in a number of blocks from 2017 to 2020, with certain differences among the blocks. According to Fig. 5a, there is a significant difference in the distribution of lung cancer deaths, with 78.61% being attributed to YH07 and YH08. Based on the results of the analysis, lung cancer deaths were primarily concentrated around Unit YH09 in Zhanggongshan Park and north of Unit YH08 near the Huaihe River. Bengbu's old urban area, close to Unit YH09, is characterized by high population density and serious aging. The number of deaths is higher in the area surrounding the old urban area and the Huaihe River.

The normalized lung cancer mortality index showed spatial auto-correlation between 2017 and 2020 according to the global Moran's I index (Moran's $I > 0$, $Z = 2.367$, $P < 0.05$). The probability that the spatial distribution pattern of lung cancer mortality is random is less

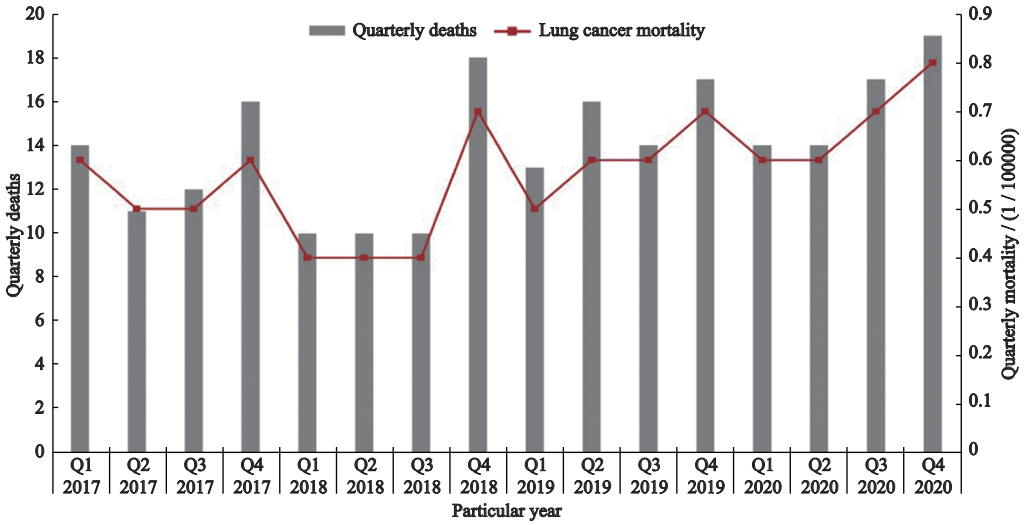


Fig. 4 Seasonal distribution characteristics of lung cancer deaths in Yuhui District, Bengbu City, China in 2017–2020; Q1 represents spring (March–May), Q2 represents summer (June–August), Q3 represents autumn (September–November), and Q4 represents winter (December to February)

Table 2 Descriptive statistics of lung cancer death cases of Yuhui District, Bengbu City, China in 2017–2020

Variable	Categories	Number of deaths	Proportion in deaths / %
Gender	Man	252	73.47
	Woman	91	26.53
Age	< 60	45	13.12
	60–69	87	25.36
	70–79	118	34.40
	≥ 80	93	27.12
Season	Spring (March–May)	77	22.45
	Summer (June–August)	90	26.24
	Autumn (September–November)	83	24.20
	Winter (December to February)	93	27.11

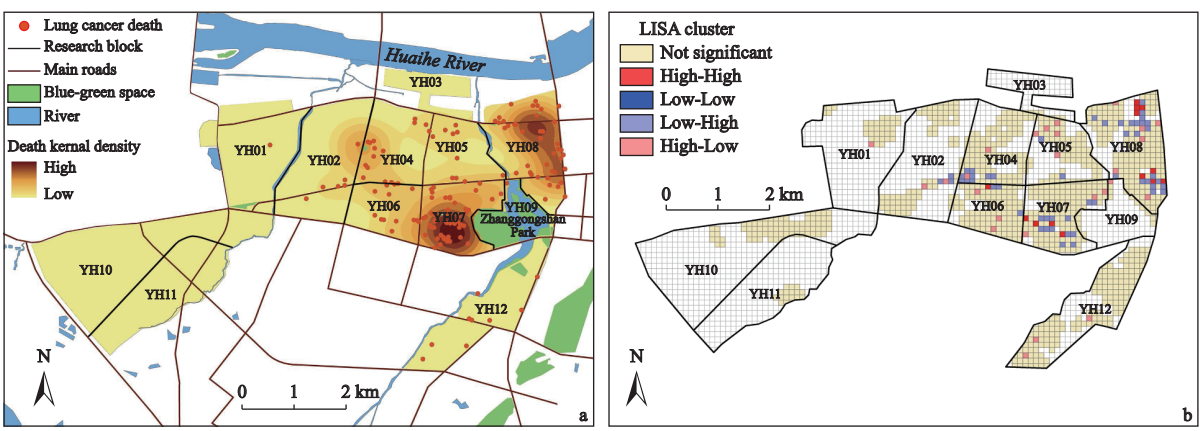


Fig. 5 Spatial distribution (a) and spatial auto-correlation (b) of lung cancer mortality in Yuhui District, Bengbu City, China in 2017–2020

than 0.01. If the probability of having a random distribution is significantly lower than that of spatial clustering, then the null hypothesis can be strongly rejected, which suggests that there is an obvious spatial clustering pat-

tern and a positive spatial correlation for lung cancer mortality.

Furthermore, the normalized mortality index exhibited local spatial auto-correlation based on the clustering and outlier analysis of the LISA clustering spatial distribution (Fig. 5b), where Low-Low clusters (0) and High-High clusters (13) were primarily located in the block units YH07 and YH08. The analysis indicates that these two blocks were the areas with the highest risk of lung cancer death, and the blocks near the old urban area and Zhanggongshan Park, which were densely populated areas, were taken into account when determining the optimal strategy. Overall, the distribution of lung cancer mortality followed the spatial characteristics of geographical proximity and network proximity of each block.

3.2 Detection of the influencing factors of lung cancer death

3.2.1 Analysis of the relationship between environmental factors and lung cancer mortality

According to Table 3, 15 environmental factors have been identified with significant correlations and statistical significance ($P < 0.05$) that may affect lung cancer mortality. However, their correlation coefficients were different. The most significant environmental factor was the residential density. The other factors followed include alcohol and tobacco facilities density, catering facilities density, bus stops density, volume ratio, road intersections density, building density, and the distance to the river, PM_{10} (inhalable particulate matter), $PM_{2.5}$ (fine particulate matter), O_3, NO_2 successively, and a significant negative correlation was found among three environmental factors, namely the (ground) surface temperature, the distance to the park, and the vegetation cover (from high to low). No correlation between industry and lung cancer mortality was found in this study ($P>0.05$) based on a difference analysis of SO_2 (sulfur dioxide). Fig. 6 illustrates the relationship between different death ① groups and environmental factors in the Yuhui District, Bengbu from 2017 to 2020.

(1) Built environment

Residencial density was significantly and positively associated with lung cancer mortality (r_s = 0.281).

Table 3 Spearman's rank correlation tests for the relationship between independent variables and lung cancer mortality in Yuhui District, Bengbu City, China

Environmental factor	Evaluation indicator	Impact factor	Scale	Correlation coefficient	Significance (two-tailed)
Built environment	Land use	Residential density	Residential density	0.281**	0.000
		Commercial density	Catering facilities density	0.240**	0.000
			Alcohol and tobacco facilities density	0.250**	0.000
	Road traffic	Road intersections density	Road intersections density	0.197**	0.000
		Bus stops density	Bus stops density	0.219**	0.000
	Spatial form	Building density	Building density (building coverage ratio)	0.179**	0.000
		Volume ratio	Volume ratio (land use intensity)	0.208**	0.000
	Blue-green space	Vegetation cover	Normalized Difference Vegetation Index (NDVI)	−0.152**	0.000
		Distance to the river	Distance from the nearest river	0.125**	0.000
		Distance to the park	Distance from the nearest park	−0.153**	0.000
Natural environment	Air pollution	Particulate matter (PM) concentration	$PM_{2.5}$ mean value	0.110**	0.000
			PM_{10} mean value	0.118**	0.000
		Gaseous pollutants concentration	SO_2 mean value	0.020	0.301
			NO_2 mean value	0.059**	0.002
			O_3 mean value	0.040*	0.039
	Temperature	Surface temperature	Mean surface temperature	−0.134**	0.000

Notes: *$P < 0.05$, **$P < 0.01$

① The death of lung cancer was divided into gender and age groups, of which gender was divided into male and female; the age group is divided into < 60, 60–69, 70–70, ≥ 80.

Therefore, the risk of death from lung cancer tends to increase when the residential density increases. There was a significant positive correlation between the density of catering facilities and alcohol and tobacco facilities and lung cancer mortality (r_s = 0.240 and r_s = 0.250, respectively), indicating that lung cancer mortality tends to increase when the density of catering facilities and alcohol and tobacco facilities increases.

In terms of road traffic, there was a significant positive correlation (r_s = 0.197) between the density of road intersections and lung cancer mortality. Therefore, lung cancer mortality tends to increase as road intersections increase. A significant positive correlation was observed between bus stop density and lung cancer mortality (r_s = 0.219). This indicates that lung cancer mortality tends to increase when the density of bus stops increases.

There was a significant positive correlation between building density and volume ratio and lung cancer mortality (r_s = 0.179, r_s = 0.208). This indicates that lung cancer mortality tends to increase when building density and volume ratio are higher.

Similar to blue-green space, vegetation cover was negatively correlated with lung cancer mortality (r_s = −0.152). Thus, when the number of green spaces increases, lung cancer mortality tends to decrease. Distance to the river was significantly correlated with lung cancer mortality (r_s= 0.125). This indicates that the risk of lung cancer mortality tends to decrease as one gets closer to the river. A statistically significant correlation was found between distance from a park and lung cancer mortality (r_s= −0.153). As a result, lung cancer mortality tends to decrease as one moves further away from the park.

(2) Natural environment

A significant positive correlation was found between PM_{10} and $PM_{2.5}$ concentrations and lung cancer mortality (r_s = 0.118 and r_s = 0.110, respectively). As a result, lung cancer mortality tends to increase when the concentration of particulate matter increases. In gaseous pollutants, NO_2 and O_3 concentrations were significantly positively related to lung cancer mortality (r_s = 0.059 and r_s = 0.040, respectively). The results indicate that the risk of lung cancer mortality tends to increase when the concentration of gaseous pollutants increases.

In terms of (ground) surface temperature, there was a significant negative correlation (r_s=−0.134) between (ground) surface temperature and lung cancer mortality. This indicates that lung cancer mortality tends to increase in colder winter months.

(3) Analysis of various lung cancer mortality

The correlation between lung cancer mortality among males and females and environmental factors was similar at bus stops density (r_s = 0.437, r_s = 0.416) and catering facilities density (r_s= 0.159, r_s= 0.306). As a result, lung cancer mortality tends to increase in old urban areas with more bus stops and catering facilities. In addition, there was a significant negative correlation between river distance and park distance. There is a lack of green space in older urban areas, resulting in a concentration of open space in the city's core area. Mortality tends to increase as people move closer to rivers and parks. Temperature and mortality had a significant negative relationship (r_s = −0.130, r_s = −0.442). As a result, lung cancer mortality tends to increase as the temperature decreases. Although there are some similarities between men and women, there are also some differences as well. A strong correlation exists between female mortality rate and SO_2 concentration. At higher concentrations, lung cancer mortality tends to increase.

People under 60-year-old had a weak correlation with environmental factors as a whole, whereas people over 60 had a strong positive correlation with bus stops density, from large to small in the age group (r_s = 0.492, r_s = 0.430, r_s = 0.447). Therefore, lung cancer mortality tends to increase when the density of bus stops increases. There was a significant negative relationship between temperature and mortality (r_s = −0.428, r_s = −0.330, r_s = −0.302), indicating that mortality tends to increase at lower temperatures. There are, however, some differences as well. A positive correlation existed between lung cancer mortality and catering facilities density (r_s = 0.390), while a negative correlation existed between lung cancer mortality and distance to the river (r_s = −0.329). As a result, the further away from the river, the lower the lung cancer mortality tends to be. The lung mortality among individuals aged 70 to 79 was negatively correlated with the density of road intersections, suggesting that the higher the density of road intersections, the lower the lung cancer mortality tends to be.

3.2.2 Analysis of spatial stratified heterogeneity of environmental impact factors

The spatial distribution of lung cancer mortality is af-

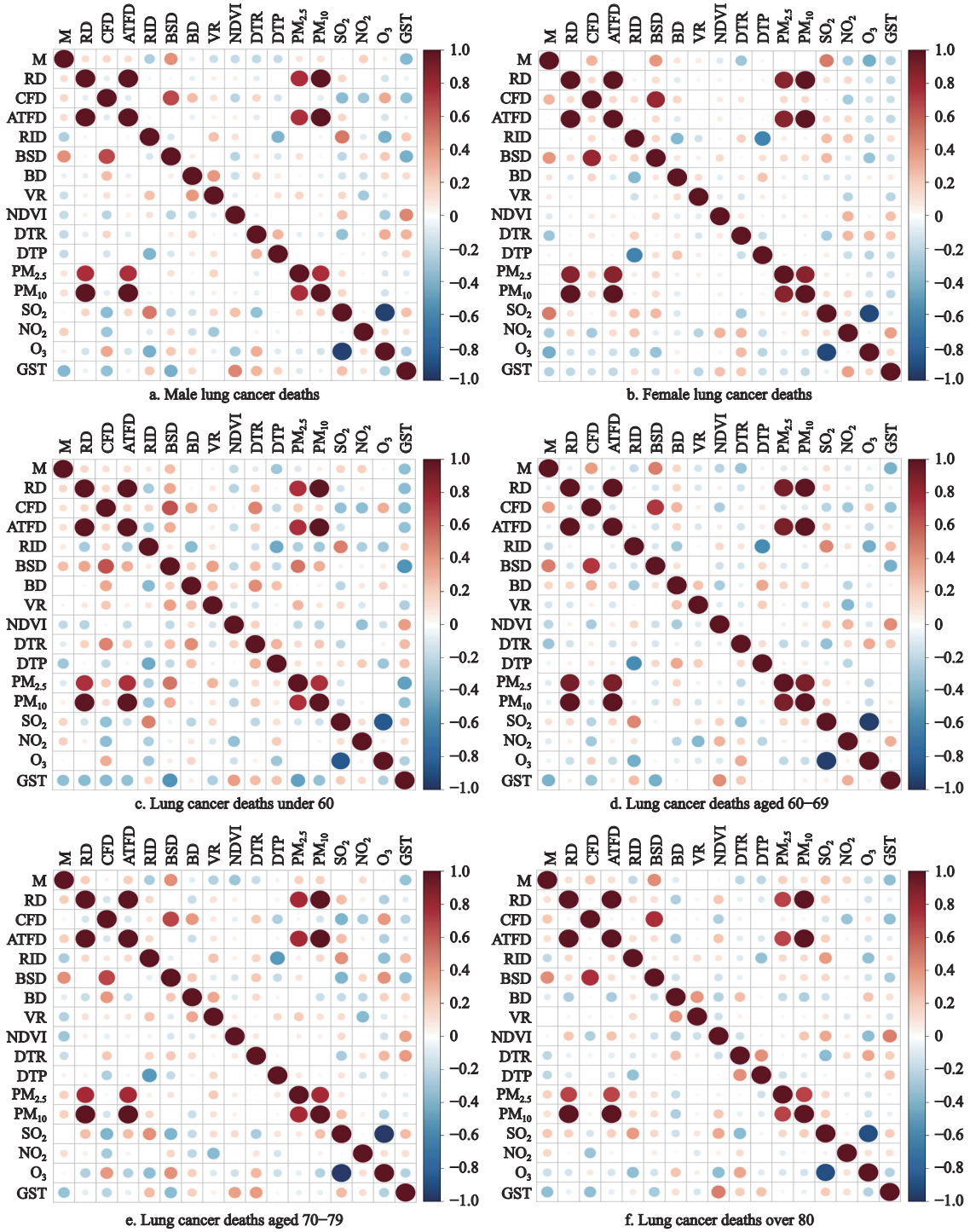


Fig. 6 Correlation coefficients between different lung cancer mortality and environmental factors in Yuhui District, Bengbu City, China in 2017–2020. M represents lung cancer mortality, RD represents residential density, CFD represents catering facilities density, ATFD represents alcohol and tobacco facilities density, RID represents road intersections density, BSD represents bus stops density, BD represents building density, VR represents volume ratio, NDVI represents the vegetation cover, DTR represents the distance to the river, DTP represents the distance to the park, $PM_{2.5}$ represents the concentration of $PM_{2.5}$, PM_{10} represents the concentration of PM_{10}, SO_2 represents the concentration of SO_2, NO_2 represents the concentration of NO_2, O_3 represents the concentration of O_3, GST represents the surface temperature

fected by different indices of spatial stratified heterogeneity. Geodetector's factor detection results indicate that all selected factors were statistically significant at $P < 0.05$. A detailed analysis of interactions between factors

impacting lung cancer mortality was conducted using the interaction detector. The effect of building density alone on lung cancer mortality was weak (q = 0.005). As shown in Table 4, when combined with other factors, the interaction between two factors has an explanatory power of 0.152. As a result, the interaction between various influencing factors was greater than their individual effects.

4 Discussion

In order to prevent diseases, it is of great importance to evaluate the risk of death. The purpose of this study was to investigate the characteristics of the spatial and temporal distribution of lung cancer mortality in the study area and the effect of the environment. In this paper, the law of disease deaths was explored from a spatial perspective at the macro level using spatial auto-correlation and other methods. Through the analysis of spatial stratified heterogeneity, we can identify the key factors of the built environment and the geographical changes in their scale and direction. These methods not only offer a new way of looking at the health of the population, but also provide more efficiency and efficiency compared to traditional census data or social and economic statistics. Studies have shown that urban built environments can affect respiratory health by altering air quality and human behavior, such as physical activity (Gottlieb, 1983).

In terms of the built environment, 1) land use: there is evidence that both high building density and volume ratio, as well as the increased pollution exposure in high-density areas, have negative effects on lung cancer mortality, which supports our conclusion that the lung cancer mortality is positively correlated with density. It is possible to integrate industrial land with residential land in the future to provide job-housing balance, reduce local car trips (Xu and Wang, 2018), and increase walking and cycling commuting, thereby reducing pollution and human exposure. 2) Road traffic: combining multiple destinations within walking distance will reduce the use of motor vehicles, thereby reducing air pollution and carbon dioxide emissions (Chen et al., 2010). In addition, walking and cycling will be promoted. Our findings indicate that lung cancer deaths are positively correlated with high road density and traffic volume. Green belts planted 50−100 m away from low urban roads are recommended for dust control and to reduce residents' exposure to high levels of motor vehicle emissions. 3) Spatial form: as a result of low frontal density, particulate matter diffuses more rapidly and is less concentrated (Wen and Malki-Epshtein, 2018). The use of land that is conducive to air pollution should be minimised, with particular emphasis on unconventional uses, such as catering facilities. In order to improve physical fitness and enhance immunity, it is necessary to reduce the density of buildings, to improve the accessibility of housing, to improve natural ventilation and to improve the interior functions of housing. 4) Blue-green space: the presence of green space and the proximity of a river can reduce air pollution and reduce lung cancer mortality. Moreover, the layout of the green space is beneficial to the greates. In summer, the more green space patches, the lower the concentration of $PM_{2.5}$, and green spaces also purify the air and adsorb dust, thus reducing the risk of lung cancer.

From the natural environment point of view, the gradual increase in lung cancer mortality is attributed to

Table 4 Results of the interaction of environmental influences on lung cancer mortality inYuhui District, Bengbu City, China

Interaction factors	Building density	Surface temperature	Catering facilities density	Alcohol and tobacco facilities density	Bus stops density	Road intersections density
Building density	0.005					
Surface temperature	0.019	0.004				
Catering facilities density	0.031	0.013	0.008			
Alcohol and tobacco facilities density	0.152	0.022	0.018	0.011		
Bus stops density	0.070	0.026	0.036	0.034	0.018	
Road intersections density	0.098	0.026	0.044	0.054	0.055	0.012

Notes: After Geodetector model interactions, six factors were found to be statistically significant, namely building density, (ground) surface temperature, catering facilities density, alcohol and tobacco facilities density, bus stops density and road intersections density.

higher concentrations of NO_2 and total suspended particles in the air. There are a number of factors that affect the generation of fine particulate matter in the atmosphere, including geographic factors, climatic conditions, and human behavior. The built environment is closely related to air pollution (Wang et al., 2016b). Air pollution affects the concentration distribution of atmospheric particulate matters through urban form, land use, development intensity, traffic, green space, and open space, thereby affecting lung cancer mortality (Ma and Gui., 2017). Human respiratory systems are the most important target organs of air pollution and atmospheric fine particulate matter exposure, and prolonged excessive exposure may result in reduced lung function. Over time, long-term exposure to this chemical may decrease lung function, trigger an inflammatory response, cause oxidative stress, and damage DNA. These mechanisms can contribute to the increase in lung cancer mortality (Vineis et al., 2006; Ren et al., 2018). In conclusion, among the natural environmental factors, the air pollution and the environment influence the death rate of lung cancer. Ultimately, it causes systemic inflammation and increases the likelihood of death. This is consistent with the findings of the study.

The study is fine-tuned and innovative in terms of the research scale; in stead of the scales of counties, states, and states, we focused on smaller scales, like communities and streets. Furthermore, we have broken the traditional one-factor model, identified 16 influential factors, classified the influential factors according to the type, and explored the variety of factors affecting the mortality of lung cancer. Based on geographical detectors, the explanation of each environmental factor and its pairwise interaction on lung cancer mortality was quantified in the discussion of the impact mechanism. Yet, there are limitations in our study. Firstly, there is a lack of information regarding smoking, genetics, and individual habit factors. Secondly, the study area is located in the old city where lacks open space. Crowd activities are largely concentrated near Zhanggongshan Park in the study area. When deciding where to live, the elderly deliberately choose to live in an open space (Wang and Pan, 2015). As a result, middle-aged and elderly individuals are at a higher risk of lung cancer death. Consequently, the results of this experiment differed from those of general research. We found that the closer to the park, the greater the risk of lung cancer. Likewise, the greater the vegetation coverage, the greater the risk of lung cancer death.

5 Conclusions

Based on discussion on the spatial and temporal distribution characteristics of lung cancer mortality in the urban residents in Yuhui District, Bengbu City, China, we examined the environmental factors impacting lung cancer mortality and their interactions, as well as factors influencing the risk of death and their mechanisms. Several conclusions have been drawn:

(1) First, there is a significant correlation betweem lung cancer mortality and the season and temporal latitude. There are a large number of patients in winter (December to February) every year, and results have shown that lung cancer mortality is highly correlated with climatic conditions.

(2) Second, there is a strong spatial clustering pattern of lung cancer mortality, which is concentrated in the old urban area and the center of Bengbu, close to the Huaihe River

(3) Finally, the interaction and integration of several factors resulted in the spatial differentiation model of lung cancer mortality, which is closely related to the environment There is a complex relationship between the built and natural environments and lung cancer mortality. Key factors include land use, road traffic, spatial form, blue-green spaces, temperature, and the concentration of pollutants. According to the analysis of the specific effects of each proxy variable on lung cancer mortality, alcohol and tobacco facilities density, road intersections density, bus stops density, catering facilities density, and building density affected spatial differentiation of lung cancer. Single-factor effects had less explanatory power than two-factor interactions.

Based on the above findings, the mortality of lung cancer exhibits distinct spatial and temporal features and is strongly correlated with multiple environmental factors. The following measures can be adopted to reduce the death rate of lung cancer in the construction of a healthy city: increase open transportation space in residential areas, reduce building density and volume ratio, increase open space to reduce pollutant concentrations, and decentralize the layout of catering facilities and alcohol and tobacco facilities. To reduce traffic and vehicle emissions, public transportation investments

should be increased in regional residential areas. The creation of networks, the systematization of layouts, and the intensification of blue-green spaces. As a result of these approaches, airborne particulate matter emissions will be significantly reduced, the urban climate will be improved, and policy advocacy will be strengthened to reduce particulate matter emissions and gaseous pollutants. Aside from smoking, genetics, and personal behavior are not the only factors that contribute to lung cancer incidence and mortality. Future studies should focus on the characteristics of the individual population.

References

Bidoli E, Pappagallo M, Birri S et al., 2016. Residential proximity to major roadways and lung cancer mortality, Italy, 1990–2010: an observational study. *International Journal of Environmental Research and Public Health*, 13(2): 191. doi: 10.3390/ijerph13020191

Booth K M, Pinkston M M, Poston W S C, 2005. Obesity and the built environment. *Journal of the American Dietetic Association*, 105(5): 110–117. doi: 10.1016/j.jada.2005.02.045

Brownson R C, Hoehner C M, Day K et al., 2009. Measuring the built environment for physical activity: state of the science. *American Journal of Preventive Medicine*, 36 (4S): S99–S123.e12. doi: 10.1016/j.amepre.2009.01.005

Cao M M, Chen W Q, 2019. Epidemiology of lung cancer in China. *Thoracic Cancer*, 10(1): 3–7. doi: 10.1111/1759-7714.12916

Cao Q L, Rui G Q, Liang Y, 2018. Study on $PM_{2.5}$ pollution and the mortality due to lung cancer in China based on geographic weighted regression model. *BMC Public Health*, 18(1): 925–934. doi: 10.1186/s12889-018-5844-4

Chen Wanqing, Zhang Siwei, Zou Xiaonong, 2010. Estimation and projection of lung cancer incidence and mortality in China. *Chinese Journal of Lung Cancer*, 13(5): 488–493. (in Chinese)

Choi W, Ranasinghe D, Deshazo J R et al., 2018. Where to locate transit stops: cross-intersection profiles of ultrafine particles and implications for pedestrian exposure. *Environmental Pollution*, 233: 235–245. doi: 10.1016/j.envpol.2017.10.055

Colditz G A, Willett W C, Stampfer M J et al., 1987. The influence of age, relative weight, smoking, and alcohol intake on the reproducibility of a dietary questionnaire. *International Journal of Epidemiology*, 16(3): 392–398. doi: 10.1093/ije/16.3.392

Fajersztajn L, Veras M, Barrozo L V et al., 2013. Air pollution: a potentially modifiable risk factor for lung cancer. *Nature Reviews Cancer*, 13(9): 674–678. doi: 10.1038/nrc3572

Flores C J, Torres-roman J S, Lopez L A M. et al., 2017. Spatiotemporal distribution of lung cancer mortality rate in Peru: 2005−2014. *Journal of Thoracic Oncology*, 12(11): S1994. doi: 10.1016/j.jtho.2017.09.917

Fu Z T, Li Y M, Lu Z L et al., 2017. Lung cancer mortality clusters in Shandong province, China: how do they change over 40 years. *Oncotarget*, 8(51): 88770–88781. doi: 10.18632/oncotarget.21144

Godden J O, 1958. The prevention of carcinoma of the lung. *Canadian Journal of Public Health*, 49(6): 232–239.

Gottlieb M S, 1983. Cancer in Louisiana (U.S.A.): an epidemiological approach to exploring environmental contributions. *Journal of Environmental Science and Health-Part C Environmental Carcinogenesis Reviews*, 1(2): 137 –174. doi: 10.1080/10590508309373315

Hällfors M H, Aikio S, Schulman L E, 2017. Quantifying the need and potential of assisted migration. *Biological Conservation*, 205: 34–41. doi: 10.1016/j.biocon.2016.11.023

Hvidtfeldt U A, Severi G, Andersen Z J et al., 2021. Long-term low-level ambient air pollution exposure and risk of lung cancer—a pooled analysis of 7 European cohorts. *Environment International*, 146: 1502112. doi: 10.1016/j.envint.2020.106249

Hong Ye, Zhang Ying, Ma Yanjun et al., 2020. Effects of air pollutants and meteorological factors on outpatient visitors for respiratory diseases in Shenyang. *China Environmental Science*, 40(9): 4077–4090. (in Chinese)

Huang J J, Deng Y Y, Tin M S et al., 2022. Distribution, risk factors, and temporal trends for lung cancer incidence and mortality: a global analysis. *Chest*, 161(4): 1101–1111. doi: 10.1016/j.chest.2021.12.655

Li C S, Song Y, Tian L et al. , 2020b. Urban form, air quality, and cardiorespiratory mortality: a path analysis. International Journal of *Environmental Research and Public Health*, 17(4): 1202–1225. doi: 10.3390/ijerph17041202

Li Rui, Li Qing, Xu Jian et al., 2020a. Regional air pollution process in winter over the Yangtze River Delta and its influence on typical northern cities. *Environmental Science*, 41(4): 1520–1534. (in Chinese)

Li X Z, Zhao Z Q, Yuan Ye et al., 2018. Heavy metal accumulation and its spatial distribution in agricultural soils: evidence from Hunan Province, China. *RSC Advances*, 8(19): 10665–10672. doi: 10.1039/C7RA12435J

Lin Yilan, Lin Fusheng, 2016. Epidemiologic study on mortality of colorectal cancer in residents in Xiamen, China. *Modern Oncology*, 24(13): 2153–2156. (in Chinese)

Liu M M, Huang Y N, Ma Z W et al., 2017a. Spatial and temporal trends in the mortality burden of air pollution in China: 2004–2012. *Environment International*, 98: 75–81. doi: 10.1016/j.envint.2016.10.003

Liu W P, Dong C L, Chen W J, 2017b. Mapping and quantifying spatial and temporal dynamics and bundles of travel flows of residents visiting urban parks. *Sustainability*, 9(8): 1296–1310. doi: 10.3390/su9081296

Liu Yaolin, Wang Huimin, Jiao Limin et al., 2015. Road central-

ity and landscape spatial patterns in Wuhan metropolitan area, China. *Chinese Geographical Science*, 25(4): 511–522. doi: 10.1007/s11769-015-0749-y

Liu Zhonggang, Li Manchun, Sun Yan et al., 2006. Study on spatial autocorrelation of urban land price distribution in Changzhou City of Jiangsu Province. *Chinese Geographical Science*, 16(2): 160–164. doi: 10.1007/s11769-006-0011-8

Loomis D, Grosse Y, Lauby-Secretan B et al., 2013. The carcinogenicity of outdoor air pollution. *The Lancet Oncology*, 14(13): 1262–1263. doi: 10.1016/S1470-2045(13)70487-X

Lu T, Yang X D, Huang Y W et al., 2019. Trends in the incidence, treatment, and survival of patients with lung cancer in the last four decades. *Cancer Management and Research*, 11: 943–953. doi: 10.2147/CMAR.S187317

Ma L, Gui H R, 2017. Anthropogenic impacts on heavy metal concentrations in surface soils from the typical polluted area of Bengbu, Anhui Province, Eastern China. *Human & Ecological Risk Assessment: An International Journal*, 23(7): 1763–1774. doi: 10.1080/10807039.2017.1344925

Mackellar L, 2015. Healthy cities: public health through urban planning. *Population and Development Review*, 41(1): 167–168. doi: 10.1111/j.1728-4457.2015.00039.x

Moore J X, Akinyemiju T, Wang H E, 2017. Pollution and regional variations of lung cancer mortality in the United States. *Cancer Epidemiology*, 49: 118–127. doi: 10.1016/j.canep.2017.05.013

Mu R, de Jong M, 2012. Establishing the conditions for effective transit-oriented development in China: the case of Dalian. *Journal of transport geography*, 24: 234–249. doi: 10.1016/j.jtrangeo.2012.02.010

National Health Commission of the People's Republic of China, 2020. *China Health Statistics Yearbook*. Beijing: China Union Medical University Press. (in Chinese)

Nielsen T S, Hansen K B, 2007. Do green areas affect health? Results from a Danish survey on the use of green areas and health indicators. *Health & Place*, 13(4): 839–850. doi: 10.1016/j.healthplace.2007.02.001

Oliveira A R, Branquinho C, Pereira M et al., 2013. Stochastic simulation model for the spatial characterization of lung cancer mortality risk and study of environmental factors. *Mathematical Geosciences*, 45(4): 437–452. doi: 10.1007/s11004-013-9443-8

Pant D K, Tenzin T, Chand R et al., 2017. Spatio-temporal epidemiology of Japanese encephalitis in Nepal, 2007–2015. *Plos One*, 12(7): e180591. doi: 10.1371/journal.pone.0180591

Pope C A, Burnett R T, Thun M J et al., 2002. Lung cancer, cardiopulmonary mortality, and long-term exposure to fine particulate air pollution. *JAMA*, 287(9): 1132–1141. doi: 10.1001/jama.287.9.1132

Ren Quanzhong, Xu Lining, Xu Ming et al., 2018. Recent progress on respiratory diseases induced by atmospheric fine particulate matters and related biological mechanisms. *SCIENTIA SINICA Chimica*, 48(10): 1260–1268. (in Chinese). doi: 10.1360/N032018-00083

Samet J M, Avila-Tang E, Boffffetta P et al., 2009. Lung cancer in never smokers: clinical epidemiology and environmental risk factors. *Clinical Cancer Research*, 15(18): 5626–5645. doi: 10.1158/1078-0432.CCR-09-0376

Song Yang, Zhang Yu, Wang Tingting et al., 2021. Spatio-temporal differentiation in the incidence of influenza and its relationship with air pollution in China from 2004 to 2017. *Chinese Geographical Science*, 31(5): 815–828. doi: 10.1007/s11769-021-1228-2

Thun M J, Henley S J, Burns D et al., 2006. Lung cancer death rates in lifelong nonsmokers. *Journal of the National Cancer Institute*, 98(10): 691–699. doi: 10.1093/jnci/djj187

Tischer C, Gascon M, Fernández-Somoano A et al., 2017. Urban green and grey space in relation to respiratory health in children. *European Respiratory Journal*, 49(6): 1502112. doi: 10.1183/13993003.02112-2015

Vandenbroucke J P, 1988. Is 'the causes of cancer' a miasma theory for the end of the twentieth century. *International Journal of Epidemiology*, 17(4): 708–709. doi: 10.1093/ije/17.4.708

Vineis P, Hoek G, Krzyzanowski M et al., 2006. Air pollution and risk of lung cancer in a prospective study in Europe. *International Journal of Cancer*, 119(1): 169–174. doi: 10.1002/ijc.21801

Wang Huiwen, Pan Xiudan, 2015. Epidemiology of lung cancer in Shenyang City, 2004–2013. *Modern Preventive Medicine*, (19): 3479–3481. (in Chinese)

Wang Lan, Jiang Xiji, Sun Wenyao et al., 2018. Impact of urban built environment on respiratory health and its planning strategy: a case study of a district in Shanghai. *City Planning Review*, 24(6): 15–22. (in Chinese)

Wang Lan, Sun Wenyao, Zhou Kaichen et al., 2019. Spatial analysis of built environment risk for respiratory health and its implication for urban planning: a case study of Shanghai. *International Journal of Environmental Research and Public Health*, 16(8): 1455–1470. doi: 10.3390/ijerph16081455

Wang Lan, Zhao XiaoJing, Jiang XiJi et al., 2016a. Study on healthy city planning from the perspective of particulate matter distribution: theoretic framework and empirical methodology. *City Planning Review*, 40(9): 39–48. (in Chinese)

Wang J F, Zhang T L, Fu B J, 2016b. A measure of spatial stratified heterogeneity. *Ecological Indicators*, 67: 250–256. doi: 10.1016/j.ecolind.2016.02.052

Wang Quan, Shen Qin, Zhang Zelin et al., 2020. Prediction of gene mutation in lung cancer based on deep learning and histomorphology analysis. *Journal of Biomedical Engineering*, 2020,37(1): 10–18. (in Chinese)

Wang Yongchuan, Wei Lijuan, Liu Juntian et al., 2012. Comparison of cancer incidence between China and the USA. *Cancer Biology and Medicine*, 9(2): 128–132. doi: 10.3969/j.issn.2095-3941.2012.02.009

World Health Organization, 2015. Tracking universal health coverage. *World Health Organization: Geneva*.

Wu S, Powers S, Zhu W et al., 2016. Substantial contribution of extrinsic risk factors to cancer development. *Nature*, 529: 43–47. doi: 10.1038/nature16166

Wen H, Malki-Epshtein L, 2018. A parametric study of the effect of roof height and morphology on air pollution dispersion in street canyons. *Journal of Wind Engineering and Industrial Aerodynamics*, 175: 328–341. doi: 10.1016/j.jweia.2018.02.006

Xu Wangyue, Wang Lan, 2018. An exploration of respiratory-health-oriented community design: based on simulation analysis of two communities in Shanghai. *New Architecture*, (2): 50–54. (in Chinese)

Xiao Hong, Yu chuanchuan, Chen Xin et al., 2022. Spatio-temporal analysis of lung cancer mortality in Jiamusi from 2008 to 2018. *Modern Preventive Medicine*, 49(8): 1365–1369. (in Chinese)

Yang D W, Liu Y, Bai C X et al., 2020. Epidemiology of lung cancer and lung cancer screening programs in China and the United States. *Cancer Letters*, 468(1): 82–87. doi: 10.1016/j.canlet.2019.10.009

Yang Xiu, Wang Jinfeng, Lei Yanhui et al., 2019. Analysis for the impact of urban built environment factors on the lung cancer incidence: an empirical study of 126 Chinese cities. *Urban Development Studies*, 26(7): 81–89. (in Chinese)

Zhao Y Q, Zu P, Zhu P et al., 2014. Changes in BMI and waist circumference among primary and secondary school students from 2005 to 2010 in Anhui, China. *Annals of Human Biology*, 41(3): 201–204. doi: 10.3109/03014460.2013.836242

water

MDPI

Article

Construction of Ecological Network Based on Multi-Scale Conversion and Nesting

Haoran Yu [1], Yongzheng Wang [1,2,*], Chan Eme [3], Xin Fan [3], Yuejing Rong [4,5], Qiang Zhang [1] and Zhe Liang [1]

1 School of Architecture and Planning, Anhui Jianzhu University, Hefei 230022, China; yuhaoran1026@yeah.net (H.Y.); zhangqiang1023@foxmail.com (Q.Z.); liazhe_320@163.com (Z.L.)
2 Anhui Urbanization Development Research Center, Hefei 230022, China
3 School of Public Administration, China University of Geosciences (Wuhan), Wuhan 430074, China; emechan340@gmail.com (C.E.); fanfx8@edu.cug.cn (X.F.)
4 State Key Laboratory of Urban and Regional Ecology, Research Center for Eco-Environmental Sciences, Chinese Academy of Sciences, Beijing 100085, China; yjrong_st@rcees.ac.cn
5 University of Chinese Academy of Sciences, Beijing 100049, China
* Correspondence: rockyhust@126.com; Tel.:+86-0551-63513049

Abstract: Ecological protection and the restoration of full-array ecosystems is an important part of ecological civilization construction, which is a powerful measure to implement the concept of green development and help bridge the gap between the respective inevitable requirements of the current ecological environment and economic development. To solve this problem, a multi-scale index system was constructed to identify ecological sources comprehensively. The minimum-cost path method, the circuit theory, and the cyclic window search method were adopted to quantitatively identify the important ecological sources and corridors in scale nesting and pinch points and barrier points that affect multi-level connectivity. Furthermore, the specific optimization layout strategy of the ecological network structure of the Hefei metropolitan area was proposed. According to the results, if ecological sources and corridors at two scales are overlaid, the coincident area of ecological sources at two scales is 1719.95 km^2. As important ecological sources, Chaohu Lake Basin, Niuwangzhai, and Wuding Mountain, which are important areas to maintain the ecological network, need to be protected. Ten overlapping ecological corridors, which are mainly distributed in Changfeng County, are easily damaged long term. As a result, ecological nodes should be set up as temporary habitats for species transfer. In addition, based on the circuit theory and the cyclic window search method, calculating areas of pinch points at two scales yields 1637.75 km^2 and 434.22 km^2, respectively, and for areas of barrier points yields 2182.75 km^2 and 126.97 km^2, respectively. The ecological pinch points at two overlapping scales among them are important areas for future protection. Due to the small and fragmented spatial distribution in the urban area, pinch points with an average size of 0.58 km^2 are easy to be restored and will greatly improve the connectivity of the ecological network after restoration. Furthermore, through the quantitative identification of ecological network elements of two scales, the paper puts forward an optimization strategy for an ecological network in the Hefei metropolitan area from three aspects of "point-line-polygon." The research results can reference decision-making concerning the delineation of urban growth boundary, regional ecological security pattern, land space renovation, and ecosystem restoration.

Keywords: multi-scale; ecological network; the circuit theory; the least-cost path method; space overlay

check for updates

Citation: Yu, H.; Wang, Y.; Eme, C.; Fan, X.; Rong, Y.; Zhang, Q.; Liang, Z. Construction of Ecological Network Based on Multi-Scale Conversion and Nesting. *Water* **2021**, *13*, 1278. https://doi.org/10.3390/w13091278

Academic Editor: Gui Jin

Received: 27 March 2021
Accepted: 28 April 2021
Published: 30 April 2021

Publisher's Note: MDPI stays neutral with regard to jurisdictional claims in published maps and institutional affiliations.

Copyright: © 2021 by the authors. Licensee MDPI, Basel, Switzerland. This article is an open access article distributed under the terms and conditions of the Creative Commons Attribution (CC BY) license (https://creativecommons.org/licenses/by/4.0/).

1. Introduction

The rapid development of urbanization caused an increasingly intense contradiction between economic development and ecological conservation. Ecological systems like forests, waters, and wetlands were destroyed, causing habitat quality to deteriorate and biodiversity decline. On the other hand, people have higher needs for life due to economic development and new demands for ecosystem services. The ecological security pattern,

the bridge between ecosystem services and societal development, is regarded as a crucial strategic tool to guarantee regional ecological security and increase well-being [1,2]. The planning of ecological security pattern (ESP) has become a key point for Chinese governments at all levels to ensure the sustainable development of the regional economy and coordinate the relationship between ecosystems and economic society. Moreover, it is regarded as a fundamental and crucial method to achieve regional ecological security and one of the strategic modes for national land development and protection [2,3]. Ecological protection and the restoration of full-array ecosystems is an important part of ecological civilization construction, which is a powerful measure to implement the concept of green development and could also solve the current ecological environment and economic development between the inevitable requirements.

In recent years, domestic and foreign scholars have constructed multi-scale ecological networks in local areas, cities, and even regions by MCR (minimum cumulative resistance), MSPA (morphological spatial pattern analysis), the circuit theory, and other methods or models from the perspective of urban planning, urban ecology, geography, landscape ecology [4–10]. Relatively, a large number of studies have provided mature methods and planning models for the construction of ecological networks, which are regarded as an important basis for constructing the ecological security pattern and the strategic deployment of ecological planning [9]. However, only a single scale was taken in most of the existing studies as the research perspective and the research units were relatively closed. As a result, some problems and deficiencies remained [7,9–11]. For example: (1) The single-scale ecological network rarely involves extraterritorial effects of "pattern–process" mutual feedback, which will ignore the interaction between ecosystem services of different scales [3,4,10]; (2) There is a lack of exploration and discussion on the characteristics of network nesting patterns, scale conversion rules, and interaction relationships among multi-scales [11]. In the hierarchical theory of landscape ecology, system process and property belonging to a certain scale are subject to such scales, and it is difficult for research results to be transferred between the different scales [11,12]. Only when the scale selection is consistent with the structure and function of the ecosystem can the "pattern–process" law be revealed correctly, and ecological problems can therefore be addressed effectively [12,13]. In the process of transformation from the large to medium or small scale, the proportion of natural components of the ecological network will decrease, and the proportion of artificial composition will increase accordingly. Based on this trend, we can judge and understand structural network patterns of different scales and correctly grasp the connection model between the main structure of the upper and lower levels in scale nesting. By organizing the connection elements between scales to construct the ecological network system, we cannot only maintain the pattern characteristics of the ecological network within each limited scale, but also ensure the effective connection of the ecological network between scales, so that the ecological network has greater stability and resilience [14]. The construction of a traditional ecological network constructs the ecological network locally, ignoring the structure of scale nesting, the ecological network structure is therefore dislocated in the scale connection of upper and lower levels [15]. As a result, it makes it impossible to use scale deduction for hierarchical linkage to solve the ecological problems at a lower level. On the other hand, it is not conducive for scale generalization to promote regional ecological security [16–18]. Therefore, according to the differences in the characteristics and mechanisms of ecological problems in different characteristic scales, a multi-level ecological network is constructed in a targeted manner, and the continuity points and barrier points of the ecological network in the conversion of different scales are found through overlay analysis. The safety pattern is regarded as the framework, practice plan, and restoration strategy are implemented and adjusted at a small scale, the hierarchical nesting structure of the ecological network is therefore optimized, and the organic coupling of structure–process–function for landscape ecology is achieved [15,19–25].

The Hefei Metropolitan Area is not only a high-level, multi-functional and international opening platform in Anhui Province, and even the central region, but also an

important asset for the country to participate in global competition. At present, the natural ecosystem is affected by the rapid expansion of urban construction based on traditional growth, causing its ecological continuity and integrity to be damaged to a certain extent. Various ecological crisis risk factors have increased significantly, and ecological security is still facing threats and challenges. Since the current development context is different from that of the past, it is necessary to ensure high-quality economic development and ecological protection. Therefore, the construction of a two-scale ecological network of the "metropolitan area–city area" to protect the regional ecological security pattern is to ensure its order—and is a necessary condition for development. Based on this, this article takes the Hefei metropolitan area as an example and: (1) Attempts to evaluate the ecological importance of the study area and identify the ecological source from two aspects—the importance of ecosystem services and ecological sensitivity; (2) Uses NPP-VIIRS(NPP-Visible infrared Imaging Radiometer) night light data, the impervious surface and topographical level index modify the landscape resistance surface and use the circuit theory and the moving window search method to quantitatively identify the important transition nodes in the scale nesting, the pinch points, and obstacles that affect the multi-level connection, to build a multi-scale ecological network; (3) Proposes relevant strategies to provide a scientific reference for protecting the ecological safety of the Hefei metropolitan area and promote its sustainable development.

2. Materials and Methods

2.1. The Study Area and Data

Hefei metropolitan area is located at the western end of the Yangtze River Delta along the middle and lower reaches of the Yangtze River. The land area and the population account for 40.6% and 43.2%, respectively, of the whole province, and the total economy accounts for nearly 59% of the whole province. It is one of the five metropolitan areas in the urban agglomerations of the Yangtze River Delta. Hefei metropolitan area is planned to be an international metropolitan area with strong influence and a core growth pole that supports the development of the whole province. The Dabie mountainous area, as the source of many small and medium-sized rivers in the Yangtze River, in addition to the Huaihe River, Xin'an River systems, and the reservoir water conservation area, as the source of many small and medium-sized rivers and reservoirs of the Yangtze, Huai, and Xin'an River systems, as well as a key area for biodiversity conservation in China, are currently facing serious soil erosion problems. Due to lake reclamation, environmental pollution, infrastructure construction, and urbanization, the biodiversity maintenance and flood regulation functions of many wetlands have been weakened. It is an urgent problem to solve how the issue of maintaining and improving the ecological service capacity of the Hefei metropolitan area to ensure regional ecological security; however, the multi-scale ecological network planning has provided an effective solution. Therefore, it has a certain degree of representativeness to take the Hefei metropolitan area as a research area and has demonstrative significance for urban sustainable construction and ecological space optimization in other areas with a damaged ecological environment. The geographical location and elevation of the study area are shown in Figure 1.

The data used in this study mainly include land use data with a resolution of 30 m and NDVI(Normalized Difference Vegetation Index) data with a resolution of 1 km in the study area in 2018, were obtained the Resource and Environmental Science Data Center of the Chinese Academy of Sciences (http://www.resdc.cn/, accessed on 20 May 2020). Elevation data (DEM) were obtained from the website of Geospatial Data Cloud (http://www.gscloud.cn/, accessed on 20 October 2018). The meteorological data, such as rainfall and temperature in the study area from 1980 to 2017, were obtained from Anhui Surface Climate Data Monthly Value Data Set of the website of China Meteorological Data Network (http://data.cma.cn/, accessed on 20 May 2020). The actual evapotranspiration data, with 30 m precision through ArcGIS10.6 (Esri, https://www.esri.com/en-us/home) Kriging interpolation of the Hefei metropolitan area, were quoted from the National Qinghai–Tibet Plateau Scientific Data

Center (http://data.tpdc.ac.cn/zh-hans/, accessed on 20 May 2020). The relevant soil data of the Hefei metropolitan area is quoted from China Soil Data Collection (1: 1 million) of the World Soil Database (HWSD), which can be found in the International Food and Agriculture Organization (FAO) (http://www.fao.org/, accessed on 13 July 2019). The night light data in 2018 and the national terrestrial ecosystem classification were, respectively, obtained from the National Oceanic and Atmospheric Administration and the China Terrestrial Ecosystem Database (http://www.ecosystem.csdb.cn/, accessed on 13 July 2019). Relevant planning texts and other data of the research area were obtained from government departments. With the support of ArcGIS 10.2 software, all spatial data were unified into Albers Conic Equal Area (Albers Conic Equal Area) and then resampled into 30 m × 30 m grid unit size for calculation. Detailed descriptions of the research data are shown in Table 1.

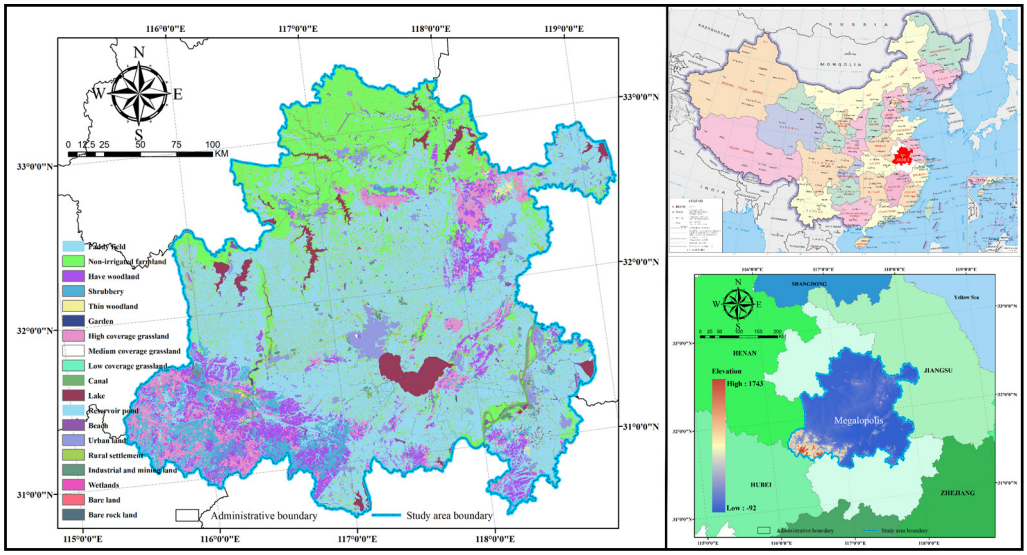


Figure 1. Location and elevation of the study area.

Table 1. The data sources for research.

Data Name	Resolution	Format	Data Description
Land use	30 m	Grid	Generated by human visual interpretation based on the Landsat 8 remote sensing image, used to calculate habitat quality
Annual average precipitation	30 m	Grid	Obtained by calculating multi-year average after interpolation of data from national meteorological station, used to calculate rainfall erosivity factor and water conservation capacity
Soil	1000 m	Grid	Obtained based on the soil type map (1:1,000,000) and the data of the second soil survey, used to calculate the soil erodibility factor
DEM	30 m	Grid	Obtained from the STRM DEM data products, from which the LS factors are calculated
NDVI	1000 m	Grid	Generated by maximum value synthesis method based on the SPOT/VEGETATION NDVI satellite remote sensing data of continuous time series
Actual evapotranspiration	30 m	Grid	Cut according to the mask of the study area based on the actual land evapotranspiration data of the whole country, the 30 m precision data of the study area are obtained by using Kriging interpolation
National terrestrial ecosystem classification	—	Vector	Used to calculate water conservation capacity

Table 1. *Cont.*

Data Name	Resolution	Format	Data Description
Planning text	—	Paper character-istics	Obtained from the government planning department
Ecological Red Line of Anhui Province	—	Vector	Obtained from the government planning department
basic geographic data	—	Vector	Include the distribution data of administrative divisions, road traffic, river systems, etc.

2.2. Research Method

Ecological security patterns of different scales do not exist independently but are connected and influenced by each other, and certain scale feature boundaries for some ecosystem services are relatively obscure [17]. For example, ecosystem services, such as water conservation and biodiversity, may have similar spatial scale features and ecosystem structures, and function at both the metropolitan and urban scales [18]. Therefore, it is necessary to select the ecological sources of the Hefei metropolitan area and urban area based on the actual situation of the study area and considering its functional positioning at different scales. Then, according to different scales, the corresponding identification methods of ecological sources were constructed to provide favorable spatial support for the ecological process behind the stable network pattern [19]. The research method consists of three parts: the comprehensive identification of ecological sources; the ecological network construction; and the nesting optimization of a multi-scale ecological network. The technical roadmap is shown in Figure 2.

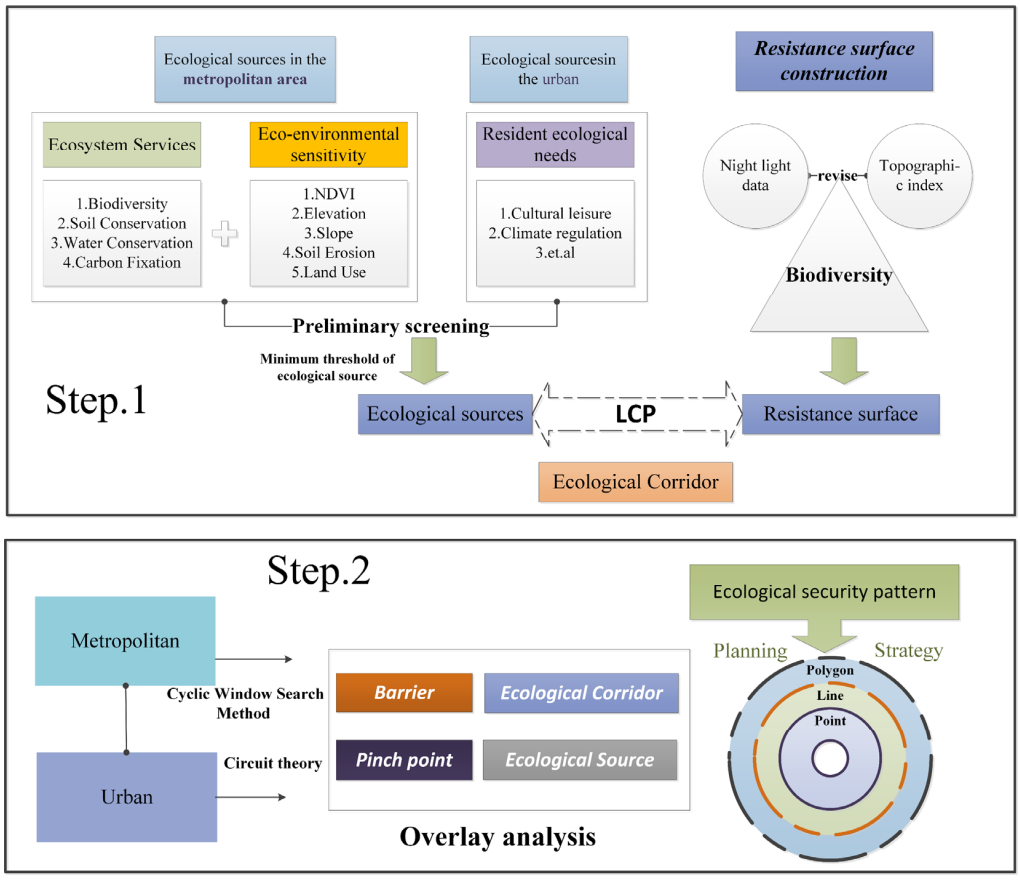


Figure 2. The technical roadmap.

2.2.1. The Comprehensive Identification of Ecological Sources

On the scale of the metropolitan area, the construction of an ecological network should be combined with the actual situation of the region and the ecological service functions to select appropriate ecological source evaluation indicators. According to related studies [16–18] and the function positioning of ecological service for the Hefei, Metropolitan Area clarified in the *Guidelines for Delineation of Ecological Protection Red Lines in Anhui Province*, four types of ecosystem service functions including water conservation, biodiversity maintenance, water and soil conservation, carbon fixation and oxygen release, as well as water and ecological environment-sensitive evaluation factors such as soil erosion and plant cover, are regarded as ecological source selection indicators. After using ArcGIS 10.2 tools, the extremely important ecosystem service functions and the extremely sensitive ecological environment were superimposed and the ecological source was extracted. By comparing and analyzing the contribution of ecological sources, the minimum threshold for selecting the area of ecological sources was determined and then checked with various protected land to obtain the ecological sources of the Hefei metropolitan area. The specific index selection and calculation formula are shown in Tables 2 and 3.

Table 2. Ecosystem service assessment method and calculation process.

Ecosystem Services	Principles and Methods	Calculation Process
Water conservation	Model of water conservation [20]	$TQ = \sum_{i=1}^{j} (P_I - R_i - ET_i) \times A_i \times 10^3$ (1) In this formula, TQ represents the total water conservation (m^3), P_I represents rainfall (mm), R_i represents surface runoff, ET_i represents evapotranspiration (mm), A_i represents the area of type i ecosystem (km^2), i represents the i-th type of ecosystem type in the study area, and j represents the number of ecosystems in the study area.
Soil and water conservation	Model of soil and water conservation [21]	The soil and water conservation service model is modified by the revised universal soil loss equation (RUSLE) to carry out the evaluation, the formula is as follows: $A_c = A_p - A_r = R \times K \times LS \times (1 - C \times P)$ (2) In this formula, A_c represents the amount of soil and water conservation, A_p represents the potential soil erosion amount, A_r represents the actual soil erosion amount, R represents the rainfall erosivity factor (MJ·mm/(hm2·h·a)), K represents the soil erodibility factor (t·hm2·h/(MJ·hm2·mm)), LS represents the slope length and slope factor (dimensionless), C represents the vegetation cover and crop management factor (dimensionless).
Carbon fixation and oxygen release (NPP)	Carbon module of InVEST model, specific parameter settings are obtained from related studies [22,23]	$C = C_{above} + C_{soil} + C_{dead} + C_{below}$ (3) In this formula, C represents the total carbon sequestration, C_{above} represents the aboveground carbon sequestration, C_{soil} represents the soil carbon sequestration, C_{dead} represents the dead carbon sequestration, C_{below} represents the underground carbon sequestration.
Habitat quality	Habitat Quality module of InVEST model, specific parameter settings are obtained from related studies [24]	$Q_{xj} = H_j\left(1 - \frac{D_{xj}^2}{D_{xj}^2 + k^2}\right)$ (4) In this formula, Q_{xj} represents the habitat quality index of the grid x of the habitat type j, H_j represents the habitat suitability of the habitat type j, D_{xj} represents the habitat stress level of the grid x of the habitat type j, K represents the half-saturation constant.

Table 3. Classification and weighting of ecological sensitivity evaluation factors.

Evaluation Factor/Unit	Sensitivity Assignment					Weights
	9	7	5	3	1	
NDVI	> 0.75	(0.65, 0.75)	(0.65, 0.75)	(0.35, 0.50)	≤ 0.35	0.20
Elevation (m)	≤ 500	(500, 800)	(800, 1100)	(1100, 1400)	>1400	0.15
Slope	≤ 5	(5, 10)	(10, 15)	(15, 25)	> 25	0.15
Land use type	Forest land or waterbody	Grassland	Cropland	Construction land	Unuse land	0.20
Soil erosion intensity	Extremely strong erosion	Strong erosion	Moderate erosion	Mild erosion	Slight erosion	0.30

In terms of the Hefei urban area, the main consideration is the urban climate regulation, cultural leisure, and improvement of the living environment, and other ecosystem service functions. Based on the macro-scale ecological evaluation, natural reserves, large reservoirs, forest parks, and wetlands in the urban area are included in the source selection set,

combined with the *Hefei City Ecological Network Planning*, and the ecological sources at the scale of the urban area are obtained after revision.

2.2.2. Construction of Ecological Network

(1) Construction and Optimization of Landscape Resistance Surface

The difficulty of species movement in patches of different habitats is reflected by the setting of resistance surfaces, which describe the impact of landscape heterogeneity on the flow of ecological processes [25]. The resistance value is not only related to the distance between ecological sources but is also related to land use and human disturbance. For example, human activities may harm the material circulation and the energy exchange between different landscape patches. Therefore, the traditional resistance surfaces cannot accurately simulate the distribution of resistance surfaces, because they mainly simulate the ecological resistance of patches based on land use. Generally speaking, the higher the habitat quality in the area, the more complex the biodiversity and the smoother the migration of species in the area [26,27]. Referring to the related studies [10,28–30] and taking the actual situation of the Hefei metropolitan area into account, this paper simultaneously uses luminous data and the terrain location index as correction factors to construct the resistance surface of the Hefei metropolitan area through the reciprocal of the quality of human settlements. Luminous data can indicate the intensity of human activity. The influence of topography on land use changes is the result of the full effects of different topography factors, while a single topography factor cannot fully reflect the impact of topography. The topographic index, combining elevation and slope to analyze the impact of terrain gradient on land use, is currently a widely used method. Considering that the value may appear to be zero, the data are processed into non-zero values without affecting the composition of actual resistance surfaces:

$$R_Z = R_0 \times OLS \times TL \tag{5}$$

$$TL = \ln\left[\left(\frac{E}{\overline{E}} + 1\right) \times \left(\frac{S}{\overline{S}} + 1\right)\right] \tag{6}$$

In the formula, R_Z represents the resistance value after the calibration of each grid in the study area. R_0 represents the initial resistance value constructed based on the reciprocity habitat quality. OLS represents the night light index. TL represents the topographic position index. E and $\overline{E}$, respectively, represent the elevation value of any grid and the average elevation value of the study area. S and $\overline{S}$, respectively, represent the gradient value of any grid and the average gradient value of the study area.

(2) Identification of Ecological Network and Key node based on Circuit Theory

The connectivity model of the circuit theory defines the movement behavior of the species based on the random walk theory. According to the model, there is a lack of foreknowledge about the landscape traversed for the species. Therefore, the optimal path may not be chosen because there are multiple paths to choose from, and the random walk hypothesis may be more in line with the behavioral characteristics of the organism [31–33]. Based on the LCP(least-cost path) method, the Linkage Mapper Tool, (https://circuitscape.org/linkagemapper/) is utilized to extract corridors of least resistance for species migration and diffusion on ArcGIS 10.2. The width of ecological corridors and the potential ecological corridors is set as 5000 weighted-cost distance and 20,000 weighted-cost distance, respectively.

According to the circuit theory model, the higher the current density is, the greater the possibility for species to pass through [31–33]. Pinch points are important areas that affect regional connectivity; once damaged, they may cause the failure of species migration. By using the Pinchpoint Mapper module in the plug-in of Circuitscape and selecting "All to One" mode and "Pairwise" mode to perform iterative calculations, respectively, the ecological pinch points can be obtained by combining and processing the highest level of the two results according to three categories of Nature Breaks. Barrier points indicate areas

with greater resistance to species movement between ecological sources. After removing such areas, it will increase the possibility of connectivity between ecologically important areas. The Barrier Mapper module of the Circuitscape plug-in is used to identify ecological barriers. Through superimposing with the current situation of land use, the intersection condition of land use and infrastructure of the barrier points can be determined.

(3) Construction and Optimization of Multi-scale Ecological Network Nesting Pattern

With the integral and dynamic feature, ecosystem services are generated based on specific ecosystem structures, processes, and functions. Different ecosystem services involve ecological processes of different scales [34,35]. Ecological networks of different scales may form a "multi-scale spatial nesting body" through organic connections [36], which cannot only maintain the dominant regulation of large-scale to small-scale but also transmit ecological efficiency through cross-scale shared key elements [37].

According to the overlay analysis of ecological sources, ecological corridors, pinch points, and barrier points in the multi-scale ecological networks, the nesting relationships and structural characteristics of ecological networks at different scales are determined and explained. The ratio of common ecological elements to higher-level ecological elements is used as the basis for judging the continuation of small-scale versus large-scale functional structures. The higher the proportion of common elements in the structural elements of the higher-level ecological network, the better the functional conductivity of the small-scale to the large-scale ecological network structure, and the greater the support for the regional ecological pattern, and correspondingly, the stronger the improvement effect of small-scale ecological network optimization on a large-scale ecological network. Taking the large-scale ecological network as the framework and carrying out the targeted protection of the ecological elements with a high proportion at a small scale, the optimization and reorganization strategy of the ecological spatial structure elements is proposed from the "point-line-polygon" level to, respectively, promote the construction of a multi-level, complex and networked ecological spatial structure system of the metropolitan area.

3. Results

3.1. The Spatial Distribution Pattern of Ecosystem Services and Ecological Sensitivity Evaluations

According to the calculation and evaluation of related models, it was found that the ecosystem services and ecological environment sensitivity of the Hefei metropolitan area showed strong spatial heterogeneity in 2018 (Figure 3). The places with high scores for ecosystem services are mainly distributed in Dabie Mountains in the southwest, Chaohu Lake in the middle, and Langya Mountain–Huangfu Mountain in the northeast, most of which are woodland and water area. Ecologically sensitive areas are mainly distributed in the mountains and waters around the mountain–plain interlaced zone in the southwest and the mountainous areas around the urban built-up area.

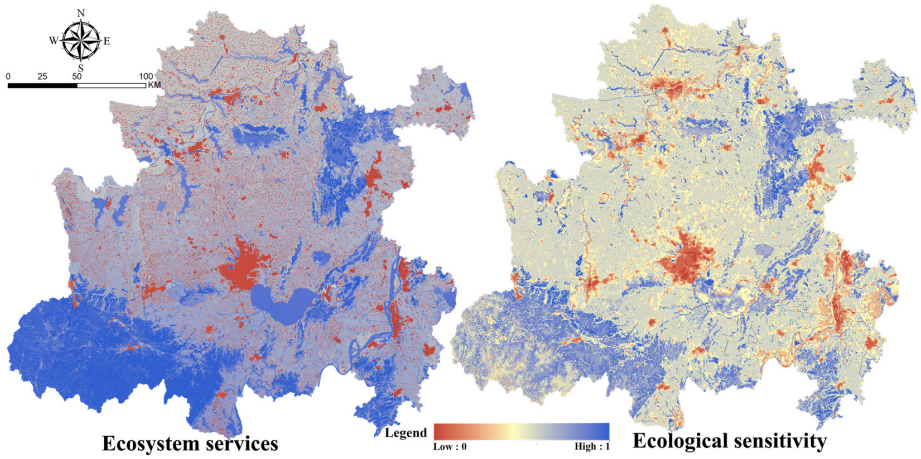


Figure 3. Spatial distribution pattern of ecosystem service and ecological sensitivity evaluation.

3.2. Extraction and Verification of Ecological Sources in Metropolitan Areas and Their Distribution

As an important support for the regional ecological security pattern, the ecological network of the metropolitan area is particularly significant for the reliability in determining its ecological sources [31–34]. Based on the evaluation of the importance of ecological service functions and ecological sensitivity, according to the natural breakpoint classification method of the ArcGIS 10.2 software, it is divided into three categories: unimportant, important, and extremely important. The areas with extremely important ecological service functions and extremely sensitive ecological environments are extracted, superimposed, and combined. It can be found that from the cumulative proportion of ecological element patches of both metropolitan area and urban area to the total area of ecological sources, there are 9010 patches less than 10 km^2 in the metropolitan area, accounting for less than 12% of the area of ecological sources. There are 1328 patches less than 5 km^2 within the ecological sources of the urban area, with the contribution to the area of the ecological source less than 15%. The size of the area has a decisive effect on the habitat heterogeneity and species carrying capacity, while the scattered and small patches only have a limited impact on maintaining regional ecological security and fulfilling ecosystem functions. Based on the analysis above, the sizes of 10 km^2 and 5 km^2 were selected as the smallest areas for ecological sources in the metropolitan area and the urban area, respectively, to determine the composition of ecological sources for two scales with the fragmented patches eliminated.

The Ecological Protection Red Line (EPRL) includes the Ecological Red Lines of prohibited development zones, important ecological function areas, sensitive areas, and vulnerable areas. Within such areas, industrialization and urbanization are prohibited to effectively protect the rare, endangered animal and plant species and ecosystems of the country, and to maintain the leading functions of important regional ecosystems. It is an important strategic measure for the Chinese government to build ecological civilization and is of great significance for the sustainable development of territorial space. To verify the scientificity and rationality of the ecological source extraction, the final ecological source was verified with the EPRL in the urban area of Hefei, as shown in Figure 4. The total area of the EPRL and the ecological sources in the Hefei metropolitan area is 8189.2 km^2 and 15,538.74 km^2, respectively. According to the spatial overlay analysis of the two areas, the overlapping part is 7094.86 km^2, accounting for 86.6% of the total area of the EPRL. It can be seen that the mining of ecological sources is scientific and practical, which plays an important role in maintaining regional ecological security.

Based on the selection criteria of the ecological sources in the metropolitan area, combined with the ecological network planning of the Hefei urban area, sources larger than 5 km^2 are selected as the ecological sources in this study. Except for the Chaohu Lake, the patches in the urban area are all small and scattered, forming a patch distribution centered on Chaohu Lake. From the perspective of administrative divisions, Chaohu City at the county level occupies most of the water area of Chaohu Lake, making it the administrative unit with the largest ecological source area in the city—followed by Lujiang County, with Chaohu Lake in the north, Yefu Mountain and Huangpi Lake in the middle, Niuwangzhai in the west, and Wuding Mountain in the south. Within the area, the mountains and rivers are criss-crossed and the ecosystem is stable. However, within the urban area, Changfeng County has the most deficient ecological sources due to its development orientation designed early by Hefei city, namely, the heavy industry and high energy-consuming industry. It urgently requires environmental improvement and ecological restoration. The distribution pattern of ecological sources in metropolitan areas and urban areas is shown in Figure 5.

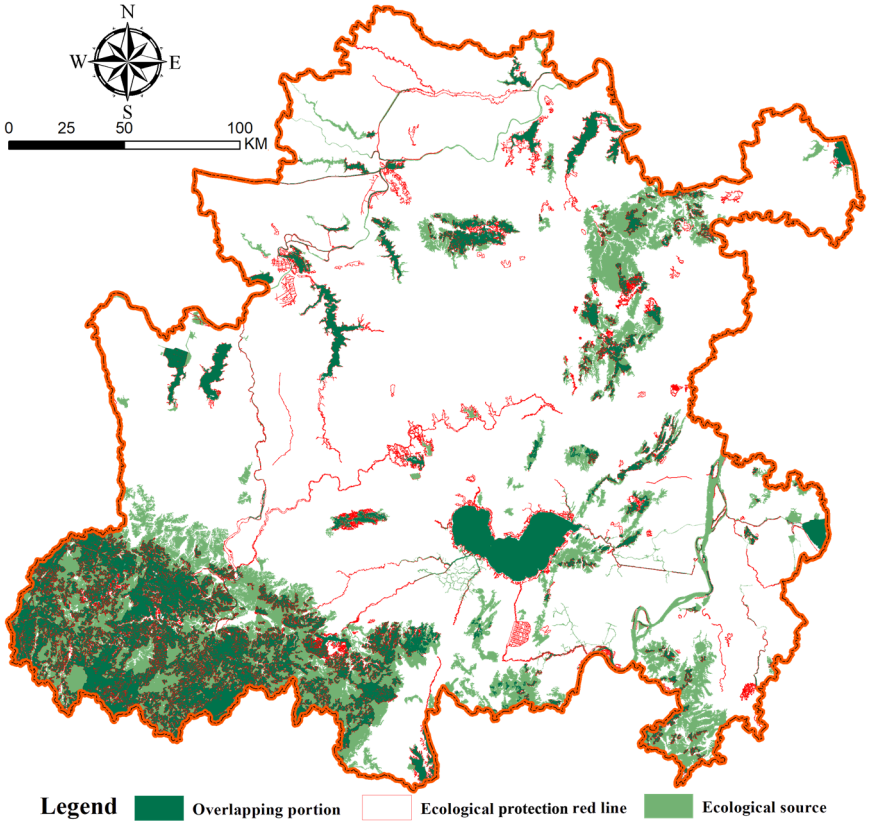


Figure 4. Rationality verification of the extraction of ecological sources.

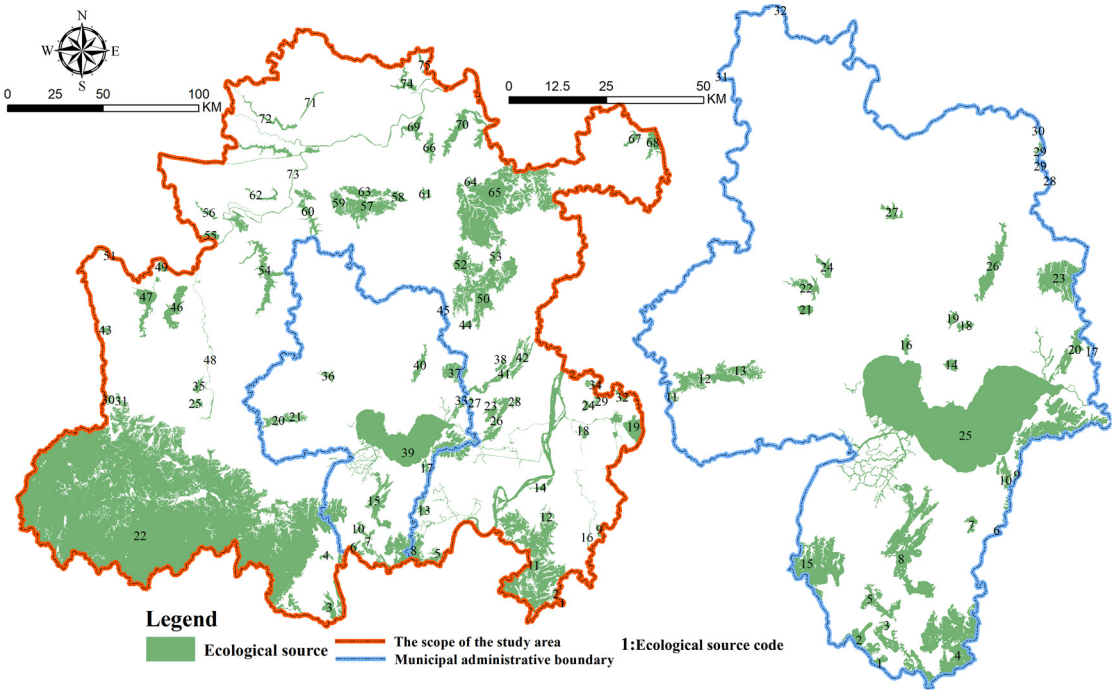


Figure 5. The spatial distribution of ecological sources in metropolitan areas and urban areas.

3.3. Establishment of the Minimum Cumulative Landscape Resistance Surface

The minimum cumulative resistance surfaces for the expansion of ecological sources are shown in Figure 6d. The areas with larger resistance values in the minimum cumulative resistance surface are mainly manifested in the central urban areas and built-up areas of subordinate counties. The southwestern part of the Hefei metropolitan area is high in terrain and mostly woodland, which makes the area's habitat quality high (Figure 6a), human activities have less impact on it. Correspondingly, the minimum cumulative resistance value is low, which has a positive impact on the spread of surrounding species and is conducive to ecological flow. The data of night lights can comprehensively reflect the urban expansion and urbanization level in the region. According to Figure 6b, the night light brightness value of the central urban area in Hefei city is the highest, that is to say, the urbanization level is the highest and it spreads around. The topographic level index reflects the degree of topographical undulations. According to Figure 6c, the Dabie Mountains and Langya Mountain–Huangfu Mountain of Chuzhou in the western Anhui province have large topographical undulations, where the range of general human activities will be restricted. This may also affect the choice of migration paths for other species to a certain extent.

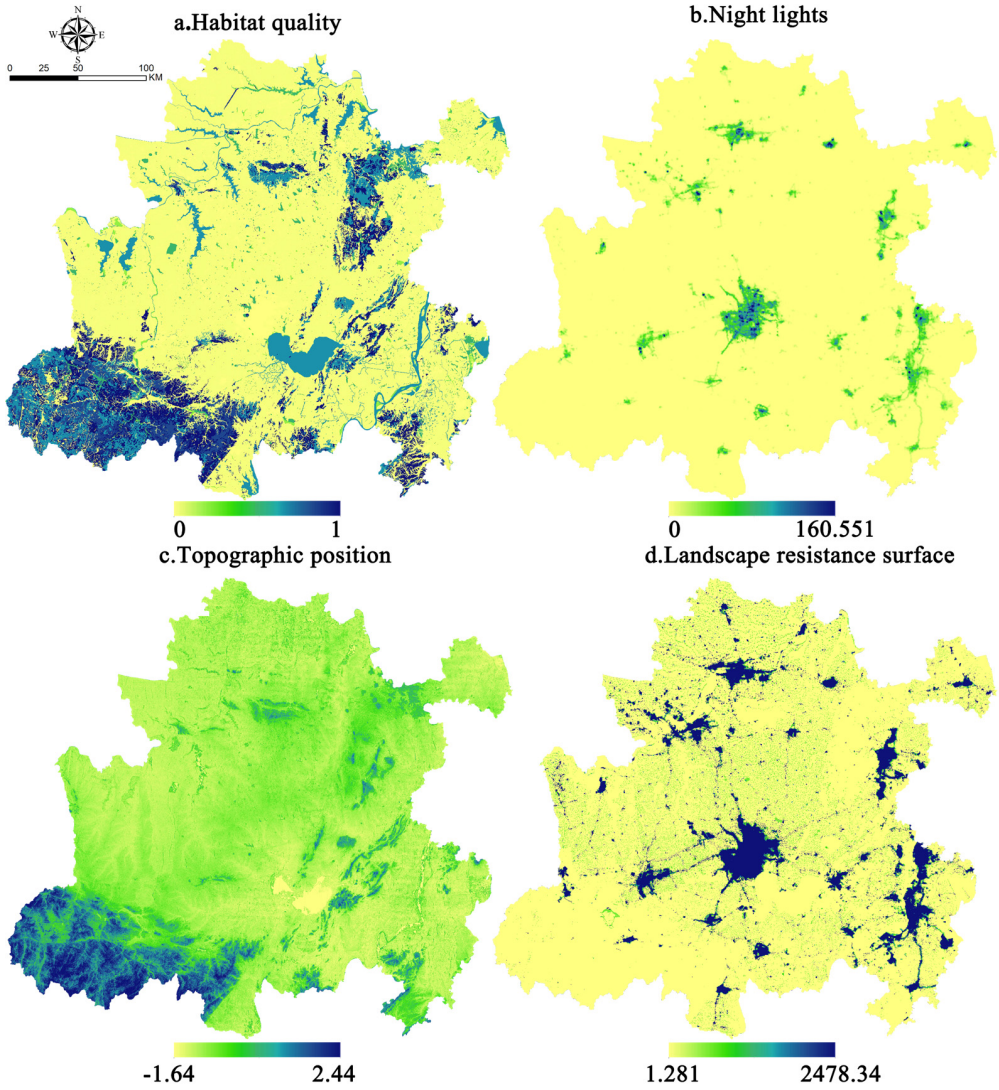


Figure 6. The minimum cumulative resistance surface of the Hefei metropolitan area. (**a**) Habitat quality; (**b**) Night light index; (**c**) Topographic index; (**d**) Landscape resistance surface.

3.4. Construction of Ecological Networks under Multi-Scale Nesting

3.4.1. Ecological Corridor Construction of the Metropolitan Area and the Urban Area

The value of ecological corridors is to connect gardens, grasslands, areas, etc., to form a more complete ecosystem and improve its spatial service value. It is mainly responsible for the basic functions such as transmission channels for species migration and habitats for biological survival and reproduction, as well as ecological restoration functions such as windproof, filtration, and ecological landscape construction. According to the GIS tool, Linkage Mapper, the LCP could be created through the vector map of the ecological sources and the grid map of the resistance surfaces, which is regarded as the ecological corridors between the ecological sources. The results are shown in Figure 7.

According to statistics, there are 155 ecological corridors in the Hefei metropolitan area, with a total length of 2272.12 km, the longest of which is 87.75 km and the average length of which is 14.65 km. There are 60 ecological corridors in the Hefei urban area, with a total length of 867.64 km. The longest corridor is 85.76 km and the average length is 14.46 km. The ecological corridor in the middle of the Hefei metropolitan area is relatively long and lacks transit stations for species transfer. Once affected by human activities, the species transfer corridors may disappear. However, they are important areas for maintaining the structures and functions of the ecological networks in the future and need to be rehabilitated by appropriate measures.

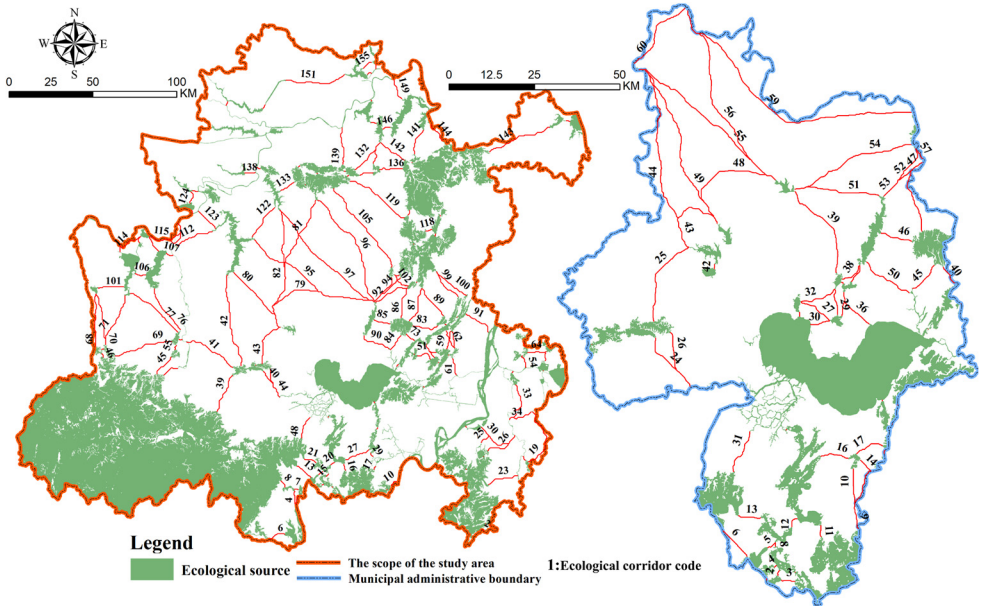


Figure 7. Spatial distribution of ecological corridors in the metropolitan area and urban area.

3.4.2. Space Characteristics of Pinch Points and Barrier Points

With the help of the Circuit Theory Model, 247 ecological pinch points were identified within the Hefei metropolitan area, with a total area of 1637.75 km^2, accounting for 2.5% of the study area. The largest and average pinch area is 187 km^2 and 6.63 km^2, respectively. There are 44 pinch points with an area larger than the average size, which are important areas for maintaining regional connectivity in the future. One hundred and eighty-nine ecological barrier points were identified within the Hefei metropolitan area, the total area of which is 2182.75 km^2, accounting for 3.4% of the study area. Forty-eight ecological pinch points and 218 barrier points are identified within the Hefei urban area, with a total area of 434.22 km^2 and 126.97 km^2, respectively. The average area of barrier points in the urban area is 0.58 km^2, and there are 177 barrier points smaller than the average patch area.

Cultivated lands and water areas constitute most of the ecological pinch points of both metropolitan areas and urban areas. The barrier points are mostly distributed on the edge of ecological sources or in ecological corridors. According to the image map of Figure 8, most of the barrier points are construction lands and road lands, with several appearing on the edge of mountains. For example, some small barrier points can be found around Dashu Mountain. In addition, it can be found that some ecological pinch points are overlapped with barrier points.

At the same time, it can be found that larger barriers mostly appear in areas where natural and artificial ecosystems converge, while relatively small barriers mostly appear in areas with frequent human activities, most of which are construction lands for urban residents. The ecological corridors within such areas are relatively short and narrow, which may directly cut off the ecological corridor with the increase in the resistance value of the barrier point. Therefore, the improvement and restoration of barrier points is the key to optimizing ecological networks.

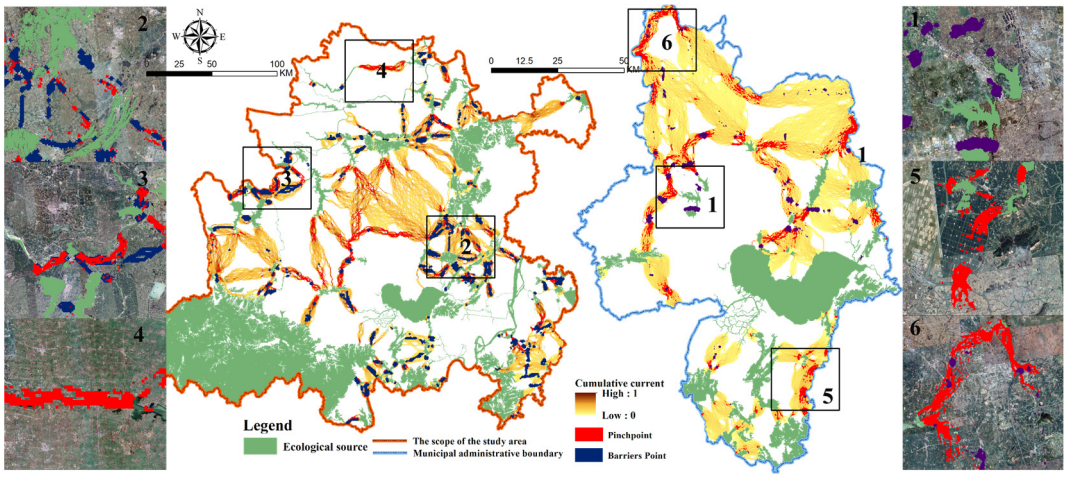


Figure 8. Identification of pinch points and barrier points at different scales.

3.5. Nesting Analysis and Optimization of Ecological Network between Scales

3.5.1. Nesting Analysis of Ecological Sources and Ecological Corridors

After superimposing the ecological corridors of the Hefei metropolitan area and urban area (Figure 9), it can be seen that there are 19 ecological sources with an area of 1719.95 km^2 shared by two scales. In addition, the largest ecological source where the two scales overlap is the Chaohu Lake Basin. The Chaohu Lake Basin is not only a key development zone but also an important ecological function zone defined in the *National Plan for Major Functional Zones* and *National Ecological Function Zoning*. It is the area with the most prominent contradictions in the spatial allocation of land resources. In recent years, while rapid urbanization and industrialization have promoted social and economic development, human activities have strongly interfered with the land use and landscape pattern of the watershed, resulting in significant impacts on the function of the ecosystem. The ecological vulnerability of the landscape has been fluctuating towards a downwards trend since 1970. As the most important ecological source in Hefei urban area, it is not only a place for people to relax and be entertained, but also a key to maintaining the stability of the regional ecosystem. Therefore, in the future, attention should be paid to the restoration of the wetland ecosystem around Chaohu Lake and the water resources environment. As an important ecological connection between the two scales, Niuwangzhai and Wuding Mountain are important sources connecting the Dabie Mountains and the Yangtze River Wetland in the urban area, and they are also of great significance to the mutual influence of the two scales of ecological networks.

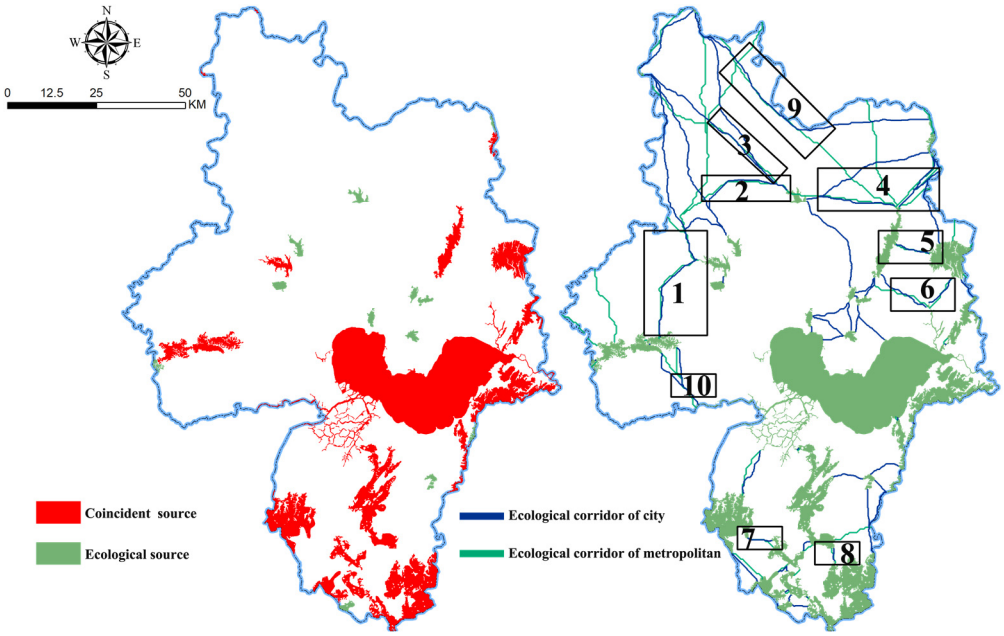


Figure 9. Superposition analysis of ecological core areas and corridors of different scales.

3.5.2. Nesting Analysis of Ecological Pinch Points and Barrier Points

By superimposing two scales of ecological pinch points and barrier points, it can be seen that (Figure 10) there are 39 overlapping ecological pinch points with an area of 134.8 km^2, accounting for 31% of the area of the urban pinch points. There are 17 overlapping barrier points with an area of 40.7 km^2, accounting for 32.1% of the area of urban barrier points.

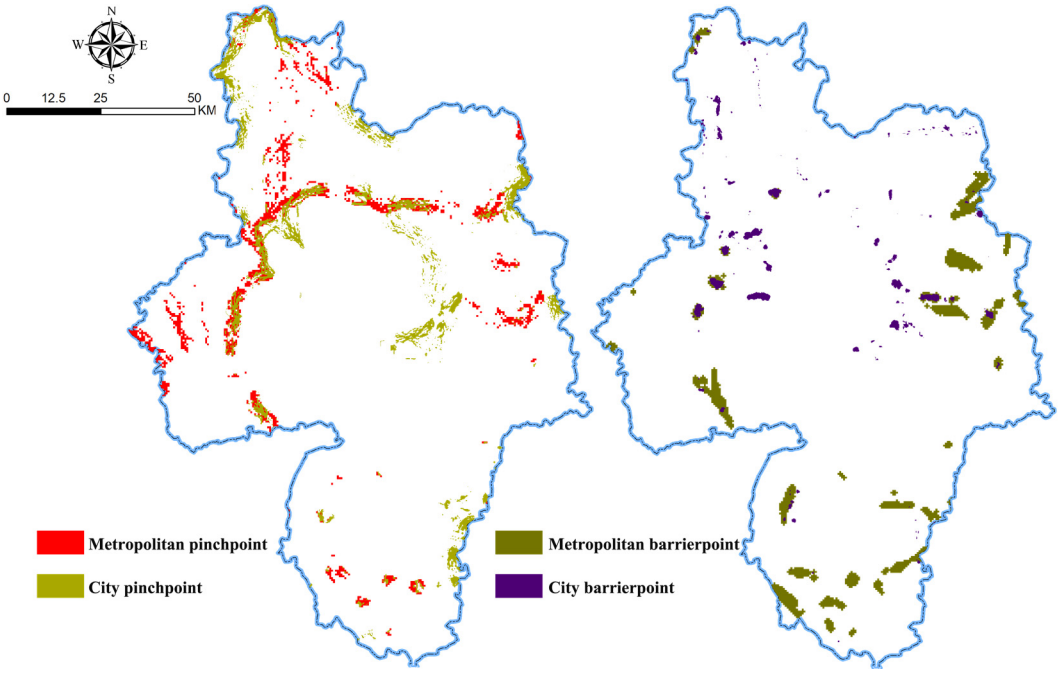


Figure 10. Comparative analysis of the superimposed areas of pinch points and barrier points.

The ecological pinch points located in the northwest and north of the Hefei urban area are highly overlapped with the scale of the metropolitan area, showing the consistency of the ecological characteristics of the nested network structure, and the ecological processes

between the two scales are significantly related. To solve the ecological problems of the metropolitan area and the exchange of material and energy of the regional ecosystem, it requires support from the urban area, and the protection for key pinch points and the restoration for barrier points in the urban area plays an important role in ensuring the connection and connectivity of the overall ecological network. Through utilizing the superposition of multi-scale ecological networks to analyze key nodes, we will play an important role at both scales and we can effectively guide the scientific investment of ecological protection and restoration funds, not to mention that providing prior restoration to such key areas can significantly improve the ecological service functions of the ecological networks.

3.6. Suggestions for Optimizing the Ecological Network of Hefei Metropolitan Area

Concerning the self-design theory and artificial design theory in the principles of restoration ecology, we considered restoring and rebuilding the ecosystem, repairing the diversity and dynamic process of the original ecosystem damaged by humans, or rebuilding a completely different or even a brand-new ecosystem. The following specific suggestions for the restoration of the ecological networks of the Hefei metropolitan area are proposed from "point–line–polygon" levels, respectively:

Level of "point": to take the lead in repairing the overlapping areas between the ecological pinch points and barrier points of the urban area and the metropolitan area, adjust the local ecological process, and drive the optimization of the regional landscape pattern. Considering the ecological problems existing in the land use mode of Hefei urban area, the surrounding protection of the traffic fields and stations and the constructions of landscape green space should be strengthened, and scattered habitat patches within the large land should be connected by the green spaces along the street. It is also necessary to pay attention to the protection and quality improvement of existing ecological sources, the control of the internal disturbance caused by human activities to large-scale sources, enriching the structure of vegetation communities, as well as improving the habitat quality of small patches.

Level of "line": It is necessary to delineate the control range of important ecological corridors, strictly control the intensity of land construction and development methods in the ecological corridors that overlap between the metropolitan area and the urban area. Moreover, according to the quality and construction conditions of the ecological corridor, it is important to cultivate the potential ecological corridor and strengthen the ecological corridor without a clear path. As for fragile points or places that are prone to breakage of the long corridors, "stepping stones" such as pocket parks and wetland waters should be considered to improve the stability of the source structure and strengthen to improve the overall structure of the ecological networks.

Level of "surface": taking the regional ecological network structure as the framework, can effectively guide the structural layout and element adjustment of the urban ecological network to ensure that the regional landscape pattern and ecological functions are effectively continued and exerted at the central city level through scale conversion and scale deduction. At the municipal level, it is necessary to improve the connectivity of the source, guarantee and support the realization of regional ecological process, and protect and optimize the key areas while repairing the problem areas.

4. Discussion

Affected by the scale effect, the interaction between the landscape pattern and the ecological process produces variability with the change of the scale, and the structures and functions of the ecological network constructed at different scales are different [38–41]. At present, most of the constructions and simulations of ecological networks are based on a single scale, so the difference and cohesion of ecological network structures between different scales are not well considered. The incoordination and dislocation of the network structures between scales will reduce the support of the local network to the regional network. The investment of capital and technology to manage, control and restore the

corridors and important nodes in the local ecological network may have a limited effect on the overall optimization of the region. This paper constructs a "source–corridor–point" ecological network structure, based on a comprehensive source identification framework. With the goal of multi-scale ecological network nesting and overall optimization, it also puts forward the ecological strategy that ecological sources and ecological corridors that overlap between the scales, as well as areas where the ecological pinch points and barriers overlap, should be given priority to be protected and restored. It can not only provide a scientific basis and technical support for the determination of control boundaries of urban development, the delineation of the EPRL, the identification, protection, and restoration of important ecological spaces in the land and space planning, but also promote the rational construction and optimization of the multi-scale ecological network nesting structure.

The regional ecological network runs through ecological space, production space, and living space. The main functions carried by different spatial locations are different, so the functions required of the ecological network are significantly different. This paper currently constructs an ecological network from the perspective of regional ecological security and stability at the regional scale and considers the composite functions of recreational activities, humanistic aesthetics as well as economic development at an urban scale. However, at a smaller scale, questions such as how to connect the ecological environment in the urban built-up areas with the higher-level network have not yet been discussed. In the construction of urban and regional ecological networks in the future, LID (low impact development) facilities such as green roofs, permeable ground, rainwater gardens, and grass ditches in urban built-up areas should be integrated into the ecological network structure to meet people's diversified needs, such as ecological improvement, economic development, and social justice. As a result, the construction of a composite ecological network can be promoted.

At present, the concept of the life community of mountains, rivers, forests, fields, lakes, and grasses and its system governance is one of the core pillars of China's ecological civilization construction. There are two realistic paths to promote the management of landscape, forest, field, lake, and grass systems: Firstly, in the context of global climate and environmental changes, coordinated governance focusing on watershed management and ecological environment restoration, to restore and improve various natural ecological subsystems as well as service functions and enhance its climate adaptability; Secondly, in the context of new urbanization and green development transformation, a coordinated plan focusing on natural capital and green infrastructure investment to cultivate ecological dividends and realize ecological economy.

5. Conclusions

Taking the Hefei metropolitan area as an example, this paper emphasizes multi-scale collaborative planning and multi-disciplinary integration, building an ecological network of two scales of "metropolitan area–urban area". Based on the LCP, the circuit theory, and the cyclic window search method, the important transfer nodes in the scale nesting, the pinch points, and barrier points that affect multi-level connectivity are quantitatively identified. The specific optimization layout plan for the ecological network structure of the Hefei metropolitan area is further proposed. The main conclusions are as follows:

(1) In the two-scale ecological network of the metropolitan area and the urban area constructed based on the "source–corridor–key point" paradigm, the overlapping area of ecological sources is 1719.95 km^2, and 10 ecological corridors overlap with each other. Longer ecological corridors should be protected to prevent the corridor from breaking and affecting the normal progress of ecological processes. The overlapping area of the two scales needs special protection because it is a key area to realize the stability of the overall ecological security pattern and the continuity of biological processes of the region.

(2) Ecological pinch points and barrier points are respective areas where species easily migrate from source to source and movement is strongly hindered, so protection and restoration should be given priority: 247 and 48 pinch points were, respectively, identified

in the metropolitan area and the urban area, and 39 of them overlapped. Moreover, there were 189 and 218 barrier points in the two areas, respectively, 17 of which overlapped. It is more important to prioritize the restoration of pinch points or barrier points that overlap between the two regions for maintaining regional ecological stability. Furthermore, building a multi-level ecological structure and function nesting, and formulating a corresponding optimization as well as a coordination plan for the cross-scale pattern can effectively deal with ecological problems.

Author Contributions: Conceptualization, H.Y., and Y.W.; methodology, H.Y., and Q.Z. and Z.L.; software, H.Y., and Q.Z.; writing—original draft preparation, H.Y., X.F. and Y.R.; writing—review and editing, H.Y., C.E. All authors have read and agreed to the published version of the manuscript.

Funding: This research was funded by the National Natural Science Foundation of China (Grant No. 51778002).

Institutional Review Board Statement: Not applicable.

Informed Consent Statement: Not applicable.

Data Availability Statement: Data sharing is not applicable to this article.

Conflicts of Interest: The authors declare no conflict of interest.

References

1. Dong, Y.; Jin, G.; Deng, X.; Wu, F. Multidimensional measurement of poverty and its spatio-temporal dynamics in China from the perspective of development geography. *J. Geogr. Sci.* **2021**, *31*, 130–148. [CrossRef]
2. Jin, G.; Shi, X.; Zhang, L.; Hu, S. Measuring the SCCs of different Chinese regions under future scenarios. *Renew. Sustain. Energy Rev.* **2020**, *130*, 109949. [CrossRef]
3. Elmqvist, T.; Andersson, E.; Mcphearson, T.; Bai, X.; Leeuw, S. Urbanization in and for the Anthropocene. *NPJ Urban Sustain.* **2021**, *1*, 7. [CrossRef]
4. Piao, S.; Ciais, P.; Huang, Y.; Shen, Z.; Peng, S.; Li, J.; Zhou, L.; Liu, H.; Ma, Y.; Ding, Y.; et al. The impacts of climate change on water resources and agriculture in china. *Nature* **2010**, *467*, 43–51. [CrossRef] [PubMed]
5. Bennett, A.F. Habitat corridors and the conservation of small mammals in a fragmented forest environment. *Landsc. Ecol.* **1990**, *4*, 109–122. [CrossRef]
6. Cunha, N.S.; Magalhaes, M.R. Methodology for mapping the national ecological network to mainland portugal: A planning tool towards a green infrastructure. *Ecol. Indic.* **2019**, *104*, 802–818. [CrossRef]
7. Zhang, J.; Jiang, F.; Cai, Z.; Dai, Y.; Liu, D.; Song, P.; Hou, Y.; Gao, H.; Zhang, T. Resistance-Based Connectivity Model to Construct Corridors of the Przewalski's Gazelle (Procapra Przewalskii) in Fragmented Landscape. *Sustainability* **2021**, *13*, 1656. [CrossRef]
8. Rohr, R.P.; Saavedra, S.; Bascompte, J. On the structural stability of mutualistic systems. *Science* **2014**, *345*, 1253497. [CrossRef]
9. Peng, J.; Zhao, H.J.; Liu, Y.X.; Wu, J.S. Research progress and prospect on regional ecological security pattern construction. *Geogr. Res.* **2017**, *36*, 407–419.
10. Jin, G.; Deng, X.; Zhao, X.; Guo, B.; Yang, J. Spatiotemporal patterns in urbanization efficiency within the Yangtze River Economic Belt between 2005 and 2014. *J. Geogr. Sci.* **2018**, *28*, 1113–1126. [CrossRef]
11. Wu, J.S.; Zhang, L.Q.; Peng, J.; Feng, Z.; Liu, H.M.; He, S.B. The integrated recognition of the source area of the urban ecological security pattern in Shenzhen. *Acta Ecol. Sin.* **2013**, *33*, 4125–4133.
12. Liu, J.; Yin, H.W.; Kong, F.H.; Li, M.H. Structure optimization of circuit theory-based green infrastructure in Nanjing. *China. Acta Ecol. Sin.* **2018**, *38*, 4363–4372.
13. Li, H.; Yi, N.; Yao, W.J.; Wang, S.Q.; Li, Z.Y.; Yang S, H. Shangri-La county ecological land use planning based on landscape security pattern. *Acta Ecol. Sin.* **2011**, *31*, 5928–5936.
14. Zhang, Z.; Chen, Y.; Wang, P.; Zhang, S.; Tao, F.; Liu, X. Spatial and temporal changes of agro-meteorological disasters affecting maize production in china since 1990. *Nat. Hazards* **2014**, *71*, 2087–2100. [CrossRef]
15. Peng, J.; LYU, D.N.; Dong, J.Q.; Liu, Y.X.; Liu, Q.Y.; Li, B. Processes coupling and spatial integration: Characterizing ecological restoration of territorial space in view of landscape ecology. *J. Nat. Resour.* **2020**, *35*, 3–13.
16. Wu, J.G. *Landscape Ecology: Pattern; Process; Scale and Hierarchy*; Higher Education Press: Beijing, China, 2007.
17. Li, Y.; Wang, X.; Dong, X. Delineating an Integrated Ecological and Cultural Corridor Network: A Case Study in Beijing, China. *Sustainability* **2021**, *13*, 412. [CrossRef]
18. Ouyang, X.; Wang, Z.; Zhu, X. Construction of the Ecological Security Pattern of Urban Agglomeration under the Framework of Supply and Demand of Ecosystem Services Using Bayesian Network Machine Learning: Case Study of the Changsha–Zhuzhou–Xiangtan Urban Agglomeration, China. *Sustainability* **2019**, *11*, 6416. [CrossRef]
19. Yue, B.R.; Liu, Z.Y. From ecological scale to spatial scale: Application of scale effect in landscape architecture planning and design. *Chin. Landsc. Archit.* **2017**, *33*, 77–81.

20. Huber, P.R.; Greco, S.E.; Thorne, J.H. Spatial scale effects on conservation network design: Trade-offs and omissions in regional versus local scale planning. *Landsc. Ecol.* **2010**, *25*, 683–695. [CrossRef]
21. Liu, Y.H.; Fu, B.J. Ecological scale and scaling. *Acta Ecol. Sin.* **2000**, *21*, 2096–2105.
22. Hoppert, M.; Bahn, B.; Bergmeier, E.; Deutsch, M.; Epperlein, K.; Hallmann, C.; Müller, A.; Platz, T.V.; Reeh, T.; Stück, H.; et al. The Saale-Unstrut cultural landscape corridor. *Environ. Earth Sci.* **2018**, *77*, 1–12. [CrossRef]
23. Cabeza, M.; Moilanen, A. Design of reserve networks and the persistence of biodiversity. *Trends Ecol. Evol.* **2001**, *16*, 242–248. [CrossRef]
24. Parent, J.R.; Volin, J.C. Validating Landsat-based landscape metrics with fine-grained land cover data. *Ecol. Indic.* **2016**, *60*, 668–677. [CrossRef]
25. Jiang, C.; Guo, H.; Wei, Y.P.; Yang, Z.Y.; Wang, X.C.; Wen, M.; Yong, L.; Zhao, L.L.; Zhang, H.Y.; Zhou, P. Ecological restoration is not sufficient for reconciling the trade-off between soil retention and water yield: A contrasting study from catchment governance perspective. *Sci. Total Environ.* **2021**, *754*, 142139. [CrossRef]
26. Zakeri, E.; Mousavi, S.A.; Karimzadeh, H. Scenario-based modelling of soil conservation function by rangeland vegetation cover in northeastern Iran. *Environ. Earth Sci.* **2020**, *79*, 665–675.
27. Li, J.P.; IA, S.X.; Yu, X.B. Evaluation of Carbon Storage on Terrestrial Ecosystem in Hebei Province Based on InVEST Model. *J. Ecol. Rural Environ.* **2020**, *36*, 854–861.
28. Wang, Y.G.; Luo, G.P.; Feng, Y.X.; Han, Q.F.; Fan, B.B.; Chen, Y.L. Effects of Land Use/Land Cover Change on Carbon Storage in Manas River Watershed over the Past 50 Years. *J. Nat. Resour.* **2013**, *28*, 994–1006.
29. Huang, M.Y.; Yue, W.Z.; Feng, S.R.; Zhang, J.H. Spatial-temporal evolution of habitat quality and analysis of landscape patterns in Dabie Mountain area of west Anhui province based on InVEST model. *Acta Ecol. Sin.* **2020**, *40*, 2895–2906.
30. Kong, F.H.; Yin, H.W.; Nakagoshi, N.; Zong, Y.G. Urban green space network development for biodiversity conservation: Identification based on graph theory and gravity modeling. *Landsc. Urban Plan.* **2010**, *95*, 16–27. [CrossRef]
31. Zhu, J.; Su, J.; Yin, H.W.; Kong, F.H. Construction of Xuzhou ecological network based on comprehensive sources identification and multi-scale nesting. *J. Nat. Resour.* **2020**, *35*, 1986–2001.
32. Linkage Mapper User Guide. Available online: https://circuitscape.org/linkagemapper/ (accessed on 20 March 2019).
33. Mcrae, B.H.; Dickson, B.G.; Keitt, T.H.; Shah, V.B. Mcrae bh, dickson bg, keitt th, shah vb. using circuit theory to model connectivity in ecology, evolution, and conservation. *Ecology* **2008**, *89*, 2712–2724. [CrossRef]
34. Peng, J.; Yang, Y.; Liu, Y.X.; Hu, Y.N.; Du, Y.Y.; Meersmans, J.; Qiu, S.J. Linking ecosystem services and circuit theory to identify ecological security patterns. *Sci. Total Environ.* **2018**, *644*, 781–790. [CrossRef] [PubMed]
35. Lee, S.W.; Hwang, S.J.; Lee, S.B.; Hwang, H.S.; Sung, H.C. Landscape ecological approach to the relationships of land use patterns in watersheds to water quality characteristics. *Landsc. Urban. Plan.* **2009**, *92*, 80–89. [CrossRef]
36. Nathwani, J.; Lu, X.L.; Wu, C.Y.; Fu, G.; Qin, X.N. Quantifying security and resilience of Chinese coastal urban ecosystems. *Sci. Total Environ.* **2019**, *672*, 51–60. [CrossRef] [PubMed]
37. Cheng, F.Y.; Liu, S.L.; Hou, X.Y.; Dong, S.K.; Ana, C.X.X. The effects of urbanization on ecosystem services for biodiversity conservation in southernmost Yunnan Province, Southwest China. *J. Geogr. Sci.* **2019**, *29*, 1159–1178. [CrossRef]
38. Li, J.; Xu, J.; Chu, J. The Construction of a Regional Ecological Security Pattern Based on Circuit Theory. *Sustainability* **2019**, *11*, 6343. [CrossRef]
39. Song, L.L.; Qin, M.Z. Identification of ecological corridors and its importance by integrating circuit theory. *Chin. J. Appl. Ecol.* **2016**, *27*, 3344–3352.
40. Zhao, W.W.; Fu, B.J.; Chen, L.D. Some fundamental issues in scaling. *Adv. Earth Sci.* **2002**, *6*, 905–911.
41. Xu, K.P.; Wang, J.N.; Wang, J.J.; Wang, X.H.; Chi, Y.Y.; Zhang, X. Environmental function zoning for spatially differentiated environmental policies in China. *J. Environ. Manag.* **2020**, *255*, 109485. [CrossRef] [PubMed]

Journal of Intelligent & Fuzzy Systems 40 (2021) 733–743
DOI:10.3233/JIFS-200712
IOS Press

Research on spatial planning evaluation of Beijing Shanghai high speed railway station based on node-place model

Wangyang Gui[a,*], Xu Zhang[b] and Ai Wang[a]
[a]*Doctor, School of Architecture and Planning, Anhui Jianzhu University, China*
[b]*Master, School of Architecture and Planning, Anhui Jianzhu University, China*

AUTHOR COPY

Abstract. The construction of high-speed rails is regarded as a major opportunity for urban development by local governments in China, so various grand development plans are actively formulated to promote urban economic development. In this paper, the development of station space is evaluated empirically based on the calculated node and place values of 24 high-speed rail stations along the Beijing-Shanghai line and Bertolini's "node-place" model. The results show that: (1) The 24 stations along the Beijing-Shanghai line have different development scale, which mostly act as sub-centers of the city, where the real estate industry, modern service industry and cultural industry are dominated in station space planning. Moreover, local governments are optimistic about the accelerant effect of high-speed rail stations whose functional configuration along the line is relatively repeated, because all 24 stations are basically set with business centers. (2) The size of cities along the Beijing-Shanghai line is related to the node value, the higher the urban function level, the greater the node value, with great differences among cities. The node value of big cities is far higher than that of small and medium-sized cities, hence there are node-oriented station areas in big cities and place-oriented ones in middle-sized and small cities. However, there is no direct relationship between the urban function level of stations along the line and the value of urban places. In some small and medium-sized cities, the planning and development intensity and scale of station areas even exceed that of big cities. (3) Only Wuxi station and Nanjing station are in a balanced development state in the space planning of railway stations along the Beijing-Shanghai line. Therefore, the risk of long-term development of station area should be considered in the planning, and reasonable measures should be formulated to promote the sustainable development of station area, so as to form the overall development of Station City.

Keywords: High speed railway, station area, Beijing-Shanghai line, node-place model

The key to play the role of railway stations accelerant lies in the overall development of them and the surrounding areas, thus promoting the overall economic and social development of the city, while the core of sustainable development of station areas is the balance of their functions. Therefore, the sustainable development of station space should not only focus on the construction of passenger stations, but also give full play to their accelerant role in promoting urban economic and social development. At present, with the rapid development of high-speed rails in China, a large number of high-speed rail new towns have been built. Therefore, it is a key issue to correctly understand the evolution mechanism of high-speed rail station area and explore the new characteristics of interactive development of stations-cities in China to establish a healthy and sustainable new urban space.

*Corresponding author. Wangyang Gui, Anhui Jianzhu University, 856 Jinzhai South Road, Baohe District, Hefei City, Anhui Province, China. E-mail: 21356364@qq.com.

ISSN 1064-1246/21/$35.00 © 2021 – IOS Press. All rights reserved.

1. Literature review

Does the construction of high-speed rail really play a role in the development of cities along the line? What is the relationship between its driving role and city size? Different scholars have different understanding, mainly in the following two aspects.

1.1. Study on the relationship between regional benefits and city size

Scholars who hold the theory of benefits to small and medium-sized cities: Allport R.J. and Brown M.E pointed out in 1993 that the construction of high-speed rail cannot bring great development in large cities because the original transportation facilities system has been relatively perfect. However, for small and medium-sized cities where original transportation facilities system is relatively immature, the construction of high-speed rail will improve the accessibility between them and large cities, and bring more favorable location conditions for small and medium-sized cities [1]. Urena's research on French high-speed rail in 2009 found that medium-sized cities between big cities are the biggest beneficiaries of high-speed rail compared with big cities and small cities [2].

Scholars who hold the theory of benefits to big cities believe that the development of high-speed rail will bring spatial polarization in the region, so that big cities can get more benefits. Sasaki's research shows that Tokyo has the largest growth among the cities along the Shinkansen line after the completion, which shows that the construction of high-speed rail can not solve the problem of excessive concentration of regional resources to large cities [3]. Kim, a Korean scholar, also believed that after the construction of high-speed railway, the surrounding population tends to gather in large cities [4]. Wichmann, a British scholar, also proved that the construction and opening of high-speed rail will lead to the concentration of economic activities and social resources to large cities along the line [5].

1.2. Advantages and disadvantages of passenger stations on urban spatial development pattern

Those who hold the view of positive effect think that the construction of passenger station enhances the accessibility of the region, affects the degree of employment, mixed land development and traffic demand, and promotes the development of the region and the upgrading of the industry [6]. Tim Lynch (1998) found that high-speed rail has a great role in promoting the economic and technological development along the line [7]. PMJ Pol (2003) believed that high-speed rail has a catalytic effect on regional economy, which is mainly manifested in two aspects: the generation of new economic activities and the construction of new infrastructure, so as to promote the economic growth of a region [8]. Oscar (2005) pointed out that the influence of the station on the surrounding areas mainly includes two aspects: on the one hand, the station construction has a great impact on the living and work in the city; on the other hand, the high-speed rail can improve the use efficiency of public transport facilities in the surrounding areas, which is conducive to the alleviation of urban traffic congestion and the development of urban economy and society [9]. Marc Guigon (2011) found that high-speed rail led to the rapid development of the tertiary industry and promoted the regional development through the study of the southern city of Valens in France.

Those who hold the view of negative effects have criticized and questioned the development of high-speed rail. Through the research of European high-speed rail network, Roger Vickerman (1997) pointed out that due to the lack of overall systematic research, the construction and opening of high-speed rail did not solve the problems existing in the development along the line as expected, but caused the continuous accumulation of large cities [10]. Ryan (1999) believed that only being close to a transportation facility locally does not necessarily increase its value, but only when the means of transportation can save travel costs can it really improve the property value. The research of Marc Guigon (2011) shows that high-speed rail will speed up the development of the region, but may cause "tunnel effect" if the local development is in a dilemma. PMJ Pol pointed out in 2003 that the construction and opening of high-speed railway will be more beneficial to those cities with good basic conditions, but the impact on those cities with relatively poor basic conditions is not necessarily so positive. In other words, "it does not mean that every station on the high-speed railway can have a huge impact on the economic development of the city" [11, 12].

Bertolini L thinks that the railway station area is not only the node in the transportation network, but also the place in the urban space, which embodies the transport and functional value of the railway station,

AUTHOR COPY

and that the balanced development of the node and the place function is the ideal state of the station area. The "node-place" model is a practical theoretical model for evaluating the development of the station area, which is widely used to evaluate the development of the transport hub areas in foreign countries [13, 14], but at present, the research on it only stays in theoretical interpretation in China. In this paper, taking the Beijing-Shanghai line as an example, the transport and functional value of nodes in the high-speed railway station area are calculated respectively, and the sustainability of the planning and development there is evaluated through the "node-place" model, so as to provide basis and suggestions for the planning and development of high-speed railway new towns [6].

2. Methodology

2.1. Node-place model

Under the support of TOD concept, Bertolini L put forward the "node-place" structure model of railway passenger station (Fig. 1), and he thought that the most basic function of passenger station is to strengthen the integration of transportation and provide basic transportation services for the emerging multi-center cities. However, with the increase of complexity of railway station area, more attention should be paid to the space development strategy of balanced node and place in railway station area. According to the model, the spatial function of station can be divided into five categories [15]: ① Station areas of balanced development, where the transport node function and urban place function of station area have achieved strong development, the developed node is the guarantee of system maintenance and environmental quality improvement in the area where node value and place value are equal and the two functions support each other. ② The dependent type station area in a free space without competition, with low traffic demand, not very convenient traffic, and relatively less urban functions, has no demand for further development of traffic due to the lack of local development potential. ③ Tension type station area that will be in a tense situation with the development potential of efficient use of land which has been explored because the diversity of transportation facilities and land use are close to the maximum. ④ The station area with node function as the main part has very developed traffic facilities,

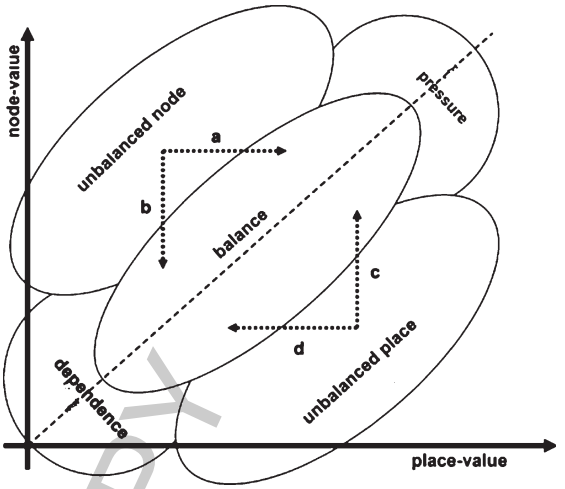


Fig. 1. Node—Place Model. Source: Refer to Ari Hynynen. Node-Place-Model; A Strategic Tool for Regional Land Use Planning. Nordic Journal of Architectural Research, 2006,4:21-29.

which are higher than land use activities, and has a small number of urban functions. This imbalance is manifested in the degradation of environmental quality caused by the fragmented land use brought by traffic facilities and traffic jams. But from a development point of view, they are worthy of attention because there may be opportunities to create new functions here. ⑤ The place function-oriented station area, where active land-use activities are stronger than the supply of transportation facilities, which has a variety of urban functions and relatively fewer transportation facilities, mainly in those areas where entrepreneurship relies on traditional technology support, because it is too remote for economic flow and a large number of infrastructure construction. They deserve attention from a transport perspective, as there may be opportunities to develop new transport facilities.

According to the model, the space node function and the place function of the ideal station area should be roughly balanced, that is, in the "rugby" area, there is no dependence or tension in this area, and the traffic is convenient, while the environmental quality of the station area can be better guaranteed.

2.2. Calculation method of node value

The node (transport) value reflects the transport attribute of the station, and the accessibility is its main measure index, which is commonly calculated by potential accessibility, weighted average travel time

AUTHOR COPY

Table 1
Assignment table of planning strength coefficient

Summary of High-Speed	Grade factor value	Functions	Value of function coefficient
City sub center	1.0	Comprehensive Function	0.2
City Portal, New district,	0.8	Single Function	0
Functional demonstration	0.6		
City windows,	0.4		
Residential community	0.2		

Source: Wenjie Song, Yujin Shi, Qing Zhu, etc. Evaluation of high-speed rail station area planning based on node-site model——Taking the Yangtze River Delta as an example [J]. Economic Geography, 2016 (10): 18-25.

/ cost, daily accessibility distance [16] and gravity model method [17]. Among them, potential accessibility is the most widely used method to calculate the regional accessibility of transport nodes [16, 19]. Therefore, in this paper, accessibility is taken as the calculation index of node value, according to the principle that the smaller the distance is, the higher the accessibility level is. The potential economic impact of accessibility on urban development decreases with distance. That is to say, the potential economic impact of j City on i city is directly proportional to the economic scale of j City and inversely proportional to the distance between them. In addition, due to the large correlation between the node accessibility and the economic attraction scale of each node itself, that is, the greater the economic attraction among nodes, the higher the accessibility level. Therefore, in this paper, the potential accessibility calculation method improved by gravity model method is adopted [20]. The formula is as follows:

$$A_i = PA_i D_i = \Sigma \frac{D_i D_j}{t_ij^{\alpha}}$$

Where,

A_i = accessibility of station i;

PA_i = potential accessibility of station i;

D_i, D_j = economic attraction of stations i and j respectively, and the GDP data of the city where the station is located (2016) is substituted into the calculation, GDP comes from the yearbook data published on the website of the National Bureau of statistics of China;

t_{ij} = travel time from stations i to j (based on the time cost data between stations, the shortest time of high-speed rail between two cities can be obtained on 12306 website);

α = friction coefficient of distance, and the accessibility of regional economic activities is usually taken as 1 [21], so $\alpha = 1$.

2.3. Calculation of place value in station area

The place (function) value reflects the functional attribute of the station area, which is an assessment of the density and intensity of regional activities, taking into account the planning, as well as the development orientation, main functions, land use and other indicators of the station area [20]. The formula is as follows:

Place functional value of the station = scale of land use × planning intensity factor

Planning strength coefficient = grade coefficient + function coefficient

Where, the scale of land use is the planned land area of high-speed railway new town; the grade coefficient represents the positioning of its own grade and level in the planning of high-speed railway new town, and the higher the positioning is, the larger the value is; the function coefficient represents the degree of diversification of regional functions undertaken by the new high-speed railway city, and the more types of functions, the greater the value (Table 1) [20].

3. Research object

Beijing-Shanghai high-speed railway runs through 24 stations in four provinces and three municipalities directly under the central government, connecting the two largest cities in China, Beijing and Shanghai, as well as the Yangtze River Delta and Bohai rim economic zones. Along the way, there are not only developed coastal economic zones, but also underdeveloped areas such as Northern Jiangsu and Northern Anhui. Its completion marks the coming of China's high-speed railway era and is of great significance to the development of China's high-speed railway. Moreover, after more than 10 years of development, it has formed a certain scale in the station area, with strong representativeness, which provides

AUTHOR COPY

conditions for space development research in the station area (Table 2). In this paper, 24 stations of Beijing-Shanghai railway are taken as the research object to analyze the spatial evolution characteristics of the station area of Beijing-Shanghai railway and the development status of the railway station and its surrounding areas, which is of great significance to understand the role of accelerant in China's high-speed railway station and the development status of the station area.

4. Planning status of station areas along Beijing-Shanghai high speed railway

Through the study of 24 stations along the Beijing-Shanghai line, it is found that all stations have corresponding plans (Table 2), and the development scale of them varies greatly. The largest planning area is Hongqiao Station in Shanghai, with a total planning area of 1,563km^2, followed by Beijing south station, with a planning area of 1,268km^2, and the smallest is Dingyuan station, with a planning area of 12km^2, followed by Qufu station, with a planning area of 23km^2. Thus it is clear that if the city scale and economic development level are high, the agglomeration capacity is strong, and the radiation scope is wide, the planning scope will be large; the planning scope of small city with a weak economic foundation is smaller.

In terms of planning positioning, there are urban new areas, urban sub-centers, urban portals, new urban centers, urban business centers, integrated transportation hubs, international business centers and residential communities. Among them, urban sub-center is the most commonly known. The planning positioning shows that the local government is optimistic about the accelerant effect of high-speed rail, and generally prefers the modern business center and urban sub-center, so as to drive the adjustment of urban structure and develop from a single center to multi centers [22].

In terms of function orientation, it is found that business office function, residential function, business trade function, leisure and entertainment function are the main planning functions of the station area. Real estate industry, modern service industry and cultural industry have become the main industries of station space planning, while exhibition industry, tourism industry, financial industry, education industry and high-tech industry have not been paid attention to, which however can form a good coordinated development with high-speed rail thanks to its rapid distribution of people flow, logistics, information flow, capital flow, to give full play to the accelerant effect of high-speed rail. Therefore, these functions can be added appropriately when conditions are available.

From the perspective of functional structure configuration along the Beijing-Shanghai line, the functional positioning is more repetitive, because business centers are all basically set up. Taking the passenger stations on the edge of the built-up areas of six major cities along the line as an example: Jinan West Railway Station is positioned as a sub-center of the city dominated by business, exhibition and culture; Tai'an railway station is positioned as a new town, a high-end business area and a leisure and living area suitable for business and living; Xuzhou station is positioned as an ecological business district of high-speed railway; Suzhou north station is positioned as a new city integrating commerce, scientific research, residence, office, culture, tourism and other functions; Tianjin south station is positioned as a commercial, residential and cultural town. Commerce and residence have become the main functional formats of such stations, with serious homogenization. The similarity of functions will inevitably lead to the surplus of urban competitiveness, resulting in the narrow way of follow-up development.

5. Calculation of node-place value of stations along the Beijing-Shanghai line

5.1. Calculation of node value of Beijing-Shanghai line

It is found after the value of the nodes is calculated by the calculation formula and then arranged from large to small according to the planning data of the station (Table 2) that, the scale of cities along the Beijing-Shanghai line is related to the node value; the higher the urban functional level is, the greater the node value is; and there are great differences between big and small cities; the node value of big cities is much higher than that of small and medium-sized cities (Table 3, Fig. 2), for example, the node value of Shanghai Hongqiao Station, North Suzhou Station, West Tianjin Station, East Wuxi Station and South Beijing Station is much higher than that of Chuzhou Station, East Suzhou Station, South Bengbu Station, East Tengzhou Station, East Qufu Station and Dingyuan Station, which

AUTHOR COPY

Table 2
Basic situation of site area planning of Beijing Shanghai line

Site	City	City type	Planning area (km^2)	Location	Major function
South BeiJing	BeiJing	Mega	1268	Modern comprehensive transportation hub, Capital image window	Business center functions
Langfang	Langfang	Big	61.3	City window	Comprehensive business center
Tianjin West	Tianjin	Mega	605	Comprehensive city sub center	Business trade, business finance, leisure, culture, residence
Tianjin South				Iconic business portal, Ecologically stylish livable place	Business, housing, cultural leisure, information media industry
Cangzhou West	Cangzhou	Medium-sized	47.1	Urban New Area	Transportation hub, business service and residence
Dezhou East	Dezhou	Medium-sized	66	City New Area	New industry, transportation hub, export-oriented industry
Jinan West	Jinan	Big city	310	Qilu New Gateway, Quancheng New Commercial Port, Urban Sub-center	Business, exhibition and culture as the leading functions
Taian	Taian	Big city	81.1	Gateway new urban area	Business, high-end business, residence and leisure
Qufu East	Qufu	Medium-sized	23	Urban Comprehensive Development Zone	Business, residence, leisure and entertainment
Tengzhou East	Tengzhou	Medium-sized	46	Comprehensive Development Zone	Residence, business, leisure and entertainment
Zaozhuang	Zaozhuang	Big	36.1	City-level city center, modern new urban area	Business exhibition, administrative office, entertainment, sports and residence
Xuzhou East	Xuzhou	Big	108	Comprehensive transportation hub and city gateway	Eco business district, high-end service industry and high-tech industry
Suzhou East	Suzhou	Small	27.3	Comprehensive new town	Production, residence, transportation, commerce, logistics and leisure
Bengbu South	Bengbu	Medium-sized	53.3	City New Area	High end service, R & D, ecology and housing
Dingyuan	Dingyuan	Small	12	Transportation portal hub	Transportation hub, scientific research
Chuzhou South	Chuzhou	Medium-sized	36.5	New urban area, business and logistics center	Business, transportation, culture, entertainment and residence
Nanjing South	Nanjing	Mega	502	Southern new center, hub-type business center	Modern service industry, commerce and commerce, headquarters economy, culture, tourism, exhibition industry and residence
Zhenjiang South	Zhenjiang	Big	52.3	Urban sub center, gateway hub	Administration, office, business, culture, shipbuilding industry, residence
Danyang North	Danyang	Medium-sized	33.2	Business Information Port	Business, information service, cultural tourism and residence
Changzhou North	Changzhou	Big	307	International Business City	Finance, commercial commerce, comprehensive transportation hub, public service and scientific research and development
Wuxi East	Wuxi	Big	372	Wuxi City Sub Center	Administrative, cultural, business center, service industry and regional passenger transport hub
Suzhou North	Suzhou	Mega City	411	New portal, internationalization, informatization and modern new city	Commerce, scientific research, residence, office, culture and Tourism
Kunshan South	Kunshan	Big city	150	Urban external transportation hub, urban portal	Business, business, mixed community
Hongqiao	Shanghai	Mega City	1563	Business center facing Yangtze River Delta	Headquarters office, commercial trade, modern business, medical treatment, education, residence

Source : The area of the built-up area is based on the data of China's urban built-up area. According to the Ministry of Housing and Urban-Rural Developmen, China Urban Construction Statistical Yearbook 2006–2018.

AUTHOR COPY

Table 3
Calculated value of node value

Station area	Calculated value of node value	Normalized value	Station area	Calculated value of node value	Normalized value
South BeiJing	31335437.27	0.626708745	Suzhou East	1998028.164	0.039960563
Langfang	3668196.025	0.073363921	Bengbu South	1991831.278	0.039836626
Tianjin West	39053514.07	0.781070281	Dingyuan	242067.0902	0.004841342
Tianjin South	43550044.36	0.871000887	Chuzhou	2529603.584	0.050592072
Cangzhou West	3736085.762	0.074721715	Nanjing South	18235056.75	0.364701135
Dezhou East	5303230.098	0.106064602	Zhenjiang South	8514069.151	0.170281383
Jinan West	10162646.44	0.203252929	Danyang North	3171007.311	0.063420146
Taian	5465878.767	0.109317575	Changzhou North	16298514.77	0.325970295
Qufu East	686948.9581	0.013738979	Wuxi East	32239403.67	0.644788073
Tengzhou East	1684043.562	0.033680871	Suzhou North	45896807.75	0.917936155
Zaozhuang	3335298.181	0.066705964	Kunshan South	13625657.59	0.272513152
Xuzhou East	7905125.891	0.158102518	Shanghai	46161299.1	0.923225982

Source: Author's own.

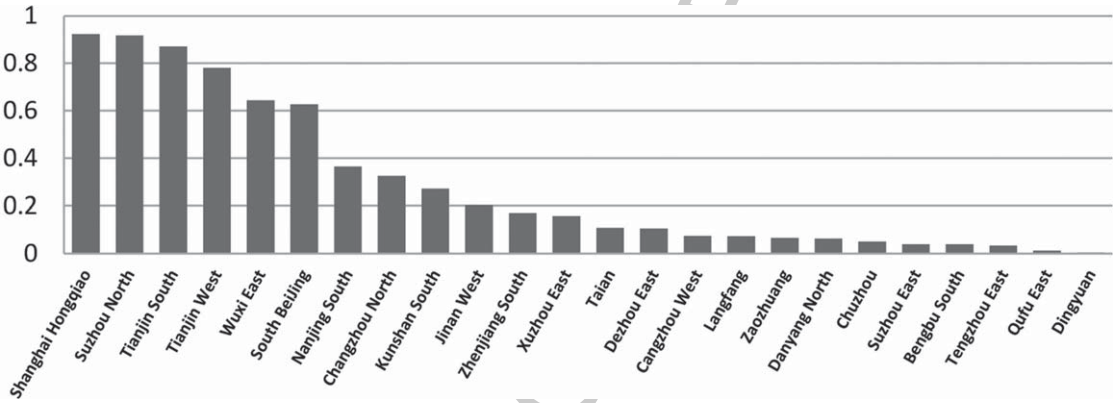


Fig. 2. Node value ranking Source: Author.

also shows that the accessibility of big cities is much higher than that of small and medium-sized cities. In addition, the node value of Beijing-Shanghai line is not evenly distributed among stations in big cities, such as Shanghai Hongqiao Station, North Suzhou Station, West Tianjin Station and south Tianjin Station, which are significantly higher than those of South Nanjing Station and West Jinan Station. In contrast, the node value of Beijing-Shanghai line is more evenly distributed in small and medium-sized cities, such as Cangzhou West Station, Langfang Station, Zaozhuang Station and Danyang North Station, which are close in node values.

5.2. Calculation method of place value

According to the station planning data and the place (function) value calculation formula, the place value is calculated (Table 4). In the formula, the scale of land use comes from the planning of high-speed rail new towns of 24 stations, which is mainly reflected in the planned land area of the station area (Table 2); the grade coefficient is the positioning of the station area in the planning, the higher the level is, the larger the value is based on the planning of each station area (Table 1, Table 2); the function coefficient is the diversity degree of the function positioning of the station area, the more diversified the function is, the greater the value is, based on the planning of each station area (Table 1, Table 2).

Table 4 and Fig. 3 show that the site value of Jinan West Station, Dezhou East Station, Xuzhou East Station and Nanjing South Station is significantly higher than that of other stations, while the planning scale of Changzhou North Station, Zhenjiang South Station, Dingyuan Station, Tianjin South Station and Kunshan South Station is small with low place value, and the place value distribution of other stations is relatively balanced and the difference is not significant. In addition, there is no direct relationship between the urban functional level of stations along the line and the value of urban places. In some small and

Table 4
Site value of Beijing Shanghai railway station

City	Calculated value of node	Normalized value	City	Calculated value of node	Normalized value
South BeiJing	31335437.27	0.020571429	Suzhou East	1998028.164	0.428571429
Langfang	3668196.025	0.057142857	Bengbu South	1991831.278	0.197142857
Tianjin West	39053514.07	0.171428571	Dingyuan	242067.0902	0.011428571
Tianjin South	43550044.36	0.008142857	Chuzhou	2529603.584	0.312857143
Cangzhou West	3736085.762	0.4	Nanjing South	18235056.75	0.548571429
Dezhou East	5303230.098	0.714285714	Zhenjiang South	8514069.151	0.016114286
Jinan West	10162646.44	0.942857143	Danyang North	3171007.311	0.020571429
Taian	5465878.767	0.357142857	Changzhou North	16298514.77	0.018285714
Qufu East	686948.9581	0.5	Wuxi East	32239403.67	0.781714286
Tengzhou East	1684043.562	0.117714286	Suzhou North	45896807.75	0.325942857
Zaozhuang	3335298.181	0.142857143	Kunshan South	13625657.59	0.008
Xuzhou East	7905125.891	0.714285714	Shanghai Hongqiao	46161299.1	0.222857143

Source: Author.

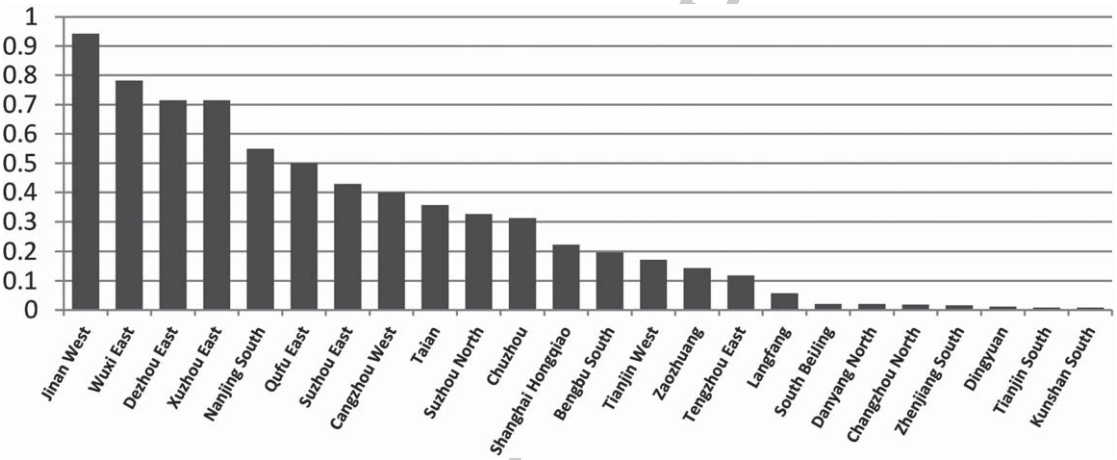


Fig. 3. Place value ranking Source: Author.

medium-sized cities, the planning and development intensity and scale of the station area even exceed that of large cities. For example, although Beijing South Railway Station is located in the center of the city, the place value is relatively low due to the limitation of the place and the extremely limited development area of the station area. Suzhou East Railway Station is located in a small and medium-sized city, but the planned area of the new town in the station area is far larger than that of Suzhou north railway station, Shanghai Hongqiao Station, Tianjin west station, etc.

6. Evaluation of node-place value of stations along the Beijing-Shanghai line

The calculated node value and place value is divided by the corresponding normalization parameters (normalization is to convert the calculated value to 0-1, and the normalization parameter is equal to or slightly greater than the maximum value of all calculated values) to get the normalized node value and place value (range: 0-1), as shown in Table 3 and Table 4. According to the normalized data, the "node-place" model map is established, with the horizontal axis representing the place value and the vertical axis representing the node value (Fig. 4).

6.1. A few stations in the balanced development zone

The node-place model map shows that (Fig. 4, Fig. 5), of the 24 stations along the Beijing-Shanghai line, there are two stations with basically balanced value, namely Nanjing Station and Wuxi East Station, accounting for 8.3% of the stations along the line, which are in a relatively balanced development mode, reflecting that the planning of these stations

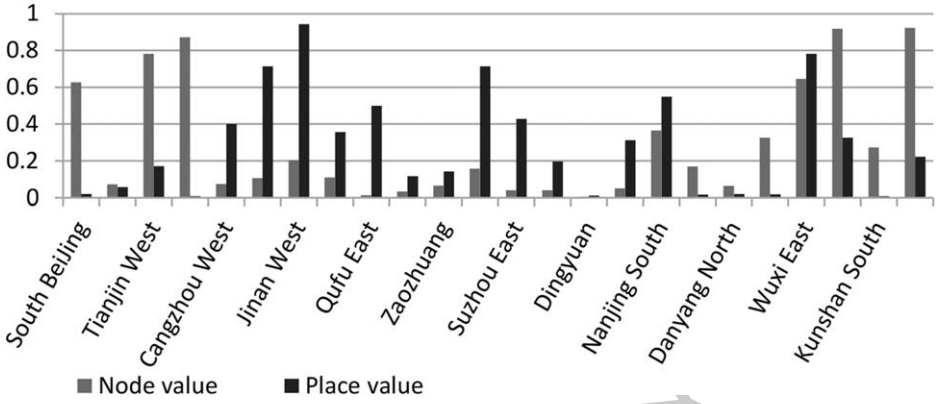


Fig. 4. Value ranking of node and place Source: Author.

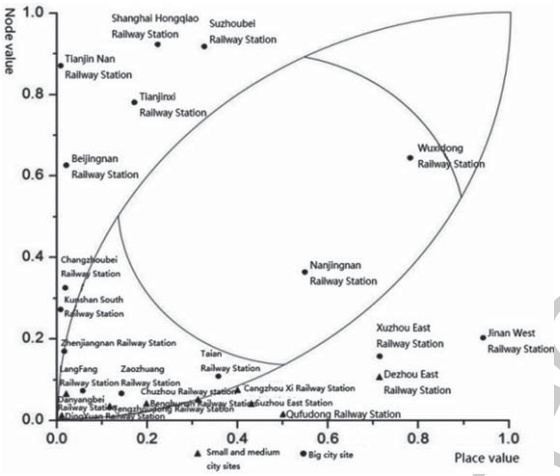


Fig. 5. Beijing-Shanghai Line Station Node-Place Model Evaluation Results.

is relatively reasonable. The development of the station area should not only include basic infrastructure projects such as comprehensive transportation, but also focus on the planning, investment and construction of public service projects, so as to form the core attraction of high-speed rail new town by improving the infrastructure. Taking Wuxi East Railway Station as an example, in the 0.533km^2 core area around the passenger station, a centralized transportation facilities land and a large-scale station square are set up, and the high-speed railway station is taken as the core to vigorously develop exhibition, tourism distribution center, bus terminal, long-distance passenger station, rail transit, etc., so as to strengthen the node function and enhance the connection between the passenger station and the city. In the second circle of 3.98km^2, a business office area, a business and tourism service area are set in the north of the station area, and a small exhibition area, a commercial shopping center, a specialized market, a large supermarket, hotels, apartments, office buildings, a culture and art center and a square are set in the south of the station area, forming a good symbiotic relationship. In the third circle of 45.62km^2, a comprehensive culture and sports area and an international comprehensive area are arranged, mainly including an Olympic Sports Center, leisure and entertainment businesses, hotels and guesthouses, international clubs, large-scale public space high-level hotel apartments, large residential areas, neighborhood service centers, etc., extending the traffic driving role of the station. Good functional configuration increases the vitality of station space and promotes the sustainable development of station area.

6.2. *Most stations deviating from the balanced development zone*

There are 9 stations in the dependent station area, namely Dingyuan Station, Danyang North Station, Tengzhou East Station, Langfang Station, Zaozhuang Station, Bengbu South Station, Chuzhou South Station, Zhenjiang Station and Tai'an Station, accounting for 37.5% of the stations along the line. They are in the low development area, with low traffic demand and lack of local development demand and potential. The main stations with node function are Kunshan South Station, Changzhou North Station, Beijing South Station, Tianjin West Station, Tianjin South Station, Suzhou North Station and Shanghai Hongqiao Station, accounting for 16.7% of the stations along the line; the main stations with

AUTHOR COPY

place function are Cangzhou West Station, Suzhou East Station, Qufu East Station, Xuzhou East Station, Dezhou East Station and Jinan West Station, accounting for 25% of the stations along the line. In addition, due to the short development time of station space, there is no tense station space. The results further show that although the station areas of Beijing-Shanghai railway in China have been developed for decades, most of them are still in the initial state; the development of space function value of the station area is relatively unbalanced; there are node-oriented station areas in big cities and place-oriented ones in middle-sized and small cities.

7. Conclusions

In this paper, the regional planning of 24 high-speed rail stations along the Beijing- Shanghai line is empirically analyzed based on the "node-place" model, and the following conclusions are drawn:

(1) The 24 stations along the Beijing-Shanghai line have different development scale, which mostly act as sub-centers of the city, where the real estate industry, modern service industry and cultural industry are dominated in station space planning. Moreover, local governments are optimistic about the accelerant effect of high-speed rail stations whose functional configuration along the line is relatively repeated, because all 24 stations are basically set with business centers.

(2) The size of cities along the Beijing-Shanghai line is related to the node value, the higher the urban function level, the greater the node value, with great differences among cities. The node value of big cities is far higher than that of small and medium-sized cities, hence there are node-oriented station areas in big cities and place-oriented ones in middle-sized and small cities. Additionally, the node value of Beijing Shanghai line is not evenly distributed among stations in big cities, but equally distributed in small and medium-sized cities whose node values are close to each other. Moreover, there is no direct relationship between the urban function level of stations along the line and the value of urban places. In some small and medium-sized cities, the planning and development intensity and scale of station areas even exceed that of big cities.

(3) The evaluation results of the "node-place" model show that a few of the 24 high-speed railway stations along the Beijing-Shanghai line are reasonably planned, and the station planning function is compatible with the actual node transport value, which is in a state of balanced development. However, the planning of most station areas cannot match the node transport value,, deviates from the value balance area, in shortage of understanding of the internal development value of this area, which is in an unsustainable development state.

AUTHOR COPY

Fund Project

Key research projects of Natural Science in Anhui colleges and Universities:

1. Research on the coupling development of high-speed railway hub and urban space from the perspective of system integration–Taking Hefei high speed railway hub as an example, KJ2019A0750.

2. Spillover effect of urban water landscape on residential land price: a case study of Hefei City, KJ2019A0752.

Fund Project of Anhui Jianzhu University introduces talents and doctors:

3. Research on the coupling development of high-speed railway hub and urban space from the perspective of system integration: Taking Hefei high-speed railway hub as an example, 2018qd34.

4. Anhui Province Housing and Urban-Rural Construction Science and Technology Plan Project, 2020-YF27.

5. Provincial Natural Science Research Projects of Universities in Anhui Province-Key Projects, KJ2019A0750.

6. The school introduced talents and doctoral start-up fund projects-natural sciences, 2018QD34.

References

[1] R.J. Allport and M. Brown, Economic benefits of the European highspeed rail network [J], *Transportation Research Record* **1381** (1993), 1–11.

[2] J.M. Urena, P. Menerault and M. Garmendia, The high-speed rail challenge for big intermediate cities: A national, regional and local perspective [J], *Cities* **26** (2009), 266–279.

[3] K. Sasaki and T.A.A. Ohashi High-speed rail transit impact on regional systems: does the Shinkansen contribute to dispersion? [J], *The Annals of Regional Science* **31** (1997), 77–98.

[4] K.S. Kim, High-speed rail developments and spatial restructuring: A case study of the Capital region in South Korea [J], *Cities* **17**(4) (2000), 251–262.
[5] M. Janic, A model of competition between high speed rail and air transport[J], *Transportation Planning and Technology* **17**(1) (1993), 1–23.
[6] W. Song, Q. Zhu, Y. Zhu, C. Kong, Y. Shi and Y. Gu, The impact of high-speed rail on the development of cities of different scales[J], *Economic Geography* **35**(10) (2015), 57–63.
[7] T. Lynch, Analysis of the Economic Impacts of Florida High-speed Rail[R]. Berlin:Inno Trans, UIC, CCFE-CER-GEB and UNIFE, 1998.
[8] PMJ Pol, The Economic Impact of the High-Speed Train on Urban Regions [J], *General Information* **10**(1) (2003), 4–18.
[9] O. Froidh, Market effects of regional high-speed trains on the Svealand line[J], *Journalof Transport Geography* **13** (2005), 352–361.
[10] R. Vickerman, High-speed Rail in Europe: Experience and Issues for Future Development[J], *The Annal of Regional Science Association* (2003), 9.
[11] PMJ Pol, The Economic Impact of the High-Speed Train on Urban Regions [J], *General Information* **10**(1) (2003), 4–18.
[12] L. Wang, W. Xia and Y. Ning, Analysis of the disequilibrium of the distribution pattern of China's high-speed rail cities: based on the perspective of comparison with ordinary railways[J], *Urban Development Research* **24**(07) (2017), 68–78.
[13] L. Bertolini, Spatial development patterns and public transport: The application of an analytical model in the Netherlands [J], *Planning Practice and Research* **14** (1999), 199–210.
[14] G.J. Peek, L. Bertolini and H. De Jonge, Gaining insight in the development potential of station areas: A decade of node- place modelling in The Netherlands [J], *Planning, Practice & Research* **21**(4) (2006), 443–462.
[15] A. Hynynen, Node-Place-Model: A Strategic Tool for Regional Land Use Planning, *Nordic Journal of Architectural Research* **4** (2006), 21–29.
[16] J. Cao, X.C. Liu, Y. Wang, et al., Accessibility impacts of China's high- speed rail network [J], *Journal of Transport Geography* **28** (2013), 12–21.
[17] J. Chen, F. Lu and C. Cheng, Review on the research progress of accessibility measurement methods and applications [J], *Progress in Geographical Sciences* **26**(5) (2008), 100–110.
[18] J. Gutiérrez, Location, economic potential and daily accessibility: an analysis of the accessibility impact of the high-speed line Madrid-Barcelona-French border [J], *Journal of Transport Geography* **9**(4) (2001), 229–242.
[19] A. Holl, Twenty years of accessibility improvements, The case of the Spanish motorway building programme [J], *Journal of Transport Geography* **15**(4) (2007), 286–297.
[20] W. Song, Y. Shi, Q. Zhu, Evaluation of high-speed rail station area planning based on node-site model: A case study of the Yangtze River Delta [J], *Economic Geography* **2016**(10), 18–25.
[21] F. Bruinsma and P. Rietveld, Urban agglomerations in European in-frastructure networks [J], *Urban Studies* **30**(6) (1993), 919–934.
[22] S. Ji and J. Duan, Planning and design strategies for the high-speed rail hub area: Taking Nanjing South Railway Station as an example [J], *Planner* **32**(03) (2016), 68–74.

AUTHOR COPY

Nature Environment and Pollution Technology
An International Quarterly Scientific Journal

p-ISSN: 0972-6268
(Print copies up to 2016)
e-ISSN: 2395-3454

Vol. 20 | No.3 | pp. 1115-1126 | 2021

Original Research Paper

https://doi.org/10.46488/NEPT.2021.v20i03.019

Open Access Journal

The Construction of Regional Ecological Security Pattern Based on a Multi-Factor Comprehensive Model and Circuit Theory

H.R. Yu*, Y.Z. Wang*(**) †, Z. Liang*and C.K. Min***

*School of architecture and planning, Anhui Jianzhu University, Hefei 230022, China
**Anhui Urbanization Development Research Center, Hefei 230022, China
***School of English, Welsh School of Architecture, Cardiff University, Cardiff CF10 3BA, UK
†Corresponding author: Y.Z. Wang; rockyhust@126.com

Nat. Env. & Poll. Tech.
Website: www.neptjournal.com

Received: 19-11-2020
Revised: 09-12-2020
Accepted: 22-02-2021

Key Words:
Regional Security pattern
Circuit theory
Residents' needs
Development strategy

ABSTRACT

Various ecological problems have become increasingly prominent due to the accelerated growth of urbanization. Ecological security and ecological conservation have become an important topics in the current scenario. This study took southern Anhui as an example, constructing comprehensive assessment models to conduct source identification from three perspectives, i.e. ecosystem services, ecological sensitivity and residents' ecological needs. Landscape resistance surface was built based on the reciprocal of habitat quality and night-time light data. According to the circuit theory, the ecological process in the heterogeneous landscape was simulated to identify ecological corridors, extract pinch points and divide barriers that need improvement, thereby to construct the southern Anhui ecological security pattern (ESP). The pattern comprised 20 ecological sources, 37 ecological corridors, 9 pinch points and 2 levels of improvement areas. Specifically, ecological sources were mainly distributed within the area of Huangshan city and Xuancheng city, mostly covered with trees; ecological corridors were mostly located in the northern part of the research area; pinch points were mainly farmland or beside construction land; the primary improvement area was mainly in Chaohu city and Maanshan city, while the secondary improvement area was distributed around the primary area. The study discussed the diversified improvement strategies of different barriers and introduced the optimization scheme "one centre, two wings, one belt", providing planning advice for decision-makers. The study expanded the construction of regional ESP, and partly guided the steady development of ESP of southern Anhui.

INTRODUCTION

The rapid development of urbanization has caused an increasingly intense contradiction between economic development and ecological conservation. Ecological systems like forests, waters, and wetlands have been destroyed, causing deterioration in the habitat quality and a decline in the biodiversity. On the other hand, people have higher needs for life thanks to the economic development, as well as new demands for ecosystem services. Ecological security pattern, the bridge between ecosystem services and societal development, is regarded as a crucial strategic tool to guarantee regional ecological security and increased well-being. The planning of ecological security pattern (ESP) has become a key for the Chinese governments at all levels to ensure the sustainable development of the regional economy, and coordinate the relationship between ecosystem and economic society. Also, it is regarded as a fundamental and a crucial method to realize regional ecological security, and one of the strategic modes for national land development and protection (Nathwani et al. 2019, Huang et al. 2020).

Currently, scholars in various fields at home and abroad have discussed the structure (He et al. 2020) and function (Song et al. 2020) of ESP, as well as its construction (Xun et al. 2018) and assessment (Yin et al. 2011, Schröter et al. 2020). In addition, scholars have conducted massive research concerning biodiversity conservation (Chen et al. 2017), nature reserve planning (Jia et al. 2005), remedy for ecosystem (Meng et al. 2012), etc. The research on ESP construction in China has formed a mainstream paradigm of "source identification—resistance surface construction—corridor construction". Generally speaking, the identification of sources should provide important ecological services and own nice landscape connectivity, greatly needed in regions. Traditional ecological source identification mostly comprises two methods: the first is to directly determine natural reserves, national parks, scenic spots, etc. as an ecological source. Though convenient to operate, it may lack the accuracy of patch assessment. Some scholars chose patches with a relatively stable type of eco-utilization in the long term as ecological sources, for example, woodland, grassland, farmland, etc. However, this method does not take land-use heterogeneity

into account, as a land of the same type in different regions still differs to a certain degree. Another more scientific method is to construct a comprehensive indicator system to assess regional parcels, and then to determine ecological sources. The chosen indicators are determined by the functional importance of ecosystem services, ecological sensitivity, etc. (Peng et al. 2018). The weight and constitution of indicators in different areas are determined according to the local situation. Specifically speaking, indicators comprises important ecosystem services indicators like water conservation, biodiversity, carbon fixation ability, soil conservation, etc. (Gao et al. 2020), and ecological sensitivity indicators like elevation, slope, etc. However, scholars at home and abroad have not thoroughly considered the relationship between ecosystem services, ecological sensitivity and residents' needs for ecosystem services. The natural ecosystem cannot survive without "people", which means that a sustainable society needs a balanced development between ecological basic services and residents' ecological needs (Li et al. 2020). The construction of ESP is a multi-goal optimization process based on the coordinated "society-economy-ecology" development. In this regard, this study considered residents' needs for ecosystem services when selecting ecological sources.

The key to the ecological corridor selection is to simulate species migration and construct a resistance surface. Currently, scholars mainly apply circuit theory (Guo et al. 2020), minimum cumulative resistance (MCR) model (Li et al. 2007), and cellular automaton (Zhou et al. 2020) to simulate the movement of species migration. MCR model and ant colony optimization algorithms can only determine the position of the ecological source, as well as the position and direction of ecological corridor, unable to further identify patches and corridors that are more crucial. While circuit theory can be applied to study the movement pattern of ecological flow in a heterogeneous landscape, identify important patches and corridors by calculating isolation degree between patches, and then determine the range of corridor. For resistance surface construction, researchers often determine the resistance value of each patch based on their experience, leading to relatively large differences in the resistance value of different regions. The relatively more scientific method at present is to construct a resistance surface based on the reciprocal of habitat quality coupling with night-time light data (Wang et al. 2019).

This study chose southern Anhui as a research area and attempted to: (1) comprehensively consider the coordination between ecosystem services and residents' needs in the construction of ESP, determine ecological sources and verify their rationality; (2) based on the reciprocal of habitat quality, utilize the modification of night-time light data to construct regional landscape resistance surface; (3) based on circuit theory, select ecological corridor and its range, determine the pinch points that could influence the connectivity of ecological corridor and barrier, and study diversified strategies of ecological conservation, to provide advice for the planning of regional ecological conservation.

MATERIALS AND METHODS

Study Area and Data Sources

Southern Anhui, located in southern Anhui Province (29°31'-31°N, 116°31'-119°45'E) (Fig. 1), has an area of 31.2 thousand km^2. It has abundant forest resources and soils, with 20.5 thousand km^2 forest area, accounting for 45.7% of the total forest area in Anhui province. Southern Anhui is an important ecological source of the Yangtze River Delta, and also one of the most famous tourist spots in China. Long-term land development has caused severe

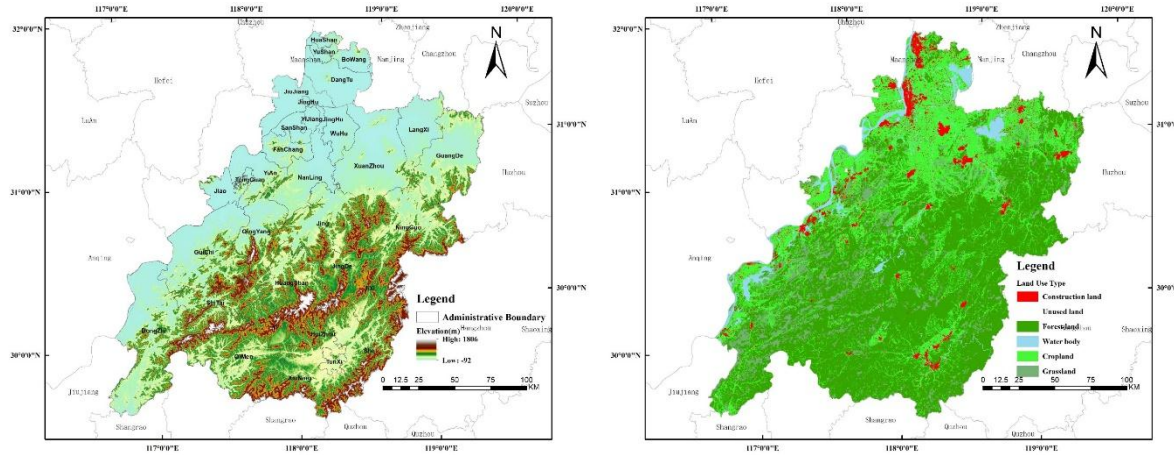


Fig. 1: Land-use type and elevation in southern Anhui.

influences on the ecosystem in southern Anhui, causing problems like habitat deterioration, biodiversity loss, deforestation, soil erosion, etc. Relatively large differences in environment exist within the region. Also, southern Anhui has not formed an interconnected ecological network.

The data sources used in this study were as follows: (1) the 2018 land use and NDVI database was provided by the Resource and Environment Data Cloud Platform; (2) digital elevation model (DEM) data was obtained from the Geospatial Data Cloud website at a spatial resolution of 90m; (3) meteorological data from National Tibetan Plateau Data; (4) soil data from Food and Agriculture Organization of the United Nations (FAO). (5) the 2018 NPP-Virrss was provided by the National Oceanic and Atmospheric Administration. We reclassified all data using the nearest-neighbour to ensure that the spatial resolution was 30m × 30m.

Research Framework and Methods

Identification of the ecological source: The ecological source refers to the area that, from the perspective of human services, plays a decisive role in maintaining regional ecological stability. It normally consists of ecological patches that have relatively important ecosystem services, high ecological sensitivity, and can satisfy residents' ecological needs (Dondina et al. 2016). The methodological framework is shown in Fig. 2, and each process has been described in detail thereafter.

This study applied relevant assessment models (InVEST model (Tallis et al. 2011), CASA model and water and soil conservation model (Zhang et al. 2019)) to quantitatively assess the ecosystem services in southern Anhui. According to the previous research and the local situation of the research area, the study gave four types of ecosystem services the weights of 0.2, 0.3, 0.2, and 0.3 respectively, and divided them into five levels based on natural breakpoint method. The assessment of ecosystem services in southern Anhui was then generated after overlaying the weights.

Ecological sensitivity reflects the complexity and probability of regional ecological problems. Its degree reflects the probability of ecological problems in the disturbance of unreasonable activities (Peng et al. 2018). To maintain regional ecological stability, it is supposed to protect areas with relatively high sensitivity. Southern Anhui is a hilly and mountainous region. According to relevant research (Zhang et al. 2011, Peng et al. 2018, Peng et al. 2017) and the actual situation of the research area, five types of indices, i.e. soil erosion intensity, vegetation coverage, land use type, elevation and slope were selected as assessment factors. The analytic hierarchy process was adopted to determine the weight of each indicator, and then the sensitivity of five

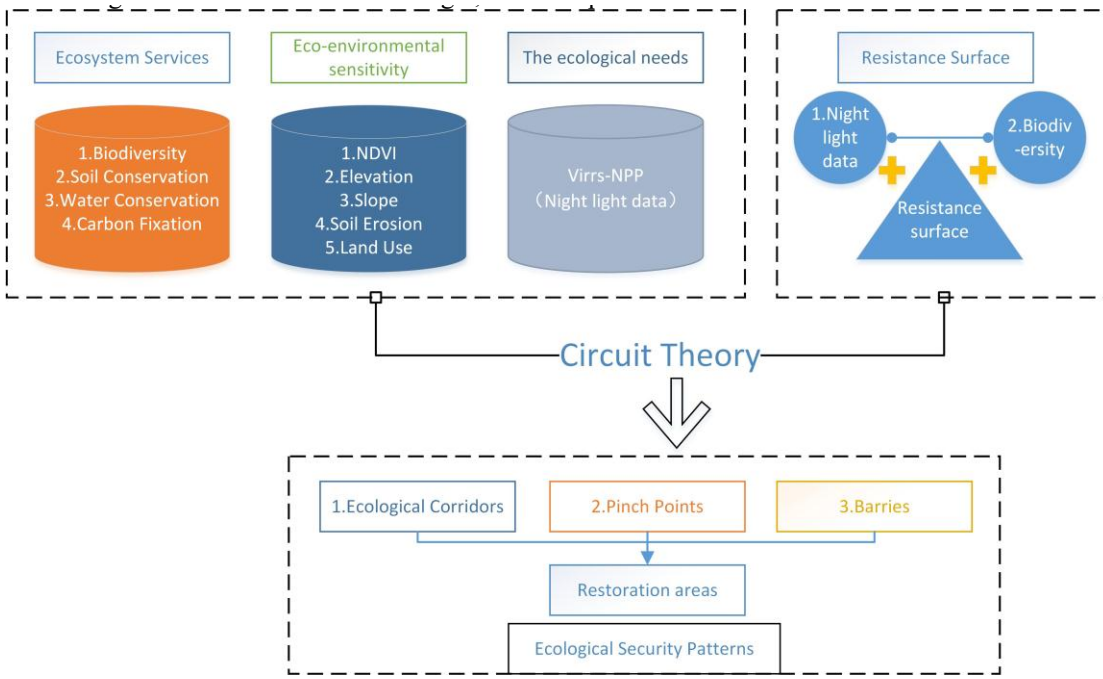


Fig. 2: Construction framework of ecological security pattern in southern Anhui.

Table 1: Classification and weighting of ecological sensitivity evaluation factors.

Evaluation factor/unit	Sensitivity assignment					Weights
	9	7	5	3	1	
NDVI		(0.65, 0.75]	(0.65, 0.75]	(0.35, 0.50]		0.20
Elevation (m)		(500, 800]	(800, 1100]	(1100, 1400]	1400	0.15
Slope		(5, 10]	(10, 15]	(15, 25]		0.15
Land-use type	Forest land or Waterbody	Grassland	Cropland	Construction land	Unuse land	0.20
Soil erosion intensity	Extremely strong erosion	Strong erosion	Moderate erosion	Mild erosion	Slight erosion	0.30

factors was valued and calculated according to their weight. According to the natural breakpoint method, five levels including no sensitivity, light sensitivity, medium sensitivity, high sensitivity and extreme sensitivity were divided to assess the ecological sensitivity. The specific valuation and weights are shown in Table 1.

Generally, land of ecological services with a closer distance towards human activities are applied by residents more often, accordingly with higher ecological importance. Therefore, further analysis based on population density distribution data is required to acquire the spatial distribution of ecological needs. As night-time light data based on VIIRS-NPP has proven to be accurate in reflecting the intensity and range of human activities, the nuclear density analysis was applied to calculate the aggregated intensity of ecological needs in different expanded radii. The radium of needs was set to be 10 km to calculate night-time aggregated intensity. The specific equations and explanations have been mentioned in some research (Peng et al. 2018, Peng et al. 2017).

At last, three assessment results, i.e. ecosystem services, ecological sensitivity and residents' ecological needs were valued respectively, based on the reference to associated statistics, at the weights of 0.5, 0.3 and 0.2, thereby generating the final result of the importance to protect the ecological sources. According to the natural breakpoint method, five levels were divided, and patches that were greater than level three were selected as an ecological source candidate. Considering that ecological source needs certain habitat area and is capable of providing important ecological services, some relatively small patches were eliminated according to the actual situation. In the meantime, patches that are relatively aggregated were combined with other patches, thereby generating the southern Anhui ecological source.

The construction of ecological resistance surface: The difficulty of species migrating to patches of different habitats can be reflected by the resistance surface. Resistance surface depicts the influence of landscape heterogeneity towards ecological process flow. The resistance value is related not only to the distance to the ecological source but also to the land use and human disturbance. For example, human activities will prevent material circulation and energy exchange between different landscape patches. Therefore, traditional resistance surfaces were mainly applied to simulate ecological resistance according to the land use of patches, and could not accurately simulate the distribution of resistance surface. Generally speaking, the higher of the habitat quality in the region, the more complex will be the biodiversity in the region, and easier will be the migration of species. Regarding relevant research (Zhou et al. 2020, Peng et al. 2017), the study considered the actual situation in southern Anhui and adopted the reciprocal of habitat quality to construct a resistance surface. In the meantime, night-time light data were applied as a calibration factor. Considering that the value can be zero, the study assigned the data at no-zero value, and it exerted no influence to the construction of the actual resistance surface.

$$R_Z = R_0 \times OLS$$

In the equation, R_Z represents the resistance value after the calibration of each grid, R_0 represents the original resistance value constructed based on land use type, OLS represents night-time light index.

Ecological corridor and security pattern: Circuit theory is generally required to identify sticking points and pinch points, and thereby to construct the complete regional ecological security pattern, as shown in Fig. 3 (Dondina et al. 2016). In the construction of an ecological corridor, the tool Linkage Mapper developed based on circuit theory can explicitly depict the exact positions of barriers and pinch points. Sticking points are the barriers to effective species migration and ecological process. Under the circumstances of high urbanization, it is of great significance to determine and ameliorate sticking points. Pinch points are the area of too frequent ecological processes, and also the key node of ESP construction, unable to eliminate or hamper. Circuit theory can identify the ecological corridors that suit real species migration routes, combined with the improvement of sticking points and the protection of nodes, and it helps scholars to have a clear understanding towards ESP construction and propose targeted advice for protection (Liu et al. 2018).

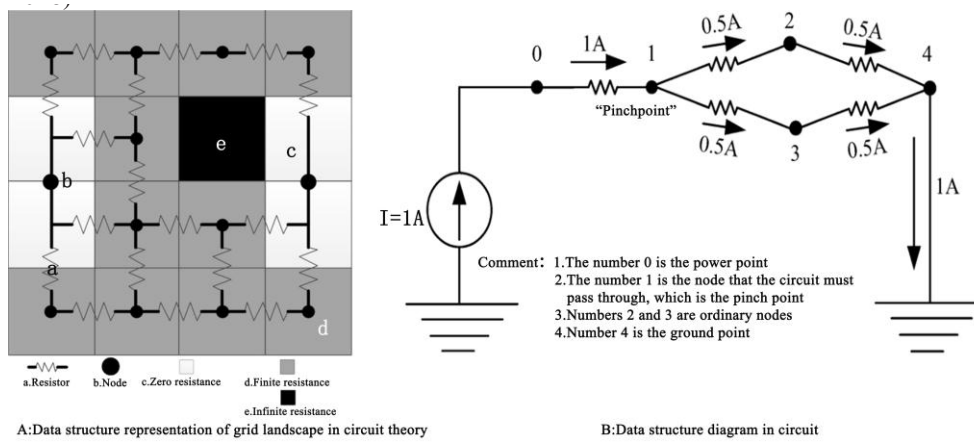


Fig. 3: Circuit theory grid circuit expression and resistance distribution diagram.

RESULTS AND DISCUSSION

Spatial Distribution Pattern of Factors

Every ecosystem service was divided into five levels according to the natural breakpoint method, and the significance from low to high was ranked from level one to five (Fig. 4). Results showed that ecosystem services presented a relatively significant spatial variation on overall quality which may result from the fact that the southern Anhui is higher than the northern. To analyze it in the context of the whole region, the biodiversity and water conservation of southern Anhui ranked the best, with the area greater than level three

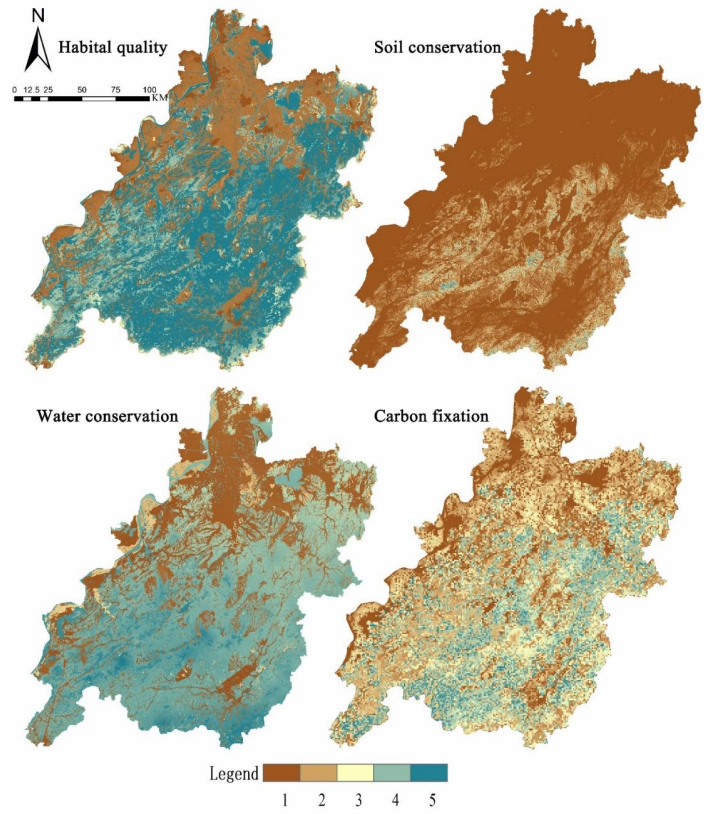


Fig. 4: Spatial distribution map of ecosystem service grades in southern Anhui.

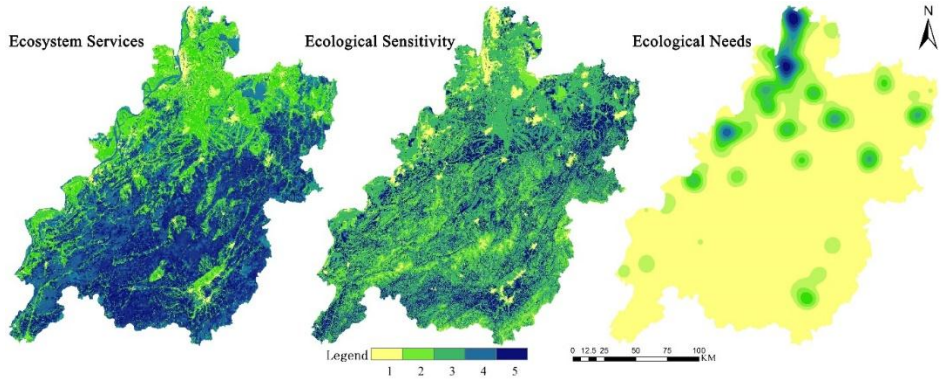


Fig. 5: The spatial distribution of factors for ecological source identification.

accounting for 62.7% and 48.5% of the total respectively, while the area of soil conservation and NPP that ranks greater than level three accounted for 1.17% and 34.6% of the total respectively. The soil conservation of southern Anhui is at serious risk, urging for certain protection strategies to renovate this function. Chaohu city and Maanshan city have high population density with rapid economic development, and face severely degenerated functions of biodiversity and water conservation and serious ecological problems, compared to Huangshan city and Xuancheng city.

Value water conservation, soil conservation, NPP and biodiversity at the weights of 0.2, 0.3, 0.2 and 0.3, and divide them respectively into five levels according to the natural breakpoint method. The assessment of ecosystem services in southern Anhui was then generated after overlaying the weights (Fig. 5). To understand the variations of ecosystem functions within the southern Anhui, the zonal statistics function in ArcGIS was applied to calculate the score of normalized ecosystem functions, as shown in Fig. 6. Qimen county ranked the highest in the assessment of ecosystem functions, while Jinghu district within Chaohu city ranked the lowest. The ecosystem functions presented an overall tendency of high in the south but low in the north. The overall ecosystem functions were related to elevation and population density.

The areas that rank greater than level three were mainly distributed in the south and the east, mostly consisting of woodland and grassland, accounting for 28.1% of the total area. The areas that have low sensitivity were mostly construction land, as well as the bare land at high elevation, located in the south of southern Anhui.

Residents' ecological needs were mainly distributed in the north and part of the east of southern Anhui, contrary to the distribution of ecosystem services and ecological

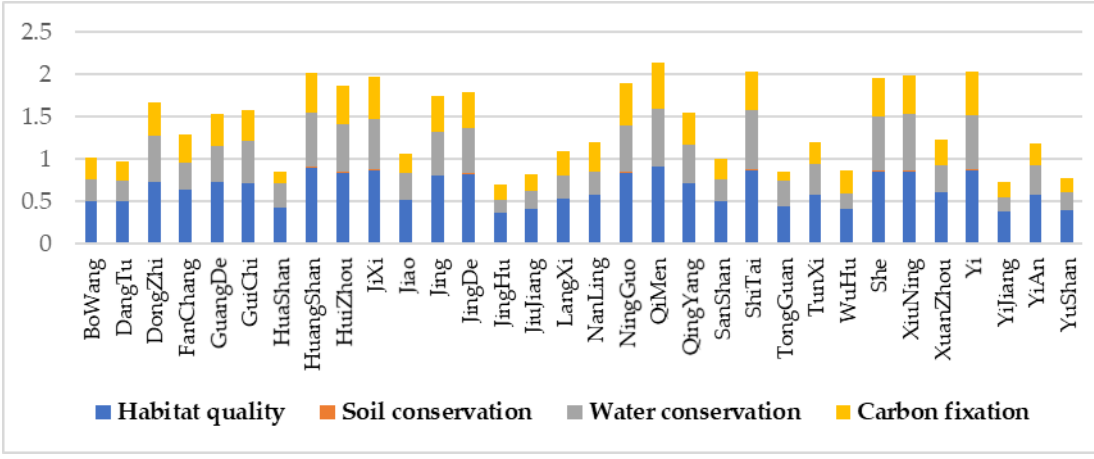


Fig. 6: The importance score of ecosystem services of counties.

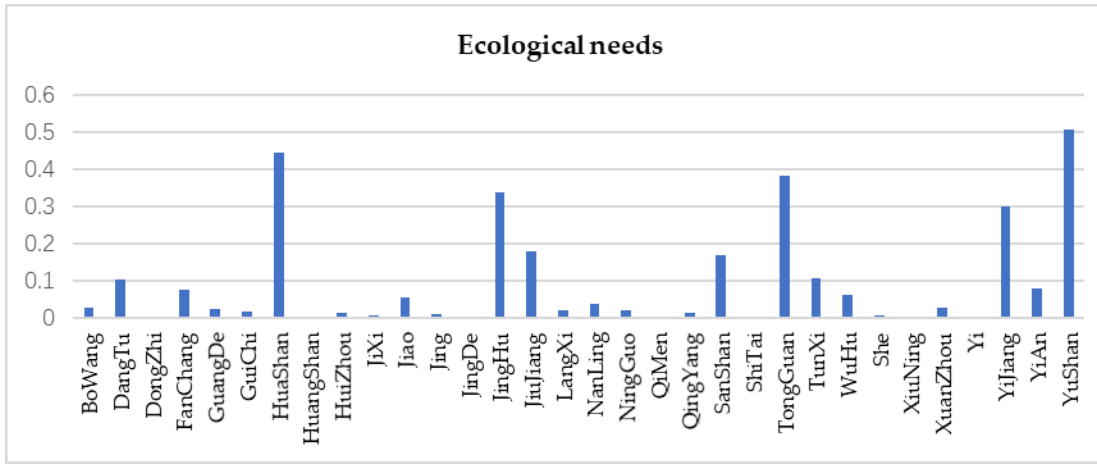


Fig. 7: The rank of residents' ecological needs in the counties and districts of southern Anhui.

sensitivity as shown in Fig. 7. For example, Jinghu district and Yunshan district are the economic centres of the region, and the ecological conditions within the region cannot satisfy the living needs of the majority; while the south and east of southern Anhui have sparse population, thereby they have relatively small residents' needs compared to the north. It means that apart from satisfying residents' needs, it is required to strengthen the connection between internal ecological lands within the region and construct a regional ecological network. It can help maintain regional ecological security and satisfy the coordinated development of "nature-society-ecology".

Ecological Source Extraction

Based on the assessment of ecosystem services, ecological sensitivity and residents' ecological needs in southern Anhui, patches that ranked greater than level three were extracted to identify the distribution of ecological sources, as shown in Fig. 8. The total area of ecological source in southern Anhui is 19269.54km^2, accounting for 51.3% of the total area. The areas are mainly distributed in the regions of Huangshan city, Xuancheng city and Chizhou city. These are the prime areas which can guarantee the ecological security of southern Anhui, as well as the ecological bottom line of urbanization

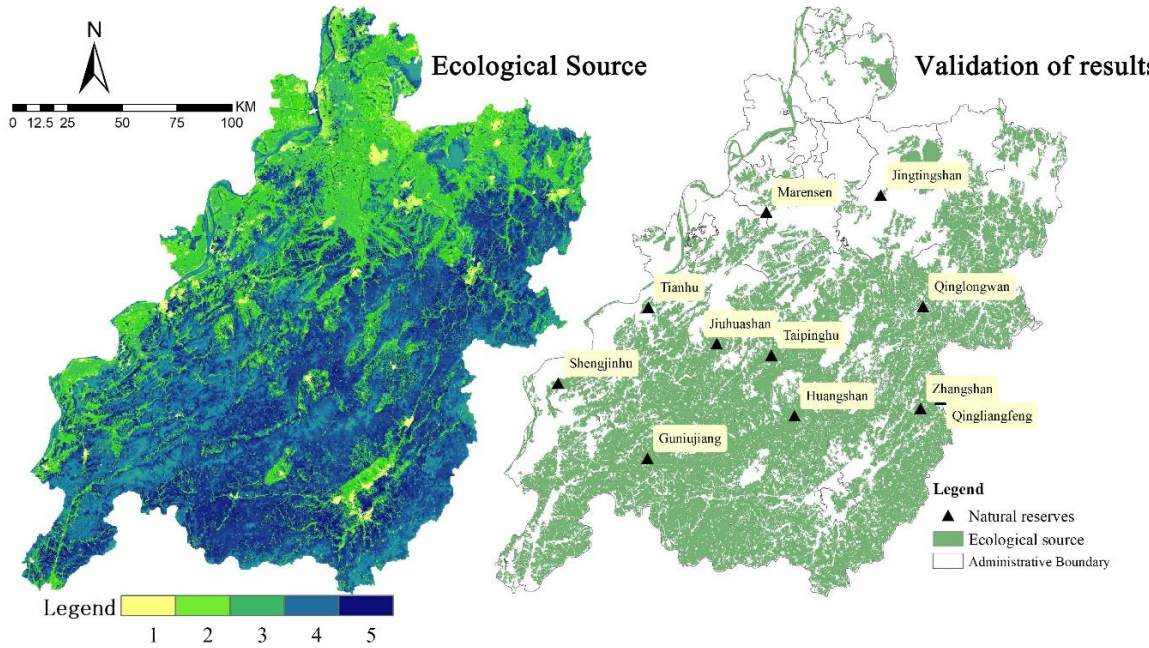


Fig. 8: Validation of results of ecological source extraction in southern Anhui.

Table 2:The area and the percentage of land-use in the ecological source region.

Land-use type	Area (km^2)	Proportion (%)
Cropland	432.34	2.2
Frost land	15369.49	79.7
Grassland	2557.99	13.3
Waterbody	896.53	4.7
Construction land	13.38	0.0995
Other land	0.1	0.0005

and environmental resource development. Exploitation and construction should be strictly prohibited in these areas. Among them, woodland was the most primary land use type, accounting for 79.7% of the total; grassland and waters accounted for 13.3% and 4.7% receptively; farmland accounted for 2.2%. It can be seen that certain ecological sources were exploited or constructed unreasonably. Besides, construction area and bare land accounted for less than 1% (Table 2).

To verify the effectiveness of the ecological source extraction based on a multi-factor comprehensive model, the study overlay the geographic position of ten national and provincial natural reserves and patches extracted from ecological sources. It can be found that natural reserves were basically within the extraction range of the ecological source, proving the validation of source extraction results.

The Construction of Minimum Accumulated Resistance Surface

The minimum accumulated resistance surface in an ecological source is shown in Fig. 9. Among them, the area along the Yangtze River, located in the north of research area, ranked the highest of the minimum accumulated resistance value, especially in the areas of Wuhu city and Maanshan city (Dangtu county, Jinghu District, Wuhu county and Fanchang county). The middle and south of the research area had complex surrounding landscape. As woodland and grassland limit human activities, thereby exerting a relatively small influence on the ecological environment, the minimum accumulated resistance surface is relatively small.

The ESP Construction of Southern Anhui

The spatial distribution of ecological corridors: The identification of the ecological corridor plays an important role in maintaining the ecological process. The ecological function of corridor closely relates to its spatial range such as the edge effect of corridor. The width of the ecological corridor based on circuit theory is determined according to the accumulated resistance and certain specific threshold. As shown in Fig.10, the range of ecological corridor was determined as the threshold of accumulated resistance increased from 1000 to 6000, and the ratio of the ESP area increased accordingly. The figure shows that as threshold increases, the area of ecological corridor increases accordingly, while there is slight or no change in the ecological corridor's spatial distribution.

Considering the urgent need for economic development, the limitation of financial investment in ecological conservation in southern Anhui, as well as the discussion of relevant research on ecological corridor, this study assumed that the investment in ecological conservation supported 10% of the whole research area, and applied threshold 3000 to determine the spatial range of ecological corridor. There were 37 ecological corridors determined, with a total length of 440.42

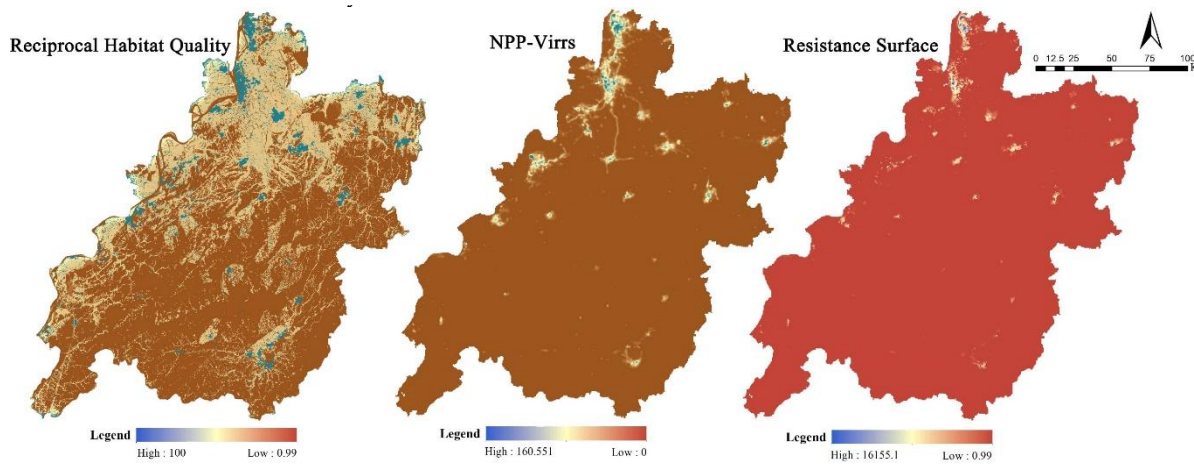


Fig. 9: Ecological resistance surface in southern Anhui.

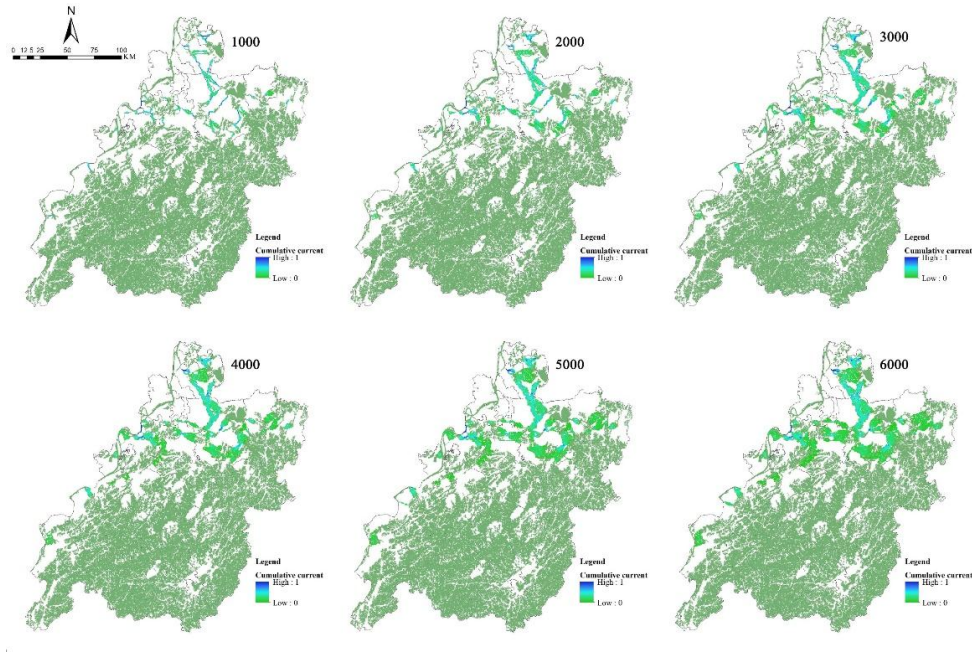


Fig. 10: Spatial distributions of ecological corridors for thresholds from 1000 to 6000.

km, mostly consisting of farmland. The ecological corridors in the south had high current density and presented a shape of cobweb, while the southwest and east had relatively small current density and presented a clustered distribution. The longest ecological corridor in the region was 59 km; the shortest 1.2 km.

The spatial distribution of barriers and pinch points: Linkage Mapper tool developed based on circuit theory was applied to determine the barriers that could influence the connection quality of ecological corridors, divide improvement areas in ecological corridors, and identify pinch points based on current corridors. The method is applied to give priority to the areas that are important to the connectivity of the research area, as shown in Fig. 11.

The ecological corridor barriers in southern Anhui were divided into primary and secondary improvement areas. The

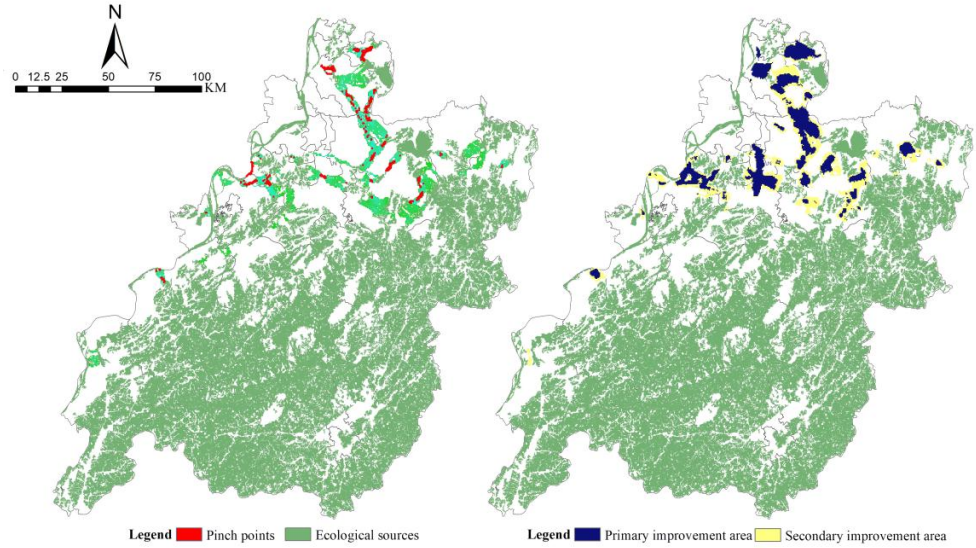


Fig. 11: Spatial distribution of pinch points and improvement areas.

area of the primary area was 1144.42 km^2, mostly distributed between sources or in the fringe area of sources; the area of the secondary area was 969.18km^2, mainly distributed around the primary improvement area. The range of secondary area depended on the number of connective sources and the distance between sources, influenced by both construction land and farmland.

According to the natural breakpoint method, the area with the highest ecological corridor density of the three levels was regarded as a pinch point area, with a total area of 119.24 km^2. The pinch points were mainly distributed close to the fringe area of the northern research area, with many cornerstones–small ecological sources within. The pinch points of the southwest were mainly distributed between the Yangtze River and ancient forests in southern Anhui, with a complete ecological conservation system and good landscape connectivity. According to the distribution of pinch points, 9 important pinch points were extracted for ecological conservation and improvement.

The Construction and Planning Strategies for ESP in Southern Anhui

The construction of ESP in southern Anhui is based on the comprehensive consideration of the ecological corridor, improvement area and the pinch point. There were 20 ecological sources, 37 ecological corridors, 9 important pinch points and 2 levels of improvement areas. The ecological corridors, pinch points and improvement areas were mainly distributed in the north, relating to the actual situation of southern Anhui. Southern Anhui, the important area with ecological functions of the Yangtze River Delta, has a major district of woodland and grassland, mostly distributed within Huangshan city, Chizhou city and Xuancheng city. Maanshan city and Wuhu city in the region are the bridge between southern Anhui and the external area. The rapid economic development causes significant ecological degradation in the area. To maintain the ecological connection of southern Anhui to the outside world and perform its important ecological function of serving residents, the ESP of southern Anhui is designed accordingly (Fig. 12).

Currently, scholars believe that barrier improvement, ecological pinch point protection and buffering zone construction are effective methods to optimize regional ESP under the circumstances of urbanization. In this study, the improvement area in southern Anhui mainly consisted of farmland and construction land. The improvement area was

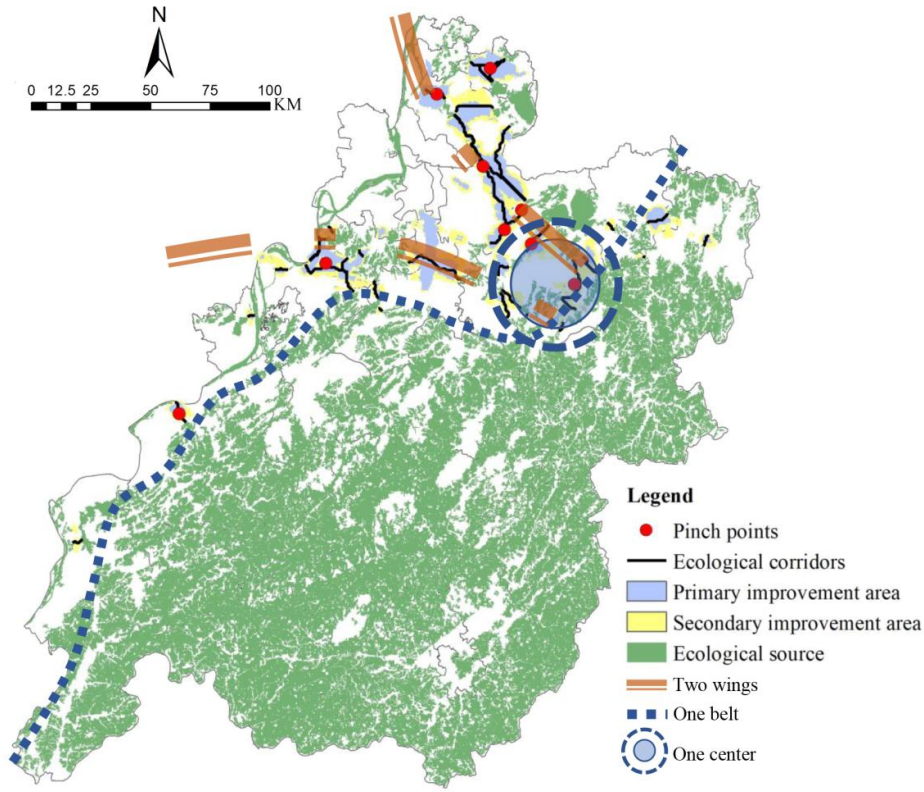


Fig. 12: Spatial distribution map of ecological security patterns.

located in the construction area, mainly around the urban area of Maanshan city of Wuhu city. The urban areas are the center for economic and population growth. Therefore, it is inappropriate to eliminate barriers in practical improvement strategies. Generally speaking, setting urban green belts in an economically developed area is a proper method to deal with the problem. Barriers besides farmland or sources should be eliminated in place, to enhance corridor connectivity. For pinch points that are important to the connection to the ecological source, the development-prohibited area should be set. In the meantime, unified planning at the provincial, city and county level should be conducted to ensure the connectivity of the ecological corridor. In this regard, a comprehensive spatial pattern of "one centre, two wings, one belt" should be generated at the regional level. "One centre" refers to the intersection of Chaohu city, Maanshan city and the southern mountainous area, regarded as an important node allowing species to accept ones from other sources; "two wings" refers to the ecological corridors from the southern mountainous area to Chaohu city and Maanshan city. Due to the overlength of the corridor, policymakers should adopt effective methods to ensure the connectivity of corridor and safeguard species to successfully migrate to the intersection of the southern mountainous area; "one belt" refers to the biological buffering zone that should be set between the southern mountainous area and northern plain area, to prevent the land expansion or population increase in the plain area and thereby avoiding the ecological degradation in the southern mountainous area.

Currently, there is no unified agreement about the method and indices of source extraction at home and abroad. Therefore, it is necessary to conduct validation after indices construction. The study overlaid the geographic positions of national and provincial natural reserves on source identification results, partly verifying the reasonability of the indices extracted from ecological sources. However, limited by manpower and material resources, the study did not construct a quantitative assessment standard of long-term dynamic monitoring. It is required to conduct more in-depth research to verify the reasonability of extracted indices.

Besides, southern Anhui is a region that has a close connection to its surrounding cities, and it surely could be influenced by the outside material and energy flow. Therefore, further research should consider breaking the boundaries of administrative divisions, as well as the influence of surrounding ecological factors on the ecological pattern of the research area.

CONCLUSION

The study constructed identification indices of "people-oriented" ecological source based on ecosystem services, ecological sensitivity and residents' needs and applied the reciprocal of habitat quality and night-time light data to construct landscape resistance surface. At last, based on circuit theory, ESP of southern Anhui was constructed, and then the optimization scheme was generated accordingly.

The main conclusion comprises: (1) the multi-factor comprehensive assessment model based on ecosystem services, ecological sensitivity and residents' needs was applied to identify 20 ecological sources in southern Anhui that suited "nature-ecology-society". Compared with the geographic positions of national and provincial nature reserves, the feasibility and rationality of the model were verified. The area of ecological source accounted for 51.3% of the total, mainly consisting of woodland and grassland; (2) the regional landscape resistance surface in the study was built according to the reciprocal of habitat quality and night-time light data. Compared with the valuation that only considers the land-use type, this valuation considered the important influence of human activities on the ecological process. Therefore, this construction of resistance surface is more reasonable; (3) the range and direction of 37 ecological corridors in southern Anhui were identified according to circuit theory, and then two levels of improvement areas and 9 important pinch points were divided accordingly. The area of the primary improvement area was 1144.42km^2, mainly distributed in the north of southern Anhui; the area of the secondary area was 969.18km^2, mostly consisting of farmland and construction land.

REFERENCES

Chen, X., Peng, J., and Liu, Y. 2017. Construction of Ecological Security Pattern of Yunfushan City Based on the Framework of "Importance-Sensitivity-Connectivity". Geogr. Res., 36(3):471-484.

Dondina, O., Kataoka, L., Orioli, V., and Bani, L. 2016. How to manage hedgerows as effective ecological corridors formammals: A two-species approach. Agric. Ecosyst. Environ., 231, 283–290.

Gao, J., Zou, C., Zhang, K., Xu, M., and Wang, Y. 2020.The establishment of Chinese ecological conservation redline and insights into improving international protected areas. J. Environ. Manag., 264:110505.

Guo, X., Zhang, X., and Du, S. 2020. The impact of onshore wind power projects on ecological corridors and landscape connectivity in Shanxi., Chin. J. Clean. Prod., 254.

He, J., Pan, Y., Liu, D. 2020. Analysis of the wetland ecological pattern in Wuhan from the perspective of an ecological network. Acta Ecologica Sinica, 40(11):3590-3601.

Huang, J., Hu, Y., and Zheng, F. 2020. Research on recognition and protection of ecological security patterns based on circuit theory: a case study of Jinan City. Environ. Sci. Pollut. Res. Int, 27(11):12414-12427.

Jia, L., OuYang, Z., Zhao, T. 2005. The ecological function regionalization of Anhui Province., Acta Ecologica Sinica, 25(2):254-260.

Li, Z., and Li, M. 2020. Spatio-temporal dynamics of ecological security pattern of the Pearl River Delta urban agglomeration based on LUCC simulation. Ecol. Indic., 114.

Li, Z., Yang, G., and Dong, Y. 2007. Establishing the ecological security pattern in rapidly developing regions: A case in the AYRAP. J. Nat. Res. 22(1): 106-113.

Liu J, Yin H W., Kong F H., and Li M H. 2018. Structure optimization of circuit theory-based green infrastructure in Nanjing, China. Acta Ecologica Sinica, 38(12):4363-4372.

Meng, J., Zhu, L., and Yang, Q. 2012. Construction of the ecological security pattern of land use in Ordos City. Acta Ecological Sinica, 32(21):6755-6766.

Nathwani, J., Lu X., Wu, C., Fu, G., and Qin, X. 2019. Quantifying security and resilience of Chinese coastal urban ecosystems. Sci. Total Environ., 672:51-60.

Peng, J., Yang, Y., and Liu, Y. 2018. Linking ecosystem services and circuit theory to identify ecological security patterns. Sci Total Environ, 644(10):781-790.

Peng, J., Yang, Y., Liu, Y., Hu, Y., Du, Y., Meersmans, J., and Qiu S. 2018. Linking ecosystem services and circuit theory to identify ecological security patterns. Sci. Total Environ., Dec 10,644:781-790.

Peng, J., Zhao, H., and Liu, Y. 2017. Urban ecological corridors construction: a review. Acta Ecologica Sinica, (37):23-30.

Schröter, M., Kraemer, R., Remme, and R.P. 2020. Distant regions underpin interregional flows of cultural ecosystem services provided by birds and mammals. Ambio, 49(5).

Song, T., Li, D., Zhang, L. 2020.Evaluation of the importance of regional ecosystem services in the Qinba Mountains and construction of ecological security patterns. Eng. Sci. 22(01): 64-72.

Wang, Y., Jin, X., and Shen, C. 2019. The construction of ecological security pattern in the developed areas in the east—A Case Study in southern Jiangsu. Acta Ecologica Sinica, 39(07):2298-2310.

Xiaona L., Chunlan L., and Long C. 2020. Gradient effects and ecological zoning of ecosystem services in transition zone of Beijing Bay. Transactions of the Chinese Society of Agricultural Engineering, 36(12):276-285.

Xun, F., Luo, K., and Li, Y. 2018. Evaluation of urban water system corridor ecosystem service value based on high-score remote sensing data- Taking the water system corridor in central Beijing as an example. Chin. Gard., 34(10):50-54.

Yin, H.W., Kong F.H., Qi, Y., Wang, H.Y., Zhou, Y.N., and Qing, Z.M. 2011. Developing and optimizing ecological networks in urban agglomeration of Hunan province; China.Acta Ecologica Sinica, 31(10): 2863-2874.

Zhang, D., Qu, L., and Zhang, J. 2019. Construction and optimization of ecological security pattern based on the perspective of ecological supply and demand- Taking the Yangtze River Delta as an example. Acta Ecologica Sinica, 39(20):7525-7537.

Zhou, R., Lin, M., and Wu, Z. 2020. Construction of Ecological Security in Guangdong-Hong Kong-Macao Greater Bay Area from the Perspective of Importance of Ecosystem Services. Ecol. Econ., 36(07):189-196.

sustainability

MDPI

Article

Measuring the Relationship between Physical Geographic Features and the Constraints on Ecosystem Services from Urbanization Development

Yongzheng Wang [1,2], Yiwen Ji [1,2,3], Haoran Yu [1,2,3] and Xiaoying Lai [4,5,*]

1 School of Architecture and Planning, Anhui Jianzhu University, Hefei 230022, China; rockyhust1979@ahjzu.edu.cn (Y.W.); yiwenji@njfu.edu.cn (Y.J.); yuhaoran2021@ahjzu.edu.cn (H.Y.)
2 Collaborative Innovation Center for Urbanization Construction of Anhui Province, Anhui Jianzhu University, Hefei 230022, China
3 School of Landscape Architecture, Nanjing Forestry University, Nanjing 210037, China
4 College of Management and Economics, Tianjin University, Tianjin 300072, China
5 School of Management, Wuhan Institute of Technology, Wuhan 430205, China
* Correspondence: xiaoying.lai@tju.edu.cn

Abstract: Exploring the constraint relationship between physical geographic features and urbanization on ecosystem services is important for managing and optimizing regional ecosystem services. Taking Anhui Province as an example, we assessed the spatial and temporal evolution characteristics of five types of ecosystem services (habitat support, water production services, soil conservation, NPP, and carbon fixation) and five types of urbanization levels (population, economic, social, ecological, and spatial) in 2000, 2010, and 2020, and integrated the constraint line method, bivariate spatial autocorrelation model, and spatial regression model to measure the relationship between ecosystem services. The spatial constraints between ecosystem services and urbanization level and natural topography in Anhui Province were measured using the constraint line method, bivariate spatial autocorrelation model and the spatial regression model. The results show that: (1) the spatial distribution of the five types of ecosystem services in Anhui Province is characterized as "low in the north and high in the south". At the provincial level, the five ecosystem services in southern and central Anhui Province are synergistic, while the five ecosystem services in northern Anhui Province show a trade-off; (2) topography has different effects on the five ecosystem services with "exponential" effects on water production services and NPP, "positive convex" effects on habitat support, and "positive convex" effects on habitat support"; (3) the bivariate global autocorrelation Moran's I index between ecosystem services and urbanization level in Anhui Province is significant, confirming that ecosystem services and urbanization are spatially related, where the development of population urbanization, spatial urbanization, economic urbanization, and social urbanization leads to the decrease in ecosystem services, and ecological urbanization promotes the increase in ecosystem services. In the spatial regression model, the Spatial Lag Model passed the significance test, indicating that there is a spatial spillover effect between ecosystem services and urbanization. That is, changes in ecosystem services are influenced not only by their own urbanization elements, but also by urbanization elements in neighboring units or more distant units. Exploring the constraints of ecosystem services and identifying their interaction with urbanization can provide a scientific basis for land-use optimization, adjusting management measures and achieving regional sustainability.

Keywords: spatial effects; ecosystem services; urbanization; InVEST; constraint lines; trade-offs and synergies

check for updates

Citation: Wang, Y.; Ji, Y.; Yu, H.; Lai, X. Measuring the Relationship between Physical Geographic Features and the Constraints on Ecosystem Services from Urbanization Development. *Sustainability* **2022**, *14*, 8149. https://doi.org/10.3390/su14138149

Academic Editor: Agnieszka Bieda

Received: 10 May 2022
Accepted: 27 June 2022
Published: 4 July 2022

Publisher's Note: MDPI stays neutral with regard to jurisdictional claims in published maps and institutional affiliations.

Copyright: © 2022 by the authors. Licensee MDPI, Basel, Switzerland. This article is an open access article distributed under the terms and conditions of the Creative Commons Attribution (CC BY) license (https://creativecommons.org/licenses/by/4.0/).

1. Introduction

Ecosystem services contain numerous benefits, such as natural environmental conditions and utilities, that humans derive, directly or indirectly, from ecosystems and their

ecological processes, and provide the resources and environmental basis for human survival [1,2]. However, in the context of rapid urbanization, uncontrolled human claims on natural resources and unscientific resource use have degraded nearly 60% of global terrestrial ecosystem services [3]. In 1987, the United Nations released the study "Our Common Future", which introduced the concept of sustainable development [4]. Economic growth, social progress and environmental protection were clearly defined as the three pillars of sustainable development. By the end of 2020, 56.1% of the world's population lived in cities. Cities occupy 3% of the world's land, consume 75% of the world's natural resources, emit 50% of the world's waste and 70% of the greenhouse gases, and also generate more than 80% of the GDP. Cities have become a key factor in advancing sustainable human development. Therefore, a scientific understanding of the interaction between ecosystem services and urban development and an in-depth investigation of its "mechanism-process" mechanism of influence have become an important means of theoretical support for promoting sustainable social development.

In recent years, scholars at home and abroad have discussed the spatial and temporal evolution of ecosystem services [5–7], influencing factors [8,9] and trade-offs and synergistic relationship measurements [10–12]. A large number of studies have been conducted in recent years. For example, Geng Tengwei et al. used geographic probes to find that urbanization is a key factor affecting the value of ecosystem services, and used geographically weighted regression models (GWR) to explore the spatially divergent characteristics of the intensity of urbanization effects [13], and Zhang Yushuo et al. [14] used multiple regression models to quantitatively reveal the influence of three dimensions, land use, social and economic dimensions, on the trade-offs and synergies of ecosystem services. Li Cheng et al. [15] presented a study that used the root–mean–square error index and redundancy analysis to investigate the factors influencing ecosystem services in the Yangtze River Delta urban agglomeration, and found that the increase in construction land was an important factor affecting the decline in ecosystem services; Howe et al. [16], based on existing studies on the trade-offs and synergistic relationships of ecosystem services, found that trade-offs in ecosystem services tend to be static, while natural environmental changes, ecosystem feedback and food webs may lead to lags in shifting trade-offs in ecosystem services. Alison et al. [17] assessed the complex relationship between ecosystem services and agricultural production and found that agriculture can be a source of degradation for many ecosystem services, such as loss of wildlife habitat, nutrient runoff, watercourse deposition, greenhouse gas emissions, and pesticide poisoning by humans and non-target species. Natural geographic features have been used by researchers to explore the spatial variations in ecosystem services as important influencing factors, e.g., Yang Sun et al. [18] assessed the value of ecosystem services in the middle reaches of the Yangtze River as a logarithmic function of topographic gradient, and the value of ecosystem services was greater in mountainous areas than in plains. The authors of [19] took the western plains and eastern mountains of the South Four Lakes Basin in eastern China as an example, and proved that topography is an important factor affecting the spatial distribution of multiple hydrological ecosystem services through correlation analysis and redundancy analysis. Researchers have studied the impact factor measures of ecosystem services such as GWR and geographic probes, and used a redundancy analysis to directly express the causality and intensity of the impact, i.e., determine the heterogeneity of positive and negative impact relationships or the spatial impact magnitude of a factor on ecosystem services. Numerous studies have provided empirical evidence, showing [20–23] that the relationship between ecosystem services and influencing factors changes with spatial scale and temporal scale, and shows nonlinear influence characteristics. The degree of influence that these factors have on ecosystem services in nonlinear processes (types of constraint curves, thresholds and eigenvalues) plays an important role in managing and balancing the negative impacts of ecosystem services and human activities [24–26]. Among the many factors affecting changes in ecosystem services, physical geographic features and human construction activities are considered to be the key driving forces that change and influence

the spatial pattern of ecosystem services and trade-off relationships, meaning that physical geographic features and urbanization development are a long-standing focus of research on ecosystem service changes [27,28]. Theoretically, measuring the constraints on ecosystem services regarding physical and geographic features and urbanization development is important for enhancing the understanding of the drivers and mechanisms of ecosystem services [29,30]. To sum up, scholars pay more attention to the traditional linear regression and correlation analysis methods to measure the relationship between variables, but ignore the limiting effect of limiting variables on response variables in complex ecosystems affected by multiple factors. Scientific measurement of the limitations of natural geographical characteristics on ecosystem services is conducive to accurately understanding the marginal characteristics of the impact of urbanization on ecosystem services.

Anhui Province is located in the Yangtze River Delta city cluster, one of the six largest city clusters in the world, which is an important intersection between the Belt and Road and the Yangtze River Economic Belt, and an important platform for China's participation in international competition. The urbanization rate in Anhui Province has increased from 18.55% in 2000 to 58.33% in 2020, and the rapid urbanization activities have caused serious habitat fragmentation within the region, with an increase of 1.65% in construction land, a decrease of 0.5% in forest and grass land, and a decrease of 2.5% in arable land within the last 20 years. The spatial pattern of land cover in Anhui Province significantly varies with the changes in topography, and the altitude of the whole province gradually decreases from south to north. The southern part is mostly forested and grassland, while the northern part is mostly arable land and construction land, so it shares commonality and characteristics with cities in the lower Yangtze River basin. Against the background of the research presented above, this paper plans to conduct research focusing on three aspects: (1) At the research scale, this paper selects county administrative units (excluding municipal districts) to obtain measurements and statistics on ecosystem services and urbanization, mainly because the long-standing spatial raster data on population and economy are limited to the research scale, with limited spatial and temporal accuracy, an inconsistent data structure, and a mismatch of spatial units. (2) This paper aims to conduct a comprehensive evaluation of ecosystem services in Anhui Province during 2000, 2010 and 2020, based on the InVEST model and CASA model, and to evaluate the development level of urbanization in counties in Anhui Province during 2000, 2010 and 2020 in five dimensions: population, economy, society, space and ecology. (3) This paper aims to explore the constraints that natural topography places on ecosystems and the constraints threshold with the help of the constraint line method, based on the bivariate spatial autocorrelation model. The spatial interactions and spatial dependence between urbanization and ecosystem services in the study area were investigated based on Bivariate Moran's I, Ordinary Least Square (OLS), Spatial Lag Model (SLM), and Spatial Error Model (SEM), and the spatial interaction between urbanization and ecosystem services in the study area.

2. Materials and Methods

2.1. Overview of the Study Area

Anhui Province, located in East China, is a sub-center city of the Yangtze River Delta (Figure 1), between 114°54′–119°37′ east longitude and 29°41′–34°38′ north latitude, with a total area of 140,100,000 km^2. There are 105 counties and districts, including 60 counties and 55 municipal districts. The topography of Anhui Province is diverse, with the Yangtze River and the Huai River crossing the whole territory from west to east, dividing the province into three natural regions: HuaiBei, Jianghuai and Jiangnan. The traditional zoning concept is divided into northern Anhui, central Anhui and southern Anhui. North Anhui refers to the area north of the Huai River, including Suizhou, Huabei, Bengbu, Fuyang, Huainan, Bozhou, with six cities; Central Anhui refers to the area north of the Yangtze River and south of the Huai River, including Hefei, Liuan, Chuzhou, Anqing, with four cities. South Anhui refers to the area south of the Yangtze River, including Huangshan, Wuhu, Maanshan, Tongling, Xuancheng, Chizhou, with six cities. To the north of the Huai

River, the terrain is vast and open, and is part of the Great Plains of North China. The central part lies between Jiang and Huai, with mountainous hills. The banks of Yangtze River and around Chaohu Lake are low and flat, belonging to the famous middle and lower reaches of the Yangtze River Plain; the south is dominated by mountains and hills. It is located in the transition area between the warm temperate zone and subtropical zone. North of the Huai River is a warm, temperate, semi-humid monsoon climate, and south of the Huai River is a subtropical, humid monsoon climate, compatible with the north and south.

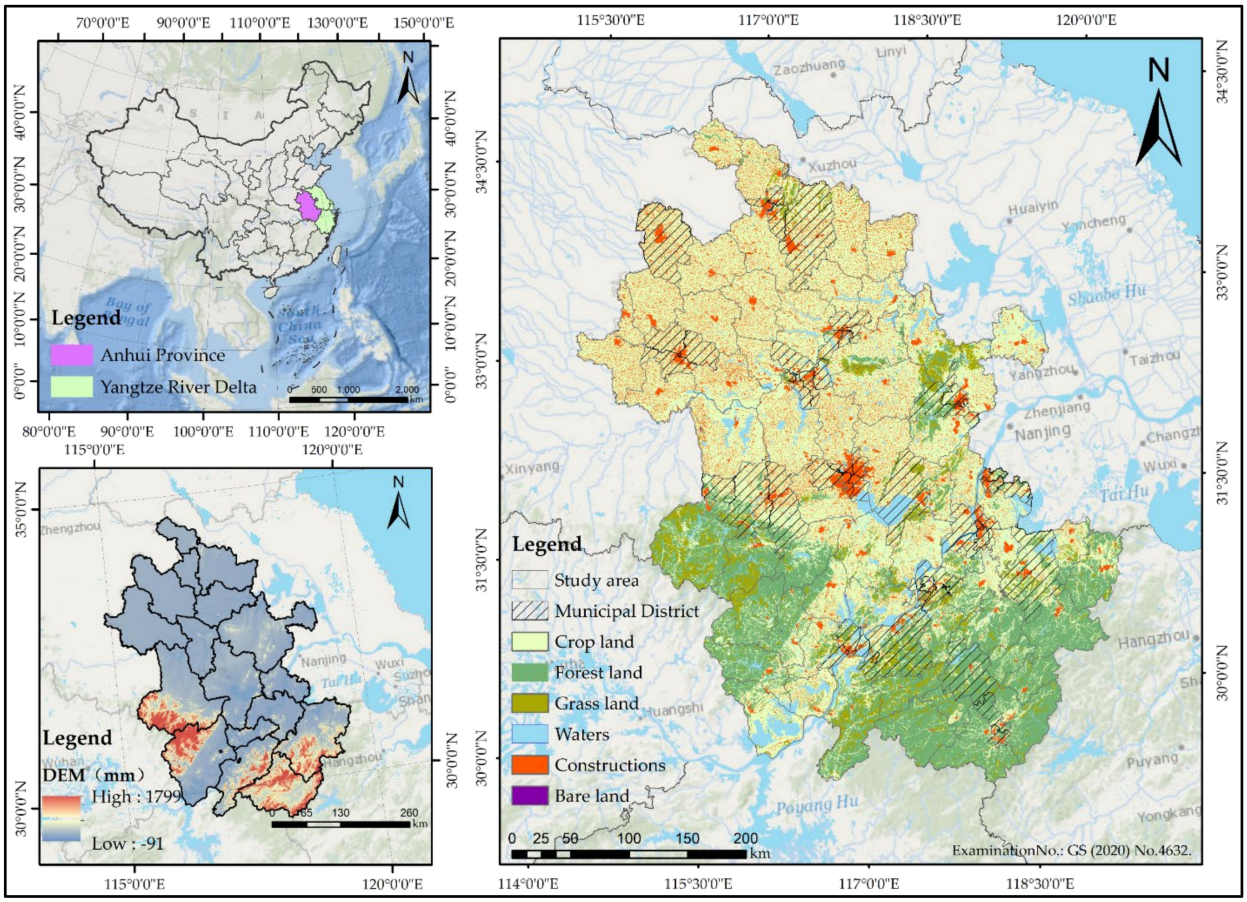


Figure 1. Geographical characteristics and spatial distribution of land use in the study area.

2.2. Data Sources and Processing

A rainfall dataset and evapotranspiration dataset from the National Earth System Science Data Center (http://www.geodata.cn/, accessed on 10 October 2021) were used to input rainfall and evapotranspiration data into the water production module of the InVEST model. The Digital Elevation Model (DEM) was obtained from the Geospatial Data Cloud website (http://www.gscloud.cn/, accessed on 20 July 2021) with a raster size of 90 m. Soil data were obtained from the Cold Region Dry Zone Science Data Center (http://data.casnw.net/portal/, accessed on 5 May 2021). Soil data were obtained from the Chinese Soil Dataset (v1.1), which was used to calculate the soil erodibility factor (K) in the soil conservation services, as well as the plant-available water content (PAWC) and depth-to-root restrictions in the water production module of the InVEST model [31]. The data of urbanization indicators were obtained from the Statistical Yearbook of Anhui Province, county statistical yearbooks and bulletins. The entropy value method was used to calculate the weights of each indicator, and the entropy value method was calculated by SPSSAU (https://www.spssau.com/, accessed on 5 May 2021). This was interpolated to 100 m and the coordinates were unified as WGS_1984.

2.3. Research Ideas and Methods

The InVEST model [32] was used to calculate habitat support services (HQ), soil conservation services (SDR), water production services (WY), and carbon fixation (CF) in the study area in 2000, 2010, and 2020. The CASA model was also used [33]. The NPP of the study area in 2000, 2010, and 2020 was calculated to replace the organic matter production function, and the five types of ecosystem services were weighted and calculated until the integrated ecosystem services. (2) Based on the statistical yearbooks and statistical bulletins of the study area in 2000, 2010 and 2020, we obtained the relevant evaluation indicators, and used the entropy value method to calculate the indicators at all levels to obtain the spatial and temporal evolution patterns of the five types of urbanization levels and the comprehensive urbanization level in the study area. (3) Based on the constraint line method [34,35], the spatial regression model was used to measure the spatial constraint relationship between integrated ecosystem services and five urbanization spatial subtypes(Figure 2).

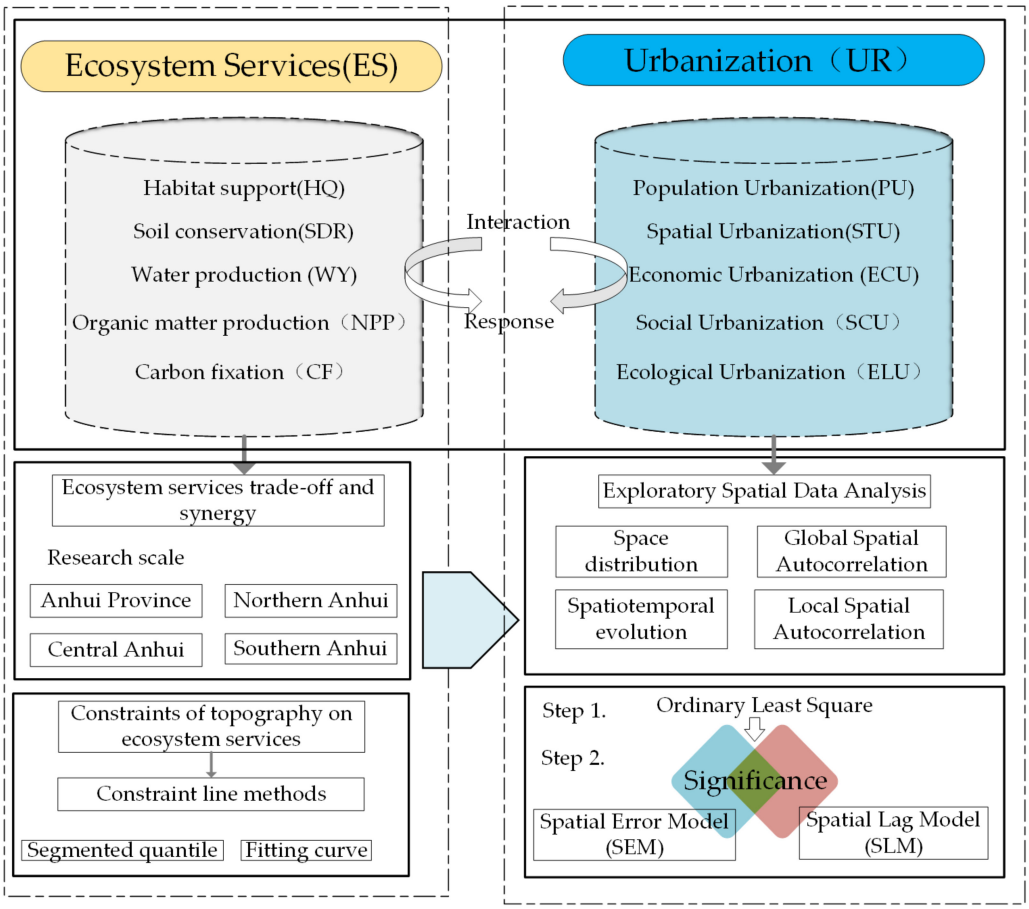


Figure 2. Research Technology Route.

2.3.1. Ecosystem Service Evaluation Methods

1. Habitat Quality (Habitant Quality)

The InVEST model is used for ecosystem service function assessment, in which the habitat quality evaluation module is based on the link between land cover and habitat threat sources. It calculates the intensity of threat sources by considering the radius of stress, spatial weights, spatial attenuation types, etc., and combining the habitat adaptation

of other land types and sensitivity to threat sources to obtain the habitat quality of the area using the following equation.

$$Q_{xj} = H_j \left[1 - \left(\frac{D_{xj}^z}{D_{xj}^z + k^z} \right) \right] \tag{1}$$

where Q_{xj} represents the type of landscape in the study area, while j in x represents the habitat quality index of the raster H_j. The value range of $[0, 1]$ represents the habitat suitability score of the landscape type j in the habitat suitability scores; k is the half-saturation constant, which is set according to the accuracy of data in the study area and is 50.5 in this paper; z. In this study, the Habitat Quality module parameter table was set based on the InVEST model manual and related studies.

2. Water Yield (WY)

In this study, the water production service refers to the surface water production in a certain area. The calculation of surface water production is based on a simplified hydrological cycle model that ignores the influence of groundwater and is determined by a combination of numerous parameters, such as rainfall, evapotranspiration, soil depth, and plant-available water. The assessment was performed using the water yield module of the InVEST model, which is mainly based on the Budyko hydrothermal coupling equilibrium assumption equation.

$$Y(x) = \left(1 - \frac{AET(x)}{P(x)} \right) \times P(x) \tag{2}$$

$$\frac{AET(x)}{P(x)} = 1 + \frac{PET(x)}{P(x)} - \left[1 + \left(\frac{PET(x)}{P(x)} \right)^W \right]^{\frac{1}{w}} \tag{3}$$

$$PET(x) = Kc(x) \times ETo(x) \tag{4}$$

$$W(x) = \frac{AWC(x) \times Z}{P(x)} + 1.25 \tag{5}$$

where $Y(x)$ is each raster cell in the watershed x of annual water production (mm) $AET(x)$ is the raster cell$x$ of the actual annual evapotranspiration (mm). $P(x)$ is the annual precipitation of the raster cell, x is the annual precipitation of the raster cell (mm), $PET(x)$ is the annual evapotranspiration of the grid cell, and x is the potential evapotranspiration of the raster cell. $Kc(x)$ is the crop evapotranspiration coefficient, $ETo(x)$ is the crop evapotranspiration coefficient of the raster cell, and x is the reference crop evapotranspiration of the raster cell. $AWC(x)$ is the effective soil water content (mm), determined by the plant-use water content (PAWC), the maximum root burial depth of the soil and the minimum value of the plant root depth. $W(x)$ indicates the non-physical parameters of natural climate-soil properties; Z is set using the relevant literature that is available for the study area [26].

3. Soil retention (SDR)

The assessment of the soil retention function in the study area is based on the sediment retention module of the InVEST model, which is mainly calculated using the universal soil loss equation (USLE). The calculation equation is as follows.

$$SC = Ap - Ar = R \times K \times L \times S \times (1 - C \times P) \tag{6}$$

where SC is the amount of soil retention t/hm^2, which is composed of potential soil erosion Ap and actual soil erosion. Ar is determined by the difference between potential and actual soil erosion. R is the rainfall erosion factor. This paper is limited by the rainfall process data; the R value is estimated and verified according to different types of rainfall data [36]. K is the soil erodibility factor, which is calculated using the erosion-productivity evaluation model (EPIC) proposed by Williams et al. in 1990 [37]. The LS is the slope length slope factor; C is the vegetation cover and management factor; P is the soil conservation measure

factor. In the model, *P* and *C* values are fixed values, which are used to reconcile the actual deviations in the calculation of soil conservation (see Table 1) and are mainly determined by referring to the USDA Handbook 703 and the related literature [38–40].

Table 1. P and C values for different land-use types.

Land Use	Cropland	Forest	Grass	Waters	Constructions	Bareland
P	0.29	0.7	0.5	0.2	0.16	0.27
C	0.27	0.01	0.06	0	0.2	0.35

4. Net Primary Productivity (NPP)

Net primary production (NPP) refers to the net primary productivity of vegetation and is used to characterize ecosystem carbon storage services. The calculation equation is as follows.

$$NPP(x,t) = APAR(x,t) \times \varepsilon(x,t) \quad (7)$$

where $NPP(x,t)$ is x location, t is net primary productivity at the moment of time $\left(\mathrm{gc/m^2}\right)$; $APAR(x,t)$ is x location, t is photosynthetically active radiation at the moment of time $\left(\mathrm{MJ/m^2}\right)$; $\varepsilon(x,t)$ is x location, t is the light energy utilization at the moment of time.

5. Carbon Fixation Services (CF)

Ecosystem carbon stocks are composed of four main components: aboveground biomass (C_{above}), below-ground biomass (C_{below}), soil carbon (C_{soil}), and dead organic matter (C_{dead}). Aboveground biomass includes all aboveground living organic matter, such as tree trunks, branches, leaves, etc.; below-ground biomass is the living plant roots that are located underground; soil organic matter includes the organic matter fraction in the soil; dead organic matter includes dead branches and leaves, dead standing trees, etc. In addition to this, the carbon stock module of the InVEST model considers the carbon stored in the wood harvest or the associated wood products. Since this study aims to explore the status of carbon stock in the study area, the fifth carbon pool is not taken into account. The relevant equations are as follows.

$$C_{total} = C_{above} + C_{below} + C_{soil} + C_{dead} \quad (8)$$

where C_{total} is the total carbon stock in the study area. C_{above} is the aboveground biomass carbon stock. C_{below} is the belowground biomass carbon stock. C_{soil} is the soil carbon stock. C_{dead} is the dead organic carbon stock. The carbon density of different land-use types and different soil types in each carbon pool is mainly obtained from the relevant literature for the study area [26], where the subsurface carbon stock is converted from the aboveground carbon stock in a certain proportion.

2.3.2. Evaluation Index Construction of Urbanization Development Level

Urbanization is a complex system which mainly refers to the process of rural populations moving to cities, the expansion of the urban scale and the series of social changes caused by this. Based on the connotations of urban development and related research results, a relatively systematic and complete urbanization level evaluation index system was constructed. The urbanization system is divided into five dimensions, including population urbanization subsystem, economic urbanization subsystem, social urbanization subsystem and spatial urbanization subsystem, and ecological urbanization, Therefore, the evaluation of the comprehensive urbanization level (UR) needs to measure the level of the five urbanization subsystems. First, the study needs to construct an evaluation index system for urbanization development level. Demographic urbanization is the core of urbanization, and indicators reflecting the civilization of the rural population and the degree of urban population agglomeration should be considered. Economic urbanization is the driving force, and indicators reflecting regional economic development and financial income should be considered. Spatial urbanization is the guarantee, and indicators

carrying human activities and guaranteeing urban development should be considered. Demographic urbanization and economic urbanization lay the foundation for urbanization and lifestyle transformation, and social urbanization lays the foundation for urbanization and lifestyle transformation. The urbanization of the population and economic urbanization lay the foundation for urbanization and lifestyle transformations; social urbanization and land-use urbanization are the expressions of society and space, respectively; ecological urbanization is an important factor in guaranteeing residents happiness, and indicators reflecting the sustainable and high-quality development of cities need to be selected. In this paper, we will follow the principles of comprehensiveness, accessibility and scientificity. We will look at the existing evaluation results of urbanization development, evaluate five different levels (population, economy, society, ecology and space), streamline and adjust their indicators, and construct an evaluation index system for urbanization level in this paper, considering development mechanisms. We will assign weights to each indicator based on the entropy value method due to their possible covariance problem, i.e., a linear relationship between the indicators. As the covariance of each index needs to be less than 7.5, the final indexes characterizing urbanization development were obtained as shown in Table 2.

Table 2. Evaluation index system of urbanization development level.

Target Layer	Guideline Layer	Indicator Layer
Urbanization (UR)	Population urbanization (PU)	Urban population share (0.03), urban population density (0.06)
	Economic urbanization (ENU)	GDP (0.14), GDP per capita (0.14), fiscal revenue per capita (0.21)
	Social urbanization (SCU)	Total retail sales of consumer goods per capita (0.0527), health technicians per 10,000 people (0.05), school students per 10,000 people (0.02)
	Spatial urbanization (STU)	Urban road area per capita (0.06), built-up area owned per capita (0.11)
	Ecological urbanization (ECU)	Greening coverage rate of built-up areas (0.11), park green space per capita (0.02)

2.3.3. Exploratory Spatial Data Analysis (ESDA)

Exploratory Spatial Data Analysis (ESDA) is centered on measuring the degree of spatial association between things or phenomena, which compensates for the shortcomings of traditional statistical analysis, which ignores the spatially dependent properties embedded in the data [41]. ESDA analysis can be used to determine whether urbanization development has geographic clustering characteristics and spatial anomalies at ecosystem service levels, and then to explore the spatial processes in more depth. The two methods are Global Spatial Autocorrelation and Local Spatial Autocorrelation.

(1) Global spatial autocorrelation analysis is used to test whether the level of urbanization development and the level of ecosystem services are spatially correlated and spatially clustered across the study area, and is generally more commonly applied to the Global Moran's I index, with the following formula.

$$I = \frac{n\sum_{i=1}^{n}\sum_{i\neq j}^{n} w_{ij}(x_i-\overline{x})(x_j-\overline{x})}{\sum_{i=1}^{n}\sum_{j\neq i}^{n} w_{ij}\sum_{i=1}^{n}(x_i-\overline{x})^2} = \frac{\sum_{i=1}^{n}\sum_{j\neq i}^{n} w_{ij}(x_i-\overline{x})(x_j-\overline{x})}{s^2\sum_{i=1}^{n}\sum_{j\neq i}^{n} w_{ij}} \quad (9)$$

where $S^2 = \frac{1}{n}\sum(Y_i-\overline{Y})^2$ denotes the variance in urbanization development and ecosystem service level values, n is the total number of study units. W_{ij} is the standardized spatial adjacency weight matrix, selected based on the first-order common boundary Rook weights. When the area is adjacent to i and j, $W_{ij} = 1$; otherwise, 0. Y_i indicates the regional i. Y, denotes the average value of urbanization development and ecosystem service level in the study area. For I, a positive value indicates the spatial similarity of the variables, while a negative value indicates no similarity.

By the significance test of Moran's I index, if Moran's I is significant and positive at a given confidence level, it means that the level of urbanization development and the level of ecosystem services are positively correlated (higher or lower) and clustered in space, and the closer the value is to 1, the smaller the spatial difference between the level of urbanization development and the level of ecosystem services in If Moran's I is significant and negative, it indicates that the level of urbanization development and the level of ecosystem services are negatively correlated (higher or lower) between regions, and the closer the value is to −1, the greater the spatial difference between them.

(2) Local spatial autocorrelation analysis reflects the degree and significance of spatial differences between each region and its neighboring regions by measuring the significance level of spatially correlated local indicators, which is often measured by scatter plots and Local Moran's I statistics, calculated as follows:

$$I_i = \frac{(x_i - \overline{x}) \sum_{i=1}^{n} W_{ij}(x_j - \overline{x})}{\sum_{i=1}^{n} (x_i - \overline{x})^2}, \; i \neq j \tag{10}$$

among them, w_{ij} is the spatial weight matrix, and n is the total number of study units.

By visualizing the Moran scatter plot and LISA clustering map, four major types of spatial aggregation for urbanization development level and ecosystem service level can be identified, namely, high–high aggregation, high–low aggregation, low–high aggregation, and low–low aggregation types.

2.3.4. Constraint Line Methods

Since the introduction of boundary lines in 1972, constraint line methods have been increasingly used in ecology to compensate for the shortcomings of traditional statistical methods in deciphering the distribution of scatter cloud data. Compared to traditional linear regression and correlation methods, constraint line methods can better characterise the limiting effects of limiting variables on response variables in complex ecosystems due to multiple factors. There are four main methods of drawing constraint lines: parametric, scatter cloud grid, quantile regression and quantile partitioning. In this paper, the quantile partitioning method was chosen to extract the constraint lines [42]. Based on the scatter plot between ecosystem services, the range of ecosystem services on the x-axis was divided into 100 equal parts to obtain 100 columns, and 99% of the quantile of each column was taken as the boundary point to obtain 100 boundary points to fit each constraint line using Origin 2021 software (www.originlab.com, accessed on 2 March 2022). The optimal constraint lines were obtained from simulations based on the shape and goodness—of-fit of the scattered point cloud to explore the constraint effects of topographic factors on ecosystem services.

2.3.5. Spatial Regression Model

Classical linear regression models cause the misestimation of model parameters and reduce the validity of the model when solving problems due to the presence of spatial autocorrelation; therefore, there is a need to construct regression models that are applicable to spatial data [41,43]. Anselin provided the general form of spatial regression models.

$$Y = \rho W_1 + X\beta + u \tag{11}$$

$$\mu = \lambda W_2 \varepsilon + \mu, \mu \sim N\left[0, \sigma^2 I\right] \tag{12}$$

where Y is the dependent variable, X is the explanatory variable, β is the spatial regression coefficient of the explanatory variable, u is the spatially varying error term, μ is the white noise, W_1 is the spatial weight matrix reflecting the spatial decease of the dependent variable itself. W_2 is the spatial weight matrix reflecting the spatial trend of the residuals, which is usually determined based on the adjacency or distance function relationship. ρ is the coefficient of the spatial lag term, whose value ranges from 0 to 1. The closer the value is to 1, the more similar the values of the dependent variables taken in adjacent areas. λ is

the coefficient of spatial error, whose value ranges from 0 to 1, and the closer the value is to 1, the more similar the values of the explanatory variables taken in adjacent regions, where W_1 can be equal to W_2.

The following models can be derived from the general form of the spatial autoregressive model when ρ and β are not equal to 0 and λ. When these are equal to 0, the spatial lag model (SLM) is used, in which the dependent variable of the region under study is not only related to the explanatory variables in this region, but also to the dependent variables in the neighboring regions. When ρ equals 0, β and λ are not equal to 0. Therefore, a spatial error model (SEM) is used, which means that the dependent variable Y in the studied region is not only related to the explanatory variable X in the region, but is also related to the dependent variable and the explanatory variables in the neighboring regions. Spatial dependence not only implies a lack of spatial independence in observations, but also shows the structure of the data underlying this spatial correlation, that is, the strength and pattern of spatial correlation are determined by both absolute location (pattern) and relative location (distance). In this paper, we used spatial regression simulations to explore the interaction mechanisms between county-scale urbanization and ecosystem service values.

3. Results

3.1. Spatial and Temporal Evolutionary Characteristics of Various Ecosystem Services in the Study Area and County

Based on the above ecosystem service evaluation methods, the spatial pattern of five types of ecosystem services at the county scale in Anhui Province were obtained and the mean values of each ecosystem service in the corresponding years were used to describe the changes in ecosystem services in the study area during the 20 years of study. The study showed that the overall performance of the five ecosystem services at the county scale in Anhui Province was "low in the north and high in the south" during the period 2000–2020 (Figure 3).

Among them, the average level of habitat support services in the study area increased and then decreased at 0.486, 0.490, and 0.485, respectively; the capacity of carbon storage services continued to decrease, with average values of 12.58 ($t{\cdot}ha^{-2}$), 12.54 ($t{\cdot}ha^{-2}$), 12.49 ($t{\cdot}ha^{-2}$). Water production service capacity increases year by year, with county average water production values of 758.07 mm, 901.87 mm and 1007.08 mm during 2000, 2010 and 2020; soil conservation function increases year by year, with county average values of 782.92 ($t{\cdot}ha^{-2}$), 782.95 ($t{\cdot}ha^{-2}$), 783.35 ($t{\cdot}ha^{-2}$). Organic matter production function first decreases and then increases, with county average values of 512.59 ($gc{\cdot}m^{-2}$), 504.98 ($gc{\cdot}m^{-2}$), 564.60 ($gc{\cdot}m^{-2}$). The overall trend of changes in ecosystem services across types showed inconsistency, mainly due to the existence of different degrees of trade-offs among ecosystem services.

(1) Analysis of synergistic relationships of ecosystem service trade-offs in the study area under different regions.

Based on the above analysis, it is worth exploring whether trade-off relationships occur among the five types of ecosystem services in the study area. Therefore, Spearman's correlation measure was used to explore the average ecosystem service correlations in different regions in Anhui Province from 2000 to 2020 at the study-area-wide scale, covering South Anhui, North Anhui, and Central Anhui (Figure 4). The study showed that the five types of ecosystem services showed strong synergistic correlations at the global scale, as well as for South Anhui and Central Anhui, while some ecosystem services showed trade-offs in North Anhui, and the overall synergistic correlations showed Anhui Province > South Anhui > Central Anhui > North Anhui. The synergistic correlation between soil conservation and carbon storage function was the best (0.75) and the synergistic relationship between soil conservation and water production was the weakest (0.58) at the whole-area scale. The synergistic relationship between habitat support services and water production services was the weakest (0.48 and 0.27) in South and Central Anhui. The water production service in this study refers to rainfall minus evapotranspiration and does not consider

surface runoff, which may increase the regional water production capacity to some extent due to the increase in construction land or agricultural land. In northern Anhui, except for the strong synergy between habitat support services and carbon storage, water production services and NPP, the remaining ecosystem services showed a weak synergy and weak trade-off. The shift in the relationship between ecosystem services varied widely, e.g., soil conservation and carbon storage had the best synergy at the provincial scale, while they showed a trade-off in northern Anhui (−0.10). This is more strongly related to the different physical geographic characteristics of Anhui Province, where the northern Anhui Province is mostly plain, and its land cover/use is mostly arable land and construction land, with a smaller proportion of woodland and grassland, while the amount of woodland and grassland in the hilly areas of central Anhui and the mountainous areas of southern Anhui has a much higher proportion than that of construction land.

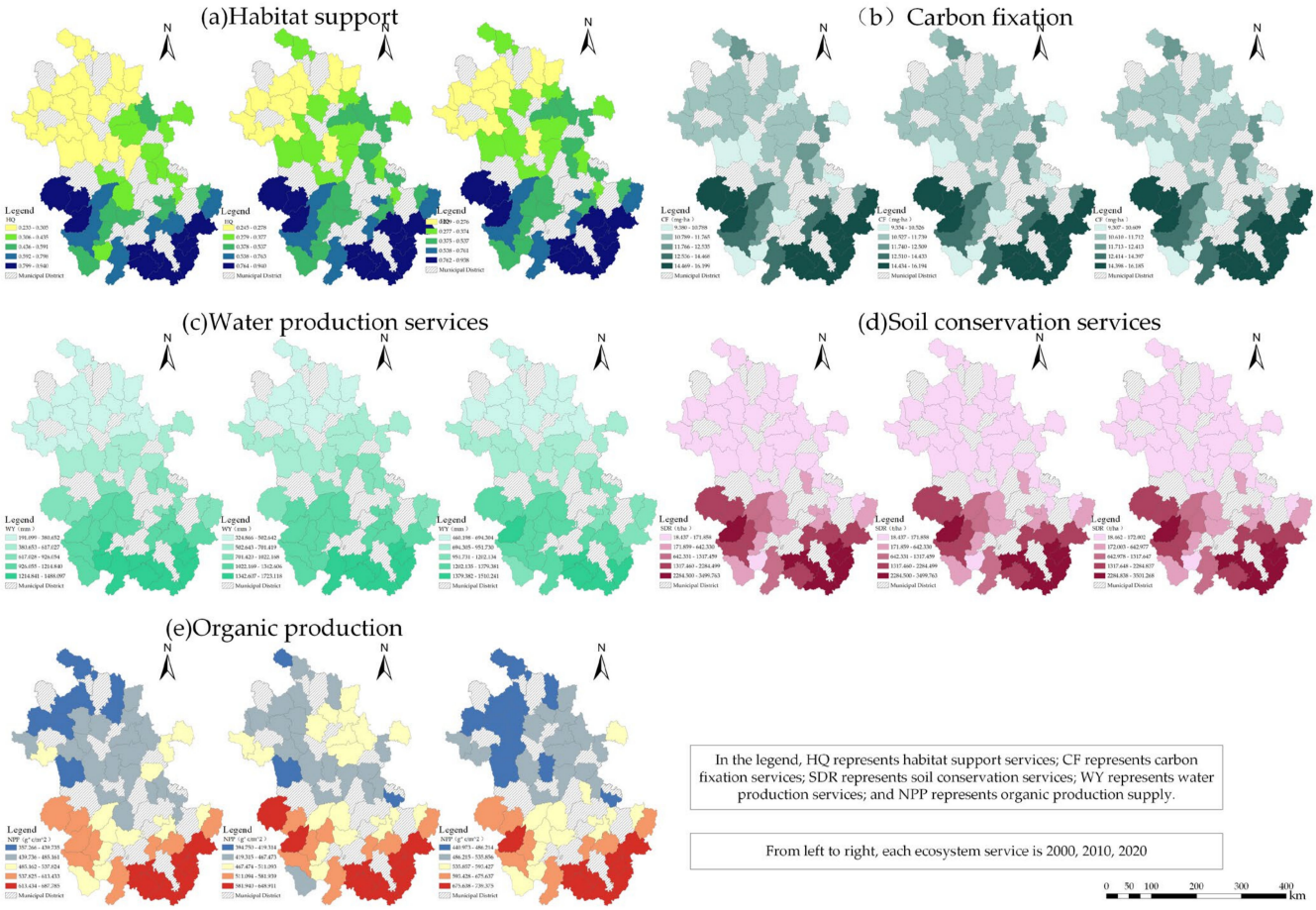


Figure 3. Evolutionary characteristics of five types of ecosystem services at the county level in the study area during 2000, 2010 and 2020.

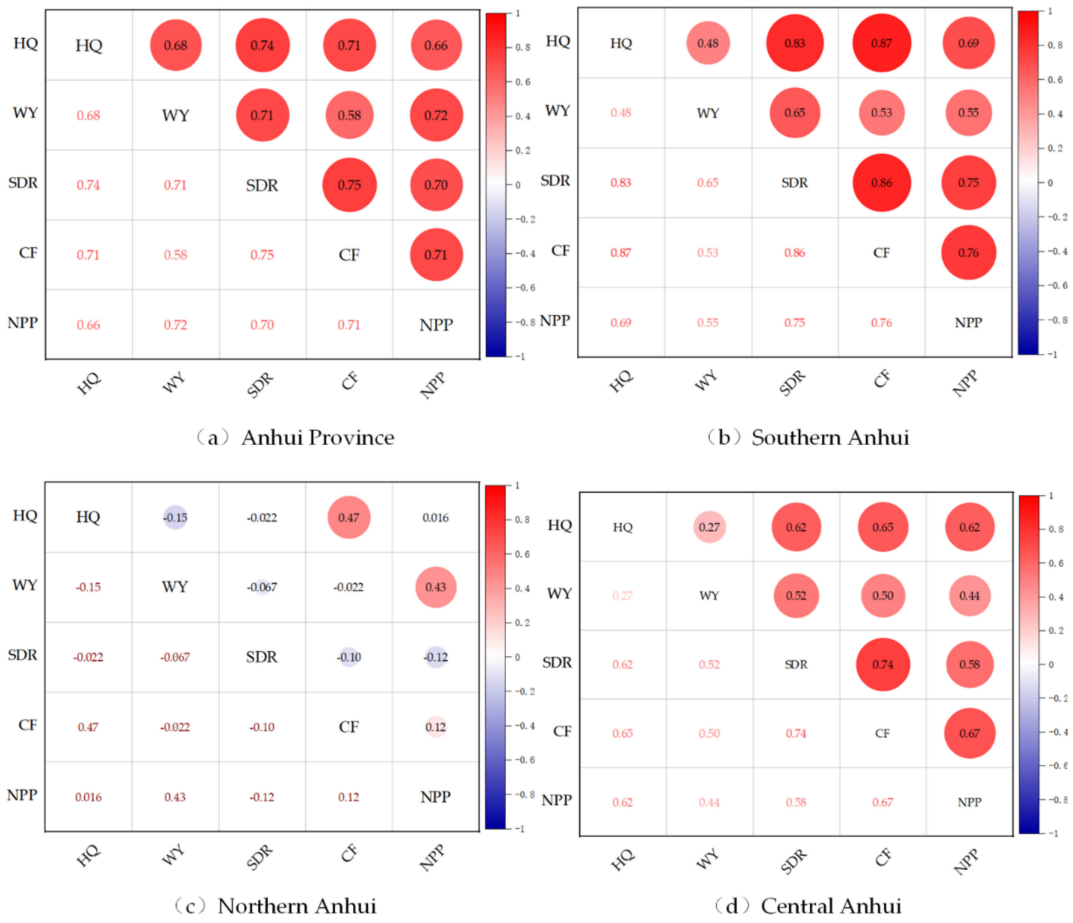


Figure 4. Measurements of synergies and trade-offs among multi-scale ecosystem services in the study area.

(2) Measurement of the effect of physical and geographical features on ecosystem service constraints.

While the relationships among the five types of ecosystem services in the study area have been discussed, whether the physical geographic characteristics of the study area are important factors affecting the trade-off relationships of ecosystem services in the study area needs to be further explored. In addition to their interactions, ecosystem service relationships are influenced by many other factors, such as meteorological factors, topographic factors, and land cover factors. The complexity of these factors also means that the relationship between ecosystem services is not simple and linear. The constraint line approach provides a new way of understanding the relationships among ecosystem services and the related ecological processes that influence them. Ecosystem patterns and processes are often influenced by a combination of factors, so a scatter plot reflecting the relationship between two ecological variables often appears as a bounded scatter cloud. Scatter clouds do not represent correlations between two variables, but instead represent constraining relationships. The constraint line approach has great potential to address the trade-offs of ecosystem services, and this section aims to explore the role of topographic factors in constraining five types of ecosystem services to better understand why relationships between ecosystems shift (Figure 5).

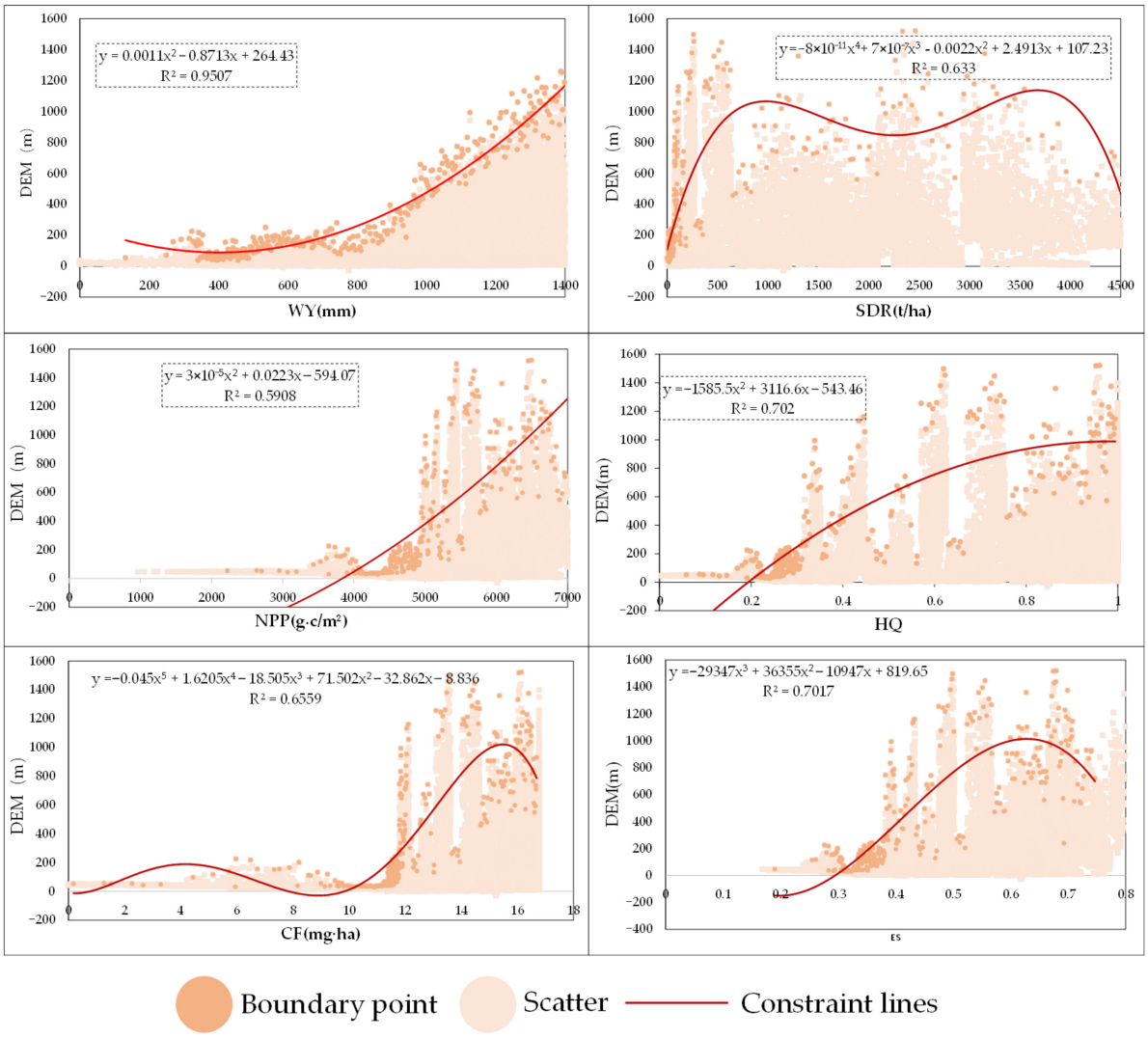


Figure 5. Spatial and temporal evolutionary characteristics of urbanization levels and subtypes at the county level in the study area during 2000, 2010 and 2020.

The results show that the constraint line of water production service according to the topography factor is "exponential"; that is, the constraint effect of topography factor on water production service continuously decreases with the rise in the topography of the whole study area ($R^2 = 0.9507$ The constraint line of terrain factor on soil conservation function is "convex wave type", and the constraint effect of terrain factor on soil conservation shows fluctuating characteristics ($R^2 = 0.633$). The topographic factor on the NPP constraint line is "exponential", and the correlation between water production service and NPP is synergistic (0.43). The two are of the same type in terms of constraint line ($R^2 = 0.5908$); the constraint line of topography on habitat support is "positively convex", i.e., topography effectively constrains habitat support services and proportionally increases the constraint effect, while the overall constraint line of topography on carbon storage is "convex wave" ($R^2 = 0.6559$). However, Figure 4 shows that the carbon storage constraint line is "open downward parabolic" at altitudes below 200 m, and the hump is low, which differs from the overall trend of soil conservation. After the elevation rises to 200 m, the constraint line fits experience a rapid rise and reach their peak at about 1000 m. The constraint fitting curve of the integrated ecosystem service function becomes "S-shaped" as the topography increases, and the constraint effect of the topography factor decreases extremely rapidly in the range of 0.6~0.7 as the integrated ecosystem service increases.

3.2. Analysis of Spatial and Temporal Changes in the Level of Urbanization Development and Subsystems in the Study Area

The population urbanization, economic urbanization, social urbanization, spatial urbanization, and ecological urbanization scores for the three period nodes of 2000, 2010, and 2020 were calculated by the weights of each index, and the spatial and temporal evolution characteristics of urbanization in the three periods were obtained from the statistical comprehensive urbanization level (Figure 6) and divided into five levels using the natural breakpoint grading method.

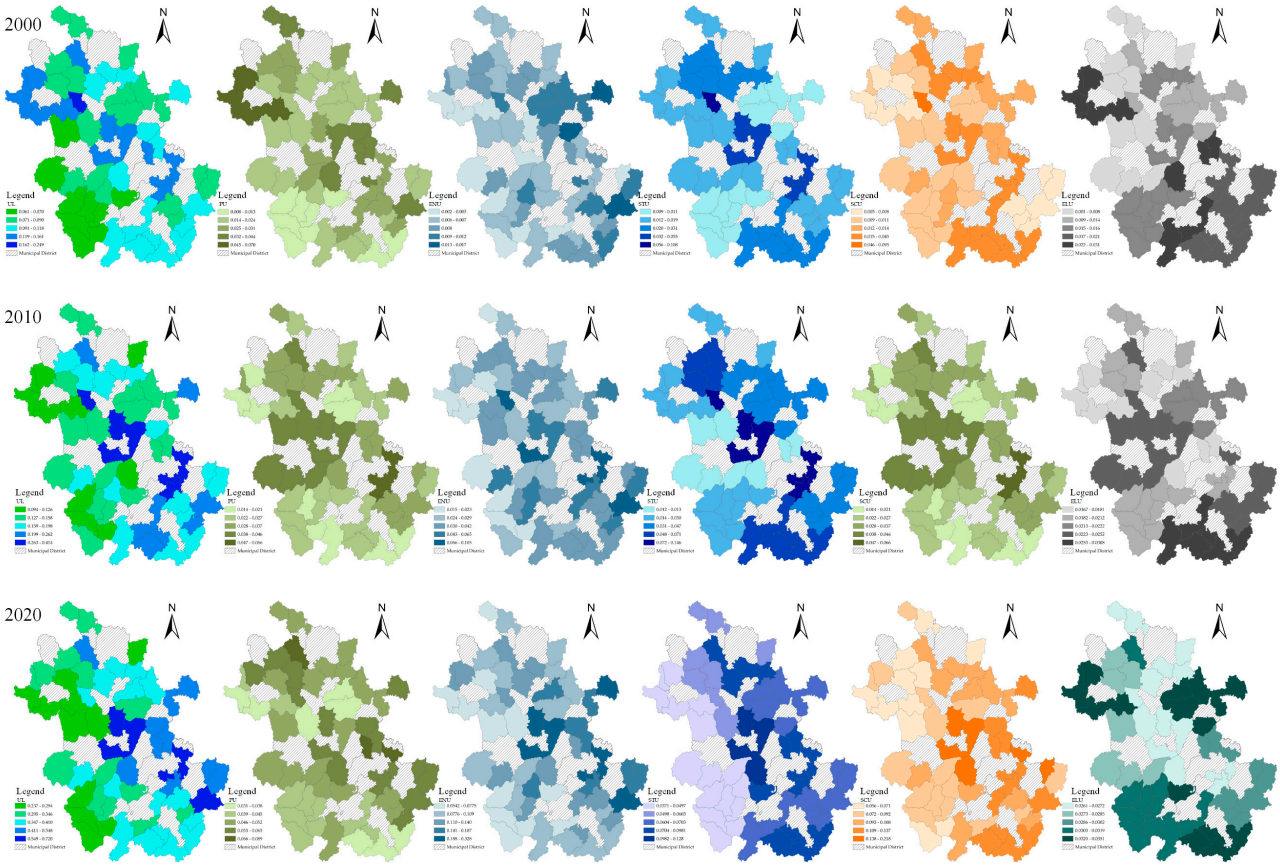


Figure 6. Scatter plot and constraint lines between topography and ecosystem services in the study area (UR: urbanization; PU: population urbanization; ENU: economic urbanization; STU: spatial urbanization; SCU: social urbanization; ELU: ecological urbanization).

The results show that the average level of comprehensive urbanization gradually increased between 2000, 2010 and 2020 (0.100, 0.187 and 0.382), and the center of gravity of the highest level of county urbanization shifted from northern Anhui (2000) to central Anhui (2010) to southern Anhui (2020). The spatial pattern and evolution of various urbanization subsystems differ significantly, with the high value of population urbanization subsystems in 2000 occurring in the counties belonging to Fuyang in northern Anhui. The highest values in terms of economic urbanization areas were found in Tianchang, Chaohu, and Ningguo under Maanshan; among the spatial urbanization county evaluation units, Fengtai County had the highest level in 2000, followed by Feidong, Feixi, and Fanchang counties. In the five urbanization subsystems between 2010 and 2020, the center of gravity for population urbanization gradually shifted from north to south, and spatial urbanization developed from a single point to a multi-point pattern; the pattern of economic urbanization remained the same after Hefei. The pattern of economic urbanization later maintained two major development areas around Hefei City and Wuhu City. The most dramatic change in the development level of ecological urbanization occurred in the central Anhui region, with the average level of each year rising and then falling between 2000 and 2020. In

general, the comprehensive urbanization development level of counties in Anhui Province significantly increased during 2000–2020, which is in line with the normal economic and social development trends. The urbanization development in northern Anhui started to decline compared with that in central and southern Anhui, and the change in county urbanization development level levels within the region was relatively flat. The spatial pattern of development of each subsystem in Central and Southern Anhui region changed more drastically.

3.3. Measurement of the Spatial Spillover Effect of Urbanization Development on Ecosystem Services

Based on GeoDa 1.18 software (http://geodacenter.github.io/, accessed on 2 May 2021), the bivariate global autocorrelation Moran's I index between the integrated level of urbanization and the integrated level of ecosystem services in counties was measured for the years 2000, 2010, and 2020. The bivariate global autocorrelation of Moran's I index between the combined level of urbanization and the combined level of ecosystem services was −0.310, −0.312, and −0.108 in 2000, 2010, and 2020, respectively, which passed the significance test at the 0.001 level. The overall negative correlation increased and then decreased. There was a significant negative spatial correlation between urbanization level and ecosystem services during the study period, indicating that the development of urbanization leads to the deterioration of ecosystem services. The bivariate spatial autocorrelation test indicated a significant spatial dependence effect between the value of ecosystem services and urbanization, which generated a significant negative externality during the study period. This is mainly due to the rapid expansion of land for construction in the period of urbanization, which causes strong disturbance to ecosystem services. The existence of spatial spillover effects is mainly due to the flow of material, energy and information flows between neighboring regions. In addition, natural processes (e.g., atmospheric circulation, temperature, precipitation) and human activities (e.g., urbanization, economic development, population migration) also lead to the spatial spillover of ecosystem services. Therefore, ecosystem protection and management cannot be limited to a single unit, and collaborative management across regions and different levels of government departments is an effective means of ecosystem protection.

In order to further investigate the impact of urbanization development on ecosystem services, this study used a spatial regression model to investigate the impact of five types of urbanization subsystems on integrated ecosystem services (ES) to more accurately understand the impact of different urbanization types on ecosystem services. The general process of spatial regression modeling was judged with the help of Lagrange multiplier statistic (LM) in spatial econometrics. The OLS regression model was built, and the spatial autocorrelation diagnosis of the regression results was made with the help of LM-lag and LM-error (Table 3). Comparing the test statistics of LM-lag and LM-error, the spatial regression model with a better significance was selected. The results showed that both LM-lag and LM-error were significant during 2000–2020; therefore, to continue comparing the significance of Robust LM (error) and Robust LM (lag), it was found that Robust LM (error) was not significant during 2000 and 2020, and Robust LM during 2010 (error) and Robust LM (lag) were both significant, but Robust LM (lag) was more significant. Therefore, the relationship between urbanization development and ecosystem services during 2000, 2010, and 2020 was modeled using a spatial lag model (Table 4).

Table 3. Regression results of OLS models for 2000, 2010 and 2020 in the study area.

Variables	2000			2010			2020		
R-squared	0.377 ***			0.342 ***			0.258 ***		
Adjusted R-squared	0.320			0.575			0.190		
Akaike info criterion	−94.0367			−122.247			−85.027		
Coefficient	PU	−4.095 *		PU	−0.898 *		PU	−3.593 *	
	ENU	1.218 *		ENU	0.939 *		ENU	0.389 *	
	ELU	1.734 *		ELU	2.755 *		ELU	−0.219 *	
	STU	−0.521 *		STU	−1.380 *		STU	−0.240 *	
	SCU	−1.125 *		SCU	0.520 *		SCU	0.052 *	
DIAGNOSTICS FOR SPATIAL DEPENDENCE	MI/DF	VALUE	PROE	MI/DF	VALUE	PROE	MI/DF	VALUE	PROE
Moran's I (error)	0.7556	6.1458	0.00	0.4852	4.019	0.00	0.7975	6.5551	0.00
Lagrange Multiplier (lag)	1	37.747	0.00	1	28.263	0.00	1	0.1680	0.00
Robust LM (lag)	1	6.524	0.01	1	17.131	0.00	1	0.0086	0.92
Lagrange Multiplier (error)	1	31.514	0.00	1	12.995	0.00	1	6.0741	0.00
Robust LM (error)	1	0.292	0.59	1	1.864	0.04	1	5.9147	0.01
Lagrange Multiplier (SARMA)	2	38.0386	0.00	2	30.127	0.00	2	6.0827	0.00

Notes: *** $p \leq 0.001$, ** $p \leq 0.01$, * $p \leq 0.05$.

Table 4. Regression results based on spatial error model and spatial lag model.

Variables	2000 (SLM & SEM)				2010 (SLM & SEM)				2020 (SLM & SEM)			
R-squared	0.867 ***		0.823 ***		0.888 ***		0.881 ***		0.875 ***		0.852 ***	
Akaike info criterion	−160.871		−174.283		−122.247		−166.276		−89.5468		−67.527	
Coefficient	PU	−1.029 ***	PU	−1.029 ***	PU	−0.341 ***	PU	0.419	PU	−2.862 ***	PU	−1.372 **
	ENU	−0.312 **	ENU	−0.912	ENU	−0.097 *	ENU	1.076	ENU	0.353 *	ENU	0.123
	ELU	0.481 **	ELU	0.401 **	ELU	1.059 **	ELU	0.626	ELU	0.295 ***	ELU	1.520
	STU	−0.140 **	STU	−0.153 **	STU	−0.509 ***	STU	−0.207 ***	STU	−0.101 *	STU	−0.223 *
	SCU	−0.127 *	SCU	−0.127	SCU	0.229 *	SCU	0.005	SCU	0.036 *	SCU	0.256 *
CONSTANT	0.106		0.306		0.108		0.412		0.638		0.504	
Schwarz criterion	−146.21		−155.62		−162.228		−153.71		−76.981		−50.981	
Log likelihood	95.444		91.233		95.4441		89.138		50.773		88.773	

Notes: *** $p \leq 0.001$, ** $p \leq 0.01$, * $p \leq 0.05$.

The study shows that the effects of population urbanization and spatial urbanization on ecosystem services during 2000–2020 are negatively correlated. After interpreting the regression coefficients measured by the SLM model, each 1% increase in population urbanization in 2000, 2010, and 2020 was shown to lead to a −1.029%, −0.341%, and −2.862% decrease in ecosystem services in that year. Each 1% increase in urbanization led to a decrease in ecosystem services of −0.140%, −0.509%, and −0.101%; social urbanization and economic urbanization led to a decrease in ecosystem services in the early stage, and each 1% increase in social urbanization will led to a −1.125% decrease in ecosystem services in that year, respectively. With social and economic development, social urbanization and economic urbanization contribute to ecosystem services. The effects of ecological urbanization on ecosystem services were all positive, with each 1% increase in ecological urbanization leading to 0.481%, 1.059%, and 0.295% increases in ecosystem services in that year. After measuring the spatial spillover effects of the five types of urbanization on ecosystem services, population concentration, economic development, and the expansion of urban construction land were found to lead to a decrease in ecosystem services. However, it is important to note that population and economic agglomeration do not necessarily lead to the degradation of ecosystem services. This is mainly due to the fact that population and economic agglomeration cannot directly interfere with ecological services, but can affect them by promoting the expansion of land for construction. The expansion of urban construction land will reduce ecological services, but inner urban waters, wetlands and green areas will mitigate the degradation of ecosystem functions to some extent; therefore, eco-urbanization promotes the improvement of ecosystem services at any stage. The spatial

error term was significant during 2010 and 2020; however, in 2000 the spatial error term was not significant. This indicates that changes in ecosystem services are also influenced by other, non-urbanization factors (policies, natural environment, etc.) (Figure 7).

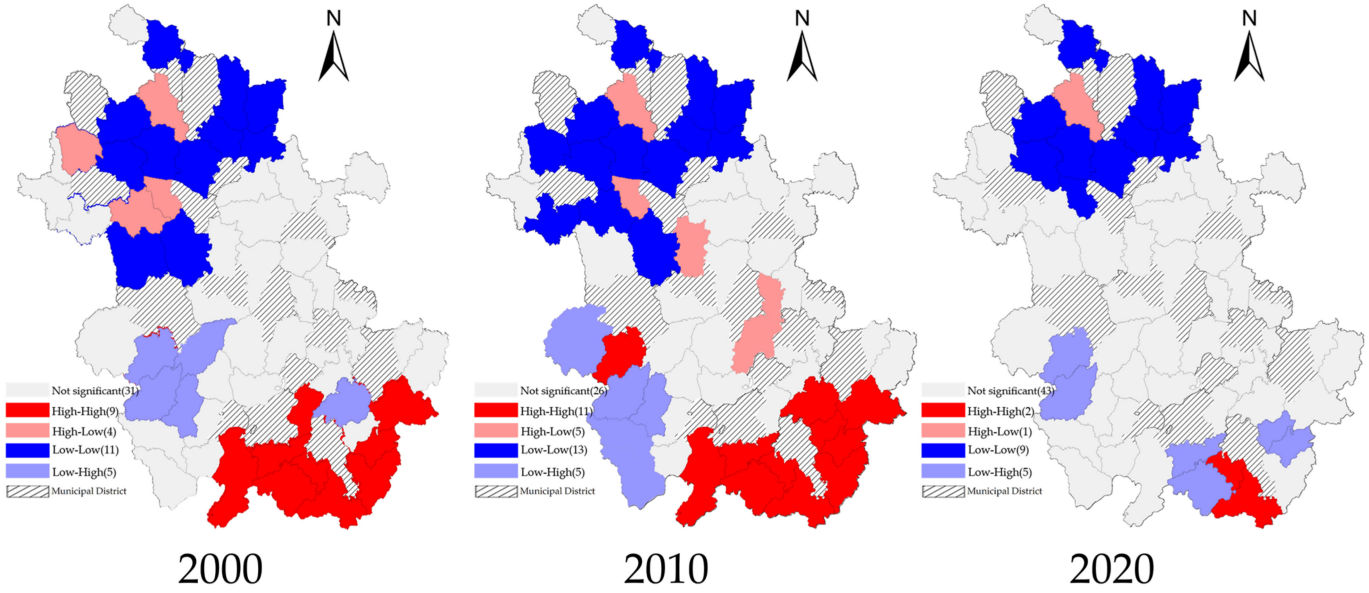


Figure 7. LISA diagram of integrated level of urbanization and integrated level of ecosystem services between 2000, 2010 and 2020.

4. Discussion

4.1. Transformation of the Relationship Development between Urbanization Development Patterns and Ecosystem Services in the New Era

In recent decades, the rapid development of urbanization in China has caused great disturbances to regional ecological security and seriously affected the well-being of regional people. Frequent and intense urbanization activities have led to a significant increase in land for construction, which previously had mainly shifted from arable land, forest land, and grassland, and a shift in land use driven by natural geographic features due to planning (government and residential construction needs) has begun to occur (Figure 8a). This shift involves both temporal and spatial dimensions, resulting in multiple complex adaptive changes in ecosystem services (linear, nonlinear, hysteresis, etc.). In the new era of China's national policy development shift, the development model of urbanization has shifted from the crude development of large-scale demolition and construction that occurred in the past to high-quality development. This change requires that some cities face a certain degree of actual demand for construction land, which is less than the existing construction land, resulting in the phenomenon of "hollow cities". Urbanization is the inevitable result of social development; however, in the future, there is a need to establish a long-term mechanism for the efficient, intensive and economical use of land, to fully explore the potential of urban land, to make intensive and economical use of land, to promote the more efficient allocation of resources in cities and towns, and to reduce energy consumption in the process of urbanization. In terms of urban construction patterns, there is a need to establish a compact and efficient land-use pattern to prevent excessive urban sprawl and disorderly development (Figure 8b).

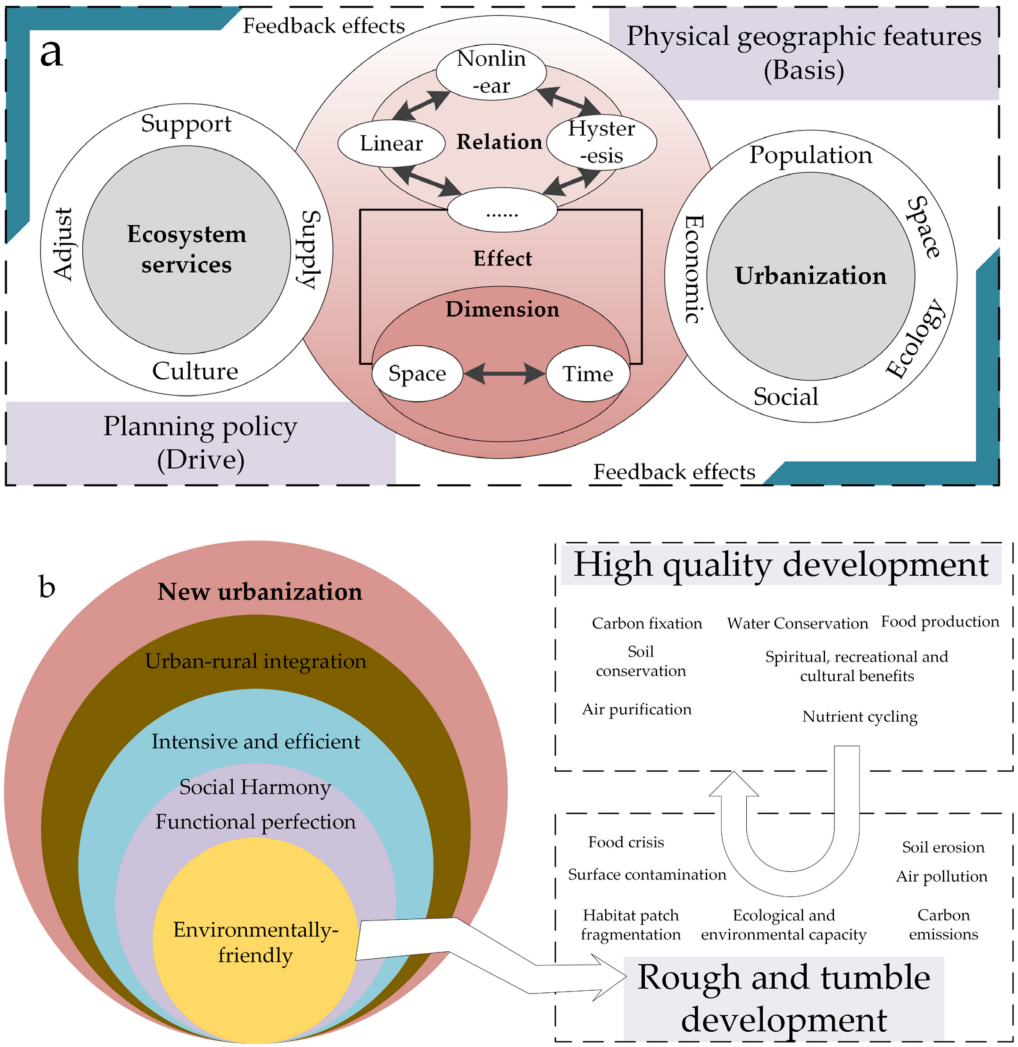


Figure 8. An analysis of the relationship between urbanisation patterns and ecosystem services.

Under the condition of resource and energy constraints, China is facing the big challenge of high resource consumption, high energy consumption, and high carbon emissions in urbanization development. As the world's largest greenhouse-gas-emitting economy, China has made a commitment to be "peak carbon and carbon neutral". Therefore, the future development pattern of urbanization and ecosystem service enhancement needs to change from antagonistic to synergistic effects. According to existing studies, China's urbanization rate is expected to reach 75% in 2035 and 80% in 2050 according to the high-level scenario of China's urbanization development, with an additional 150–200 million people to be added in the future. This study confirms that the development of urbanization in Anhui Province has led to different degrees of decline in regional ecosystem services over the past 20 years. In terms of the development trend of the five types of urbanization subsystems, the urbanization development rate of northern Anhui may continue to lag behind that of the Hefei periphery, the Wanjiang urban belt, and southern Anhui. The large population shift to developed cities in China will cause the actual urban land demand in this area to weaken, but will increase the ecological and environmental pressure in the inflowing areas. The future urbanization development mode of the population outflow areas should focus on the transformation of the land stock to avoid the disorderly increase in urban area and waste of resources. For the county cities in southern Anhui with good economic development and an excellent ecological background, the future direction of urban construction should consider increasing the green spaces to carry out urban functions. Ecological resources such as rivers, lakes and water systems are no longer just embellish-

ments for cities, but need to be transformed into important spaces that can carry industries and convert ecological values.

4.2. Conservation Strategies for Ecosystem Services in Different Regions

At present, numerous studies have shown that ecological restoration policies have positive effects on environmental quality improvements [44–46]. However, specific policy implementation programs need to be continuously optimized. In this paper, we investigated the nonlinear relationship between topographic factors and ecosystem services, and confirmed that the constraints of physical geography on ecosystem services are consistent with the academic understanding that natural factors, as formative factors, determine the state of the ecological background to a certain extent, and provide a quantitative basis for the implementation of future ecosystem service protection policies in the study area. The Spearman correlation was used to measure the trade-offs and synergistic relationships among ecosystem services, and it was found that the five types of ecosystem services in the study area showed synergistic relationships overall; however, some ecosystem services in northern Anhui showed trade-offs. In addition, this paper was unable to measure food production as a food supply service in the ecosystem due to the limited research data. However, related studies in this region show that there is a conflict between the ecosystem services provided by agricultural land and ecological land (woodland and grassland), which reflects the objective existence of a competitive relationship between food production and ecological conservation. Therefore, policymakers often address the possibility that ecosystem regulating services such as the conservation of regional biodiversity, air purification, and carbon sequestration and oxygen release may affect grain production. The northern Anhui region is an important supply area for grain production, so the trade-off between grain production and other ecosystem services needs to be emphasized while improving the quality of the ecological environment. The hilly area in central Anhui is the core area of development in Anhui, with high demands for urban construction and development. In the future, not only should the expansion of construction land be reasonably arranged, a certain proportion of ecological land be maintained, and low-pollution and low-consumption green industries be developed, but the improvement of internal habitat quality can be achieved by constructing ecological corridors, reducing landscape fragmentation, and increasing the connectivity of ecological land. The mountainous areas in southern Anhui Province have a high vegetation coverage, but less farmland and a smaller proportion of construction land and play an important ecological service function in Anhui Province and even in the Yangtze River Delta urban agglomeration. Therefore, attention should be paid to protecting the ecological environment in the mountainous areas of southern Anhui, and avoiding the expansion of large-scale construction land, which would block species migration corridors and destroy species diversity.

4.3. Shortcomings and Prospects

This paper measured the spatial and temporal evolution characteristics of the five types of ecosystem services in the study area at the county level during 2000, 2010, and 2020 using the InVEST model and CASA model, and explored the constraint effects of physical geographic features on the five types of ecosystems in the study area based on the constraint line method. The spatial distribution of the five types of urbanization in the county study unit was measured using the entropy method. The spatial regression model was used to measure the effects of population, economic, social, spatial, and ecological urbanization on ecosystem services, and a spatial spillover effect was found between urbanization development and ecosystem services. Additionally, various factor flows between regions were shown to affect each other in neighboring regions. Due to the difficulty of data acquisition, there are limitations in the selection of urbanization evaluation indicators in this paper, which do not fully represent the full significance of the five types of urbanization: demographic, economic, social, spatial, and ecological. Ecosystem services include provisioning services (water production), regulating services (carbon fixation, soil conservation), cultural

services (spiritual, cultural and cultural benefits, etc.), and supporting services (habitat support, organic matter production), which involve many subtypes of ecosystem services. In this paper, only those ecosystem services that are closely linked to human activities in the study area were selected; this did not include plant pollination, pest and disease pests, cultural services, etc. In the future, a more comprehensive assessment of ecosystem services could be conducted using different research methods.

5. Conclusions

In this study, the spatial and temporal variation characteristics of the five subtypes of urbanization and ecosystem services of county units in the study area were evaluated based on the InVEST model, CASA model, constraint line method and entropy method between 2000, 2010 and 2020, and the spatial relationship between integrated ecosystem services and urbanization subtypes was further explored using spatial regression models. The main conclusions are as follows:

(1) At the county scale of Anhui Province in 2000, 2010 and 2020, the overall performance of the five ecosystem services was "low in the north and high in the south". The overall trend of each type of ecosystem services was inconsistent, mainly due to the different degrees of trade-offs among ecosystem services. Using the constraint line method to measure the topography of the five ecosystem services, we found that the constraint effect of topography on the five ecosystem services is an important factor leading to the existence of different degrees of trade-offs among the ecosystem services;

(2) Based on the five dimensions of population, economy, society, space, and ecology, we measured the comprehensive level of urbanization and the spatial and temporal development of subtypes in Anhui counties and found that the average level of comprehensive urbanization gradually increased (0.100, 0.187, 0.382) and the center of gravity of the highest level of county urbanization shifted from northern Anhui (2000) to central Anhui (2010) to southern Anhui (2020);

(3) Based on the spatial autocorrelation model and spatial regression model, which were used to measure the spatial relationship and influence degree of integrated ecosystem services and urbanization subtypes, a significant negative spatial correlation was found between urbanization level and ecosystem services during the study period, indicating that the development of urbanization would lead to the deterioration of ecosystem services. The flow between county elements would also cause a decline in ecosystem services in the surrounding counties.

Author Contributions: Conceptualization, Y.W. and Y.J.; methodology, H.Y.; software, H.Y. and X.L.; validation, H.Y. and Y.W.; formal analysis, Y.J.; investigation, Y.W.; resources, Y.W.; data curation, Y.W.; writing—original draft preparation, Y.W.; writing—review and editing, Y.J.; visualization, X.L.; supervision, H.Y.; project administration, Y.W. and X.L.; funding acquisition, Y.W. and X.L. All authors have read and agreed to the published version of the manuscript.

Funding: This research was supported by the Key Project of Provincial Humanities and Social Sciences Research in Anhui Universities (Grant Number: SK2020A0257) and the National Natural Science Foundation of China (Grant Number: 42071286).

Institutional Review Board Statement: Not applicable.

Informed Consent Statement: Not applicable.

Data Availability Statement: Not applicable.

Conflicts of Interest: The authors declare no conflict of interest.

References

1. Liu, S.; Costanza, R.; Farber, S.; Troy, A. Valuing ecosystem services: Theory, practice, and the need for a transdisciplinary synthesis. *Ann. N. Y. Acad. Sci.* **2010**, *1185*, 54–78. [CrossRef] [PubMed]
2. Harrington, R.; Anton, C.; Dawson, T.P.; de Bello, F.; Feld, C.K.; Haslett, J.R.; Kluvankova-Oravska, T.; Kontogianni, A.; Lavorel, S.; Luck, G.W. Ecosystem services and biodiversity conservation: Concepts and a glossary. *Biodivers. Conserv.* **2010**, *19*, 2773–2790. [CrossRef]
3. Liu, H.; Liu, L.; Ding, S. The impact of human activities on ecosystem services flow. *Acta Ecol. Sin.* **2017**, *37*, 3232–3242.
4. Keeble, B.R. The brundtland report: 'Our common future'. *Med. War* **1988**, *4*, 17–25. [CrossRef]
5. Hao, Z.; Jian, S.; Wei, D.; Li, P. Ecosystem health: Assessment framework, spatial evolution, and regional optimization in southwest china. *Chin. Geogr. Sci.* **2020**, *30*, 142–156.
6. Che, L.; Zhou, L.; Xu, J. Integrating the ecosystem service in sustainable plateau spatial planning: A case study of the yarlung zangbo river basin. *J. Geogr. Sci.* **2021**, *31*, 281–297. [CrossRef]
7. Li, P.; Liu, C.; Liu, L.; Wang, W. Dynamic analysis of supply and demand coupling of ecosystem services in loess hilly region: A case study of lanzhou, china. *Chin. Geogr. Sci.* **2021**, *31*, 276–296. [CrossRef]
8. Han, H.-Q.; Yang, J.-Q.; Liu, Y.; Zhang, Y.-J.; Wang, J.-W. Effect of the grain for green project on freshwater ecosystem services under drought stress. *J. Mt. Sci.* **2022**, *19*, 974–986. [CrossRef]
9. Xie, J.; Lu, Z.; Xiao, S.; Yan, C. Driving force and ecosystem service values estimation in the extreme arid region from 1975 to 2015: A case study of alxa league, china. *Chin. Geogr. Sci.* **2021**, *31*, 1097–1107. [CrossRef]
10. Zheng, Z.; Fu, B.; Feng, X. Gis-based analysis for hotspot identification of tradeoff between ecosystem services: A case study in yanhe basin, china. *Chin. Geogr. Sci.* **2016**, *26*, 466–477. [CrossRef]
11. Zheng, H.; Wang, L.; Wu, T. Coordinating ecosystem service trade-offs to achieve win–win outcomes: A review of the approaches. *J. Environ. Sci.* **2019**, *82*, 103–112. [CrossRef]
12. Wang, X.; Zhang, X.; Feng, X.; Liu, S.; Yin, L.; Chen, Y. Trade-offs and synergies of ecosystem services in karst area of china driven by grain-for-green program. *Chin. Geogr. Sci.* **2020**, *30*, 101–114. [CrossRef]
13. Geng, T.W.; Chen, H.; Zhang, H.; Shi, Q.Q.; Liu, D. Spatiotemporal evolution of land ecosystem service value and its influencing factors in shaanxi province based on gwr. *J. Nat. Resour.* **2020**, *35*, 1714–1727.
14. Zhang, Y.; Wu, D. Multi-scale analysis of ecosystem service trade-offs and associated influencing factors in beijing-tianjin-hebei region. *Areal Res. Dev.* **2019**, *38*, 141–147.
15. Cheng, L.; Jie, Z.; Zhi, Z.; Si, G. Spatiotemporal dynamics and influencing factors of ecosystem service trade in the yangtze river delta urban agglomeration 2022, 1–13, 1000–0933. *Acta Ecol. Sin.* **2022**, *1–13*, 1000–0933.
16. Howe, C.; Suich, H.; Vira, B.; Mace, G.M. Creating win-wins from trade-offs? Ecosystem services for human well-being: A meta-analysis of ecosystem service trade-offs and synergies in the real world. *Glob. Environ. Chang.* **2014**, *28*, 263–275. [CrossRef]
17. Power, A.G. Ecosystem services and agriculture: Tradeoffs and synergies. *Philos. Trans. R. Soc. B Biol. Sci.* **2010**, *365*, 2959–2971. [CrossRef]
18. Yang, S.H.; Hu, S.G.; Qu, S.J. Terrain gradient effect of ecosystem service value in middle reach of yangtze river, china. *J. Appl. Ecol.* **2018**, *29*, 976–986.
19. Choi, S.; Lee, W.K.; Son, Y.; Yoo, S.; Lim, J.H. Changes in the distribution of south korean forest vegetation simulated using thermal gradient indices. *Sci. China Life Sci.* **2010**, *53*, 784–797. [CrossRef]
20. Jian, X.; Ji, C.; Yanxu, L.; Fei, F.; Jian, W. Spatio-temporal differentiation of interaction of ecosystem services and regional responses in the"belt and road"area. *Acta Ecol. Sin.* **2020**, *40*, 3258–3270.
21. Cao, J.; Zhang, Z.; Cui, F.; Chen, S.; Yang, Y.; Kuang, T.; Chen, Y. Response of ecosystem services to landscape pattern changes in the new york bay area from 1996 to 2015. *World Reg. Stud.* **2021**, *30*, 826–838.
22. Long-Hui, L.; Fu-Jun, C.; Yue-Qing, X.; An, H.; Ling, H. Ecosystem services transition in beijing-tianjin-hebei region and its spatial patterns. *J. Nat. Resour.* **2020**, *35*, 532–545. [CrossRef]
23. Juan, Z.; Fan, C.; Yuan, J.; Cheng, L.; Dong, Z.; Zhi, L.; Qi, X.; Ying, Q. Impacts of village land use change on ecosystem services and human well-being under different tourism models in hani rice terrace. *Acta Ecol. Sin.* **2020**, *40*, 5179–5189.
24. Yan, L.; Dan, Y.; Bo, F.; Ming, C.; Ji, C. Research progress on the biodiversity and ecosystem service scenario simulations. *Acta Ecol. Sin.* **2020**, *40*, 5863–5873.
25. Bo, F.; Han, T.; Fu, Z.; Wen, Z.; Shuai, W. The impact of global change on ecosystem services. *China Basic Sci.* **2017**, *19*, 14–18.
26. Yu, H.; Gu, X.; Liu, G.; Fan, X.; Zhao, Q.; Zhang, Q. Construction of regional ecological security patterns based on multi-criteria decision making and circuit theory. *Remote Sens.* **2022**, *14*, 527. [CrossRef]
27. Jie, G.; Ling, Y.; Chai, X.; Qing, G. A comparative review of research highlights on ecosystem services of china and USA in the latest 30 years. *Acta Ecol. Sin.* **2020**, *40*, 3537–3547.
28. Liu, Y.; Fu, B.-J.; Zhao, W.; Wang, S. Ecological asset accounting and ecosystem services evaluation: Concept intersection and key research priorities. *Acta Ecol. Sin.* **2018**, *38*, 8267–8276.
29. Zhong, L.; Teng, F.; Li, Z.; Wang, J. Tourism-oriented urbanization from the perspective of ecosystem services: Research framework and prospect. *Ecol. Environ. Sci.* **2020**, *29*, 2130–2140.
30. Les, D.; Hai, L.; Jing, X.; Feng, Z.; Jun, L. Review of bidirectional effects of urbanization and ecosystem services. *Ecol. Sci.* **2017**, *36*, 233–240.

31. Xia, Z.; Nan, H. Study on classification and applicability of comprehensive evaluation methods. *Stat. Decis.* **2022**, *38*, 31–36.
32. Sharp, R.; Tallis, H.; Ricketts, T.; Guerry, A.; Wood, S.A.; Chaplin-Kramer, R.; Nelson, E.; Ennaanay, D.; Wolny, S.; Olwero, N. *Invest User's Guide*; The Natural Capital Project: Stanford, CA, USA, 2014.
33. Potter, C.; Klooster, S.; Hiatt, C.; Genovese, V.; Castilla-Rubio, J.C. Changes in the carbon cycle of amazon ecosystems during the 2010 drought. *Environ. Res. Lett.* **2011**, *6*, 034024. [CrossRef]
34. Guo, Q.; Rundel, P.W. Self-thinning in early postfire chaparral succession: Mechanisms, implications, and a combined approach. *Ecology* **1998**, *79*, 579–586. [CrossRef]
35. Thomson, J.D.; Weiblen, G.; Thomson, B.A.; Alfaro, S.; Legendre, P. Untangling multiple factors in spatial distributions: Lilies, gophers, and rocks. *Ecology* **1996**, *77*, 1698–1715. [CrossRef]
36. Yu, W. Comparison of different methods for estimating average annual rainfall erosivity. *J. Soil Water Conserv.* **2001**, *15*, 31–34.
37. Williams, J.; Jones, C.; Kiniry, J.; Spanel, D.A. The epic crop growth model. *Trans. ASAE* **1989**, *32*, 497–511. [CrossRef]
38. Lin, M.; Liu, H.; Zhou, R.; Gong, J. Evaluation and trade-offs of ecosystem services in guangdonghong kong-macao greater bay area under multi-scenario simulation. *Geogr. Res.* **2021**, *40*, 2657–2669.
39. Meng, F.; Wen, T.; Wei, L.; Yue, H.; Yan, Z. Ecological risk assessment and spatial identification of ecological restoration from the ecosystem service perspective: A case study in source region of yangtze river. *Acta Ecol. Sin.* **2021**, *41*, 3846–3855.
40. Dan, W.; Chang, Z.; Nai, L.; Meng, X. Tradeoffs and synergies among ecosystem services in the yangtze river economic belt, china. *Environ. Ecol.* **2021**, *3*, 1–7.
41. Anselin, L. Interactive techniques and exploratory spatial data analysis. In *Regional Research Institute Working Papers*; Regional Research Institute: Morgantown, WV, USA, 1996.
42. Medinski, T.; Mills, A.; Esler, K.; Schmiedel, U.; Jürgens, N. Do soil properties constrain species richness? Insights from boundary line analysis across several biomes in south western africa. *J. Arid Environ.* **2010**, *74*, 1052–1060. [CrossRef]
43. Anselin, L. Spatial regression. In *The SAGE Handbook of Spatial Analysis*; Sage: Newcastle upon Tyne, UK, 2009; Volume 1, pp. 255–276.
44. Lichang, Y.; Xiaofeng, W.; Kun, Z.; Feiyan, X.; Changwu, C.; Xinrong, Z. Trade-offs and synergy between ecosystem services in national barrier zone. *Geogr. Res.* **2019**, *38*, 2162–2172.
45. Baker, S.; Eckerberg, K. A policy analysis perspective on ecological restoration. *Ecol. Soc.* **2013**, *18*, 17. [CrossRef]
46. Borgström, S.; Zachrisson, A.; Eckerberg, K. Funding ecological restoration policy in practice—patterns of short-termism and regional biases. *Land Use Policy* **2016**, *52*, 439–453. [CrossRef]

sustainability

MDPI

Article

Assessment of the Urban Expansion and Its Impact on the Eco-Environment—A Case Study of Hefei Municipal Area

Xiamei Yao [1,†], Yuanyuan Chen [1,†], Qingyi Zhang [1], Zhongqiong Mou [2], Xiaojie Yao [1,*] and Chun Ou [3,*]

[1] School of Architecture and Urban Planning, Anhui Jianzhu University, Hefei 230601, China
[2] School of Foreign Languages, Shandong University of Science and Technology, Qingdao 266510, China
[3] School of Biology and Food Engineering, Fuyang Normal University, Fuyang 236037, China
* Correspondence: yaoxj661@sina.cn (X.Y.); ouchun_2007@163.com (C.O.)
† These authors contributed equally to this work.

Abstract: With the advancement of urbanization, the ecological environmental changes caused by the continuous expansion of cities have become a major concern. Thus, this study is based on a remote sensing image map of Hefei city from 1984 to 2020, which is now in the process of rapid development. We constructed an index system with ecological land, ecosystem service value, ecological environment quality, urban land expansion coefficient, urban heat island rate index, total pollutant emissions, ecological pressure, and ecological deficit, and then evaluated the ecological environment of Hefei city with the help of the entropy weight comprehensive evaluation method. The results show that (1) in the positive evaluation index, the ecological land area was reduced to half of the original area, the ecological service value was reduced by 0.37 times its initial value, and the eco-environmental index was <35 and still decreasing. (2) In the negative evaluation index, the urban heat island ratio index increased by nearly 10 times its initial value, the total emission of various pollutants increased by 6.64 times its initial value, the ecological deficit increased year by year after 1999, and the ecological pressure in 2020 increased to 3 times that in 1999. (3) The overall environmental score of the Hefei urban area has decreased by 48.6 times its initial value. The values of positive evaluation indexes are decreasing, whereas the values of negative evaluation indexes are increasing, and both these items are moving backward, leading to the decrease in the comprehensive ecological environmental score. It can be noticed that the urban expansion of Hefei has had a severe impact on the ecological environment, resulting in the continuous reduction in the ecological land area, a serious urban heat island effect, and continuous weakening of regional ecological service functions. The study results can be used for reference in alleviating the impacts of urban expansion on the environment, promoting the optimization of the urban landscape and the sustainable development of the social economy and environment.

Keywords: urban expansion; Hefei municipal area; entropy weight method; eco-environment

check for updates

Citation: Yao, X.; Chen, Y.; Zhang, Q.; Mou, Z.; Yao, X.; Ou, C. Assessment of the Urban Expansion and Its Impact on the Eco-Environment—A Case Study of Hefei Municipal Area. *Sustainability* **2022**, *14*, 10613. https://doi.org/10.3390/su141710613

Academic Editors: Daniela Baldantoni and Alessandro Bellino

Received: 13 July 2022
Accepted: 22 August 2022
Published: 25 August 2022

Publisher's Note: MDPI stays neutral with regard to jurisdictional claims in published maps and institutional affiliations.

Copyright: © 2022 by the authors. Licensee MDPI, Basel, Switzerland. This article is an open access article distributed under the terms and conditions of the Creative Commons Attribution (CC BY) license (https://creativecommons.org/licenses/by/4.0/).

1. Introduction

The continuous expansion of cities and the impact on the ecological environment has become an important element in the study of global environmental changes. Along with the significant spatial expansion of cities and the conversion of land types, the structure, function, and pattern of cities [1,2] change, which can lead to changes in the ecological environment. For example, some studies suggest that the expansion of cities leads to increased pollutant emissions and reduced ecosystem resilience [3,4], which are important factors leading to the poor ecological environment of cities in developing countries such as China, India, and Laos [5–7]. It is estimated that China's urbanization rate will reach 70% in 2035 and 80% in 2050 [8]. By then, as urbanization continues, the impact of urban expansion on the ecological environment will continue, which is a more complex issue for most developing regions regarding how they should face this environmental degradation.

Research on the impact of urban spatial expansion on the ecological environment has received much attention. In previous studies, the evaluation was mainly based on unilateral index evaluation, such as the evaluation and analysis from the perspective of the landscape pattern index [9], land use change [10], and urban surface temperature [11] with the help of 3S technology; however, in reality, the impact of urban expansion on the ecological environment is very complex and strongly variable, and is difficult to evaluate by individual indexes. The international community has some comprehensive ecological evaluation models for the ecological environment, such as the remote sensing-based ecological index (RSEI) [12], eco-environmental effects of urban sprawl (EEUS) [13], and other models. Based on remote sensing and spatial analysis techniques, ecological environment quality evaluation indexes are selected and a comprehensive evaluation method is used to quantitatively evaluate the impact of urban spatial expansion on regional ecological environment changes. Some scholars have also constructed models to evaluate the impact of urban spatial expansion on regional natural geographic and environmental elements and natural disasters and the analysis and evaluation of their resource and energy effects with the help of officially released socioeconomic statistics [14,15]. However, these methods also have certain limitations and cannot highlight the impact of urban spatial expansion on the dynamics of the ecological environment, and these methods also ignore the ecological indicators with large differences in values. The entropy-weighted comprehensive evaluation method is a more widely used comprehensive evaluation method [16,17], and is more objective compared to other comprehensive evaluation methods because it determines the indicator weights based on the changes in the indicators. In addition, current research still focuses on cities that are already relatively developed, while less research has been conducted on rapidly expanding cities. If such urban expansion and environmental changes are evaluated and defined, it can help fast-growing cities such as Hefei, in China and Pushkar in India protect the local environment in their future development, constituting a reference value for future urban planning.

Therefore, taking as an example the Hefei municipal area in China, which has been rapidly urbanized in recent years, and combining eight remote sensing images from 1984 to 2020 and social development data from government statistics, the entropy weight method was used to construct a comprehensive evaluation index system, with ecological land, ecosystem service value, ecological environment quality, urban land expansion coefficient, urban heat island rate index, total pollutant emissions, ecological pressure, and ecological deficit as evaluation indexes. The analysis was conducted to ensure that the possible impacts of urban expansion on the urban environment of Hefei can be comprehensively analyzed in terms of resources, environment, ecosystem service capacity, ecological security, and other aspects. This study provides new evidence for the ecological and environmental changes caused by urban expansion, and provides a theoretical reference for ecological environment protection in developing countries such as China.

2. Materials and Methods

2.1. Study Area

As of 2020, Hefei has a total area of 11,445.1 km^2 and a built-up area of 528.5 km^2. Its total population is 8.189 million, and its urbanization rate is as high as 76.33% [18]. Hefei is located in the middle and lower reaches of the Yangtze River in China and belongs to the Jianghuai region, located northwest of Chaohu Lake, as shown in Figure 1. The Feixi River is around the center of the city, and the land has a subtropical humid monsoon climate [19]. Its economic development, political status, and education popularization occupy a leading position in Anhui Province, China. Hefei is also the main transportation and communication hub in the middle and lower reaches of the Yangtze River. With the growing demand for the economic development of the middle and lower reaches of the Yangtze River and Anhui Province in China in recent years, the urban space of Hefei keeps expanding, leading to some major changes in the urban land structure and certain impacts on the environment. Hefei is a relatively developed city in the middle and lower

reaches of the Yangtze River, and it is also a sub-central city in the region [20], with an important position in the ecological aspect. Hence, the environmental situation of Hefei has an important impact on the environment of the middle and lower reaches of the Yangtze River and even China as a whole. The study of urban expansion and its ecological and environmental benefits is of great significance to regulate the blind expansion of urban construction land and safeguard the regional environment.

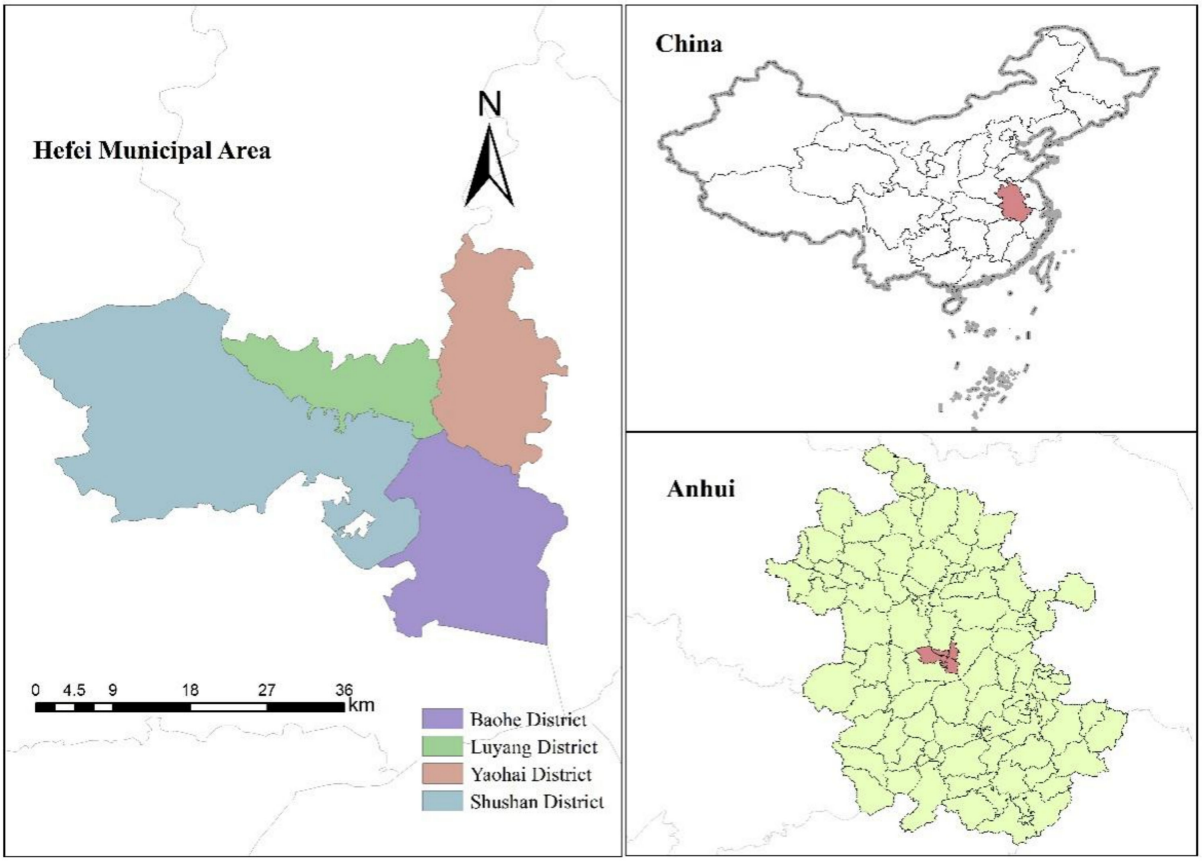


Figure 1. Hefei municipal area location map.

2.2. Data Source and Landscape Information Extraction

This study is based on the fall data of remote sensing images of the Landsat series, including the following years: 1984, 1989, 1994, 1999, 2004, 2009, 2014, and 2020. The remote sensing image data of the first six periods were recorded by Landsat 5, and 2014 and 2020 were recorded by Landsat 8, with resolutions of 30 and 15 m, respectively, meeting the research requirements. The analysis was also conducted with the help of relevant socioeconomic statistics and aided by software such as ArcGIS and ENVI.

According to the current land use classification system [21], the surface landscape types were classified into five categories—construction land, forest land, water area, cultivated land, grassland, and unused land—by combining the actual situation of regional land use and remote sensing image maps. The supervised classification results are shown in Figure 2. Several local high-definition image maps were selected for sampling and verification, and the kappa coefficient and image classification accuracy of the land use classification maps were >80% and 90%, respectively, meeting the classification accuracy requirements of this study.

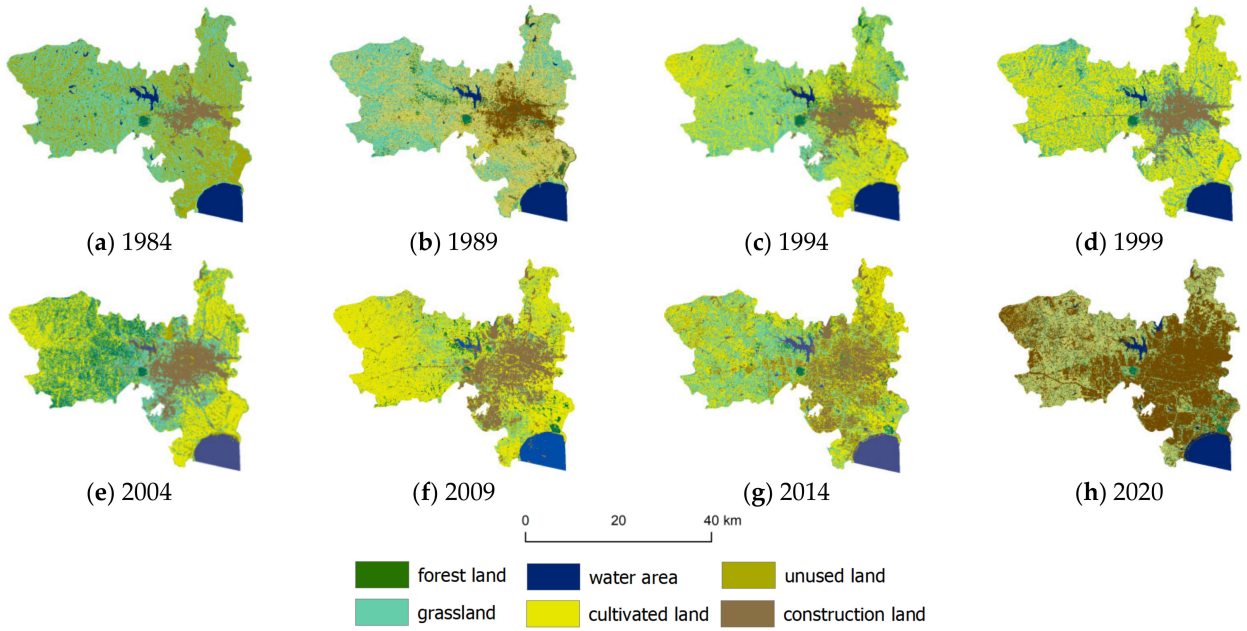


Figure 2. Land-use distribution of Hefei municipal area from 1984 to 2020.

2.3. Comprehensive Evaluation Method Based on Entropy Weight Method

The entropy method is determined according to the degree of variation of the index value, which is an objective empowerment method and avoids the bias caused by human factors [22]. The numerical gap between the various indicators in this study is large, so the entropy weight method was used.

Through the entropy weight method, we selected appropriate indicators and constructed an evaluation index system to comprehensively evaluate the urban ecological benefits of Hefei. The positive indicators of ecological benefits are ecological land area (ELA), ecosystem service value (ESV), and eco-environmental index (EI). The negative indicators include urban land expansion coefficient (K), urban heat island ratio index (URI), total pollutant emission (PE), ecological pressure (EP), and ecological deficit (ED), as shown in Figure 3.

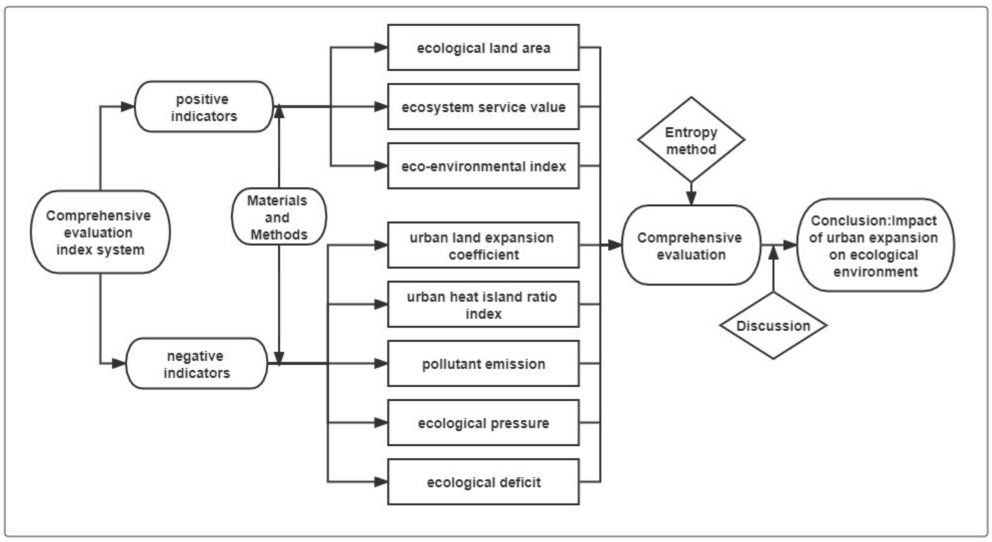


Figure 3. Research design.

The extreme value method was used to conduct dimensionless treatment of the data, and then the weight of each index was obtained through the entropy weight method. Finally, the contribution degree of each index was multiplied by the weight and summed to obtain the comprehensive score. The calculation formula is as follows:

(1) Proportion

$$P_{ij} = \frac{x_{ij}}{\sum_{i=1}^{n} xij} \quad (1)$$

where P_{ij} is the contribution degree, X_{ij} is the dimensionless processed data, i is the year, and j is the index [23].

(2) Information entropy of the system

$$e_j = -\frac{1}{\ln\ n} \sum_{i=1}^{n} P_{ij} \ln(P_{ij}) \quad (2)$$

where e_j is the information entropy of the system.

(3) Weight of each index

$$w_j = \frac{(1 - ej)}{\left(n - \sum_{j=1}^{n} ej\right)} \quad (3)$$

where w_j is weight value of index.

(4) Comprehensive score of the eco-environment.

$$S = \sum_{j=1}^{m} w_j P_{ij} \quad (4)$$

where S is the comprehensive score. According to Equations (1)–(3), the weight vector of m targets can be obtained. The weight values and proportion values of each index are shown in Table 1.

Table 1. Proportion values and weights of each indicator.

Assessment Index	Years	ELA	ESV	EI	K	URI	PE	EP	ED
Indicator effect		+	+	+	-	-	-	-	-
Proportion value (P_{ij})	1999	0.029	0.037	0.028	0.029	0.032	0.045	0.069	0.127
	2004	0.026	0.029	0.028	0.026	0.025	0.043	0.053	0.075
	2009	0.021	0.02	0.019	0.021	0.021	0.04	0.025	0.02
	2014	0.017	0.017	0.019	0.017	0.017	0.001	0.01	0.007
	2020	0.001	0.001	0.001	0.001	0.001	0.008	0.001	0.001
Weight value (w_i)		0.094	0.103	0.093	0.094	0.095	0.136	0.158	0.229

Note: ELA, ecological land area; ESV, ecosystem service value; EI, eco-environmental index; K, urban land expansion coefficient; URI, urban heat island ratio index; PE, total pollutant emission; EP, ecological pressure; ED, ecological deficit.

2.4. Calculation Method of the Positive Indicators

2.4.1. Ecosystem Service Value

Based on the equivalent coefficient table for ESV per unit area of terrestrial ecosystem in China [24,25], combined with the economic value of natural food production of farmland in Hefei, the ecosystem service value coefficients of each landscape type in Hefei were estimated: forest land 851,668/km^2, grassland 282,011/km^2, arable land 269,157/km^2, water area 1,790,617/km^2, and unused land 16,359/km^2. Due to the special nature of construction land, its ecosystem service value is not estimated for the time being. The specific ecosystem service value coefficients are shown in Table 2.

Table 2. Ecosystem service value coefficients of Hefei municipal area from 1984 to 2020 (USD).

	Forest Land	Grassland	Cultivated Land	Water Area	Unused Land
Gas regulation	1362.79	311.50	194.68	0.00	0.00
Climatic regulation	1051.30	350.43	346.54	179.11	0.00
Water conservation	1245.98	311.50	233.62	7935.36	11.68
Soil formation and protection	1518.54	759.27	568.48	3.89	7.79
Waste disposal	510.07	510.07	638.57	7078.74	3.89
Biodiversity protection	1269.35	424.41	276.45	969.53	132.39
Food production	38.94	116.81	389.37	38.94	3.89
Raw and processed material	1012.36	19.47	38.94	3.89	0.00
Entertainment culture	498.39	15.57	3.89	1689.86	3.89
Total	8507.73	2819.04	2690.55	17,899.33	163.53

The value of ecosystem services is calculated as follows:

$$ESV = \sum_{i=1}^{n} (D_i \times S_i) \quad (5)$$

where ESV is the ecosystem service value; i and n are the landscape type and quantity in the region, respectively; Di is the ecosystem value coefficient of the ith landscape type; and S_i is the area occupied by the ith landscape type [26–28].

2.4.2. Eco-Environmental Index

The eco-environmental index model is a standardized model proposed by the Chinese Environmental Protection Department to evaluate the ecological environmental status in China. According to the eco-environmental index model, the ecological environmental quality of Hefei is evaluated based on the ecological environmental status of the region [29]. The calculation formula is as follows:

$$EI = 0.25 \times BI + 0.2 \times VI + 0.2 \times WI + 0.2 \times (100 - LI) + 0.15 \times PI \quad (6)$$

$$\begin{aligned} BI = (&0.35 \times S(\text{forest land}) + 0.21 \times S(\text{grassland}) + 0.28 \times S(\text{water area}) \\ &+0.11 \times S(\text{cultivated land}) + 0.01 \times S(\text{unused land}) \\ &+0.04 \times S(\text{building land}))/S(\text{Hefei}) \end{aligned} \quad (7)$$

$$\begin{aligned} VI = (&0.38 \times S(\text{forest land}) + 0.34 \times S(\text{grassland}) + 0.19 \times S(\text{cultivated land}) \\ &+0.07 \times S(\text{building land}) \\ &+0.02 \times S(\text{unused land}))/S(\text{Hefei}) \end{aligned} \quad (8)$$

$$WI = S(\text{water area})/S(\text{Hefei}) \quad (9)$$

$$\begin{aligned} PI = 0.4 \times (100 - 1.726 \times EM(SO_2)/S(\text{Hefei})) + 0.4 \times (100 - 0.53 \times \\ EM(\text{COD})/P) + 0.2 \times (100 - 2.425 \times EM(\text{solid waste})/S(\text{Hefei})) \end{aligned} \quad (10)$$

$$\begin{aligned} LI = \text{Aero} \times (&0.05 \times S(\text{mild erosion}) + 0.25 \times S(\text{moderate erosion}) \\ &+0.7 \times S(\text{severe erosion}))/S(\text{Hefei}) \end{aligned} \quad (11)$$

EI is the eco-environmental index, BI is the biological abundance index, VI is the vegetation cover index, WI is the water density index, PI is the environmental quality index, LI is the land degradation index, S refers to an area, EM refers to emission, and P refers to annual precipitation.

Aero is the normalization coefficient of the land degradation index, and the degree of soil erosion [30] can be determined according to the soil erosion index table of the Ministry of Water Resources, that is, by overlaying the vegetation coverage map and slope map. According to the current situation of the study area, the fractional vegetation cover percentages are >75, 60–75, 45–60, 30–45, and <30, which are rated as 1, 2, 3, 4, and 5, respectively. The areas with slopes <5°, 5–8°, 8–15°, 15–25°, and >25° are graded as 1, 2, 3, 4, and 5, respectively. Then, the two maps after grading are added, and the obtained value is the basic data of soil erosion degree grading. The values of 2, 3, 4, 5, and 6 are classified

as mild erosion; 7 and 8 are classified as moderate erosion; 9 and 10 are classified as heavy erosion. The soil erosion indicators are shown in Table 3.

Table 3. Table of soil erosion indicators.

FVC (%)	Slope				
	<5°	**5–8°**	**8–15°**	**15–25°**	**>25°**
>75	Mired	Mired	Mired	Mired	Mired
60–75	Mired	Mild	Mild	Mild	Moderate
45–60	Mired	Mild	Mild	Moderate	Moderate
30–45	Mired	Mild	Moderate	Moderate	Heavy
<30	Mired	Moderate	Moderate	Heavy	Extremely heavy

Note: FVC, fractional vegetation cover.

According to the *Technical Specification for Eco-environmental Quality Assessment* [31], the index is divided into the following five grades, as shown in Table 4.

Table 4. Criteria for eco-environmental quality assessment.

Rank	Extremely Bad	Bad	Moderate	Good	Excellent
Index range	EI < 20	20 ≤ EI < 35	35 ≤ EI < 55	55 ≤ EI < 75	EI ≥ 75

2.4.3. Urban Land Expansion Coefficient

The urban land expansion coefficient can be used to determine whether the expansion speed of the construction land within the city is reasonable.

$$K = V/UPR \times 100\% \quad (12)$$

$$V = \Delta A/\Delta t \quad (13)$$

K is the expansion coefficient of urban land, V is the urban expansion rate, and UPR is the average annual growth rate of the urban population. When the value of K is closer to 1.12, the urban land scale expansion tends to be more reasonable; when the value of K is greater than 1.12, the expansion is too fast; and when the value of K is <1.12, the expansion is too slow [32].

2.4.4. Urban Heat Island Ratio Index

The urban heat island ratio index shows the areas of the city that are affected by the heat island effect, which are significantly warmer than the rest of the region and seriously affect the quality of the ecological environment. The steps of urban surface temperature inversion are as follows.

With the help of thermal infrared band data in remote sensing images, the single window algorithm with high accuracy is used in the research [33,34]. At the same time, for Landsat TM and OLI remote sensing image data, the inversion formulas are different:

$$(TM)\ TS = K2/\ln(K1/B(TS) + 1) - 273.15, \quad (14)$$

$$(OLI)\ TS = [a \times (1 - C - D) + (b \times (1 - C - D) + C + D) \times T6\text{-}D \times T6]/C - 273.5. \quad (15)$$

For different types of image data, K1 and K2 values also vary (please refer to the data header file). B (TS) is the thermal infrared radiation brightness value, and a and b values are constants. For the specific case of the Hefei municipal area, a = −67.35535, b = 0.458606 [35], T6 is the satellite brightness temperature of TM6, Ta is the average atmospheric action temperature in the local actual situation, and C and D are the intermediate variables, calculated as follows.

$$T6 = K2/\ln(1 + K1/b1), \quad (16)$$

$$B(TS) = [b1 - lu - \tau \times (1 - \varepsilon) \times ld]/(\tau - \varepsilon), \quad (17)$$

$$C = \tau \times \varepsilon \quad (18)$$

$$D = (1 - \tau) \times [1 + \tau \times (1 - \varepsilon)]. \quad (19)$$

where b1 is the thermal infrared radiation calibration value, ε is the surface-specific radiation rate [36], lu is the radiant intensity of the upward atmosphere, τ is the atmospheric transmission, and ld is the radiant intensity of the downward atmosphere (data source: http://atmcorr.gsfc.nasa.gov/, accessed on 12 March 2021).

ε is closely related to the normalized difference vegetation index (NDVI), which is the normalized vegetation index.

Surface emissivity on the natural surfaces is calculated as follows:

$$\varepsilon = 0.9625 + 0.0614 \times FVC0.0461 \times FVC \times FVC \quad (20)$$

Surface emissivity on the town surface is calculated as follows:

$$\varepsilon = 0.9589 + 0.086 \times FVC{-}0.0671 \times FVC \times FVC \quad (21)$$

$$FVC = (NDVI - NDVI_S) / (NDVI_V - NDVI_S) \quad (22)$$

The FVC indicates the fractional vegetation cover [37]. NDVIv represents the NDVI value when the site is completely covered by vegetation, whereas $NDVI_S$ represents the NDVI value when the site is bare. These two values need to be determined according to the actual situation of different years.

$$URI = \frac{1}{100\ m} \sum_{i=1}^{n} w_i \times p_i \quad (23)$$

where URI is the urban heat island ratio index [38]; m is the normalized grade index, the equal series of temperature classification; i and n are the target temperature grade and grades within the urban heat island, respectively; w_i is the weight value, taking the grade i value; and p_i is the percentage of grade i area.

2.4.5. Ecological Deficit and Ecological Pressure

Ecological deficit and ecological pressure can satisfactorily show the impact of human activity on the ecological environment in cities. The formulas are as follows:

$$EF = \sum_{j=1}^{6} \left(r_j \times \sum_{i=1}^{n} (c_i / p_i) \right) \quad (24)$$

$$EC = \sum_{J=1}^{6} a_j \times r_j \times y_j \quad (25)$$

$$ED = ed \times N = (EF - EC) \times N \quad (26)$$

$$EP = EF/EC \quad (27)$$

where EF is the per-capita ecological footprint, j is an ecologically productive land type, i is the type of goods and inputs consumed, r_j is the equilibrium factor, c_i, p_i are the per-capita consumption of the ith consumer goods and its global average productivity, EC is the per-capita ecological carrying capacity, a_j is the per-capita ecological productive land area, y_j is the yield factor, the values of r_j and y_j refer to previous research results, ed is ecological deficit or profit, ED stands for the total ecological deficit, and EP is the ecological pressure [39,40].

ED is an important indicator to measure the level of the ecological carrying capacity of a region [35]. If ED > 0, it is an ecological deficit, indicating that the ecological trace of

the region exceeds its ecological carrying capacity and the regional ecosystem is unsafe. If ED < 0, it is ecological profit and loss, which indicates that the ecological carrying capacity of the region exceeds the ecological footprint, and the regional ecosystem is relatively safe.

EP is an important index to observe regional ecological risk, which can quantitatively reveal the differences in regional ecological risk in time and space. The ecological risk is divided into the following five levels according to the range of T value: if the value is >1, the ecological risk is extremely high; 0.8–1.0, high risk; 0.6–0.8, medium risk; 0.4–0.6, low risk; <0.4, extremely low risk [41,42].

3. Results

3.1. Analysis of Positive Indicators of Eco-Efficiency

3.1.1. Ecological Land

Ecological land refers to the land type with an ecological service function. According to the specific situation of the study area and the existing classification methods of ecological land in China, the types of ecological land in the study area can be divided into forest land, cultivated land, water area, grassland, and unused land [43]. As shown in Figure 4, the ecological land within the jurisdiction of Hefei has decreased significantly from 1194 to 602 km^2, of which grassland and cultivated land decreased the most by 318.71 and 258.42 km^2, respectively. During this period, the area of construction land increased sharply until it exceeded the area of ecological land. In the past 36 years, a total of 592 km^2 of ecological land was transformed into construction land. As shown in Figure 3, most of the construction land was originally cultivated land and grassland. The aforementioned situation made the ecological service function of the land in the urban area of Hefei decline sharply and the ecological regulation function weaken, which will inevitably threaten the urban environment and ecological security.

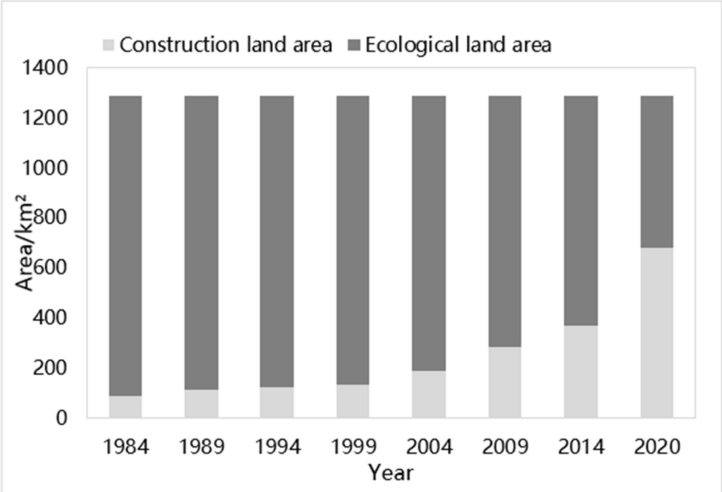


Figure 4. Area change in the construction land and ecological land in Hefei municipal area.

3.1.2. Ecosystem Service Value

As shown in Table 5, the value of ecosystem services in the Hefei municipal area fluctuated and decreased with time. During the study period, the value of ecosystem services decreased from USD 487.75 million to USD 309.42 million, with an average annual decrease of USD 4.95 million. At the same time, the service value of each landscape type also changes to some extent. Among them, the ecosystem service value of grassland decreased the most, by USD 59.73 million, and the proportion decreased from 25.4% to 6.98%, which indicates that the supply position of grassland ecosystem service value in the whole ecosystem is gradually declining. In addition, although the service value of forest land and water area is barely decreasing or changing, the proportion is increasing, from

7.24% and 34.26% to 11.85% and 47.30%, respectively, indicating that the supply position is improving and gradually tends to be dominant.

Table 5. Ecosystem services value (million USD).

	Grassland	Cultivated Land	Unutilized Land	Waters Area	Forest Land	Total
1984	123.81	161.19	0.36	167.11	35.32	487.75
1989	106.93	161.56	0.81	144.71	42.05	456.11
1994	109.77	153.90	0.93	151.43	48.40	464.41
1999	95.43	165.44	0.93	135.60	48.01	445.45
2004	85.13	147.16	0.82	138.14	43.01	414.14
2009	98.27	112.63	0.72	133.21	37.56	382.42
2014	81.84	93.73	0.70	159.35	36.65	372.19
2020	34.05	91.65	0.70	146.36	36.69	309.42

By observing the landscape distribution map, it can be noticed that the aforementioned changes are mainly caused by the following: ① in the process of urban expansion, a large number of cultivated land and grassland are occupied, resulting in the decline in the service value of cultivated land and grassland. ② The service value of forest land increased first and then decreased because the newly built Hefei Binhu National Forest Park and other wetland parks increased the area of forest land and then decreased the service value because of the continuous expansion of the city. ③ The supply of water service value increases and tends to dominate, mainly because the water area covers a large area in the jurisdiction of Hefei, and the area change is small during the study period. Therefore, when the overall ecological service value decreases, the proportion of water service value can rise.

3.1.3. Eco-Environmental Index

It can be observed from Table 6 that in the past 36 years, the biological abundance index and vegetation coverage index in the region have shown decreasing trends. The main reason is that the rapid expansion of construction land has occupied the grassland, forest land, and cultivated land that contribute greatly to the biological abundance and vegetation coverage, resulting in the reduction in the two indexes by 0.38 and 0.41 times their initial values; the rest of the indexes barely changed. The aforementioned index changes resulted in the continuous reduction in the eco-environmental index. As shown in Table 4, the Hefei municipal area is always at the bad level, which is not the best ecological quality for human habitation, mainly because the urban expansion occupies the land, resulting in the reduction in green space and land degradation, while the increase in population and the need for economic development lead to an increase in the emission of various pollutants.

Table 6. EI in Hefei municipal area from 1984 to 2020.

YEAR	BI	VI	WI	LI	PI	EI
1984	0.16	0.22	0.07	92.68	—	—
1989	0.15	0.21	0.06	92.68	—	—
1994	0.15	0.21	0.07	92.68	—	—
1999	0.14	0.21	0.06	92.68	99.99	33.62
2004	0.13	0.19	0.06	92.68	99.99	33.62
2009	0.13	0.18	0.06	92.68	99.98	33.61
2014	0.12	0.16	0.07	92.68	99.96	33.61
2020	0.10	0.13	0.06	92.68	99.95	33.59

3.2. Analysis of Negative Indicators of Eco-Efficiency

3.2.1. Urban Land Expansion Coefficient

According to Figure 5, it can be clearly seen that the expansion rate of urban space in Hefei city shows obvious phase characteristics, first slowly decreasing, then dramatically increasing, then having a slight decrease and finally a sudden increase, in chronological order: In the low-speed expansion phase from 1984 to 1989, the expansion rate was 5 km^2/a;

in the slow expansion phase from 1989 to 1999, the average expansion rate and expansion intensity index were 1.9 km^2/a; in the rapid expansion period from 1999 to 2014, the average expansion rate of urban construction land was 18.1 km^2/a; in the period from 2014 to 2020, the expansion reached 51.8 km^2/a. The phase characteristics of the expansion coefficient and the expansion rate are relatively similar, and before 1994 are much smaller than the critical value of 1.12, indicating that the expansion of the Hefei city area is slow. Between 1994 and 1999, the expansion coefficient value is close to 1.12, which is more reasonable, after which the expansion rate accelerates, far exceeding 1.12, indicating that the expansion is too fast and unreasonable. In general, from 1984 to 2020, the construction land area of Hefei city expanded dramatically, from 90 km^2 to 681 km^2, which is 7.58 times that of the original area, with an average annual expansion rate of 16.42 km^2/a and an expansion coefficient of 2.83, which are too fast and unreasonable.

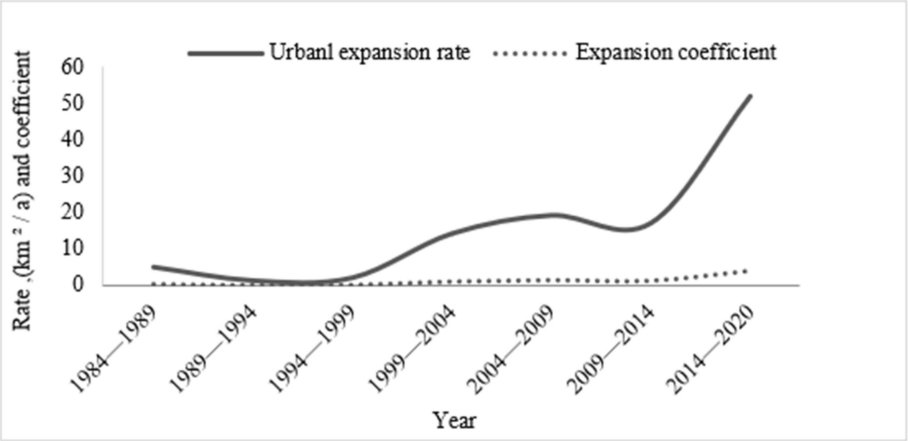


Figure 5. Characteristic values of construction land expansion.

Exploration has revealed that after Hefei broke through the 2005 master plan index, the preparation of the *Hefei City Master Plan (2006–2020)* [44] was completed, and in the subsequent period, according to the new master plan requirements, the Hefei city urban area has entered a state of rapid expansion.

3.2.2. Urban Heat Island Ratio Index

According to the actual situation of the surface temperature in the study scope, the surface temperature is divided into seven grades by the natural breakpoint method, as shown in Table 7.

Table 7. Land surface temperature area statistics and URI (km^2).

Year		Lowest	Low	Medium Low	Medium	Medium High	High	Highest	URI
1984	Area (km^2)	0.07	125.8	433.89	485.46	223.79	45.7	0.01	0.03
	PREC (%)	0.01	12.91	33.77	32.34	17.42	3.56	0.01	
1989	Area (km^2)	3.43	168.13	417.93	377.95	241.64	69.72	5.91	0.05
	PREC (%)	0.27	11.53	32.53	30.98	18.81	5.43	0.46	
1994	Area (km^2)	2.32	140.87	376.89	395.30	267.74	83.22	18.62	0.07
	PREC (%)	0.18	10.97	29.34	30.77	20.84	6.48	1.45	
1999	Area (km^2)	0.10	125.79	351.13	385.54	282.14	95.89	44.12	0.1
	PREC (%)	0.01	9.79	27.33	30.01	21.96	7.46	3.43	
2004	Area (km^2)	2.96	186.05	352.06	335.50	195.18	172.14	40.81	0.15
	PREC (%)	0.23	14.48	27.40	26.11	15.19	13.40	3.18	
2009	Area (km^2)	7.22	121.05	228.63	352.71	325.06	178.30	71.70	0.17
	PREC (%)	0.56	9.42	17.80	27.45	25.30	13.88	5.58	
2014	Area (km^2)	1.19	116.16	221.59	346.55	305.36	236.08	57.37	0.2
	PREC (%)	0.09	9.04	17.25	26.97	23.77	18.38	4.47	
2020	Area (km^2)	4.12	89.87	184.90	228.25	304.12	405.25	67.82	0.32
	PREC (%)	0.32	7.00	14.39	17.77	23.67	31.54	5.28	

Note: URI, urban heat island ratio index.

The area of surface temperature and the proportion are calculated through the inversion data. The high-temperature area and highest-temperature area represent the range of the urban heat island, which is substituted into the formula to calculate the proportion index of the heat island, as shown in Table 6.

During the study period, the high-temperature area and highest-temperature area in the study area increased by 9 times their initial values, and the URI increased from 0.03 to 0.32, which is a 10-fold increase. The urban heat island effect was severe, and the regulation of surface temperature was out of balance.

According to Figure 6, comparing the landscape pattern map and surface temperature in the same year, it can be seen that different temperature zones and different landscape land types, such as the high-temperature zone and highest-temperature zone, are mainly distributed in the built-up area of Hefei. Moreover, the temperature difference in the suburban area is large, where the highest-temperature zone is mainly distributed in the Shushan Economic Development Zone, the Baohe Industrial Zone, etc., which have a large proportion of construction land and little green land and water. The lowest-temperature zone and low-temperature zone are mainly distributed in waters and woodlands, such as the area surrounding Chaohu Lake, Dashu Mountain, and cultivated land in suburban areas. In addition, it can also be found that the diffusion of construction land and surface temperature in Hefei has a certain consistency from the central city surrounded by the Inter River to the four sides, mainly to the southwest and southeast, and the city center shifts to the south, so it can be inferred that the urban heat island effect is positively related to the extent of urban construction land.

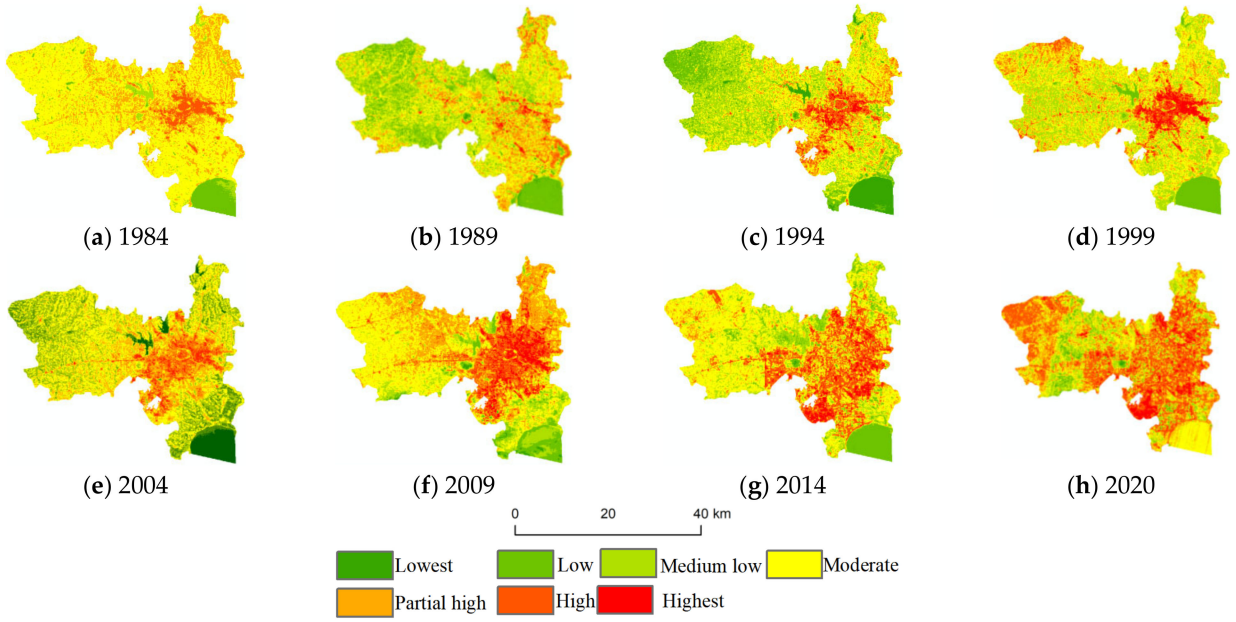
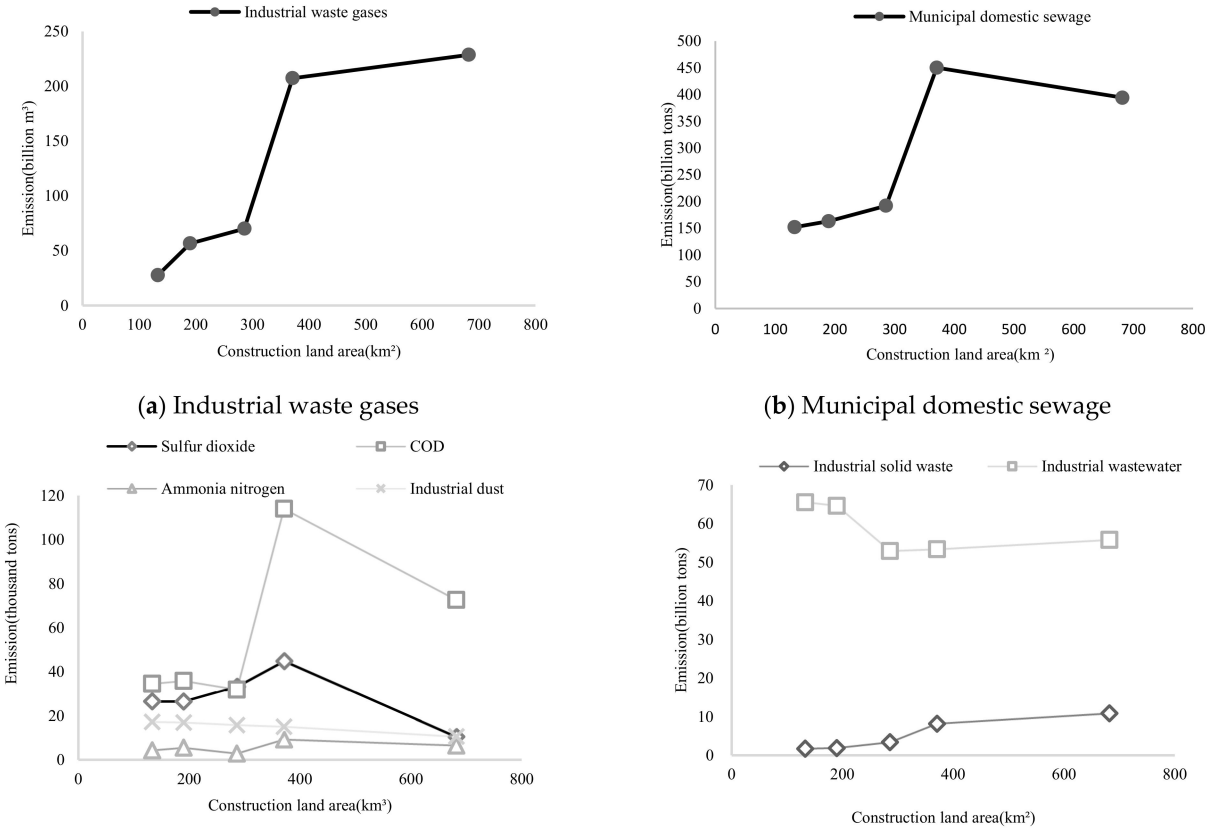


Figure 6. Spatial distribution of land surface temperature.

3.2.3. Urban Pollutant Discharge

The discharge of urban pollutants can more clearly reflect the impact of human activities and urban development on the ecological environment. To examine the relationship between urban expansion and ecological environmental changes, we used the area of construction land as the independent variable and the emission of pollutants as the dependent variable. During the period from 1999 to 2020, the emissions of urban pollutants showed a phase escalation with the continuous expansion of construction land. As shown in Figure 7, the emissions of ammonia nitrogen and industrial soot dust remained unchanged, but the emissions of urban domestic sewage increased to 2.77 times the original amount, and the emissions of industrial waste gas increased by 4 times the original amount. In addition, the

emissions of sulfur dioxide show a decline, decreasing by 1.5 times the original amount. Meanwhile, according to the figure, the emission of pollutants has certain stages, and the stages of different pollutants have a high degree of similarity. For example, industrial solid emissions before the area reached 371 km^2 increased rapidly with the increase in land area, reaching 29,300 tons/km^2, after which the speed slowed down to 0.86 million tons/km, and the emissions of urban domestic sewage and industrial waste gas were highly similar. The reason is because Hefei proposed the Hefei City Air Pollution Prevention and Control Act Plan in late 2013 and established the Hefei Environmental Protection Committee in 2014 to study and develop major environmental protection measures and review the ecological master plan situation within the city. These policies or measures have aided in curtailing pollutant emissions in the area surrounding the city of Hefei after 14 years.



(**a**) Industrial waste gases

(**b**) Municipal domestic sewage

(**c**) SO_2, COD, NH_3-N, industrial dust

(**d**) Industrial solid waste, industrial wastewater

Figure 7. Change in urban construction land and amount of various pollutant discharges.

3.2.4. Ecological Pressure and Ecological Deficit

In Table 8, it can be observed that during the period from 1999 to 2020, the per-capita ecological footprint of the region increased by a total of 0.66 times its initial value, whereas the per-capita ecological carrying capacity decreased by half. The contradictory changes in these two indicators led to the rising per-capita ecological deficit and ecological stress index, which increased by 0.68 and 3 times their initial values, respectively. According to the evaluation criteria of ecological deficit and ecological stress index, during the study period, the ecological deficit was always greater than 0 and increased year by year, indicating the dangerous ecological situation of the Hefei municipal district. As the per-capita ecological stress index is much greater than 2, the ecological stress is too high, and the Hefei municipal district is at extremely high ecological risk. Because of the increasing population in the region, the total ecological footprint and ecological carrying capacity of the Hefei area have increased to 3.5 and 1.2 times their initial values, respectively, and the ecological deficit

has increased from 1,854,513.1 to 7,108,753.3. The ecological risks of this region are also gradually increasing.

Table 8. EF, EC, ed, and EP in Hefei municipal area.

Years	1999	2004	2004	2014	2020
EF	1.587	1.976	2.380	2.465	2.515
EC	0.137	0.115	0.088	0.077	0.070
ed	1.450	1.861	2.292	2.388	2.444
EP	11.576	17.190	26.970	32.179	35.685

Note: EF, per-capita ecological footprint; EC, per-capita ecological carrying capacity; ed, ecological deficit or profit; EP, ecological pressure.

3.3. Comprehensive Evaluation Results

The evaluation system was constructed with the aforementioned indicators, the weight and proportion values of each indicator were obtained and calculated (29), and the comprehensive score for each year was calculated. The final results are shown in Table 9.

Table 9. The comprehensive scores.

Years	Comprehensive Scores (S)
1999	0.397
2004	0.305
2009	0.187
2014	0.104
2020	0.008

The comprehensive score of Hefei's environment decreased from 0.397 to 0.008, a decrease of 48.6-fold, which indicates the continuous decline in Hefei's environmental quality, and this decline is the largest from 2014 to 2020.

4. Discussion

4.1. Selection of Evaluation Index

In the study of urban expansion, many scholars are studying the structure of cities, such as Yu et al. (2022), who proposed a framework of an assessment process of polycentric structure based on spatial distribution and interaction [45], but did not propose how the development and change in urban structure caused changes in the local ecological environment. Camille et al. (2020) started to study the changes in the ecological environment with the change in urban structure [46], and found that the type of urban structure influences the environmental conditions of cities, especially the irrational expansion of cities, which may seriously lead to the deterioration of the urban ecological environment [47,48].

Therefore, we explored the changes in the ecological environment from the perspective of urban surface land-use type. To avoid the singularity of the experiment, the selection of indicators takes into account many aspects related to the urban environment, such as urban pollutant emissions, population, resource output, and urban surface temperature. In the study of positive indicators, not only land-use changes are taken into account, but also pollutant emissions, regional slope, regional consumption capacity, population, etc. For example, the urban expansion coefficient was chosen to determine the urban expansion by combining urban population and urban construction land, and the ecosystem service value coefficient was calculated by using the 2020 food prices and land types. The constructed evaluation system provides a reference basis for macroeconomic control of the urban environment and urban planning and makes the evaluation results more comprehensive and fairer.

4.2. Impact of Urban Expansion on the Ecological Environment

The study of the impact of urban expansion on the ecological environment highlights the impact of human development on the ecological environment. The continuous expansion of cities leads to the deteriorating condition of the urban environment year by year. During the study period, 592 km^2 of ecological land was converted into construction land, the total value of regional ecosystem services decreased from USD 487.75 million to 309.42 million, and the eco-environmental index also kept decreasing, which shows that the situation of construction land encroaching on ecological land is critical, especially the decrease in grassland and arable land with high ecological functions [49], which make up the regional biodiversity. This is similar to the findings of Yang and Rotich et al., that urban expansion leads to a reduction in biodiversity and vegetation cover in the region, ultimately leading to a reduction in the supply of urban ecosystem services and a deterioration in the quality of the ecological environment [50].

At the same time, the increase in population, the decrease in ecological land, and the acceleration of urbanization have led to a 6.64-fold increase in total urban pollutant emissions, a 10-fold increase in the heat island ratio index, and an increase in ecological pressure and ecological deficit per capita to 35.685 and 2.444, respectively, in Hefei. The industrial wastewater, urban domestic sewage, industrial waste gas, and industrial solid waste emissions in the city increased 0.1, 1.77, 4, and 8 times their initial values, respectively, showing a positive correlation with the expansion of the construction land area, indicating that the expansion of the city and the increase in industrial land led to the intensification of environmental pollution. The comparison of the spatial distribution of surface temperature and the landscape classification map revealed the spread of construction land and the high-temperature zone. The spread shows a high similarity. The area of the construction site is too large for fertilization, and Dimitra, Mizbah, and other scholars mentioned that the main constituents in the construction land, such as concrete, asphalt, and other impermeable materials, absorb heat quickly and have a small specific heat capacity, and warm up faster than the natural sub-base [51,52]. Moreover, the green space system within the urban area is underdeveloped, and the distribution of green space is scattered within the jurisdiction of Hefei and cannot be systematically linked, making it difficult to mitigate the urban heat island effect. At the same time, the increasing ecological pressure and ecological deficit indicate that with the economic development and urbanization process, the human impact on the ecological environment is expanding, and the ecological carrying capacity is broken but decreasing. This results in the difficulty in regulating the impact caused by humans on the environment, giving rise to ecological security problems, excessive ecological pressure, and extremely high and rising ecological risk.

4.3. Importance of Hefei's Development

The city of Hefei has urbanized at a fast pace and has been able to continuously absorb the population of the surrounding areas, making the urban population grow significantly, which has now exceeded 70% [53], as shown in Figure 8. This is still far from developed cities. Using the data of developed countries instead of the standard of developed cities, as of 2020, the data of GDP per capita, urbanization rate, and Engel coefficient of developed countries are >USD 46,350, >80%, and <30%, respectively, while those of Hefei are USD 18,784, 76.33%, and 33.8%.

The rapid urbanization of Hefei is related to its special position, as Hefei is located in the middle of China. The rise of central China is crucial to China, and Anhui Province needs a city as its representative, so the development of Hefei is fundamental to China's development. For a provincial capital in an area such as Anhui Province, which does not have too many characteristics, the only way to create a "star city" is to implement a strong provincial capital strategy. This is the right choice for the capital of Anhui Province. Only through the implementation of the strategy of strengthening the provincial capital and creating a star city can the development of the prefecture-level cities in Anhui Province be stimulated. By studying the ecological impact of Hefei's urban expansion and how to

preserve the environment in the process of urbanization, we can guide other areas in the Yangtze River Delta region and even the rapidly expanding cities in the world [54].

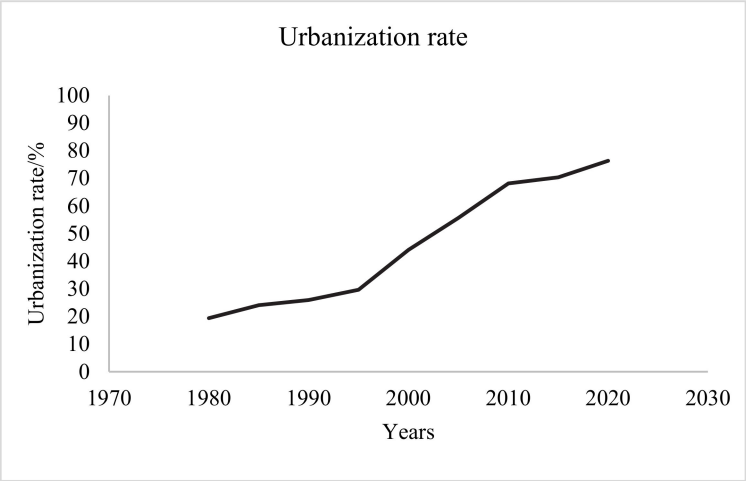


Figure 8. Hefei urbanization rate progress.

4.4. Limiting Factors

This study has some limitations. Firstly, we examined a long period of time, and we can clearly see the evolution of urbanized Hefei, but this also leads to the low resolution of the obtained Landsat series remote sensing images, which has some influence on the land classification and surface temperature inversion. The second limitation is that some indicators that can adequately evaluate the state of the urban ecological environment are not available or cannot be described quantitatively due to some missing data, such as the carbon sequestration and humidification capacity of vegetation in the whole city, thus leading to some limitations of the study. Finally, this study only considered the rate of urban expansion, while the urban structure in the process of urban expansion was not included in the evaluation system because it could not be quantitatively described. However, the impact of urban structure on the ecological environment is not small, and it can be realized by regulating the distribution and size of various types of land. Future research would benefit from a comprehensive evaluation of the ecological environment of Hefei, China, for more in-depth studies, including the use of higher-resolution remote sensing imagery, and the use of more accessible indicators. We hope that in the future, there will be ways to quantify the urban structure and use it in research.

5. Conclusions and Outlook

In this study, we constructed an evaluation index system from ecological land area, ecosystem service value, eco-environmental index, urban land expansion coefficient, urban heat island proportion index, total pollutant emissions, ecological pressure, and ecological deficit and comprehensively evaluated the impact of urbanization expansion on the ecological environment with the help of the entropy weight method. The results show that the ecological land area in the positive indicators decreases from 1194 to 602 km^2, the value of ecosystem services decreases from USD 487.75 million to 309.42 million, and the eco-environmental index decreases by 0.03. In the negative indicators, the urban expansion coefficient increases to nearly 10 times its initial value. The heat island ratio index also increases from 0.03 to 0.32, the pollutant emission increases by 6.64 times its initial value, and the ecological pressure and ecological deficit increase to 3.1 and 3.85 times their initial values, respectively. The decrease in positive indicators and the increase in negative indicators in the evaluation system finally lead to the decrease in the overall ecological environmental score of Hefei from 0.397 to 0.008.

As a subcenter city of the Yangtze River Delta urban agglomeration in China, Hefei city has been developing rapidly in recent years. This study can provide a quantitative basis

for optimizing the existing urban construction pattern and future sustainable development construction, improving the ecological environment of urban green space, and effectively improving the quality of people's living environment.

Author Contributions: Conceptualization, X.Y. (Xiaojie Yao) and C.O.; methodology, X.Y. (Xiamei Yao) and Y.C.; software, Y.C.; validation, Y.C.; formal analysis, Q.Z.; investigation, X.Y. (Xiamei Yao); data curation, X.Y. (Xiamei Yao); writing—original draft preparation, Y.C. and X.Y. (Xiamei Yao); writing—review and editing, C.O.; visualization, Z.M.; supervision, X.Y. (Xiaojie Yao). All authors have read and agreed to the published version of the manuscript.

Funding: This work was financially supported by the Key Project of Natural Science Research of Anhui Provincial education department (KJ2020A0519, KJ2020A0456), the Doctoral Research Foundation of Anhui Jianzhu University (2020QDZ15), the Social Science Innovation and Development Research Project in Anhui Province (2021CX182), the Youth Fund Project of Humanities and Social Sciences Research of Ministry of Education (18YJC760117), the Excellent Youth Talent Support Program of Universities in Anhui Province (gxyq2021197), and the peak discipline cultivation project of Anhui Province (2021-138, 2021-136).

Institutional Review Board Statement: Not applicable.

Informed Consent Statement: Not applicable.

Data Availability Statement: Not applicable.

Conflicts of Interest: The authors declare that they have no known competing financial interests or personal relationships that could have appeared to influence the work reported in this paper.

References

1. Muhamad Nor, A.N.; Abdul Aziz, H.; Nawawi, S.A.; Muhammad Jamil, R.; Abas, M.A.; Hambali, K.A.; Yusoff, A.H.; Ibrahim, N.; Rafaai, N.H.; Corstanje, R.; et al. Evolution of Green Space under Rapid Urban Expansion in Southeast Asian Cities. *Sustainability* **2021**, *13*, 12024. [CrossRef]
2. Ying, X.; Yun, C.; Fen, P.; Jingzhi, L.; Xiaojing, Y. Analog simulation of urban construction land supply and demand in Chang-Zhu-Tan Urban Agglomeration based on land intensive use. *J. Geogr. Sci.* **2019**, *29*, 1346–1362.
3. Zhang, H. The Impact of Urban Sprawl on Environmental Pollution: Empirical Analysis from Large and Medium-Sized Cities of China. *Int. J. Environ. Res. Public Health* **2021**, *18*, 8650. [CrossRef] [PubMed]
4. Yang, D.Y.; Ye, C.; Xu, J. Land-Use Change and Health Risks in the Process of Urbanization: A Spatiotemporal Interpretation of a Typical Case in Changzhou, China. *Land* **2021**, *10*, 820. [CrossRef]
5. Jun, W.; Lichun, S.; Xiaomei, Y.; Zhihua, W.; Dazhuan, G.; Junmei, K.; Fengshuo, Y.; Yueming, L.; Bin, L. Economic Globali-zation Impacts on the Ecological Environment of Inland Developing Countries: A Case Study of Laos from the Perspective of the Land Use/Cover Change. *Sustainability* **2019**, *11*, 3940.
6. De Jong, M. From Eco-Civilization to City Branding: A Neo-Marxist Perspective of Sustainable Urbanization in China. *Sustainability* **2019**, *11*, 5608. [CrossRef]
7. Priyanka, M.; Naresh, K. Impact of Urban Sprawl on the Environment of Rohtak City. *Appl. Ecol. Environ. Sci.* **2021**, *9*, 336–339.
8. Qiao, W.Y.; Li, Y.; Guan, W.H.; Wang, X.; Wang, X. Forecast of China's urbanization level in 2016–2050. *Econ. Geogr.* **2018**, *38*, 51–58.
9. Zubair, O.A. Investigating Urban Growth and the Dynamics of Urban Land Cover Change Using Remote Sensing Data and Landscape Metrics. *Pap. Appl. Geogr.* **2021**, *7*, 67–81. [CrossRef]
10. Kim, J.-H.; Kwon, O.-S.; Ra, J.-H. Urban Type Classification and Characteristic Analysis through Time-Series Environmental Changes for Land Use Management for 31 Satellite Cities around Seoul, South Korea. *Land* **2021**, *10*, 799. [CrossRef]
11. Ronald, C.E.; Yuji, M.; Soe, W.M. Effects of landscape composition and pattern on land surface temperature: An urban heat island study in the megacities of Southeast Asia. *Sci. Total Environ.* **2017**, *577*, 349–359.
12. Hanqiu, X.; Yifan, W.; Huade, G.; Tingting, S.; Xisheng, H. Detecting Ecological Changes with a Remote Sensing Based Ecological Index (RSEI) Produced Time Series and Change Vector Analysis. *Remote Sens.* **2019**, *11*, 2345.
13. Danling, C.; Xinhai, L.; Xu, L.; Xue, W. Measurement of the eco-environmental effects of urban sprawl: Theoretical mechanism and spatiotemporal differentiation. *Ecol. Indic.* **2019**, *105*, 6–15.
14. Li, H.W.; Xu, E.; Zhang, H. Examining the coupling relationship between urbanization and natural disasters: A case study of the Pearl River Delta, China. *Int. J. Disaster Risk Reduct.* **2021**, *55*, 102057. [CrossRef]
15. Kassouri, Y. Monitoring the spatial spillover effects of urbanization on water, built-up land and ecological footprints in sub-Saharan Africa. *J. Environ. Manag.* **2021**, *300*, 113690. [CrossRef]
16. Cunha, Z.G.; Guidolini, J.F.; Branco, E.A.; Ometto, J.P. How sustainable is the nitrogen management in Brazil? A sustainability assessment using the Entropy Weight Method. *J. Environ. Manag.* **2022**, *316*, 115330. [CrossRef]

17. Xianqi, Z.; Chenbo, W.; Enkuan, L.; Cundong, X. Assessment Model of Eco environmental Vulnerability Based on Improved Entropy Weight Method. *Sci. World J.* **2014**, *2014*, 797814.
18. Hefei Bureau of statistics. *Hefei Statistical Yearbook*; Anhui people's Statistics Press: Hefei, China, 1984–2020.
19. Wu, J. Physical and geographical conditions and urban construction of Hefei. *Res. Urban Constr. Arch.* **1999**, *4*, 12–13.
20. Zhu, D.; Sun, J.; Lu, L. Study on spatial correlation and temporal and spatial evolution of Hefei Economic Circle. *Geoscience* **2017**, *37*, 738–747.
21. *GB/T 21010-2017*; Classification of Land Use Status. Department of Cadastral Management, China Standards Press: Beijing, China, 2007.
22. Gzyl, H.; Mayoral, S.; Gomes-Gonçalves, E. *Loss Data Analysis: The Maximum Entropy Approach*; De Gruyter: Berlin, Germany, 2018.
23. Yancang, L.; Lei, Z.; Juanjuan, S. Comprehensive Assessment on Sustainable Development of Highway Transportation Ca-pacity Based on Entropy Weight and TOPSIS. *Sustainability* **2014**, *6*, 4685–4693.
24. Wei, X.; Zhao, L.; Cheng, P.; Xie, M.; Wang, H. Spatial-Temporal Dynamic Evaluation of Ecosystem Service Value and Its Driving Mechanisms in China. *Land* **2022**, *11*, 1000. [CrossRef]
25. Minglei, R.; Yingfei, L.; Xiaodi, F.; Liuqian, D.; Gang, W.; Guangyuan, K.; Liping, Z.; YaFeng, Z. The changeable degree assessment of designed flood protection condition for designed unit of inter-basin water transfer project based on the entropy weight method and fuzzy comprehensive evaluation model. *IOP Conf. Ser. Earth Environ. Sci.* **2021**, *826*, 012029. [CrossRef]
26. Peng, H.; Hua, L.; Zhang, X.; Yuan, X.Y.; Li, J.H. Evaluation of ESV Change under Urban Expansion Based on Ecological Sensi-tivity: A Case Study of Three Gorges Reservoir Area in China. *Sustainability* **2021**, *13*, 8490. [CrossRef]
27. Xie, G.D.; Zhen, L.; Lu, C.; Xiao, Y.; Chen, C. A valuation method of ecosystem services based on expert knowledge. *J. Nat. Resour.* **2008**, *5*, 911–919.
28. Binod, B.; Qiuhong, T.; Yadu, P.; Ximeng, X. Vegetation dynamics and ecosystem service values changes at national and provincial scales in Nepal from 1999 to 2017. *Environ. Dev.* **2019**, *32*, 100464.
29. Yao, Y.; Wang, S.; Zhou, Y.; Liu, R.; Han, X. The Application of Ecological Environment Index Model on the National Evaluation of Ecological Environment Quality. *Remote Sens. Inf.* **2012**, *27*, 93–98.
30. Lei, S.; Lin, Z.; Li, G.; Yao, H. Evaluation of Regional Ecological Environment Based on Landsat7 ETM+. *Remote Sens. Data Beijing Surv. Mapp.* **2014**, *3*, 69–72.
31. Ministry of Environmental Protection. *Technical Specification for Ecological Environment Assessment (Trial) (HJ/t192-2006)*; China Environmental Science Press: Beijing, China, 2006.
32. Li, Z.; Kuang, W.; Zhang, S. Remote Sensing Monitoring and Spatiotemporal Pattern of Land Use/Cover Change in Built-up Area of Tianjin in the Past 70 Years. *Remote Sens. Technol. Appl.* **2020**, *35*, 527–536.
33. Tasya, B.; Rokhmatuloh, A.W. Comparison Spatial Pattern of Land Surface Temperature with Mono Window Algorithm and Split Window Algorithm: A Case Study in South Tangerang, Indonesia. *IOP Conf. Ser. Earth Environ. Sci.* **2018**, *149*, 012066–012076.
34. Qingyu, X.; Xiong, X.; Huan, X.; Xiaochun, Z.; Yuting, H. A New Strategy for Comparison of Land Surface Temperature Re-trieval Methods with Landsat Remote Sensing Images Considering Regional Consistency. *IOP Conf. Ser. Earth Environ. Sci.* **2021**, *687*, 012166. [CrossRef]
35. Jiang, Y.; Lin, W. A Comparative Analysis of Retrieval Algorithms of Land Surface Temperature from Landsat-8 Data: A Case Study of Shanghai, China. *Int. J. Environ. Res. Public Health* **2021**, *18*, 5659. [CrossRef] [PubMed]
36. Fei, W.; Zhihao, Q.; Caiying, S.; Lili, T.; Arnon, K.; Shuhe, Z. An Improved Mono-Window Algorithm for Land Surface Temperature Retrieval from Landsat 8 Thermal Infrared Sensor Data. *Remote Sens.* **2015**, *7*, 4268–4289.
37. Mu, X.; Zhao, T.; Ruan, G.; Song, J.L.; Wang, J.D.; Yan, G.J.; Mcvicar, T.R.; Yan, K.; Gao Zhan, L.; Yao, K.; et al. High Spatial Resolution and High Temporal Frequency (30-m/15-day) Fractional Vegetation Cover Estimation over China Using Multiple Remote Sensing Datasets: Method Development and Validation. *J. Meteorol. Res.* **2021**, *35*, 128–147. [CrossRef]
38. Han-qiu, X.; Ben-qing, C. Remote sensing of the urban heat island and its changes in Xiamen City of SE China. *J. Environ. Sci.* **2003**, *16*, 276–281.
39. Lingna, L.; Yalin, L. Dynamic changes of the ecological footprint in the Beijing-Tianjin-Hebei region from 1996 to 2020. *Ecol. Indic.* **2020**, *112*, 106142.
40. Girili, A.; Mubarek, A. Regional ecological security assessment on Central Asia based on ecological footprint analysis. *Geogr. Res.* **2008**, *6*, 1308–1320.
41. Xia, Q. Study on Land Ecological Carrying Capacity of Hefei Based on Ecological Footprint Xia Qian. Master's Thesis, Anhui Agricultural University, Hefei, China, 2019.
42. Li, X.F.; Song, L.; Xie, Z.B.; Gao, T.; Wang, T.T.; Zheng, X.; Liu, J.; Liu, L. Assessment of Ecological Vulnerability on Northern Sand Prevention Belt of China Based on the Ecological Pressure–Sensibility–Resilience Model. *Sustainability* **2021**, *13*, 6078. [CrossRef]
43. Li, Y.-Y.; Liu, Y.; Ranagalage, M.; Zhang, H.; Zhou, R. Examining Land Use/Land Cover Change and the Summertime Surface Urban Heat Island Effect in Fast-Growing Greater Hefei, China: Implications for Sustainable Land Development. *ISPRS Int. J. Geo-Inf.* **2020**, *9*, 568. [CrossRef]
44. State Council. Reply of the State Council on the overall urban planning of Hefei. *Bull. State Counc. People's Repub. China* **2016**, *14*, 49–51.
45. Yu, H.S.; Yang, J.; Li, T.; Jin, Y.; Sun, D.Q. Morphological and functional polycentric structure assessment of megacity: An integrated approach with spatial distribution and interaction. *Sustain. Cities Soc.* **2022**, *80*, 103800. [CrossRef]

46. Camille, R.; Sophie, L. Urban Structure and Environmental Externalities. *Environ. Resour. Econ.* **2018**, *70*, 31–52.
47. Mukherjee, F. Environmental Impacts of Urban Sprawl in Surat, Gujarat: An Examination Using Landsat Data. *J. Indian Soc. Remote Sens.* **2022**, *50*, 1003–1020. [CrossRef]
48. Zhao, Y.; Zhong, L.; Ma, Y.; Fu, Y.; Chen, M.; Ma, W.Q.; Zhao, C.; Huang, Z.; Zhou, K. WRF/UCM simulations of the impacts of urban expansion and future climate change on atmospheric thermal environment in a Chinese megacity. *Clim. Chang.* **2021**, *169*, 38. [CrossRef]
49. Ma, S.; Huang, J.; Chai, Y.Y. Proposing a GEE-Based Spatiotemporally Adjusted Value Transfer Method to Assess Land-Use Changes and Their Impacts on Ecosystem Service Values in the Shenyang Metropolitan Area. *Sustainability* **2021**, *13*, 12694. [CrossRef]
50. Rahman, M.M.; Szabó, G. Impact of Land Use and Land Cover Changes on Urban Ecosystem Service Value in Dhaka, Bangladesh. *Land* **2021**, *10*, 793. [CrossRef]
51. Sresto, M.A.; Morshed, M.M.; Siddika, S.; Almohamad, H.; Al-Mutiry, M.; Abdo, H.G. Impact of COVID-19 Lockdown on Vegetation Indices and Heat Island Effect: A Remote Sensing Study of Dhaka City, Bangladesh. *Sustainability* **2022**, *14*, 7922. [CrossRef]
52. Founda, D.; Katavoutas, G.; Pierros, F.; Mihalopoulos, N. The Extreme Heat Wave of Summer 2021 in Athens (Greece): Cumulative Heat and Exposure to Heat Stress. *Sustainability* **2022**, *14*, 7766. [CrossRef]
53. National Bureau of Statistics. *China Statistical Yearbook*; China Statistics Press: Beijing, China, 2000–2020.
54. Basu, T.; Das, A. Systematic review of how eco-environmental transformation due to urbanization can be investigated in the sustainable development of Indian Cities. *Environ. Chall.* **2021**, *4*, 100099. [CrossRef]



环境科学
Environmental Science
ISSN 0250-3301,CN 11-1895/X

《环境科学》网络首发论文

题目：城市空间格局与热环境响应关系：以合肥市区为例
作者：陈媛媛，姚侠妹，偶春，张清怡，姚晓洁
DOI：10.13227/j.hjkx.202207042
收稿日期：2022-07-04
网络首发日期：2022-09-20
引用格式：陈媛媛，姚侠妹，偶春，张清怡，姚晓洁．城市空间格局与热环境响应关系：以合肥市区为例[J/OL]．环境科学. https://doi.org/10.13227/j.hjkx.202207042



网络首发：在编辑部工作流程中，稿件从录用到出版要经历录用定稿、排版定稿、整期汇编定稿等阶段。录用定稿指内容已经确定，且通过同行评议、主编终审同意刊用的稿件。排版定稿指录用定稿按照期刊特定版式（包括网络呈现版式）排版后的稿件，可暂不确定出版年、卷、期和页码。整期汇编定稿指出版年、卷、期、页码均已确定的印刷或数字出版的整期汇编稿件。录用定稿网络首发稿件内容必须符合《出版管理条例》和《期刊出版管理规定》的有关规定；学术研究成果具有创新性、科学性和先进性，符合编辑部对刊文的录用要求，不存在学术不端行为及其他侵权行为；稿件内容应基本符合国家有关书刊编辑、出版的技术标准，正确使用和统一规范语言文字、符号、数字、外文字母、法定计量单位及地图标注等。为确保录用定稿网络首发的严肃性，录用定稿一经发布，不得修改论文题目、作者、机构名称和学术内容，只可基于编辑规范进行少量文字的修改。

出版确认：纸质期刊编辑部通过与《中国学术期刊（光盘版）》电子杂志社有限公司签约，在《中国学术期刊（网络版）》出版传播平台上创办与纸质期刊内容一致的网络版，以单篇或整期出版形式，在印刷出版之前刊发论文的录用定稿、排版定稿、整期汇编定稿。因为《中国学术期刊（网络版）》是国家新闻出版广电总局批准的网络连续型出版物（ISSN 2096-4188，CN 11-6037/Z），所以签约期刊的网络版上网络首发论文视为正式出版。

网络首发时间：2022-09-20 08:57:25
网络首发地址：https://kns.cnki.net/kcms/detail/11.1895.X.20220919.1413.053.html

城市空间格局与热环境响应关系：以合肥市区为例

陈媛媛[1]，姚侠妹[1*]，偶春[2]，张清怡[1]，姚晓洁[1]
(1. 安徽建筑大学建筑与规划学院，合肥 230601；2. 阜阳师范大学生物与食品工程学院，阜阳 236037)

摘要：随着城市不断扩张，区域的地表覆盖类型发生转变，大量自然景观被人造景观所替代，环境温度随之上升。研究城市空间格局与热环境之间的响应关系，对于改善生态环境、优化城市空间布局有一定的指导意义。基于合肥市区 2020 年的 Landsat 8 系列遥感影像数据及 ENVI 和 ARCGIS 等分析平台，采用皮尔逊相关性与剖面线反映两者之间的关联性，再选取关联性最大的 3 个空间格局组成要素构建多元回归函数，以探究城市空间格局对城市热环境的影响及其作用机制。结果表明：①2013—2020 年间，随着时间推进，合肥市高温区明显增加。对于不同的季节，热岛效应呈现出夏季>秋季>春季>冬季。②中心城区内，建筑占比、建筑高度、不透水占比和人口密度明显高于郊区，而植被覆盖度呈现出郊区高于城区，且在城区主要呈现出点状分布，水体呈不规则分布。③城市高温区主要分布在城区各类开发区内，而城区内其他地方则以中高温及以上温度分区为主，郊区以中低温为主。④各要素的空间格局与热环境之间的皮尔逊系数为正相关的有建筑占比（0.395）、不透水面占比（0.333）、人口密度（0.481）和建筑高度（0.188），负相关的为植被覆盖度（−0.577）和水体占比（−0.384）。构建的夏季热环境多元回归函数，包括建筑占比、人口密度和植被覆盖度的系数分别为 8.372、0.295 和−5.639，常数为 38.555。研究结果能够为优化城市空间布局和提高城市居住品质提供参考依据。

关键词：城市空间格局；热环境；相关性分析；合肥市区；多元线性回归
DOI:10.13227/j.hjkx.202207042

Relationship Between Urban Spatial Pattern and Thermal Environment Response in Summer: A Case Study of Hefei City

CHEN Yuan-yuan[1], YAO Xia-mei[1]*, OU Chun[2], ZHANG Qing-yi[1], YAO Xiao-jie[1]
(1. School of Architecture and Urban Planning, Anhui Jianzhu University, Hefei 230601, China; 2.School of Biology and Food Engineering, Fuyang Normal University, Fuyang 236037, China)

Abstract: With the continuous expansion of cities, the land cover type of the region is transformed, a large number of natural landscapes are replaced by man-made landscapes, and the environmental temperature rises. The study of the response relationship between urban spatial pattern and thermal environment has some guidance for improving ecological environment and optimizing urban spatial layout. Based on the Landsat 8 series remote sensing image data of Hefei City in 2020 and analysis platforms such as ENVI and ARCGIS, Pearson correlation and profile lines were used to reflect the correlation between the two, and then the three components of spatial pattern with the greatest correlation were selected to construct multiple regression functions to investigate the influence of urban spatial pattern on urban thermal environment and its mechanism of action. The results show that: ①The high temperature area of Hefei City increases significantly with the advance of time during 2013-2020. For different seasons, the urban heat island effect shows summer > autumn > spring > winter. ②In the central urban area, the building occupancy, building height, imperviousness occupancy and population density are significantly higher

收稿日期：2022-07-04；**修订日期：**2022-09-06
基金项目：教育部人文社会科学研究青年基金项目（18YJC760117）；安徽省社会科学创新发展研究课题项目（2021CX182）；安徽建筑大学博士科研启动基金项目（2020QDZ15）；安徽省高峰学科培育课题项目（2021-138）；安徽省高校自然科学研究项目（KJ2020A0456）；安徽省高校优秀青年人才支持计划项目（gxyq2021197）
作者简介：陈媛媛（1998～），女，硕士研究生，主要研究方向为城市热环境和景观生态，E-mail:2965705275@qq.com
*通信作者，E-mail:yaoxiamei@126.com

than those in the suburbs, while fractional vegetation coverage presents a higher suburban than urban area, and mainly shows a point distribution in the urban area and an irregular distribution of water bodies. ③The urban high temperature zone is mainly distributed in various development zones in urban areas, while other places in urban areas are dominated by medium-high temperature and above temperature zoning, and suburban areas are dominated by medium-low temperature. ④The Pearson coefficients between the spatial pattern of each element and the thermal environment are positively correlated with the building occupancy (0.395), impervious surface occupancy (0.333), population density (0.481), and building height (0.188), and negatively correlated with fractional vegetation coverage (−0.577) and water occupancy (−0.384). The coefficients of the constructed multiple regression functions, including building occupancy, population density and fractional vegetation coverage, are 8.372, 0.295 and −5.639 respectively, with a constant of 38.555. The results of the study can provide a reference basis for optimizing urban spatial layout and improving urban living quality.
Key words: urban spatial pattern; thermal environment; correlation analysis; Hefei City; multiple linear regression

城市化进程的主要特点是非农业人口大量增长、城市空间不断扩张和社会经济持续聚集等[1]，导致大量的建筑和不透水面覆盖了原用地，林地和草地等绿色空间面积降低，同时工业、人口、车辆和污染物排放等热源的激增[2,3]，导致城市热环境温度不断攀升，与城市扩展前的热环境温度形成鲜明对比，影响了生态环境以及人居环境质量[4]。而城市内的绿色空间已被证明具有降温增湿和气候改良[5]等功能，对于缓解城市热岛效应有着积极的作用。研究城市空间格局与热环境之间的响应关系，对于构建城市绿地系统和建设宜居城市有一定的借鉴意义。

目前针对城市空间与热环境的影响研究已经较为多样。对于城市热环境情况的获取方法包括地表监测[6]和遥感数据反演[7]等。热环境的影响因素研究则包括从绿地的面积和形状等形态特征[8]，绿地和水体占比和垂直结构等结构[9]，水体和绿地等的缓冲区效应及其空间布局[10]等多方面探讨中微观角度下绿地或水体的空间结构对城市热环境的影响；而近些年则主要是从整个城市的景观格局[11]、建筑结构[12]、不透水面[13]和城市下垫面参数[14,15]等城市形态要素作为切入点从宏观角度展开研究；在研究方法上，大部分学者会在区域内选择多个随机点或者随机区域，再取其内的平均温度值以及影响因素值，通过空间自相关[16~18]和皮尔逊相关性分析[19]等研究两者关联程度，并利用最小二乘法[20]和空间滞后模型[21]等回归模型构建函数，进而探究两者关系。由此可见，目前关于热环境的影响研究多样且深刻，但是缺少多个城市空间格局影响因子对热环境的响应关系研究，同时目前的研究多针对上海、纽约等较为发达的城市，对正处于快速扩展中的合肥市区热环境的研究还较少。

综上所述，研究基于合肥市区的遥感影像数据及 ARCGIS 和 ENVI 等分析平台，反演出往年地表温度，观察合肥市历年和不同季节的热环境空间格局，随后取热岛效应最为严重的季节内多个时间点的地表温度，并取其平均值，再对建筑高度、建筑占比、不透水面占比、水体面积占比、植被覆盖度和人口密度的空间格局要素进行定量化处理，再利用剖面线和皮尔逊相关性分析，剖析上述空间格局要素分别对城市热环境的影响程度，最后通过综合考量，选取影响程度最大的 3 个要素构建多元回归函数，以探究城市热环境与空间格局之间的关系，以期为建设生态宜居型城市提供理论依据。

1 材料与方法

1.1 研究区域概况

合肥市位于中国的华东地区、安徽省中部、江淮之间，市域范围在东经 116°41′~117°58′，北纬 30°57′~32°32′之间[22]；截止到 2020 年，常住人口 936.99 万，城镇化率 76.33%，建成区面积 528.5km²[23]；合肥市交通便捷，航路、水路和公路等各类道路在空间上形成纵横交

错的三维交通网络，是全国的综合交通枢纽；境内主要有丘陵岗地、低洼平原和低山残丘这3类地貌，地形起伏不大，内含巢湖和江淮水系的部分河流，地表水系发达[24]；本文研究区域是合肥市区，包括蜀山区、包河区、瑶海区和庐阳区这4个市辖区，区域内拥有合肥经开区和蜀山高新区等多个开发区，内含产业园和工业用地等；除了致力于产业、经济发展，市区内还含有合肥滨湖湿地森林公园和方兴湖公园等多个公园绿地，立志于将合肥打造成生态宜居城市。合肥是合肥都市圈的中心城市[25]，长三角城市群的副中心城市[26]，其城区内的良好热环境状态能够保证居民的舒适生活环境和整个合肥市乃至长江流域的良性发展。

1.2 数据来源及预处理

基础数据采集于地理空间数据云（www.gscloud.cn）的遥感数据，借助ENVI和ARCGIS对遥感影像图进行大气校正、裁剪等预处理，并将其地表土地覆盖类型划分为绿地、水体、不透水面，经实地抽样调查验证，数据总体分类精度达到 80%，符合实验要求。人口数据来源于Worldpop 官网（www.worldpop.org），建筑高度通过爬取百度地图现有的建筑位置、范围和高度，并对其进行补充以及异常值剔除。

1.3 研究方法

1.3.1 地表温度反演

反演采用的是单窗算法[27~29]，对于采集到的Landsat 8 OLI数据，采用以下计算：

$$TS(OLI) = [a \times (1 - C - D) + (b \times (1 - C - D) + C + D) \times T_6 - D \times Ta] / C - 273.5 \quad (1)$$

式中，对于Landsat 8 OLI类型的遥感影像，a和b常量根据合肥市区的具体情况和遥感影像图采集时间定为−67.35535和0.45860[30]；T_6为TM6卫星亮度温度；C和D为中间变量；计算公式分别如下：

式中，K_1和K_2的值分别为774.89和1321.08[31]，L_γ为辐射定标后的热红外波段；ε为地表比辐射率[32]；τ为大气透射率（数据来源：美国国家航空航天局官网）。

$$T_6 = K_2 / \ln(1 + K_1 / L_\gamma) \quad (2)$$

$$C = \tau \times \varepsilon \quad (3)$$

$$D = (1 - \tau) \times [1 + \tau \times (1 - \varepsilon)] \quad (4)$$

其中ε与归一化植被指数NDVI有密切关系[33]:

自然表面与城镇表面的地表发射率分别为：

$$\varepsilon = 0.9625 + 0.0614 \times FVC - 0.0461 \times FVC \times FVC \quad (5)$$

$$\varepsilon = 0.9589 + 0.086 \times FVC - 0.0671 \times FVC \times FVC \quad (6)$$

式中，ε为地表比辐射率；FVC为区域的植被覆盖度。

1.3.2 城市空间形态定量化表达

参考其他学者在空间格局对于热环境的影响上的研究，以及研区域实际情况，将研究尺度确定为120m，并将研究区域划分为120×120m的方格，以便对空间形态进行量化。选取表达城市空间格局的要素有：水体面积占比(WP)、不透水面占比(ISP)、建筑高度(BH)、建筑占比(BD)、植被覆盖度(FVC)和人口密度(PD)。空间量化公式如下所示。

（1）WP、ISP和BD

$$D = S / S_i \quad (7)$$

式中，D为统计单元的占比（包含：水体面积占比、不透水面占比和建筑占比）；S为统计单元面积；S_i为第i个统计单元内水体（不透水面和建筑）面积。

（2）BH

$$H = \frac{\sum_{i=1}^{n} H_i \times A_i}{\sum_{i=1}^{n} A_i} \quad (8)$$

式中，H 为统计单元内平均建筑高度；H_i 为第 i 栋建筑的高度；A_i 为第 i 栋建筑的占地面积；

（3）FVC

植被覆盖度（FVC）的计算公式为：

$$FVC = (NDVI - NDVI_S) / (NDVI_V - NDVI_S) \quad (9)$$

式中，NDVI 为归一化的植被指数；$NDVI_V$ 为区域被植被全部覆盖时的 NDVI 值，而 $NDVI_S$ 为区域未被植被覆盖时的 NDVI 值[34]。

（4）PD

从 Worldpop 官网下载的栅格数据，其内每一个像元的值为像元大小面积内的人口数量，该像元大小为 100m×100m。为方便研究，将其转化为密度值，再将其转化为 120m 分辨率。

$$P = \frac{\sum_{i=1}^{n} G_i}{n} \quad (10)$$

$$G_i = m_i / S \quad (11)$$

式中，P 为统计单元的人口密度；G_i 为第 i 个原像元内的人口密度；n 为统计单元内包含的原像元个数。m_i 为第 i 个原像元内的人口数量；S 为原像元大小。

1.3.3 皮尔逊相关性分析

皮尔逊相关性分析可以较为直观的反映每一对自变量对因变量的影响程度[35]。计算公式如下：

$$R_{xy} = \frac{\sum_{i=1}^{n}(x_i - \overline{x})(y_i - \overline{y})}{\sqrt{\sum_{n=1}^{n}(x_i - \overline{x})^2 \sum_{n=1}^{n}(y_i - \overline{y})^2}} \quad (12)$$

式中，R_{xy} 为两个变量 x 和 y 之间的相关性系数；x_i 为水体面积占比、不透水面占比、建筑高度等空间格局要素；y_i 为温度数值。

2 结果与分析

2.1 地表热环境及城市空间格局要素特征

2.1.1 合肥热环境空间格局演变概况

利用单窗算法，借助 ARCGIS 和 ENVI 软件，反演出合肥市区 2013 年、2015 年、2018 年和 2020 年的地表温度，获取到城市热环境空间格局演变概况，如图 1 所示。

从 2013—2020 年，市区内的中高温区围绕中心城区不断向四周蔓延，侵占了大量的低温区域，主要是往西南与东南方向扩散，热岛重心逐渐想南部转移，表现在蜀山高新区、滨湖新区等区域由低温区转为中高温区，和大量的市区西部地表温度由低温转为中温。同时原本中心城区与周边郊区的温差较小，但是随着城市空间的扩展，郊区与中心城区的温差越来越大，象征着合肥市区的热岛效应越来越严重，亟待缓解。

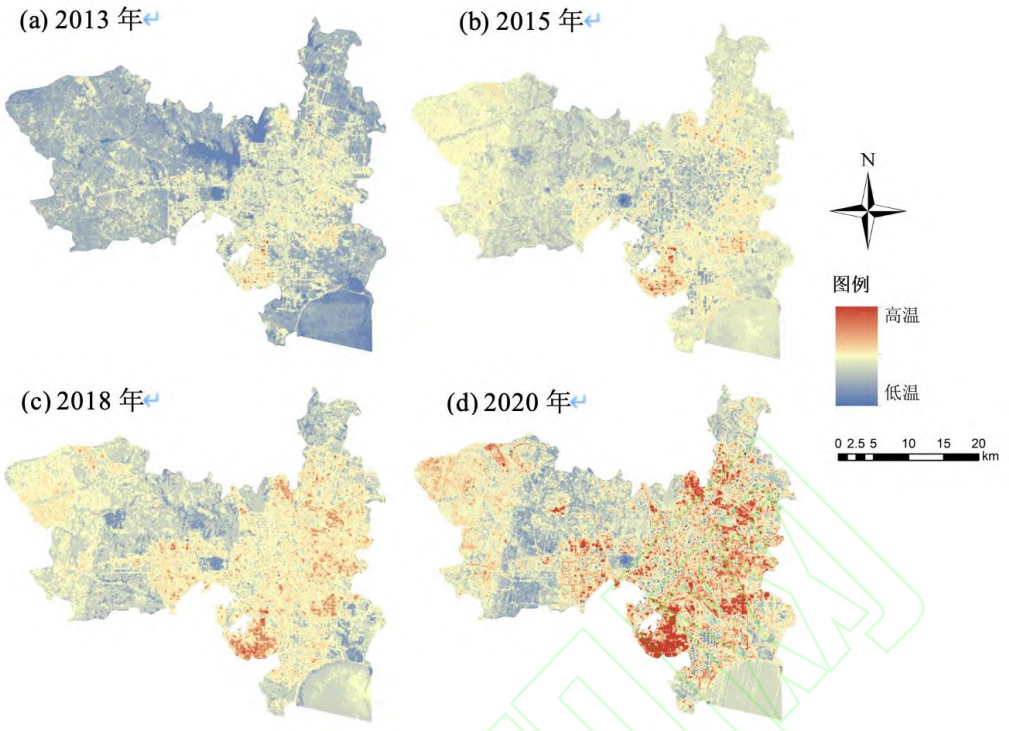


图 1　2013~2020 年热环境空间格局

Fig. 1 Spatial pattern of thermal environment from 2013 to 2020

2.1.2 合肥市区热环境格局四季演变

根据数据的可获取性、云量、天气和分辨率等原因，反演了 2020 年的 1 月 12 日、4 月 21 日、6 月 5 日和 10 月 27 日这 4 个时间点的地表温度，分别代表合肥市冬季、春季、夏季和秋季的热环境情况，结果如图 2 所示。

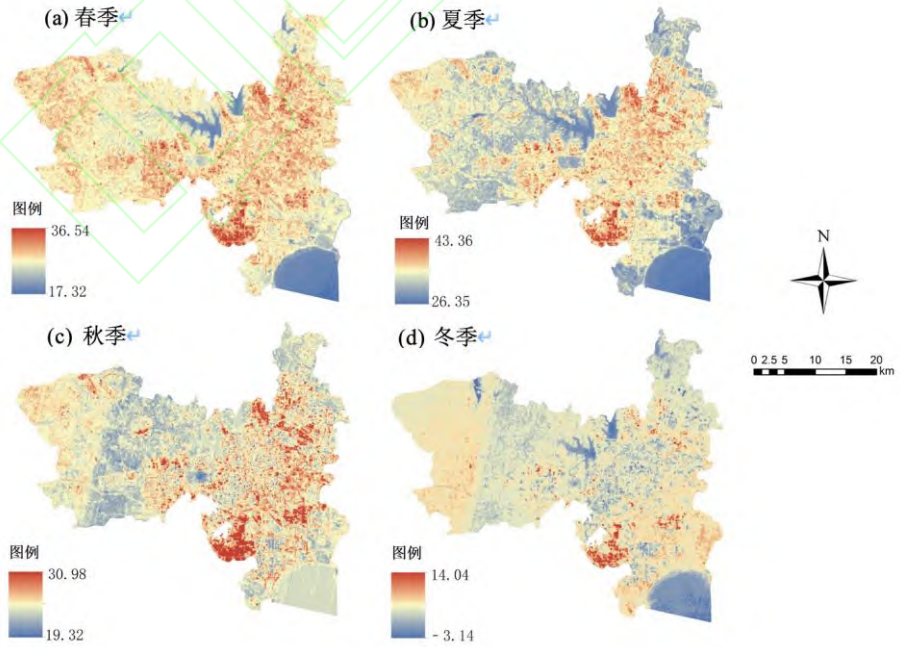


图 2　2020 年四季的热环境空间格局

Fig. 2 Spatial pattern of the thermal environment for all seasons in 2020

由图 2 可知，4 个季节的高温区和低温区的大小和范围均不一样，其中可发现夏季的城区与郊区的温差最大，中高温区的轮廓最为显著，与城区范围高度重合，其次是秋季和春季，冬天最小，冬季的城区内除开经开区、高新区等开发区外，低温区范围甚至多余高温区，与郊区温度相差无几，且没有了清晰轮廓。综上所述，合肥市热岛效应最强的是夏季，其次是秋季、春季以及冬季。

2.1.3 城市空间格局分布特征

利用 ARCGIS 的空间统计分析工具，对合肥市区的空间格局要素进行定量化处理，处理结果如图 3 所示。

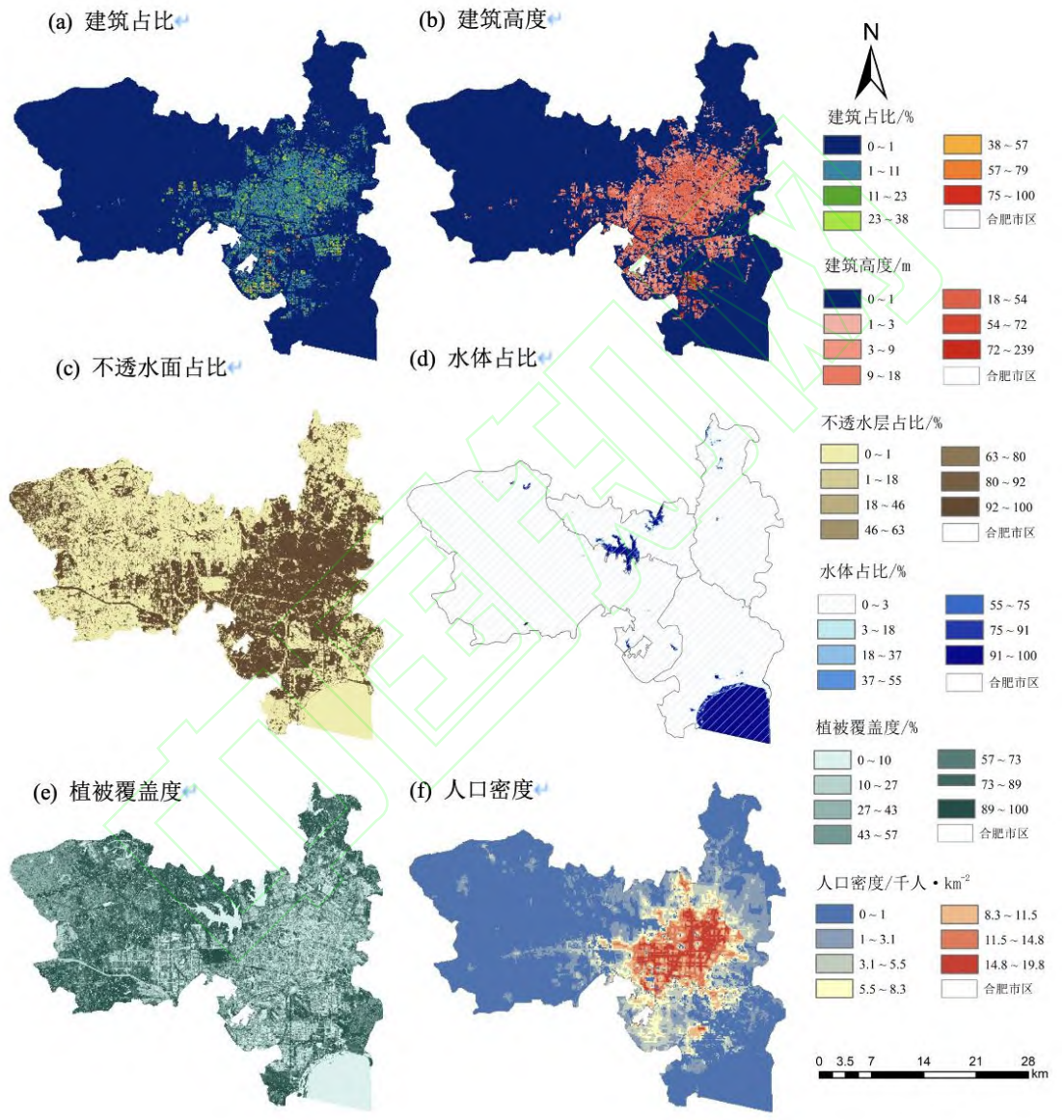


图 3　城市空间格局分布特征

Fig. 3 Distribution characteristics of urban spatial pattern

合肥市区的建筑占比分布与其所在区域有密切关系，城市大部分区域建筑占比在 18%以下，新建成的住宅区、商业区建筑占比在 18%~23%之间，而合肥蜀山经开区、包河工业区和经开区等开发区，建筑占比普遍在 23%以上，占比高于 57%的区域面积达到 2.36km²。从图 3(b)中可以看出，老城区内的建筑高度普遍位于 54m，围绕老城区、滨湖新区等区域内新建的住宅楼、商业楼等建筑高度较高，而工业厂区等地内的建筑具有占地面积大，高度低

的特点，高度在 72m 以上的建筑占地面积达 12.28km²。在图 3(c)中，不透水面大致呈现出以围绕中心城区向周围扩展并不断减少，是较为显著的单核扩展模式，高不透水面占比地区主要分布在蜀山经开区、高新区等地，在整体上有 31%的区域不透水面积占比大于 92%。合肥室内水体主要以巢湖、董铺水库、大房郢水库等大面积水体为主，水体总面积占据了合肥市区的 6.3%。

植被主要覆盖在城市建成区周边，覆盖度在 89%以上的区域占据了 13.1%，其中包括大蜀山国家森林公园、南艳湖、植物园、滨湖国家森林公园等高植被覆盖区域，而建成区内的植被覆盖度普遍低于 43%。合肥市区人口密度在 11.5 千人·km^{-2} 以上的区域主要分布在合肥中心城区内，人口分布格局与街道布局有关，主要分布在街道两侧，这些区域主要以多层住宅、高层住宅为主，占据了 6.7%的区域，而大部分开发区内虽然建筑占比高，但人口稀疏。

2.2 城市空间格局对城市热环境的影响

2.2.1 空间格局与城市内部温度的相关性

（1） 夏季平均地表温度

从对合肥市四季的热环境分析来看，其夏季的热岛效应更为严重，城市中心与郊区的温差更大，对人居环境的影响更为强烈，所以文章选取了合肥市的夏季作为研究时间点，同时为避免单个时间点时出现的由天气原因造成的误差，反演了 2020 年夏季（5 月 21 日至 9 月 20 日）的 3 个时间点的地表温度，随后利用波段计算，取这 3 个时间点的地表温度的平均值，结果如图 4 所示。以下的相关性研究均是基于图 4 进行。

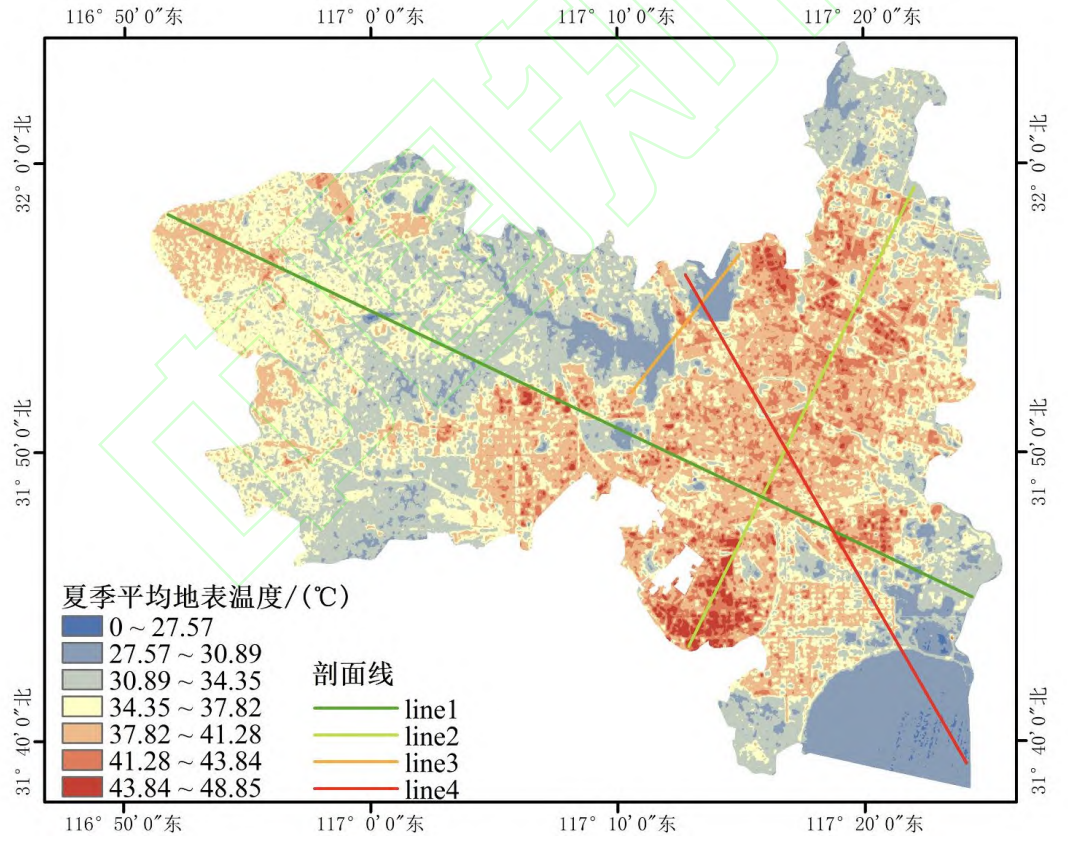


图 4 夏季地表平均温度空间格局

Fig. 4 Spatial pattern of the average surface temperature in summer

将地表温度按照自然断点法划分为 7 个等级，如图 4 和表 1 所示。从图 4 可以看出，从西至东，大致为中温区-低温区-高温区。西部虽远离主城区，但是由于西部与淮南、六安城市连接，拥有发达的交通线路，且具有机场、各类工业园以及高刘镇等较为发达的小镇，这

些区域不透水面和建筑较多，植被少，导致温度升高。结合表 1 可以得出，中高温区、高温区和极高温区，总面积达到了 427.57km²，在研究区域内占比 33.28%，地理位置主要分布在城市建成区内，与郊区温度差距较大，其中高温密集区主要分布在蜀山经开区、包河工业区、庐阳产业园和瑶海产业园等，这些区域位于城市中心周边，温度比城市中心高，而中心城区内部零散分布着一些低温区，这些区域大部分为水体和公园。

表 1　地表温度等级

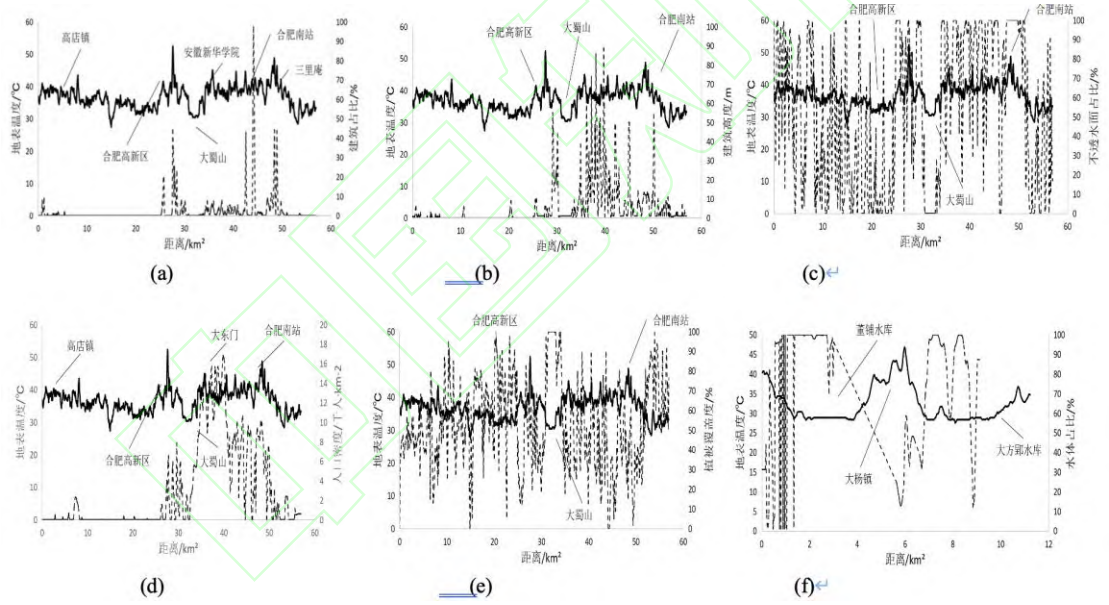
Table 1 Surface temperature level

项目	极低温区	低温区	中低温	中温	中高温	高温区	极高温区
面积/km²	2.380	142.604	361.432	350.729	322.019	90.136	15.419
占比/%	0.185	11.100	28.133	27.300	25.065	7.016	1.200

2.2.2 空间格局与城市内部温度的相关性

（1）剖面线

在研究区域内划取两条空间格局最为复杂且垂直相交的剖切线（见图 4 中的 line1 和 line2），同时由于水体分布极其的不均匀，所以对水体的研究另外选取了两条垂直相交的剖切线(见图 4 中的 line3 和 line4)。line1 起于合肥河东村，止于大圩镇；line2 起于合肥张店村，止于吴郢村；line3 起于大杨镇，止于巢湖内部；line4 起于东大荒，止于高桥村。4 条剖切线均途径中心城区，具体位置见图 4。最后获取到 4 条线上对应的空间格局指数和地表温度值，并将其制剖面折线图，结果如图 5 和图 6 所示。

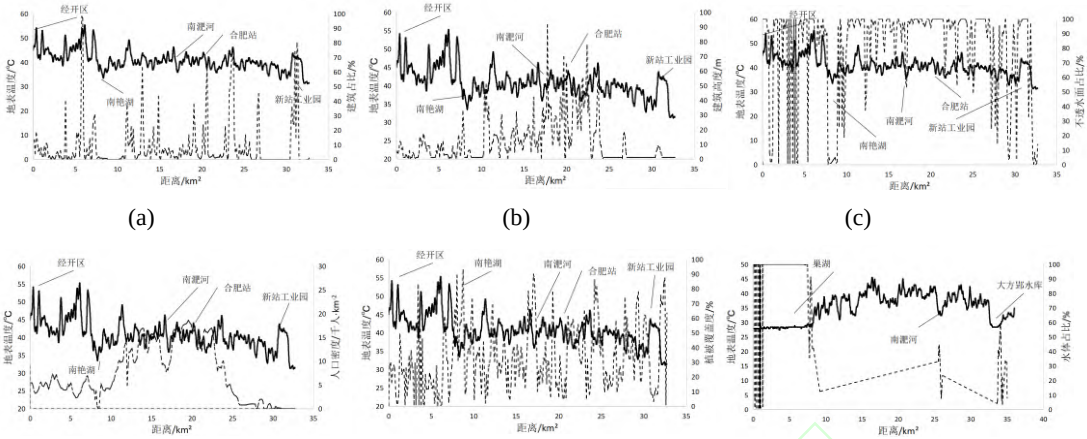


图例：　——— 地表温度；－－－ 空间格局要素

(a)建筑占比，(b) 建筑高度，(c) 不透水面占比，(d) 人口密度，(e) 植被覆盖度，(f) 水体

图 5　line1 和 line3 的空间格局与地表温度剖面线

Fig. 5 Spatial pattern of line1 and line3 with the profile line of surface temperature



(a) (b) (c)

(d) (e) (f)

图例： ——— 地表温度；– – – 空间格局要素

(a)建筑占比，(b) 建筑高度，(c) 不透水面占比，(d) 人口密度，(e) 植被覆盖度，(f) 水体

图 6　line2 和 line4 的空间格局与地表温度剖面线

Fig. 6 Spatial pattern of line2 and line4 with the profile line of surface temperature

从 line1 下的地表温度剖面线先呈现出中温，再降低，最后剧烈升高，分别对应着低密度建设用地区域、耕地及建成区，这与 line1 下的建筑占比、不透水面和人口密度的变化呈现出高度的一致性，与植被覆盖度则相反，如到了高新区，建筑密度与不透水面增高，温度也随之上升，而到了大蜀山、郊区等高植被覆盖度区域则显示出明显的降温趋势；line3 对应的温度为先升温再降温，对应着先经过巢湖、滨湖新区和中心城区再到大杨镇，水体占比先高后低，最后再增高的趋势；line2 为先高温，然后降温，再有所升高，对应着依次途径了蜀山经开区、中心城区和新站工业园，分别对应着建筑占比高、人口密度大但是植被覆盖度较开发区高以及高建筑占比区域；line4 为低温，增温再降温，对应着依次经过董铺水库、大杨镇和大房郢水库，水体占比先增高，后降低，再增高。

结合 line1 和 line2、line3 和 line4 的剖面线可以得出，建筑占比、建筑高度、不透水面和人口密度这 4 要素的波段曲线与城市地表温度的波段曲线具有相似的走向，当上述 4 要素升高时，地表温度也会升高，反之则降低，表明这 4 个要素与地表温度正相关。而水体和植被覆盖度的剖切线波动与地表温度的剖切线波段走向相反，当这 3 个要素升高时，地表温度降低，反之温度升高，表明该 3 要素与地表温度负相关。

（2）皮尔逊相关性分析

为更加深层次的研究不同空间格局要素对城市地表温度的影响，针对不同的空间格局要素，在区域内生成 1800 个随机点，获取到各随机点对应的各空间格局要素的值和地表温度值，并筛选无效值与重复值，形成实验数据组，最终得出各空间格局要素与地表温度之间的皮尔逊相关性系数，如表 2 所示。

表 2　空间格局与地表温度的皮尔逊相关性

Table 2 Pearson's correlation of spatial patterns and surface temperature

项目	建筑高度	建筑占比	不透水面占比	水体占比	植被覆盖度	人口密度
Pearson 相关性系数	0.188	0.395	0.333	−0.384	−0.577	0.481
显著性水平（双侧）	0.01	0.01	0.01	0.01	0.01	0.01
实验数据组数	46	406	430	52	1498	172

系数的绝对值大小代表了空间格局要素对城市热环境的影响程度。如表 2 所示，在上述

要素中，对地表温度影响有正面影响是人口密度、建筑占比、不透水面和建筑高度，相关性系数值依次降低分别为 0.481、0.395、0.333、0.188，代表了城市内的人口密度和建筑占比是导致城市热环境温度上升，致使城市出现热岛效应的主要因素，当两者在城市中占比越大，城市热源增多，散热能力降低，热环境温度就越高。而对地表温度呈现出负相关的要素有植被覆盖度、水体，相关性系数值依次为−0.577 和−0.384，均为负数，代表了上述要素能够降低城市地表温度，当其在城市中占比越高时，植物和水体的降温增湿效益越显著，越能够缓解城市热岛效应。

2.2.3 回归分析

综合考虑研究区域实际情况以及剖切线与皮尔逊的相关性分析，从这 7 个要素中选出对地表温度影响程度最大的 3 个要素，即植被覆盖度、人口密度和建筑占比，构建多元线性回归方程，并选取了 1500 个随机点，获取到该 1500 个点下的要素值和地表温度值。同时研究考虑到空间格局要素和地表温度的值属于连续型随机变量，因而采用多元线性回归分析。最终得到 2020 年合肥市区夏季城市热环境的多元线性函数模型，如公式（13）所示。

$$T = 38.555 + 8.372\mathrm{BD} + 0.295\mathrm{PD} - 5.639\mathrm{FVC} \quad (13)$$

式中，T 为合肥市夏季地表温度；各要素定义域分别为｛BD|0≤BD≤1｝，｛FVC|0≤FVC≤1｝和｛PD|0≤PD≤19.8｝。该模型中的 R^2=0.481，Durbin-Waston=2.048，且各个要素的 VIF≪5，说明模式回归拟合效果较好，具有统计学意义，同时每一组观测值独立，不存在多重共线性。同时，根据变量的累积比例与指定分布的累积比例之间的关系所绘制了 P-P 图，如图 7 所示，其中的点接近一条直线，且基本都落在或者靠近对角线上，说明数据服从正态分布。

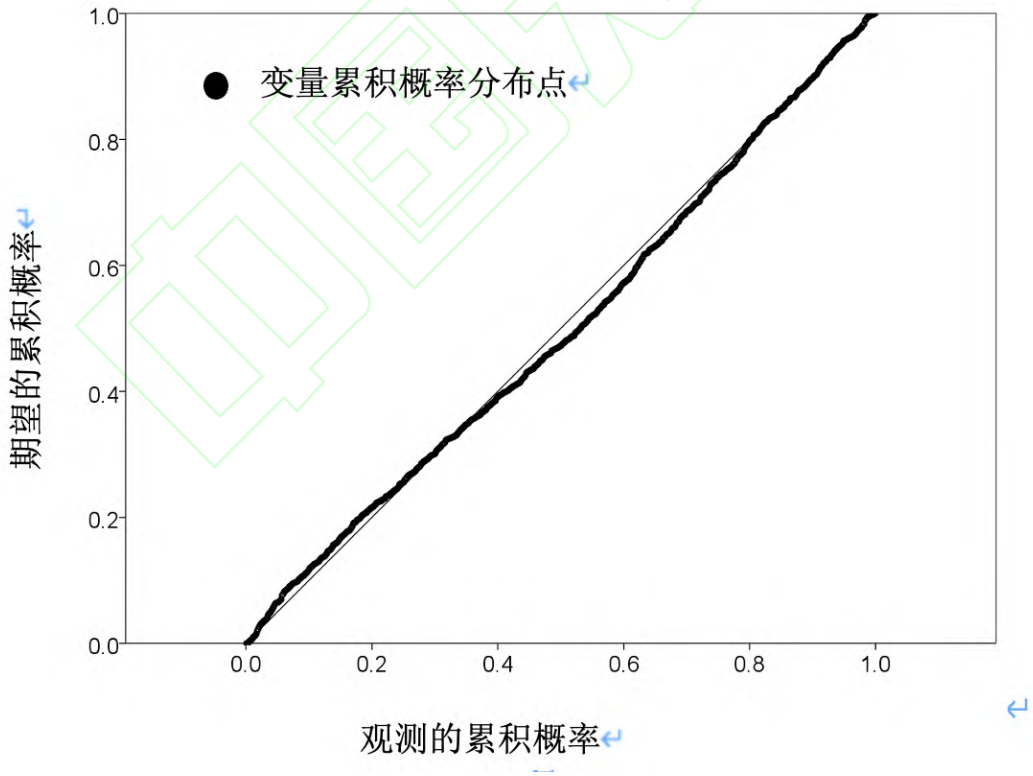


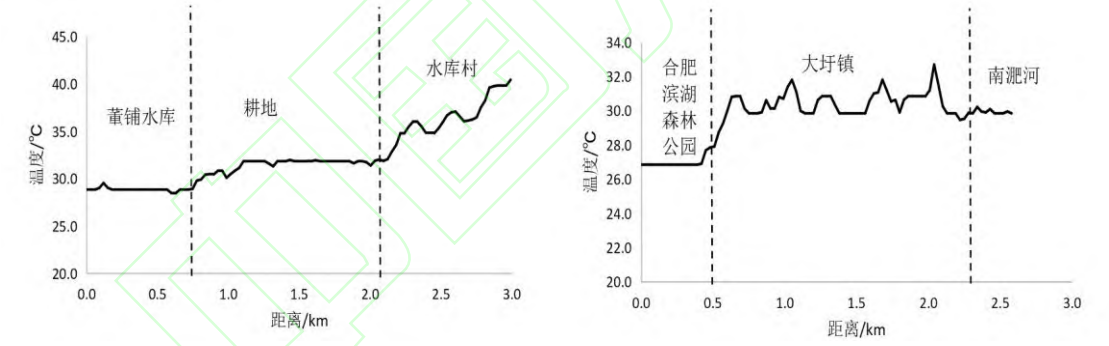
图 7　要素与温度的回归标准化残差 P-P 图

Fig. 7 P-P diagram of the standardized residuals of the regression of the elements on temperature

3 讨论

在不同的季节中，合肥市区的热岛效应显现出不同程度，其中夏季最为明显，冬季不明显，这也是本文在相关性研究中选取夏季作为研究时间点的原因。但是在对于北方的城市的热环境研究里，还存在冬季热岛效应比夏季明显的情况，例如刘勇洪等[36]提到在同样的情况下北京的热岛效应为：冬季>秋季>春季>夏季，这主要是是由于北方城区冬季取暖，人口密集，高楼耸立，导致城区空气不流通，同时北方郊区冬季植被枯萎多数枯萎，地面裸露，导致郊区降温比城区多，进而导致热岛效应明显。而本文研究的合肥位于北亚热带，属南方城市，以亚热带常绿阔叶林为主，使得冬季城区内也种植有许多的常绿树种，起到了降温增湿的作用，与郊区温差小，而夏季郊区的耕地里面的农作物正处于成长中后期，植被旺盛，城区相对于郊区植被面积少很多，同时城区被大面积的不透水面覆盖，建筑密集，从而使得夏季热岛效应严峻，这与葛静茹等[37]和李莹莹等[38]的研究结果相似。

城市中的绿地与水体都具有显著的降温效应，能够改善城市生态环境与局部气候，提供人居环境的舒适性[39]。有研究发现，城市地表温度的分布与其空间格局有着一定关系，从相关性分析来看，绿地和水体具有较强的降温作用，而以水泥、沥青、砖瓦为主的不透水面、建筑具有升温的的作用，而人口作为城市热源，又经常位于多建筑、高不透水面区域，导致人类聚集地温度也较高[40]。同时距离绿地、水体的远近也对温度有着一定的影响，采用对大蜀山、巢湖周边具有稳定情况的区域进行剖面，如图 8 所示，当观测点处于绿地和水体的内部时，温度低且较为稳定，温度变化不大，当观测点位于绿地和水体外时，温度逐渐上升。除此之外绿地与水体的规模、形状等，都对其降温效应有着不同程度的影响，合理的规划建设能够在一定的土地规模内使得两者生态效益最大化，这与陈斌等[41]和张晓东等[42]的研究结果基本一致。



(a) 董铺水库　　(b) 合肥滨湖森林公园

图 8　水体、绿地及周边区域的温度剖面线

Fig. 8 Temperature profile of green space, water area and surrounding area

4 建议

随着城市化进程的推进，建设用地与城市绿地之间的矛盾越发突出[43,44]，城市内部发展在水平面上愈加局促和紧凑，为避免人居环境恶劣，对于合肥这种南方城市，应该增加城区内部的常绿阔叶树种的种植，减少大面积的不透水面区域，减缓夏季的热岛效应，例如可以减少例如大面积水泥地或瓷砖广场等不必要的不透水面的使用，将类似用地改造成疏林广场；同时进行城市规划时合理分布城市绿地及水体空间，且使其形状复杂化，蔓延至更为宽阔的区域，尽可能发挥出绿地内部的降温效应，影响更多的区域，可以在开发区等建筑占比大的地方可以通过扩展道路两侧绿化带或定距建立小型公园及湿地等方式，以达到降温的目的；未来的城市绿色空间进应当从二维空间上延伸至三维立体空间上，有助于绿色空间从地面延

伸到垂直面以及空中[45,46]，这有利于增加城市内的绿色空间，增加绿量，以达到更优化的降温效果，详细措施为：对于建筑高度以及面积要合理控制，增加天空开阔度，降低建筑占比，同时增加垂直绿化以及屋顶绿化，降低热岛效应；对于住宅区，增加区内的平面绿化面积和立体绿化量。

目前对于城市热岛效应的减缓措施研究已经较为多样了，但是很多城市面临着已建成区区域无法拆除，公园和湿地等无法在内部建立，立体绿化对于这类似的区域是很好的选择，但是国内的立体绿化的景观营造、管理养护等技术还不成熟，无法大面积投入使用，但是相信随着相关研究的不断深入，这将为未来解决城市严重的热岛效应提供更加完善的解决方案。

5 结论

（1）2013—2020 年间，合肥市区高温范围随着城市扩展而蔓延至滨湖新区、长江西路等区域，城市热环境愈发恶劣。对于 2020 年的 4 个季节，研究区域的热岛效应呈现出夏季>秋季>春季>冬季。

（2）城市空间格局主要与土地利用类型有关，大部分开发区的具有建筑占比高(>23%)、不透水面占比高(>92%)、建筑高度普遍偏低(<18m)、植被覆盖率低(<27%)，住宅区和商业区建筑高度较高(>18m)、建筑占比中等(18%~23%)和人口密度较大(11.5 千人·km^{-2})的特点；公园、湿地和郊区等地的植被覆盖度高，分别大于 57%，而不透水面少(<18%)。同时城市热环境空间格局显示，高温区主要分布在工业园、产业园等，低温区分布在公园、水体和郊区等。

（3）在研究时间节点上，研究区域内各空间格局要素与地表温度的剖面线走向有一定的规律，建筑占比、建筑高度、不透水面占比、人口与地表温度为正相关，植被覆盖度和水体为负相关；同时各空间格局要素与地表温度之间的皮尔逊相关性分析的绝对值依次为：植被覆盖度（−0.577）>人口密度（0.481）>建筑占比（0.395）>水体占比（−0.384）>不透水面占比（0.333）>建筑高度（0.188），由上述两种相关性分析结果可见建筑占比、人口密度和植被覆盖度与城市热环境的相关性最强。在以上基础上构建了多元回归线性方程，建筑占比、人口密度和植被覆盖度的系数分别为 8.372、0.295 和−5.639，常数为 38.555。

参考文献：

[1] Zhang S L, Zheng H Q, Zhou H Y, *et al*. Sustainable land urbanization, urban amenities, and population urbanization: Evidence from city-level data in China[J]. Social Science Quarterly,2021,**102**(4):1686-1698.

[2] 鹿广利,刘传印,孙鑫鑫,等.移动热源对巷道热环境影响的动态模拟研究[J].煤炭技术,2022,**41**(2):157-161.

Lu G L, Liu C Y, Sun X X, *et al*. Dynamic simulation study on influence of moving heat source on tunnel thermal environment [J]. Coal Technology, 2022,**41**(2):157-161.

[3] Christopher G H, Mikhail V C, Andrew M F, *et al*. Valley of the sun-drenched parking space: The growth, extent, and implications of parking infrastructure in Phoenix[J]. Cities,2019,**89**:186-198.

[4] Luo X, Yang J, Sun W, *et al*. Suitability of human settlements in mountainous areas from the perspective of ventilation: A case study of the main urban area of Chongqing[J]. Journal of Cleaner Production,2021, **310**, doi: 10.1016/J.JCLEPRO.2021.127467.

[5] Zhu C Y, Ji P, Li S H. Effects of urban green belts on the air temperature, humidity and air quality[J]. Journal of Environmental Engineering and Landscape Management,2017,**25**(1):39-55.

[6] 程志刚,李炬,周明煜,等.北京中央商务区(CBD)城市热岛效应的研究[J].气候与环境研究,2018,**23**(6):633-644.

Cheng Z G, Li J, Zhou M Y, *et al*. A study on urban heat island effect in Beijing central business district (CBD) [J]. Climate and Environmental Research, 2018,**23** (6):633-644.

[7] 雷金睿,陈宗铸,吴庭天,等.1989～2015 年海口城市热环境与景观格局的时空演变及其相互关系[J].中国环境科学,2019,**39**(4):1734-1743.

Lei J R, Chen Z Z, Wu TT, *et al*. Spatio-temporal evolution and interrelationship between thermal environment and landscape patterns of Haikou City, 1989~2015[J]. China Environmental Science, 2019,**39** (4):1734-1743.

[8] Chang C R, Li M H, Chang S D. A preliminary study on the local cool-island intensity of Taipei city parks[J]. Landscape and Urban Planning,2006,**80**(4):386-395.

[9] Edward A G, David J C.Urban forest structure and land cover composition effects on land surface temperature in a semi-arid suburban area[J]. Urban Forestry & Urban Greening,2017,**28**:28-35.

[10] 刘艳红,郭晋平,魏清顺.基于 CFD 的城市绿地空间格局热环境效应分析[J].生态学报,2012,**32**(6):1951-1959.

Liu Y H, Guo J P, Wei Q S. Analysis of the thermal environment effect of urban green space spatial pattern based on CFD [J]. Acta Ecologica Sinica, 2012,**32** (6): 1951-1959.

[11] Xiao R, Cao W, Liu Y, *et al*. The impacts of landscape patterns spatio-temporal changes on land surface temperature from a multi-scale perspective: A case study of the Yangtze River Delta[J]. Science of the Total Environment, 2022, **821**, doi: 10.1016/J.SCITOTENV.2022.153381.

[12] Lirong D, Chun C. Thermal environment optimization and energy saving of residential buildings under the demand of low-carbon operation[J]. International Journal of Heat and Technology,2021,**39**(2):659-668.

[13] Xiao R B, Ouyang Z Y, Zheng H, *et al*. Spatial pattern of impervious surfaces and their impacts on land surface temperature in Beijing, China[J]. Journal of Environmental Sciences,2007,**19**(2):250-256.

[14] 姚晓洁,王霞,姚侠妹.基于 RS 技术的皖北城市阜阳市主城区热环境效应分析[J].生态学杂志,2021,**40**(10):3290-3303.

Yao X J, Wang X, Yao X M. Thermal environmental effect of the main urban area of Fuyang City in northern Anhui based on RS technology[J]. Chinese Journal of Ecology, 2021,**40**(10):3290-3303.

[15] Guha S, Govil H, Dey A, *et al*. A case study on the relationship between land surface temperature and land surface indices in Raipur City, India[J]. Geografisk Tidsskrift-Danish Journal of Geography,2020,**120**(1):35-50.

[16] 王鹏龙,张建明,吕荣芳.基于空间自相关的兰州市热环境[J].生态学杂志,2014,**33**(4):1089-1095.

Wang P L, Zhang J M, Lü R F. Urban thermal environment pattern with spatial autocorrelation in Lanzhou[J]. Chinese Journal of Ecology,2014,**33**(4):1089-1095.

[17] 林晋大,多玲花,邹自力.城市扩张背景下景观破碎化动态演变及空间自相关分析——以南昌市为例[J].水土保持研究,2022,**29**(4):362-369.

Lin J D, Duo L H, Zhou Z L. Dynamic evolution and spatial autocorrelation analysis of landscape fragmentation under the

background of urban expansion——A case study of Nanchang City[J]. Research of Soil and Water Conservation,2022,**29** (4): 362-369.

[18] 沈中健,曾坚.闽南三市城镇发展与地表温度的空间关系[J].地理学报,2021,**76**(3):566-583.
Shen Z J, Zeng J. Spatial relationship of urban development to land surface temperature in three cities of southern Fujian[J]. Acta Geographica Sinica, 2021,**76**(3):566-583.

[19] 冯悦怡,胡潭高,张力小.城市公园景观空间结构对其热环境效应的影响[J].生态学报,2014,**34**(12):3179-3187.
Feng Y Y, Hu T G, Zhang L X. The influence of spatial structure of urban park landscape on its thermal environmental effects[J]. Journal of Ecology,2014,**34**(12):3179-3187.

[20] Zheng Z, Zhou W Q, Yan J L, *et al*. The higher, the cooler? Effects of building height on land surface temperatures in residential areas of Beijing[J]. Physics and Chemistry of the Earth,2018,**110**:149-156.

[21] 宋鑫博,黄鹤,郭军,等.城市形态对夏季热环境影响研究——以天津中心城区为例[J].生态环境学报,2021,**30**(11):2165-2174.
Song X B, Huang H, Guo J, *et al*. Research on the impact of urban morphology on thermal environment in summer:A case of Tianjin Central City[J]. Ecology and Environmental Sciences,2021,**30**(11):2165-2174.

[22] 邬晓光.合肥市城市地理空间基础框架的建设与应用[J].城市勘测,2007,**22**,(6):23-25.
Wu X G. Construction and application of urban geospatial infrastructure framework in Hefei [J]. Urban Geotechnical Investigation & Surveying,2007,**22**,(6):23-25.

[23] 合肥市统计局.合肥统计年鉴[M].合肥:中国统计出版社,2020.

[24] 李莹莹,尤罗利,陈永生,等.环巢湖地区多水塘景观时空格局演变特征及其驱动因素[J].生态学报,2018,**38**(17):6280-6291.
Li Y Y, Yu R L, Chen Y S, *et al*. Spatial-temporal characteristics of multi-pond landscape change and their driving factors in the Chaohu Basin, China[J]. Acta Ecologica Sinica,2018,**38**(17):6280-6291.

[25] 陈晓华,吴仕嫱.南京——合肥双都市圈区域空间格局研究——基于城市流的视角[J].华东经济管理,2021,**35**(11):35-44.
Chen X H, Wu S Q. Research on the regional spatial pattern of Nanjing-Hefei double metropolitans:Based on the perspective of urban flow[J]. East China Economic Management,2021,**35**(11):35-44.

[26] 宋炳林,陈琳.长三角五大都市圈中心城市国际化水平比较研究[J].浙江社会科学,2017,**33**,(6):57-64,156-157.
Song B L, Chen L. A comparative study of the internationalization level of the central cities in the five metropolitan areas of the Yangtze River Delta[J]. Zhejiang Social Science,2017,**33**(6):57-64,156-157.

[27] Jiang Y, Lin W P. A comparative analysis of retrieval algorithms of land surface temperature from Landsat-8 data: A case study of Shanghai, China[J]. International Journal of Environmental Research and Public Health, 2021, **18**(11), doi:10.3390/IJERPH18115659.

[28] 胡光庭,王刚,杨崇俊.阳江市绿地空间分布及其热环境分析[J].遥感信息,2017,**32**(2):156-161.
Hu G T, Wang G, Yang C J. Analysis of green landscape distribution and thermal environment of Yangjiang City [J]. Remote Sensing Information, 2017,**32**(2): 156-161.

[29] Niloufar S, Touraj N, Shahrzad F, *et al*. Evaluating the spatial distribution and the intensity of urban heat island using remote sensing, case study of Isfahan city in Iran[J]. Sustainable Cities and Society,2019,**45**: 686-692.

[30] Wang F, Qin Z H, Song C Y, *et al*. An improved mono-window algorithm for land surface temperatu reretrieval from Landsat 8 thermal infrared sensor data[J].Remote Sensing ,2015,**7**(4):4268-4289.

[31] Zheng W W, Zeng Y N. Comparative analysis of two land surface temperature retrieval algorithms based on multi-source remote sensing data[J]. Applied Mechanics and Materials,2011,**130-134**,doi,10.4028/WWW.SCIENTIFIC.NET/AMM.130-134.4130.

[32] 孙艳伟,王润,郭青海,等.基于人居尺度的中国城市热岛强度时空变化及其驱动因子解析[J].环境科学,2021,**42**(1):501-512.
Sun Y W, Wang R, Guo Q H, *et al*. Estimation of the urban heat island intensity change and its relationships with driving factors across China based on the human settlement scale[J]. Environmental Science, 2021,**42**(1): 501-512.

[33] Qiao R R, Dong C Y, Ji S X, *et al*. Spatial scale effects of the relationship between fractional vegetation coverage and land surface temperature in Horqin Sandy Land, North China[J]. Sensors,2021,**21**,doi,10.3390/S21206914.

[34] 王晓蕾,石守海.基于 GEE 的黄河流域植被时空变化及其地形效应研究[J].地球信息科学学报,2022,**24**(6):1087-1098.

Wang X L,Shi S H. Spatio-temporal changes of vegetation in the yellow river basin and related effect of landform based on GEE[J]. Journal of Geo-information Science,2022,**24**(6):1087-1098.

[35] Zhu B,Yuan J Q. Pressure transfer modeling for an urban water supply system based on pearson correlation analysis[J]. Journal of Hydroinformatics,2015,**17**(1):90-98.

[36] 刘勇洪,徐永明,张方敏,等.北京城市空间形态对热岛分布影响研究[J].地理学报,2021,**76**(7):1662-1679.

Liu Y H, Xu Y M, Zhang F M, *et al.* Influence of Beijing spatial morphology on the distribution of urban heat island[J]. Acta Geographica Sinica, 2021,**76**(7): 1662-1679.

[37] 葛静茹,王海军,贺三维,等.武汉市都市发展区地表温度季节性空间分布与驱动力分析[J].长江流域资源与环境,2021,**30**(2):351-360.

Ge J R, Wang H J, He S W, *et al*. Seasonal-spatial distribution and driving forces of land surface temperature in the urban development area of Wuhan[J]. Resources and Environment in the Yangtze Basin,2021,**30**(2):351-360.

[38] 李莹莹,邓雅云,陈永生,等.基于卫星遥感的合肥城市绿色空间对热环境的影响评估[J].生态环境学报,2018,**27**(7):1224-1233.

Li Y Y, Deng Y Y, Chen Y S, *et al*. Analysis on cooling effect of urban parks on urban thermal environment in Yinchuan City based on remote sensing [J]. Ecology and Environmental Sciences, 2018,**27**(7):1224-1233.

[39] 孔繁花,尹海伟,刘金勇,等.城市绿地降温效应研究进展与展望[J].自然资源学报,2013,**28**(1):171-181.

Kong F H, Yin H W, Liu J Y, *et al.* A review of research on the urban green space cooling effect[J]. Journal of Natural Resources,2013,**28**(1):171-181.

[40] Sresto M A, Morshed M M, Siddika S, *et al.* Impact of COVID-19 lockdown on vegetation indices and heat island effect: A remote sensing study of Dhaka City, Bangladesh[J]. Sustainability,2022,**14**(13),doi:10.3390/SU14137922.

[41] 陈斌,徐尚昭,杨顶田,等.武汉市主城区公园景观的热环境效应[J].遥感信息,2021,**36**(3):58-66.

Chen B, Xu S Z, Yang D T, *et al.* Thermal environmental effects of park landscape of main urban region in Wuhan[J]. Remote Sensing Information, 2021,**36**(3): 58-66.

[42] 张晓东,赵银鑫,马风华,等.基于遥感数据的银川市城市公园对城市热环境降温效应分析[J].水土保持通报,2021,**41**(5):338-347.

Zhang X D, Zhao Y X, Ma F H, *et al.* Analysis of cooling effect of Yinchuan urban park on urban thermal environment based on remote sensing data [J]. Bulletin of Soil and Water Conservation, 2021,**41**(5):338-347.

[43] 王莹书,石培基,赵武生,等.兰州市热环境时空特征及影响因素研究[J].生态科学,2022,**41**(2):59-65.

Wang Y S, Shi P J, Zhao W S, *et al.* Spatial-temporal characteristics and influencing factors of thermal environment in Lanzhou[J]. Ecological Science,2022,**41**(2):59-65.

[44] 梁建设,白永平,杨雪荻,等.基于多源数据的城市扩张中热环境演变及响应[J].环境科学,2022,**43**(6):3365-3374.

Liang J S, Bai Y P, Yang X D, *et al*. Evolution and response of the thermal environment in urban expansion based on multi-source data [J]. Environmental Science, 2022,**43**(6): 3365-3374.

[45] 史宝刚,尹海伟,孔繁花,等.基于 ENVI-met 模型的南京市新街口地区垂直绿化降温效应评价[J].现代城市研究,2021,**35**(12):125-132.

Shi B G, Yin H W, Kong F H, *et al.* Assessment of the cooling effect for urban facade greening in Xinjiekou District, Nanjing, China[J]. Modern Urban Research,2021,**35**(12):125-132.

[46] 丁威,王鹏,黄威,邓剑,等.考虑局域气候影响的海绵城市垂直绿化技术应用[J].中国给水排水,2019,**35**(12):85-87.

Ding W, Wang P, Huang W, *et al.* Application of vertical greening technology in sponge city with influence of local climate[J]. China Water & Wastewater, 2019,**35**(12):85-87.

第51卷第11期 中国科学技术大学学报 Vol. 51, No. 11
2021年11月 JOURNAL OF UNIVERSITY OF SCIENCE AND TECHNOLOGY OF CHINA Nov. 2021
Received: 2021-04-21; Revised: 2021-08-09 doi: 10.52396/JUST-2021-0114

Summer thermal performance study on pipe-embedded PCM composite wall in existing buildings

CHEN Sarula[1,4], CHANG Tianxin[1], YANG Yang[2*], PAN Chao[1], WU Yunfa[1,3,4]
1. College of Architecture and Urban Planning, Anhui Jianzhu University, Hefei 230601, China;
2. College of Architecture and Art, Hefei University of Technology, Hefei 230009, China;
3. State Key Laboratory of Fire Science, University of Science and Technology of China, Hefei 230027, China;
4. China-Portugal Joint Laboratory of Cultural Heritage Conservation Science, Suzhou 215031, China
* Corresponding author. E-mail: yangyang2017@tju.edu.cn

Abstract: Pipe-embedded building envelope is a heavyweight thermo-activated building system (TABS) that has its pipe circuits inside the building envelope, which has been seldom studied in existing buildings. In this context, the pipe-embedded PCM composite wall (PEPCW) in which the pipe-embedded interlayer is relocated to the outside of the load-bearing layer and replaced by macro-encapsulation-based pipe-embedded PCM panel is proposed to address the retrofitting challenges. In this paper, the summer thermal performance and energy saving potential of PEPCW are evaluated through a validated mathematical model. The simulation tests verify the effectiveness of PEPCW in cooling load reduction, and the corresponding amplitude value of interior surface temperature and heat flux can be decreased by 1.1 ℃ and 9.9 W·m^{-2}, respectively. Besides, the parametric tests indicate that the pipe interval has a more obvious influence than PCM thickness, and the value of 300/30 mm (pipe interval/PCM thickness) is recommended. Furthermore, the effectiveness of PEPCW is proved to be satisfactory in the three different cities (i.e., Tianjin, Nanjing, and Guangzhou), and the maximum heat gain reduction (i.e., 39.30 kWh·m^{-2}) is observed in hot summer and warm winter region (i.e., Guangzhou). In addition, the influence of solar absorbance on conditioned space at different orientations can be remarkably reduced through PEPCW, and the reduction in the three sunny sides are relatively higher than the dark side (i.e., north). Overall, the proposed PEPCW presents a satisfactory thermal behavior in the cooling season and could contribute to the progress of energy saving retrofit in the vast existing buildings.

Keywords: thermal performance; TABS; PCM; mathematical model; existing buildings
CLC number: TU111.4 **Document code**: A

1 Introduction

The building sector is one of the three major non-renewable energy consumers, causing about 40% of all terminal energy need around the world[1,2]. Statistics data shows that up to 50% of primary energy has been consumed to thermally regulate the heating/cooling load and condition indoor environment[3]. Actually, the external envelope, as an interface directly connects the inside and outside space, can highly affect the total energy demand and comfort feeling of users[4]. It should be noted that most of the existing buildings no doubt have a higher energy consumption rate than new-built buildings, especially those with a little or without any energy saving measures[5]. These affirm the urgency of exploring appropriate retrofitting measures to realize high-efficient existing buildings in either China or other countries.

Traditionally, insulating the building fabric and increasing the total thermal resistance is a common practice among designers and service engineers. This is usually effective in the heating season, however, it may also have a negative impact on heat dissipation in transition and cooling season when theoutdoorenvironment is suitable for exploiting the natural coldness resource (NCR). For example, Ji et al[6] reported that the dwelling buildings in the UK with a high level of insulation are often facing the problem of summer overheating, and the internal heat, therefore, has to be conditioned by chillers which no doubt would increase the energy consumption. Besides, increasing the insulation thickness is also limited by the aging and fire safety, lower heat capacity and the home builders' desire to provide maximum internal space[1].

Citation: Chen Sarula, Chang Tianxin, Yang Yang, et al. Summer thermal performance study on pipe-embedded PCM composite wall in existing buildings. J. Univ. Sci. Tech. China, 2021, 51(11): 840-856.

(C)1994-2022 China Academic Journal Electronic Publishing House. All rights reserved. http://www.cnki.net

Nomenclature

T	temperature, ℃		*Greek symbols*
T_F	melting/solidifying temperature, ℃	ρ	density, kg · m^{-3}
T_e	outdoor temperature, ℃	ρ_s	surface absorptance, –
T_{in}	room temperature, ℃	λ	thermal conductivity, W · m^{-1} · ℃$^{-1}$
$T_{x=0}$	interior surface temperature	η	efficiency, –
$T_{x=L}$	exterior surface temperature	Γ_Φ	diffusion coefficient, –
R_{ES}	radiation heat exchange, W · m^{-2}	α	heat transfer coefficient, W · m^{-2} · ℃
H	pump head, m	θ_e	exterior surface temperature, ℃
G	design capacity, m^3 · h^{-1}	Φ	common variable
L	length, m		
c_p	specific heat capacity, J · kg^{-1} · ℃$^{-1}$		Abbreviation and subscripts
h	enthalpy, J · kg^{-1}	TABs	thermo-activated building system
U	velocity vector, –	PEPCW	pipe-embedded PCM composite wall
S_Φ	source term	GSHE	ground-source heat exchanger
r	volume liquid fraction, –	MRT	mean radiant temperature
L	latent heat, J · kg^{-1}	PVR	photovoltaic radiant panel
q	heat flux, W · m^{-2}	NCR	natural coldness resource
I	solar radiation, W · m^{-2}	PCM	phase change material
t	time, minute or hour	XPS	extruded polystyrene foam boards
b	thickness	ASHP	air-source heat pump
l/s	liquid/solid state of PCM	HVAC	heating, ventilation and air conditioning
U	velocity vector, –	ref	reference
S_Φ	source term	k/i	Water/ PCMs
r	liquid fraction, –	j	cement (j=1), XPS (j=2) and brick (j=3)

Thermal mass application is another common approach, which is functioning in dampening the temperature fluctuations within a building based on its ability to absorb and store heat. Among different thermal mass applications, PCM is regarded as a novel energy-saving approach due to its capacity of being able to store and release the heat to reduce the load caused by building envelopes[7]. It is reported that the energy storage capacity of a 5.0 mm PCM composite wall almost equals to an 8.0 cm thick concrete wall, and the energy storing capacity of a 1.5 cm thick gypsum-based PCM wall is 5-times higher than a usual gypsum board and equals to a 12.0 cm thick wall[8,9]. Meanwhile, macro-encapsulation PCM has been regarded as one kind of feasible package methods in building areas[10-13]. For example, Vicente et al[11] reported that the combination of macro-encapsulated PCM wall and 10.0 cm XPS external insulation could result in an 80% reduction of thermal amplitude. Despite the many advantages of PCM, the passive application of PCM is usually limited to a mild climate region where the external temperature is near to the melting/solidification zone[14,15]. That is why more than one kinds of PCM are integrated into the same building envelope to achieve year-round thermal management[16,17].

Therefore, new cost-effective alternatives to traditional thermal insulation and thermal mass approaches are required. The thermo-activated building system (TABs) appears to be an attractive technology by integrating the building structure to act as an energy-storage to make useful reductions in domestic energy use[18]. Primarily, TABs is a water-based regulating circulatory system coupled with the heavy building thermal mass (usually thick concrete slabs in ceilings or floors). And the replacement of the old air-based paradigm with water-based paradigm as well as the use of the building structure for energy storage is the two keys of TABs. Recently, the pipe-embedded building envelope in walls and windows, as a new type of heavyweight TABS, has gained increased attention[19,20]. Owing to its high efficiency under a small temperature difference condition, pipe-embedded building envelope greatly relaxes the restrictions on heat source temperature. This allows for the utilization of widespread close-to-free energy sources: e. g. solar energy, shallow geothermal energy and industrial waste heat in the heating season[21]; and NCR stored by ground source heat exchangers (GSHE) or radiate cooling through radiant panels in the cooling season[22,23].

For the pipe-embedded exterior wall, Zhou et al[19] reviewed the heat transfer calculation models of TABS and brought forward the early concept of the pipe-embedded building envelope coupled with GSHE and

(C)1994-2022 China Academic Journal Electronic Publishing House. All rights reserved.　http://www.cnki.net

solar collectors. They also developed different validated frequency-domain finite-difference (FDFD) models to predict heat transfer performances[24]. A thermal-water activated wall outfitted with mini-tube capillary-network is presented by Yu et al[25] and its transient thermal behavior influenced by water temperature and the flow rate was numerically examined in the summer condition. Their results supported the advantage of this type of composite wall in stabilizing the interior wall surface temperature and reducing the building energy consumption. Shen et al[26] utilized the air source heat pumps (ASHP), evaporative cooling (cooling tower) and natural heat sources (underground soil and water) as the source of low-temperature hot water or high-temperature cold water and comprehensive parametric studies (including climate regions, orientations, water temperatures) of the composite transparent/opaque building envelopes were conducted both in the heating and cooling season through numerical methods.

The pipe-embedded interlayer is usually not visible owing to the water-carrying pipes are placed inside the building envelope, which is of particular interest to architects[27]. Meanwhile, the above studies also have clearly highlighted the energy saving potential of the pipe-embedded building envelope. However, some limitations still exist in current studies and the application challenges of the pipe-embedded building envelope also will potentially prevent its large-scale promotion in practice. On the one hand, almost all previous studies focus on new-built buildings. Obviously, configurations of the pipe-embedded building envelopes for new-built buildings are not suitable for the existing buildings that lack the condition of reconfiguring its structures. Also, applications of the pipe-embedded building envelope in the current configurations usually presents a disadvantage in the aspect of malfunctions[28], making repairs difficult without major interventions on site. Though a closed pipe-embedded exterior wall system (with water pipe outside of the concrete layer) to harvest and absorb the solar heat gain in the south to intercept the heat loss in the north is proposed by Reference [21], this system can only play a limited role in a certain condition in the winter. On the other hand, the aforementioned studies on the pipe-embedded building envelopes have placed more focus on the thermal behavior and energy saving potential at the component level, and further savings and heat transfer enhancement through system operation control have merely been mentioned. Actually, the intermittent operation mode has been adopted in diverse fields including radiant ceilings/floors[18], which could effectively enhance the heat transfer and economic performance. It also should be pointed out that "clean energy heating/cooling" has earned abundant government supports especially in China that is suffering from serious air pollution[29]. Recently, a package of clean energy policies has been released by the Chinese government related to "peak-valley time-of-use price", "replacing heating coal with electricity" and "replacing heating coal with natural gas"[29], etc. These affirm the enormous potential of utilizing the pipe-embedded system with a cheaper electricity price during the valley period.

Despite the significant number of works in the literature dealing with the utilization of PCM in passive applications, not so many articles can be found on PCM in active building systems[30]. Current studies almost are all about PCM in ceiling panels or radiant floors[31-35]. Mazo et al[30] described a model developed to simulate a radiant floor system with PCM in simple building types. The PCM radiant floor model was based on a one-dimensional finite difference scheme where the effective capacity method is used for PCM simulation. To shift the cooling/heating load from the peak period to the off-peak period and also address the application problem of the radiant PCM floor in areas which both need cooling and heating in different seasons, Zhang et al[33-34] proposed and numerically studied a double layer PCM floor with different melting temperature. Koschenz et al[35] proposed a chilled ceiling panel coupled with PCM, this chilled ceiling panel device was designed to absorb a heat flux of 40 $W \cdot m^{-2}$ during 8.0 h without producing an increase in temperature above the comfort range. Therefore, the effectiveness of an active building system integrated with PCM for cooling and heating has been verified.

As illustrated in Figure 1, in this paper, a macro-encapsulated PCM based pipe-embedded composite wall (PEPCW) is proposed as a feasible and cost-effective energy saving retrofit idea for building designers and engineers, which can decrease the heat/cold loss through the building envelope in winter/summer by relocating the pipe-embedded interlayer to the outside of the load-bearing layer. To verify its effectiveness, an experimentally validated mathematical model has been developed to explore the transient summer thermal performance of the PEPCW and the corresponding potential to reduce the cooling load. Further, a comprehensive parametric study is carried out to reveal the influence of some key design parameters, including pipe interval and PCM thickness, which is useful for engineers and architects to evaluate the impact of these parameters on heat loss through practical PEPCW. Besides, the effect of the climate region and building orientation on the thermal performance is also evaluated. This research seeks to enrich the existing energy saving retrofit approaches for the vast existing buildings, supplement the current academic research in

(C)1994-2022 China Academic Journal Electronic Publishing House. All rights reserved. http://www.cnki.net

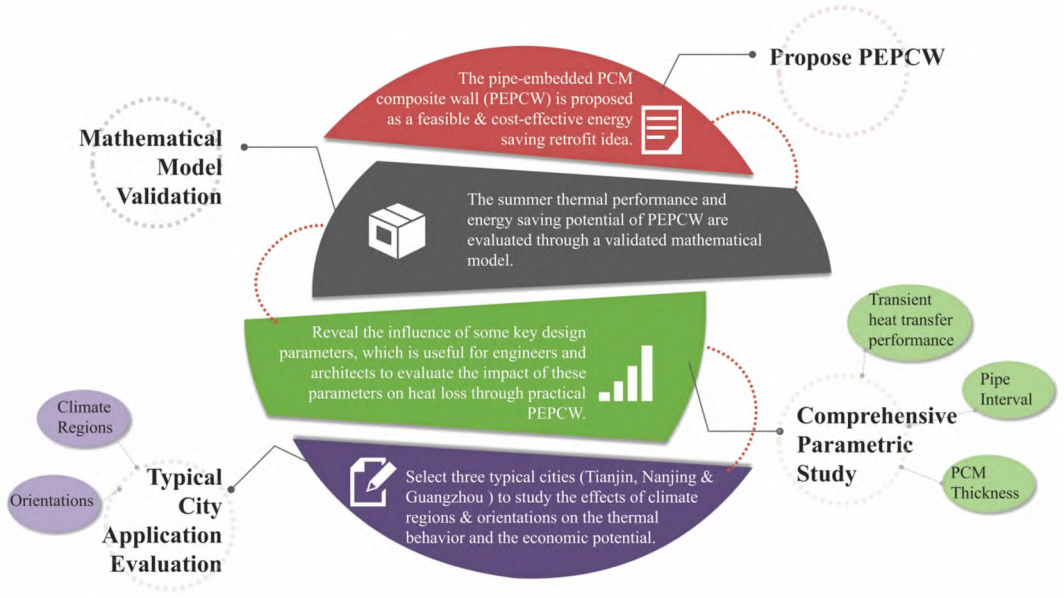


Figure 1. The main works done in the study.

the field of pipeline embedded building envelope structures, and provide the data and theoretical guidance for further research on PEPCW.

2 Mathematical model and validation

2.1 Geometric description

The PEPCW system basically consists of pipe-embedded PCM composite wall and local low-grade water source. In this paper, the embedded pipe is circulated with high-temperature cold water produced from GSHE or PVR during valley period to take away the heat inside of the wall and finish the coldness charging process simultaneously. As illustrated in Figure 2, the studied PEPCW is a typical 240 mm wall unit integrated with PCM interlayer and serpentine polythene pipes. The dimensions of the studied control volume are 2800 mm (length, i. e., room height), 350 mm (width, i. e., wall thickness) and 300 mm (height, i. e., pipe interval). The diameter of the embedded pipe is 20 mm. Due to the different U-value limit requirements in different climate regions[36], the insulation layer thicknesses for the three studied Chinese cities are 64 mm (cold/Tianjin), 36 mm (hot summer and cold winter/Nanjing) and 22 mm (hot summer and warm winter/Guangzhou). Macro-encapsulated organic paraffin RT24[37] through shaped aluminum plates is selected as the PCM interlayer. As such, modular production, installation and leakage risk of PEPCW could be well addressed and the building structure also would not be much affected. The material properties and geometric dimensions of PEPCW unit are given in Table 1.

2.2 Governing equations and boundary conditions

The three-dimensional heat transfer process of PEPCW is illustrated in Figure 2. In order to simplify the numerical process, some necessary assumptions are made as follows: ① Symmetry boundary conditions are considered between the serpentine pipes[21], as shown in Figure 2 (b); ② the longwave radiation heat exchange between the exterior wall surface and outdoor environment is considered in the form of sol-air temperature (T_o)[38]; ③ the thermophysical properties of materials are constant and they are thermally homogenous and isotropic except for the PCM in the phase change process[39]; ④ the thermal contact resistance between inner layers of PEPCW are ignored; ⑤ thermal expansion of PCM is neglected; ⑥ when the water inlet velocity is 0.5 m·s^{-1} from 23:00-06:00, it is the valley period that the PEPCW is deactivated (mass flow = 0), and the fluid inside the pipes is assumed to be a solid zone until 06:00-23:00 when the water velocity is 0 m·s^{-1}, PEPCW is reactivated (mass flow>0)[40].

The computation domain for PEPCW mainly consists of three parts (the PCM region, solid region and fluid region). For PCM region, two methods (enthalpy-porosity method and equivalent heat capacity method) are provided in Fluent solver in order to model the solidification/melting process[41]. Among them, the enthalpy-porosity method which determines the enthalpy value in the energy equation is proved to be better by numerically solving Navier-Stokes partial differential equations of mass, energy, and momentum[42,43]. The total enthalpy value covers both sensible and latent parts in which the latent enthalpy is evaluated as a percentage of the latent heat of

(C)1994-2022 China Academic Journal Electronic Publishing House. All rights reserved.　http://www.cnki.net

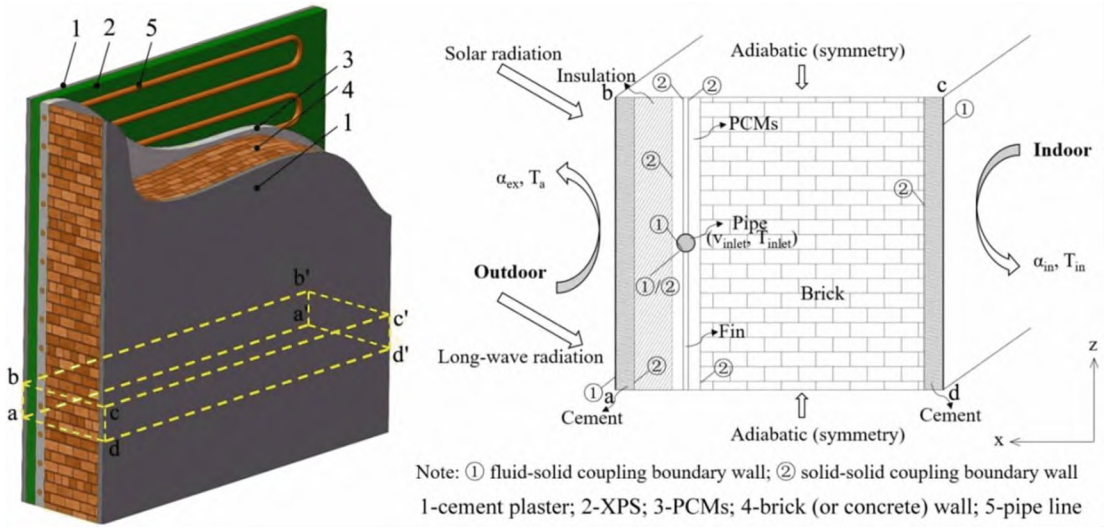


Figure 2. Geometry model and heat transfer process of PEPCW.

Table 1. Thermophysical properties and geometric size of PEPCW model.

Material	Density ρ (kg · m^{-3})	Thermal conductivity λ(W · m^{-1} · ℃$^{-1}$)	Specific heat c_p(J · kg^{-1} · ℃$^{-1}$)	Latent heat L (kJ · kg^{-1})	Thickness b(mm)	Melting/ Congealing T_F (℃)
Cement plaster	1800	0.930	1050	/	20	/
XPS	30	0.042	1380	/	64(Tianjin) 36 (Nanjing) 22(Guangzhou)	/
Brick	1500	0.640	879	/	120	/
Copper pipe	8978	387.600	381	/	2	/
PCMs	880 (l) 770 (s)	0.200 (l) 0.200 (s)	2000	260	30, 40, 50	21–25 (l) 25–21 (s)
PCM container	2719	202.400	871	/	1	/

$$\rho_i \frac{\partial h}{\partial t} = \lambda_i \left(\frac{\partial^2 T}{\partial x^2} + \frac{\partial^2 T}{\partial y^2} + \frac{\partial^2 T}{\partial yz^2} \right) \quad (1)$$

where ρ is the density (kg · m^{-3}) , λ is the thermal conductivity coefficient (W · m^{-1} · ℃$^{-1}$) , C_p is the specific heat capacity at constant pressure (J · kg^{-1} · ℃$^{-1}$) and h is the enthalpy (J · kg^{-1}) . The subscript i represents the PCM.

Further, the enthalpy of the PCM interlayer is computed as follows:

$$h = h_{ref} + \int_{T_{ref}}^{T} C_p dT + rL \quad (2)$$

where T_{ref} is the reference temperature when the specific enthalpy is zero (T_{ref} = 0℃) . H_{ref} is the specific enthalpy at the reference temperature (H_{ref} = 0 kJ · kg^{-1}) . r is the local liquid fraction in the calculation region of PCM interlayer. L is the latent heat of PCM in the whole phase change process (J · kg^{-1}) .

Besides, the volume liquid fraction of the PCM domain is defined as:

$$r = \begin{cases} 0, \text{if } T < T_F(s) \\ 1, \text{if } T > T_F(l) \end{cases} \quad (3)$$

where T_F is the melting and solidifying temperature (℃) .

For the solid area, the energy controlling equation is written as follows:

$$(\rho c_p)_j \frac{\partial T}{\partial t} = \lambda_j \left(\frac{\partial^2 T}{\partial x^2} + \frac{\partial^2 T}{\partial y^2} + \frac{\partial^2 T}{\partial yz^2} \right) j = 1,2,3 \quad (4)$$

where j represents the cement plaster(j = 1) , XPS (j = 2) and clay brick (j = 3) , respectively.

For fluid area, the energy governing equation is given as:

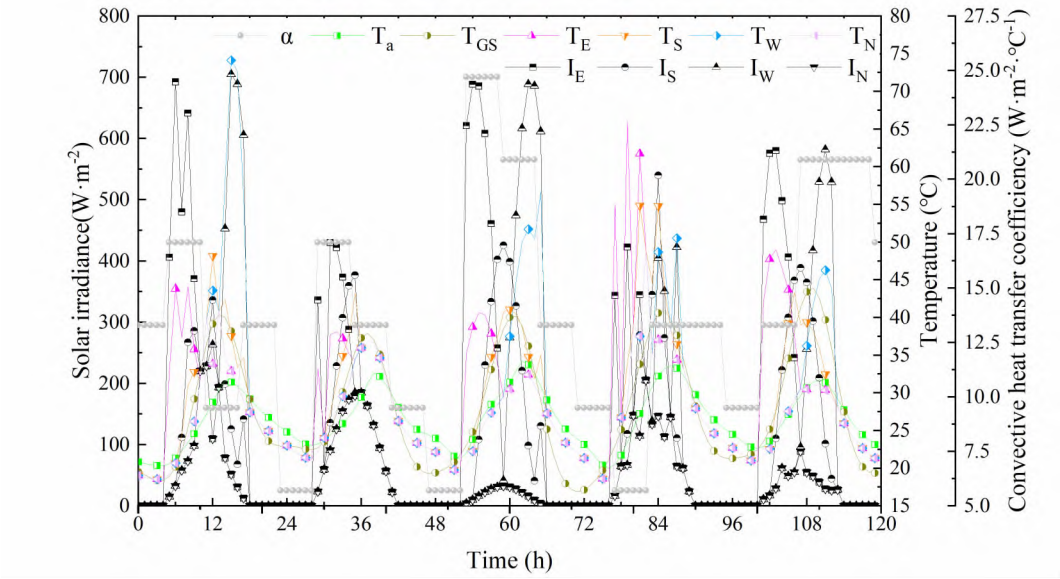
$$\frac{\partial(\rho_k \Phi)}{\partial t} + \nabla(\rho \overline{U} \Phi) = \nabla(\Gamma_\Phi grad \Phi) + S_\Phi \quad (5)$$

The boundary condition for the interior surface is defined as:

$$\lambda \left. \frac{\partial T}{\partial x} \right|_{x=0} = \alpha_{in}(T_{in} - T_{x=0}) \quad (6)$$

where λ_0(W · m^{-1} · ℃$^{-1}$) is the thermal conductivity coefficient of internal cement plaster. α_{in}(W · m^{-2} · ℃$^{-1}$) is the synthetic surface heat transfer coefficient, here the value is set to 8.7[44]. T_{in} is the indoor temperature setpoint (26 ℃) and $T_{x=0}$ (℃) is the interior wall surface temperature recorded in the Fluent solver.

(C)1994-2022 China Academic Journal Electronic Publishing House. All rights reserved. http://www.cnki.net



Appendix 1. Meteorological data of typical five days in Tianjin

For the boundary exposed to the ambient, it is defined as:

$$\lambda \left.\frac{\partial T}{\partial x}\right|_{x=L} = \alpha_{ex}(T_a - T_{x=L}) + \rho_s I - R_{ES} \quad (7)$$

where λ_L(W · m^{-1} · ℃$^{-1}$) is the thermal conductivity of external cement plaster. α_{ex}(W · m^{-2} · ℃$^{-1}$) is the exterior surface heat transfer coefficient, and the α_{ex} is calculated by Eq. (8)[45]. T_a and $T_{x=L}$(℃) is the outdoor temperature and the exterior wall surface temperature, respectively. ρ_s is the external surface solar absorptance, which is 0.65 according to the Chinese code[46]. I (W · m$^{-2)}$ is the solar irradiation. R_{ES}(W · m$^{-2)}$ is the longwave radiation heat transfer between the external surface and ambient.

$$\alpha_{ex} = 5.62 + 3.9v \quad (8)$$

The sol-air temperature (T_o, ℃) is given as follows[46]:

$$T_o = \frac{I \cdot \rho_s}{\alpha_{ex}} + T_a \quad (9)$$

The boundary condition for the inside contact interfaces where there is no phase change transition to occur is defined as:

$$-\lambda \left.\frac{\partial T}{\partial x}\right|_{x,\text{layer1}} = -\lambda \left.\frac{\partial T}{\partial x}\right|_{x,\text{layer2}} \quad (10)$$

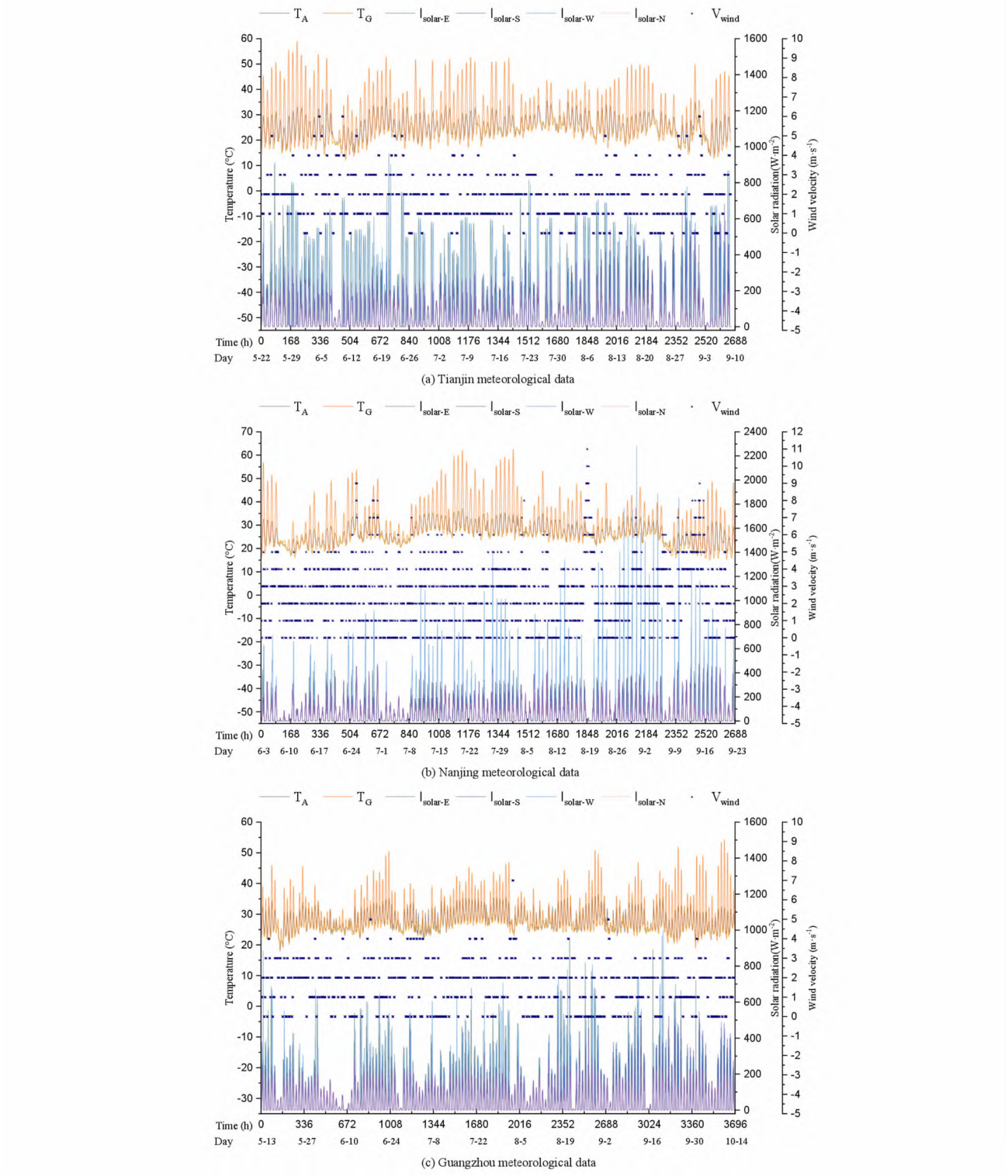
Otherwise, the boundary condition for the contact interface is given as:

$$-\lambda \left.\frac{\partial T}{\partial x}\right|_{x,\text{layer1}} = L\rho_j \frac{\partial r}{\partial t} - \lambda \left.\frac{\partial T}{\partial x}\right|_{x,\text{layer2}} \quad (11)$$

2.3 Numerical procedure

The numerical computation is carried out with the commercial CFD software, i. e., Fluent. Before the simulation, grid independence has been checked, and the total element and the node number of the PEPCW unit are 112750 and 119340, respectively. The governing equations are discretized by the second-order upwind scheme for advection terms and central differencing scheme, and the coupling of the velocity and pressure fields was carried out by using the SIMPLE algorithm. Due to the turbulence of cycling water, the standard $k-\varepsilon$ model (STD$k\varepsilon$) coupled with enhanced wall treatment (EWT) method is employed. All the meteorological data used in the simulation in the full text are from the special meteorological dataset for building thermal environment analysis of China[46]. Among them, the transient thermal performance of the TAPCW system in section 3.1 and a parametric study about pipe interval and PCM thickness in section 3.2 was firstly evaluated under Tianjin climate scenario. Correspondingly, the chosen meteorological data (i. e., solar irradiance, outdoor environment temperature and wind velocity) and calculated sol-air temperature from August 9 to 13 in Tianjin is showed in appendix 1. Following that the whole cooling season evaluation was taken in to account to evaluate the influence of climate and orientation of three typical cities in section 3.3 and 3.4. The cooling season in the mentioned three cities is May 22- Sep. 09 (Tianjin, 111 days) , Jun. 03- Sep. 24 (Nanjing, 114 days) and May 13 - Oct. 19 (Guangzhou, 160 days) , respectively. For details of the meteorological data is showed in appendix 2. During the simulation, the water temperature is 21 ℃ and the velocity is 0.5 m · s^{-1}. The characteristic change inside of the water zone as well as the boundary conditions is accomplished automatically through recorded journal-files and user-defined functions (UDF) . The time step size is defined as 15 seconds and the boundary

(C)1994-2022 China Academic Journal Electronic Publishing House. All rights reserved.　http://www.cnki.net



Appendix 2. Meteorological data for three typical cities

conditions are changed every 60 minutes according to the available meteorological data. The convergence criteria are 10^{-7} for the residuals of the energy equation. To eliminate the thermal storage effect on the simulation results, the simulation for all of the cases has already calculated 5 days before the actual starting date[10].

2.4 Model validation

To verify the numerical model of PEPCW, a validation test is done and compared with the experiment result and simulation results presented in Reference [48]. Figure 3 shows a pipe-embedded PCM hot water wall mainly used for indoor radiant heating. The PEPCW studied in

(C)1994-2022 China Academic Journal Electronic Publishing House. All rights reserved. http://www.cnki.net

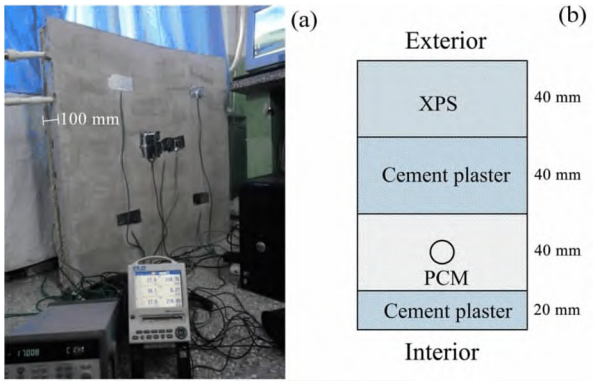


Figure 3. Test rig (left) and configuration of the radiant PCM wall (right) for validation.

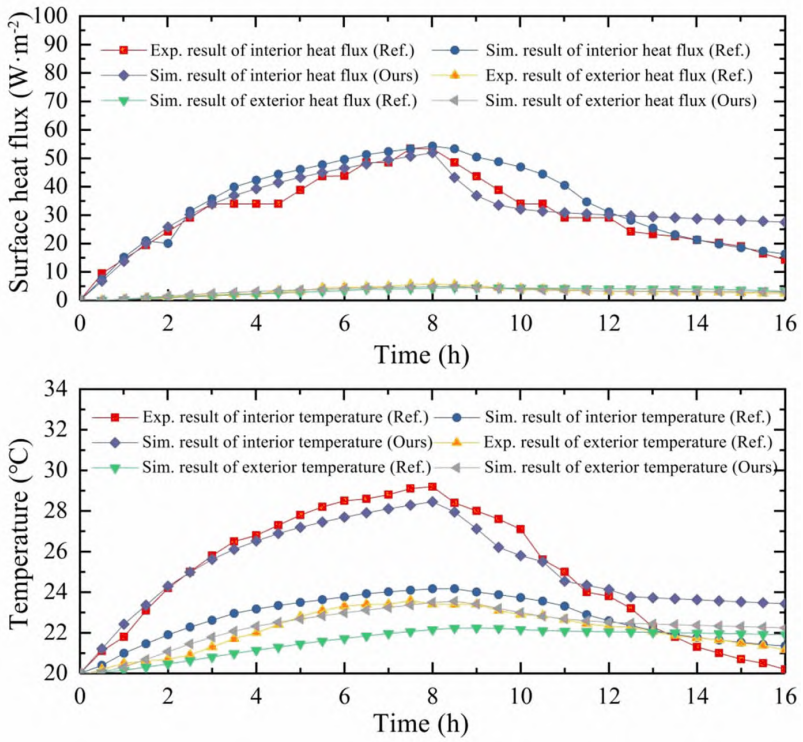


Figure 4. Comparison of the numerical and experimental results.

this paper is similar to the pipe-embedded PCM hot water wall in the aspect of structure, heat transfer process and boundary conditions. Usually, the parameter change (including the position, thermophysical and geometric) of the non-core structural layer has a slight impact on the numerical model. For the research object that has a similar heat transfer process and boundary conditions, lots of researchers have adopted this method in their parametric studies and comparative studies[26]. As shown in Figure 3 (a) , the dimension of the experimental radiant wall unit is 1000 mm × 1000 mm × 100 mm. The test wall unit consisted of a 40 mm XPS (exterior) followed by two layers of cement plaster that are 40 mm and 20 mm thick with a 40mm layer of PCM layer between them. The PCMs adopted in the referenced test is the mixture of 48 # solid paraffin and liquid paraffin provided by Sinopharm Chemical Reagent Beijing Co. , Ltd, and the melting temperature and latent heat of fusion are 27. 8 ℃ and 145. 4 kJ · kg^{-1}. The external diameter and internal diameter of the PE pipe are 20 mm and 17. 4 mm, respectively. The pipe interval is 150 mm. During the whole indoor test period, the indoor air temperature is kept constant at 20 ℃. 10 thermocouples and multi-point heat flow meter (KEM-HFM-215) distributed as Figure 3 (b) are fixed at both side of the interior and exterior surface to monitor the dynamic temperature and heat flux profile during the test. The initial temperature of the test wall unit is 20 ℃. The whole intermittent operation test lasts 16 hours with a continuous hot water

(C)1994-2022 China Academic Journal Electronic Publishing House. All rights reserved.　http://www.cnki.net

charging (50 ℃) during the first 8 hours.

Regarding the validation, a geometry model with the same dimensions of experimental test rig of Huo [48] is built in ANSYS. After that, the numerical results of the validation test are validated against both the experimental and numerical data. As can be seen in Figure 4, both the heat flux and temperature at the interior and exterior surface keep the same trend and agree well with the experimental result. Also, the simulation results obtained by us have an obvious improvement compared with that of Huo [48]. However, there also exists some difference between the experimental and numerical (ours) results. Taking their experimental results as the benchmark, the average relative value of the temperature and heat flux at the interior/exterior surface are 4.1%/2.7% and 17.4%/14.4% respectively. Compared with the average relative value of temperature, the relative value of heat flux is bigger. It should be noted that the value difference in the first 12 h is obvious than the last 4 h, which indicates that the calculation precision is different at different times. This could be attributed to the reasons as follows: (1) the thermophysical properties of the PCM given in the literature is not exactly accurate, especially in the melting/solidification temperature range, which may result in the value difference in heat charge/discharge process; (2) the installation error and cavities inside the PCM layer cannot be avoided in the experimental test especially for a macro-encapsulated PCM application, which may also change the equivalent thermophysical properties of PCM as the PCM layer is treated as an ideal PCM region without any thermal expansion or cavities in the simulation. In view of that, the accuracy of the numerical model is satisfying for engineering application with a macro-encapsulated PCM interlayer. The model can be used to study the thermal behavior of PEPCW and carry out parameter studies.

3 Results and discussion

3.1 Transient heat transfer performance analysis

In this section, the composite wall in south orientation is examined as an example in a typical day in the hottest month of Tianjin (Aug 13, the meteorological data is showed in appendix 1). It should be noted that a five day's simulation is conducted in all studied cases and only the results the last cycle are used for further analysis. For the PEPCW wall, the pipe interval is 300 mm and the PCM thickness is 30 mm. Hourly variations of surface heat flux, temperature and the liquid fraction inside of the PCM layer are presented in Figure 5. When the interior surface heat flux is negative, it means that the thermal energy is released to the indoor space, which is the so-called building cooling load. Conversely, when this value is positive, it states that the interior surface temperature is lower than the indoor setting point and therefore it absorbs heat from the room space, representing a supplementary cooling process. As is shown in Figure 5 (a), the interior surface of PEPCW is significantly 'decreased' during the simulation test and the maximum value difference of interior heat flux between the PEPCW and the ordinary wall is up to 9.9 $W \cdot m^{-2}$. It could be found in Figure 5 (b) that the PEPCW exhibits a much lower maximum interior surface temperature. In detail, the peak value of the interior surface temperature decreased by 1.1 ℃ compared with the ordinary wall. It also could be observed that the interior surface temperature of the ordinary wall shows a time lag of 12 h, which usually causes extra and unnecessary cooling measures during the nighttime due to the higher mean radiant temperature (MRT). With the pipe-embedded PCM layer, the interior surface temperature is lower than 26 ℃ throughout the test, which means the MRT could be significantly reduced. Consequently, the PEPCW system could not only cut down the energy consumption

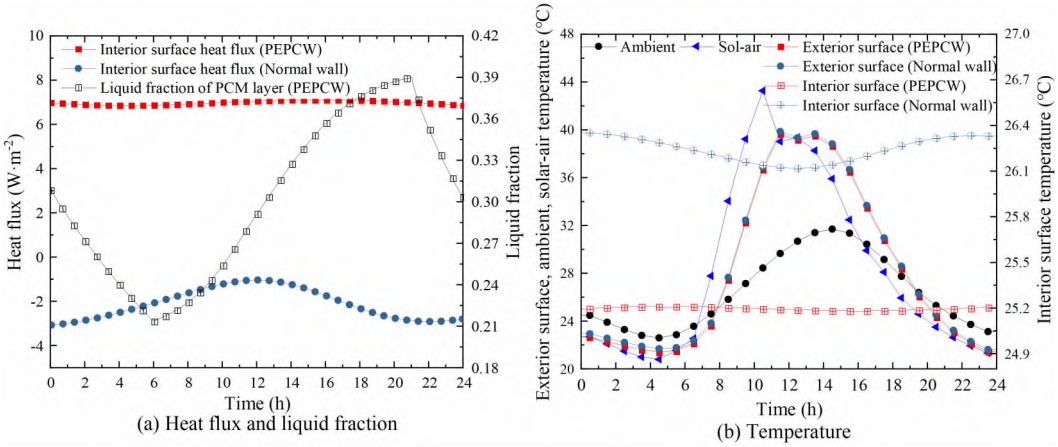


Figure 5. Heat flux and temperature variation of the PEPCW.

(C)1994-2022 China Academic Journal Electronic Publishing House. All rights reserved. http://www.cnki.net

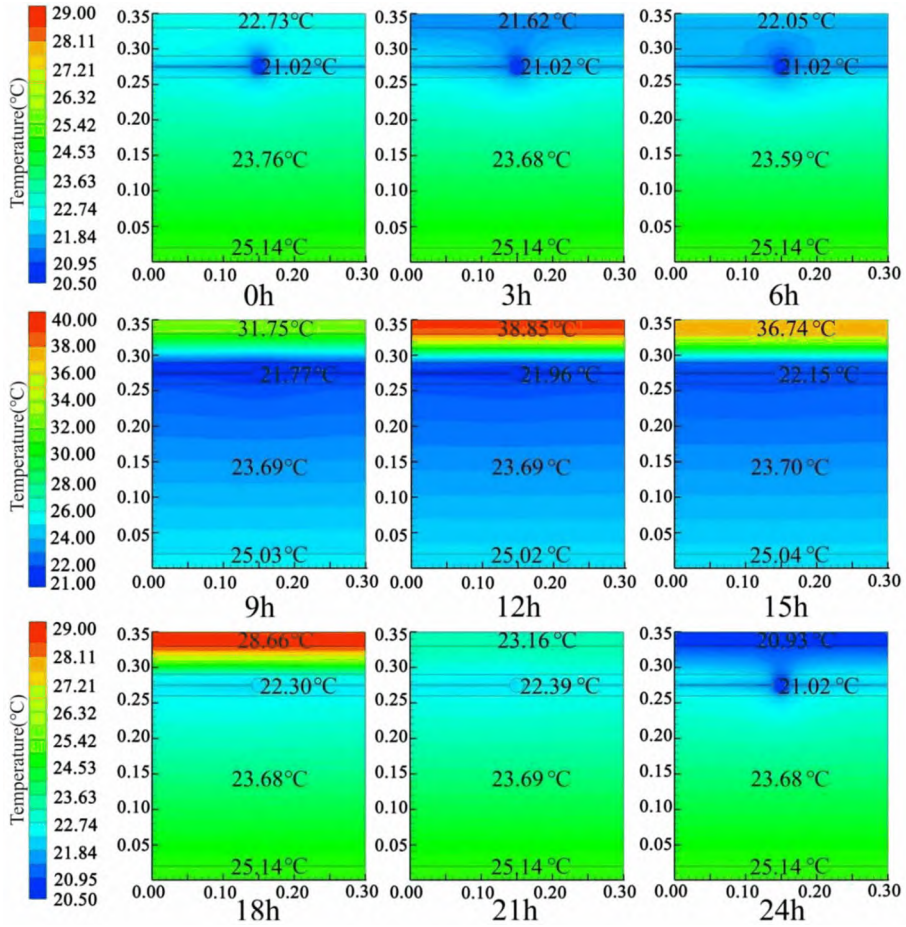


Figure 6. Variation of the temperature field at the cross-section of PEPCW.

but lift the indoor thermal comfort level at the same time. Results also show that the PCM inside of PEPCW could keep a dynamic balance during the test. And this could be regarded as another evidence of the effectiveness of PEPCW in building energy management because a stable melting/solidification cycle is a key index to evaluate the effectiveness of the PCM application. In a word, the PEPCW could act as a thermal barrier role between the indoor and outdoor environment, offsetting the heat gain through the building envelope and even supplying cooling energy to the indoor space. Accordingly, the initial investment and operating costs for a traditional HVAC system could be reduced correspondingly.

The variation of the temperature field at the cross-section of PEPCW is illustrated in Figure 6. It could be found that an obvious thermal stratification phenomenon of the composite wall is shown in the pipe-embedded zone. Temperature difference between the external cement and PCM layer varied from −0.1 ℃ to 16.9 ℃, while this value between the internal cement and PCM layer is within the range of 1.6−4.1 ℃. This implicates that the heat absorbed from the ambient can hardly pass through the PEPCW, thereby the interior surface temperature could be effectively controlled. Meanwhile, Figure 7 shows the temperature profile variation of the PEPCW and ordinary wall, where the dotted line (except for the monitoring points) is an indirect reference and not a direct simulation monitoring result. It could be seen that the temperature of the PCM layer remain at the melting/solidification zone throughout the whole day. The pipe-embedded PCM interlayer could significantly diminish the amplitude of temperature swing at the right side of PCM layer, making the temperature variation go flat between x =0.09 m and x = 0.35 m, while the temperature profile in the left side does not decline seriously. This also indicates that relocating the pipe-embedded interlayer to the position between the load-bearing layer and the external XPS is technically feasible.

3.2 Effect of pipe interval and PCM thickness

Following the last section, the influence of pipe interval and PCM thickness under Tianjin condition is evaluated here. Figure 8 shows the heat flux and temperature variation of the interior surface as well as the liquid fraction inside of the PCM layer under different pipe interval and PCM thickness conditions. In Figure 8, the interior surface temperature for all of the nine studied

(C)1994-2022 China Academic Journal Electronic Publishing House. All rights reserved.　http://www.cnki.net

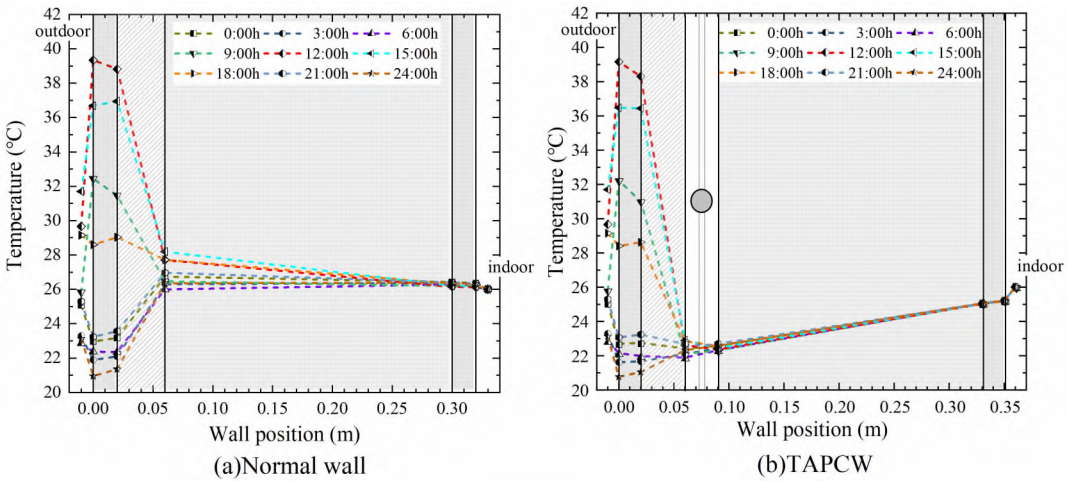


Figure 7. Temperature profile variation for the normal wall and PEPCW.

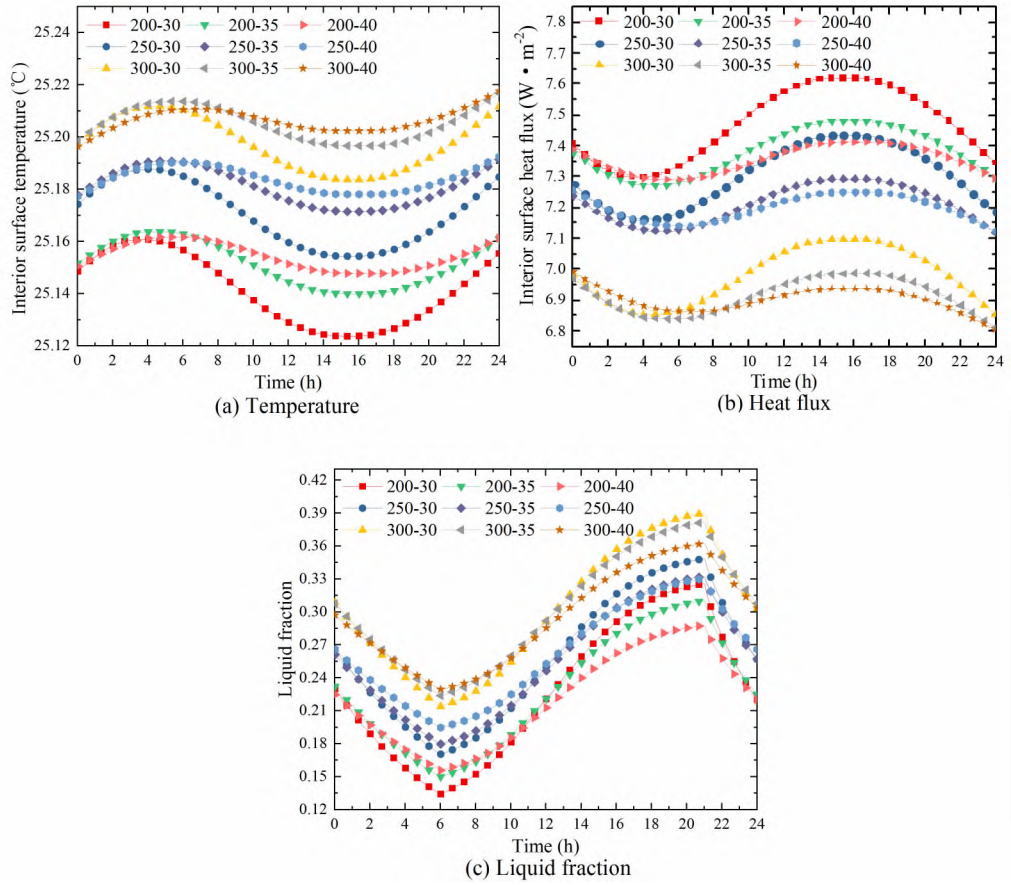


Figure 8. Influence of the pipe interval and PCM thickness on heat transfer performance.

cases are both lower than that of the indoor setting point and the interior surface heat flux is positive during the test, which means the nine studied cases are all effective. Further observation shows that when keeping PCM thickness constant and increasing the pipe interval, the interior surface temperature is also increased but the increment is reduced gradually. When keeping the pipe interval constant and increasing the PCM thickness, the interior surface temperature is increased instead of decreasing. The heat flux variation of interior surface in Figure 8 (b) also shows the same phenomenon. This could be probably attributed to the thermal conductivity of PCMs, which is lower than the bricklayer and the cement layer. That is to say, increasing the PCM thickness will also increase the thermal resistance between the pipe and the interior surface. Actually, a

(C)1994-2022 China Academic Journal Electronic Publishing House. All rights reserved. http://www.cnki.net

lower thermal conductivity coefficient is desirable for energy-saving of ordinary buildings, because the heat transfer resistance is raised. Whereas, for PEPCW with intermittent thermal storage, both the heat transfer intercepting capacity and heat charge/discharge capacity are crucial. Besides, as is shown in Figure 8 (c), though steady phase change process occurs in all cases, a thinner PCM shows a higher utilization ratio. Therefore, though a thick PCM layer represents a higher energy storage potential, the balance between the heat charge/discharge and thermal intercepting capacity should be taken into account simultaneously, or it would be count-productive and also would bring in unnecessary material waste.

The impact of the pipe interval and PCM thickness on daily heat gain is illustrated in Figure 9. Results show that the daily accumulated heat gain of PEPCW is far less than the traditional one. For the ordinary wall, this value is positive and is around 0.05 kWh · m^{-2}, while these value for the studied PEPCW are both negative. Compared with the ordinary wall, the reduction ratio of this value is around 427.9-454.9% for PEPCW. Besides, though a closer arrangement of the embedded pipe and a thinner PCM layer shows a smaller accumulated heat gain value, the maximum percentage difference between the case of 200-30 and case 300-40 is only 27 which is not obvious compared with the overall decline ratio. As a result, a thinner PCM layer of 30 mm and a larger pipe interval of 300 mm are recommended here.

3.3 Effect of climate region

As is shown in appendix 2, different cities located in different climate region usually have different thermal insulation requirement and cooling demand. In this section, three typical Chinese cities are selected to evaluate the thermal performance of PEPCW. The three cities are Tianjin (cold region; latitude: 39.12° N), Nanjing (hot summer and cold winter region; latitude: 32.03° N) and Guangzhou (hot summer and warm winter region; latitude: 23.13° N), which distribute from south to north in China. Thus, cities in other countries have similar latitude or climate characteristic could also find valuable references in practice.

As is shown in Figure 10, the interior surface heat flux of PEPCW in three typical cities, compared with the ordinary wall, are both turned into positive and remain in a relatively stable status in the cooling season. Meanwhile, the interior surface temperature also could be controlled below the indoor setting point, which is beneficial for improving the indoor thermal comfort level. Figure 11 shows the monthly accumulated heat gain and the corresponding reduction of PEPCW. The simulation results state that when a higher heat gain is formed in a cooling month, a greater heat gain reduction will also be obtained. Therefore, though the heat gain varies greatly in different months of the cooling season, the PEPCW system could satisfy the heat gain reduction demand well and even provide extra cooling for the indoor space. Besides, due to the different primary meteorological conditions in different regions, the amount of heat reduction required for the building to achieve indoor thermal comfort is different. For areas with higher temperatures, the demand for heat reduction is higher; places with lower temperatures have the lower need, so the adjustment effect of TAPCW varies in different climate regions. The result shows that the total

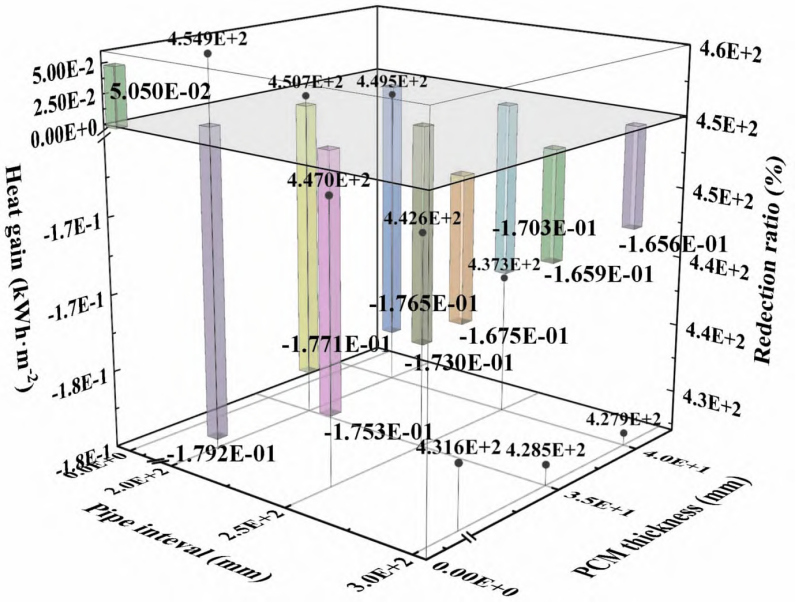


Figure 9. Influence of the pipe interval and PCM thickness on accumulated heat gain.

(C)1994-2022 China Academic Journal Electronic Publishing House. All rights reserved.　http://www.cnki.net

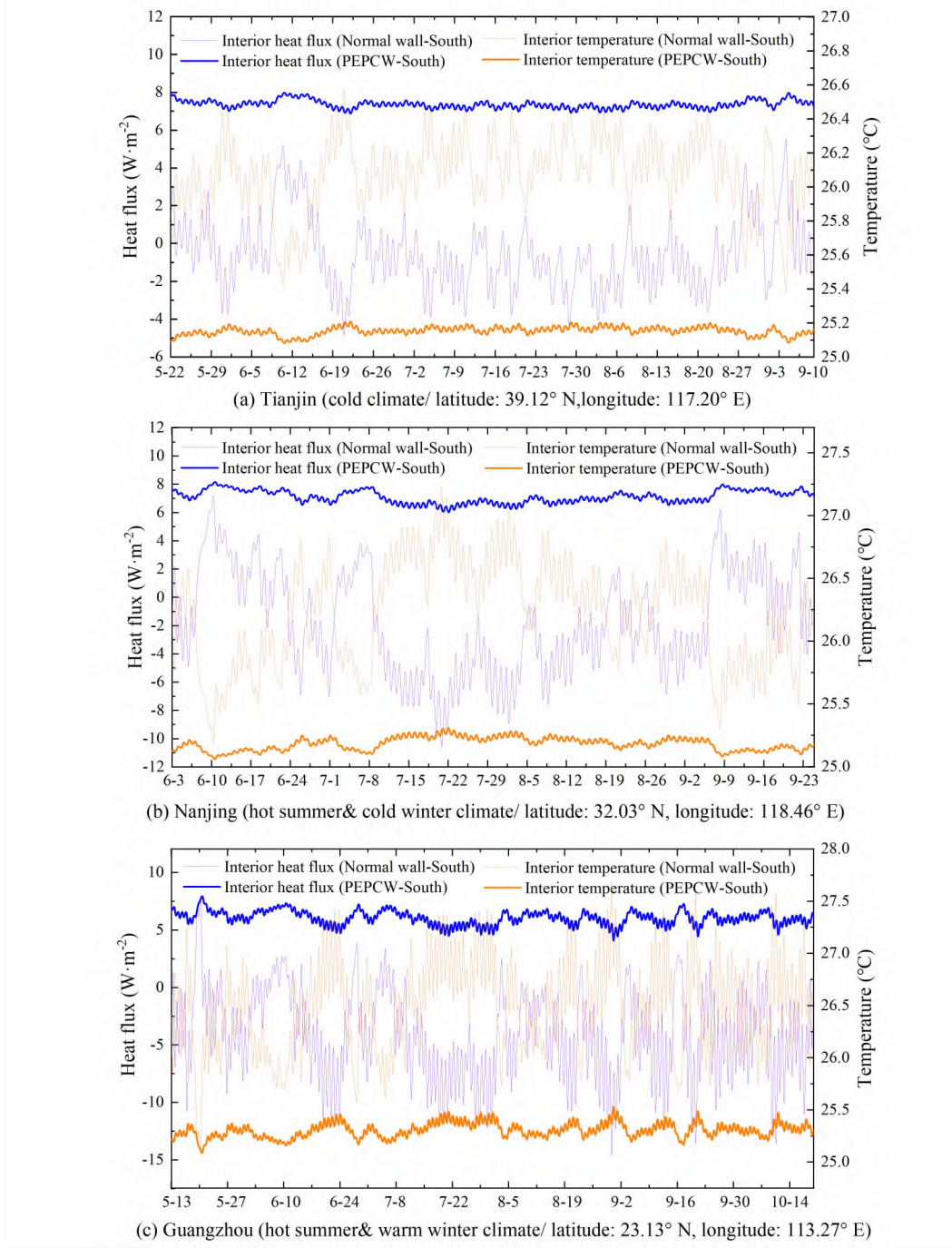


Figure 10. Hourly variation of the interior surface heat flux and temperature in typical cities.

heat gain of the ordinary wall in Tianjin is the smallest one (i. e., 1. 69 kWh · m^{-2}), and this value for Guangzhou application is the highest one (i. e., 16. 10 kWh · m^{-2}). While, for PEPCW, the heat gain of Guangzhou is lower than that of Tianjin and Nanjing, but their difference is not too much. The maximum heat gain reduction appears in Guangzhou, i. e. ,39. 30 kWh · m^{-2}, and the heat gain reduction in Tianjin and Nanjing is similar. Therefore, the PEPCW system is proved to be satisfactory in all of the selected cities.

3.4 Effect of orientation

The solar radiation varies with the building orientation, which usually brings about the different thermal impact on the exterior wall for different orientations as well as the indoor environment. Thus, the impact of orientation on PEPCW is investigated in this section. Figure 12 show the orientation influence on heat gain and the corresponding reduction in typical cities. It could be seen that the accumulated heat gain of the ordinary wall at different orientations is significantly affected by solar

(C)1994-2022 China Academic Journal Electronic Publishing House. All rights reserved. http://www.cnki.net

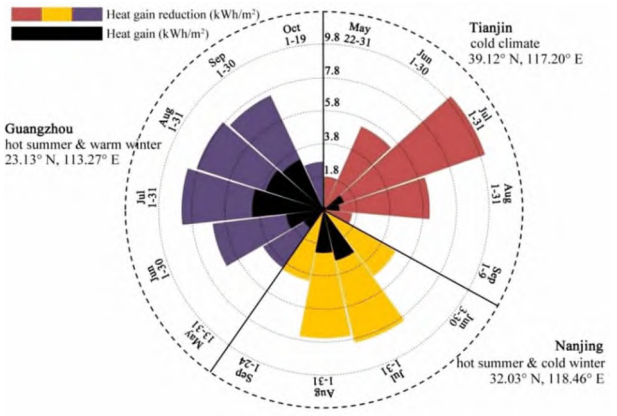


Figure 11. The monthly accumulated heat gain in typical cities.

absorbance. When the pipe-embedded PCM interlayer is added, the influence of solar irradiance is reduced remarkably. And the accumulated heat gain in different orientations is both turned into negative, which means the interior wall surface will take away the heat from the room instead of transferring the environment heat into the room. The simulation results also indicate that due to the differences in primary meteorological conditions in different cities, the cumulative heat gains in the four directions in the same city are slightly different. Obviously, the accumulated heat gain at different orientations in Guangzhou is higher than Tianjin and Nanjing due to a longer cooling season. From the perspective of orientation, because the dark side (i.e., the North) of the building gets less heat and needs less heat reduction to improve indoor thermal comfort, the reduction of cumulative heat gain in the north of the building is relatively less than that of the other three sunny sides, while the south side of the main sunny side gets the most heat, and the reduction effect of cumulative heat gain is very obvious. In a word, it is convincing that PEPCW system is effective in all of the four orientations, especially in the sunny side where the heat gain reduction is greater.

4 Conclusions

The concept of thermo-activated PCM composite wall (PEPCW) is proposed to address the shortcomings existed in traditional energy saving retrofit measures and to solve application challenges of pipe-embedded building envelope facing the vast existing buildings. In this paper, the heat transfer performance of the PEPCW driven by the intermittent high-temperature cold water and its effectiveness in the aspect of energy saving are examined, which is accomplished by using a validated numerical model. Furthermore, the effects of pipe interval, PCM thickness, climate region and the orientation on the thermal behavior and the energy saving and economic potential are also numerically investigated. The main conclusions are as follows: Select three typical cities to study the effects of climate regions and orientations on the thermal behavior and the energy saving and economic potential.

(Ⅰ) The comparative study between PEPCW and normal wall preliminarily verify the effectiveness of PEPCW in stabilizing the interior surface temperature, offsetting the cold loss through the building envelope and even supplying coldness energy to the indoor space of the existing buildings needed to be retrofitted. With the pipe-embedded PCM system, the temperature and heat flux amplitude of interior surface of PEPCW under Tianjin conditions can be decreased by 1.1 ℃ and 9.9 $W \cdot m^{-2}$, respectively.

(Ⅱ) Results show that the pipe spacing has a more obvious influence than PCM thickness. Considering the cost performance, a thinner PCM layer (e.g., 30 mm) and a larger pipe interval (e.g., 300 mm) is recommended though a closer arrangement of the embedded pipe and a thinner PCM layer shows a smaller accumulated heat gain value.

(Ⅲ) The summer thermal performances of PEPCW

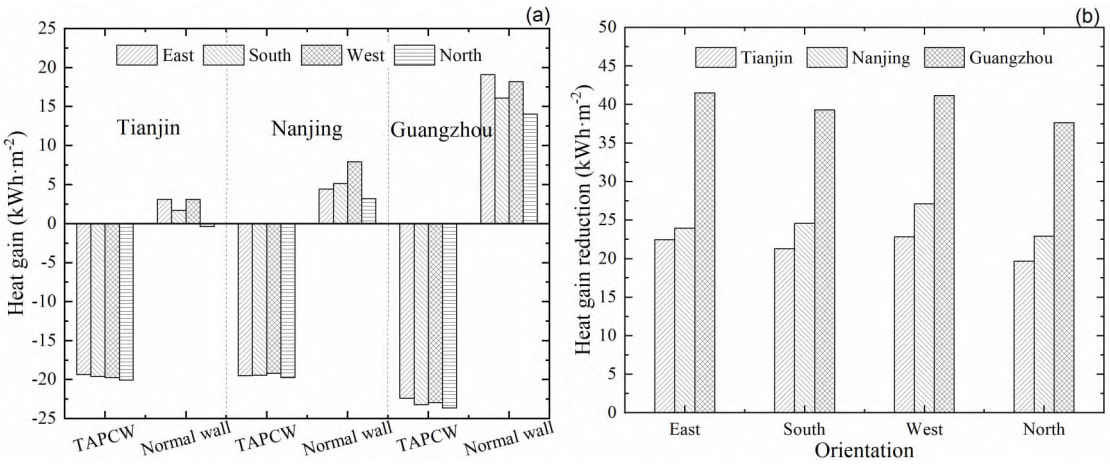


Figure 12. (a) Effect of the orientation on accumulated heat gain; (b) Effect of the orientation on accumulated heat gain reduction.

(C)1994-2022 China Academic Journal Electronic Publishing House. All rights reserved.　http://www.cnki.net

in retrofitting buildings are proved satisfactory in all the studied three cities. Results show that the maximum heat gain reduction (i. e., 39. 30 kWh · m^{-2}) after applying PEPCW appears in hot summer and warm winter (i. e., Guangzhou).

(Ⅳ) Compared with the static ordinary wall, the influence of solar radiation on the indoor thermal environment could be remarkably reduced. Results show that the PEPCW applied in the three sunny orientations are more effective than the the dark orientation (i. e., north).

The above results and conclusions obtained from numerical research have specific theoretical guiding significance for further research and application of PEPCW. However, there are still several issues that need to be further resolved: (1) Many factors affect the thermal performance of PEPCW, including cold/heat source temperature, installation area, thermal physical parameters of phase change materials, indoor set temperature and existing building enclosure Structural types, etc., need to be further analyzed in conjunction with actual projects; (2) PEPCW systems should be applied to the actual reconstruction of existing buildings In the case, the overall thermal performance of the reconstructed building was experimentally verified and long-term tested, and its application effects were more comprehensively evaluated to give more targeted guidance on the technology.

Acknowledgments

This work is supported by the Youth Fund of Anhui Natural Science Foundation (2108085QE241), National Key Research and Development Program of China (2021YFE0200100), Fundamental Research Funds for the Central Universities (PA2021KCPY0038), Department of Housing and Urban-Rural Development of Anhui Province (2020-YF36) and Anhui Natural Science Research Projects of Universities (KJ2020A0462).

Conflict of interest

The authors declare no conflict of interest.

Author information

CHEN Sarula received her PhD in Architecture from Tianjin University. She is a master supervisor at Anhui Jianzhu University. She is a specialist in building energy-saving and ultra-low energy consumption fields.

YANG Yang (corresponding author) received his PhD in Architecture from Tianjin University. He is a specialist in building energy-saving and ultra-low energy consumption fields.

References

[1] IEA. World Energy Statistics 2020. Paris: International Energy Agency, 2021.

[2] Li N, Liu X, Yu B. The performance analysis on a novel purified PV-Trombe wall for electricity, space heating, formaldehyde degradation and bacteria inactivation. Journal of University of Science and Technology of China, 2021, 51: 308-318.

[3] Ye R, Lin W, Fang X, et al. A numerical study of building integrated with $CaCl_2 \cdot 6H_2O$/ expanded graphite composite phase change material. Applied Thermal Engineering, 2017, 126: 480-488.

[4] MaPugsley A, Zacharopoulos A, Mondol J, et al. Vertical Planar Liquid-Vapour Thermal Diodes (PLVTD) and their application in building facade energy systems. Applied Thermal Engineering, 2020, 179: 115641.

[5] Lodi C, Magli S, Contini F, et al. Improvement of thermal comfort and energy efficiency in historical and monumental buildings by means of localized heating based on non-invasive electric radiant panels. Applied Thermal Engineering, 2017, 126: 276-289.

[6] Ji Y, Fitton R, Swan W, et al. Assessing overheating of the UK existing dwellings-A case study of replica Victorian end terrace house. Building and Environment, 2014, 77: 1-11.

[7] Ye H, Wang Z, Wang L, et al. Effects of PCM on thermal control performance of a thermal control system subjected to periodic ambient conditions. Journal of University of Science and Technology of China, 2016, 46: 845-852.

[8] Yang Z, Zhang Q, Zhang W, et al. Research progress on heat transfer enhancement methods for medium temperature latent heat thermal energy storage systems. Chemical Industry and Engineering Progress, 2019, 38: 4389-4402.

[9] Oliver A. Thermal characterization of gypsum boards with PCM included: Thermal energy storage in buildings through latent heat. Energy and Buildings, 2012, 48: 1-7.

[10] Zhu L, Yang Y, Chen S, et al. Numerical study on the thermal performance of lightweight temporary building integrated with phase change materials. Applied Thermal Engineering, 2018, 138: 35-47.

[11] Vicente R, Silva T. Brick masonry walls with PCM macrocapsules: An experimental approach. Applied Thermal Engineering, 2014, 67: 24-34.

[12] Gholamibozanjani G, Farid M. Application of an active PCM storage system into a building for heating/cooling load reduction. Energy, 2020, 210: 118572.

[13] Rathore P, Shukla S K. An experimental evaluation of thermal behavior of the building envelope using macroencapsulated PCM for energy savings. Renewable Energy, 2020, 149: 1300-1313

[14] Fateh A, Borelli D, Devia F, et al. Summer thermal performances of PCM-integrated insulation layers for light-weight building walls: Effect of orientation and melting point temperature. Thermal Science and Engineering Progress, 2018, 6: 361-369.

[15] Zhu N, Ma Z, Hu P, et al. Energy performance of double shape-stabilized phase change materials wallboards in office building. Applied Thermal Engineering, 2016, 105: 180-188.

[16] Yu N, Chen C, Lin J, et al. Thermal properties of phase change materials used in buildings for solar phase change thermal storage curing of precast concrete components. Chemical Industry and Engineering Progress, 2021, 40: 297-304.

(C)1994-2022 China Academic Journal Electronic Publishing House. All rights reserved. http://www.cnki.net

[17] Romani J, Cabeza L, Perez G, et al. Experimental testing of cooling internal loads with a radiant wall. Renewable Energy, 2017, 116: 1-8.
[18] Zhou L, Li C. Study on thermal and energy-saving performances of pipe-embedded wall utilizing low-grade energy. Applied Thermal Engineering, 2020, 176: 115477.
[19] Luo Y, Zhang L, Bozlar M, et al. Active building envelope systems toward renewable and sustainable energy. Renewable and Sustainable Energy Reviews, 2019: 470-491.
[20] Ibrahim M, Wurtz E, Anger J, et al. Experimental and numerical study on a novel low temperature façade solar thermal collector to decrease the heating demands: A south-north pipe-embedded closed-water-loop system. Solar Energy, 2017, 147: 22-36.
[21] Rayegan S, Motaghian S, Heidarinejad G, et al. Dynamic simulation and multi-objective optimization of a solar-assisted desiccant cooling system integrated with ground source renewable energy. Applied Thermal Engineering, 2020, 173: 115210.
[22] Jeong S, Tso C, Zouagui M, et al. A numerical study of daytime passive radiative coolers for space cooling in buildings. Building Simulation, 2018, 11: 1011-1028.
[23] Xie J, Zhu Q, Xu X, et al. An active pipe-embedded building envelope for utilizing low-grade energy sources. Journal of Central South University, 2012, 19: 1663-1667.
[24] Yu Y, Niu F, Guo H, et al. A thermo-activated wall for load reduction and supplementary cooling with free to low-cost thermal water. Energy, 2016, 99: 250-265.
[25] Shen C, Li X, Yan S, et al. Numerical study on energy efficiency and economy of a pipe-embedded glass envelope directly utilizing ground-source water for heating in diverse climates. Energy Conversion and Management, 2017, 150: 878-889.
[26] Jiang S, Li X, Lyu W, et al. Numerical investigation of the energy efficiency of a serial pipe-embedded external wall system considering water temperature changes in the pipeline. Journal of Building Engineering, 2020, 31: 101435.
[27] Prieto A, Knaack U, Auer T, et al. Solar coolfacades: Framework for the integration of solar cooling technologies in the building envelope. Energy, 2017,137: 353-368.
[28] Silvero F, Lops C, Montelpare S, et al. Impact assessment of climate change on buildings in Paraguay—Overheating risk under different future climate scenarios. Building Simulation, 2019, 12: 1-18.
[29] National Development and Reform Commission (NDRC). Opinions on Clean Heating Price Policy in North China. [2021-03-01]. http://www.ndrc.gov.cn/zcfb/zcfbtz/201709/t20170925_861387.html.
[30] Mazo J, Delgado M, Marin J, et al. Modeling a radiant floor system with Phase Change Material (PCM) integrated into a building simulation tool: Analysis of a case study of a floor heating system coupled to a heat pump. Energy and Buildings, 2012, 47: 458-466.
[31] Zhao M, Zhu T, Wang C, et al. Numerical simulation on the thermal performance of hydraulic floor heating system with phase change materials. Applied Thermal Engineering, 2016, 93: 900-907.
[32] B González, Prieto M. Radiant heating floors with PCM bands for thermal energy storage: A numerical analysis. International Journal of Thermal Sciences, 2021, 162: 106803.
[33] Xia Y, Zhang X. Experimental research on a double-layer radiant floor system with phase change material under heating mode. Applied Thermal Engineering, 2016, 96: 600-606.
[34] Fu W, Zou T, Liang X, et al. Thermal properties and thermal conductivity enhancement of composite phase change material using sodium acetate trihydrate-urea/expanded graphite for radiant floor heating system. Applied Thermal Engineering, 2018, 138: 618-626.
[35] Koschenz M, Lehmann B. Development of a thermally activated ceiling panel with PCM for application in lightweight and retrofitted buildings. Energy and Buildings, 2004, 36: 567-578.
[36] Shen C, Li X. Energy saving potential of pipe-embedded building envelope utilizing low-temperature hot water in the heating season. Energy and Building, 2017, 138: 318-31.
[37] Rubitherm. Techdata-RT18HC. [2021-03-01]. https://www.rubitherm.eu/en/.
[38] Ocallaghan P, Probert S. Sol-air temperature. Applied Energy, 1977, 3: 307-311.
[39] Kong X, Lu S, Li Y, et al. Numerical study on the thermal performance of building wall and roof incorporating phase change material panel for passive cooling application. Energy and Buildings, 2014, 81: 404-415.
[40] Nageler P, Schweiger G, Pichler M, et al. Validation of dynamic building energy simulation tools based on a real test-box with thermally activated building systems (TABS). Energy and Buildings, 2018, 168: 42-55.
[41] ANSYS. Ansys Fluent Theory Guide. Canonsburg, PA, 2011.
[42] Faheem A, Ranzi G, Fiorito F, et al. A numerical study on the thermal performance of night ventilated hollow core slabs cast with micro-encapsulated PCM concrete. Energy and Buildings, 2016, 127: 892-906.
[43] Du R, Li W, Xiong T, et al. Numerical investigation on the melting of nanoparticle-enhanced PCM in latent heat energy storage unit with spiral coil heat exchanger. Building Simulation, 2019, 12: 869-879.
[44] China Academy of Building Research (CABR). Design code for heating ventilation and air conditioning of civil buildings (GB50736-2012). Beijing: China Building Industry Press, 2012.
[45] Blanco J, Arriaga P, Roji E, et al. Investigating the thermal behavior of double-skin perforated sheet façades: Part A: Model characterization and validation procedure. Building and Environment, 2014, 82: 50-62.
[46] China Academy of Building Research (CABR). Code for thermal design of civil buildings (GB50176-2016). Beijing: China Building Industry Press, 2016.
[47] Kharbouch Y, Ouhsaine L, Mimet A, et al. Thermal performance investigation of a PCM-enhanced wall/roof in northern Morocco. Building Simulation, 2018, 11: 1083-1093.
[48] Huo R. Study on thermal storage properties of phase change material wallboard with water-heating system. Beijing: Beijing University of Civil Engineering and Architecture, 2012.

(C)1994-2022 China Academic Journal Electronic Publishing House. All rights reserved. http://www.cnki.net

既有建筑嵌管式相变复合墙体夏季热特性研究

陈萨如拉[1,4],常甜馨[1],杨洋[2*],潘超[1],吴运法[1,3,4]

1. 安徽建筑大学建筑与规划学院,安徽合肥 230601
2. 合肥工业大学建筑与艺术学院,安徽合肥 230009
3. 中国科学技术大学火灾科学国家重点实验室,安徽合肥 230027
4. 中国-葡萄牙文化遗产保护科学"一带一路"联合实验室,江苏苏州 215031

* 通讯作者. E-mail: yangyang2017@tju.edu.cn

摘要: 管道嵌入式建筑围护结构作为一种重质热激活建筑系统(TABS),由于其管道内嵌于建筑围护结构内部,故目前在既有建筑改造中应用较少. 本文提出了管道嵌入式相变复合墙体(PEPCW)的概念,其主要利用基于宏观封装的嵌管式相变板代替传统嵌管夹层,并将嵌管夹层移至承重层外侧,为解决既有建筑改造中应用这一技术提供了创新解决思路. 本文利用经实验验证的数学模型评估了PEPCW的夏季热性能和节能潜力,结果表明,复合墙体内表面温度和热流可分别降低1.1℃和9.9 W·m^{-2}. 参数化模拟结果表明,管道间距相比相变夹层厚度对复合墙体热性能影响更为明显,所研究条件下的管道间距和相变层厚度建议取值为300/30 mm. 通过对三个不同气候分区的典型城市(即天津、南京和广州)开展的应用评估结果还表明,PEPCW在改善室内热舒适度方面可以取得令人满意的效果,尤其是在夏热冬暖地区. 此外,应用PEPCW可显著降低太阳辐射吸收率对不同朝向墙体热负荷的影响,三个向阳朝向的指标下降幅度高于北面. 综合来看,PEPCW在供冷季节表现出令人满意的热性能,有助于推动嵌管式建筑围护结构在既有建筑中的节能改造应用.

关键词: 热性能; TABS; 相变材料; 数值模型; 既有建筑

(C)1994-2022 China Academic Journal Electronic Publishing House. All rights reserved. http://www.cnki.net

引文格式：王爱，张强，储金龙，等．轨道交通沿线不同区段土地利用的差异性测度［J］．测绘科学，2021，46(9)：190-198，217.(WANG Ai，ZHANG Qiang，CHU Jinlong，et al. Study on difference measurement of the impact of rail transit on land use in different sections［J］. Science of Surveying and Mapping，2021，46(9)：190-198，217.)DOI：10.16251/j.cnki.1009-2307.2021.09.025.

轨道交通沿线不同区段土地利用的差异性测度

王　爱[1,2]，张　强[1]，储金龙[1]，孙　圳[1]，季顾烽[3]

（1. 安徽建筑大学 建筑与规划学院，合肥　230601；2. 安徽省城镇化发展研究中心，合肥　230022；
3. 东北师范大学 地理科学学院，长春　130024）

摘　要：为了研究轨道交通沿线的土地利用差异性变化，该文提出了一种面向城市总规用地、遥感影像数据探讨土地利用差异性的分析方法，为引导城市与轨道交通协同发展提供支撑，以合肥 1 号轨道交通为例，运用了 ArcGIS 空间和 SPSS 统计分析方法。研究表明，在时间维度方面：①用地的动态度、变化率和变化量大小排序均呈现出二环以外＞一二环之间＞一环以内。②在用地面积变化上，相交于二环以外，一环以外、一二环之间区域的用地面积变化不突出；空间维度方面：①轨道交通各站点周边用地均呈现多元复合型，而不同站点周边用地的主导功能有所差异。②各站点 400～600 m 范围用地的信息熵和均衡度大小趋于较高值的平稳状态，200 m 范围内信息熵和均衡度波动大。③各站点周边商业、居住和道路用地半径维数较高，道路、商业用地边界维数较高。

关键词：轨道交通；土地利用；时空维度；差异性；合肥市

【中图分类号】P208　　**【文献标志码】**A　　**【文章编号】**1009-2307(2021)09-0190-09

Study on difference measurement of the impact of rail transit on land use in different sections

WANG Ai[1,2]，*ZHANG Qiang*[1]，*CHU Jinlong*[1]，*SUN Zhen*[1]，*JI Gufeng*[3]

（1. School of Architecture & Urban Planning，Anhui Jianzhu University，Hefei 230601，China；
2. Anhui Urbanization Development Research Center，Hefei 230022，China；
3. School of Geographical Sciences，Northeast Normal University，Changchun 130024，China）

Abstract：In order to study the differential changes of land use along the rail transit，this paper proposed an analysis method for exploring the difference of land use based on urban master plan land and remote sensing image data to provide support for guiding the coordinated development of urban and rail transit. This paper took the Hefei No. 1 rail transit as an example，using ArcGIS spatial analysis and SPSS statistical analysis methods. The research showed that，in terms of time dimension：① The order of land use dynamics，rate of change and magnitude of change was outside the second ring road＞between the first and second ring roads＞within the first ring road. ②In terms of land area changes，intersect outside the second ring road，the area of land outside the first ring road and between the first ring road and the second ring road did not change significantly；In terms of spatial dimensions：①The surrounding land of each rail transit station was in a diversified and complex type，while the dominant functions of the surrounding land of different stations were different. ② The information entropy and equilibrium degree of the land in the range of 400～600 m at each station tend to be higher. The information entropy and equilibrium degree fluctuate greatly within the range of 200 m. ③ The radius dimension of commercial，residential and road land around each site was relatively high，and the boundary dimension of road and commercial land was relatively high.

Keywords：rail transit；land use；space-time dimension；difference；Hefei city



作者简介：王爱（1985—），男，安徽合肥人，博士，主要研究方向为城市地理与城市规划。
E-mail：520wangai@163.com

收稿日期：2020-04-15
基金项目：国家自然科学基金项目(51678001)；安徽省自然科学基金项目(2008085QE241)；安徽省高校自然科学研究重点项目(KJ2019A0752)；安徽建筑大学博士科研基金项目(2018QD56)
通信作者：张强 硕士研究生 E-mail：1336135170@qq.com

(C)1994-2022 China Academic Journal Electronic Publishing House. All rights reserved.　http://www.cnki.net

0　引言

交通网络构成城市发展的空间骨架，城市交通工具与运输方式的转变和升级，对城市土地利用方式的变化和空间结构的发展有深远的影响[1]。轨道交通作为大运量的交通运输方式，在降低城市污染排放、提升城市交通效率等方面发挥着重要的作用，是城市绿色发展、低碳节能的必由之路。随着新型城镇化战略的推进，各级政府推出一系列以轨道交通建设为导向的发展政策，北京、上海、苏州、合肥等城市陆续兴起建设轨道交通的热潮。

国内外学者对于轨道交通的研究课题主要集中在以轨道交通的投资运营[2-4]、轨道交通与城市土地开发利用的内在逻辑[5-6]、轨道交通与生态环境保护的关联性[7-9]、轨道交通与出行结构的耦合关系[10-12]4 个方面。由于土地资源作为不可再生的生产要素，是城市建设发展的主要物质载体。如何利用好不可再生的土地资源，是我国正在处于城镇化加速期和将长期面临人多地少矛盾大背景下的必然要求[13]。关于轨道交通与城市土地开发利用方面的研究一直是学术界研究的重点。文献［14］基于廊道效应理论对轨道交通沿线用地进行了比较分析，据此探索合理的城市土地利用模式。文献［15］基于地价和开发强度两个要素，从时间维度上探讨轨道交通影响下城市空间结构动态演变过程。文献［16］定量分析了西安轨道交通 2 号线沿线站点的用地功能。文献［17］就城市地铁环线对城市空间结构与土地利用的影响进行了探讨。文献［18］分析了地铁站点沿线的土地利用和交通的协调关系，并建构了协调程度的评价模型。文献［19］基于不同的空间尺度，分析了轨道交通站点对商业地产和物业的差异性影响。

总体来说，国内外对于城市轨道交通与土地利用的研究，呈现出多学科交叉，集成研究的特点。在数据获取、影响效应的研究上更多地采用了现代化技术和模拟分析方法，对于轨道交通的研究也日趋成熟。但学术界对于在轨道交通与土地利用关系方面的研究，较多关注城市尺度下轨道交通与土地利用的协调关系，针对站点周边用地的差异性深入探讨较少。本文从时空两个维度，探讨轨道交通沿线土地利用的差异性，综合分析站点周边用地的面积、功能和形态等方面的变化特征，不仅能为评估和优化站点周边空间环境提供参考，也有利于科学规划轨道交通体系，提高土地资源的集约节约。

1　研究区域与研究方法

1.1　研究区域

本研究以合肥市主城区为研究区域，其作为安徽省的省会，在建国之初，是一座“五平方千米、五万人、五条马路”的江淮小邑。改革开放以来，合肥市的社会经济迅速发展，合肥的建成空间从“环城”扩展到“滨湖”空间，城市主要职能从科教基地到科学中心。城市空间不断拓展，城市体量和运行结构日益庞杂。目前合肥有 6 条轨道交通线同时在建，至 2019 年 12 月已开通运营 3 条轨道交通线，线路总长 89.58 km。基于轨道交通的建设速度和规模，研究轨道交通沿线不同区段土地用地的差异性，对于指导轨道交通沿线土地的合理利用，提升土地价值具有重要意义。研究选取合肥地铁 1 号线为案例，其于 2015 年开通运营，开通前后时间跨度大，已对沿线各类用地和经济活动产生了显著影响。地铁 1 号线的具体线型走向串联了合肥站、老城区、合肥南站枢纽地区、骆岗机场和滨湖新区等城市重要的功能空间(图 1)。



图 1　合肥市 1 号轨道交通与城市功能区的关系

Fig. 1　The Relationship between No. 1 Rail Transit and the Urban Functional Area in Hefei

1.2　研究思路及方法

定量测度轨道交通沿线的土地利用情况，首先需要明确具体的空间尺度范围。通过梳理相关

(C)1994-2022 China Academic Journal Electronic Publishing House. All rights reserved.　http://www.cnki.net

研究文献[20-22]，研究基于轨道交通 2 000 m 的最大服务半径，并结合最新的《城市居住区规划设计标准》(GB 50180—2018)内确定的 5、10、15 min 生活圈的服务半径，将缓冲区设置为 200、400、600 和 2 000 m 等不同空间尺度，探析合肥市轨道交通 1 号线沿线不同区段的土地利用情况。主要内容包括：①根据合肥城市空间格局的特征，以主城区一环路、二环路构成城市圈层的基本架构，选取轨道交通开工前 2009 年和建成运行后 2019 年的 2 个时间节点，对轨道交通 1 号线站点 2000 m 范围内的一环以内、一二环之间、二环以外 3 个区段的各类用地进行统计，比较分析土地利用的面积、程度和变化空间等方面的变化情况；②以 2019 年轨道交通站点周边 0～200、200～400、400～600 m 的 3 个范围内的区域，针对站点周边土地利用的功能、结构和形态 3 方面进行探讨，研究轨道交通不同区段土地利用的差异性。具体研究思路见图 2，通过 ArcGIS 空间分析方法和 SPSS 统计分析方法，构建地理模型揭示轨道交通不同区段各类用地的差异。具体分析模型释义见表 1。

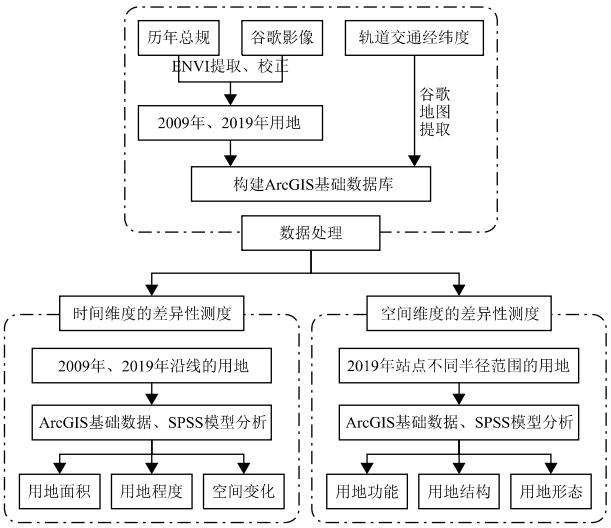


图 2 研究思路

Fig. 2 Research Ideas

表 1 地理模型及释义

Tab. 1 Geographical Model and Interpretation

名称	模型	模型释义	地理意义
动态度(式(1))	$K=\frac{A_e-A_b}{A_b}-\frac{1}{t_e-t_b}\times 100\%$	K 为某地类的动态度；A_b、A_e 分别为前后两时期某类用地的面积；t_e、t_b 为时间	其大小反映某类用地面积的变化速率
综合指数、变化量、变化率(式(2))	$I=\sum_{i=1}^{4}(L_i\times P_i)\times 100$ $\Delta I=I_y-I_x$ $R_c=\frac{\Delta I}{I_x}$	I 为土地利用程度综合指数；ΔI 为变化量；R_c 为变化率；L_i 为 i 用地分级指数；P_i 为 i 用地面积占比；Pix(Piy)为 $x(y)$时间 i 用地面积占比	若 $\Delta I>0$ 或 $R_c>0$，则该区域用地处于发展期，否则处于调整期
相对变化率(式(3))	$R_r=\left\lvert\frac{A_e-A_b}{A_b}\right\rvert/\left\lvert\frac{T_e-T_b}{AT_b}\right\rvert$	R_r 为某用地相对变化率；A_e、A_b 为局部区域某用地不同时间的面积；T_e、T_b 为全区域该用地不同时间的面积	若 $R_r=1$ 表示该区域与全区域的变化一致；若 $R_r>1$ 则变化大；反之则变化小
信息熵(式(4))	$H=-\sum_{i=1}^{n}(P_i\times\ln P_i)$ $P_i=A_i/\sum_{i=1}^{n}A_i$	H 为城市用地数量结构信息熵；P_i 为各用地面积占总面积的比例；A_i 为 i 用地的面积	熵值越高，表明用地分布越均衡
均衡度(式(5))	$J=\left[\sum_{i=1}^{n}(P_i\times\ln P_i)\right]/\ln n$	J 为城市土地利用结构均衡指数；n 为城市用地职能数	均衡度越大表明城市用地的均质性越强
半径维数(式(6))	$\ln S(r)=\ln\eta+D\ln r$	r 为半径；$S(r)$是半径为 r 的圆中某地类型的面积；η 为常数；D 为半径维数	半径维数越大，该类型土地的向心聚集越强
边界维数(式(7))	$\ln P=\ln\varphi+D/2\ln A$	P 与 A 分别为某用地类型斑块的周长和面积；φ 为常数；D 为边界维数	边界维数越大，各用地类型形态越复杂

1.3 数据收集及处理

研究数据主要包括合肥遥感影像、土地利用现状、1 号轨道交通建设情况 3 方面数据。①合肥市建成区 2009 年和 2019 年遥感影像数据，来源于谷歌历史影像；②合肥市 2009 年和 2019 年建成区土地利用现状，来源于合肥市自然资源规划局编制的历年城市总体规划；③1 号轨道交通站点位置及线性走向，来源于合肥市轨道交通近期建设规划(2009—2016 年)，并结合谷歌地图获取其经纬度。

(C)1994-2022 China Academic Journal Electronic Publishing House. All rights reserved. http://www.cnki.net

基于以上收集数据，利用 AutoCAD 软件将各类用地导出为 JPG，并利用 Photoshop 软件将 JPG 各类用地的颜色对比度进行适当调整，以便于各地类的区分。通过 ENVI 遥感软件提取 2009 年、2019 年 1 号轨道交通周边 2 000 m 范围内的现状土地利用类型进行识别和提取，结合历史影像进行用地的纠正调整。导入 ArcGIS 进行坐标空间配准和要素转矢量等处理。在此基础上，通过谷歌地图收集 1 号轨道交通的各个站点及线型的经纬度，导入 ArcGIS 进行矢量化定位处理，构建合肥市 1 号轨道交通的空间属性数据库，并对 1 号轨道交通空间特征进行可视化表达和研究(图 3)。

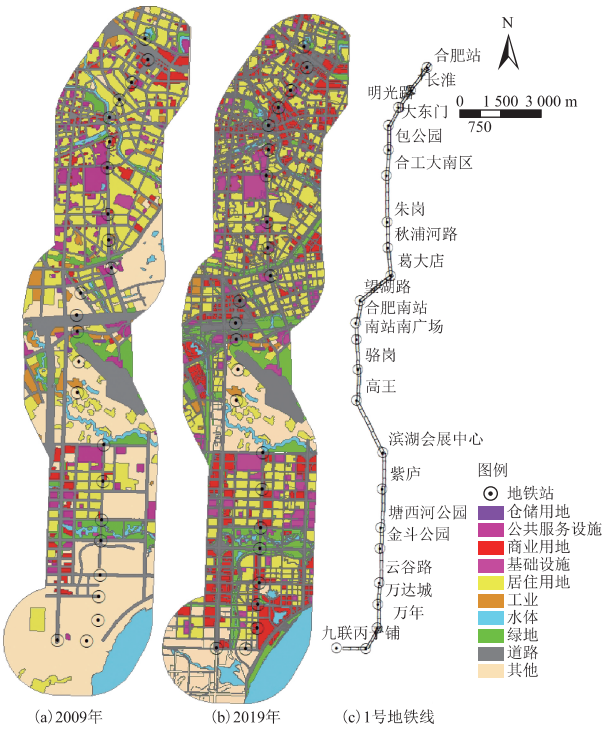


图 3　合肥市 1 号轨道交通沿线用地类型

Fig. 3　Types of Land Use Along No. 1 Rail Transit in Hefei

2　时间维度的不同区段用地的差异性

结合研究区域情况，并参考城市建设用地分类标准，在将各类用地进行适当整合后划分为道路、工业(工业用地与仓储用地)、公服(公共服务设施与基础设施用地)，居住、绿地、商业(商业和商务用地)、水域以及其他(主要包括城市待建设用地、农村耕地等)。

2.1　用地面积变化

利用表(1)中式(1)计算各类用地的动态度，把握不同区段各类用地面积变化差异，分析结构见表 2。可以发现 2009—2019 年合肥 1 号轨道交通线沿线 2 000 m 范围内各类用地都产生了显著变化。城市二环以外区段的其他用地、商业用地、居住用地动态度分别高达－20 859.592%、6 712.707%、5 292.855%，道路、工业及仓储、公服等各类用地动态度均高于其他环线区域。并且其他用地和工业及仓储用地动态度为负数，说明其他用地和工业及仓储用地不断被道路用地、公服、居住、绿地、商业等占据。一环、二环之间的区域整体动态度次于二环外区域，商业用地、道路用地、居住用地动态度分别达到 859.472%、664.248%、－629.507%，一环、二环之间道路用地和商业用地在不断增加，居住用地、工业及仓储用地等在不断减少。一环内相比动态度最低，部分居住用地不断赋予商业服务的功能并转换成商业用地。

表 2　不同区段各类用地动态度

Tab. 2　Land Use Dynamics Degree in Different Locations

用地类型	一环以内	一环、二环之间	二环以外
道路	83.996	664.248	1 599.795
工业	－3.604	－622.404	－969.821
公服	－183.011	－190.633	1 143.003
居住	－1 168.935	－629.507	5 292.855
绿地	251.618	352.488	5 918.616
其他	－150.306	－399.204	－20 859.592
商业	1 229.998	859.472	6 712.707
水域	－59.756	－34.458	1 162.436

综上所述，二环外的动态度＞一二环之间动态度＞一环以内动态度，表明随着中心城区距离的增大，轨道交通周边用地的动态度呈现逐步减小的趋势。轨道交通对非中心城区的各类用地面积变化影响较大，因为中心城区在轨道交通建成前已具备较好的城市建设，交通便捷、人口和经济活动较为集中，形成一个成熟的功能区域，轨道交通建设对其影响相对而言不明显。而二环外的区域距离城市中心区较远，该区域开发强度不高，加上交通不便和区位条件差。轨道交通的修建提高了该区域的通达性，加之地价的廉价和政策的倾向，促使城市人口和经济的不断集聚，因此各用地的动态度相对较大。

2.2　用地程度变化

结合研究区的情况分级指数进行修正，道路、工业、公服、居住和商业为 4，绿地为 3，其他用地和水体为 2，并通过表 1 中的式(2)计算得出不同环线范围的各类用地程度变化量和变化率。由表 3 可知，二环外的各类用地程度变化量为 45.825，变化率为 0.125，两者远高于其他环线的

(C)1994-2022 China Academic Journal Electronic Publishing House. All rights reserved.　http://www.cnki.net

区域。因为用地程度变化与初期的城市开发强度和开发成熟度有关，各环线区域各类用地程度的增加主要是由于用地类型的转换。二环以外区域主要是由于其他用地向建设用地的转换。一环、二环之间主要是其他用地、工业仓储用地及居住用地向商业、道路、绿地用地转换。一环外主要是居住、公服、其他用地置换为商业、道路用地。总的来说，变化量(变化率)的大小顺序：二环以外>一环、二环之间>一环以内，说明轨道交通周边用地的程度变化与离中心城区距离呈现负相关。

表 3 不同区段各类用地程度变化情况

Tab. 3 Changes in Land Use Degree in Different Sections

环线范围	综合指数 I		变化量	变化率
	2009 年	2019 年	ΔI	R_c
一环以内	380.356	382.215	1.859	0.005
一环、二环之间	392.539	394.789	2.251	0.006
二环外	291.664	337.489	45.825	0.157

2.3 用地的空间变化

通过表 1 的式(3)计算出不同环线范围的用地类型相对变化率 R_r，进一步探讨全域范围内的站点周边的用地变化情况。由表 4 可知，整体来看二环外的用地相对变化率较高，除了工业用地、其他用地外，另外 6 类用地的相对变化率均大于 1，表明变化率高于全域水平。一环、二环之间道路、工业、水域的相对变化率均高于全域水平，其中工业的相对变化率更是达到 7.151。一环以内的公服、居住用地相对变化率高于全域水平。总的来说，一环以外、一环、二环之间区域的用地面积变化不突出，均与全域水平较为接近，同时也说明轨道交通的建设对于远离城市中心的二环外区域影响较大。

表 4 不同区段各类土地利用类型相对变化率

Tab. 4 The Relative Change Rate of Land Use Types in Different Sections

用地类型	一环以内	一环、二环之间	二环外
道路	0.476	1.007	1.058
工业	0.226	7.151	0.650
公服	2.096	0.740	2.693
居住	2.917	0.534	2.765
绿地	0.579	0.641	1.069
其他	0.000	0.000	0.974
商业	0.909	0.471	1.193
水域	0.919	1.937	1.180

3 空间维度的不同区段用地的差异性

利用 ArcGIS 空间分析工具，提取出 2019 年各站点 0～200、200～400、400～600 m 的用地情况。结合 1 号轨道交通实际情况，排除待开发的站点：望湖路、南站南广场、骆岗、高王、丙子铺、九联圩。

3.1 用地功能

研究不同站点周边用地占比情况，可以明确该站点的主要功能，并针对不同站点的用地结构进行分析(表 5)。可以发现：①紫庐、秋浦河路、长淮、朱岗、葛大店、包公园的居住用地占比大，且有一定的服务配套功能，主要提供居住功能；合肥站、合肥南站、大东门交通用地占比大，主要承担交通枢纽功能；②金斗公园、会展中心、塘西河公园绿地占比大，主要提供绿地游憩功能；③万年埠、明光路、云谷路商业商务用地占比大，承担着各个片区主要的商业购物功能；张洼站主要为工业生产功能。

表 5 不同区段各类用地构成

Tab. 5 Composition of Land for Different Sections

站名	半径/m	道路/(%)	工业/(%)	公服/(%)	居住/(%)	绿地/(%)	其他/(%)	商业/(%)	水域/(%)
包公园	200	18.588	0.000	0.366	29.155	2.443	0.000	49.448	0.000
	200～400	19.426	1.583	20.518	19.913	9.519	0.000	21.985	7.056
	400～600	20.639	0.049	3.943	45.998	9.625	0.000	5.297	14.450
滨湖会展中心	200	33.492	0.000	14.665	0.000	41.874	0.000	9.970	0.000
	200～400	15.096	0.000	21.744	0.160	42.503	0.000	17.776	2.722
	400～600	11.255	0.000	29.067	9.814	43.376	0.000	2.414	4.074
长淮	200	36.531	0.000	4.781	21.252	0.000	0.000	37.436	0.000
	200～400	15.602	0.000	13.272	39.257	0.140	0.000	31.728	0.000
	400～600	9.770	2.438	4.214	73.234	0.001	0.000	10.343	0.000

(C)1994-2022 China Academic Journal Electronic Publishing House. All rights reserved. http://www.cnki.net

续表

站名	半径/m	道路/(%)	工业/(%)	公服/(%)	居住/(%)	绿地/(%)	其他/(%)	商业/(%)	水域/(%)
	200	41.944	0.000	0.165	0.000	14.012	0.000	26.289	17.589
大东门	200～400	47.255	0.003	2.063	8.321	9.247	0.000	27.544	5.566
	400～600	26.347	0.000	4.086	7.140	9.021	0.000	39.787	13.619
	200	37.392	0.000	22.619	22.553	14.782	0.000	2.653	0.000
葛大店	200～400	33.133	0.000	20.198	27.611	15.547	0.000	3.510	0.000
	400～600	26.538	0.000	3.907	46.088	20.875	0.000	2.592	0.000
	200	98.203	0.000	0.000	0.000	1.797	0.000	0.000	0.000
合肥南站	200～400	59.181	0.000	0.008	0.000	15.087	0.000	25.724	0.000
	400～600	77.478	0.000	0.013	0.000	13.643	0.000	8.866	0.000
	200	61.673	0.000	0.199	0.000	0.000	0.000	38.128	0.000
合肥站	200～400	73.125	0.000	0.267	2.289	0.000	0.000	24.319	0.000
	400～600	51.593	0.000	2.011	16.246	0.663	0.000	29.487	0.000
	200	36.366	0.000	22.067	20.619	4.624	0.000	16.324	0.000
合工大南区	200～400	16.798	0.000	40.968	32.371	1.695	0.000	8.167	0.000
	400～600	12.310	3.914	42.270	39.029	0.739	0.000	1.738	0.000
	200	40.282	0.000	0.000	0.000	59.718	0.000	0.000	0.000
金斗公园	200～400	19.479	0.000	2.006	8.380	58.498	0.000	7.586	4.051
	400～600	13.687	0.000	8.564	22.050	37.810	0.000	7.179	10.711
	200	34.782	0.012	13.459	0.000	9.559	0.000	42.187	0.000
明光路	200～400	20.822	0.000	3.840	3.443	2.262	0.000	66.871	2.761
	400～600	26.051	0.004	4.711	18.862	6.053	0.000	39.389	4.930
	200	28.067	0.000	17.940	26.006	3.525	0.000	24.462	0.000
秋浦河路	200～400	12.594	3.447	0.825	67.703	0.603	0.000	14.829	0.000
	400～600	16.711	1.276	13.704	51.849	4.668	0.000	11.792	0.000
	200	30.323	0.000	0.000	0.835	40.224	0.000	28.619	0.000
塘西河公园	200～400	15.219	0.000	8.290	10.502	35.815	0.000	22.592	7.583
	400～600	12.835	0.000	3.816	34.233	29.179	0.000	5.841	14.096
	200	29.003	0.000	0.048	0.000	14.025	0.000	48.385	8.540
万达城	200～400	23.564	0.000	0.004	16.416	6.272	0.000	50.510	3.235
	400～600	26.331	0.000	2.763	31.603	0.440	0.000	33.104	5.760
	200	21.586	0.000	0.012	0.000	2.853	0.000	75.549	0.000
万年埠	200～400	16.715	0.000	0.004	33.557	0.847	0.000	48.877	0.000
	400～600	23.384	0.000	4.699	31.635	2.071	0.000	38.212	0.000
	200	34.329	0.000	0.000	0.000	8.248	0.000	57.423	0.000
云谷路	200～400	20.448	0.000	0.010	14.523	5.269	0.000	59.750	0.000
	400～600	21.016	0.000	0.023	51.542	1.094	0.000	20.006	6.319
	200	33.030	0.000	32.998	5.493	0.000	0.000	28.479	0.000
朱岗	200～400	15.032	0.002	21.280	53.563	0.323	0.000	9.800	0.000
	400～600	18.618	2.478	7.461	63.674	1.055	0.000	6.715	0.000
	200	26.112	0.000	0.000	44.796	7.193	0.000	21.898	0.000
紫庐	200～400	16.996	0.000	0.490	58.937	2.359	0.000	21.218	0.000
	400～600	21.775	0.000	17.905	45.823	2.131	0.000	12.366	0.000

(C)1994-2022 China Academic Journal Electronic Publishing House. All rights reserved.　http://www.cnki.net

不同用地性质的空间分布分析。①交通用地、绿地和水域各半径范围内所占比例相当，也存在距离站点越近交通用地所占比例越大的趋势；②公共服务设施用地的占比视具体的站点功能有所差异，呈现出公服用地占比离站点越远越大的趋势；③居住用地呈现距离地铁站越远所占比例递增的趋势；④商业用地0～200、200～400 m半径范围内的比例远高于400～600 m范围。总之，轨道交通各站点周边用地均呈现多元复合型，而不同站点周边用地的主导功能有所差异，主要包括居住、商业、交通3类，个别站点公园和工业用地占主导。

3.2 用地结构

通过表1中式(4)、式(5)计算出不同半径范围用地的信息熵和均衡度，结果见表6。同一半径不同站点的对比。400～600 m信息熵和均衡度大小趋于较高值的平稳状态，表明站点400～600 m范围内不同职能的用地更多，土地分布更均衡。200～400 m范围内信息熵和均衡度有一定的波动。

表6 站点用地结构的信息熵、均衡度统计

Tab. 6 Information Entropy and Equilibrium Degree of Site Land m

站名	400～600		200～400		200	
	信息熵	均衡度	信息熵	均衡度	信息熵	均衡度
包公园	1.475	0.709	1.774	0.853	1.132	0.544
滨湖会展中心	1.415	0.681	1.396	0.671	1.242	0.597
长淮	0.914	0.440	1.298	0.624	1.210	0.582
大东门	1.878	0.903	1.378	0.662	1.307	0.629
葛大店	1.257	0.605	1.451	0.698	1.419	0.682
合肥南站	0.685	0.330	0.946	0.455	0.090	0.043
合肥站	1.109	0.533	0.675	0.325	0.678	0.326
合工大南区	1.223	0.588	1.304	0.627	1.465	0.704
金斗公园	1.612	0.775	1.244	0.598	0.674	0.324
明光路	1.494	0.719	1.022	0.491	1.227	0.590
秋浦河路	1.363	0.655	0.995	0.478	1.477	0.711
塘西河公园	1.557	0.749	1.629	0.783	1.126	0.542
万达城	1.369	0.658	1.267	0.609	1.200	0.577
万年埠	1.295	0.623	1.056	0.508	0.645	0.310
云谷路	1.217	0.585	1.068	0.514	0.891	0.429
朱岗	1.115	0.536	1.195	0.575	1.249	0.601
紫庐	1.338	0.643	1.056	0.508	1.232	0.593

200 m范围内信息熵和均衡度波动最大，主要是由于其不同职能用地相对最少，且各个站点主要职能的差异导致。

同一站点不同半径的对比。大致呈现出信息熵和均衡度从站点由内而外升高的趋势。仅合工大南区、琼海公园、大东门、长淮不同，由于其站点周边主要功能性质的影响。总的来说，各个范围的信息熵和均衡度趋势接近，且整体值较高，说明用地结构已发展完善，均质性较高。

3.3 用地形态

通过表1中式(6)、式(7)计算得到各站点不同半径范围内用地的半径维数和边界维数。根据前文分析，站点周边工业、水域、绿地等并非都有，因此各类用地形态的分析针对交通、公服、居住和商业用地这4类用地进行分析，计算结果见表7。

同一站点不同用地性质的对比。①半径维数方面。大小排序为：交通＞商业＞居住＞公管。半径维数总体是随着距离站点越近越大，表明用地向心集中程度越强。②边界维数各站点趋势较为一致，大小排序为：交通＞商服＞居住＞公管。站点各类用地的形状复杂程度相当，其中交通用地的形态最为复杂。边界维数大体上呈现随距离站点越近越大，即各类用地形态越复杂。

同一性质不同站点的对比。①半径维数：道路用地半径维数最高，均在5以上，表面其向心程度较高。公服用地，合肥南站、云谷路的半径维度最低，其分别主要提供交通换乘功能和商业功能。居住用地和商业用地半径维度整体上较高，均在3以上。总的来说，各站点道路、商业、居住用地半径维数较大，向站点集中的趋势明显；②边界维数：包公园、长淮、合工大南校区、朱岗的用地形态整体比较规整。道路用地，各个站点半径维数均在4.5以上，道路交通设施完善。公服用地除了合肥南站、万达城、万年埠、云谷路外，其他站点边界维数较高。居住和商业各站点半径维数整体较高，较为趋近。

综上所述，商业、居住和道路用地半径维数较高，表明向心聚集程度较强，公服用地半径维数较低，表明向心聚集程度较弱。道路、商业用地边界维数较高即形态复杂，公服、居住用地较为规则。

(C)1994-2022 China Academic Journal Electronic Publishing House. All rights reserved. http://www.cnki.net

表 7　站点用地形态的半径维数、边界维数统计

Tab. 7　Radial Dimension and Boundary Dimension of Site Land

站名	半径维数				边界维数			
	道路	公服	居住	商业	道路	公服	居住	商业
包公园	5.009	4.018	5.223	5.001	4.867	3.167	4.943	4.565
滨湖会展中心	5.045	5.099	2.456	4.603	4.510	4.068	1.892	3.460
长淮	5.061	4.518	5.427	5.193	4.994	3.740	5.398	4.980
大东门	5.434	3.575	3.096	5.320	5.719	2.873	2.921	5.346
葛大店	5.309	4.832	5.269	4.071	5.167	4.036	4.968	2.845
合肥南站	5.806	0.928	0.000	3.306	5.808	0.481	0.000	3.223
合肥站	5.748	3.221	3.065	5.386	6.272	2.571	2.921	5.432
合工大南区	5.070	5.317	5.253	4.492	4.852	4.773	4.962	3.681
金斗公园	5.122	2.822	3.208	3.016	4.683	2.328	2.812	2.306
明光路	5.204	4.475	3.038	5.500	5.346	3.791	2.769	5.682
秋浦河路	5.003	4.433	5.446	4.950	4.839	3.569	5.377	4.508
塘西河公园	5.072	2.989	4.485	5.003	4.590	2.498	3.694	4.144
万达城	5.188	2.162	3.380	5.448	5.100	1.373	3.378	5.193
万年埠	5.068	2.014	3.506	5.561	4.833	1.401	3.647	5.064
云谷路	5.203	1.052	3.477	5.472	5.048	0.610	3.540	5.233
朱岗	5.131	5.046	5.196	4.872	4.969	4.233	5.022	4.368
紫庐	5.123	2.737	5.549	5.038	4.759	2.279	5.164	4.138

4　结束语

合肥市 1 号轨道交通对沿线各类用地的影响，时间维度方面：①各类用地面积变化方面，轨道交通对非中心城区的各类用地面积变化影响较大，用地的动态度、变化率和变化量大小排序均呈现出二环以外＞一二环之间＞一环以内。其中，二环以外区段的商业、居住、其他用地动态度分别高达 −20 859.592%、6 712.707%、5 292.855%；②用地利用程度变化差异方面，变化率和变化量的大小顺序均为二环以外＞一环、二环之间＞一环以内。其中，二环以外的用地程度变化量为 45.825，变化率为 0.125，远高于其他环线区域；③各类用地变化空间差异方面，一环以外、一环、二环之间区域的用地面积变化不突出，二环以外用地面积变化较大，远大于全域变化水平。

空间维度方面：①用地功能方面，轨道交通各站点周边用地均呈现多元复合型，而不同站点周边用地的主导功能有所差异，主要包括居住、商业、交通 3 类，个别站点公园和工业用地占主导；②各轨道站点 400～600 m 范围用地的信息熵和均衡度大小趋于较高值的平稳状态，200 m 范围内信息熵和均衡度波动最大，主要是由于其不同职能用地相对最少，且各个站点主要职能的差异导致。用地呈现出距离站点越远，其信息熵和均衡度越高的趋势，表明用地类型越多，结构均衡性越强；③商业、居住和道路用地半径维数较高向心聚集程度较强，道路、商业用地边界维数较高形态较复杂。边界维数大体呈现随着距离站点越近越大，即各类用地形态越复杂。

在城镇化快速发展的时代背景下，城市土地利用变化主要是在规划引导下，受人口增长、经济发展、产业结构调整等因素的综合作用，并致城市空间的外围拓展和城市内部土地的更新。本文仅是基于单元同构的城市土地使用性质数据进行空间分析，探讨了轨道交通沿线土地利用的变化情况，为提升土地使用效率，引导城市与轨道交通协同发展提供了支撑。而随着数据获取渠道的丰富，在既有研究的基础上，基于多元异构数据，从空间相互作用与网络的视角，针对轨道站点沿线土地变化的驱动因素，以及轨道交通与城市发展的协调关系的研究是未来值得深入探讨的方向。

参考文献

[1] 邓羽. 轨道交通站域的城市物质空间更新轨迹与组织模式:以北京为例[J]. 地理科学,2017,37(6):14-21.(DENG Yu. The spatial succession and organization model of the urban material space within the rail transit station:a case in Beijing[J]. Scientia Geographica Sinica,2017,37(6):817-824.)

[2] 何冬华. 土地增值收益再分配的博弈与干预:刍议广州 TOD 的竞合关系[J]. 城市规划,2018,42(7):

(C)1994-2022 China Academic Journal Electronic Publishing House. All rights reserved.　http://www.cnki.net

79-85.(HE Donghua. Benefit game and intervention on the redistribution of land value increment:discussion on competition and cooperation of the transitoriented development in Guangzhou[J]. City Planning Review,2018,42(7):79-85.)

[3] 林雄斌,杨家文,李贵才,等. 跨市轨道交通溢价回收策略与多层级管治:以珠三角为例[J]. 地理科学,2016,36(2):222-230.(LIN Xiongbin,YANG Jiawen,LI Guicai,et al. Land value capture and multi-level governance for inter-city passenger rail transit in the Zhujiang River Delta[J]. Scientia Geographica Sinica,2016,36(2):222-230.)

[4] WANG Y,LIANG Z. The dynamic research on investment/financing management system of regional inter-city rail transit engineering[EB/OL].(2019-10-29). https://kns.cnki.net/KCMS/detail/detail.aspx?dbcode=IPFD&filename=MGKY201003001437.

[5] 吴佳明,陈鹏,周军. 深圳轨道交通一期站点地区土地利用变化特征研究[J]. 规划师,2010,26(S2):201-204.(WU Jiaming,CHEN Peng,ZHOU Jun. Land use changes along Shenzhen subway the first stage station area development[J]. Planners,2010,26(S2):201-204.)

[6] 郭源园,李莉,李贵才,等. 国内外城市土地利用与交通相互作用研究综述[J]. 国际城市规划,2015,30(3):29-36.(GUO Yuanyuan,LI Li,LI Guicai,et al. Overview of interaction between urban land use and transportation[J]. Urban Planning International,2015,30(3):29-36.)

[7] LIN J J,GAU C C. A TOD planning model to review the regulation of allowable development densities around subway stations[J]. Land Use Policy,2006,23(3):1-36.

[8] 冯国强,李菁. 城市轨道交通减排治污效应评估[J]. 中国人口·资源与环境,2019,29(10):143-151.(FENG Guoqiang,LI Jing. Assessment of emission reduction effect of urban rail transit[J]. China Population,Resources and Environment,2019,29(10):143-151.)

[9] 梁若冰,席鹏辉. 轨道交通对空气污染的异质性影响:基于RDID方法的经验研究[J]. 中国工业经济,2016,336(3):83-98.(LIANG Ruobing,XI Penghui. Heterogeneous effects of rail transit on air pollution:an empirical study with RDID[J]. China Industrial Economics,2016,336(3):83-98.)

[10] CHAN S,MIRANDA-MORENO L. A station-level ridership model for the metro network in Montreal,Quebec[J]. Canadian Journal of Civil Engineering,2013,40(3):254-262.

[11] 梁明瑗,王观. 成都市中心城区轨道交通站点周边共享单车停放空间研究[J]. 规划师,2019,35(18):54-61.(LIANG Mingyuan,WANG Guan. A study of parking space of shared bikes near rail transit stations,Chengdu[J]. Planners,2019,35(18):54-61.)

[12] 申犁帆,张纯,李赫,等. 城市轨道交通通勤与职住平衡状况的关系研究:基于大数据方法的北京实证分析[J]. 地理科学进展,2019,38(6):791-806.(SHEN Lifan,ZHANG Chun,LI He,et al. Relationship between urban rail transit commuting and jobs-housing balance:an empirical analysis from Beijing based on big data methods[J]. Progress in Geography,2019,38(6):791-806.)

[13] 王爱,陆林,包善驹. 合肥市地价的空间格局与影响因素研究[J]. 经济地理,2016,36(10):84-92.(WANG Ai,LU Lin,BAO Shanju. Study on land price spatial pattern and its influencing factors in Hefei[J]. Economic Geography,2016,36(10):84-92.)

[14] 王锡福,徐建刚,李杨帆. 南京城市轨道交通建设潜在影响下的土地利用分异研究[J]. 人文地理,2005,10(3):112-116.(WANG Xifu,XU Jiangang,LI Yangfan. Potential influences of rail transportation construction to land use differentiation in Nanjing[J]. Human Geography,2005,10(3):112-116.)

[15] 乐晓辉,陈君娴,杨家文. 深圳轨道交通对城市空间结构的影响:基于地价梯度和开发强度梯度的分析[J]. 地理研究,2016,35(11):2091-2104.(LE Xiaohui,CHEN Junxian,YANG Jiawen. Impact of rail transit on urban spatial structure in Shenzhen:analysis based on land parcel price and far gradients[J]. Geographical Research,2016,35(11):2091-2104.)

[16] 段德罡,张凡. 土地利用优化视角下的城市轨道站点分类研究:以西安地铁2号线为例[J]. 城市规划,2013,37(9):39-45.(DUAN Degang,ZHANG Fan. Study on classification of urban rail transit stations from theperspective of land use optimization:a case study on Xi'an subway line 2[J]. City Planning Review,2013,37(9):39-45.)

[17] 何冬华,袁媛. 轨道交通环线沿线的土地利用空间特征分析:以广州市轨道交通11号环线为例[J]. 现代城市研究,2010,25(9):90-95.(HE Donghua,YUAN Yuan. Analysis of the spatial characteristics of land-use led by ring rail line:a case study in Guangzhou[J]. Modern Urban Research,2010,25(9):90-95.)

[18] 周青峰,刘苏,王耀武. 城市轨道交通站点周边土地利用与交通协调关系研究[J]. 铁道运输与经济,2018,40(4):100-106.(ZHOU Qingfeng,LIU Su,WANG Yaowu. A study on the coordinative relation of land use and transport around the metro station[J]. Railway Transport and Economy,2018,40(4):100-106.)

[19] DEBREZION G,PELS E,RIETVELD P. The impact of railway stations on residential and commercial property value:a meta-analysis[J]. The Journal of Real Estate Finance and Economics,2007,35(2):161-180.

(下转第217页)

(C)1994-2022 China Academic Journal Electronic Publishing House. All rights reserved. http://www.cnki.net

based on spatial analysis: a case study of Xi'an[J]. City Planning Review, 2016, 40(8): 59-64.)

[7] 陆相林，苗长虹. 小城镇应急设施选址等级优化配置模型与实证：以北京市房山区消防站点布局优化为例[J]. 安全与环境工程，2016，23(2)：96-101.（LU Xianglin, MIAO Changhong. Hierarchical optimization allocation of emergency facility location in small towns: a case study of fire stations in Fangshan district in Beijing[J]. Safety and Environmental Engineering, 2016, 23(2): 96-101.)

[8] 徐智邦，周亮，蓝婷，等. 基于 POI 数据的巨型城市消防站空间优化：以北京市五环内区域为例[J]. 地理科学进展，2018，37(4)：535-546.（XU Zhibang, ZHOU Liang, LAN Ting, et al. Spatial optimization of mega-city fire station distribution based on point of interest data: a case study within the 5th Ring Road in Beijing [J]. Progress in Geography, 2018, 37(4): 535-546.)

[9] 肖大威. 试论城市防火规划[J]. 城市规划，1985(3)：61-63.（XIAO Dawei. On urban fire prevention planning[J]. City Planning Review, 1985(3): 61-63.)

[10] UNO T, KATO K, KATAGIRI H. An application of interactive fuzzy satisficing approach with particle swarm optimization for multiobjective emergency facility location problem with a-distance[C]// Proceedings of the 2007 IEEE Symposium on Computational Intelligence in Multicriteria Decision Making (MCDM2007). New York: IEEE Press, 2007: 368-373.

[11] CHANDRAMOULI M, LIU N, HUANG B. Optimal siting of fire stations using GIS and ANT algorithm [J]. Journal of Computing in Civil Engineering, 2006, 20(5): 361-369.

[12] 詹庆明，杨爽. 村镇应急公共设施选址布局优化研究[J]. 地球信息科学学报，2019，21(5)：15-27.（ZHAN Qingming, YANG Shuang. Optimization of emergency facilities layout in villages [J]. Journal of Geo-information Science, 2019, 21(5): 15-27.)

[13] 陈韶阳，程镇燕，D K L. 基于 SAVEE 方法的海岛空间价值评价：以南沙群岛为例[J]. 海洋环境科学，2012，31(1)：107-110.（CHEN Shaoyang, CHENG Zhenyan, DOUGLAS K L. Islands valuation of spatial appraisal based on SAVEE method: with the Nansha Islands as an example[J]. Marine Environmental Science, 2012, 31 (1): 107-110.)

[14] LOH D K, HSIEH Y T C, CHOO Y K, et al. Integration of a rule-based expert system with GIS through a relational database management system for forest resource management [J]. Computers and Electronics in Agriculture, 1994, 11(2-3): 215-228.

[15] LOH D K, HOLTFRERICH D R, VAN STIPDONK S E P. Automated construction of rule bases for forest resource planning[J]. Computers and Electronics in Agriculture, 1998, 21(2): 117133.

[16] 武汉市测绘研究院. 武汉市地理国情监测与城市协调发展研究 2018[M]. 北京：测绘出版社，2018.（Wuhan Geomatic Institute. Study on geographical conditions monitoring and urban harmonious development of Wuhan 2018[M]. Beijing: Surveying and Mapping Press, 2018.)

[17] 王磊. 历史钩沉：武汉市早期的城市设计回顾[J]. 华中建筑，2001，19(5)：102-106.（WANG Lei. History retrospection: a recalling about Wuhan's city design in the early days[J]. Huazhong Architecture, 2001, 19 (5): 102-106.)

[18] 姜昀呈，孙立坚，王涛涛，等. 兰州市中心城区犯罪分布与城市环境的关系[J]. 测绘科学，2021，46(5)：167-174.（JIANG Yuncheng, SUN Lijian, WANG Taotao, et al. The coupling relationship between crime distribution and urban environment in Lanzhou city center[J]. Science of Surveying and Mapping, 2021, 46(5): 167-174.)

[19] 毛峰. 基于多源轨迹数据挖掘的居民通勤行为与城市职住空间特征研究[D]. 上海：华东师范大学，2015.（MAO Feng. Mining commuting pattern and urban jobs-housing balance from multi-source mobile trajectory data[D]. Shanghai: East China Normal University, 2015.)

（责任编辑：路素军）

（上接第 198 页）

[20] 魏中宇，苏惠敏，黄荣静. 西安地铁二号线建设对土地利用变化的影响[J]. 生态学杂志，2018，37(8)：2472-2482.（WEI Zhongyu, SU Huimin, HUANG Rongjing. The influence of the construction of Xi'an metro line 2 on land use change[J]. Chinese Journal of Ecology, 2018, 37(8): 2472-2482.)

[21] 洪涛. 南京中心城轨道站点周边商业用地开发强度研究[D]. 南京：南京工业大学，2018.（HONG Tao. Research on the development intensity of commercial land around the orbit sites of the central urban area of Nanjing[D]. Nanjing: Nanjing University of Technology, 2018.)

[22] 张艳，曹康，何奕苇，等. 土地使用与轨道交通的空间适配探讨：深圳地铁 2 号线的实证分析[J]. 城市规划，2017(8)：107-115.（ZHANG Yan, CAO Kang, HE Yiwei, et al. Discussion on spatial match between land use and rail transit: a case study of Shenzhen subway line 2[J]. City Planning Review, 2017(8): 107-115.)

（责任编辑：路素军）

(C)1994-2022 China Academic Journal Electronic Publishing House. All rights reserved.　http://www.cnki.net

大型铁路客站站域空间步行网络构建研究

桂汪洋,张旭

(安徽建筑大学 建筑与规划学院,合肥 230601)

摘要: 新时期我国对新型客站的巨大投入,其目标不是一个自我满足的一站式服务的交通枢纽,而是期望其作为城市触媒带动其周边城市片区的协同发展,这需要客站与城市空间的有机衔接和互动,步行网络的构建是影响站城融合的关键要素。本文基于我国站域空间活力提升的需求,通过国内外站域案例的比较,剖析步行网络与站域空间发展的互馈机制,探讨点块、点轴和点网 3 种站域步行系统结构模式的特征,分析了站域肌理、土地利用、开发强度、功能空间和交通规划 5 种步行网络建构要素,并在此基础上提出了性能化设计、分层分流、链接成网、资源链接、统一规划 5 种优化策略,可促进站域步行网络的建构,提升站域活力,实现站域协同发展和客站的可持续建设。

关键词: 站域; 步行系统; 网络化; 协同; 站城融合

中图分类号: TU91 **文献标识码:** A **文章编号:** 1673-0836(2022)01-0020-08

Research on Construction of Spatial Pedestrian Network in Large Railway Passenger Station

Gui Wangyang, Zhang Xu

(*School of Architecture and Planning, Anhui Jianzhu University, Hefei* 230601, *P.R. China*)

Abstract: In the new era, our country's huge investment in new passenger stations does not aim to be a self-satisfied one-stop service transportation hub, but to act as an urban catalyst to drive the coordinated development of its surrounding urban areas. This requires an organic connection between the passenger station and the urban space. Interaction, the construction of a pedestrian network is a key element that affects the integration of stations and cities. Based on the demand for improving the vitality of the station space in China, this paper analyzes the mutual feedback mechanism of the pedestrian network and the development of the station space through the comparison of the domestic and foreign station area cases. It discusses the three structural modes of the station area pedestrian system of the point block, point axis and point network. The characteristics of the station area, land use, development intensity, functional space, and transportation planning five pedestrian network construction elements are analyzed. On this basis, performance-based design, hierarchical distribution, link formation, resource link, and unified plan five optimization strategies are proposed to promote the construction of the station area pedestrian network, enhance the station area's vitality, and realize the coordinated development of the station city and the sustainable construction of the passenger station.

Keywords: station domain; walking system; networking; collaboration; station-city integration

收稿日期: 2021-10-30(修改稿)

作者简介: 桂汪洋(1976—),男,安徽霍山人,博士,副教授,主要从事城市设计研究。E-mail: 21356364@qq.com

基金项目: 安徽省高校省级自然科学研究项目(KJ2019A0750,KJ2019A0752);校引进人才及博士启动基金项目(2018QD34);安徽省住房城乡建设科学技术计划项目(2020-YF27)

(C)1994-2022 China Academic Journal Electronic Publishing House. All rights reserved. http://www.cnki.net

0　引言

如何提升站域空间活力已成为城市管理者和规划者所共同关心的问题。随着高铁时代的到来，我国新建了大量的高铁客站，但城市居民除了非必要性活动依然不愿意进入这个片区，形成了站房新、广场大、站域空间活力低的局面。而步行网络建立的意义正在于缝合和激发活力，通过网络化的步行系统，将客站与其他城市功能要素系统链接，放大客站服务的强度和能级，形成促进区域增长的内核。基于我国站域活力提升的诉求，本文提出站域步行网络的建构，界定其空间分布，剖析其形成机制，并进一步提出相应的完善策略。

1　步行网络与站域发展的契合

步行系统网络化发展是站域高效集约化发展的必然需求，而站域的集约化发展又会促进步行系统网络化发展。客站带来大量的人口聚集和流动必然促使站域土地结构调整和重新分配，对有限的土地进行集约化利用的需求也进一步增强。集约化最主要的表现就是土地的立体化使用，立体化发展必须以客站为基础，向空中、地下和站点周边地区辐射，这种功能的拓展与延伸催化了步行系统的蔓延和网络的形成。城市轨道交通在地下和空中的分层，拓展了地下和空中行走的需求；其次，大型铁路客站各种交通设施（公交、出租、私家车等）在不同标高城市基面之间的换乘，成为了步行系统网络化发展的重要动力。而利用地下和空中空间承接部分地面功能，不但可以扩大站域空间容量，还可以有效地改善地面环境品质，带来更多的商机，促进站域空间的集约化发展。如日本，规模前十位的地下街有 8 个是结合铁路客站而发展起来的（图 1），形成了步行适宜的集约化发展的站域空间。

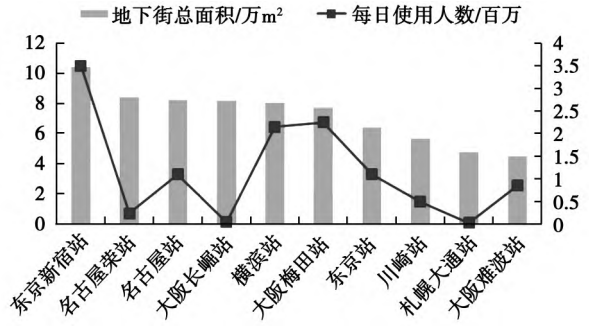


图 1　日本高铁站

Fig. 1　Japan high speed rail station

2　结构模式

由于站域存在“核心-扩展”的组合关系，客站与步行系统的基本空间组合模式为“生长点”与“发展轴”，这两者所构成的结构由于发展阶段、传统结构和所处区位等的不同，往往呈现出不同的结构模式，通过对国内外客站与周边城市空间发展模式的归纳总结，可将结构模式分为点块、点轴、点网 3 种类型（图 2）。

2.1　点块模式

点块模式即在步行核心区内（200～400 m 以内），将客站与各种城市功能通过合理的组织和有序的交通联系形成一个有机的整体（图 2）。主要特征是把站前广场、站房和站场作为一个整体，将地下、地面、地上进行统一设计，使之成为一个立体的、高效的城市公共空间体系。但其产权关系、建设时序与运营管理等方面较为复杂，常见于城市中心地段用地较为紧张的地区。地下空间与地上空间立体化整合，提升了区域步行系统的完整性和连续性，改善了城市交通环境。比较典型的如日本京都站，将站房、站场和站前广场一体化设计，通过层叠手法，形成了连续的步行空间，创造了丰富多彩的城市生活场所。

2.2　点轴模式

点轴模式是以客站为依托，沿着单一轴线，通过地下街与地面空间有机结合，塑造地上、地面和地下共同承载城市各种活动的公共空间结构（图 2）。此模式主要特征是地下空间结合车站一体化开发，步行系统和城市功能以站点为中心沿轴线发展，将地面作为城市广场，地下用作商业开发、人流集散和与周边区域的连接通道，形成连接范围更广、功能更复杂、规模更大的“城市发展轴”。此模式常见于城市边缘区新建客站，利用客站带动新城建设。比较典型的如杭州东站，结合客站利用地下步行系统联系客站南北，形成南北向的发展轴，带动新城的发展。

2.3　点网模式

点网模式是以客站为核心，在核心区和影响区（1 500 m 以内），通过步行系统进行有机联系，形成功能多样、空间立体的整体（图 3）。主要特征是在站域步行可达范围内，将车站、城市存在的问题一体化解决，车站发展上升到地段的高度，通过多组建筑来综合解决区域问题，促进站城一体化发

(C)1994-2022 China Academic Journal Electronic Publishing House. All rights reserved.　http://www.cnki.net

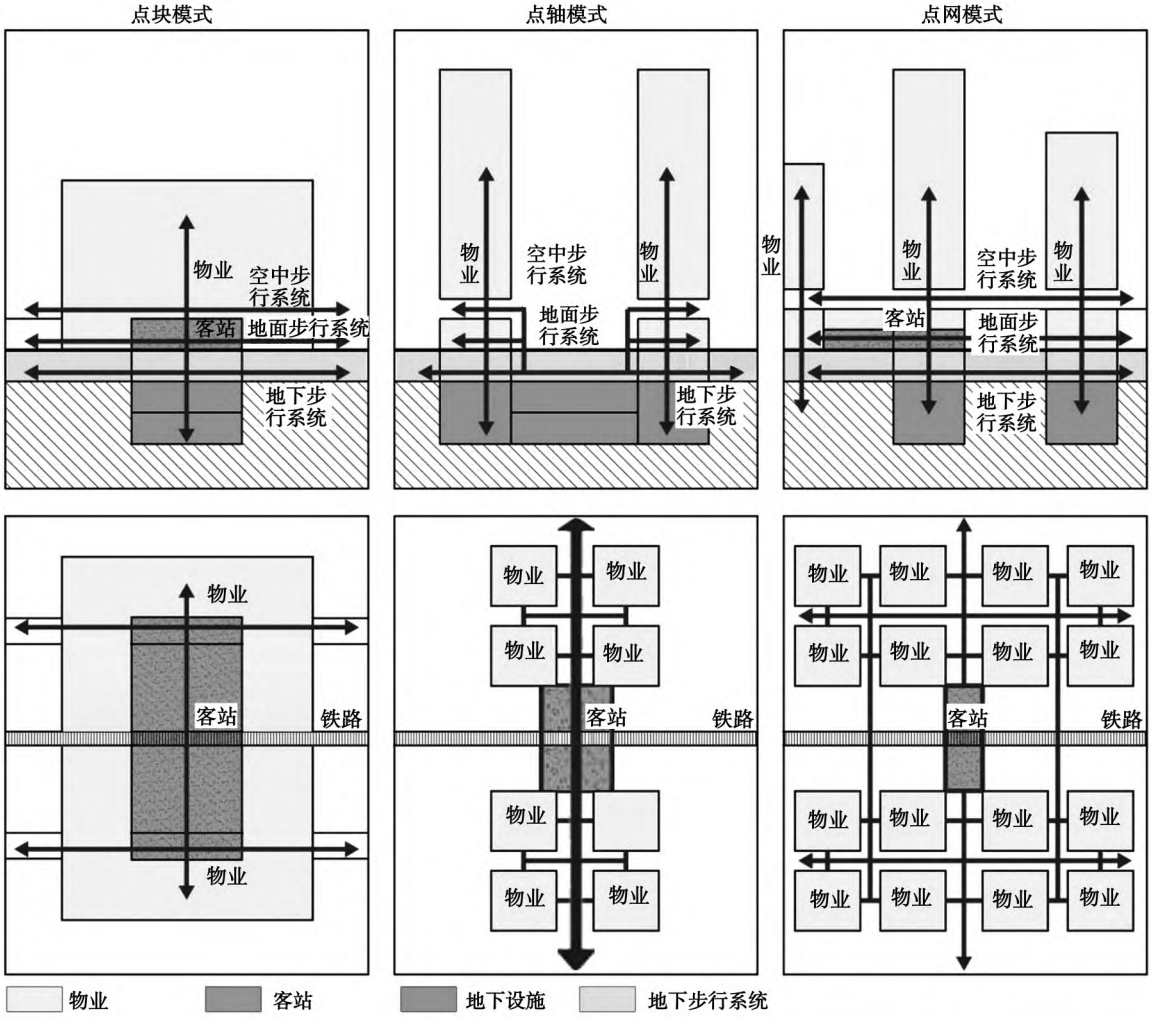


图2 站域步行系统的结构模式

Fig. 2 Structural model of the station-domain walking system

展[1]。步行系统的发展不再拘泥于客站本身，而是结合城市空间，形成有机渗透、交叠的延展性关系，成为一个功能复合而统一的城市空间系统。此模式常见于城市中心再发展区域，以客站的改扩建为机遇，通过区域整合，提升中心区活力。比较典型的如日本大阪站，通过站域统一规划设计，利用步行动线整合和广场、建筑中庭、连廊等的运用，形成连续、舒适的步行空间，焕发区域活力。

3 建构要素

铁路客站如果仅仅考虑自身发展需求，很容易形成一个自我封闭的系统，导致城市人流导入不足，空间活力低。因此，步行网络系统的建立更加需要将客站与周边城市空间作为一盘棋，从区域乃至城市的视角统筹考虑。

3.1 站城肌理

城市肌理作为城市设计的基本要素，反映了由建筑群决定的外部空间形态。通过国内外典型客站的对比可以发现，在步行核心圈层内(500 m)，国内铁路客站除去本身的综合开发以及配套外，周边城市建筑与铁路客站基本是两套相互独立的空间体系，城市肌理也因站场和线路的割裂而呈现出明显的城市板块和客站板块(图3)。

以杭州东站为例，空间结构等级分化明显，与周边建筑超长的步行距离和道路的阻隔，地面步行难以成行，地下步行系统基本成为了仅服务于客站的交通通廊，客站与城市人流难以相互转换[2]。而日本客站站场和站前广场占地面积均较小，空间密度较为平均，空间结构等级不明显，线路两侧的城市肌理往往得以延续，形成了连续的街道。不同的肌理往往反映了客站与周边城市空间联系的强弱，也决定了步行系统的发展方向。因此，客站与周边城市空间的肌理在步行网络设计中应当给予足够的重视。

(C)1994-2022 China Academic Journal Electronic Publishing House. All rights reserved. http://www.cnki.net

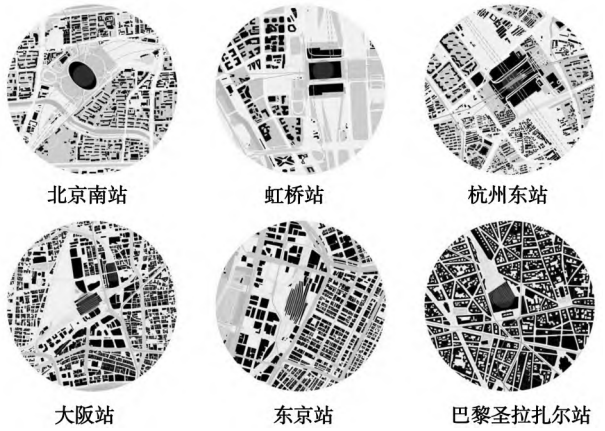


图 3　国内外不同站域的站城肌理

Fig. 3　Station-city texture in different station regions at home and abroad

3.2　土地利用

通过对比可以发现，我国目前站域空间土地利用呈现出了单一的特征（图 4），客站周边多为商务办公楼和住宅开发。以北京南站为例，其周边除了少量零碎的商业空间外，基本都是封闭的居住区。市场、酒店、办公和居住 4 种功能业态已经成为了我国高铁站点区域的主要类型，所占比例平均值分别为 7.71%、6.95%、25.27%和 56.17%[3]。日本铁路客站周边建筑基本以组团的形式呈现，并且土地利用较为多元化，大多为商业、酒店、办公、休闲娱乐等城市功能，公共性极强。以大阪站为例，在步行可达范围内，形成了高端办公、商业的梅北地区，面向年轻人的阪急梅田站、茶屋町地区，面向成人的高档酒店、餐厅、精品屋和演奏厅的西梅田地区，融合全球潮流与本地特色的 JR 大阪站南地区和商店、电影院、健身房等设施齐全的大阪站地区。

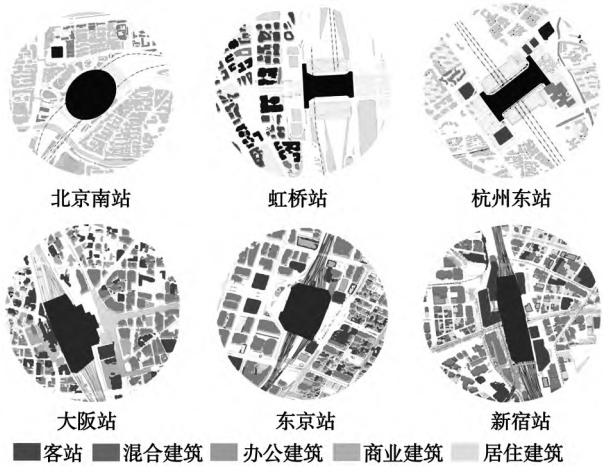


图 4　国内外不同站域的土地利用

Fig. 4　Land use in different stations at home and abroad

这 5 个各具特色的街区，提高了城市生活的效率和便利，也提升了区域活力。

3.3　开发强度

我国内地目前站域规划容积率一般规定在2.5左右，甚至更低。而从日本和我国香港等人口高密度地区来看，一般开发强度都在 8～10 之间（表 1）。以香港为例，香港通过《建筑物（规划准则）》法规的确立，将轨道交通车站周边列为一类住宅用地，均采用高容积率开发。在都会区，建议商业容积率在 10.0～15.0，住宅容积率为 8.0～10.0；新区和综合发展区住宅容积率为 6.5；在新市镇商业容积率建议 8.0～10.0，住宅容积率建议为8.0，这种结合车站土地高强度利用导向，确保了 3/4 居民住在轨道交通站点 500 m 以内，55%的商办写字楼集中在站点 200 m 以内。在步行范围内高强度开发，不但保证了土地利用价值的最大化，而且为客站带来了大量的客流，增加设施使用几率[4]。

表 1　东京各等级枢纽 400 m 圈层容积率分析

Table 1　Volume ratio analysis of 400 m circle layers of various levels of Tokyo

地段	地区	站点周边土地用途	容积率
一级中心	银座	娱乐、零售、商业为主	10～15
	新宿	商业、餐饮、娱乐、文化为主	10～15
	涩谷	商业、餐饮、娱乐、文化为主	9.5～12
	池袋	商业、餐饮、娱乐、文化为主	10.5～12
二级中心	上野	商业、餐饮为主	8～10
	浅草	商业、餐饮为主	8～10
三级中心	中野	商业、餐饮为主	5～8

3.4　功能空间

通过对比发现，国内的客站更多地表现为交通节点，国外的客站更加关注交通节点与城市场所功能的均衡。

客站作为城市的触媒，不应该仅仅是交通功能的载体，也是办公、零售、娱乐、居住、文化艺术、购物和公共服务设施等融合聚集的场所（图 5）。为了满足人们出行过程中的多样化需求，同时也充分发挥客站的综合效益，大型铁路客站站域的功能日益复合化。这种复合化不仅表现在土地利用的多元化，也表现在功能空间的立体化，将交通设施、商业、办公、旅馆、集散广场等多种用地进行竖向叠加发展，如交通+商业+居住，交通+办公+居住，交通+

(C)1994-2022 China Academic Journal Electronic Publishing House. All rights reserved.　http://www.cnki.net

文化设施+办公等多种组合模式，将客站地区基本功能和从属功能整合到以站点为核心的综合系统中，转变站点地区单一土地利用[5]。如涩谷既是多条铁路、地铁、公交的交汇处，也是城市商业、文娱、会议和展览中心，因乘客在换乘过程中可完成日常购物活动，故成为了市民良好的休闲活动场所，在提高了服务质量的同时，也增加了乘客的回流(图6)。

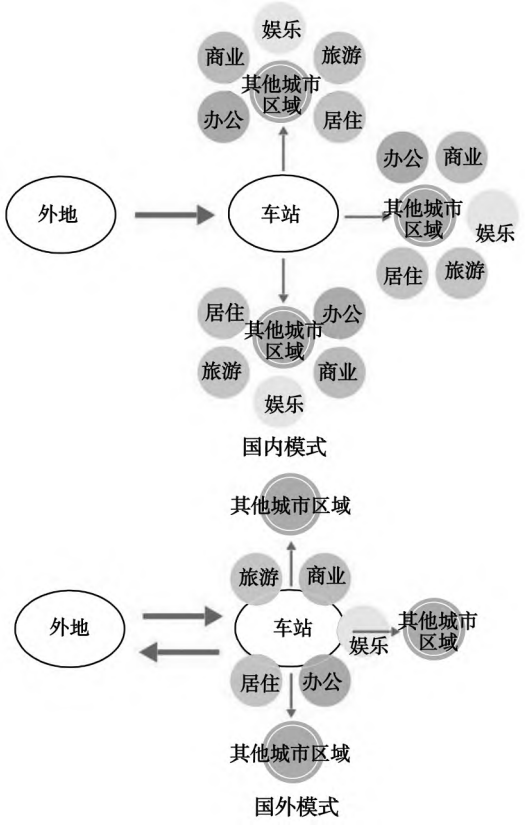


图5 国内外客站发展模式对比

Fig. 5 Comparison of the development model of passenger stations at home and abroad

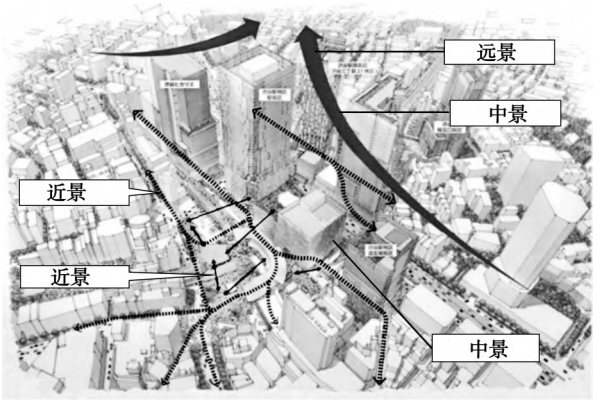


图6 涩谷站

Fig. 6 Shibuya station

3.5 交通规划

功能集聚必然会带来大量人流和物流，这些要素一方面是活力产生的根源，另一方面也意味着混乱。就像国内大多数客站一样，为了快进快出，客站周边被城市主干道和专向通道环绕，导致了客站与周边城市空间的割裂(图7)，城市人流和客站人流难以转换，空间活力低。因此，合理的路网结构是站域活力提升的根本。通过对比发现，国内客站周边路网密度低，道路等级高，次干道和支路网密度低，客站两侧联系薄弱(图7)。不合理的路网结构降低了步行的安全性和舒适性，限制了步行活动的产生。另外，国内客站更多的职能是城际间的交通联系，而日、法、德等地区的客站则更加致力于换乘效率的提升，因此更加倾向于将客站设于城市中心。如东京站不仅是城际铁路的枢纽站，也是城市轨道交通的重要节点和生活中心，轨道交通线路密集，每天乘降人数约为110万人次，即使没有庞大的城际交通客流支撑，也拥有巨大的客流量，而这些客流便是站域活力提升的根源，而且多条城市线路的集聚也为客站人流高效疏解提供了保障。

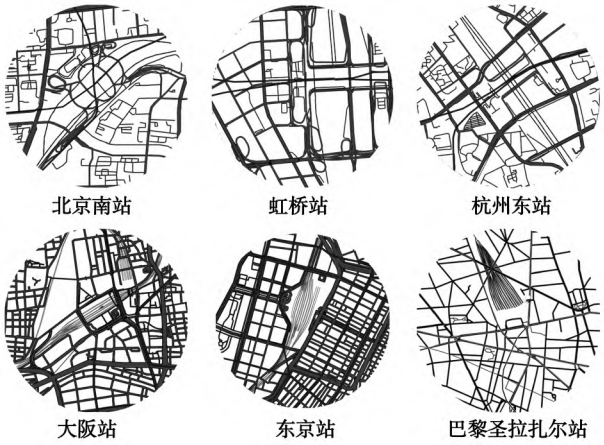


图7 国内外不同站域的交通组织

Fig. 7 Transportation organization in different station areas at home and abroad

4 建构策略

网络的建立需要在水平和垂直两个维度来加强链接，形成交通、空间、功能配置、土地利用等多方面的协同，通过资源的共享和各功能之间的相互作用，进而提升区域活力。

4.1 性能化设计

地下和空中步行系统在水平向伸展和连接的同时，必须与地面的步行网络形成舒适便捷的交通

(C)1994-2022 China Academic Journal Electronic Publishing House. All rights reserved. http://www.cnki.net

联系，而且在这种节点引入广场、绿化、阳光和休息设施，不但可以打破地下空间的封闭性和强化各层面之间的联系，还可以形成富有变化和趣味的特色空间。因此，这种贯通地下、地面以及地上多个空间层次，联系城市多个层面的节点空间，往往布置大量的垂直交通设施形成上下空间的核心节点，在为市民步行提供了多样化的选择的同时，成为了集散和转换的核心场所[6-7]。比如涩谷站围绕山谷状地形以及周边轨道交通网汇集的特点，设置了纵向的城市核（图 8），在 1 层、2 层和 3 层强化与周边道路的连续性和可通过性，在地下 3 层则提供了东急东横线与副都心线直接连通的场所，为乘客提供便利和舒适的空间，并在周边项目中也设置了这种跨越地下、地面和地上的城市核，最终形成了从车站延伸到周边的立体步行网络，确保了客站与周边城区的顺畅衔接，强化了客站与周边区域的环游性。这种节点空间一般设置于连通城市重要设施和公共空间的交叉点上，便于市民流动与集散，具有较强的标识性，便于人们寻找，同时要加强节点与地面城市设置和步行空间体系的联系，促进地下横向联系向竖向联系流动，并在满足功能的基础上，创造出富有特色和趣味的节点空间。

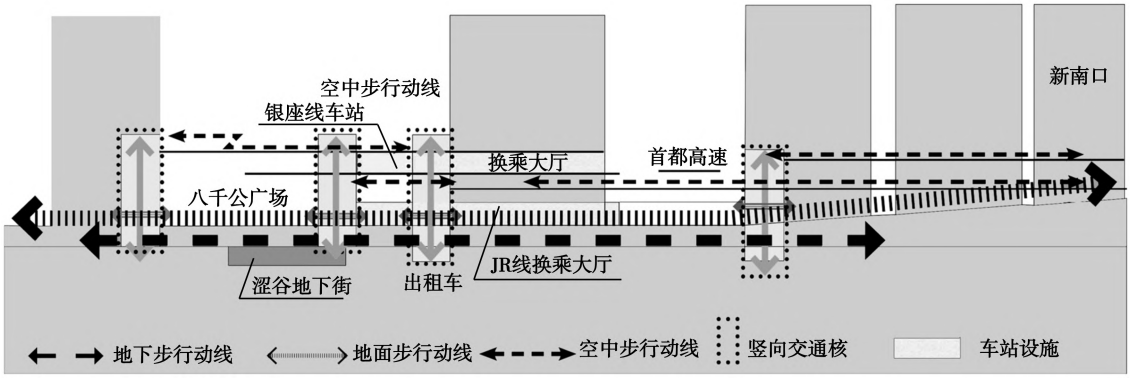


图 8　涩谷站多基面步行系统链接

Fig. 8　Shibuya station multi-basic walking system link

4.2　分层分流

如今在日本和香港站点区域，通过分层分流人们的活动可以分为 3 个层面，市民来往家、购物中心、写字楼、交通站点等场所可以完全不落地，同时行车道路很少出现拥堵状况，路面、地下铁和空中连廊在建筑群间立体交织（图 9）。空中步行系统跨越多个街区，同时将多种类型的建筑群联系到一起，形成客站社区。空中连廊接入建筑后形成空中入口，因此连廊空间也复合了门厅空间的功能，最后客站、过街天桥、大厦中的二层走廊及各种零售店等活动场所，有机地连接在一起，加上地下街的分流，形成了一个立体分流的步行系统，可以有效地疏散客站人流，促进城市人流与客站人流的转换，并减少地面人流，提高交通效率。港铁公司借鉴这种模式大量运用到了轨道交通物业开发上，形成地下、地面和空中与城市空间立体衔接的建筑群组，这种立体接驳提高空间使用效率的开发模式为站点地区一体化发展提供了极好的范本[8]。

4.3　联结成网

步行系统联结成网是提高交通效率和站城协同发展成功的先决条件[9]。因此，站域步行系统

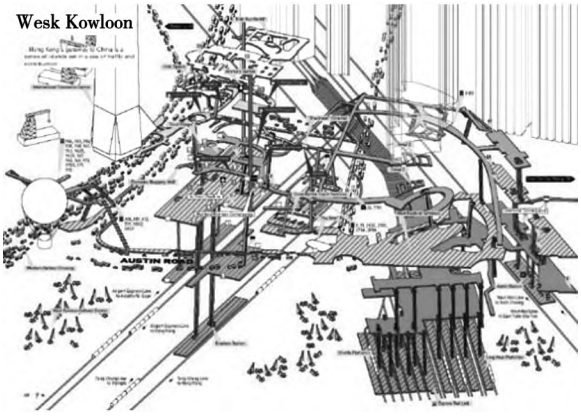


图 9　西九龙步行体系的分层

Fig. 9　Stratification of the West Kowloon pedestrian system

完整性和连续性的建设，成为了当今站域活力提升的重要因素。步行体系作为交通系统的组成部分和街道的延伸，可以提供从建筑内部穿越的通道（中庭、架空层、内街等），在多个城市基面之间（地面、地下和空中）将客站与区域内的建筑连接起来，形成层次清晰、立体高效的网络体系。通过这种立体化整合，可以实现乘客向潜在消费者的转化，以及客站与周边城市空间的“共生”[10]。比较典型的如大阪站，为完善步行网络，一是提高客

(C)1994-2022 China Academic Journal Electronic Publishing House. All rights reserved.　http://www.cnki.net

站周边区域的路网密度，完善道路等级，减轻了道路的交通负担，增加市民步行可达性和交通的多样性；二是增加建筑密度，客站周边有铁道站、办公楼、商业设施和酒店等，创造连续的城市界面和清晰的外部空间；三是减小街区尺寸和周边公共建筑体量来调整城市尺度，防止高层建筑形成壁垒现象。通过对区域的格局的调整，建立了完整的步行网络(图10)。

4.4 资源链接

步行系统构成的慢速公共空间连接周边公共服务设施以及公共绿地，能使客站地区成为具有强大吸引力的公共交往场所，这也将成为考验客站地区能否充分具有城市活力的关键。如多摩新城中心车站，利用抬起的平台，将车站和城市公园、美术馆、商场、办公楼、停车场等连在一起，营造良好的步行空间，形成了一个富有活力的社区中心。再如京都站，利用站前广场设置城市综合体，在中庭内集合了博物馆、购物中心、剧院、酒店、百货商场、派出所等城市公共服务设施，形成了极具魅力的城市



图10 大阪站的交通调整

Fig. 10 Traffic adjustment at Osaka Station

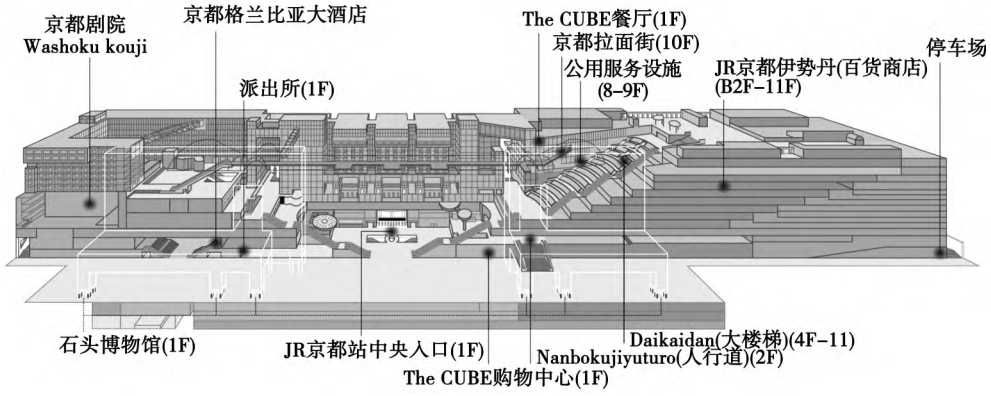


图11 京都站的功能空间

Fig. 11 Functional space of Kyoto Station

(C)1994-2022 China Academic Journal Electronic Publishing House. All rights reserved. http://www.cnki.net

节点(图 11)。提高站域空间步行范围内各种功能区的联系，创造完善通畅的步行网络，可以有效地提升设施的使用效率，形成一个交通便利、功能完善的站域经济圈[11]。

4.5　统一规划

首先，应遵循地下空间与地面和地上空间统筹规划，互补发展，地下空间与地上空间实施一体化开发与管理，避免各自孤立，各行其政; 另外，应明确地下空间规划制度与法规。完善的规划编制可以避免盲目开发和秩序混乱。以日本为例，其地下空间规划体系包括 5 个部分，分别是地下都市计划、地下利用的总体规划、地下空间、地下街规划和地下交通网络规划。从总体层面到区域层面分层控制，有效地提高了城市机能，促进了区域步行网络发展。再者，地下空间法规包含了地下空间建设与运营的各个方面，为地下空间开发提供了有效的保障。而且，地下空间规划是以城市规划为基础制定，其目的是提高城市活性。可见，地下空间法规体系的完整，也是让步行系统能够得以完整的主要因素。

5　结语

新时期我国对新型客站的巨大投入，其目标不是一个自我满足的一站式服务的交通枢纽，而是期望能作为城市触媒带动其周边城市片区的协同发展，这需要客站与城市空间的有机衔接和互动，步行网络的建立无疑是提升站域活力的一剂良药，有助于实现站域协同发展和客站建设的可持续性。

参考文献(References)

[1] 桂汪洋，程泰宁. 由站到城: 大型铁路客站站域公共空间整体性发展途径研究[J]. 建筑学报，2018(6): 36-39. (Gui Wangyang, Cheng Taining. From station to city: research on the integral development of public space in large railway passenger stations [J]. Architecture Journal, 2018(6): 36-39.(in Chinese))

[2] 刘皆谊. 城市立体化的视角[M]. 南京: 东南大学出版社，2009. (Liu Jieyi. The perspective of the three-dimensional urbanization [M]. Nanjing: Southeast University Press, 2009. (in Chinese))

[3] 林辰辉，马璇.. 中国高铁枢纽站区开发的功能类型与模式[J]. 城市交通 2012(9): 41-49. (Lin Chenhui, Ma Xuan. Types and modes of development of China's high-speed rail hub station area [J]. Urban Transportation, 2012(9): 41-49. (in Chinese))

[4] 谢晶晶，何芳，李云. 我国 TOD 导向土地复合利用存在问题与模式探析[J]. 城市规划，2013(11): 54-61. (Xie Jingjing, He Fang, Li Yun. Problems and models of TOD-oriented land composite utilization in my country [J]. Urban Planning, 2013 (11): 54-61. (in Chinese))

[5] 李胜全，张强华. 高速铁路时代大型铁路枢纽的发展模式探讨——从"交通综合体"到"城市综合体"[J]. 规划师，2011，27(7): 26-30. (Li Shengquan, Zhang Qianghua. Discussion on the development model of large-scale railway hubs in the era of high-speed railways—from " transportation complex " to " urban complex" [J]. Planner, 2011, 27(7): 26-30. (in Chinese))

[6] 刘皆谊，杨陈婷. 运用空间叙事营造场景的地下空间研究[J]. 地下空间与工程学报，2020，16(3): 647-655. (Liu Jieyi, Yang Chenting. Research on underground space using space narration to create scenes [J]. Chinese Journal of Underground Space and Engineering, 2020, 16(3): 647-655. (in Chinese))

[7] 刘皆谊. 地下街结合城市场所精神的演变趋势探讨[J]. 地下空间与工程学报，2009，5(4): 645-650. (Liu Jieyi. Discussion on the evolution trend of underground streets combined with the spirit of urban places [J]. Chinese Journal of Underground Space and Engineering, 2009, 5(4): 645-650. (in Chinese))

[8] 马路明，董春方. 香港都市综合体与城市交通的空间驳接[J]. 建筑技艺，2014(11): 34-39. (Ma Luming, Dong Chunfang. Spatial connection between Hong Kong urban complex and urban transportation [J]. Architectural Skills, 2014(11): 34-39. (in Chinese))

[9] 杨熹微. 首屈一指的交通枢纽——涩谷站周边大规模再开发项目正式启动[J]. 时代建筑，2009(5): 77-79. (Yang Xiwei. The premier transportation hub—the large-scale redevelopment project around Shibuya station is officially launched [J]. Times Architecture, 2009(5): 77-79. (in Chinese))

[10] 胡映东，张昕然. 初探城市轨道交通与建筑综合体的共生[J]. 华中建筑，2013(6): 89-93. (Hu Yingdong, Zhang Xinran. A preliminary study on the symbiosis of urban rail transit and architectural complex [J]. Huazhong Architecture, 2013(6): 89-93. (in Chinese))

[11] Fröidh O. Market effects of regional high-speed trains on the Svealand line [J]. Journal of Transport Geography, 2005, 13(4): 352-361.

(C)1994-2022 China Academic Journal Electronic Publishing House. All rights reserved.　http://www.cnki.net

生态环境学报 2021, 30(6): 1321-1332
Ecology and Environmental Sciences
http://www.jeesci.com
E-mail: editor@jeesci.com

基于CiteSpace的城市环境中细颗粒物研究进展的可视化分析

王薇[1,2]，张蕾[1]

1. 安徽建筑大学建筑与规划学院，安徽 合肥 230022；2. 安徽建筑大学建成环境与健康重点实验室，安徽 合肥 230022

摘要：细颗粒物（$PM_{2.5}$）在城市发展进程中，对城市环境空气质量和居民健康的影响程度日益上升。文章数据来源于1971—2020年WOS和CNKI数据库中城市环境中细颗粒物相关研究主题的文献样本数据，利用CiteSpace软件，通过区域分布特征分析、关键词共现分析、突现词探测、文献共被引分析和多维尺度分析等，系统梳理了城市环境中细颗粒物研究领域的前沿、知识基础、热点现状与发展趋势，得出以下结论：（1）在研究趋势方面，中国学者近年来在国际上发表论文的占比逐年递增，国内外研究内容稍有差异，但总体趋同；（2）在研究性质方面，国内研究侧重于描述细颗粒物的产生原因及表现特征方面，国外则多运用动力学和沉积原理对场域中的细颗粒物运动规律做出解析；（3）在研究对象方面，国内的源解析案例较多，而国外则推进交通排放空间格局的研究；（4）在研究前沿方面，国内研究主要关注主成分分析的细化和室内空气质量的优化，国外研究则更倾向于从可持续发展、人类健康及改善人居环境角度研究细颗粒对人体的影响。最后，文章认为应加强多学科交叉与合作，拓展人居环境视角下细颗粒物的系统性研究，综合关注其在不同城市和功能区的水平运动和垂直扩散规律，有效优化绿色基础设施的空间配置，准确地从源头控制环境污染，从而改善城市的空气质量，维护城市生态平衡。

关键词：城市环境；细颗粒物；可视化分析；科学知识图谱；CiteSpace；CNKI

DOI: 10.16258/j.cnki.1674-5906.2021.06.024

中图分类号：X51　　**文献标志码：**A　　**文章编号：**1674-5906（2021）06-1321-12

引用格式：王薇, 张蕾, 2021. 基于 CiteSpace 的城市环境中细颗粒物研究进展的可视化分析[J]. 生态环境学报, 30(6): 1321-1332.

WANG Wei, ZHANG Lei, 2021. Visual analysis of research progress of fine particles in urban environment based on CiteSpace [J]. Ecology and Environmental Sciences, 30(6): 1321-1332.

在快速发展的工业化和城市化进程中，城市环境问题逐渐成为现阶段的突出热点，空气质量更是影响了人居环境和居民健康，成为影响中国城市居住质量和可持续发展不可忽视的问题。而空气质量的评价及污染防治由于大量化石燃料的燃烧、工矿业发展以及机动车尾气排放的影响，已成为大气污染研究和城市气候领域的主要课题之一（赵晨曦等，2014）。研究表明，相对于PM_{10}、TSP等较大细颗粒物，$PM_{2.5}$由于粒径小，在大气中的存留时间长，对有毒物质的吸附性和呼吸系统对其的吸收率大，因此对人体健康、空气污染、大气能量平衡以及大气能见度的影响严重（胡元洁，2018）。近年来出现的海平面上升、洪水和干旱、极端高温、热岛效应、空气污染等各类气候灾害都是由全球气候变化导致，对城市居民的健康和生存环境产生了严重影响。例如中国长三角区域在2013年夏季出现持续性热浪，2015年冬季受强厄尔尼诺现象影响在全国范围出现连续的雾霾现象（Manfred et al.，2013；郭飞，2017；任思佳，2018），2016—2017年台风14号“莫兰蒂”等相继登陆带来了大规模大范围的沙尘和持续降雨天气，灾情严重；2018年中东部地区持续低温雪灾，江西大部分地区出现强降雨，洪涝严重等（赵晨曦等，2014）持续的自然灾害。

多数学者对细颗粒物进行了总结和归纳（金嘉恒等，2017；邹佳乐等，2019），从空间规划的角度阐述了城市颗粒物空气污染的控制策略（戴菲等，2019），从生态学领域研究细颗粒物与植被关系（赵晨曦等，2013），从化学领域研究$PM_{2.5}$的来源解析方法（郑玫等，2014），但多局限于对细颗粒物的控制技术、检测方法、相关性、解析技术等方面的综述。本文结合了文献计量法、知识可视化图谱分析法与传统文献梳理法，对城市环境中细颗粒物研究的整体特征、热点前沿、路径演化与发

基金项目：国家自然科学基金项目（51778001）；2018年安徽省教育厅高校优秀拔尖人才培育项目（gxbJZD23）；2021年安徽省重点研究与开发计划项目“绿墙建筑一体化及生态绿墙环境效应计算分析”

作者简介：王薇（1975年生），女，教授，博士，硕士研究生导师，国家一级注册建筑师，研究方向建筑技术和人居环境。E-mail: vivi.gan@126.com

收稿日期：2021-02-24

(C)1994-2022 China Academic Journal Electronic Publishing House. All rights reserved.　http://www.cnki.net

展趋势进行分析，旨在推动城市中细颗粒物研究向多元化、纵深化与国际化方向发展。

1 数据与方法

1.1 数据采集

检索时间截至 2020 年 9 月 30 日，数据来源于 Web of Science 核心合集（SCI 与 SSCI 来源）和中国学术期刊网络出版数据（CNKI）（核心期刊与 CSSCI 来源期刊），通过以下方式进行文献检索（郭琳琳等，2017）。

1.1.1 直接检索

运用 2 组专业术语“建筑、微环境、微气候、绿化”与“雾霾、颗粒物、PM、空气质量、空气污染”，“building、micro-environment、microclimate、building environment、urban environment”与“PM、haze、air pollution、particulate matter、air quality”，在检索式中对其进行交集运算。

1.1.2 追溯检索

由于 WOS 中英文关键词与中文关键词有出入，在上一步检索到的与城市环境密切相关的文献中，利用相似关键词“residential areas、urban vegetation、urban park、road-side、green infrastructure、street canyon”等，重复追溯检索。

1.1.3 循环检索

循环前 2 步的检索，纳入相关度高的文献，删除无作者及与城市环境等不相关文献，最终筛选出中、英相关文献样本各 329、558 篇，输出格式为 download_*.txt，运行 CiteSpaces 进行去重处理。

1.2 研究工具与方法

CiteSpace 软件通过分析信息知识单元的测度和相似性，采用不同技术形成多途径的可视化知识网络，对学科的研究热点、发展前沿和演化路径进行梳理（Chen，2006；Chen et al.，2010）。数据源为 1971—2020 年 WOS 和 CNKI 数据库中的文献样本，使用 Citespace 软件计算、统计并绘制出关键词、区域分布、突现词探测、作者共被引等可视化图谱，以分析结果作为城市环境视角下颗粒物研究的知识基础、前沿热点、发展趋势探测的重要参考依据，结合传统文献梳理法，对研究价值较高文献的内容及观点进行剖析，从发展趋势、研究性质、对象演变等方面揭示城市环境中颗粒物研究的前沿动态和发展趋势，为探索研究动态与发展趋势提供建议与参考。

1.3 国内外研究整体特征分析

1.3.1 发文量

由图 1 可知，基于城市环境视角的颗粒物研究于 1971 年初现，1971—1995 年间总体文献数量偏少，1995—2005 年间增幅较平缓，2005 年后总体呈现出持续增长的态势，表明国内外对建筑环境中颗粒物的关注度逐渐增加。2017—2018 年后，国内外发表论文均有一定程度的减少。国内研究从 1993—2013 年间论文数量与增幅均较小，2013 年后呈井喷式增长，说明在颗粒物污染加重的环境下，社会和学者们提高了关注度，并研究相应的解决方法与措施。

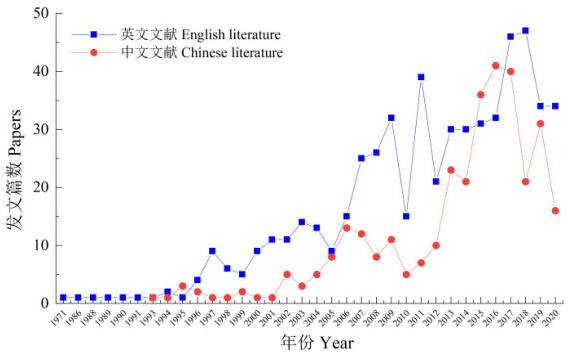


图 1 文献数量年度分布图

Fig. 1 Annual distribution map of literature quantity

对比图 1 中数量和发展趋势上的异同，可知以下 3 点，其一，国外最早开始城市环境中的颗粒物研究，经历了近 50 年的发展，影响力日趋增大，吸引了越来越多专家学者。其二，国内外细颗粒物文献在发展过程中早期增幅较小，可能是前期对于细颗粒物的研究尚未广泛触及相关学科领域，随着学科的交叉与发展，在城市环境中解决空气质量问题逐渐获得学者们的重视。其三，早期国内对细颗粒物的研究来自国外相关研究与实践，并得到了持续关注；随着城市化进程的迅速发展，并伴随着空气质量的污染，在 2003 年后掀起研究浪潮，近年研究数量增长率逐渐加快，说明该领域的国内研究趋势与社会需求紧密相关。

1.3.2 区域分布的特征

由图 2 可知，中国对该领域研究关注度极高，是在此领域发文量最大的国家；国外细颗粒物研究的对象主要集中在美国、德国、英国和意大利。但对比聚类可知中国虽与多国进行合作交流，但合作数量较少，英国则是进行国际合作最多的国家。

德国对颗粒物的研究多集中于 20 世纪，是该领域的前期探索者，可能是由于 19 世纪末工业革命后，烟囱工业带来的污染在欧洲尤以德国与比利时最盛。美国宾夕法尼亚州及俄亥俄州受其影响巨大，20 世纪 40 年代后美国发生多次大型烟雾事件，更加引起了学者的重视。英国作为世界上第一个工业化国家，面对严重的环境污染问题，开始研究空气质量的改善，推动了世界上首部空气污染防治法

(C)1994-2022 China Academic Journal Electronic Publishing House. All rights reserved. http://www.cnki.net

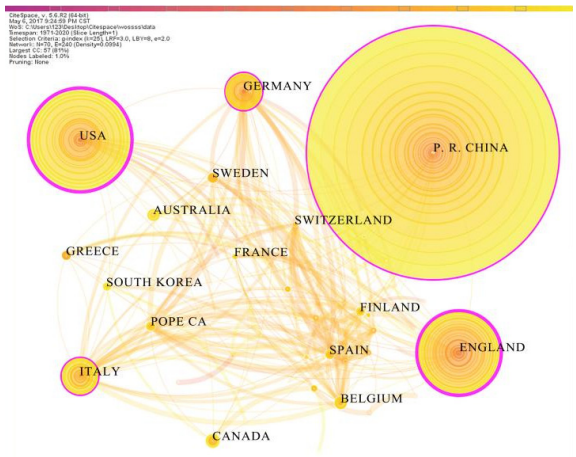


图 2 英文文献区域分布知识图谱

Fig. 2 Knowledge map of regional distribution of English literature

《清洁空气法》的诞生（王越，2018）。1918 年，英国化学物理学家唐南（Frederick George Donnan）发现胶体化学过程和有云的大气过程有许多相似之处，因此依据“Hydrosol（水溶胶）”引入了“Aerosol（气溶胶）”术语。中国对于颗粒物研究集中于近 20 年，上世纪 80 年代后中国学者开始了对大气颗粒物的研究工作，对细颗粒物的关注较晚，因此研究成果相对较少（谢心庆等，2015）。

1.3.3 代表人物、观点

由于国外文献作者数较多，因此将时间切片设为每两年，并通过寻径算法修剪切片网络，得到作者共被引知识图谱（图 3）。由图 3 可以看出，在英文文献中，该研究领域的研究学者之间形成了相互影响的复杂网络。Vardoulakis 对该领域影响最大，他曾发表多篇该领域的综述；2003 年他发表的《街道峡谷的空气质量模拟：综述》（谢心庆等，

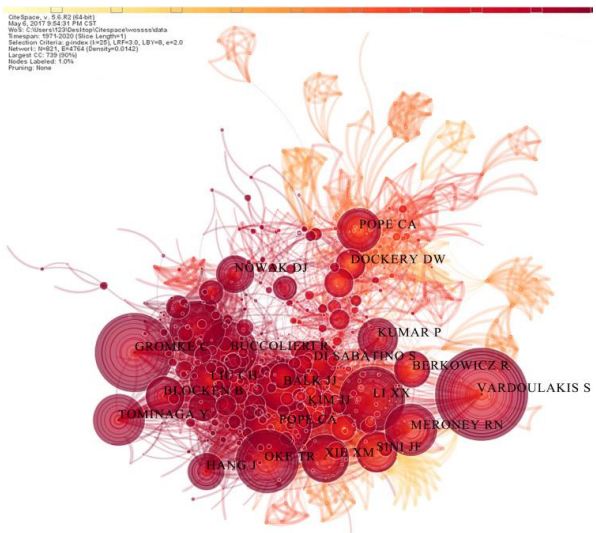


图 3 英文文献作者共被引知识图谱

Fig. 3 Knowledge map of co-cited authors in English literature

2015）对研究评估空气质量的不同扩散建模方法，包括数学模型、物理模型和化学算法模型，以及监测技术进行了整理和比较；此外，他还发表了多篇高频被引文章。影响力为第二的是 Gromke，他通过风洞和数值调查方法获得实验数据，对树木种植的街道峡谷中进行扩散研究，并对 CFD 数据结果进行评估（Gromke et al.，2008）。Oke（1988）则在 1988 年通过回顾当时城市峡谷实地研究的成果，结合尺度和数学模型对街道设计与城市冠层气候的影响进行了探讨（Gromke et al.，2008），在城市气候研究领域奠定了知识基础。

中文文献作者之间的合作关系并不复杂，可以看出几个明显的集聚关系。由图 4 可以看出，影响力较大的作者间存在合作关系，高被引文献重复较高，因此以团体为单位进行分析。其中影响力最大的是以赵力、陈超、王清勤为核心的科研团队，该团队合作研究了不同结构类型的建筑中，窗隙通风对室内细颗粒物（$PM_{2.5}$）浓度的影响（陈超等，2016），并对北京市某办公建筑夏冬季室内外 $PM_{2.5}$ 浓度变化特征进行实时监测与数据分析（赵力等，2015）。其次是冯银厂和吴建会的课题团队所进行的 $PM_{2.5}$ 和 PM_{10} 污染特征及来源解析研究（王敬等，2014），该团队在杭州、宁波、天津、济南、乌鲁木齐等地均进行了采样及解析（冯银厂等，2004；吴琳等，2009；包贞等，2010；肖致美等，2012）。冯银厂的研究成果被其他研究者实践于多数城市。鲁绍伟、李少宁、陈波等主要研究城市绿化空间在不同时段或不同天气下的 $PM_{2.5}$ 浓度变化（陈波等，2016c；陈波等，2016b），并对该地区常见绿化树种的 $PM_{2.5}$ 吸滞能力进行定量分析（陈波等，2016a）。由图 4 可知，课题团队仅在本课题深入研究，而鲜少与其他领域有知识交叉，主要是由于国内研究多来自现实需求，缺乏长期、全面的研究，以及缺乏与国外深度研究的交流互动，因此各课题团队的关联性较少，无法形成复杂的知识网络。

2 国际研究前沿与热点分析

2.1 研究前沿与知识基础

本文梳理了 1971—2020 年国际上对城市环境中颗粒物研究的前沿演化特征与知识基础，见图 5。该网络分为 17 个聚类，本文选择最大的 6 个主要聚类进行分析。

2.1.1 聚类#0（dispersion modelling）

聚类#0 主要致力于研究城市环境中颗粒物的扩散模式和规律。该聚类的知识基础源于 Kim et al.（2004）通过建立具有重整化群 k-epsilon 湍流格式的三维流体动力学计算模型，开展环境风向对城市

(C)1994-2022 China Academic Journal Electronic Publishing House. All rights reserved. http://www.cnki.net

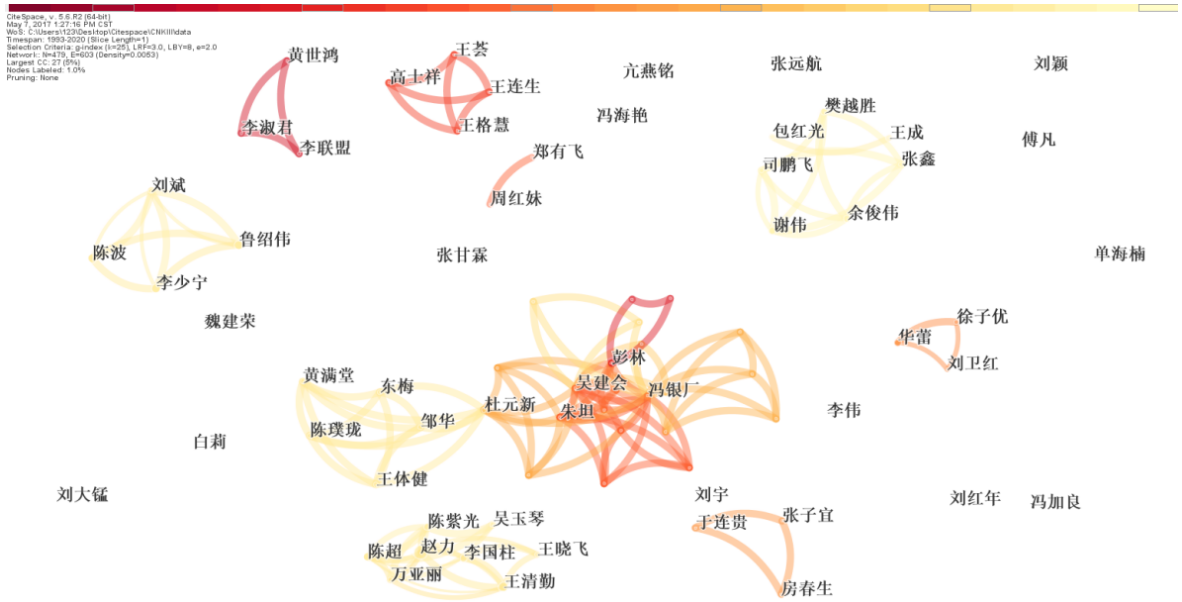


图 4 中文文献作者合作知识图谱

Fig. 4 Collaborative relationship knowledge graph of Chinese literature authors

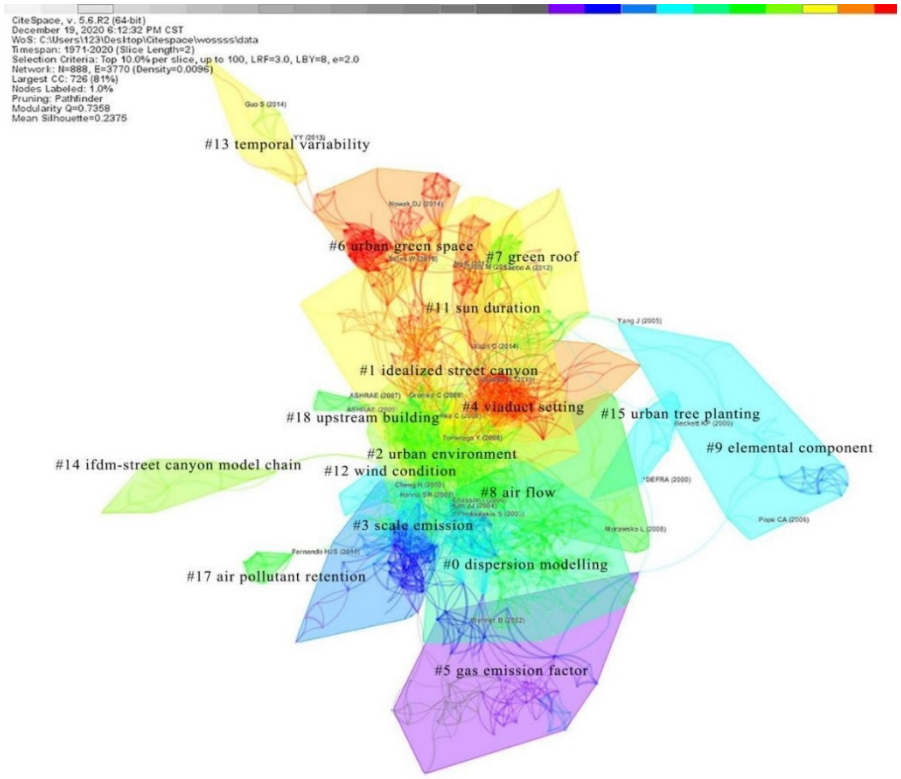


图 5 1971—2020 年基于 WOS 的文献共被引网络聚类图谱

Fig. 5 Clustering map of the articles' co-citation network based on Web of Science (WOS), 1971–2020

街道峡谷流动和扩散影响的数值研究。例如 Kumar et al.（2011）对城市道路交通中细颗粒物的动力学和扩散模型的研究进行了综述；Salmond et al.（2010）研究了街道峡谷与城市边界层堆积模式粒子的垂直输运；Mazzeo et al.（2011）根据来自 4 个街道峡谷的全尺度数据，分析了自然以及交通产生的气体流动。

2.1.2 聚类#1（idealized street canyon）

聚类#1 主要依据建立理想化的街道峡谷模型，研究城市植被、大气环境与交通等影响因素对空气污染的消减作用。该聚类的知识基础源于 Gromke et al.（2008）在城市街道峡谷对街道式绿化的交通流

(C)1994-2022 China Academic Journal Electronic Publishing House. All rights reserved. http://www.cnki.net

和交通尾气扩散规律进行的研究，并提出了一种新的方法来模拟多孔植物结构，如树冠小规模风洞应用（Gromke et al.，2009）。例如 Badach et al.（2020）综述了近年来有关城市绿化因沉积和空气动力作用而减轻空气污染的研究，并尝试通过合理设计和保护植被系统，提出空间规划策略以改善城市空气质量；Salim et al.（2011）运用两种方法 rans（标准 k-epsilon 模型和 RSM 模型）和 les（大型涡流模拟）比较城市街道峡谷中树木种植的污染物扩散数值模拟；Janhall（2015）以城市街道峡谷或交叉路口的植被屏障为重点，依据模型与实验得出城市植被对微粒空气污染沉积与扩散的作用。

2.1.3 聚类#2（urban environment）

聚类#2 主要强调了细颗粒物污染在城市环境中的表现。该聚类的知识基础源于 Li et al.（2006）在街道峡谷风场与污染物输运 CFD 模拟研究上的进展，以及 Sabatino et al.（2007）在 2007 年通过 CFD 和积分模型对城市理想几何形状内的污染物扩散模拟。例如 Tominaga et al.（2013）综述了目前 CFD 模拟城市环境近场污染物扩散的建模技术，对以往研究中近场污染物在建筑物周围扩散的主要特征进行了识别和讨论；Ramponi et al.（2015）对不同城市密度、相同和不同街道宽度下一般城市布局室外通风进行了 CFD 模拟；Buccolieri et al.（2010）主要研究了城市空气的可呼吸性及其与模拟城市几何形状内污染物浓度分布的关系。

2.1.4 聚类#3（scale emission）

聚类#3 主要研究城市大气细颗粒物污染的扩散和排放程度。该聚类的知识基础源于 Vardoulakis et al.（2003）在 2003 年对街道峡谷空气质量模型的研究综述，包括对不同扩散建模方法以及监测技术的整理和比较。例如 Assimakopoulos et al.（2003）研究了不同二维街道峡谷配置下大气污染物扩散的数值；Tay et al.（2010）将街道峡谷中的城市气溶胶通量与更大规模的排放关联起来；Britter et al.（2003）从区域、城市、邻里和街道 4 个不同的尺度研究城市区域的污染物流动与扩散问题。

2.1.5 聚类#4（viaduct setting）

聚类#4 聚焦于高架桥或建筑造成的不同峡谷空间对气流及污染物扩散的影响。该聚类的知识基础源于 Hang et al.（2012）和 Baik et al.（1999）的不同研究。Hang 等研究建筑物高度差异性对城市理想高层建筑区域污染物扩散和行人通风的影响，阐明了建筑布局、高度差异性和高层城市几何体中地面污染物去除潜力之间的关系；Baik et al.（1999）通过城市街道峡谷气流和污染物扩散特性的数值研究，得出了街道峡谷污染物浓度在连续排放和非排放阶段的分布结论。例如 Hang et al.（2019）研究了高宽比和墙体加热条件对二维典型街道峡谷气流和被动污染物暴露的影响；He et al.（2017）研究了不同街道高宽比和高架桥下的高层深街峡谷气流和被动污染物暴露数值；Duan et al.（2020）研究了高架走道内外的湍流和扩散。

2.1.6 聚类#5（gas emission factor）

聚类#5 重视分析不同城市环境下的细颗粒物排放因子分析。Wallace（2012）在 1996 年对室内颗粒物的综述，以及 Wehner et al.（2002）在 2002 年通过实测和简单模型研究街道峡谷中粒子数大小分布及其对城市空气环境的转化，构成了该领域的知识基础。例如 Ketzel et al.（2003）基于街道和屋顶的水平观测，分析了哥本哈根交通源附近的颗粒物和微量气体排放因子；Monn（2001）描述了空气污染物的小尺度空间变化以及室内外和个人实测的数据库，研究聚焦在悬浮颗粒物、较小程度的二氧化氮和光化学污染物；Longley et al.（2003）以英国曼彻斯特为例，实测研究了繁忙街道峡谷内气溶胶（4.6 nm d-p 10 mu m）的数量和质量大小分布。

从近 50 年聚类的时间分布可见，最初对城市中颗粒物的分析局限于气体排放因子（1997）和排放规模（2000）等微观角度，2000 年后逐渐走向对城市风况到气流流向规律的研究，2009 年起大量使用 CFD 研究城市中细颗粒物的论文成为热门话题；对城市的客体研究也从单个个体，如城市植树（2002）、上游建筑物（2007）、绿色屋顶（2010）等对颗粒物的影响或改善作用，扩大到街道峡谷（2012）、城市绿色空间（2016）等城市规划宏观角度的研究。

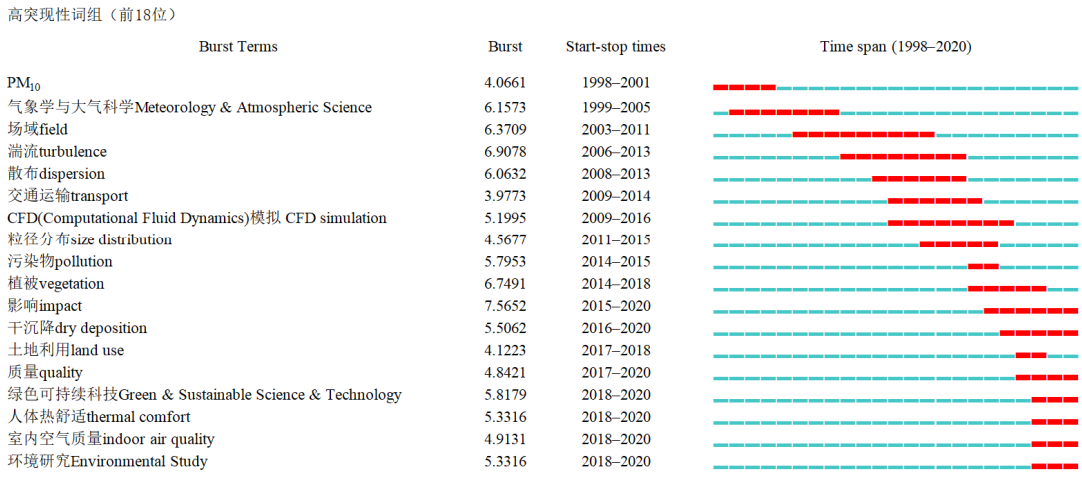
2.2 研究热点与发展趋势

本文利用 CiteSpace 软件引文的突现词探测算法，对其同义词和相近词进行归拢，得出城市环境中细颗粒物研究领域的突现词图谱，见图 6。

1998—1999 年的突现词为 PM_{10} 和气象学与大气科学。该时期重点关注气象学角度 $PM_{2.5}$ 和 PM_{10} 的污染状况。如 Putaud et al.（2009）研究了欧洲 60 个农村、城市和道路颗粒物的物理和化学特征；Chan et al.（2007）介绍了中国特大城市空气污染的现状。

2003—2009 年的突现词为场域、湍流、散布、交通运输和 CFD 模拟。该时期常以 CFD 模拟来探索某场域内颗粒物的运动规律和交通排放的空间分析。如计算无限长街谷中街道内与屋顶上方大气层界面处污染物的流动和垂直交换（Sini et al.，1996），以及交通排放空间格局模拟（Requia et al.，

(C)1994-2022 China Academic Journal Electronic Publishing House. All rights reserved. http://www.cnki.net



引文年份始自 1971 年，但至 1998 年才出现满足突现条件的词汇，因此以 1998—2020 年作为分析的时间跨度

图 6 基于 WOS 的城市环境中颗粒物研究中的突现词图谱

Fig. 6 Burst terms in the study of the particulate matter in urban environment based on Web of Science

2017），或是研究气象因素对大气生物气溶胶（花粉、真菌孢子、细菌、病毒或动植物碎片）浓度释放、扩散的影响（Jones et al.，2004）。

2011—2014 年的突现词为粒径分布和污染物。重点关注对城市中污染物气体的数量检测、成分分析和变化预测。例如收集大量数据研究 $PM_{2.5}$ 在北京、天津、承德和石家庄的时空变化及其化学成分（Zhao et al.，2013），或结合卫星遥感等新技术对区域表面的 $PM_{2.5}$ 进行估算（Ma et al.，2014）。

2014—2017 年的突现词为植被、影响、干沉降、土地利用和质量。该时期基于干沉降原理的植物除尘以及人为或自然现况对 $PM_{2.5}$ 浓度的影响研究成为研究热点。如利用 CFD 方法评估路边树木对街道峡谷空气动力学和沉积的影响（Xue et al.，2017），从城市规划的角度评价土地利用和景观格局与 $PM_{2.5}$ 浓度之间的相关性（Feng et al.，2017），研究不同气象参数与大气污染物浓度的影响等（Zhang et al.，2015）。

2018 年后的突现词为绿色可持续科技、人体热舒适、室内空气质量、环境研究，逐渐倾向于从可持续发展、人类健康以及改善人居环境角度研究细颗粒物对人体的影响，技术上也不再局限于单一分析手段。Pettit et al.（2018）开展了实用性植物对室内空气修复作用的综述研究；Ghaffarianhoseini et al.（2018）研究分析了 SBS（病态建筑综合症）的症状和负面影响，强调了建筑环境的作用，针对健康室内环境的研究提出了可行的解决方案；Weerasuriya et al.（2019）集成了计算流体动力学模拟、多区域空气流动模型和建筑能量模拟来计算风、浮力以及风和浮力驱动通风机制下的通风率，利用自然通风优化高层住宅的能源性能。

3 国内研究热点与路径演化

研究主题的分布和演变可以直观地反映不同时段中的分析视角、研究方法、热点领域的变化。而研究主题可以通过中心度较高的关键词展现，关键词间的相关性一定范围内能够表达学科领域中知识的相互关联（秦晓楠等，2014）。本文利用关键词共现分析梳理了国内对于城市环境中颗粒物研究的主要热点、研究倾向和结构发展变化，使用寻径算法对片状网络与合并网络进行修剪，绘制出研究主题演化路径及关键词中心性排序列表，见图 7 和表 1。可视后的图谱共包含关键词节点 59 个，连线 49 条。

3.1 研究主题与热点分析

本文以中心度为指标，对关键路径图谱中的关键词排序得出表 1，以此识别并整理不同时段的城市环境中颗粒物的研究主题。

1993—2010 年间具有中心性的关键词较少，说明该时段处于城市环境中细颗粒物研究的起步阶段，核心关键词为 $PM_{2.5}$、PM_{10}、源解析和可吸入性颗粒物等基础性词汇。大多集中于对某地区污染程度的评估与颗粒物的浓度与成分分析，如朱易等（2004）对南宁市大气颗粒物（TSP、PM_{10}、$PM_{2.5}$）的污染程度进行了监测；华蕾等（2006）利用源解析技术对北京市 PM_{10} 的主要排放源进行了成分分析；董雪玲等（2009）研究了北京市大气 PM_{10} 和 $PM_{2.5}$ 中有机物的时空变化。

2011—2014 年间对细颗粒物的研究逐渐发展，在短期内热点词迅速增多，该时段的核心关键词为粒径分布、空气污染、相关性和功能区，除了对不同区域细颗粒物浓度、粒径分布、排放因子和化学成分的分析外，细颗粒物与气象要素（李绥等，

(C)1994-2022 China Academic Journal Electronic Publishing House. All rights reserved. http://www.cnki.net

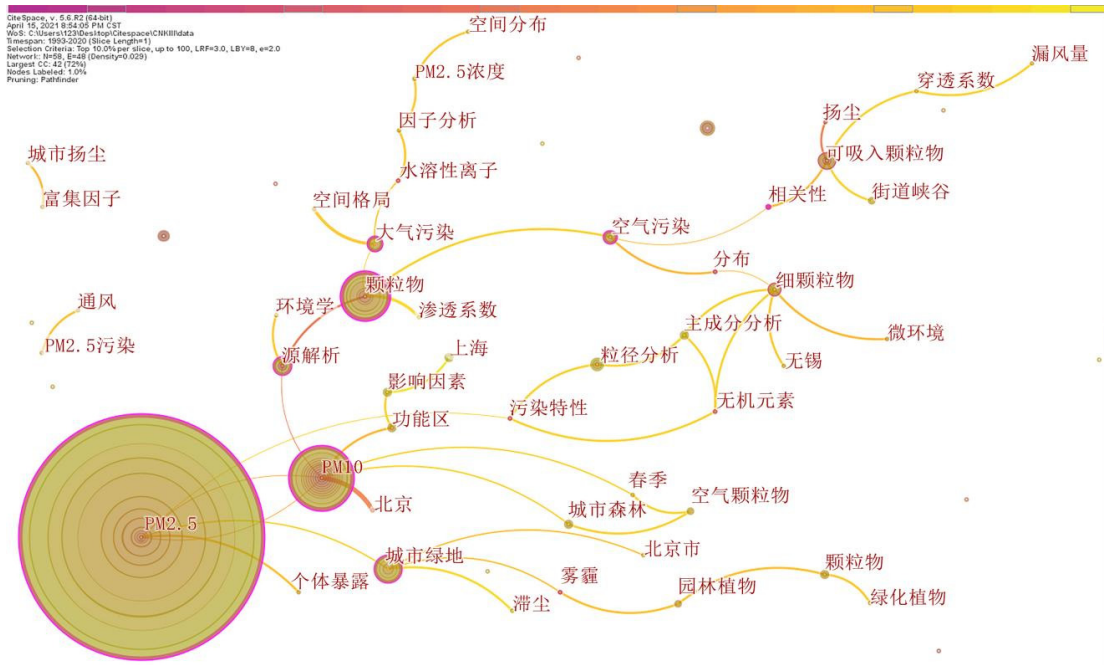


图 7　国内城市环境中细颗粒物研究领域研究主题演化路径

Fig. 7　The research themes evolution path of field of fine particulate matter in domestic urban environment

表 1　城市环境中细颗粒物研究关键词共现网络的关键词中心性排序列表

Table 1　The keyword centre index rank of study on fine particulate matter in urban environment co-occurrence network

年份 Year	关键词 Key word	中心度 Centre	年份 Year	关键词 Key word	中心度 Centre
2004	PM_{10}	0.77	2015	滞尘能力 Dust detaining abilities	0.05
2004	$PM_{2.5}$	0.36	2016	大气污染 Atmospheric pollution	0.23
2005	源解析 Source analysis	0.37	2016	水溶性离子 Soluble ions	0.14
2005	可吸入颗粒物 Inhalable particles	0.19	2016	因子分析 Factor analysis	0.1
2011	粒径分布 Particle size distribution	0.22	2016	$PM_{2.5}$浓度 Concentration of $PM_{2.5}$	0.05
2014	分布 Distribution	0.3	2016	城市森林 Prban forest	0.02
2014	空气污染 Air pollution	0.26	2017	污染特征 Pollution characteristics	0.22
2014	相关性 Correlation	0.22	2017	主成分分析 Principal component analysis	0.2
2014	功能区 Functional zone	0.1	2017	无机元素 Inorganic elements	0.2
2015	城市绿地 Urban green space	0.27	2017	春季 Springtime	0.06
2015	园林植物 Ornamental plants	0.1	2017	影响因素 Influence factor	0.05
2015	雾霾 Haze	0.14	2017	穿透系数 Penetration factor	0.05

2014）、土地利用类型以及功能区规划之间的相关性的研究也成为了研究热点，并常使用模型作为相关性分析的技术方法（阳海鸥等，2017）。

2015—2016 年间该领域研究进展迅速，两年内出现大量的核心热点词，分别为城市绿地、园林植物、雾霾、滞尘能力、大气污染、水溶性离子、因子分析、$PM_{2.5}$ 浓度以及城市森林，研究集中在城市绿化对大气污染滞尘能力的分析，其中包括大尺度的环城绿地（肖玉等，2015）、绿化设施（韩晔等，2015）、城市森林（陈波等，2016）以及小尺度的园林植物（张桐等，2017），此外对细颗粒物中水溶性离子的污染特征研究也得到了关注（陈金媛等，2016）。

2017 年后的核心热点词为污染特征、主成分分析、无机元素、春季、影响因素和穿透系数，除往年关注过的热点话题外，对颗粒物的基础研究开始倾向于季节性的变化特征（杜万光等，2017）以及不同季节的特征对比（王的等，2017）。另外由于室内空气质量受到不断关注，对可吸入颗粒物围护结构渗透机理的研究（张辉辉等，2017），以及基于建筑漏风量与围护结构穿透系数的室内细颗粒物防控设计研究（李景广等，2017）取得了进展。

3.2　研究方向与路径演化

由图 7 可知，根据主题词的节点分布与联系，梳理出国内该领域研究 3 条重要的演化路径。

3.2.1　“细颗粒物（PM_{10}/$PM_{2.5}$）−大气污染−因子分析−浓度−空间分布”研究路径

该路径主要对细颗粒物进行基础性研究，从城市空气质量监测的需求出发，逐渐发展为对细颗粒

(C)1994-2022 China Academic Journal Electronic Publishing House. All rights reserved. http://www.cnki.net

物的产生原因及表现特征的分析，主要集中以下 4 个方面的研究：（1）浓度监测：主要采取实测-数据分析（毛慧伦等，2019）的方式；（2）空间格局：主要采取遥感影像数据收集（$PM_{2.5}$浓度反演影像和 DMSP-OLS 夜间灯光数据集）（吴健生等，2016）、模型分析（重力模型、ESDA 模型（杨帆等，2016）、Fluent）、数值分析（GIS 空间统计分析、克里金插值法（戴昭鑫等，2016））等方法；（3）产生因子：一般采取源解析法分析其因，如离子色谱法从其化学成分分析（陈金媛等，2016）、化学质量平衡模型（CMB model）和二重源解析（冯银厂等，2005）的方式；（4）影响因子：主要集中在地理位置、气象因素（空气温度、相对湿度、风速）（刘晴等，2019）、人文因素（鲁绍伟等，2017）的相关性分析，采取因子分析、聚类分析及空间相关性分析（吴健生等，2016）等主要技术手段。

3.2.2 “细颗粒物（$PM_{10}/PM_{2.5}$）−空气颗粒物−城市绿地/城市森林−园林植物−滞尘能力”研究路径

该路径更倾向于研究植物在人类活动高度影响下对颗粒物的消减作用，分为城市森林、景观绿化和植物叶片 3 个尺度的研究。对城市森林植被区的研究主要集中在不同生境类型下城市森林大气颗粒物的变化特征及其影响因素（段文军等，2017）；对景观绿化的研究包括绿地植物滞尘作用的机理、植物个体和群落的滞尘能力以及绿地滞尘的影响因素（孙晓丹等 2015），以及不同绿地结构对大气颗粒物的消减能力（孙晓丹等，2015）；对植物叶片的研究大多为分析绿化植物叶片表面特征对滞尘效应的影响（柴一新等，2002）。

3.2.3 “细颗粒物（$PM_{10}/PM_{2.5}$）−污染特征−粒径分析−可吸入性颗粒物−街道峡谷/扬尘/穿透系数−漏风量”研究路径

该路径从细颗粒物的污染特征细化至粒径分布（王申博等，2017），关注了城市中颗粒物分布不均衡问题（吴正旺等，2014），主要包括，（1）街道峡谷：主要关注街区尺度的颗粒物污染的空间分布，通过模型模拟和评估街道空气质量，4 种常用模型包括 ENVI-met、FLUENT、MISKAM 和 OSPM（周姝雯等，2017），研究变量常为建筑物间隔（即建筑间距与街道总长之比）、街道峡谷高宽比和风（刘建峰等，2017）。（2）扬尘：主要关注建筑施工扬尘对城市环境的影响，可以通过高斯面源反演法计算扬尘污染源，建立开放源可吸入颗粒物污染源强数据库，进一步分析城市扬尘污染（刘彩霞，2006）。（3）穿透系数-漏风量：主要从室内空气质量出发，通过质量平衡方程分析室内颗粒物浓度的主要影响因素，研究颗粒渗透研究中穿透系数、渗透因子和室内外颗粒物浓度比的关系，以及打印复印设备集中局部排风、人体活动影响的室内污染物分布变化（李景广等，2017），研究手段包括现场测试、实验室研究、模型研究（张辉辉等，2017）。

4 结论与展望

4.1 结论

（1）在研究整体特征方面，国内外对于城市环境中的细颗粒物研究内容稍有差异，但总体趋势相近，在发展过程中的增幅都呈现缓步上升、井喷增长和相对减少 3 个阶段。起步阶段国内对细颗粒物的基础性研究较少，自 2004 年后关注点紧跟前沿，研究重心的趋同与中国学者近年来在国际上发表论文的占比逐年递增有显著关系。相较国外，国内对该领域研究是由于现实需求而出发的，缺乏长期、全面的研究，缺少与国外深度研究的交流互动，因此各课题间的关联性较少，未形成复杂的知识网络。

（2）在研究性质方面，国内研究侧重细颗粒物的产生原因及表现特征方面，在对空间分布和时空变化的研究中，多数为基于实测与模型分析得出数据结论与环境评价的定量分析；国外则多定量分析，运用动力学和沉积原理，研究场域中细颗粒物的运动规律。

（3）在研究对象方面，国内的源解析案例较多，而国外对交通排放空间格局的研究居于前沿。在人为影响因素的分析中，国内较关注建筑施工扬尘对居民生活的影响，而国外则更多聚焦于研究个体暴露对细颗粒物的影响。

（4）在研究前沿趋势方面，对细颗粒物的浓度、因子、空间分布、源解析等基础性研究，城市绿地对细颗粒物的消减作用，以及人居环境和室内空气质量的改善是近 20 年的主要研究内容。2017 年后国内外前沿话题出现异端，国内研究在主成分分析的基础上对不同成分的细颗粒物做细化研究，室内空气质量的优化得到了关注；国外研究则从更倾向于可持续发展、人类健康以及改善人居环境角度研究细颗粒对人体的影响。

4.2 展望

（1）城市环境中细颗粒物的研究涉及到环境科学、城市规划、建筑学、化学、力学、生态学、计算机科学等众多学科，需要数据处理、源解析、计算流体动力学、遥感等多项技术支撑，因此需要加强多学科交叉与合作，以拓展人居环境视角下细颗粒物的系统性研究。

（2）可持续发展和人类健康学视角下的细颗粒物研究已成为国际研究关注的热点，应当综合关注

(C)1994-2022 China Academic Journal Electronic Publishing House. All rights reserved. http://www.cnki.net

其在不同城市和功能区的水平运动和垂直扩散规律。同时有效优化绿色基础设施的空间配置，准确地从源头控制环境污染，从而改善城市空气质量及维护城市生态平衡。

参考文献：

ASSIMAKOPOULOS V D, APSIMON H M, MOUSSIOPOULOS N, 2003. A numerical study of atmospheric pollutant dispersion in different two-dimensional street canyon configurations [J]. Atmospheric Environment, 37(29): 4037-4049.

BADACH J, DYMNICKA M, BARANOWSKI A, 2020. Urban Vegetation in Air Quality Management: A Review and Policy Framework [J]. Sustainability, 12(3): 1258.

BAIK J J, KIM J J, 1999. A numerical study of flow and pollutant dispersion characteristics in urban street canyons [J]. Clarivate Analytics Web of Science, 38(11):1576-1589

BRITTER R E, HANNA S R, 2003. Flow and dispersion in urban areas [J]. Annual REVIEW of Fluid Mechanics, 35(1): 469-496.

BUCCOLIERI R, SANDBERG M, SABATINO S D, 2010. City breathability and its link to pollutant concentration distribution within urban-like geometries [J]. Atmospheric Environment, 44(15): 1894-1903.

CHAN C K, YAOX H, 2007. Air pollution in mega cities in China [J]. Atmospheric Environment, 42(1): 1-42.

CHEN C M, IBEKWE-SANJUAN F, HOU J H, 2010. The structure and dynamics of co-citation clusters: A multiple-perspective co-citation analysis [J]. Journal of the American Society for Information Science and Technology, 61(7): 1386-1409.

CHEN C M, 2006. CiteSpace II: Detecting and visualizing emerging trends and transient patterns in scientific literature [J]. Journal of the American Society for Information Science and Technology, 57(3): 359-377.

DUAN G, BRIMBLECOMBE P, CHU Y L, et al., 2020. Turbulent flow and dispersion inside and around elevated walkways [J]. Building and Environment, 173: 1-14.

FENG H H, ZOU B, TANG Y M, 2017. Scale- and Region-Dependence in Landscape-$PM_{2.5}$ Correlation: Implications for Urban Planning [J]. Remote Sensing, 9(9): 1-20.

GHAFFARIANHOSEINI A, ALWAER H, OMRANY H, et al., 2018. Sick building syndrome: are we doing enough? [J]. Architectural Science Review, 61(3): 99-121.

GROMKE C, BUCCOLIERI R, SABATINO S, et al., 2008. Dispersion study in a street canyon with tree planting by means of wind tunnel and numerical investigations—Evaluation of CFD data with experimental data [J]. Atmospheric Environment, 42(37): 8640-8650.

GROMKE C, RUCK B, 2009. On the Impact of Trees on Dispersion Processes of Traffic Emissions in Street Canyons [J]. Boundary-Layer Meteorology, 131(1): 19-34.

HANG J, CHEN X Y, CHEN G W, et al., 2019. The influence of aspect ratios and wall heating conditions on flow and passive pollutant exposure in 2D typical street canyons [J]. Building and Environment, 168: 1-20.

HANG J, LI Y G, SANDBERG M, et al., 2012. The influence of building height variability on pollutant dispersion and pedestrian ventilation in idealized high-rise urban areas [J]. Building and Environment, 56: 346-360.

HE L J, HANG J, WANG X M, et al., 2017. Numerical investigations of flow and passive pollutant exposure in high-rise deep street canyons with various street aspect ratios and viaduct settings [J]. The Science of the total environment, 584-585: 189-206.

JANHALL S, 2015. Review on urban vegetation and particle air pollution-Deposition and dispersion [J]. Clarivate Analytics Web of Science, 105: 130-137.

JONES A M, HARRISON R M, 2004. The effects of meteorological factors on atmospheric bioaerosol concentrations——a review [J]. The Science of the Total Environment, 326(1-3): 151-180.

KETZEL M, WÅHLIN P, BERKOWICZ R, et al., 2003. Particle and trace gas emission factors under urban driving conditions in Copenhagen based on street and roof-level observations [J]. Atmospheric Environment, 37(20): 2735-2749.

KIM J J, BAIK J J, 2004. A numerical study of the effects of ambient wind direction on flow and dispersion in urban street canyons using the RNG k-ε turbulence model [J]. Atmospheric Environment, 38(19): 3039-3048.

KUMAR P, KETZEL M, VARDOULAKIS S, et al., 2011. Dynamics and dispersion modelling of nanoparticles from road traffic in the urban atmospheric environment——A review [J]. Journal of Aerosol Science, 42(9): 580-603.

LI X X, LIU C H, DENNIS Y C, et al., 2006. Recent progress in CFD modelling of wind field and pollutant transport in street canyons [J]. Atmospheric Environment, 40(29): 5640-5658.

LONGLEY I D, GALLAGHER M W, DORSEY J R, et al., 2003. Inglis. A case study of aerosol (4.6 nm<D_p<10 μm) number and mass size distribution measurements in a busy street canyon in Manchester, UK [J]. Atmospheric Environment, 37(12): 1563-1571.

MA Z W, HU X W, HUANG L, et al., 2014. Estimating ground-level $PM_{2.5}$ in China using satellite remote sensing [J]. Environmental Science & Technology, 48(13): 7436-44.

MANFRED N, HANNS M, DANIEL R, 2013. Acute and subacute effects of urban air pollution on cardiopulmonary emergencies and mortality: time series studies in austrian cities [J]. International Journal of Environmental Research and Public Health, 10(10): 4728-4751.

MAZZEO N A, VENEGAS L E, 2011. Study of natural and traffic-producing turbulences analysing full-scale data from four street canyons [J]. International Journal of Environment and Pollution, 47(1-4): 290-301.

MONN C, 2001. Exposure assessment of air pollutants: a review on spatial heterogeneity and indoor/outdoor/personal exposure to suspended particulate matter, nitrogen dioxide and ozone [J]. Atmospheric Environment, 35(1): 1-32.

OKE T R, 1988. Street design and urban canopy layer climate [J]. Elsevier, 11(1-3): 103-113.

PETTIT T, IRGA P J, TORPY F R, 2018. Towards practical indoor air phytoremediation: A review [J]. Chemosphere, 208: 960-974.

PUTAUD J P, DINGENEN R, ALASTUEY A, et al., 2009. A European aerosol phenomenology-3: Physical and chemical characteristics of particulate matter from 60 rural, urban, and kerbside sites across Europe [J]. Atmospheric Environment, 44(10): 1308-1320.

RAMPONI R, BLOCKEN B, COO L D, et al., 2015. CFD simulation of outdoor ventilation of generic urban configurations with different urban densities and equal and unequal street widths [J]. Building and Environment, 92: 152-166.

REQUIA W, ROIG H, KOUTRAKIS P, et al., 2017. Modeling spatial patterns of traffic emissions across 5570 municipal districts in Brazil [J]. Journal of Cleaner Production, 148: 845-853.

SABATINO S D, BUCCOLIERI R, PULVIRENTI B, et al., 2007. Simulations of pollutant dispersion within idealised urban-type geometries with CFD and integral models [J]. Atmospheric Environment, 41(37): 8316-8329.

SALIM S M, CHEAH S C, CHAN A, 2011. Numerical simulation of dispersion in urban street canyons with avenue-like tree plantings: Comparison between RANS and LES [J]. Building and Environment, 46(9): 1735-1746.

SALMOND J A, PAUSCHER L, PIGEON G, et al., 2010. Vertical transport of accumulation mode particles between two street canyons and the urban boundary layer [J]. Atmospheric Environment, 44(39):

(C)1994-2022 China Academic Journal Electronic Publishing House. All rights reserved. http://www.cnki.net

5139-5147.

SINI J F, ANQUETIN S, MESTAYER P G, 1996. Pollutant dispersion and thermal effects in urban street canyons [J]. Atmospheric Environment, 30(15): 2659-2677.

TAY B K, MCFIGGANS G B, JONES D P, et al., 2010. Linking urban aerosol fluxes in street canyons to larger scale emissions [J]. Atmospheric Chemistry and Physics, 10(5): 2475-2490.

TOMINAGA Y, STATHOPOULOS T, 2013. CFD simulation of near-field pollutant dispersion in the urban environment: A review of current modeling techniques [J]. Atmospheric Environment, 79: 716-730.

VARDOULAKIS S, FISHER B, PERICLEOUS K, et al., 2003. Modelling air quality in street canyons: A review [J]. Atmospheric Environment, 37(2): 155-182.

WALLACE L, 2012. Indoor Particles: A Review [J]. Journal of the Air & Waste Management Association, 46(2): 98-126.

WEERASURIYA A U, ZHANG X L, GAN V J L, et al., 2019. A holistic framework to utilize natural ventilation to optimize energy performance of residential high-rise buildings [J]. Building and Environment, 153: 218-232.

WEHNER B, BIRMILI W, GNAUK T, et al., 2002. Particle number size distributions in a street canyon and their transformation into the urban-air background: measurements and a simple model study [J]. Atmospheric Environment, 36(13): 2215-2223.

XUE F, LI X F, 2017. The impact of roadside trees on traffic released PM_{10} in urban street canyon: Aerodynamic and deposition effects [J]. Sustainable Cities and Society, 30: 195-204.

ZHANG H L, WANG Y G, HU J L, et al., 2015. Relationships between meteorological parameters and criteria air pollutants in three megacities in China [J]. Environmental Research, 140: 242-254.

ZHAO P S, DONG F, HE D, et al., 2013. Characteristics of concentrations and chemical compositions for $PM_{2.5}$ in the region of Beijing, Tianjin, and Hebei, China [J]. Atmospheric Chemistry and Physics, 13(9): 4631-4644.

包贞, 冯银厂, 焦荔, 等, 2010. 杭州市大气 $PM_{2.5}$ 和 PM_{10} 污染特征及来源解析[J]. 中国环境监测, 26(2): 44-48.
BAO Z, FENG Y C, JIAO L, et al., 2010. Characteristics and source analysis of atmospheric $PM_{2.5}$ and $PM_{2.5}$ pollution in Hangzhou [J]. Environmental Monitoring in China, 26(2): 44-48.

柴一新, 祝宁, 韩焕金, 2002. 城市绿化树种的滞尘效应——以哈尔滨市为例[J]. 应用生态学报, 13(9): 1121-1126.
CHAI Y X, ZHU N, HAN H J, 2002. Dust Catching Effect of Urban Greening Tree Species: A Case Study of Harbin City [J]. Chinese Journal of Applied Ecology, 13(9): 1121-1126.

陈波, 李少宁, 鲁绍伟, 等, 2016. 北京大兴南海子公园 $PM_{2.5}$ 和 PM_{10} 质量浓度变化特征[J]. 生态科学, 35(2): 104-110.
CHEN B, LI S N, LU S W, et al., 2016. Variation characteristics of $PM_{2.5}$ and PM_{10} mass concentrations in Nanhaizi Park, Daxing, Beijing [J]. Ecological Science, 35(2): 104-110.

陈波, 刘海龙, 赵东波, 等, 2016. 北京西山绿化树种秋季滞纳 $PM_{2.5}$ 能力及其与叶表面 AFM 特征的关系[J]. 应用生态学报, 27(3): 777-784.
CHEN B, LIU H L, ZHAO D B, et al., 2016. Relationship between $PM_{2.5}$ capacity and leaf surface AFM characteristics of green tree species in the Western Hills of Beijing in autumn [J]. Chinese Journal of Applied Ecology, 27(3): 777-784.

陈波, 鲁绍伟, 李少宁, 2016. 北京城市森林不同天气状况下 $PM_{2.5}$ 浓度变化[J]. 生态学报, 36(5): 1391-1399.
CHEN B, LU S W, LI S N, 2016. Variation of $PM_{2.5}$ concentration in urban forest under different weather conditions in Beijing [J]. Acta Ecologica Sinica, 36(5): 1391-1399.

陈超, 王平, 陈紫光, 等, 2016. 不同结构型式建筑外窗缝隙通风对建筑室内细颗粒物 ($PM_{2.5}$) 浓度的影响[J]. 北京工业大学学报, 42(4): 601-608.
CHEN C, WANG P, CHEN Z G, et al., 2016. Effect of gap ventilation on indoor fine particulate matter ($PM_{2.5}$) concentration in buildings with different structural types [J]. Journal of Beijing University of Technology, 42(4): 601-608.

陈金媛, 唐凯杰, 朱莹, 等, 2016. 杭州市 $PM_{2.5}$ 中水溶性离子的污染特征研究[J]. 浙江工业大学学报, 44(4): 410-416.
CHEN J Y, TANG K J, ZHU Y, et al., 2016. Study on pollution characteristics of water-soluble ions in $PM_{2.5}$ in Hangzhou [J]. Journal of Zhejiang University of Technology, 44(4): 410-416.

戴菲, 陈明, 傅凡, 等, 2019. 基于城市空间规划设计视角的颗粒物空气污染控制策略研究综述[J]. 中国园林, 35(2): 75-80.
DAI F, CHEN M, FU F, et al., 2019. A review of particulate air pollution control strategies from the perspective of urban spatial planning and design [J]. Chinese Landscape Architecture, 35(2): 75-80.

戴昭鑫, 张云芝, 胡云锋, 等, 2016. 基于地面监测数据的 2013—2015 年长三角地区 $PM_{2.5}$ 时空特征[J]. 长江流域资源与环境, 25(5): 813-821.
DAI Z X, ZHANG Y Z, HU Y F, et al., 2016. Temporal and spatial characteristics of $PM_{2.5}$ in the Yangtze River Delta from 2013 to 2015 based on surface monitoring data [J]. Resources and Environment in the Yangtze Basin, 25(5): 813-821.

董雪玲, 刘大锰, 袁杨森, 等, 2009. 北京市大气 PM_{10} 和 $PM_{2.5}$ 中有机物的时空变化[J]. 环境科学, 30(2): 328-334.
DONG X L, LIU D M, YUAN Y S, et al., 2009. Temporal and spatial variation of organic compounds in atmospheric PM_{10} and $PM_{2.5}$ in Beijing [J]. Environmental Science, 30(2): 328-334.

杜万光, 王成, 王茜, 等, 2017. 春季旗山福建柏林内外空气颗粒物变化特征[J]. 环境科学与技术, 40(10): 176-184.
DU W G, WANG C, WANG Q, et al., 2017. Characteristics of airborne particulate matter in spring in Qishan, Fujian and Berlin [J]. Environmental Science and Technology, 40(10): 176-184.

段文军, 王成, 张昶, 等, 2017. 夏季 3 种生境森林内空气颗粒物变化特征[J]. 北京林业大学学报, 39(5): 73-81.
DUAN W J, WANG C, ZHANG C, et al., 2017. Characteristics of airborne particulate matter in three habitats in summer [J]. Journal of Beijing Forestry University, 39(5): 73-81.

冯银厂, 彭林, 吴建会, 等, 2005. 乌鲁木齐市环境空气中 TSP 和 PM_{10} 来源解析[J]. 中国环境科学, 25(Z1): 30-33.
FENG Y C, PENG L, WU J H, et al., 2005. Sources of TSP and PM_{10} in ambient air of Urumqi [J]. China Environmental Science, 25(S1): 30-33.

冯银厂, 吴建会, 朱坦, 等, 2004. 济南市环境空气中 TSP 和 PM_{10} 来源解析研究[J]. 环境科学研究, 17(2): 1-5.
FENG Y C, WU J H, ZHU T, et al., 2004. Analysis of sources of TSP and PM_{10} in ambient air in Ji'nan [J]. Research of Environmental Sciences, 17(2): 1-5.

郭飞, 2017. 基于 WRF 的城市热岛效应高分辨率评估方法[J]. 土木建筑与环境工程, 39(1): 13-19.
GUO F, 2017. High-resolution evaluation method of urban heat island effect based on WRF [J]. Journal of Civil, Architectural and Environmental Engineering, 39(1): 13-19.

郭琳琳, 李保峰, 陈宏, 2017. 我国在街区尺度的城市微气候研究进展[J]. 城市发展研究, 24(1): 75-81.
GUO L L, LI B F, CHEN H, 2017. Research progress of urban microclimate at block scale in China [J]. Urban Development Research, 24(1): 75-81.

韩晔, 周忠学, 2015. 西安市绿地景观吸收雾霾生态系统服务测算及空间格局[J]. 地理研究, 34(7): 1247-1258.
HAN Y, ZHOU Z X, 2015. Estimation and spatial pattern of haze absorption ecosystem services of green space landscape in Xi'an City [J]. Geographical Research, 34(7): 1247-1258.

胡元洁, 2018. 室内外大气颗粒物和典型有机污染物的环境行为及人体呼吸暴露风险[D]. 广州: 中国科学院大学(中国科学院广州地球化学研究所): 175-176.
HU Y J, 2018. Environmental behavior of indoor and outdoor

(C)1994-2022 China Academic Journal Electronic Publishing House. All rights reserved. http://www.cnki.net

atmospheric particulate matter and typical organic pollutants and human respiratory exposure risk [D]. Guangzhou: University of Chinese Academy of Sciences (Guangzhou Institute of Geochemistry, Chinese Academy of Sciences): 175-176.

华蕾, 郭婧, 徐子优, 等, 2006. 北京市主要 PM_{10} 排放源成分谱分析[J]. 中国环境监测, 22(6): 64-71.
HUA L, GUO J, XU Z Y, et al., 2006. Composition spectrum analysis of main PM_{10} emission sources in Beijing [J]. Environmental Monitoring in China, 22(6): 64-71.

金嘉恒, 张根茂, 李倩, 2017. $PM_{2.5}$ 的综述与进展[J].科技创新导报, 14(3): 74-75, 139.
JIN J H, ZHANG G M, LI Q, 2017. Review and progress of $PM_{2.5}$ [J]. Science and Technology Innovation Review, 14(3): 74-75, 139.

李景广, 黄衍, 李旻雯, 2017. 建筑室内细颗粒物($PM_{2.5}$)防控设计研究[J]. 暖通空调, 47(1): 109-112, 73.
LI J G, HUANG Y, LI M W, 2017. Control design of indoor fine particulate matter ($PM_{2.5}$) in buildings [J]. Heating Ventilating & Air Conditioning, 47(1): 109-112, 73.

李绥, 杨二东, 石铁矛, 等, 2014. 商业街区可吸入颗粒物空间分布及其气象要素的相关性[J]. 沈阳建筑大学学报(自然科学版), 30(5): 923-930.
LI S, YANG E D, SHI T M, et al., 2014. Spatial distribution of inhalable particulate matter and its correlation with meteorological factors in commercial districts [J]. Journal of Shenyang Jianzhu University (Natural Science Edition), 30(5): 923-930.

刘彩霞, 2006. 天津市开放源可吸入颗粒物污染问题分析[J]. 中国环境监测, 22(4): 80-83.
LIU C X, 2006. Analysis of open source inhalable particulate pollution in Tianjin [J]. Environmental Monitoring in China, 22(4): 80-83.

刘建峰, 王宝庆, 牛宏宏, 等, 2017. 计算流体力学模拟街道峡谷特征和风向对细颗粒物污染扩散的影响[J]. 环境污染与防治, 39(4): 367-374.
LIU J F, WANG B Q, NIU H H, et al., 2017. Computational fluid dynamics simulation of the effects of street canyon characteristics and wind direction on the diffusion of fine particulate matter pollution [J]. Environmental Pollution & Control, 39(4): 367-374.

刘晴, 高鹏, 李成, 等, 2019. 泰安市典型生态功能区空气负离子的时空分布及影响因素分析[J]. 环境化学, 38(1): 169-176.
LIU Q, GAO P, LI C, et al., 2019. Spatial and temporal distribution and influencing factors of air anions in Tai'an City typical ecological function area [J]. Environmental Chemistry, 38(1): 169-176.

鲁绍伟, 蒋燕, 陈波, 等, 2017. 北京城市植被区 $PM_{2.5}$ 浓度时空变化及影响因素分析[J]. 环境科学与技术, 40(1): 180-187.
LU S W, JIANG Y, CHEN B, et al., 2017. Spatiotemporal variation and influencing factors of $PM_{2.5}$ concentration in urban vegetation areas of Beijing [J]. Environmental Science and Technology, 40(1): 180-187.

毛慧伦, 何红弟, 2019. 上海黄浦江轮渡颗粒物污染状况的分布特征[J]. 大连海事大学学报, 45(2): 113-122.
MAO H L, HE H D, 2019. Distribution characteristics of particulate matter pollution in Shanghai Huangpu River ferry [J]. Journal of Dalian Maritime University, 45(2): 113-122.

秦晓楠, 卢小丽, 武春友, 2014. 国内生态安全研究知识图谱——基于 Citespace 的计量分析[J]. 生态学报, 34(13): 3693-3703.
QIN X N, LU X L, WU C Y, 2014. Knowledge map of ecological security research in China: A quantitative analysis based on CiteSpace [J]. Acta Ecologica Sinica, 34(13): 3693-3703.

任思佳, 2018. 城市街谷绿化形式对机动车尾气扩散影响的数值模拟研究[D]. 武汉: 华中农业大学: 37-39.
REN S J, 2018. Numerical simulation study on the influence of greening forms on vehicle exhaust diffusion in urban street canyons [D]. Wuhan: Huazhong Agricultural University: 37-39.

孙晓丹, 李海梅, 周春玲, 等, 2015. 园林植物消减大气颗粒物研究进展[J]. 北方园艺 (24): 184-188.
SUN X D, LI H M, ZHOU C L, et al., 2015. Research progress on reduction of atmospheric particulate matter by garden plants [J]. Northern Horticulture, (24): 184-188.

王的, 冯海艳, 景慧敏, 2017. 北京市冬季、春季 PM_{10} 和 $PM_{2.5}$ 中元素地球化学特征[J]. 地球科学进展, 32(8): 850-858.
WANG D, FENG H Y, JING H M, 2017. Geochemical characteristics of PM_{10} and $PM_{2.5}$ in winter and spring in Beijing [J]. Advances in Earth Sciences, 32(8): 850-858.

王敬, 毕晓辉, 冯银厂, 等, 2014. 乌鲁木齐市重污染期间 $PM_{2.5}$ 污染特征与来源解析[J]. 环境科学研究, 27(2): 113-119.
WANG J, BI X H, FENG Y C, et al., 2014. Characteristics and source analysis of $PM_{2.5}$ pollution during heavy pollution period in Urumqi [J]. Research of Environmental Sciences, 27(2): 113-119.

王申博, 余飞, 燕启社, 等, 2017. 典型背景区大气颗粒物中元素粒径分布特征[J]. 环境科学与技术, 40(6): 133-140.
WANG S B, YU F, YAN Q S, et al., 2017. Element size distribution characteristics of atmospheric particulate matter in typical background area [J]. Environmental Science and Technology, 40(6): 133-140.

王越, 2018. 英国空气污染防治演变研究(1921—1997)[D]. 西安: 陕西师范大学: 1-7.
WANG Y, 2018. Evolution of air pollution control in UK (1921–1997) [D]. Xi'an: Shaanxi Normal University: 1-7.

吴健生, 许娜, 张曦文, 2016. 中国低碳城市评价与空间格局分析[J]. 地理科学进展, 35(2): 204-213.
WU J S, XU N, ZHANG X W, 2016. Evaluation and spatial pattern analysis of low-carbon cities in China [J]. Progress in Geography, 35(2): 204-213.

吴琳, 冯银厂, 戴莉, 等, 2009. 天津市大气中 PM_{10}、$PM_{2.5}$ 及其碳组分污染特征分析[J]. 中国环境科学, 29(11): 1134-1139.
WU L, FENG Y C, DAI L, et al., 2009. Characteristics of atmospheric PM_{10}, $PM_{2.5}$ and its carbon component pollution in Tianjin [J]. China Environmental Science, 29(11): 1134-1139.

吴正旺, 王岩慧, 单海楠, 2014. 北京市 $PM_{2.5}$ 分布的不均匀现象[J].环境科学与技术, 37(S1): 87-91, 95.
WU Z W, WANG Y H, SHAN H N, 2014. Unevenness of $PM_{2.5}$ distribution in Beijing [J]. Environmental Science and Technology, 37(S1): 87-91, 95.

肖玉, 王硕, 李娜, 等, 2015. 北京城市绿地对大气 $PM_{2.5}$ 的削减作用[J]. 资源科学, 37(6): 1149-1155.
XIAO Y, WANG S, LI N, et al., 2015. Effects of urban green space on atmospheric $PM_{2.5}$ reduction in Beijing [J]. Resources Science, 37(6):1149-1155.

肖致美, 毕晓辉, 冯银厂, 等, 2012. 宁波市环境空气中 PM_{10} 和 $PM_{2.5}$ 来源解析[J]. 环境科学研究, 25(5): 549-555.
XIAO Z M, BI X H, FENG Y C, et al., 2012. Sources of PM_{10} and $PM_{2.5}$ in ambient air in Ningbo City [J]. Research of Environmental Sciences, 25(5): 549-555.

谢心庆, 郑薇, 2015. 国内外 $PM_{2.5}$ 研究进展综述[J]. 电力科技与环保, 31(4): 17-20.
XIE X Q, ZHENG W, 2015. Research progress of $PM_{2.5}$ at home and abroad [J]. Electric Power Technology and Environmental Protection, 31(4): 17-20.

阳海鸥, 陈文波, 梁照凤, 2017. LUR 模型模拟的南昌市 $PM_{2.5}$ 浓度与土地利用类型的关系[J]. 农业工程学报, 33(6): 232-239.
YANG H L, CHEN W B, LIANG Z F, 2017. Relationship between $PM_{2.5}$ concentration and land use types simulated by LUR model in Nanchang City [J]. Transactions of the Chinese Society of Agricultural Engineering, 33(6): 232-239.

杨帆, 周亮, 林蔚, 等, 2016. 2001—2010 年非洲大气 $PM_{2.5}$ 污染浓度空间格局演化[J]. 世界地理研究, 25(3): 30-39.
YANG F, ZHOU L, LIN W, et al., 2016. Evolution of spatial pattern of $PM_{2.5}$ pollution concentration in Africa during 2001–2010 [J]. World Regional Studies, 25(3): 30-39.

张辉辉, 王芳, 王砚玲, 等, 2017. 可吸入颗粒物围护结构渗透机理研究进展[J]. 建筑科学, 33(4): 134-141.

(C)1994-2022 China Academic Journal Electronic Publishing House. All rights reserved. http://www.cnki.net

ZHANG H H, WANG F, WANG Y L, et al., 2017. Research progress on permeation mechanism of respirable particulate matter envelope [J]. Building Science, 33(4): 134-141.

张灵艺, 秦华, 2015. 城市园林绿地滞尘研究进展及发展方向[J]. 中国园林, 31(1): 64-68.
ZHANG L Y, QIN H, 2015. Research on Progress of Dust-Retention for Urban Green Space [J]. Chinese Landscape Architecture, 31(1): 64-68.

张桐, 洪秀玲, 孙立炜, 等, 2017. 6 种植物叶片的滞尘能力与其叶面结构的关系[J]. 北京林业大学学报, 39(6): 70-77.
ZHANG T, HONG X L, SUN L W, et al., 2017. Particle-retaining characteristics of six tree species and their relations with micro-configurations of leaf epidermis [J]. Journal of Beijing Forestry University, 39(6): 70-77.

赵晨曦, 王玉杰, 王云琦, 等, 2013. 细颗粒物($PM_{2.5}$)与植被关系的研究综述[J]. 生态学杂志, 32(8): 2203-2210.
ZHAO C X, WANG Y J, WANG Y Q, et al., 2013. Research review on the relationship between fine particulate matter ($PM_{2.5}$) and vegetation [J]. Chinese Journal of Ecology, 32(8): 2203-2210.

赵晨曦, 王云琦, 王玉杰, 等, 2014. 北京地区冬春 $PM_{2.5}$ 和 PM_{10} 污染水平时空分布及其与气象条件的关系[J]. 环境科学, 35(2): 418-427.
ZHAO C X, WANG Y Q, WANG Y J, et al., 2014. Spatial and temporal distribution of $PM_{2.5}$ and PM_{10} pollution levels in winter and spring in Beijing and their relationship with meteorological conditions [J]. Environmental Science, 35(2): 418-427.

赵力, 陈超, 王平, 等, 2015. 北京市某办公建筑夏冬季室内外 $PM_{2.5}$ 浓度变化特征[J]. 建筑科学, 31(4): 32-39.
ZHAO L, CHEN C, WANG P, et al., 2015. Variation characteristics of indoor and outdoor $PM_{2.5}$ concentration in an office building in Beijing in summer and winter [J]. Architectural Science, 31(4): 32-39.

郑玫, 张延君, 闫才青, 等, 2014. 中国 $PM_{2.5}$ 来源解析方法综述[J]. 北京大学学报(自然科学版), 50(6): 1141-1154.
ZHENG M, ZHANG Y J, YAN C Q, et al., 2014. A review of $PM_{2.5}$ source analysis methods in China [J]. Acta Scientiarum Naturalium Universitae Pekinensis, 50(6): 1141-1154.

周姝雯, 唐荣莉, 张育新, 等, 2017. 城市街道空气污染物扩散模型综述[J]. 应用生态学报, 28(3): 1039-1048.
ZHOU S W, TANG R L, ZHANG Y X, et al., 2017. Review on diffusion models of urban street air pollutants [J]. Chinese Journal of Applied Ecology, 28(3): 1039-1048.

朱易, 胡衡生, 张新英, 等, 2004. 南宁市大气颗粒物 TSP、PM_{10}、$PM_{2.5}$ 污染水平研究[J]. 环境污染与防治, 26(3): 176-178, 242.
ZHU Y, HU H S, ZHANG X Y, et al., 2004. Study on atmospheric particulate matter TSP, PM_{10}, $PM_{2.5}$ pollution levels in Nanning City [J]. Environmental Pollution & Control, 26(3): 176-178, 242.

邹佳乐, 林尧林, 杨薇, 2019.中国近年 $PM_{2.5}$ 污染研究进展[J]. 环境污染与防治, 41(3): 357-361, 366.
ZOU J L, LIN Y L, YANG W, 2019. Research progress of $PM_{2.5}$ pollution in China in recent years [J]. Environmental Pollution & Control, 41(3): 357-361, 366.

Visual Analysis of Research Progress of Fine Particles in Urban Environment Based on CiteSpace

WANG Wei[1, 2], ZHANG Lei[1]

1. School of Architecture and Urban Planning, Anhui Jianzhu University, Hefei 230022, China;
2. Key Laboratory of Built Environment and Health, Anhui Jianzhu University, Hefei 230022, China

Abstract: In the process of urban development, the impact of fine particulate matter ($PM_{2.5}$) on urban environmental air quality, residents' health and sustainable development is increasing. The paper is based on literature sample data from WOS database and CNKI database from 1971 to 2020, including literature sample data on research topics related to fine particulate matter in urban environment. Based on the analysis of regional distribution characteristics, co-citation analysis of literatures, detection of emerging words, co-occurrence analysis of keywords and multi-dimensional scale analysis in CiteSpace software, this paper systematically sorted out the frontiers, knowledge bases, hot spots and development trends in the research field of fine particulate matter in urban environment. The following conclusions are drawn: (1) In terms of research trend, as the proportion of Chinese scholars' papers published in international journals has been increasing year by year, the research contents at home and abroad are slightly different but generally convergent;(2) In terms of research properties, domestic studies focus on describing the causes and characteristics of fine particulate matter, while foreign studies mostly use dynamics and deposition principles to analyze the movement rules of fine particulate matter in the field. (3) In terms of research objects, there are more source analysis cases in China, while the studies on the spatial pattern of traffic emissions in foreign countries are at the forefront. And (4) in terms of research frontier, domestic researches mainly focus on the refinement of principal component analysis and the optimization of indoor air quality, while foreign researches are more inclined to study the impact of fine particles on human body from the perspective of sustainable development, human health and improvement of human living environment. Finally, it is suggested that we should strengthen interdisciplinary cooperation and expand the systematic study of fine particulate matter from the perspective of human settlement environment. It is necessary to pay comprehensive attention to its horizontal movement and vertical diffusion in different cities and functional areas. At the same time, we need to effectively optimize the spatial configuration of green infrastructure and accurately control environmental pollution from the source to improve urban air quality and maintain urban ecological balance.

Keywords: urban environment; fine particulate matter; visual analysis; mapping knowledge domains; CiteSpace; CNKI

(C)1994-2022 China Academic Journal Electronic Publishing House. All rights reserved. http://www.cnki.net

生态环境学报 2021, 30(11): 2157-2164 http://www.jeesci.com
Ecology and Environmental Sciences E-mail: editor@jeesci.com

城市街道峡谷$PM_{2.5}$时空分布特征与空气质量评价
——以合肥市长淮街道为例

王薇[1, 2]，程歆玥[1]，胡春[1, 2]，夏斯涵[1]，王甜[1]

1. 安徽建筑大学建筑与规划学院，安徽 合肥 230022；2. 安徽建筑大学建成环境与健康重点实验室，安徽 合肥 230022

摘要：以 $PM_{2.5}$ 为代表的空气污染对城市居民的生活产生了巨大的影响。街道峡谷是城市的重要构成部分，是城市居民生活的主要场所之一。以 $PM_{2.5}$ 为研究对象，于 2021 年 1 月 22—24 日在合肥市瑶海区长淮街道的街道峡谷设立 7 个固定式监测点，并以附近的三里街国控点为参照，分析冬季合肥市街道峡谷的 $PM_{2.5}$ 污染水平及其影响因素。研究表明，（1）街道峡谷内 $PM_{2.5}$ 日均质量浓度呈现“W”型变化特征。在街道峡谷非必要通勤市民，应避免在工作日午高峰出行，可以选择在 15:00—16:00 出行。（2）不同街道峡谷内 $PM_{2.5}$ 质量浓度大小趋势为：道路交叉口>道路旁>小区公园绿地>一般街道峡谷。风速越大，距离排放污染源越远，距离绿化植物越近，$PM_{2.5}$ 质量浓度越低。公园绿地、宽阔型街道峡谷、降低迎风面建筑高度和增加街道宽度都能降低街道峡谷内部的 $PM_{2.5}$ 质量浓度。上升型街道峡谷的背风侧易造成高质量浓度 $PM_{2.5}$ 累积。（3）对合肥市长淮街道冬季而言，$PM_{2.5}$ 的空气质量水平为中度污染，空气质量级别为四级。湿度对街道峡谷的 $PM_{2.5}$ 质量浓度贡献度比温度更大，湿度和温度对街道峡谷的 $PM_{2.5}$ 质量浓度贡献度分别为 80.5%和 54.7%。

关键词：街道峡谷；$PM_{2.5}$；时空分布；空气质量评价；温湿度；风速；车流量

DOI: 10.16258/j.cnki.1674-5906.2021.11.006

中图分类号：X16 **文献标志码：**A **文章编号：**1674-5906（2021）11-2157-08

引用格式：王薇, 程歆玥, 胡春, 夏斯涵, 王甜, 2021. 城市街道峡谷$PM_{2.5}$时空分布特征与空气质量评价——以合肥市长淮街道为例[J]. 生态环境学报, 30(11): 2157-2164.

WANG Wei, CHENG Xinyue, HU Chun, XIA Sihan, WANG Tian, 2021. Spatio-temporal distribution characteristics of $PM_{2.5}$ and air quality evaluation in urban street canyons: Take Changhuai street in Hefei as an example [J]. Ecology and Environmental Sciences, 30(11): 2157-2164.

2019 年末中国常住人口城镇化率达到 60.60%（中央人民政府，2020），高城镇化率在提高居民生活质量的同时，也带来了城市大气污染、交通拥堵、热岛效应等一系列问题。其中，机动车尾气排放及其形成的二次污染，是城市大气污染的主要来源。常见的大气污染物有 SO_2、NO_2、CO、O_3 和颗粒物，但现阶段国内最为关注的是 $PM_{2.5}$。2018 年，$PM_{2.5}$ 导致过早死亡人数有 1 368 200 人，据预测，大气 $PM_{2.5}$ 质量浓度 2025 年需降至 40 μg·m^{-3} 以下，其导致的过早死亡人数才能与 2018 年接近（郭云等，2021）。

城市街道峡谷是城市居民生活的主要场所之一，街道峡谷在城市建成环境中占比高达三成（于洋等，2020）。街道峡谷是指两侧具有连续高大建筑物的狭长街道（Nicholson，1975）。1993 年，街道峡谷这一概念被引入中国，后被进一步扩展，即使街道两旁的建筑物高低不平、不连续甚至有一定的缺口，也可称作街道峡谷（周洪昌等，1994；王宝民等，2005）。街道峡谷内污染物的扩散主要受交通量、气象条件、天空开阔度、街道峡谷高宽比和朝向等影响（邓寄豫等，2017；葛晓燕，2018）。由于两侧建筑的阻挡，传输的污染物难以扩散，进而产生累积效应；同时由于街道峡谷附近人口较多，街道峡谷内的污染物不仅影响室外环境质量，又会作为置换源影响室内空气质量，进而影响城市居民的身体健康。

2020 年合肥市全市 $PM_{2.5}$ 质量浓度年均值为 36 μg·m^{-3}，未达到国家二级标准，超标 3%（合肥市生态环境局，2021）。目前相关研究大多集中在省市的宏观层面研究，对与人体接触紧密的街道峡谷 $PM_{2.5}$ 质量浓度的探讨较少。因此，本研究以城市内典型街道峡谷为例，采用固定式监测点的方式实测街道峡谷内 $PM_{2.5}$ 质量浓度，分析 $PM_{2.5}$ 在街道峡谷的时空分布规律，对于改善城市街道峡谷的

基金项目：国家自然科学基金项目（51778001）；国家重点研发计划（2017YFC0702503）；安徽省教育厅高校优秀拔尖人才培育资助项目（gxbJZD23）

作者简介：王薇（1975年生），女，教授，博士，研究方向为建筑技术和人居环境。E-mail: vivi.gan@126.com

收稿日期：2021-06-11

(C)1994-2022 China Academic Journal Electronic Publishing House. All rights reserved. http://www.cnki.net

空气质量具有积极意义，同时为街道峡谷空气污染防治提供对策。

1 研究概况与方法

1.1 研究对象概况

合肥市地处中纬度地带，31°52′N，117°17′E，是季风气候最明显的区域之一，属于典型的夏热冬冷气候区城市，全年气温夏热冬冷，春秋温和，年平均气温在 15—16 ℃之间，夏季平均气温为 27.5—28.5 ℃，冬季平均气温为 1.5—5.0 ℃，相对湿度与温度的年变化相一致，夏季最大，冬季最小。城市主导风向为东南风，其中夏季东南风，冬季东北风，年平均风速在 1.6—3.3 $m·s^{-1}$ 之间。

合肥市作为安徽省会城市，人口城镇化率高。合肥全市人口密度为 1.0 万人/平方千米，建筑密度为 41.2%（李小东等，2018）。合肥市规划类型始于“风扇式”布局，城市街道以东北—西南走向为主。瑶海区位于合肥市东部，总面积为 64.4 km^2，是合肥四大老城区之一且是国字号老工业基地。据统计，瑶海区已开发建设用地面积超过可开发用地面积的 90%以上，呈现出建设用地人口密度和建筑密度“双高”的局面。瑶海区长淮街道位于北一环内，其建设用地人口密度达到 3.5 万人/平方千米，建筑密度达到 52.6%（黄慧芬，2019）。

研究表明（王飞等，2014），合肥市区空气首要污染物主要为 $PM_{2.5}$，其来源与汽车尾气排放有很大关系；其次，合肥市冬季雾霾情况较其他季节严重。因此，以合肥市环境保护局网站提供的全市 10 个监测点空气质量指数为依据（http://sthjj.hefei.gov.cn/index.html），确定合肥市区空气污染较严重区域，并在此基础上，研究合肥市瑶海区长淮街道冬季街道峡谷 $PM_{2.5}$ 质量浓度的时空演化特征，旨在为改善合肥市街道峡谷空气质量提供科学依据。

1.2 选点依据与测点分布

本研究根据建筑布局、建筑高宽比、街道长宽度、植物绿化、风向风速、下垫面等特征指标综合选取并确定实测样点，分析城市街道峡谷 $PM_{2.5}$ 质量浓度的时空分布特征，最终确定 7 个样点进行实地观测，并以三里街国控点（H 点）进行对照评价，如图 1 所示。

街道峡谷主要有 3 种分类标准（Hu et al.，2020）：（1）基于高宽比的分类标准，根据建筑物高度与道路宽度比值来计算高宽比；（2）基于对称性的分类标准，根据道路两旁建筑物的高度确定，如对称式、非对称式（上升型、下降型）等；（3）基于复杂几何形态的分类标准，如一般街道峡谷、道路交叉口、公园绿地、高架桥上下等。而对于现实中的街道峡谷，可能涵盖多个分类标准，上述方法不能很好地反映街道峡谷 $PM_{2.5}$ 质量浓度的空间分布效果。因此，引入街道峡谷封闭比（SCER）的概念（Wei et al.，2021），定义 SCER 为背风面建筑高度（LB）、道路宽度、迎风面建筑高度（WB）三者之比。SCER 数值由现场实测所得，背风面建筑和迎风面建筑根据监测时的主要风向确定，如图 2 所示。

1.3 监测仪器

根据街道峡谷测点的分布，配置 7 台 ONETEST 500 粉尘浓度监测仪和 7 台 KESTREL 5500 手持式风速仪进行测试。粉尘浓度监测仪测试 $PM_{2.5}$ 质量浓度及温湿度，其中 $PM_{2.5}$ 质量浓度的测量范围为 0—1 000 $\mu g·m^{-3}$，测量精度为±10% FS，分辨率为 0.1



图1 测试样点分布

Fig. 1 Distribution of test samples

(C)1994-2022 China Academic Journal Electronic Publishing House. All rights reserved. http://www.cnki.net

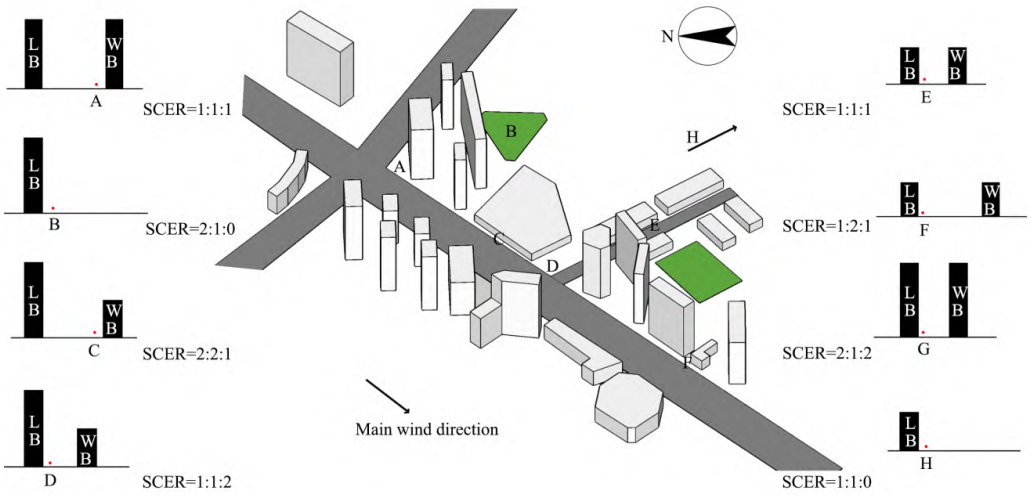


图2 街道峡谷封闭比

Fig. 2 Street Canyon Enclosure Ratios

μg·m^{-3}；温度的测量范围为−20—60 ℃，测量精度为±0.5%，分辨率为 0.1 ℃；相对湿度的测量范围为 0—100%，测量精度为±3%，分辨率为 0.1%。监测过程中每 2 秒钟记录 1 次数据。监测高度与一般人体呼吸高度一致，距离地面 1.5 m，如图 1 所示。

1.4 监测时间

实测选择在 2021 年 1 月 22—24 日进行，每天 08:00—17:00，监测街道峡谷内的 $PM_{2.5}$ 质量浓度、温湿度和风速，监测期间天气晴朗，天气状况较一致。

1.5 空气质量评价标准

根据生态环境部 2018 年发布的《环境空气质量标准》（GB 3095—2012）修改单（生态环境部，2018），空气质量指数（air quality index，AQI）是一个用来定量描述空气质量水平的数值，其等级划分为：优（AQI≤50）、良（50<AQI≤100）、轻度污染（100<AQI≤150）、中度污染（150<AQI≤200）、重度污染（200<AQI≤300）、严重污染（AQI>300）。目前，中国尚无正式的空气质量指数标准，但此修订单中 $PM_{2.5}$ 质量浓度值可用来评价不同街道峡谷的空气质量水平。空气质量指数的计算公式如下：

$$I=\frac{I_{high}-I_{low}}{C_{high}-C_{low}}(C-C_{low})+I_{low} \quad (1)$$

式中：

I——空气质量指数，即 AQI，输出值；

C——$PM_{2.5}$ 日均值质量浓度，输入值；

I_{low}——对应于 C_{low} 的指数限值，常量；

I_{high}——对应于 C_{high} 的指数限值，常量；

C_{low}——小于或等于 C 的质量浓度限值，常量；

C_{high}——大于或等于 C 的质量浓度限值，常量。

其中，指数限值和质量浓度限值的常量如表 1 所示。

表1 空气污染物的指数限值和质量浓度限值

Table 1 Index limits and mass concentration limits of air pollutants

空气质量指数 Air quality index	$PM_{2.5}$日均值 Daily mean value of $PM_{2.5}$/(μg·m^{-3})
0	0
50	35
100	75
150	115
200	150
300	250
400	350
500	500

2 结果与分析

根据不同日期和选点位置，对各个实测样点位置和每天各时间段的 $PM_{2.5}$ 质量浓度随时间和选点位置变化的趋势进行统计分析。为保证分析数据的精确性，首先在 Excle 中对各监测样点的 $PM_{2.5}$ 质量浓度、温度和相对湿度等数据进行统一，再进行筛选得到 3 天 7 个实测样点的有效数据共 48 600 条，对每天、每小时、每点分各天和 3 天整体的数据取平均值。

2.1 城市街道峡谷的PM2.5时间分布特征

时间序列指的是描述现象指标随时间变化的直观图形，利用它观察现象演变的状况（闫秀婧，2009），最终结果如图 2 所示，$PM_{2.5}$ 日均质量浓度均呈现出“W”型变化特征。

图 3 可以看出 3 d 内不同测点 $PM_{2.5}$ 质量浓度随时间变化的规律，街道峡谷 $PM_{2.5}$ 质量浓度平均值为 125.54 μg·m^{-3}。$PM_{2.5}$ 质量浓度在 12:00—13:00 区间最高，为 135.96 μg·m^{-3}；在 09:00—10:00 区间最低，为 122.15 μg·m^{-3}；在 13:00—14:00 区间次之，

(C)1994-2022 China Academic Journal Electronic Publishing House. All rights reserved. http://www.cnki.net

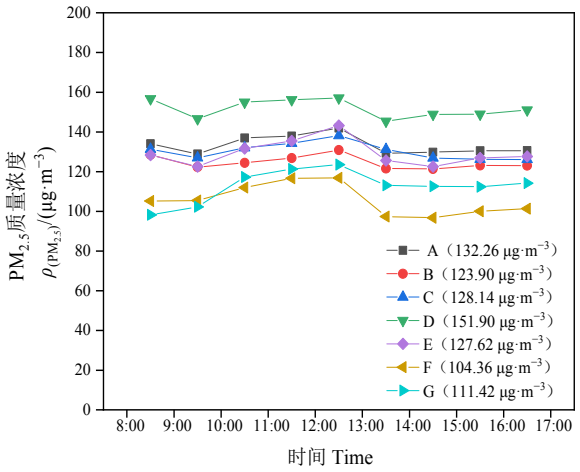


图3 $PM_{2.5}$日均质量浓度

Fig. 3 Daily average mass concentration of $PM_{2.5}$

为 122.71 μg·m^{-3}。因此建议长淮街道的市民可选择避开工作日午高峰时期出行，以降低城市街区 $PM_{2.5}$ 质量浓度。

2.2 城市街道峡谷的$PM_{2.5}$空间分布特征

空间分布指的是描述现象指标随空间变化的直观图形，利用它观察现象演变的状况（王薇等，2014）。由于各个实测样点所处的街道峡谷形态特征不同，其环境的 $PM_{2.5}$ 质量浓度也不尽相同，最终结果如图 3 所示。

2.2.1 总体分布特征

3 天内 D 点在 1 月 22 日 $PM_{2.5}$ 平均质量浓度最高，为 260.52 μg·m^{-3}；F 点在 1 月 23 日 $PM_{2.5}$ 平均质量浓度最低，为 63.17 μg·m^{-3}。同一天内 D 点 1 月 22 日 $PM_{2.5}$ 平均质量浓度最高，为 260.52 μg·m^{-3}，F 点 1 月 22 日 $PM_{2.5}$ 平均质量浓度最低，为 170.80 μg·m^{-3}，两点 $PM_{2.5}$ 平均质量浓度相差 89.72 μg·m^{-3}。其中，1 月 22 日 $PM_{2.5}$ 背景质量浓度较高。

由图 4 可知，合肥市城市街道峡谷 $PM_{2.5}$ 质量浓度的空间分布排序为：D 点（151.90 μg·m^{-3}）>A 点（132.26 μg·m^{-3}）>C 点（128.14 μg·m^{-3}）>E 点（127.62 μg·m^{-3}）>B 点（123.90 μg·m^{-3}）>G 点（111.42 μg·m^{-3}）>F 点（104.36 μg·m^{-3}）。因此，在城市设计中，建议使用 F 点和 G 点的街道峡谷空间形态，而避免使用 A 点和 D 点的街道峡谷空间形态，进而降低街道峡谷内的 $PM_{2.5}$ 质量浓度。

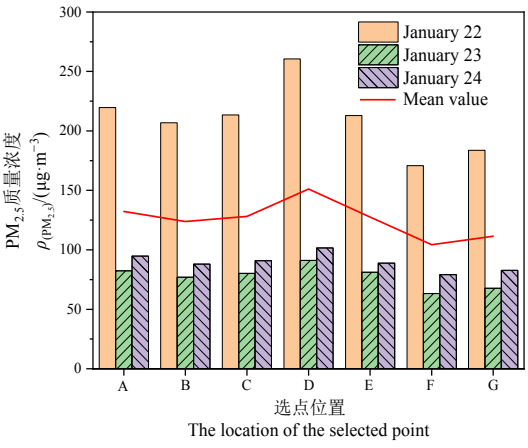


图4 各监测点$PM_{2.5}$质量浓度

Fig. 4 $PM_{2.5}$ mass concentration at each monitoring point

2.2.2 各监测点环境特征

如图 2 所示，A 点位于对称街道峡谷，SCER=1:1:1，即标准型街道峡谷。测点 A 位于道路交叉口迎风面建筑侧，周边为高层建筑，没有植物绿化，靠近汽车尾气污染源排放位置，且人流量和车流量大，汽车停留时间长，街道峡谷的 $PM_{2.5}$ 质量浓度为 132.26 μg·m^{-3}。

B 点位于非对称街道峡谷，SCER=2:1:0，即下降型街道峡谷。测点 B 位于小区公园绿地，周边乔木、灌木和草地较多，对 $PM_{2.5}$ 质量浓度起到一定的降解作用。而且测点 B 位于高层商住楼后塑胶运动场上，即高层建筑背风处，对 $PM_{2.5}$ 的传输起到一定的阻挡作用，$PM_{2.5}$ 质量浓度为 123.90 μg·m^{-3}。

C 点位于非对称街道峡谷，SCER=2:2:1，即下降型街道峡谷。测点 C 位于主干道旁迎风面建筑侧，周边为高层和多层建筑，虽人流量和车流量较大，但停留时间短，且测点周边有灌木绿化带，对 $PM_{2.5}$ 质量浓度起到一定的降解作用，$PM_{2.5}$ 质量浓度为 128.14 μg·m^{-3}。对比测点 A、C 可知，其他条件不变，降低迎风面建筑高度，能降低街道峡谷内部的 $PM_{2.5}$ 质量浓度。

D 点位于非对称街道峡谷，SCER=1:1:2，即上升型街道峡谷。测点 D 位于主次干道交叉口多层建筑侧，没有植物绿化，靠近汽车尾气污染源排放位置，且人流量和车流量大，汽车停留时间长，因此 $PM_{2.5}$ 的质量浓度高，为 151.90 μg·m^{-3}。上升型街道峡谷的背风侧易造成高质量浓度 $PM_{2.5}$ 堆积。因此建议在城市设计中，应避免设计上升型街道峡谷的背风侧建筑，同时也建议在上升型街道峡谷的背风侧增设垂直绿化以减少空气污染。

E 点位于对称街道峡谷，SCER=1:1:1，即标准型街道峡谷。测点 E 点位于次干道旁，周边为多层建筑，人流量和车流量较大，停留时间短，且测点周边有灌木绿化带，对 $PM_{2.5}$ 质量浓度起到一定的降解作用，$PM_{2.5}$ 质量浓度为 127.62 μg·m^{-3}。

F 点位于对称街道峡谷，SCER=1:2:1，即宽阔型街道峡谷。测点 F 位于主干道旁人行道一侧，虽人流量和车流量较大，但停留时间短，且靠近 1 m 宽的乔木与灌木组成的绿化带，对 $PM_{2.5}$ 的降解作

(C)1994-2022 China Academic Journal Electronic Publishing House. All rights reserved. http://www.cnki.net

用很大，因此 $PM_{2.5}$ 的质量浓度很低，为 104.36 $\mu g \cdot m^{-3}$。对比测点 E、F 可知，其他条件不变，增加街道宽度，能降低街道峡谷内部的 $PM_{2.5}$ 质量浓度。

G 点位于对称街道峡谷，SCER=2:1:2，即狭窄型街道峡谷。测点 G 位于一般街道峡谷内，人流量和车流量很小，且街道峡谷内风速较大（图 5），对 $PM_{2.5}$ 的扩散作用很大，因此 $PM_{2.5}$ 的质量浓度很低，为 111.42 $\mu g \cdot m^{-3}$。建议在城市设计中考虑主导风向，利用城市通风廊道减轻街道峡谷内的 $PM_{2.5}$ 质量浓度。

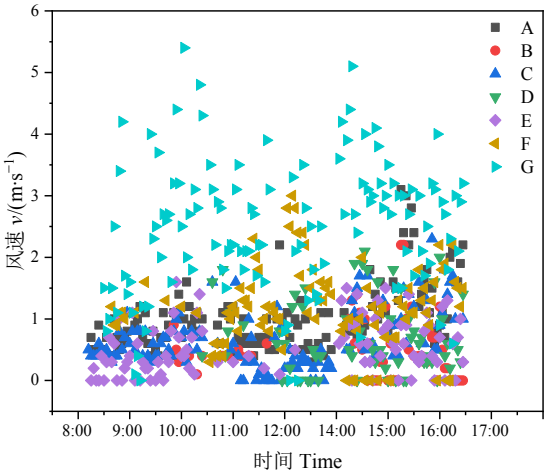


图5 街道峡谷内风速的日变化

Fig. 5 Diurnal variation of wind speed in the street canyon

H 点位于非对称街道峡谷，SCER=1:1:0，即下降型街道峡谷。测点 H 为国控点，$PM_{2.5}$ 质量浓度为 127.62 $\mu g \cdot m^{-3}$。比国控点 $PM_{2.5}$ 质量浓度更低的街道峡谷有 B、F、G 三点，说明公园绿地、宽阔型街道峡谷、较大的风速都能降低街道峡谷内部的 $PM_{2.5}$ 质量浓度。

2.3 环境影响因素分析

相关研究（Wei et al.，2021）表明，建筑环境因子如气象条件、风向风速、车流量、下垫面材料、植物绿化等，都不同程度地影响街道峡谷内 $PM_{2.5}$ 每小时质量浓度分布效果。

2.3.1 温湿度的影响

如表 2 所示，运用 SPSS 对 $PM_{2.5}$ 质量浓度和温湿度的每小时平均值进行回归分析，其中常数项远大于温湿度的系数，说明合肥市长淮街道峡谷内 $PM_{2.5}$ 的背景质量浓度较高，除机动车尾气排放外，生活源和工业源的影响较大。

在 Origin 中对 $PM_{2.5}$ 质量浓度和温湿度的每小时平均值进行线性拟合，如图 6 所示，温度和相对湿度两个建筑环境因子对 $PM_{2.5}$ 每小时质量浓度作多元线性回归，得到方程有：

表2 温湿度与$PM_{2.5}$每小时质量浓度的回归分析

Table 2 Regression analysis of temperature, humidity and $PM_{2.5}$ hourly mass concentration

因变量 Dependent variable	预测变量 Predictor variable	非标准化系数 Non-standardized coefficient		标准系数 Standard coefficient	sig.	R^2
		常量B	标准误差 Standard error	回归系数 Beta		
$PM_{2.5}$	Constant	−587.922	52.439		0.000	0.532
	Temperature	23.346	2.561	0.547	0.000	
	Humidity	6.637	0.495	0.805	0.000	

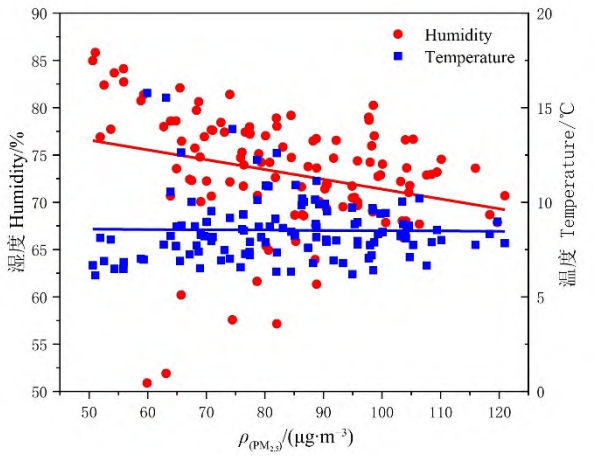


图6 $PM_{2.5}$质量浓度和温湿度的回归方程

Fig. 6 Regression equation of $PM_{2.5}$ mass concentration and temperature and humidity

$$\rho_{(PM_{2.5})} = -587.92 + 23.35 \times t + 6.64 \times H \quad (2)$$

式中：

$\rho_{(PM_{2.5})}$——$PM_{2.5}$ 每小时质量浓度值；

t——温度值；

H——湿度值。

式中 R^2=0.53，说明温湿度两个要素变量共同解释了 $PM_{2.5}$ 变化的 53%。温度对 $PM_{2.5}$ 的贡献度达 54.7%，湿度对 $PM_{2.5}$ 的贡献度达 80.5%，说明与温度相比，湿度对街道峡谷的 $PM_{2.5}$ 质量浓度贡献度比温度更大。

引起街道峡谷 $PM_{2.5}$ 每小时质量浓度周期性变化的主要原因是昼夜温差造成（张云伟等，2016），白天随着气温的升高，大气边界层开始膨胀，导致街道峡谷 $PM_{2.5}$ 质量浓度降低。由图 6 可知，湿度与 $PM_{2.5}$ 每小时质量浓度呈现显著正相关，根据有关研究结论（臧振峰等，2021），温度与 $PM_{2.5}$ 每小时质量浓度应该呈现显著负相关，而本研究中温度

(C)1994-2022 China Academic Journal Electronic Publishing House. All rights reserved. http://www.cnki.net

与 $PM_{2.5}$ 每小时质量浓度呈现微小的正相关，可能是白天背景质量浓度过大造成的。

2.3.2 风速的影响

风速与 $PM_{2.5}$ 的扩散速率有关，对街道峡谷内的 $PM_{2.5}$ 质量浓度有显著的输送、稀释和扩散作用（邱巧玲，2007）。本研究风速的测量结果以每 10 分钟作平均处理，如图 5 所示，显示了 1 月 22—24 日 3 d 内长淮街道峡谷风速的日变化，街道峡谷下午风速基本高于上午风速，说明早上街道峡谷风速较低，易发生 $PM_{2.5}$ 的滞留。因而建议在长淮街道峡谷，高峰期非必要通勤市民避免选择下午出行，以免行车拥堵造成城市空气污染。合肥市城市街道峡谷风速的空间分布排序为：G 点 (2.43 $m·s^{-1}$)>F 点 (1.16 $m·s^{-1}$)>A 点 (1.01 $m·s^{-1}$)>C 点 (0.66 $m·s^{-1}$)>D 点 (0.59 $m·s^{-1}$)>B 点 (0.46 $m·s^{-1}$)=E 点 (0.46 $m·s^{-1}$)。其中，风速越大，$PM_{2.5}$ 质量浓度越低，G 点街道峡谷的风速明显高于其他监测点，有利于降低街道峡谷内的 $PM_{2.5}$ 质量浓度。

2.3.3 车流量的影响

机动车的尾气排放主要集中在城市街道峡谷，由于街道峡谷的特殊结构，$PM_{2.5}$ 难以扩散并不断聚集，导致居民长期暴露于汽车尾气中，对人体健康产生了极大的危害。因此，街道峡谷内的车流量与 $PM_{2.5}$ 每小时质量浓度的相关性已经成为重要的研究课题之一（柴晋鹏等，2021）。本研究的街道峡谷胜利路位于合肥市瑶海区交通主干道上，以每小时记录 10 min 的车流量来估算街道峡谷每小时内车流量的大致情况。如图 7 所示，1 月 22—24 日对应周五至周日，工作日的车流量基本大于周末的车流量。街道峡谷车流量的日变化折点图基本呈现“W”型分布，即有明显的早高峰、午高峰和晚高峰分布。根据 3 d 平均值可以看出，长淮街道峡谷的车流量早高峰>晚高峰>午高峰，其中 15:00—16:00 时间段内的车流量最小。因而建议在长淮街道，非必要通勤市民可以选择 15:00—16:00 出行，以免行车拥堵造成街道峡谷环境污染。

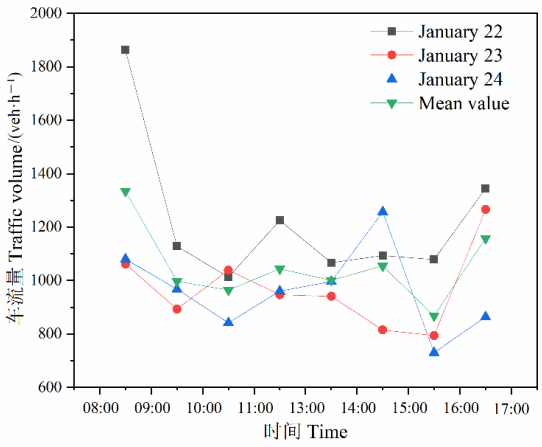


图7 街道峡谷内车流量的日变化

Fig. 7 The daily change of traffic flow in the street canyon

3 城市街道峡谷空气质量评价

对各实测样点的 48 600 条 $PM_{2.5}$ 质量浓度有效值进行统计，运用 AQI 对其数据进行计算分析，得到表 3。合肥市长淮街道峡谷 $PM_{2.5}$ 空气质量水平以中度污染为主，空气质量级别多分布在四级。根据实测数据计算得出 AQI 值为 165，三里街国控点（H 点）的 AQI 值为 166，误差值为 0.01，空气质量水平都为中度污染，空气质量级别都为四级，两者差距不大。说明采用 AQI 能较好地评价街道峡谷的空气质量。

表3 街道峡谷空气质量评价

Table 3 Air Quality Evaluation of Street Canyon

街道峡谷选点位置 Street canyon location	$\rho_{(PM_{2.5})}$/(μg·m^{-3})	AQI	空气质量水平 Air quality level	空气质量级别 Air quality level
A	132.26	174	Moderate pollution	Fourth level
B	123.90	162	Moderate pollution	Fourth level
C	128.14	168	Moderate pollution	Fourth level
D	151.09	201	Severe pollution	Fifth level
E	127.62	168	Moderate pollution	Fourth level
F	104.36	136	Light pollution	Third level
G	111.42	145	Light pollution	Third level
H	126.20	166	Moderate pollution	Fourth level

4 结论与展望

4.1 结论

（1）街道峡谷内 $PM_{2.5}$ 日均质量浓度均呈现出“W”型变化特征。街道峡谷内非必要通勤市民应避免在工作日午高峰出行，可以选择在 15:00—16:00 出行，此时风速较大、车流量较小，能减少 $PM_{2.5}$ 对空气质量的影响。

（2）对不同街道峡谷空间分布而言，$PM_{2.5}$ 质量浓度由大到小的趋势为：道路交叉口>道路旁>小区公园绿地>一般街道峡谷。风速越大，距离排放污染源越近，距离绿化植物越近，$PM_{2.5}$ 质量浓度越低。

（3）公园绿地，宽阔型街道峡谷，降低迎风面建筑高度和增加街道宽度都能降低街道峡谷内部的 $PM_{2.5}$ 质量浓度。上升型街道峡谷的背风侧易造成高质量浓度 $PM_{2.5}$ 堆积。

（4）对合肥市长淮街道冬季而言，$PM_{2.5}$ 的空气质量水平为中度污染，空气质量级别为四级。温湿度共同解释了 $PM_{2.5}$ 变化的 53%，湿度对街道峡谷的 $PM_{2.5}$ 质量浓度贡献度比温度更大，湿度和温度

(C)1994-2022 China Academic Journal Electronic Publishing House. All rights reserved. http://www.cnki.net

对街道峡谷的 $PM_{2.5}$ 质量浓度贡献度分别为 80.5% 和 54.7%。

4.2 展望

（1）在道路旁不同树种植物、街道峡谷空间形态和环境影响因素对 $PM_{2.5}$ 浓度的协同降解作用有待进一步研究。

（2）风速风向对不同类型的街道峡谷 $PM_{2.5}$ 浓度的扩散作用有待深入研究。

参考文献:

HU C B, ZHANG F, GUO F Y, et al., 2020. Classification and mapping of urban canyon geometry using Google Street View images and deep multitask learning [J]. Building and Environment, DOI: 10.1016/j.buildenv.2019.106424.

NICHOLSON S E, 1975. A pollution model for street-level air [J]. Atmospheric Environment, 9(1): 19-31.

WEI Z H, PENG J X, MA X W, et al., 2021. Toward $PM_{2.5}$ Distribution Patterns Inside Symmetric and Asymmetric Street Canyons: Experimental Study [J]. Journal of Environmental Engineering, DOI: 10.1061/(ASCE)EE.1943-7870.0001878.

柴晋鹏, 陈学刚, 赵直, 2021. 基于移动监测的城市街谷交通相关污染物浓度时空变化研究[J]. 地球与环境, 49(4): 389-399.
CHAI J P, CHEN X G, ZHAO Z, 2021. Study on the temporal and spatial variation of traffic-related pollutants concentration in urban streets and valleys based on mobile monitoring [J]. Earth and Environment, 49(4): 389-399.

邓寄豫, 郑炘, 2017. 街区层峡几何形态与微气候的关联性研究[J]. 建筑与文化, 14(5): 212-213.
DENG J Y, ZHENG K, 2017. Study on the relationship between the geometry of the block gorge and microclimate [J]. Architecture and Culture, 14(5): 212-213.

葛晓燕, 2018. 城市典型街谷道路中污染物扩散特征模拟[D]. 西安: 西安建筑科技大学: 29-56.
GE X Y, 2018. Simulation of pollutant diffusion characteristics in typical urban streets and valleys [D]. Xi'an: Xi'an University of Architecture and Technology: 29-56.

郭云, 蒋玉丹, 黄炳昭, 等, 2021. 我国大气 $PM_{2.5}$ 及 O_3 导致健康效益现状分析及未来 10 年预测[J]. 环境科学研究, 34(4): 1023-1032.
GUO Y, JIANG Y, HUANG B Z, et al., 2021. Analysis of the current health benefits of my country's atmospheric $PM_{2.5}$ and O_3 and its prediction in the next 10 years [J]. Environmental Science Research, 34(4): 1023-1032.

合肥市生态环境局, 2021. 2020 年合肥市环境状况公报[N/OL]. (2021-06-04) [2021-06-04]. http://sthjj.hefei.gov.cn/hbzx/gsgg/18085969.html.
Hefei Municipal Bureau of Ecology and Environment, 2020. Bulletin on Environmental Status of Hefei City from 2021 to 2020 [N/OL]. (2021-06-04) [2021-06-04]. http://sthjj.hefei.gov.cn/hbzx/gsgg/18085969.html.

黄慧芬, 2019. 合肥市城市空间形态演变多尺度研究（1949—2015 年）[D]. 合肥: 合肥工业大学: 21-54.
HUANG H F, 2019. Multi-scale study on the evolution of urban spatial form in Hefei (1949–2015) [D]. Hefei: Hefei University of Technology: 21-54.

李小东, 张玉鹏, 李德, 2018. 合肥瑶海区旧城更新改造规划路径探索[J]. 规划师, 34(S1): 44-49.
LI X D, ZHANG Y P, LI D, 2018. Exploration on the planning path of old city renewal and reconstruction in Yaohai District of Hefei [J]. Planner, 34(S1): 44-49.

邱巧玲, 王凌, 2007. 基于街道峡谷污染机理的城市街道几何结构规划研究[J]. 城市发展研究 (4): 78-82.
QIU Q L, WANG L, 2007. Research on Urban Street Geometric Structure Planning Based on the Pollution Mechanism of Street Canyon [J]. Urban Development Research (4): 78-82.

生态环境部, 2018. 关于发布《环境空气质量标准》（GB 3095—2012）修改单的公告[N/OL]. (2021-06-04) [2021-06-04]. http://www.mee.gov.cn/gkml/sthjbgw/sthjbgg/201808/t20180815_451398.htm.
Ministry of Ecology and Environment, 2018. Announcement on Issuing the Revision Sheet of Ambient Air Quality Standard (GB 3095—2012) [N/OL]. (2021-06-04) [2021-06-04]. http://www.mee.gov.cn/gkml/sthjbgw/sthjbgg/201808/t20180815_451398.htm.

王宝民, 柯咏东, 桑建国, 2005. 城市街谷大气环境研究进展[J]. 北京大学学报(自然科学版), 41(1): 146-153.
WANG B M, KE Y D, SANG J G, 2005. Research progress of atmospheric environment in urban street canyons [J]. Journal of Peking University (Natural Science Edition), 41(1): 146-153.

王飞, 吴开亚, 王慧慧, 等, 2014. 合肥市 $PM_{2.5}$ 与用地类型特征比较及建设性方案研究[J]. 环境科学与管理, 39(10): 73-79.
WANG F, WU K Y, WANG H H, et al., 2014. Comparison of $PM_{2.5}$ and land use type characteristics in Hefei City and study on constructive plans [J]. Environmental Science and Management, 39(10): 73-79.

王薇, 张之秋, 2014. 城市住区空气负离子浓度时空变化及空气质量评价——以合肥市为例[J]. 生态环境学报, 23(11): 1783-1791.
WANG W, ZHANG Z Q, 2014. Spatio-temporal Change of Negative Air Ion Concentration of Urban Residential Area and Air Quality Assessment——Case Study of Hefei City [J]. Journal of Ecological Environment, 23(11): 1783-1791.

闫秀婧, 2009. 青岛市森林与湿地负离子水平时空分布研究[D]. 北京: 北京林业大学: 13-14.
YAN X J, 2009. Research on the Spatial and Temporal Distribution of Anion Levels in Forests and Wetlands in Qingdao City [D]. Beijing: Beijing Forestry University: 13-14.

于洋, 刘晓宇, 田达睿, 等, 2020. 街道峡谷几何形态规划要素对太阳能潜力的影响研究[J]. 工业建筑, 50(7): 137-142.
YU Y, LIU X Y, TIAN D R, et al., 2020. Research on the influence of street canyon geometry planning elements on solar energy potential [J]. Industrial Construction, 50(7): 137-142.

臧振峰, 张凤英, 李永华, 等, 2021. 我国主要粮产区 $PM_{2.5}$、PM_{10} 时空分布特征及影响因素——以河南省为例[J]. 自然资源学报, 36(5): 1163-1175.
ZANG Z F, ZHANG F Y, LI Y H, et al., 2021. Spatio-temporal distribution and affecting factors of $PM_{2.5}$ and PM_{10} in major grain producing areas in China: A case study of Henan province [J]. Journal of Natural Resources, 36(5): 1163-1175.

(C)1994-2022 China Academic Journal Electronic Publishing House. All rights reserved. http://www.cnki.net

张云伟, 王晴茹, 陈嘉, 等, 2016. 城市街谷内 $PM_{2.5}$ 浓度时空变化及影响因素分析[J]. 中国环境科学, 36(10): 2944-2949.
ZHANG Y W, WANG Q R, CHEN J, et al., 2016. Analysis of Temporal and Spatial Changes of $PM_{2.5}$ Concentration in Urban Streets and Valleys and Influencing Factors [J]. China Environmental Science, 36(10): 2944-2949.
中央人民政府, 2020. 政府工作报告—2020年5月22日在第十三届全国人民代表大会第三次会议上[N/OL]. (2020-05-29) [2020-05-29]. http://www.gov.cn/premier/2020-05/29/content_5516072.htm.
Central People's Government, 2020. government work report—at the third session of the 13th national people's congress on May 22, 2020 [N/OL]. (2020-05-29) [2020-05-29]. http://www.gov.cn/premier/2020-05/29/content_5516072.htm.
周洪昌, 杨佩昆, 高延令, 1994. 城市街道汽车排放物扩散过程的风洞试验[J]. 同济大学学报 (自然科学版), 39(3): 306-311.
ZHOU H C, YANG P K, GAO Y L, 1994. Wind tunnel test on the diffusion process of automobile emissions from urban streets [J]. Journal of Tongji University (Natural Science Edition), 39(3): 306-311.

Spatio-temporal Distribution Characteristics of $PM_{2.5}$ and Air Quality Evaluation in Urban Street Canyons: Take Changhuai Street in Hefei as An Example

WANG Wei[1, 2], CHENG Xinyue[1], HU Chun[1, 2], XIA Sihan[1], WANG Tian[1]
1. School of Architecture and Urban Planning, Anhui Jianzhu University, Hefei 230022, China;
2. Key Laboratory of Built Environment and Health, Anhui Jianzhu University, Hefei 230022, China

Abstract: The air pollution represented by $PM_{2.5}$ has a great impact on the life of urban residents. Street canyon is an important part of the city and one of the main places where urban residents live. In this study, $PM_{2.5}$ was taken as the research object. From January 22 to January 24, 2021, seven fixed monitoring stations were set up in the street canyon of Changhuai Street, Yaohai District, Hefei City, and the pollution level of $PM_{2.5}$ in the street canyon of Hefei City in winter and its influencing factors were analyzed with reference to the national control point of Sanli Street nearby. The results show that, (1) the average daily mass concentration of $PM_{2.5}$ in street canyons presents a "W"-shaped variation. Non-essential commuters in street canyons should avoid traveling at noon peak on working days, and can choose to travel between 15:00 and 16:00. (2) The trend of $PM_{2.5}$ concentration in different street canyons was: road intersection>roadside>community park green space>general street canyons. The larger the wind speed is, the farther it is from the emission pollution source and the closer it is to the greening plants, the lower the mass concentration of $PM_{2.5}$. Park green space, wide street canyon, reducing the height of windward buildings and increasing street width can all reduce the $PM_{2.5}$ concentration in street canyon. The leeward side of the rising street canyon is easy to cause the accumulation of $PM_{2.5}$ with high mass concentration. (3) In winter, the air quality level of $PM_{2.5}$ is moderate pollution, and the air quality level is Grade 4. The contribution of humidity to $PM_{2.5}$ concentration in street canyons is greater than that of temperature, and the contribution of humidity and temperature to $PM_{2.5}$ concentration in street canyons is 80.5% and 54.7%, respectively.

Keywords: street canyon; $PM_{2.5}$; temporal and spatial distribution; air quality evaluation; temperature and humidity; wind speed; traffic flow

(C)1994-2022 China Academic Journal Electronic Publishing House. All rights reserved. http://www.cnki.net

生态环境学报 2020, 29(7): 1367-1376 http://www.jeesci.com
Ecology and Environmental Sciences E-mail: editor@jeesci.com

高密度城市住区绿地空气负离子浓度分布特征及其与微气候关系

王薇[1,2]，陈明[3]，夏斯涵[1]

1. 安徽建筑大学建筑与规划学院，安徽 合肥 230022；2. 安徽建筑大学建成环境与健康研究中心，安徽 合肥 230022；
3. 安徽安德建筑设计有限公司，安徽 合肥 230022

摘要：选取合肥市政务区天鹅湖周边 4 个高密度城市住区的不同类型绿地为研究对象，于 2016 年 7—8 月、12 月针对分别在雨后、晴天、阴天 3 种天气状况下，主要包括空气正、负离子浓度，温度，相对湿度，风速，分析了夏冬两季室内外空气负离子浓度的分布特征，结果表明，（1）夏季各样本绿地空气负离子浓度呈现雨后>晴天>阴天的趋势，冬季各样本绿地空气负离子浓度呈现出晴天>阴天>雨后的趋势。（2）空气负离子浓度总体夏季高于冬季。夏季 4 块样本绿地室外环境的空气负离子平均浓度呈现雏菊苑>丽景城>琥珀五环城>陶然居的趋势，分别为 351、292、276、260 ion·cm^{-3}；冬季呈现出陶然居>丽景城>琥珀五环城>雏菊苑的趋势，分别为 296、289、259、206 ion·cm^{-3}。（3）4 种不同类型绿地中，道路绿地的空气负离子浓度偏低，其中夏季最低值达 193 ion·cm^{-3}，冬季最低值达 171 ion·cm^{-3}；宅旁绿地、组团绿地和中心绿地的空气负离子浓度相对较高，其中夏季最高值达 405 ion·cm^{-3}，冬季最高值达 360 ion·cm^{-3}。论文进一步对空气负离子浓度与环境因子的进行相关性分析，根据以上分析得出结论，（1）晴天无尘时空气负离子浓度明显增大，雨后天晴时空气负离子比干燥晴天还要高，尤其雷雨过后空气中负离子浓度明显增高。（2）来往人员车辆较多不利于负离子的产生；植物层次结构丰富，能提高环境的空气负离子浓度。（3）室外绿地的空气负离子浓度与温度总体呈正相关，与相对湿度关系不明确，与风速总体呈正相关。（4）住区内部大面积的水体与绿地有利于激发负离子浓度。（5）住区周边的乔灌草结构，对城市主干道的灰尘起到了阻挡的作用，但也一定程度上阻挡了气流的运动。在此基础上作者进一步提出展望，建议整合住区内部的绿地或水体相贯通，形成整体化的绿地空间布局，同时采用郁闭度稍大的密林地或疏林地，在实现滞尘作用与利于气流的畅通之间寻找一个最佳的临界值。

关键词：高密度城市住区；绿地；空气负离子；分布特征；环境因子；相关性

DOI: 10.16258/j.cnki.1674-5906.2020.07.011

中图分类号：X16 **文献标志码：**A **文章编号：**1674-5906（2020）07-1367-10

引用格式：王薇, 陈明, 夏斯涵, 2020. 高密度城市住区绿地空气负离子浓度分布特征及其与微气候关系[J]. 生态环境学报, 29(7): 1367-1376.

WANG Wei, CHEN Ming, XIA Sihan, 2020. Research on distribution characteristics of negative air ions concentration in high-density urban residential green space and its relationship with microclimate [J]. Ecology and Environmental Sciences, 29(7): 1367-1376.

城市住区规划设计的首要目标就是为居民提供一个良好的居住及生活环境，住区绿地规划设计是住区规划的重要组成部分，越来越受到居民的重视。住区绿地的建设水平是居民选择住区的考虑重点之一，观念已从生存性的居住需求转变为高质量的品质需求。

绿地不仅能改善小气候、固碳释氧、减噪，还可以杀菌滞尘、增加负离子浓度。绿地产生的空气负离子具有良好的保健功能，被誉为空气中的维生素和生长素，因此常被作为衡量城市空气质量的一种重要且正面的指标（邵海荣等，2005；王薇等，2013），也直接影响了住区环境的空气质量以及人的健康和舒适程度。伴随着城市经济发展、人口增长、城市规划建设以及人们日益关注自身生活环境质量的大背景下，国内外学者开始关注空气负离子与城市环境的关系（Marko et al., 2008；Jayaratne et al.，2008；Ling et al.，2010；Ling et al.，2013；孟丽红等，2011；王薇等，2014）。因此本课题立足于拓展空气负离子在城市住区中的应用研究，根据城市住区不同绿地类型研究空气负离子浓度的分布情况，旨在优化城市住区规划设计，通过合理的空间配置和规划布局来缓解城市化引起的城市生

基金项目：国家自然科学基金项目（51778001）；安徽省教育厅 2018 年高校优秀拔尖人才培育资助项目（gxbJZD23）

作者简介：王薇（1975 年生），女，教授，博士，国家一级注册建筑师，研究方向建筑技术和人居环境。E-mail: vivi.gan@126.com

收稿日期：2020-02-14

(C)1994-2022 China Academic Journal Electronic Publishing House. All rights reserved. http://www.cnki.net

态环境问题，为城市居民提供安全、健康、方便、舒适的居住环境，促进其健康协调发展，对于提高城市住区环境和人居环境具有重要的现实意义。

1 研究区域概况和研究方法

1.1 研究区域概况

安徽省合肥市地处中纬度地带，31°52'N，117°17'E，是季风气候最为明显的区域之一，属于典型的夏热冬冷地区气候代表城市，全年气温夏热冬冷，春秋温和，年平均气温在 15—16 ℃之间，属于温和的气候型，夏季平均气温为 27.5—28.5 ℃左右，冬季月平均气温在 1.5—5.0 ℃之间，相对湿度的年变化与温度年变化相一致，夏季最大，冬季最小。城市主导风向为东南风，其中夏季东南风，冬季偏北风，年平均风速在 1.6—3.3 $m \cdot s^{-1}$ 之间。

合肥市政务文化新区位于省会合肥主城区的西南，规划面积 12.67 km^2，现有常住城市人口约 10 万人，是合肥市“141”城市空间发展战略中主城区重要组成部分，也是一座集行政办公、文教体育、金融商贸、旅游度假、居住休闲功能为一体，独具人居生态特色的魅力新区、时尚之城，已经发展成为省会合肥新的政治经济中心和商业文化中心。https://baike.so.com/doc/562883-595890.html.

合肥政务文化中心核心区有一处合肥市内最大的开放式公园，周边有大片绿地，包括各种雕塑、园林树木、人工沙滩、喷泉等景观。课题组前期开展过此区域环境的空气质量研究，本文则进一步研究此区域周边的住区绿地，以天鹅湖绿地环境的空气质量作为参考指标，探讨有利于住区居民身心健康和休闲运动的住区绿地规划与设计。

1.2 样本选择

如图 1 所示，选取合肥市政务区天鹅湖周边 4 个高密度住区：陶然居、雏菊苑、丽景城、琥珀五环城开展研究。

陶然居位于天鹅湖东部，天鹅湖路南、东至路东。占地面积 2.78×10^4 m^2，总建筑面积 9×10^4 m^2，绿化率为 40%，容积率为 2.44，基地内共有 7 栋高层住宅。雏菊苑位于天鹅湖东北部，休宁路南、石台路西。占地面积约 5.5×10^4 m^2，总建筑面积约 11×10^4 m^2，绿化率为 50%，容积率为 2.0，基地内共 9 栋高层住宅。丽景城位于天鹅湖西部，祁门路北。占地面积约 6.3×10^4 m^2，总建筑面积约 16×10^4 m^2，绿化率为 44%，容积率为 2.2，基地内共 17 栋高层住宅。琥珀五环城位于天鹅湖南部，西南临潜山路，东临金寨路高架，北临习友路。占地面积约 12.9×10^4 m^2，总建筑面积约 45.1×10^4 m^2，绿化率为 40%，容积率为 3.5，基地内共 18 栋高层住宅。

1.3 选点依据

根据城市居住区中绿地的位置和功能的不同，可分为居住区公共绿地、宅旁绿地、居住区道路绿地及公建设施绿地这 4 种类型。本文研究对象为城市居住区公共绿地，它集中反映了居住区的绿地质量水平。结合以上 4 个居住区的规划组织结构类型，最终确定了样点分布在中心绿地、组团绿地、宅旁绿地和道路绿地，见图 2。

1.4 研究方法

测试指标有正、负离子浓度，$PM_{2.5}$ 浓度，以及风速、空气温度、相对湿度。2016 年 7—8 月、12 月针对每个住区分别选取雨后、晴天、阴天 3 种不同天气状况，每天 07:00—18:00，每隔 1 h 测试 1

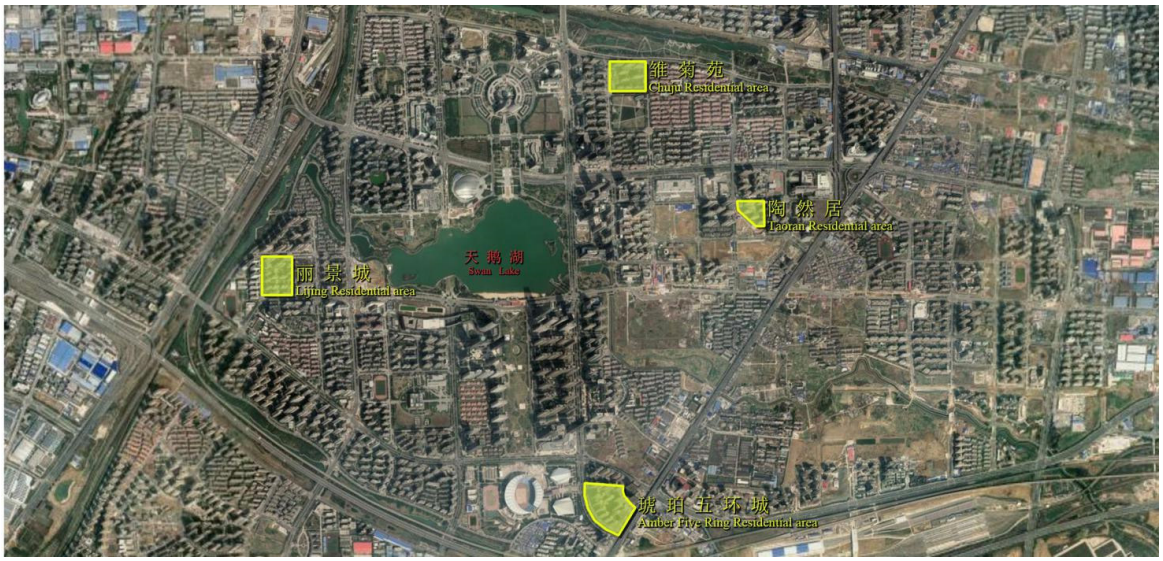


图 1 合肥市政务区天鹅湖周边样本分布图

Fig. 1 Sample distribution around Swan Lake, Hefei government district

(C)1994-2022 China Academic Journal Electronic Publishing House. All rights reserved. http://www.cnki.net

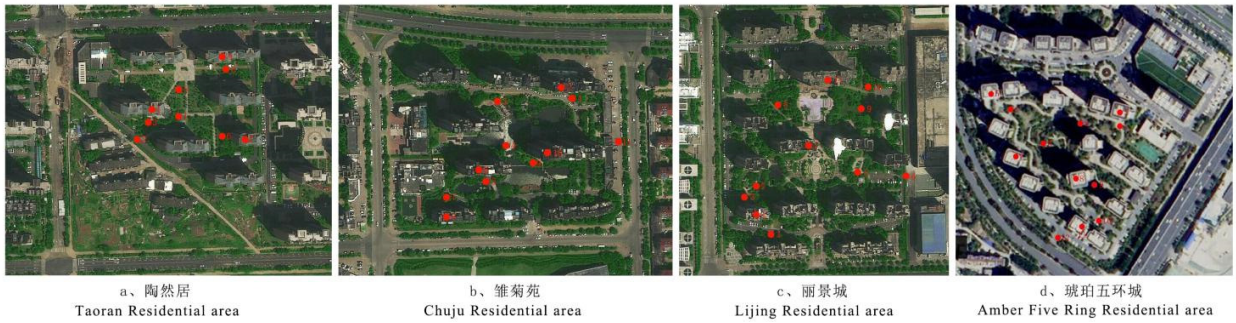


图 2 实测样地

Fig. 2 Measured sample plots

次，同时记录空气正、负离子浓度（ion·cm^{-3}）、$PM_{2.5}$浓度（μg·cm^{-3}）、温湿度和风速。空气正负离子浓度用日本原产的 COM-3200PRO 空气离子测试仪，距地面 1.5 m 处，与成人呼吸高度基本一致。风速使用三杯式风速传感器测定，用 WY-100G 数据采集记录仪连接，实时显示空气正、负离子浓度，温度，相对湿度与风速并记录，间隔 5 sec 记录一次。$PM_{2.5}$ 浓度用美国便携式 Dylos 空气质量检测仪测定，每个观测点记录 5 min，每分钟读取 1 组数据。运用 Excel 软件进行数据处理，采用 SPSS 进行统计分析。

2 样本绿地与空气负离子浓度的关系

各样本绿地由于所处的区位环境特征不同，其环境的空气负离子浓度也不尽相同。为了保证分析数据的精确，首先建立数据库对各实测样点的空气负离子、风速、温度和相对湿度数据进行统一，再进行筛选最终得到的有效数据取平均值进行分析。

2.1 陶然居

由图 2a 所示，实测样点 1 为组团绿地，位于居住区中心部位，是居民室外健身休息的场所，活动人群较多。样点 2 为道路绿地，绿地狭长，且为低矮的灌草结构，来往人员车辆较多。样点 3、6、8 为宅旁绿地。样点 5 为中心绿地，乔灌草结构，绿地配置丰富，且为疏林地，郁闭度适中。样点 4、7、9 均为室内，靠近道路，其中样点 4 东面紧邻中心绿地，四周绿地面积较大，且空间较为宽敞。

2.1.1 夏季数据

如图 3 所示，陶然居夏季室外晴天空气负离子浓度相对较高，阴天空气负离子浓度最低，呈现出晴天>雨后>阴天的趋势。同时夏季室外下午负离子浓度整体高于上午。其中夏季上午室外样点晴天空气负离子浓度最高，平均浓度达到 258 ion·cm^{-3}，雨后达到 229 ion·cm^{-3}，阴天达到 203 ion·cm^{-3}；下午室外样点雨后空气负离子浓度最高，平均浓度达到 318 ion·cm^{-3}，晴天达到 306 ion·cm^{-3}，阴天达到 246 ion·cm^{-3}。

夏季室内雨后空气负离子浓度相对较高，阴天空气负离子浓度最低，呈现出雨后>晴天>阴天的趋势。同时夏季室内下午负离子浓度整体高于上午。

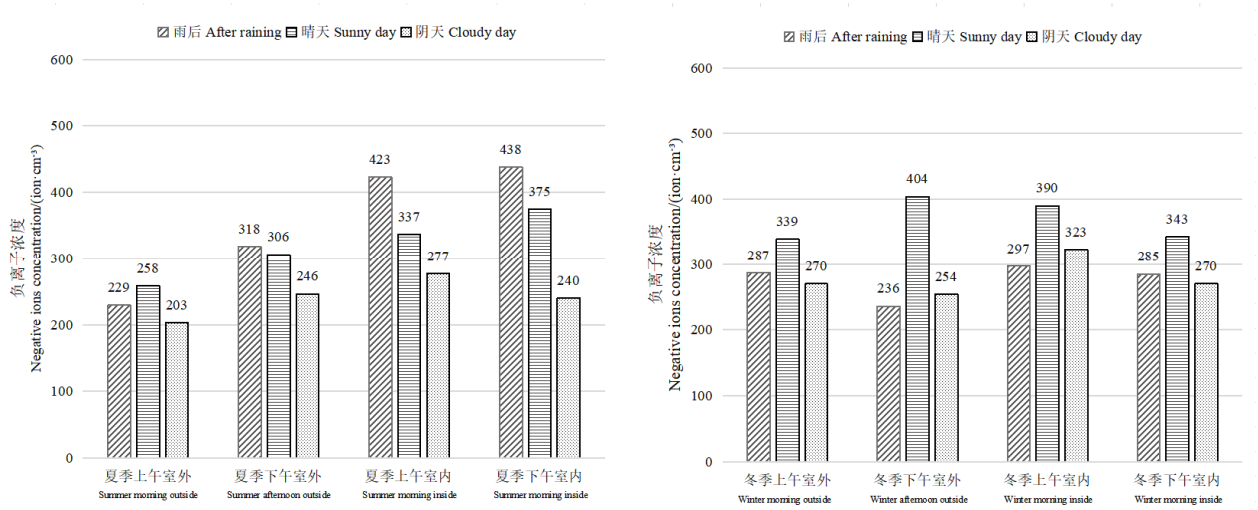


图 3 陶然居室内外环境空气负离子浓度分布图

Fig. 3 Distribution of NAI concentration in indoor and outdoor environment of Taoran Residential area

(C)1994-2022 China Academic Journal Electronic Publishing House. All rights reserved. http://www.cnki.net

夏季上午室内样点雨后空气负离子浓度最高，平均浓度达到 423 ion·cm^{-3}，晴天达到 337 ion·cm^{-3}，阴天达到 277 ion·cm^{-3}；下午室内样点雨后空气负离子浓度最高，平均浓度达到 438 ion·cm^{-3}，晴天达到 375 ion·cm^{-3}，阴天达到 240 ion·cm^{-3}。

2.1.2 冬季数据

如图 3 所示，陶然居冬季室内外晴天空气负离子浓度相对较高，阴天和雨后相对晴天较低，两者差别不大。冬季室内外上午负离子浓度整体高于下午。其中冬季上午室外样点晴天空气负离子浓度最高，平均浓度达到 339 ion·cm^{-3}，雨后达到 287 ion·cm^{-3}，阴天达到 270 ion·cm^{-3}；下午室外样点晴天空气负离子浓度最高，平均浓度达到 404 ion·cm^{-3}，阴天达到 254 ion·cm^{-3}，雨后达到 236 ion·cm^{-3}。

冬季上午室内样点 4、7、9 的晴天空气负离子浓度最高，平均浓度达到 390 ion·cm^{-3}，阴天达到 323 ion·cm^{-3}，雨后达到 297 ion·cm^{-3}；冬季下午室内样点的晴天空气负离子浓度最高，平均浓度达到 343 ion·cm^{-3}，雨后达到 285 ion·cm^{-3}，阴天达到 270 ion·cm^{-3}。

2.2 雏菊苑

如图 2b 所示，实测样点 1、5、7、9 均为宅旁绿地，样点 2、6、8、10 均为室内，样点 3 为组团绿地，样点 4 为中心绿地，样点 11 为道路绿地。

2.2.1 夏季数据

如图 4 所示，雏菊苑夏季室外雨后空气负离子浓度相对较高，阴天空气负离子浓度最低，呈现出雨后>晴天>阴天的趋势。同时夏季室内外负离子浓度上午略高于下午。其中夏季上午室外样点雨后空气负离子浓度最高，平均浓度达到 376 ion·cm^{-3}，晴天达到 351 ion·cm^{-3}，阴天达到 323 ion·cm^{-3}；下午室外样点雨后空气负离子浓度最高，平均浓度达到 410 ion·cm^{-3}，晴天达到 337 ion·cm^{-3}，阴天达到 317 ion·cm^{-3}。

夏季上午室内样点雨后空气负离子浓度最高，平均浓度达到 560 ion·cm^{-3}，晴天达到 418 ion·cm^{-3}，阴天达到 300 ion·cm^{-3}；下午室内样点雨后空气负离子浓度最高，平均浓度达到 475 ion·cm^{-3}，晴天达到 388 ion·cm^{-3}，阴天达到 305 ion·cm^{-3}。

2.2.2 冬季数据

如图 4 所示，雏菊苑冬季室内外晴天空气负离子浓度相对较高，雨后和阴天空气负离子浓度偏低，呈现出晴天>阴天>雨后的趋势。同时冬季室内外负离子浓度上午高于下午。其中冬季上午室外样点晴天空气负离子浓度最高，平均浓度达到 302 ion·cm^{-3}，阴天达到 234 ion·cm^{-3}，雨后达到 128 ion·cm^{-3}；下午室外样点雨后空气负离子浓度最高，平均浓度达到 203 ion·cm^{-3}，晴天与阴天基本一致，分别为 185 ion·cm^{-3} 和 184 ion·cm^{-3}。

冬季上午室内样点晴天空气负离子浓度最高，平均浓度达到 445 ion·cm^{-3}，阴天达到 328 ion·cm^{-3}，雨后达到 184 ion·cm^{-3}；下午室内样点晴天空气负离子浓度最高，平均浓度达到 310 ion·cm^{-3}，阴天和雨后基本一致，分别为 268 ion·cm^{-3} 和 260 ion·cm^{-3}。

2.3 丽景城

如图 2c 所示，实测样点 1、3、10 均为宅旁绿地，样点 2、8、9 均为组团绿地，4、7、11 均为室内，样点 5 为中心绿地，样点 6 为道路绿地。

2.3.1 夏季数据

如图 5 所示，丽景城夏季室内外雨后和晴天空气负离子浓度相对较高，阴天空气负离子浓度最低，呈现出雨后>晴天>阴天的趋势。同时夏季室内外负

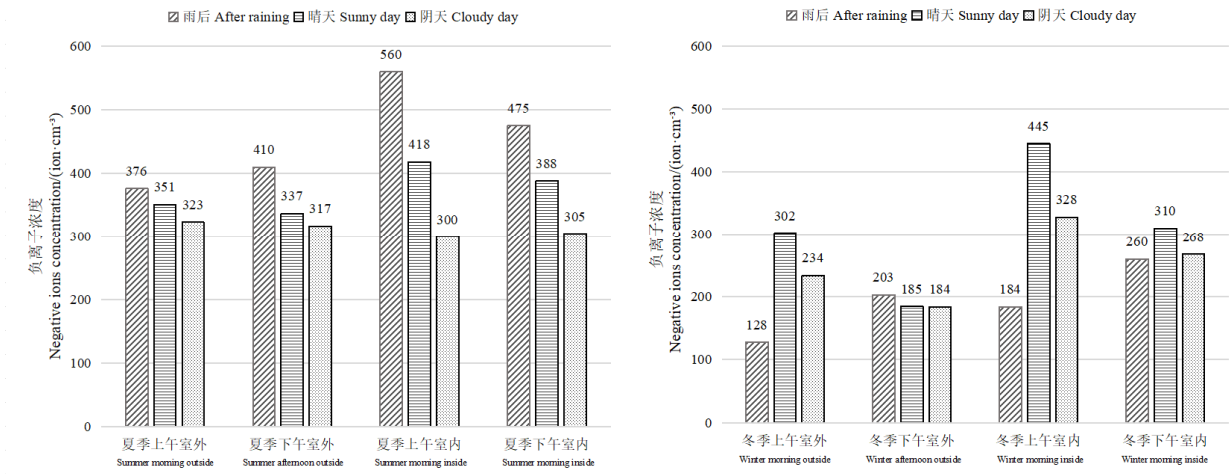


图 4 雏菊苑室内外环境空气负离子浓度分布图

Fig. 4 Distribution of NAI concentration in indoor and outdoor environment of Chuju Residential area

(C)1994-2022 China Academic Journal Electronic Publishing House. All rights reserved. http://www.cnki.net

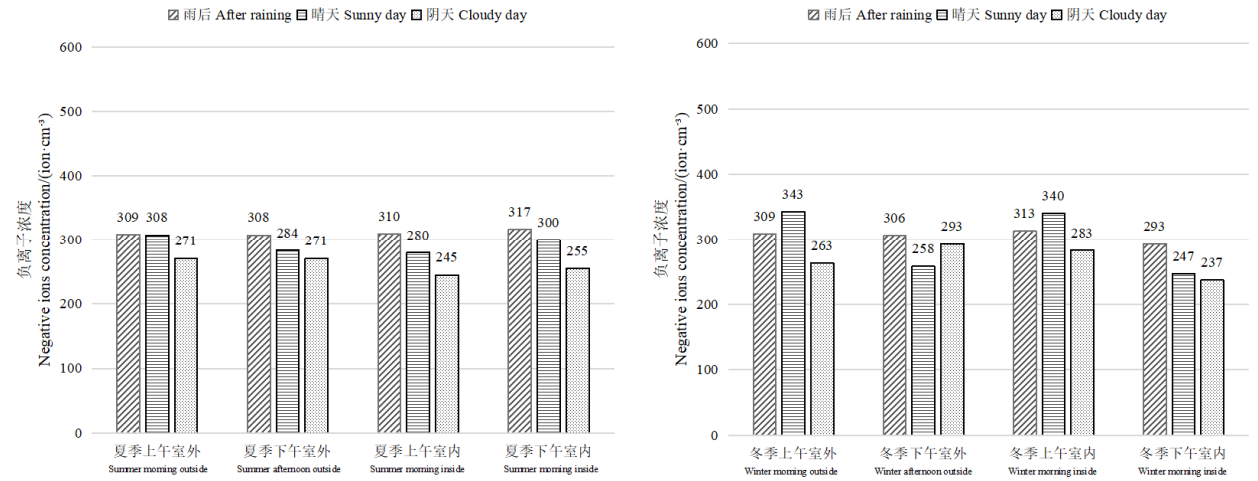


图 5　丽景城室内外环境空气负离子浓度分布图

Fig. 5　Distribution of NAI concentration in indoor and outdoor environment of Lijing Residential area

离子浓度上下午差异不显著。其中夏季上午室外样点雨后和晴天基本一致，分别为 309 ion·cm^{-3} 和 308 ion·cm^{-3}，阴天达到 271 ion·cm^{-3}；下午室外样点雨后空气负离子浓度最高，平均浓度达到 308 ion·cm^{-3}，晴天达到 284 ion·cm^{-3}，阴天达到 271 ion·cm^{-3}。

夏季上午室内样点雨后空气负离子浓度最高，平均浓度达到 310 ion·cm^{-3}，晴天达到 280 ion·cm^{-3}，阴天达到 245 ion·cm^{-3}；下午室内样点雨后空气负离子浓度最高，平均浓度达到 317 ion·cm^{-3}，晴天达到 300 ion·cm^{-3}，阴天达到 255 ion·cm^{-3}。

2.3.2　冬季数据

如图 5 所示，丽景城冬季室内外雨后空气负离子浓度相对较高，阴天空气负离子浓度最低，呈现出雨后>晴天>阴天的趋势。同时冬季室内外负离子浓度上午高于下午。其中冬季上午室外样点晴天空气负离子浓度最高，平均浓度达到 343 ion·cm^{-3}，雨后达到 309 ion·cm^{-3}，阴天达到 263 ion·cm^{-3}；下午室外样点雨后空气负离子浓度最高，平均浓度达到 306 ion·cm^{-3}，阴天达到 293 ion·cm^{-3}，晴天达到 258 ion·cm^{-3}。

冬季上午室内样点晴天空气负离子浓度最高，平均浓度达到 340 ion·cm^{-3}，雨后达到 313 ion·cm^{-3}，阴天达到 283 ion·cm^{-3}；下午室内样点雨后空气负离子浓度最高，平均浓度达到 293 ion·cm^{-3}，晴天达到 247 ion·cm^{-3}，阴天达到 237 ion·cm^{-3}。

2.4　琥珀五环城

如图 2d 所示，琥珀五环城样点 1、4、9、10 为宅间绿地，样点 2、5、7、8、11 为室内，样点 3 为组团绿地，样点 6 为中心绿地，样点 12 为道路绿地。

2.4.1　夏季数据

如图 6 所示，琥珀五环城夏季室内外雨后空气负离子浓度相对较高，阴天空气负离子浓度最低，呈现出雨后>晴天>阴天的趋势。同时夏季室内外负离子浓度下午高于上午。其中夏季上午室外样点晴天空气负离子浓度最高，平均浓度达到 296 ion·cm^{-3}，雨后达到 281 ion·cm^{-3}，阴天达到 233 ion·cm^{-3}；下午室外样点雨后空气负离子浓度最高，平均浓度达到 314 ion·cm^{-3}，晴天达到 274 ion·cm^{-3}，阴天达到 256 ion·cm^{-3}。

夏季上午室内样点雨后空气负离子浓度最高，平均浓度达到 308 ion·cm^{-3}，晴天达到 284 ion·cm^{-3}，阴天达到 262 ion·cm^{-3}；下午室内样点雨后空气负离子浓度最高，平均浓度达到 396 ion·cm^{-3}，晴天达到 304 ion·cm^{-3}，阴天达到 250 ion·cm^{-3}。

2.4.2　冬季数据

如图 6 所示，琥珀五环城冬季室内外晴天空气负离子浓度相对较高，雨后空气负离子浓度最低，呈现出晴天>雨后>阴天的趋势。同时冬季室内外负离子浓度上午高于下午。其中冬季上午室外样点晴天空气负离子浓度最高，平均浓度达到 439 ion·cm^{-3}，阴天达到 310 ion·cm^{-3}，雨后达到 145 ion·cm^{-3}；下午室外样点晴天空气负离子浓度最高，平均浓度达到 253 ion·cm^{-3}，雨后与阴天基本一致，分别为 207 ion·cm^{-3} 和 203 ion·cm^{-3}。

冬季上午室内样点晴天空气负离子浓度最高，平均浓度达到 448 ion·cm^{-3}，阴天达到 370 ion·cm^{-3}，雨后达到 166 ion·cm^{-3}；下午室内样点晴天空气负离子浓度最高，平均浓度达到 394 ion·cm^{-3}，雨后达到 252 ion·cm^{-3}，晴天达到 238 ion·cm^{-3}。

(C)1994-2022 China Academic Journal Electronic Publishing House. All rights reserved. http://www.cnki.net

2.5 结果分析

2.5.1 各样本绿地空气负离子浓度随天气变化的特征

由图 3—6 可以看出，夏季各样本绿地空气负离子浓度都呈现雨后>晴天>阴天的趋势，冬季各样本绿地空气负离子浓度都呈现出晴天>阴天>雨后的趋势。晴天空气负离子浓度高于阴天，主要由于晴天太阳辐射较强，空气对流作用也较强，植物的光合作用也相应增强，因此产生的空气正、负离子浓度也高些（吴甫成等，2006）。

夏季雨后天晴时空气负离子比干燥晴天还要高，尤其雷雨过后空气中负离子浓度明显增高。这是因为雷电的冲击带来大量的负离子，降雨的同时会增加负离子密度，降低正离子密度（王薇等，2013）。

2.5.2 各样本绿地空气负离子浓度随季节变化的特征

由图 7 可以看出，空气负离子浓度总体夏季高于冬季，与其他研究学者的结论统一。由于冬季温度低，静风频率高，大气层结构稳定，容易出现逆温现象，不利于污染物扩散。同时冬季植物处于落叶和休眠状态，光合作用微弱，导致空气负离子浓度不断降低（穆丹等，2009）。

夏季 4 块样本绿地室外环境的空气负离子浓度存在差异，空气负离子平均浓度从大到小的顺序是：雏菊苑>丽景城>琥珀五环城>陶然居，分别为 351、292、276、260 ion·cm^{-3}。雏菊苑显著高于其他 3 个样本绿地，其他 3 个样本绿地负离子浓度差别不大，主要得益于该住区内部大面积的水体与绿地，水域面积的大小与空气负离子浓度呈正相关（吴楚材等，2001）。同时东南角大量的乔灌草结构对城市主干道的灰尘也起到了阻挡的作用。

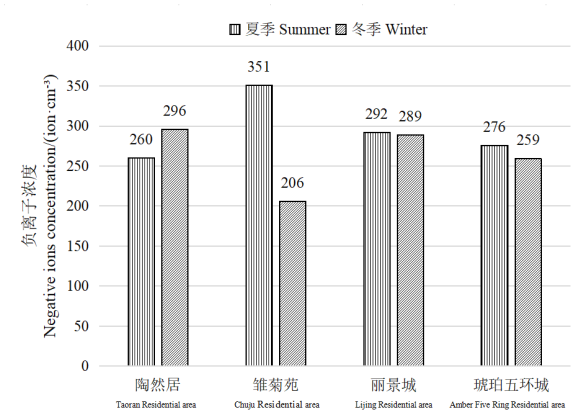


图 7 夏冬两季各样本绿地室外空气负离子浓度分布图

Fig. 7 Outdoor NAI concentration distribution of sample green space in summer and winter

冬季 4 块样本绿地室外环境的空气负离子浓度存在差异，空气负离子平均浓度从大到小的顺序是：陶然居>丽景城>琥珀五环城>雏菊苑，分别为 296、289、259、206 ion·cm^{-3}。雏菊苑显著低于其他 3 个样本绿地，其他 3 个样本绿地负离子浓度差别不大，主要由于冬季光照强度不足，不利于水体的激发，因此负离子浓度的提高有限。

2.5.3 各样本绿地空气负离子浓度随空间变化的特征

对夏冬两季住区的宅旁绿地、组团绿地、中心绿地、道路绿地 4 种不同类型的绿地空气负离子浓度进行对比分析，由图 8 可以看出，夏季陶然居宅旁绿地>中心绿地>组团绿地>道路绿地，分别为 281、277、248、193 ion·cm^{-3}；冬季组团绿地>中心绿地>宅旁绿地>道路绿地，分别为 360、332、289、231 ion·cm^{-3}。夏季雏菊苑中心绿地>组团绿地>宅旁绿地>道路绿地，分别为 405、353、346、325 ion·cm^{-3}；

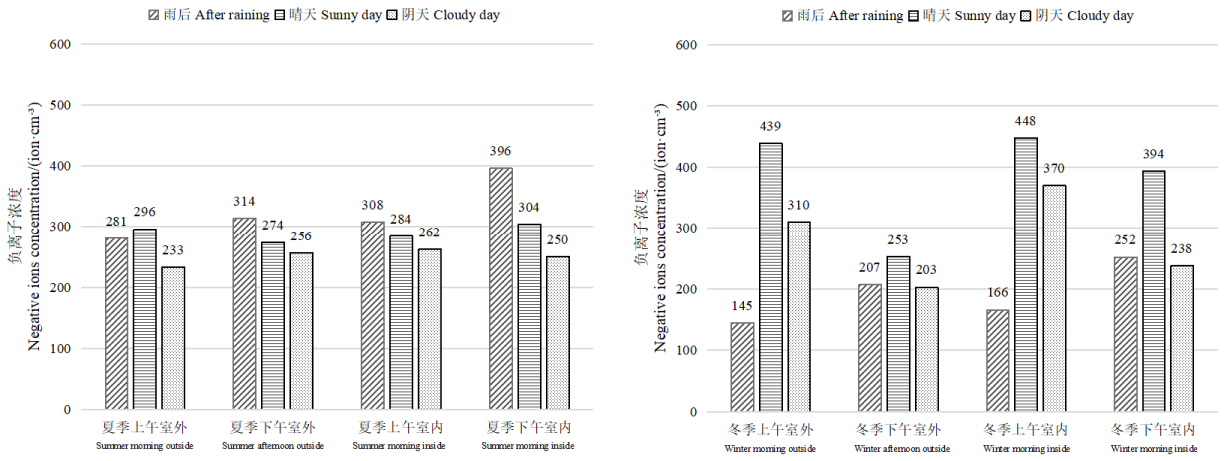


图 6 琥珀五环城室内外环境空气负离子浓度分布图

Fig. 6 Distribution of NAI concentration in indoor and outdoor environment of Amber Five Ring Residential area

(C)1994-2022 China Academic Journal Electronic Publishing House. All rights reserved. http://www.cnki.net

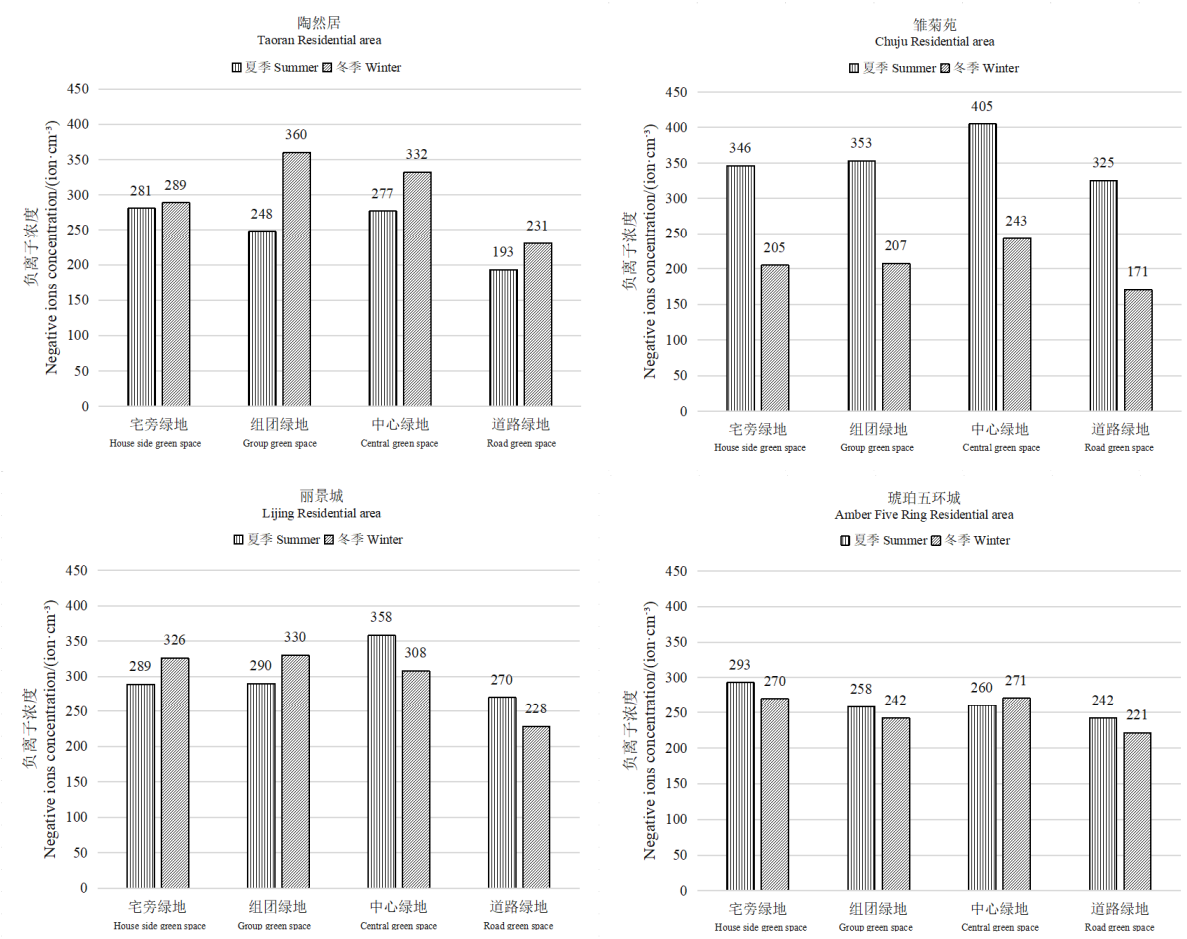


图 8　夏冬两季 4 个住区不同类型绿地室外空气负离子浓度分布图

Fig. 8　Outdoor NAI concentration distribution of different types of green space in four residential areas in summer and winter

冬季中心绿地>组团绿地>宅旁绿地>道路绿地，分别为 243、207、205、171 ion·cm^{-3}。夏季丽景城中心绿地>组团绿地>宅旁绿地>道路绿地，分别为 358、290、289、270 ion·cm^{-3}；冬季组团绿地>宅旁绿地>中心绿地>道路绿地，分别为 330、326、308、228 ion·cm^{-3}。夏季琥珀五环城宅旁绿地>中心绿地>组团绿地>宅旁绿地，分别为 293、260、258、242 ion·cm^{-3}；冬季中心绿地>宅旁绿地>组团绿地>道路绿地，分别为 271、270、242、221 ion·cm^{-3}。

总体来看，道路绿地的空气负离子浓度偏低，主要由于绿地狭长且多为低矮的灌草结构，来往人员车辆又较多，不利于负离子的产生。而中心绿地、组团绿地和宅旁绿地的配置较丰富，常采用乔灌草复层结构，郁闭度适中，有利于负离子的产生，因此空气负离子浓度较高。

3　各样本不同绿地类型室外空气负离子浓度与环境因子的相关分析

住区内部局地微气候因素如温度、湿度、风速等对空气负离子浓度有重要的影响（吴志萍等，2007）。因此基于以上 4 个住区室外绿地的实测，分别将温度、湿度、风速与空气负离子浓度进行了相关性分析，如表 1—4 所示。

表 1　陶然居室外绿地空气负离子浓度与环境因子的相关系数

Table 1　The correlation coefficient of NAI concentration with environmental factors in outdoor green space of Taoran residential area

绿地类型 Greenland Types	实测样点 Measured sample	ε 相关 (ε relevant) 温度 Temperature/℃	相对湿度 Relative humidity/%	风速 Wind speed/(m·s^{-1})
宅旁绿地 House side green space	样点 3 Sample 3	0.206**	0.154**	0.102*
	样点 6 Sample 6	0.139**	0.214**	0.270**
	样点 8 Sample 8	−0.091	0.113*	0.140**
组团绿地 Group green space	样点 1 Sample 1	0.159**	0.519**	0.125**
中心绿地 Central green space	样点 5 Sample 5	−0.039	−0.086*	0.062
道路绿地 Road green space	样点 2 Sample 2	0.248**	0.015	0.044

(C)1994-2022 China Academic Journal Electronic Publishing House. All rights reserved. http://www.cnki.net

由表 1 可以看出，陶然居室外各样点中，样点 1、2、3、6 与温度呈正相关，样点 5、8 与温度呈负相关，相关性不明确。样点 1、2、3、6 和 8 与相对湿度呈正相关，样点 5 与相对湿度呈负相关，总体呈正相关。空气负离子浓度与风速均呈正相关。

由表 2 可以看出，雏菊苑室外各样点中，除样点 11 外，其余样点空气负离子浓度均与温度呈正相关；样点 1、3、7、11 各样点空气负离子浓度与相对湿度呈负相关，样点 4、5、9 呈正相关，相关性不明确。各样点空气负离子浓度与风速均呈正相关。

由表 3 所示，丽景城室外各样点中，空气负离子浓度均与温度呈正相关；除样点 3、5 外，其余样点空气负离子浓度与相对湿度均呈负相关；样点 2、3、5、6 和 8 空气负离子浓度与风速呈正相关，样点 1、9、10 与风速呈负相关，相关性不明确。

由表 4 可以看出，琥珀五环城室外各样点中，除样点 9 外，其余样点空气负离子浓度与温度均呈正相关；除样点 4 外，其余样点空气负离子浓度与相对湿度均呈正相关；各样点空负离子浓度与风速

表 2 雏菊苑室外绿地空气负离子浓度与环境因子的相关系数

Table 2 The correlation coefficient of NAI concentration with environmental factors in outdoor green space of Chuju residential area

绿地类型 Greenland Types	实测样点 Measured sample	ε 相关 (ε relevant) 温度 Temperature/℃	相对湿度 Relative humidity/%	风速 Wind speed/(m·s^{-1})
宅旁绿地 House side green space	样点 1 Sample 1	0.275**	−0.248**	0.027
	样点 5 Sample 5	0.059	0.033	0.016**
	样点 7 Sample 7	0.140**	−0.281**	0.220**
	样点 9 Sample 9	0.262**	0.001	0.051
组团绿地 Group green space	样点 3 Sample 3	0.229**	−0.318**	0.186**
中心绿地 Central green space	样点 4 Sample 4	0.272**	0.297**	0.091*
道路绿地 Road green space	样点 11 Sample 11	−0.004	−0.121*	0.111*

表 3 丽景城室外绿地空气负离子浓度与环境因子的相关系数

Table 3 The correlation coefficient of NAI concentration with environmental factors in outdoor green space of Lijing residential area

绿地类型 Greenland Types	实测样点 Measured sample	ε 相关 (ε relevant) 温度 Temperature/℃	相对湿度 Relative humidity/%	风速 Wind speed/(m·s^{-1})
宅旁绿地 House side green space	样点 1 Sample 1	0.115*	−0.187**	−0.030
	样点 3 Sample 3	0.038	0.251**	0.093*
	样点 10 Sample 10	0.224**	−0.091**	−0.156**
组团绿地 Group green space	样点 2 Sample 2	0.157**	−0.057	0.134**
	样点 8 Sample 8	0.159**	−0.025	0.290**
	样点 9 Sample 9	0.015	−0.020	−0.247**
中心绿地 Central green space	样点 5 Sample 5	0.369**	0.569**	0.085*
道路绿地 Road green space	样点 6 Sample 6	0.187**	−0.268**	0.075*

表 4 琥珀五环城室外绿地空气负离子浓度与环境因子的相关系数

Table 4 The correlation coefficient of NAI concentration with environmental factors in outdoor green space of Amber Five Ring residential area

绿地类型 Greenland Types	实测样点 Measured sample	ε 相关(ε relevant) 温度 Temperature/℃	相对湿度 Relative humidity/%	风速 Wind speed/(m·s^{-1})
宅旁绿地 House side green space	样点 1 Sample 1	0.036	0.635**	0.098
	样点 4 Sample 4	0.272**	−0.267**	0.447**
	样点 9 Sample 9	−0.061	0.082*	0.186**
	样点 10 Sample 10	0.309**	0.331**	0.003
组团绿地 Group green space	样点 3 Sample 3	0.297**	0.135*	0.536**
中心绿地 Central green space	样点 6 Sample 6	0.173**	0.245	0.433**
道路绿地 Road green space	样点 12 Sample 12	0.066	0.181**	0.141**

(C)1994-2022 China Academic Journal Electronic Publishing House. All rights reserved. http://www.cnki.net

均呈正相关。

4 结论与建议

4.1 结论

（1）夏季各样本绿地空气负离子浓度都呈现雨后>晴天>阴天的趋势，冬季各样本绿地空气负离子浓度都呈现出晴天>阴天>雨后的趋势。晴天无尘时空气负离子浓度明显增大，雨后天晴时空气负离子比干燥晴天还要高，尤其雷雨过后空气中负离子浓度明显增高。

（2）夏季空气负离子浓度高于冬季，夏季 4 块样本绿地室外环境的空气负离子平均浓度从大到小的顺序是：雏菊苑>丽景城>琥珀五环城>陶然居；冬季 4 块样本绿地室外环境的空气负离子平均浓度从大到小的顺序是：陶然居>丽景城>琥珀五环城>雏菊苑。

（3）道路绿地的空气负离子浓度较宅旁绿地、中心绿地、组团绿地较低。来往人员车辆较多不利于负离子的产生；而植物层次结构丰富的绿地，能提高环境的空气负离子浓度。

（4）室外绿地的空气负离子浓度与温度总体呈正相关，与相对湿度关系不明确，与风速总体呈正相关。

（5）住区内部大面积的水体和绿地有利于激发负离子浓度。

（6）住区周边的乔灌草结构，对城市主干道的灰尘起到了阻挡的作用，但也一定程度上阻挡了气流的运动。

4.2 建议

（1）摒弃分散自由式的布局所造成的居住区绿地的碎片化，将住区内部各个大面积的绿地或水体相贯通，形成整体化的绿地空间布局。同时丰富绿地植物层次结构，既可以实现降尘作用，又不会造成对气流的阻挡，使居住区内部气流畅通，从而激发空气负离子浓度，改善住区空气质量。

（2）设置中心绿地空间时，建议摒弃一般大量堆积茂密高大乔木的做法，改为郁闭度稍大的密林地或疏林地。从而引导气流使居住区内部气流畅通，也不会过于遮挡阳光。乔灌草复层结构可以滞尘，避免污染被气流输送入室内，但也容易阻挡气流的运动，因此要在实现滞尘作用与利于气流的畅通之间寻找一个最佳的临界值。

参考文献：

JAYARATNE E R, J-FATOKUN F O, MORAWSKA L, 2008. Air ion concentrations under overhead high-voltage transmission lines [J]. Atmospheric Environment, 42(3): 1846-1856.

MARKO V, EHN M, PETAJA T, et al., 2008. Characteristic features of air ions at Mace Head on the west coast of Ireland [J]. Atmospheric Research, 90(2-4): 278-286.

LING X, JAYARATNE E R, MORAWSKA L, 2010. Air ion concentrations in various urban outdoor environments [J]. Atmospheric Environment, 44(18): 2186-2193.

LING X, JAYARATNE E R, MORAWSKA L, 2013. The relationship between airborne small ions and particles in urban environments [J]. Atmospheric Environment, 79(11): 1-6.

孟丽红, 张敏, 姚青, 2011. 2009 年天津城区空气负离子变化规律[J]. 气象与环境学报, 27(1): 27-29.

MENG L H, ZHANG M, YAO Q, 2011. Characteristics of air anion in 2009 in Tianjin China [J]. Journal of Meteorology and Environment, 27(1): 27-29.

王薇, 张之秋, 2014. 城市住区空气负离子浓度时空变化及空气质量评价——以合肥市为例[J]. 生态环境学报, 23(11):1783-1791.

WANG W, ZHANG Z Q, 2014. Spatio-temporal change of negative air ion concentration of urban residential area and air quality assessment: Case study of Hefei city [J]. Ecology and Environmental Sciences, 23(11): 1783-1791.

邵海荣, 杜建军, 单宏臣, 等, 2005. 用空气负离子浓度对北京地区空气清洁度进行初步评价[J]. 北京林业大学学报: 自然科学版, 27(4): 56-59.

SHAO H R, DU J J, SHAN H C, et al., 2005. Assessment of air cleanness degree in Beijing using negative air ion concentration as an index [J]. Journal of Beijing Forestry University, 27(4): 56-59.

王薇, 余庄, 2013. 中国城市环境中空气负离子研究进展[J]. 生态环境学报, 22(4): 705-711.

WANG W, YU Z, 2013. Research progress on negative air ions in urban environment in China [J]. Ecology and Environmental Sciences, 22(4): 705-711.

吴志萍, 王成, 许积年, 等, 2007. 六种城市绿地内夏季空气负离子与颗粒物[J]. 清华大学学报自然科学版, 47(12): 2153-2157.

WU Z P, WANG C, XU J N, et al., 2007. Air-borne anions and particulate matter in six urban green spaces during the summer [J]. Journal of Tsinghua University Natural Science Edition, 47(12): 2153-2157.

穆丹, 梁英辉, 2009. 佳木斯绿地空气负离子浓度及其与气象因子的关系[J].应用生态学报, 20(8): 2038-2041.

MU D, LIANG Y H, 2009. Air negative ion concentration and its relationships with meteorological factors in green belts of Jiamusi [J]. Chinese Journal of Applied Ecology, 20(8): 2038-2041.

吴甫成, 姚成胜, 郭建平, 等, 2006. 岳麓山空气负离子及空气质量变化研究[J]. 环境科学学报, 26(10): 1737-1744.

WU F C, YAO C S, GUO J P, et al., 2006. Distribution of negative air ion s and its relation to air quality of the Yuelu Mountain [J]. Journal of Environmental Science, 26(10): 1737-1744.

吴楚材, 郑群明, 钟林生, 2001. 森林游憩区空气负离子水平的研究[J]. 林业科学, 37(5): 75-81.

WU C C, ZHENG Q M, ZHONG L S, 2001. A study of the aero-anion concentration in forest recreation area [J]. Forestry Science, 37(5): 75-81.

(C)1994-2022 China Academic Journal Electronic Publishing House. All rights reserved. http://www.cnki.net

陈明, 2017. 高密度城市住区绿地空气清洁度研究[D]. 合肥: 安徽建筑大学.

CHEN M, 2017. Study on air cleanliness of high-density urban residential green space [D]. Hefei: Anhui Jianzhu University.

Research on Distribution Characteristics of Negative Air Ions Concentration in High-density Urban Residential Green Space and Its Relationship with Microclimate

WANG Wei[1, 2], CHEN Ming[3], XIA Sihan[1]

1. School of Architecture and Urban Planning, Anhui Jianzhu University, Hefei 230022, China;
2. Built Environment and Health Research Center, Anhui Jianzhu University, Hefei 230022, China;
3. Anhui ANDE Architectural Design Co., Ltd, Hefei 230022, China

Abstract: In this paper, different types of green spaces in four high-density urban residential areas around Swan Lake in Hefei government district were selected as the research objects. From July to August and December 2016, the distribution characteristics of indoor and outdoor negative air ions concentration were analyzed under three weather conditions, which included after rain, sunny and cloudy, including positive air ions (PAI) and negative air ions (NAI) concentration, temperature, relative humidity and wind speed. The distribution characteristics of indoor and outdoor NAI concentration in summer and winter, the results show that: (1) In summer, the NAI concentration of the samples showed a trend of “after rain>sunny day>after rain”, while in winter, the NAI concentration of the samples showed a trend of “sunny day>cloudy day>after rain”. (2) The NAI concentration in summer is higher than that in winter. In summer, the average of NAI concentration in the outdoor environment of the four sample greenbelts showed the trend of Chuju residential area>Lijing residential area>Amber five ring residential area>Taoran residential area, they are 351, 292, 276, 260 ion·cm^{-3}; in winter, it showed the trend of Taoran residential area>Lijing residential area>Amber five ring residential area>Chuju residential area, they are 296, 289, 259, 206 ion·cm^{-3}. And (3) among the four types of green space, the NAI concentration of road green space is relatively low, the lowest value is 193 ion·cm^{-3} in summer and 171 ion·cm^{-3} in winter; while that of residential green space, group green space and central green space is relatively high, the highest value is 405 ion·cm^{-3} in summer and 360 ion·cm^{-3} in winter. The paper further analyzes the correlation between air anion concentration and environmental factors, according to these analyses, the following conclusions can be drawn: (1) The NAI concentration in the air increases significantly in the clear sky, and even higher in the clear sky after rain than in the dry sunny day, especially in the air after thunderstorm. (2) More people and vehicles are not conducive to the production of NAI; the plant structure is rich, which can improve the NAI concentration of the environment. (3) The NAI concentration in the air of outdoor green space is positively correlated with the temperature as a whole, is not clearly correlated with the relative humidity, and is positively correlated with the wind speed as a whole. (4) A large area of water and green space in the residential area is conducive to the excitation of anion concentration. And (5) the structure of trees, shrubs and grasses around the residential area blocked the dust on the main road of the city, but also blocked the movement of air flow to a certain extent. On this basis, the author further put forward the prospect, and suggested that the green space or water body in the residential area should be integrated to form an integrated green space layout. At the same time, dense forest land or sparse forest land with a slightly larger canopy density should be used to find an optimal critical value between dust retention and air flow.

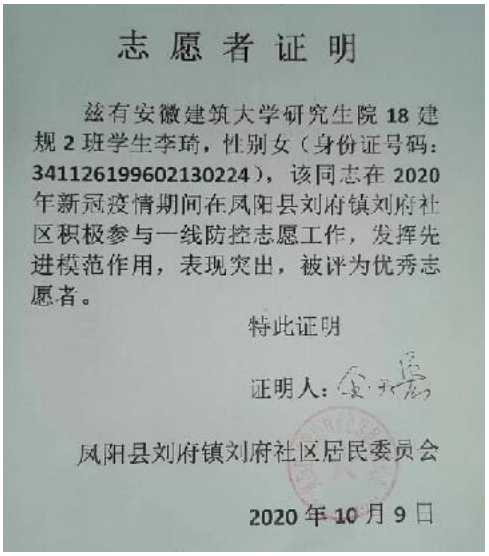
Key words: high-density urban residential area; green space; negative air ion (NAI); distribution characteristics; environmental factor; correlation

(C)1994-2022 China Academic Journal Electronic Publishing House. All rights reserved. http://www.cnki.net

2. 奖励

（优秀毕业生、国奖、优秀毕业论文等）

1.建规学子参加一线防控志愿者工作



志愿者证明

兹有安徽建筑大学研究生院18建规2班学生李琦，性别女（身份证号码：341126199602130224），该同志在2020年新冠疫情期间在凤阳县刘府镇刘府社区积极参与一线防控志愿工作，发挥先进模范作用，表现突出，被评为优秀志愿者。

特此证明

证明人：

凤阳县刘府镇刘府社区居民委员会

2020年10月9日

2. 根据安徽省教育厅、安徽省人力资源和社会保障厅、共青团安徽省委关于《安徽省普通高等学校优秀毕业生评选认定办法》（皖教学〔2021〕1号）的通知和《安徽建筑大学优秀毕业生评选认定办法》、《安徽建筑大学研究生评奖评优工作办法（校字(2014)147号）》以及学校“关于评选上报2022年省、校级品学兼优毕业生名单的通知”（校就函〔2022〕4号），我院经过各毕业班民主评议公示，经学院党政联系会议讨论通过，已初步评选出安徽省普通高等学校品学兼优毕业生研究生4人，安徽建筑大学品学兼优毕业生研究生8人。

2022年安徽省普高等学校品学兼优毕业生研究生4人（排名不分先后）

张强　　孙进　　刘子祺(女)　　刘学群

2022年安徽省普高等学校品学兼优毕业生本科生6人（排名不分先后）

17建筑学：　单姝敏(女)　　朱屠昊

17城乡规划：丁晓雅(女)　胡中昱(女)

18风景园林：朱志扬　　奚娟杰(女)

2022年安徽建筑大学品学兼优研究生8人（排名不分先后）

龚姝(女)　姜龙　章宏　解卫东　胡鑫康(女)　张文辉　刘益翔　　张旭

2022年安徽建筑大学品学兼优毕业生17人（排名不分先后）

17建筑学：汪淼(女)　黄祺越(女)　许明亮　张桂煜(女)

甄倩倩(女)　张诚

17城乡规划：潘若怡(女)　金梦媛(女)　储成伟　　潘 露(女)

冉桃滔　　胡晓敏(女)

18风景园林：钱王池(女)　　陈思亲(女)　郑子琪(女)　石荣闽

段元梅(女)

3.2019 级国家奖学金荣誉



4.安徽建筑大学 2022 年安徽省新时代育人工程项目申报

安徽建筑大学2022年安徽省新时代育人质量工程项目（研究生教育）推荐申报名单

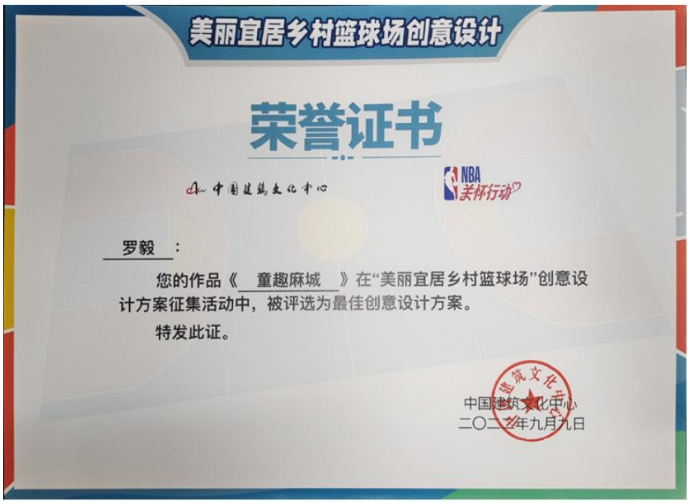
序号	选题类别	选题类型	选题名称	申报人	所在学院	备注
1	研究生思想政治教育	省级研究生课程思政示范课程	《高等热力学课》	余陶	土木学院	
2	研究生思想政治教育	省级研究生课程思政示范课程	《工程伦理》	雷经发	机电学院	
3	研究生思想政治教育	省级研究生课程思政示范课程	《土地利用与规划》	王秉义	公管学院	
4	研究生思想政治教育	省级研究生课程思政示范课程	《云计算与大数据》	张家精	电信学院	
5	研究生思想政治教育	省级研究生课程思政示范课程	《行政法》	高丽虹	公管学院	
6	研究生思想政治教育	省级研究生课程思政示范课程	《先进制造技术》	陈雪辉	机电学院	
7	研究生思想政治教育	省级研究生课程思政示范课程	《工程伦理》	罗涛	环能学院	
8	研究生思想政治教育	省级研究生课程思政示范课程	《贝叶斯统计》	谢新平	数理学院	
9	研究生思想政治教育	省级研究生课程思政示范课程	《电子政务》	钱丽	公管学院	
10	研究生思想政治教育	省级研究生课程思政示范课程	《环境生物电化学》	杨厚云	环能学院	
11	研究生思想政治教育	省级研究生课程思政教学资源库	节能工程与楼宇智能化学科研究生课程思政教学资源库	杨亚龙	电信学院	
12	研究生思想政治教育	省级研究生样板党支部	省级研究生样板党支部	汤晶晶	建规学院	
13	研究生思想政治教育	省级研究生样板党支部	省级研究生样板党支部	陈悠	环能学院	
14	研究生思想政治教育	省级研究生党员标兵	省级研究生党员标兵	徐德衡	土木学院	
15	研究生思想政治教育	省级研究生党员标兵	省级研究生党员标兵	汤晶晶	建规学院	
16	研究生思想政治教育	省级研究生党员标兵	省级研究生党员标兵	刘菲菲	公管学院	
17	研究生思想政治教育	省级研究生优秀辅导员	省级研究生优秀辅导员	贾宇枝子	研工部	
18	研究生思想政治教育	省级研究生优秀辅导员	省级研究生优秀辅导员	王艳	艺术学院	
19	研究生教育教学资源	省级优秀研究生导师团队	先进建筑材料导师团队	孙道胜	材化学院	
20	研究生教育教学资源	省级优秀研究生导师团队	“双一流”视野下的研究生能力提升导师团队	黄显怀	环能学院	

3. 新闻报道

【建功新时代】建规学子作品获“美丽宜居乡村篮球场”最佳创意设计方案

作者： 唐劲松　　发布日期： 2022-09-20　　浏览次数： 79

本网讯 近日，由住房和城乡建设部帮扶办公室指导、住房和城乡建设部直属事业单位中国建筑文化中心承办、中国青少年基金会NBA关怀行动公益基金支持的“美丽宜居乡村篮球场”创意设计方案征集结果公布，我校建规学院王昊禾老师指导的21风景园林罗毅作品《童趣麻城》、21城乡规划黄情作品《民俗大通》获最佳创意设计方案。



建规学子参加第三届亚洲建筑学生论坛并做口头汇报

作者： 唐劲松　　发布日期： 2022-08-24　　浏览次数： 173

本网讯 8月20日－21日，2022年第三届亚洲建筑学生论坛（3rd Asian Architecture Students Colloquium）在线上成功举行。本次论坛由天津城建大学主办、亚洲十余所高校协办，近150余名师生代表参加。我院王薇、周庆华、许杰青、王志鹏老师及11名研究生、本科生参加了本次论坛。

8月20日上午，主办方天津城建大学对本次论坛进行了简单的视频介绍，随后多位参会学校负责人发表了开幕致辞。邀请了来自日本北九州市立大学福田展淳教授、华侨大学姚敏峰教授、郑州大学硕士生导师陈伟莹、毕昕、天津城建大学张天宇副教授共同参与主旨演讲，其他几所院校的老师参与分论坛的点评。报告围绕着会议主题“双碳背景下的城市保护、更新与创造”展开，内容涉及如低碳建筑、虚拟现实、绿色建筑、建筑可持续性发展以及前沿国外绿色建筑设计实例等建筑学科热点问题。



【建功新时代】建规学子荣获第二届长三角大学生乡村振兴创意大赛专项赛银奖

作者： 唐劲松　　发布日期： 2022-08-19　　浏览次数： 144

本网讯　由中国城市科学研究会、浙江省教育厅、浙江省农业农村厅、浙江省文化和旅游厅主办的“第二届长三角大学生乡村振兴创意大赛平望·文化赋能空间专项赛”，2021年决赛在江苏省吴江区平望镇举办，我校风景园林研究生张敏、潘杰、王玉蓉、张晓尧、黄铖昕、常佳在冀凤全、左光之老师的指导下共同完成的项目《开“园”、截“流”——基于雨水花园的乡村公共空间活化设计》荣获银奖。



获奖证书

学生　张敏 潘杰 王玉蓉 张晓尧 黄铖昕 常佳

指导老师　冀凤全 左光之

所属项目 开“园”、“截”流——基于雨水花园的乡村公共空间活化设计

在“平望文化赋能空间专项赛”第二届长三角大学生乡村振兴创意大赛中荣获

银奖

特发此证，以资鼓励。

全国大学生乡村振兴创意大赛竞赛委员会

2022 年 4 月

我校建规学子喜获“中建海峡杯” 第九届海峡两岸大学生实体建构大赛银奖

作者： 唐劲松　　发布日期： 2022-08-05　　浏览次数： 195

为推动海峡两岸大学生的交流，展示大学生独特的建构创意，进一步推动两岸青年学生加强沟通、增进了解、深化友谊、交流互鉴。2022年8月1日至8月4日，由福建省学生联合会、中华青年交流协会、福建省土木建筑学会、中建海峡建设发展有限公司等单位联合举办的“中建海峡杯”第九届海峡两岸大学生实体建构大赛（大陆赛区）总决赛在福建省福州市永泰县梧桐镇坵演村成功举办。

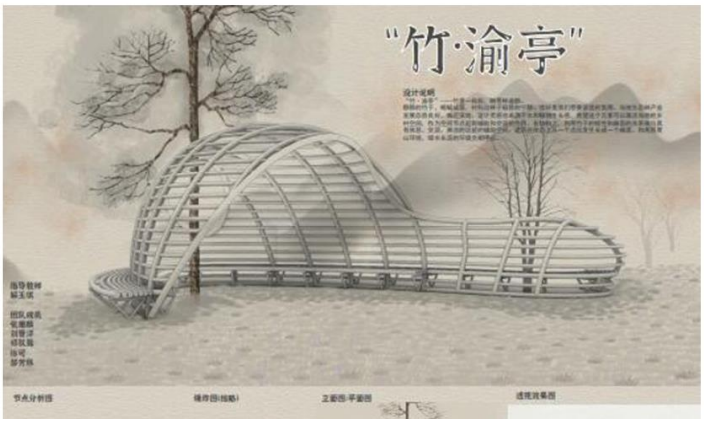


建规学院成功晋级2022年“中建海峡杯”建构大赛决赛

作者： 唐劲松　　发布日期： 2022-07-06　　浏览次数： 279

本网讯 为推动海峡两岸大学生的交流，展示大学生独特的建构创意，进一步推动两岸青年学生加强沟通、增进了解、深化友谊、交流互鉴。2022年，福建省学生联合会、中华青年交流协会、福建省土木建筑学会、中建海峡建设发展有限公司等单位将联合举办“中建海峡杯”第九届海峡两岸大学生实体建构大赛。

海峡两岸大学生实体建构大赛大陆赛区选拔赛于7月4号下午进行初赛评审，建筑与规划学院在解玉琪老师组织下，经过初赛选拔，由邹芳琳、徐可、张蕙麟、郑驭莓、刘晋洋5位同学组成的团队代表安徽建筑大学参赛，经过评委会评审，我院参赛队伍成功晋级决赛。



【学科专业竞赛】建规学子在2022年eVolo摩天大楼竞赛中获得荣誉奖

作者： 唐劲松　　发布日期： 2022-05-09　　浏览次数： 509

本网讯 5月2日，由eVolo杂志举办的国际竞赛“2022年摩天大楼竞赛”公布评选结果，获奖名额包括一、二、三等奖各1名以及荣誉奖20名。我校建规学子陈开宇、林勇、李子奕、陶志鹏团队合作完成的《The city chloroplast: a skyscrapers that absorbs CO2 and converts it into starch》，在全球427项竞赛作品中脱颖而出，获得了该国际竞赛颁发的荣誉奖奖项。



【学科专业竞赛】建规学子在2021年安徽省大学生生物标本制作大赛喜获一等奖

作者： 唐劲松　　发布日期： 2021-12-20　　浏览次数： 995

本网讯 12月20日，由安徽省教育厅主办、皖西学院承办的“2021年安徽省大学生生物标本制作大赛”在皖西学院落下帷幕，建规学子荣获一等奖两项，三等奖一项，三位老师荣获“优秀指导教师”称号。

本次大赛共有40所高校近300件作品参赛，分为植物标本组、动物标本组、创新创意组3个参赛类别。根据疫情防控的要求，本次比赛分为作品视频展示和线上答辩方式举行。参赛学生就作品立意，原料采集，制作工艺，制作过程创新点等方面进行线上介绍和答辩。参赛作品创意新颖，紧跟时代脚步，制作精美，展示了优良的标本制作水平。

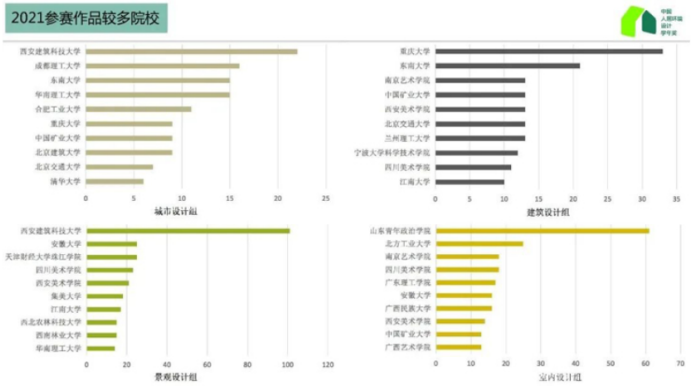
建筑与规划学院代表团队共六件作品参加比赛，建大学子在比赛各个环节表现沉着冷静，展示了良好的精神面貌与扎实的专业基础，经过大赛专家评委们的集体初审、线上评审以及评审委员会表决，我校2020级风景园林研究生陈璐、杨思嘉、陈媛媛同学的作品《多样生物，生生不息》荣获创新创意组一等奖；2021级风景园林研究生吴少微、瞿银琦、陈雅雯、张清怡同学的作品《十步茂草》荣获植物标本组一等奖，2019级风景园林本科生丁蕾、陈雨欣、陈亦菲、陈红羽同学的作品《紫蓬山国家森林公园蕨类植物》荣获植物标本组三等奖；建规学院姚晓洁、姚侠妹、王昊禾老师荣获“优秀指导教师”称号。



【学科专业竞赛】建规学院学子荣获第七届中国人居环境设计学年奖银奖

作者： 唐劲松 发布日期： 2021-11-29 浏览次数： 650

本网讯 11月28日，由清华大学和教育部高等学校设计学类专业教学指导委员会联合主办，由建筑类专业教学指导委员会所属建筑学专业教学指导分委员会、城乡规划专业教学指导分委员会、风景园林专业教学指导分委员会协办的“2021年第七届中国人居环境设计学年奖”年会暨颁奖典礼在线上落下帷幕，建规学院学子受邀参加年会暨颁奖典礼。



【学科专业竞赛】建规学子参加中日韩风景园林大学生设计竞赛荣获金奖

作者： 唐劲松　　发布日期： 2021-10-27　　浏览次数： 868

本网讯　10月23日，由中国风景园林学会（CHSLA）、日本造园学会（JILA）和韩国造景学会（KILA）共同主办，《中国园林》杂志社和《风景园林》杂志社协办的第十七届中日韩风景园林学术研讨会北京隆重举办。本届研讨会受当前疫情影响，采用线上+线下结合的形式为大家呈现，百余人相聚北京研讨会现场聆听了中日韩三国专家学者的学术报告。我院风景园林学子受邀参加竞赛颁奖典礼和学术研讨会。



【学科专业竞赛】建规学院在2021国际大学生建筑设计与数字建模竞赛中获奖

作者： 唐劲松　　发布日期： 2021-10-11　　浏览次数： 996

本网讯　近日，由联合国科教文组织支持、“一带一路”建筑类大学国际联盟发起、北京建筑大学主办的“2021国际大学生建筑设计与数字建模竞赛”公布获奖名单。建筑与规划学院提交的参赛作品《89户渔家》、《连舟浮桥·点线共生——运河上衰败码头的活力再生与生态恢复》获得建筑设计方向优秀奖；《柳江蕴物华，辉风扬日彩》、《秒土转生——老街民居遗产的数字化激活策略》分别获得建筑与场景数字建模方向二等奖、三等奖。

方向	作品名称	指导老师	参赛学生	奖项
建筑设计	89户渔家	聂玮	朱屠昊、彭程程、倪秦思、易凡、罗大昱	优秀奖
	连舟浮桥·点线共生——运河上衰败码头的活力再生与生态恢复	桂汪洋、周庆华	李成成、吴扬扬、吴静文、张辉辉、卢泉	优秀奖
	柳江蕴物华，辉风扬日彩	孙升、王艳	陈泽、胡梦婷、郝美娇、于航 、周艳冰	二等奖

【学科专业竞赛】建规学子在WUPENiCity2021城市设计及2021城市可持续调研报告竞赛中取得佳绩

作者： 唐劲松　　发布日期： 2021-09-23　　浏览次数： 1347

本网讯　9月21日“WUPENiCity2021城市设计及2021城市可持续调研报告竞赛”金奖名单公布，我校建筑与规划学院积极组织学生参与竞赛，建筑与规划学院提交的多份作品中经过与诸多高校的激烈角逐，最终我院四组参赛团队从758份作品中脱颖而出，获得2021城市可持续调研报告竞赛金奖2项，提名奖2项的佳绩。



【学科专业竞赛】建规学子在2021年全国高等院校浙东古运河（上虞段）设计竞赛中取得佳绩

作者： 唐劲松　　发布日期： 2021-09-06　　浏览次数： 816

本网讯　7月18日，“2021年全国高等院校浙东古运河（上虞段）设计竞赛”获奖名单最终揭晓。我校建规学院17级规划系本科生提交的三组作品经过与国内外诸多高校的激烈角逐，获得了优秀奖1项、佳作奖2项的佳绩。



【学科专业竞赛】建规学子在第四届安徽省高校建筑信息模型（BIM)应用大赛中取得佳绩

作者： 唐劲松　　发布日期： 2021-06-27　　浏览次数： 1007

本网讯　6月20日，第四届安徽省高校建筑信息模型(BIM)应用大赛在芜湖职业技术学院落下帷幕，我院3支参赛队伍从全省37所高校，202支参赛队伍中脱颖而出，获得了一等奖1项、二等奖2项的佳绩。在安徽省各大院校中，安徽建筑大学在本次比赛获奖的名次以及数量上名列前茅。

此次竞赛由安徽教育厅主办，芜湖职业技术学院、合肥工业大学承办；复赛分为“建筑+绿建”、“建筑+结构”、“结构+机电”、“结构+工管”4个模块，我校3支参赛队伍分别参加了“建筑+绿建”、“建筑+结构”2个模块的比赛。由于疫情防控，复赛采用“学生线上汇报，专家线下评审”相结合的方式进行评审；参赛队伍通过线上进行作品整体介绍及成果展示汇报。

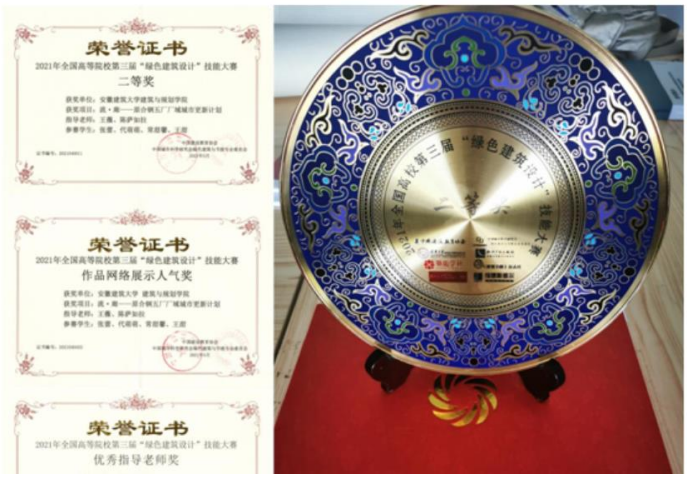
经过初赛和复赛的紧张角逐和精彩呈现，最终许杰青和韩玲老师指导，孙天泽、徐琪、张絮同学组成的安徽建筑大学sxz队在“建筑+绿建”模块获得了第1名一等奖的佳绩；王薇和陈萨如拉老师指导，常甜馨、戴雅君、倪秦思组成的安徽建筑大学安筑队在“建筑+绿建”模块获得了二等奖的佳绩；王薇和刘运林老师指导，郝北京、仇子文、彭程程同学组成的安徽建筑大学易海匠心队在“建筑+结构”模块获得了二等奖的佳绩。



【学科竞赛】建规学院在全国高等院校第三届“绿色建筑设计”技能大赛中获优异成绩

作者： 唐劲松　　发布日期： 2021-06-04　　浏览次数： 716

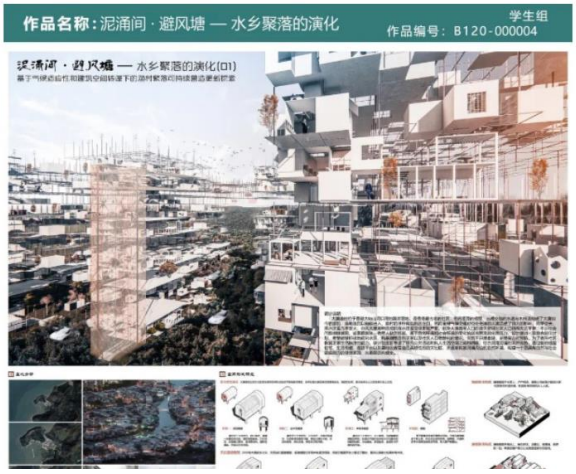
本网讯　近日，全国高等院校第三届“绿色建筑设计”技能大赛公布获奖名单，由王薇和陈萨如拉两位教师指导，我院建筑学专业研究生张蕾、代萌萌、常甜馨、王甜四位同学组队,提交的参赛作品《流·廊——原合钢五厂厂域城市更新计划》荣获二等奖以及作品网络展示人气奖，两位指导教师荣获优秀指导老师奖。



【学科专业竞赛】建规学院学子荣获紫金奖·建筑及环境设计大赛金奖

作者： 唐劲松 发布日期： 2020-12-24 浏览次数： 488

本网讯 12月19日由中共江苏省委宣传部、江苏省住房和城乡建设厅、中国建筑学会、中国勘察设计协会、中国风景园林学会主办，江苏省广播电视总台教育频道承办的第七届“紫金奖·建筑及环境设计大赛”在江苏广播电视总台教育频道演播厅圆满落下帷幕。建规学院解玉琪老师指导学生陈彦霖同学荣获紫金奖建筑及环境设计大赛金奖。



【学科专业竞赛】建规学院规划系获2020年度全国高等院校大学生乡村规划方案竞赛（安徽基地）初赛获得“两优”

作者： 唐劲松 发布日期： 2020-11-22 浏览次数： 573

本网讯 近日，2020年度全国高等院校大学生乡村规划方案竞赛（安徽基地）初赛获奖名单公布，建筑与规划学院规划系获得“两优”，“四佳”好成绩；（各基地初期评优只评选优胜奖和佳作奖，本次安徽基地第一单元共计18个高校，35个团队，共计194名学生参加竞赛，选出9份优胜奖作品，参与全国竞赛一、二、三等奖的评优）。其中肖铁桥、何颖、宋祎老师指导的17级城乡规划专业王雨滕等6位同学，提交的《“绘稻香，织渔梦”》作品，和王爱、杨新刚、侯伟老师指导的17级城乡规划专业胡晓敏等6位同学，提交的《寻“宝”环游记》作品都获得了优胜奖，后期将参与全国的竞赛评优。

2020年度全国高等院校大学生乡村规划方案竞赛安徽基地
初赛阶段评优
专家评分表

序号	作品编号	作品名称	参赛高校学院（完整名称）	指导教师及职称（按顺序）	团队成员姓名（按顺序）	评优结果
1	W11	长续技魂 寺承匠新	苏州科技大学建筑与城市规划学院	潘 斌 讲师 范凌云 教授	沈浪雁 朱承晨 黄晓雯 郑煜昂 张皓然 徐子健	优胜奖
2	W40	涨缩有序	重庆大学建筑城规学院	谭文勇 副教授 赵 强 讲 师 胡 纹 教 授	李高远 白晓丹 蔡诗韵 冯诗雁 黄 荧	优胜奖
3	W13	“绘稻乡·织渔梦”	安徽建筑大学建筑与规划学院城乡规划系	肖铁桥 副教授 何颖 讲师 宋祎 讲师	王雨滕 李 静 章慧玲 朱逸飞 潘 露	优胜奖

【学科竞赛】建规学院在2019年全国高校建筑设计教案与作业观摩和评选中获得佳绩

作者： 唐劲松　　发布日期： 2019-10-31　　浏览次数： 501

本网讯　近日，2019全国高等学校建筑教育学术研讨会暨院长系主任大会、教育部高等学校建筑学专业教学指导分委会年会在西南交通大学召开，建筑与规划学院多名教师参加了本次会议。



本次大会以“建筑教育‘通’与‘专’”为主题，由开幕式、主题报告、大会报告、颁奖仪式、海峡两岸建筑教育论坛、五大分论坛、闭幕式等部分组成。大会共包括7场主题报告、9个大会报告、5场分议题论坛及53个学术报告，涵盖建筑教育通专结合的理念、方法与模式；新工科理念下的建筑教育；建筑类专业通识平台建设；地域性人才培养模式探索；课程建设（金课、慕课）与资源共享等多个领域，多层次、多方位地展现了各高校高等教育体系和人才培养模式的方法与经验所做的探索与思考。

【专业学科竞赛】建大学子荣获第五届中国人居环境学年奖银奖

作者： 唐劲松　　发布日期： 2019-11-11　　浏览次数： 534

本网讯 2019年11月9日，2019年第五届中国人居环境设计学年奖终审暨颁奖典礼（以下简称“学年奖”）在无锡江南大学北区大学生活动中心举行。本次专题会议围绕“设计·可持续”着重探讨了在建筑、城市、景观、室内四个维度下的主题演讲和院校分享，聚焦了设计教学、课程规划、人才培养、毕业设计、城市规划、室内设计、中国传统园林等多维发展动态。



【学科竞赛】建规学院学子在2018年第四届中国人居环境设计学年奖荣获佳绩

作者： 唐劲松　　发布日期： 2018-12-25　　浏览次数： 331

本网讯 2018年12月22日至23日，在西安建筑科技大学艺术学院举办了2018年第四届“中国人居环境设计学年奖暨教育年会”，本届年会邀请了著名设计及教育专家参会，共同探讨环境设计教育的现状与未来，内容涵盖城市、建筑、景观、室内等领域的研究与实践成果，同时还有学生设计优秀成果的展示。

普通高等本科院校建筑设计组产生金奖3名、银奖6名、铜奖9名、入围12名，我院建筑系风元利、夏季芳老师指导的赵夏炎同学及其作品“高校学者工作站建筑设计”获得入围奖；景观设计组产生金奖4名、银奖6名、铜奖11名、入围20名，我院景观系张少杰老师指导的陈雨露同学及其作品“候鸟机场”上海市长兴岛湿地景观规划设计获得入围奖；景观系荣获最佳组织奖。

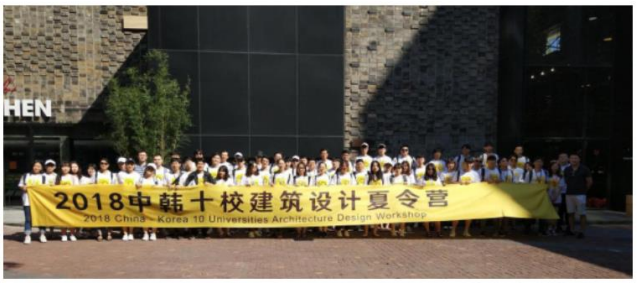
本届大赛共收到来自400余所院校的参赛作品1715件，经组委会专家评委两轮筛选，最终共有168件作品入围，入选方式以评审格式与展板结合，统一匿名网络打分。终审由庄惟敏教授主持，集合国内四个一级学科17位专家教授组成的评审委员会，严格按照评审标准，秉承公平、公正的原则，最终选出金奖13名，银奖27名，铜奖49名，入围奖79名。



【学科专业竞赛】建规学院师生参加“2018中韩建筑学生国际交流工作坊”

作者： 唐劲松　　发布日期： 2018-09-04　　浏览次数： 344

本网讯 8月23日至29日，2018中韩建筑学生国际交流工作坊（中韩十校建筑设计夏令营）在上海同济大学顺利举行。本次活动由中国建筑学会和韩国建筑院校联盟共同主办，同济大学承办，安徽建筑大学、苏州科技大学、浙江工业大学、青岛理工大学、韩国岭南大学、韩国东亚大学、韩国国立首尔科学技术大学、韩国京畿大学以及韩国东亚大学共同参与。

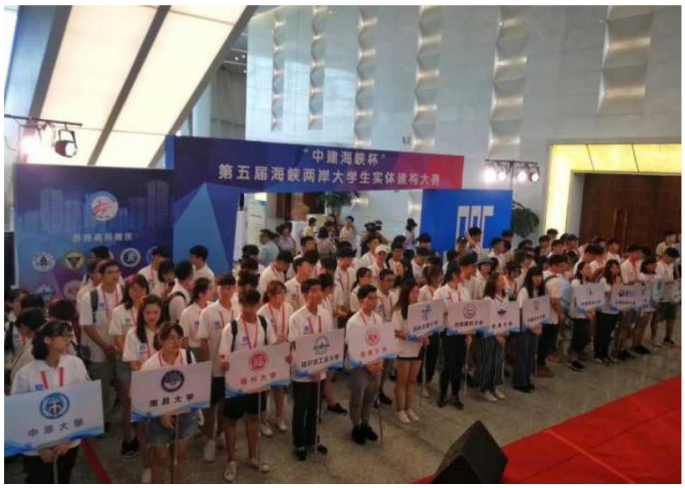


自8月23日开幕后，组委会先后安排了创意城市空间调查、专题学术讲座、中韩教师交流活动和设计工作坊及汇报评图，拓展了参赛学生的眼界，也增进了学术交流与友谊。

【学科专业竞赛】安建大学子在“中建海峡杯”第五届海峡两岸大学生实体建构大赛取得佳绩

作者： 唐劲松　　发布日期： 2018-08-29　　浏览次数： 393

本网讯　8月9日至13日，“中建海峡杯”第五届海峡两岸大学生实体建构大赛决赛在中国福州海峡青年交流营顺利举行。经过紧张激烈的角逐，安徽建筑大学建筑与规划学院参赛队表现出色，获得优秀奖。



【学科竞赛】建规学院建筑学专业学子在2017年国内外设计竞赛中屡获佳绩

作者： 唐劲松　　发布日期： 2018-01-23　　浏览次数： 905

本网讯 近年来，建筑与规划学院建筑系在全面实施专业振兴计划的背景下，积极推动教育教学改革、努力推进创新教育，通过学科竞赛，提高教学质量，增强学生的学习氛围，提升学校对外影响力。在过去的2017年，建筑系积极组织、指导学生参加各类设计竞赛，继“2017第九届中国威海国际建筑设计大奖赛”、“2017东南•中国建筑新人赛暨2017亚洲建筑新人赛中国区选拔赛”、“UIA霍普杯2017国际大学生建筑设计竞赛”、“高层建筑和城市人居委员会（CTBUH）第六届国际学生高层建筑设计大赛（澳大利亚.悉尼）”和“2017年建筑学专指委教案及优秀作业竞赛”获奖后又在第十四届“全国高等美术院校建筑与设计专业教学年会”优秀作品评选竞赛中喜获多个奖项，取得了学科竞赛年度大丰收。

2017第九届中国威海国际建筑设计大奖赛

8月31日，由中国建筑学会主办的2017全国大学生建筑设计方案竞赛公布了获奖名单。本届共收到参赛作品1007份，参赛作品来自英国爱丁堡大学、美国爱荷华州立大学、德国亚琛工业大学、意大利米兰理工大学、日本北九州市立大学、香港大学、清华大学、北京大学、同济大学、浙江大学等191所高等院校，参赛大学生3690名。本次竞赛共评出金奖1项；银奖6项；铜奖15项；优秀奖123项；“最佳指导老师奖”21项。由建规学院鲍如昕老师指导的邓宏远、汪萌同学在大赛中荣获优秀奖。

